

Crystallization

Crystallization

Fourth Edition

J. W. Mullin

*Emeritus Professor of Chemical Engineering,
University of London*



OXFORD BOSTON JOHANNESBURG MELBOURNE NEW DELHI SINGAPORE

Butterworth-Heinemann
Linacre House, Jordan Hill, Oxford OX2 8DP
225 Wildwood Avenue, Woburn, MA 01801-2041
A division of Reed Educational and Professional Publishing Ltd

 A member of the Reed Elsevier plc group

First published 1961
Second edition 1972
Third edition 1992
Reprinted 1994, 1995
Paperback edition 1997
Fourth edition 2001

© Reed Educational and Professional Publishing Ltd 2001

All rights reserved. No part of this publication may be reproduced in any material form (including photocopying or storing in any medium by electronic means and whether or not transiently or incidentally to some other use of this publication) without the written permission of the copyright holder except in accordance with the provisions of the Copyright, Designs and Patents Act 1988 or under the terms of a licence issued by the Copyright Licensing Agency Ltd, 90 Tottenham Court Road, London, England W1P 9HE. Applications for the copyright holder's written permission to reproduce any part of this publication should be addressed to the publishers

British Library Cataloguing in Publication Data

A Catalogue record for this book is available from the British Library

Library of Congress Cataloguing in Publication Data

A Catalogue record for this book is available from the Library of Congress

ISBN 0 7506 4833 3

Typeset in India at Integra Software Services Pvt Ltd, Pondicherry,
India 605005; www.integra-india.com



FOR EVERY TITLE THAT WE PUBLISH, BUTTERWORTH-HEINEMANN
WILL PAY FOR BTCV TO PLANT AND CARE FOR A TREE.

Contents

<i>Preface to Fourth Edition</i>	viii
<i>Preface to First Edition</i>	x
<i>Nomenclature and units</i>	xii
1 The crystalline state	1
1.1 Liquid crystals	1
1.2 Crystalline solids	3
1.3 Crystal symmetry	4
1.4 Crystal systems	7
1.5 Miller indices	10
1.6 Space lattices	13
1.7 Solid state bonding	15
1.8 Isomorphs and polymorphs	16
1.9 Enantiomorphs and chirality	18
1.10 Crystal habit	22
1.11 Dendrites	24
1.12 Composite crystals and twins	25
1.13 Imperfections in crystals	27
2 Physical and thermal properties	32
2.1 Density	32
2.2 Viscosity	35
2.3 Surface tension	39
2.4 Diffusivity	41
2.5 Refractive index	47
2.6 Electrolytic conductivity	48
2.7 Crystal hardness	48
2.8 Units of heat	49
2.9 Heat capacity	50
2.10 Thermal conductivity	54
2.11 Boiling, freezing and melting points	55
2.12 Enthalpies of phase change	58
2.13 Heats of solution and crystallization	62
2.14 Size classification of crystals	64
3 Solutions and solubility	86
3.1 Solutions and melts	86
3.2 Solvent selection	86
3.3 Expression of solution composition	90
3.4 Solubility correlations	92
3.5 Theoretical crystal yield	96

3.6	Ideal and non-ideal solutions	98
3.7	Particle size and solubility	108
3.8	Effect of impurities on solubility	110
3.9	Measurement of solubility	112
3.10	Prediction of solubility	120
3.11	Solubility data sources	123
3.12	Supersolubility	123
3.13	Solution structure	132
4	Phase equilibria	135
4.1	The phase rule	135
4.2	One-component systems	136
4.3	Two-component systems	139
4.4	Enthalpy–composition diagrams	146
4.5	Phase change detection	151
4.6	Three-component systems	156
4.7	Four-component systems	169
4.8	‘Dynamic’ phase diagrams	179
5	Nucleation	181
5.1	Primary nucleation	182
5.2	Secondary nucleation	195
5.3	Metastable zone widths	201
5.4	Effect of impurities	205
5.5	Induction and latent periods	206
5.6	Interfacial tension	210
5.7	Ostwald’s rule of stages	214
6	Crystal growth	216
6.1	Crystal growth theories	216
6.2	Growth rate measurements	236
6.3	Crystal growth and dissolution	260
6.4	Crystal habit modification	269
6.5	Polymorphs and phase transformations	280
6.6	Inclusions	284
7	Recrystallization	289
7.1	Recrystallization schemes	289
7.2	Resolution of racemates	295
7.3	Isolation of polymorphs	300
7.4	Recrystallization from supercritical fluids	302
7.5	Zone refining	303
7.6	Single crystals	309
8	Industrial techniques and equipment	315
8.1	Precipitation	315
8.2	Crystallization from melts	343

8.3 Sublimation	358
8.4 Crystallization from solution	368
9 Crystallizer design and operation	403
9.1 Crystal size distribution (CSD)	403
9.2 Kinetic data measurement and utilization	430
9.3 Crystallizer specification	434
9.4 Fluid–particle suspensions	451
9.5 Encrustation	459
9.6 Caking of crystals	463
9.7 Downstream processes	467
<i>Appendix</i>	478
<i>References</i>	536
<i>Author index</i>	577
<i>Subject index</i>	587

Preface to Fourth Edition

This fourth edition of *Crystallization* has been substantially rewritten and up-dated. The 1961 first edition, written primarily for chemical engineers and industrial chemists, was illustrated with practical examples from a range of process industries, coupled with basic introductions to the scientific principles on which the unit operation of crystallization depends. It was also intended to be useful to students of chemical engineering and chemical technology. The aims and objectives of the book have remained intact in all subsequent editions, although the subject matter has been considerably expanded each time to take into account technological developments and to reflect current research trends into the fundamentals of crystallization mechanisms.

The continuing upsurge in interest in the utilization of crystallization as a processing technique covers an increasing variety of industrial applications, not only in the long-established fields of bulk inorganic and organic chemical production, but also in the rapidly expanding areas of fine and specialty chemicals and pharmaceuticals. These developments have created an enormous publication explosion over the past few decades, in a very wide range of journals, and justify the large number of specialist symposia that continue to be held world-wide on the subject of crystallization.

Particular attention is drawn in this edition to such topical subjects as the isolation of polymorphs and resolution of enantiomeric systems, the potential for crystallizing from supercritical fluids, the use of molecular modelling in the search for tailored habit modifiers and the mechanisms of the effect of added impurities on the crystal growth process, the use of computer-aided fluid dynamic modelling as a means of achieving a better understanding of mixing processes, the separate and distinct roles of both batch and continuous crystallization processing, and the importance of potential downstream processing problems and methods for their identification from laboratory investigations. Great care has been taken in selecting suitable literature references for the individual sections to give a reliable guide to further reading.

Once again I want to record my indebtedness to past research students, visiting researchers and colleagues in the Crystallization Group at University College London over many years, for their help and support in so many ways. They are too numerous to name individually here, but much of their work is recorded and duly acknowledged in appropriate sections throughout this edition. I should like to express my sincere personal thanks to them all. I am also very grateful to all those who have spoken or written to me over the years with useful suggestions for corrections or improvements to the text.

Finally, and most importantly, it gives me great pleasure to acknowledge the debt I owe to my wife, Averil, who has assisted me with all four editions of

Crystallization. Without her tremendous help in preparing the manuscripts, my task of writing would not have been completed.

JOHN MULLIN
University College London
2001

Preface to First Edition

Crystallization must surely rank as the oldest unit operation, in the chemical engineering sense. Sodium chloride, for example, has been manufactured by this process since the dawn of civilization. Today there are few sections of the chemical industry that do not, at some stage, utilize crystallization as a method of production, purification or recovery of solid material. Apart from being one of the best and cheapest methods available for the production of pure solids from impure solutions, crystallization has the additional advantage of giving an end product that has many desirable properties. Uniform crystals have good flow, handling and packaging characteristics: they also have an attractive appearance, and this latter property alone can be a very important sales factor.

The industrial applications of crystallization are not necessarily confined to the production of pure solid substances. In recent years large-scale purification techniques have been developed for substances that are normally liquid at room temperature. The petroleum industry, for example, in which distillation has long held pride of place as the major processing operation, is turning its attention most keenly to low-temperature crystallization as a method for the separation of 'difficult' liquid hydrocarbon mixtures.

It is rather surprising that few books, indeed none in the English language, have been devoted to a general treatment of crystallization practice, in view of its importance and extensive industrial application. One reason for this lack of attention could easily be that crystallization is still referred to as more of an art than a science. There is undoubtedly some truth in this old adage, as anyone who has designed and subsequently operated a crystallizer will know, but it cannot be denied that nowadays there is a considerable amount of science associated with the art.

Despite the large number of advances that have been made in recent years in crystallization technology, there is still plenty of evidence of the reluctance to talk about crystallization as a process divorced from considerations of the actual substance being crystallized. To some extent this state of affairs is similar to that which existed in the field of distillation some decades ago when little attempt had been made to correlate the highly specialized techniques developed, more or less independently, for the processing of such commodities as coal tar, alcohol and petroleum products. The transformation from an 'art' to a 'science' was eventually made when it came to be recognized that the key factor which unified distillation design methods lay in the equilibrium physical properties of the working systems.

There is a growing trend today towards a unified approach to crystallization problems, but there is still some way to go before crystallization ceases to be the Cinderella of the unit operations. More data, particularly of the applied kind, should be published. In this age of prolific outputs of technical literature such a recommendation is not made lightly, but there is a real deficiency of this type

of published information. There is, at the same time, a wealth of knowledge and experience retained in the process industries, much of it empirical but none the less valuable when collected and correlated.

The object of this book is to outline the more important aspects of crystallization theory and practice, together with some closely allied topics. The book is intended to serve process chemists and engineers, and it should prove of interest to students of chemical engineering and chemical technology. While many of the techniques and operations have been described with reference to specific processes or industries, an attempt has been made to treat the subject matter in as general a manner as possible in order to emphasize the unit operational nature of crystallization. Particular attention has been paid to the newer and more recently developed processing methods, even where these have not as yet proved adaptable to the large-scale manufacture of crystals.

My thanks are due to the Editors of *Chemical Engineering Practice* for permission to include some of the material and many of the diagrams previously published by me in Volume 6 of their 12-volume series. I am indebted to Professor M. B. Donald, who first suggested that I should write on this subject, and to many of my colleagues, past and present, for helpful discussions in connection with this work. I would also like to take this opportunity of acknowledging my indebtedness to my wife for the valuable assistance and encouragement she gave me during the preparation of the manuscript.

JOHN MULLIN
London
1960

Nomenclature and units

The basic SI units of mass, length and time are the kilogram (kg), metre (m) and second (s). The basic unit of thermodynamic temperature is the kelvin (K), but temperatures and temperature differences may also be expressed in degrees Celsius ($^{\circ}\text{C}$). The unit for the amount of substance is the mole (mol), defined as the amount of substance which contains as many elementary units as there are atoms in 0.012 kg of carbon-12. Chemical engineers, however, are tending to use the kilomole (kmol = 10^3 mol) as the preferred unit. The unit of electric current is the ampere (A).

Several of the derived SI units have special names:

Quantity	Name	Symbol	SI unit	Basic SI unit
Frequency	hertz	Hz		s^{-1}
Force	newton	N		m kg s^{-2}
Pressure	pascal	Pa	N m^{-2}	$\text{m}^{-1} \text{kg s}^{-2}$
Energy, work; heat	joule	J	N m	$\text{m}^2 \text{kg s}^{-2}$
Power	watt	W	J s^{-1}	$\text{m}^2 \text{kg s}^{-3}$
Quantity of electricity	coulomb	C		s A
Electric potential	volt	V	W A^{-1}	$\text{m}^2 \text{kg s}^{-3} \text{A}^{-1}$
Electric resistance	ohm	Ω	V A^{-1}	$\text{m}^2 \text{kg s}^{-3} \text{A}^{-2}$
Conductance	siemens	S	A V^{-1}	$\text{m}^{-2} \text{kg}^{-1} \text{s}^3 \text{A}^2$
Capacitance	farad	F	C V^{-1}	$\text{m}^{-2} \text{kg}^{-1} \text{s}^4 \text{A}^2$
Magnetic flux	weber	Wb	Vs	$\text{m}^2 \text{kg s}^{-2} \text{A}^{-1}$
Magnetic flux density	tesla	T	Wb m^{-2}	$\text{kg s}^{-2} \text{A}^{-1}$
Inductance	henry	H	Wb A^{-1}	$\text{m}^2 \text{kg s}^{-2} \text{A}^{-2}$

Up to the present moment, there is no general acceptance of the pascal for expressing pressures in the chemical industry; many workers prefer to use multiples and submultiples of the bar ($1 \text{ bar} = 10^5 \text{ Pa} = 10^5 \text{ N m}^{-2} \approx 1 \text{ atmosphere}$). The standard atmosphere (760 mm Hg) is defined as $1.0133 \times 10^5 \text{ Pa}$, i.e. 1.0133 bar.

The prefixes for unit multiples and submultiples are:

10^{-18}	atto	a	10^1	deca	da
10^{-15}	femto	f	10^2	hecto	h
10^{-12}	pico	p	10^3	kilo	k
10^{-9}	nano	n	10^6	mega	M
10^{-6}	micro	μ	10^9	giga	G
10^{-3}	milli	m	10^{12}	tera	T
10^{-2}	centi	c	10^{15}	peta	P
10^{-1}	deci	d	10^{18}	exa	E

Conversion factors for some common units used in chemical engineering are listed below. An asterisk (*) denotes an exact relationship.

Length	*1 in	: 25.4 mm
	*1 ft	: 0.3048 m
	*1 yd	: 0.9144 m
	1 mile	: 1.6093 km
	*1 Å (ångstrom)	: 10^{-10} m
Time	*1 min	: 60 s
	*1 h	: 3.6 ks
	*1 day	: 86.4 ks
	1 year	: 31.5 Ms
Area	*1 in ²	: 645.16 mm ²
	1 ft ²	: 0.092903 m ²
	1 yd ²	: 0.83613 m ²
	1 acre	: 4046.9 m ²
	1 hectare	: 10 000 m ²
	1 mile ²	: 2.590 km ²
Volume	1 in ³	: 16.387 cm ³
	1 ft ³	: 0.02832 m ³
	1 yd ³	: 0.76453 m ³
	1 UK gal	: 4546.1 cm ³
	1 US gal	: 3785.4 cm ³
Mass	1 oz	: 28.352 g
	1 grain	: 0.06480 g
	*1 lb	: 045359237 kg
	1 cwt	: 508023 kg
	1 ton	: 1016.06 kg
Force	1 pdl	: 0.13826 N
	1 lbf	: 4.4482 N
	1 kgf	: 9.8067 N
	1 tonf	: 9.9640 kN
	*1 dyn	: 10^{-5} N
Temperature difference	*1 degF (degR)	: $\frac{5}{9}$ degC (K)
Energy (work, heat)	1 ft lbf	: 1.3558 J
	1 ft pdl	: 0.04214 J
	*1 cal (internat. table)	: 4.1868 J
	1 erg	: 10^{-7} J
	1 Btu	: 1.05506 kJ
	1 chu	: 1.8991 kJ
	1 hp h	: 2.6845 MJ
	*1 kW h	: 3.6 MJ
	1 therm	: 105.51 MJ
	1 thermie	: 4.1855 MJ

Calorific value (volumetric)	1 Btu/ft ³ 1 chu/ft ³ 1 kcal/ft ³ 1 kcal/m ³ 1 therm/ft ³	: 37.259 kJ m ⁻³ : 67.067 kJ m ⁻³ : 147.86 kJ m ⁻³ : 4.1868 kJ m ⁻³ : 3.7260 GJ m ⁻³
Velocity	1 ft/s 1 ft/min 1 ft/h 1 mile/h	: 0.3048 m s ⁻¹ : 5.0800 mm s ⁻¹ : 84.667 µm s ⁻¹ : 0.44704 m s ⁻¹
Volumetric flow	1 ft ³ /s 1 ft ³ /h 1 UK gal/h 1 US gal/h	: 0.028316 m ³ s ⁻¹ : 7.8658 cm ³ s ⁻¹ : 1.2628 cm ³ s ⁻¹ : 1.0515 cm ³ s ⁻¹
Mass flow	1 lb/h 1 ton/h	: 0.12600 g s ⁻¹ : 0.28224 kg s ⁻¹
Mass per unit area	1 lb/in ² 1 lb/ft ² 1 ton/mile ²	: 703.07 kg m ⁻² : 4.8824 kg m ⁻² : 392.30 kg km ⁻²
Density	1 lb/in ³ 1 lb/ft ³ 1 lb/UK gal 1 lb/US gal	: 27.680 g cm ⁻³ : 16.019 kg m ⁻³ : 99.776 kg m ⁻³ : 119.83 kg m ⁻³
Pressure	1 lbf/in ² 1 tonf/in ² 1 lbf/ft ² 1 kgf/m ² *1 standard atm *1 at (1 kgf/cm ²) *1 bar 1 ft water 1 in water 1 inHg 1 mmHg (1 torr)	: 6.8948 kN m ⁻² : 15.444 MN m ⁻² : 47.880 N m ⁻² : 9.8067 N m ⁻² : 101.325 kN m ⁻² : 98.0665 kN m ⁻² : 10 ⁵ N m ⁻² : 2.9891 kN m ⁻² : 249.09 N m ⁻² : 3.3864 kN m ⁻² : 133.32 N m ⁻²
Power (heat flow)	1 hp (British) 1 hp (metric) 1 erg/s 1 ft lbf/s 1 Btu/h 1 Btu/s 1 chu/h 1 chu/s 1 kcal/h 1 ton of refrigeration	: 745.70 W : 735.50 W : 10 ⁻⁷ W : 1.3558 W : 0.29308 W : 1.0551 kW : 0.52754 W : 1.8991 kW : 1.1630 kW : 3516.9 W

Moment of inertia	1 lb ft ²	: 0.042140 kg m ²
Momentum	1 lb ft/s	: 0.13826 kg m s ⁻¹
Angular momentum	1 lb ft ² /s	: 0.042140 kg m ² s ⁻¹
Viscosity, dynamic	*1 poise (1 g/cm s)	: 0.1 N s m ⁻² (0.1 kg m ⁻¹ s ⁻¹)
	1 lb/ft h	: 0.41338 m N s m ⁻²
	1 lb/ft s	: 1.4882 N s m ⁻²
Viscosity, kinematic	*1 stokes (1 cm ² /s)	: 10 ⁻⁴ m ² s ⁻¹
	1 ft ² /h	: 0.25806 cm ² s ⁻¹
Surface energy (surface tension)	1 erg/cm ² (1 dyn/cm)	: 10 ⁻³ J m ⁻² (10 ⁻³ N m ⁻¹)
Surface per unit volume	1 ft ² /ft ³	: 3.2808 m ² m ⁻³
Surface per unit mass	1 ft ² /lb	: 0.20482 m ² kg ⁻¹
Mass flux density	1 lb/h ft ²	: 1.3562 g s ⁻¹ m ⁻²
Heat flux density	1 Btu/h ft ² *1 kcal/h m ²	: 3.1546 W m ⁻² : 1.163 W m ⁻²
Heat transfer coefficient	1 Btu/h ft ² °F 1 kcal/h m ² °C	: 5.6784 W m ⁻² K ⁻¹ : 1.1630 W m ⁻² K ⁻¹
Specific enthalpy (latent heat, etc.)	*1 Btu/lb	: 2.326 kJ kg ⁻¹
Heat capacity (specific heat)	*1 Btu/lb°F	: 4.1868 kJ kg ⁻¹ K ⁻¹
Thermal conductivity	1 Btu/h ft°F 1 kcal/h m°C	: 1.7307 W m ⁻¹ K ⁻¹ : 1.163 W m ⁻¹ K ⁻¹

The values of some common physical constants in SI units include:

Avogadro number, N_A	$6.023 \times 10^{23} \text{ mol}^{-1}$
Boltzmann constant, k	$1.3805 \times 10^{-23} \text{ J K}^{-1}$
Planck constant, h	$6.626 \times 10^{-34} \text{ Js}$
Stefan–Boltzmann constant, σ	$5.6697 \times 10^{-8} \text{ W m}^{-2} \text{ K}^{-4}$
Standard temperature and pressure (s.t.p.)	273.15 K and $1.013 \times 10^5 \text{ N m}^{-2}$
Volume of 1 kmol of ideal gas at s.t.p.	22.41 m^3
Gravitational acceleration	9.807 m s^{-2}
Universal gas constant, R	$8.3143 \text{ J mol}^{-1} \text{ K}^{-1}$
Faraday constant, F	$9.6487 \times 10^4 \text{ C mol}^{-1}$

1 *The crystalline state*

The three general states of matter – gaseous, liquid and solid – represent very different degrees of atomic or molecular mobility. In the gaseous state, the molecules are in constant, vigorous and random motion; a mass of gas takes the shape of its container, is readily compressed and exhibits a low viscosity. In the liquid state, random molecular motion is much more restricted. The volume occupied by a liquid is limited; a liquid only takes the shape of the occupied part of its container, and its free surface is flat, except in those regions where it comes into contact with the container walls. A liquid exhibits a much higher viscosity than a gas and is less easily compressed. In the solid state, molecular motion is confined to an oscillation about a fixed position, and the rigid structure generally resists compression very strongly; in fact it will often fracture when subjected to a deforming force.

Some substances, such as wax, pitch and glass, which possess the outward appearance of being in the solid state, yield and flow under pressure, and they are sometimes regarded as highly viscous liquids. Solids may be crystalline or amorphous, and the crystalline state differs from the amorphous state in the regular arrangement of the constituent molecules, atoms or ions into some fixed and rigid pattern known as a lattice. Actually, many of the substances that were once considered to be amorphous have now been shown, by X-ray analysis, to exhibit some degree of regular molecular arrangement, but the term ‘crystalline’ is most frequently used to indicate a high degree of internal regularity, resulting in the development of definite external crystal faces.

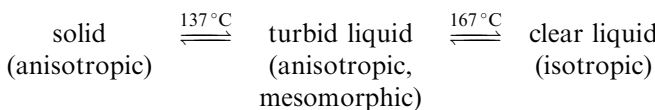
As molecular motion in a gas or liquid is free and random, the physical properties of these fluids are the same no matter in what direction they are measured. In other words, they are *isotropic*. True amorphous solids, because of the random arrangement of their constituent molecules, are also isotropic. Most crystals, however, are *anisotropic*; their mechanical, electrical, magnetic and optical properties can vary according to the direction in which they are measured. Crystals belonging to the cubic system are the exception to this rule; their highly symmetrical internal arrangement renders them optically isotropic. Anisotropy is most readily detected by refractive index measurements, and the striking phenomenon of double refraction exhibited by a clear crystal of Iceland spar (calcite) is probably the best-known example.

1.1 Liquid crystals

Before considering the type of crystal with which everyone is familiar, namely the solid crystalline body, it is worth while mentioning a state of matter which possesses the flow properties of a liquid yet exhibits some of the properties of the crystalline state.

Although liquids are usually isotropic, some 200 cases are known of substances that exhibit anisotropy in the liquid state at temperatures just above their melting point. These liquids bear the unfortunate, but popular, name ‘liquid crystals’: the term is inapt because the word ‘crystal’ implies the existence of a precise space lattice. Lattice formation is not possible in the liquid state, but some form of molecular orientation can occur with certain types of molecules under certain conditions. Accordingly, the name ‘anisotropic liquid’ is preferred to ‘liquid crystal’. The name ‘mesomorphic state’ is used to indicate that anisotropic liquids are intermediate between the true liquid and crystalline solid states.

Among the better-known examples of anisotropic liquids are *p*-azoxyphenetole, *p*-azoxyanisole, cholesteryl benzoate, ammonium oleate and sodium stearate. These substances exhibit a sharp melting point, but they melt to form a turbid liquid. On further heating, the liquid suddenly becomes clear at some fixed temperature. On cooling, the reverse processes occur at the same temperatures as before. It is in the turbid liquid stage that anisotropy is exhibited. The changes in physical state occurring with change in temperature for the case of *p*-azoxyphenetole are:



The simplest representation of the phenomenon is given by Bose’s swarm theory, according to which molecules orientate into a number of groups in parallel formation (*Figure 1.1*). In many respects this is rather similar to the behaviour of a large number of logs floating down a river. Substances that can exist in the mesomorphic state are usually organic compounds, often aromatic, with elongated molecules.

The mesomorphic state is conveniently divided into two main classes. The *smectic* (soap-like) state is characterized by an oily nature, and the flow of such liquids occurs by a gliding movement of thin layers over one another. Liquids in the *nematic* (thread-like) state flow like normal viscous liquids, but mobile threads can often be observed within the liquid layer. A third class, in which

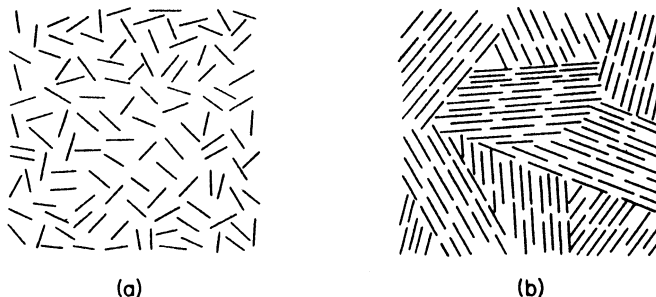


Figure 1.1. Isotropic and anisotropic liquids. (a) Isotropic: molecules in random arrangement; (b) anisotropic: molecules aligned into swarms

strong optical activity is exhibited, is known as the *cholesteric* state; some workers regard this state as a special case of the nematic. The name arises from the fact that cholestryl compounds form the majority of known examples.

For further information on this subject, reference should be made to the relevant references listed in the Bibliography at the end of this chapter.

1.2 Crystalline solids

The true solid crystal comprises a rigid lattice of molecules, atoms or ions, the locations of which are characteristic of the substance. The regularity of the internal structure of this solid body results in the crystal having a characteristic shape; smooth surfaces or faces develop as a crystal grows, and the planes of these faces are parallel to atomic planes in the lattice. Very rarely, however, do any two crystals of a given substance look identical; in fact, any two given crystals often look quite different in both size and external shape. In a way this is not very surprising, as many crystals, especially the natural minerals, have grown under different conditions. Few natural crystals have grown 'free'; most have grown under some restraint resulting in stunted growth in one direction and exaggerated growth in another.

This state of affairs prevented the general classification of crystals for centuries. The first advance in the science of crystallography came in 1669 when Steno observed a unique property of all quartz crystals. He found that the angle between any two given faces on a quartz crystal was constant, irrespective of the relative sizes of these faces. This fact was confirmed later by other workers, and in 1784 Haüy proposed his Law of Constant Interfacial Angles: the angles between corresponding faces of all crystals of a given substance are constant. The crystals may vary in size, and the development of the various faces (the crystal habit) may differ considerably, but the interfacial angles do not vary; they are characteristic of the substance. It should be noted, however, that substances can often crystallize in more than one structural arrangement (polymorphism – see section 1.8) in which case Haüy's law applies only to the crystals of a given polymorph.

Interfacial angles on centimetre-sized crystals, e.g. geological specimens, may be measured with a contact goniometer, consisting of an arm pivoted on a protractor (*Figure 1.2*), but precisions greater than 0.5° are rarely possible. The reflecting goniometer (*Figure 1.3*) is a more versatile and accurate apparatus. A crystal is mounted at the centre of a graduated turntable, a beam of light from an illuminated slit being reflected from one face of the crystal. The reflection is observed in a telescope and read on the graduated scale. The turntable is then rotated until the reflection from the next face of the crystal is observed in the telescope, and a second reading is taken from the scale. The difference α between the two readings is the angle between the normals to the two faces, and the interfacial angle is therefore $(180 - \alpha)^\circ$.

Modern techniques of X-ray crystallography enable lattice dimensions and interfacial angles to be measured with high precision on milligram samples of crystal powder specimens.

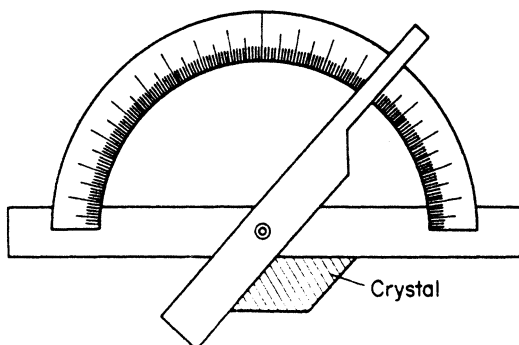


Figure 1.2. Simple contact goniometer

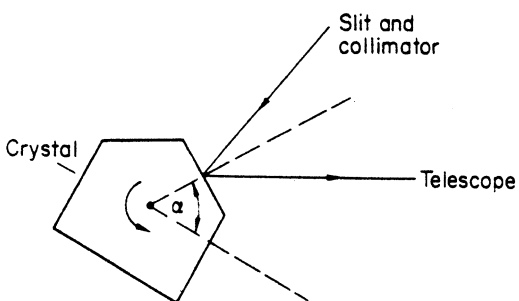


Figure 1.3. Reflecting goniometer

1.3 Crystal symmetry

Many of the geometric shapes that appear in the crystalline state are readily recognized as being to some degree symmetrical, and this fact can be used as a means of crystal classification. The three simple elements of symmetry which can be considered are:

1. Symmetry about a point (a *centre* of symmetry)
2. Symmetry about a line (an *axis* of symmetry)
3. Symmetry about a plane (a *plane* of symmetry)

It must be remembered, however, that while some crystals may possess a centre and several different axes and planes of symmetry, others may have no element of symmetry at all.

A crystal possesses a centre of symmetry when every point on the surface of the crystal has an identical point on the opposite side of the centre, equidistant from it. A perfect cube is a good example of a body having a centre of symmetry (at its mass centre).

If a crystal is rotated through 360° about any given axis, it obviously returns to its original position. If, however, the crystal *appears* to have reached its original

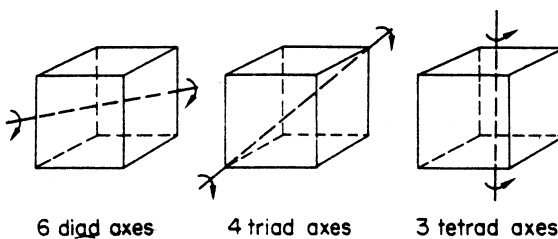


Figure 1.4. The 13 axes of symmetry in a cube

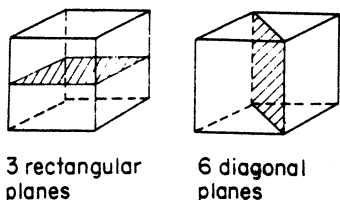


Figure 1.5. The 9 planes of symmetry in a cube

position more than once during its complete rotation, the chosen axis is an axis of symmetry. If the crystal has to be rotated through 180° ($360/2$) before coming into coincidence with its original position, the axis is one of twofold symmetry (called a diad axis). If it has to be rotated through 120° ($360/3$), 90° ($360/4$) or 60° ($360/6$) the axes are of threefold symmetry (triad axis), fourfold symmetry (tetrad axis) and sixfold symmetry (hexad axis), respectively. These are the only axes of symmetry possible in the crystalline state.

A cube, for instance, has 13 axes of symmetry: 6 diad axes through opposite edges, 4 triad axes through opposite corners and 3 tetrad axes through opposite faces. One each of these axes of symmetry is shown in *Figure 1.4*.

The third simple type is symmetry about a plane. A plane of symmetry bisects a solid object in such a manner that one half becomes the mirror image of the other half in the given plane. This type of symmetry is quite common and is often the only type exhibited by a crystal. A cube has 9 planes of symmetry: 3 rectangular planes each parallel to two faces, and 6 diagonal planes passing through opposite edges, as shown in *Figure 1.5*.

It can be seen, therefore, that the cube is a highly symmetrical body, as it possesses 23 elements of symmetry (a centre, 9 planes and 13 axes). An octahedron also has the same 23 elements of symmetry; so, despite the difference in outward appearance, there is a definite crystallographic relationship between these two forms. *Figure 1.6* indicates the passage from the cubic (hexahedral) to the octahedral form, and vice versa, by a progressive and symmetrical removal of the corners. The intermediate solid forms shown (truncated cube, truncated octahedron and cubo-octahedron) are three of the 13 Archimedean semi-regular solids which are called *combination forms*, i.e. combinations of a cube and an octahedron. Crystals exhibiting combination forms are commonly encountered (see *Figure 1.20*).

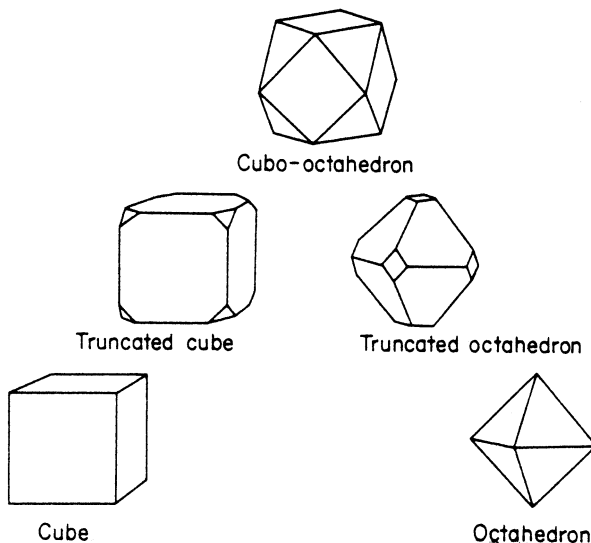


Figure 1.6. Combination forms of cube and octahedron

The tetrahedron is also related to the cube and octahedron; in fact these three forms belong to the five regular solids of geometry. The other two (the regular dodecahedron and icosahedron) do not occur in the crystalline state. The rhombic dodecahedron, however, is frequently found, particularly in crystals of garnet. *Table 1.1* lists the properties of the six regular and semi-regular forms most often encountered in crystals. The Euler relationship is useful for calculating the number of faces, edges and corners of any polyhedron:

$$E = F + C - 2$$

This relationship states that the number of edges is two less than the sum of the number of faces and corners.

A fourth element of symmetry which is exhibited by some crystals is known by the names ‘compound, or alternating, symmetry’, or symmetry about a

Table 1.1. Properties of some regular and semi-regular forms found in the crystalline state

Form	Faces	Edges	Corners	Edges at a corner	Elements of symmetry		
					Centre	Planes	Axes
<i>Regular solids</i>							
Tetrahedron	4	6	4	3	No	6	7
Hexahedron (cube)	6	12	8	3	Yes	9	13
Octahedron	8	12	6	4	Yes	9	13
<i>Semi-regular solids</i>							
Truncated cube	14	36	24	3	Yes	9	13
Truncated octahedron	14	36	24	3	Yes	9	13
Cubo-octahedron	14	24	12	4	Yes	9	13

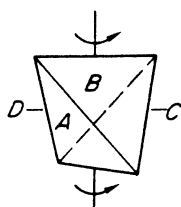


Figure 1.7. An axis of compound symmetry

'rotation–reflection axis' or 'axis of rotatory inversion'. This type of symmetry obtains when one crystal face can be related to another by performing two operations: (a) rotation about an axis, and (b) reflection in a plane at right angles to the axis, or inversion about the centre. *Figure 1.7* illustrates the case of a tetrahedron, where the four faces are marked *A*, *B*, *C* and *D*. Face *A* can be transformed into face *B* after rotation through 90° , followed by an inversion. This procedure can be repeated four times, so the chosen axis is a compound axis of fourfold symmetry.

1.4 Crystal systems

There are only 32 possible combinations of the above-mentioned elements of symmetry, including the asymmetric state (no elements of symmetry), and these are called the 32 *point groups* or *classes*. All but one or two of these classes have been observed in crystalline bodies. For convenience these 32 classes are grouped into seven *systems*, which are known by the following names: regular (5 possible classes), tetragonal (7), orthorhombic (3), monoclinic (3), triclinic (2), trigonal (5) and hexagonal (7).

The first six of these systems can be described with reference to three axes, *x*, *y* and *z*. The *z* axis is vertical, and the *x* axis is directed from front to back and the *y* axis from right to left, as shown in *Figure 1.8a*. The angle between the axes *y* and *z* is denoted by α , that between *x* and *z* by β , and that between *x* and *y* by γ . Four axes are required to describe the hexagonal system: the *z* axis is vertical and perpendicular to the other three axes (*x*, *y* and *u*), which are coplanar and inclined at 60° (or 120°) to one another, as shown in *Figure 1.8b*. Some workers

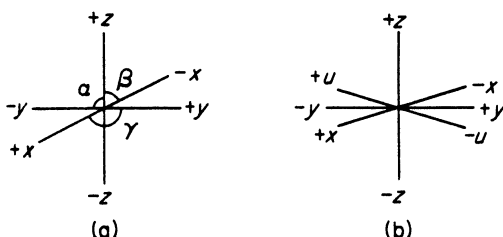


Figure 1.8. Crystallographic axes for describing the seven crystal systems: (a) three axes $\hat{y}\hat{z} = \alpha$; $\hat{x}\hat{z} = \beta$; $\hat{x}\hat{y} = \gamma$; (b) four axes (hexagonal system) $xy = \hat{y}\hat{u} = \hat{u}\hat{x} = 60^\circ$ (120°)

Table 1.2. *The seven crystal systems*

System	Other names	Angles between axes	Length of axes	Examples
Regular	Cubic	$\alpha = \beta = \gamma = 90^\circ$	$x = y = z$	Sodium chloride
	Octahedral			Potassium chloride
Tetragonal	Isometric			Alums
	Tesseral			Diamond
Tetragonal	Pyramidal	$\alpha = \beta = \gamma = 90^\circ$	$x = y \neq z$	Rutile
	Quadratic			Zircon Nickel sulphate. $7\text{H}_2\text{O}$
Orthorhombic	Rhombic	$\alpha = \beta = \gamma = 90^\circ$	$x \neq y \neq z$	Potassium permanganate
	Prismatic			Silver nitrate
	Isoclinic			Iodine
Monoclinic	Trimetric			α -Sulphur
	Monosymmetric	$\alpha = \beta = 90^\circ \neq \gamma$	$x \neq y \neq z$	Potassium chlorate
	Clinorhombic			Sucrose
Triclinic	Oblique			Oxalic acid
	Anorthic	$\alpha \neq \beta \neq \gamma \neq 90^\circ$	$x \neq y \neq z$	β -Sulphur
	Asymmetric			Potassium dichromate
Trigonal	Rhombohedral	$\alpha = \beta = \gamma \neq 90^\circ$	$x = y = z$	Copper sulphate. $5\text{H}_2\text{O}$
				Sodium nitrate
				Ruby
Hexagonal				Sapphire
	None	z axis is perpendicular to the x , y and u axes, which are inclined at 60°	$x = y = u \neq z$	Silver iodide
				Graphite
				Water (ice)
				Potassium nitrate

prefer to describe the trigonal system with reference to four axes. Descriptions of the seven crystal systems, together with some of the other names occasionally employed, are given in *Table 1.2*.

For the regular, tetragonal and orthorhombic systems, the three axes x , y and z are mutually perpendicular. The systems differ in the relative lengths of these axes: in the regular system they are all equal; in the orthorhombic system they are all unequal; and in the tetragonal system two are equal and the third is different. The three axes are all unequal in the monoclinic and triclinic systems; in the former, two of the angles are 90° and one angle is different, and in the latter all three angles are unequal and none is equal to 90° . Sometimes the limitation ‘not equal to 30° , 60° or 90° ’ is also applied to the triclinic system. In the trigonal system three equal axes intersect at equal angles, but the angles are

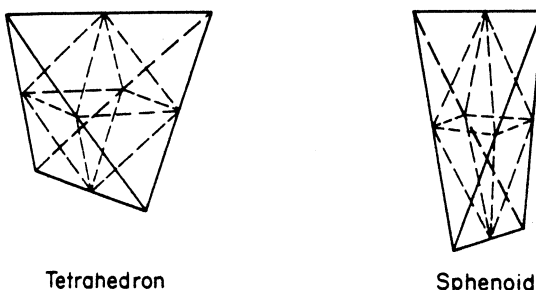


Figure 1.9. Hemihedral forms of the octahedron and tetragonal bipyramid

not 90° . The hexagonal system is described with reference to four axes. The axis of sixfold symmetry (hexad axis) is usually chosen as the z axis, and the other three equal-length axes, located in a plane at 90° to the z axis, intersect one another at 60° (or 120°).

Each crystal system contains several classes that exhibit only a partial symmetry; for instance, only one-half or one-quarter of the maximum number of faces permitted by the symmetry may have been developed. The *holohedral* class is that which has the maximum number of similar faces, i.e. possesses the highest degree of symmetry. In the *hemihedral* class only half this number of faces have been developed, and in the *tetrahedral* class only one-quarter have been developed. For example, the regular tetrahedron (4 faces) is the hemihedral form of the holohedral octahedron (8 faces) and the wedge-shaped sphenoid is the hemihedral form of the tetragonal bipyramid (*Figure 1.9*).

It has been mentioned above that crystals exhibiting combination forms are often encountered. The simplest forms of any crystal system are the prism and the pyramid. The cube, for instance, is the prism form of the regular system and the octahedron is the pyramidal form, and some combinations of these two forms have been indicated in *Figure 1.6*. Two simple combination forms in the tetragonal system are shown in *Figure 1.10*. *Figures 1.10a* and *b* are the tetragonal prism and bipyramid, respectively. *Figure 1.10c* shows a tetragonal prism that is terminated by two tetragonal pyramids, and *Figure 1.10d* the

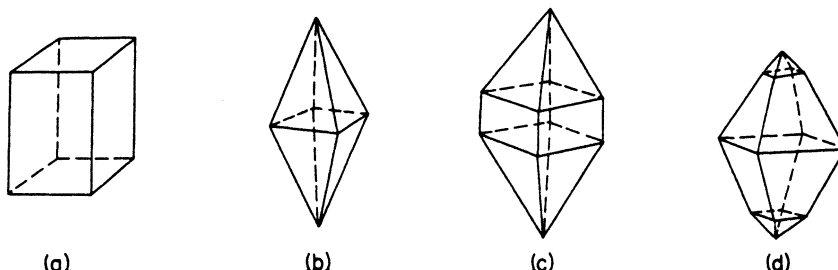


Figure 1.10. Simple combination forms in the tetragonal system: (a) tetragonal prism; (b) tetragonal bipyramid; (c) combination of prism and bipyramid; (d) combination of two bipyramids

combination of two different tetragonal bipyramids. It frequently happens that a crystal develops a group of faces which intersect to form a series of parallel edges: such a set of faces is said to constitute a *zone*. In *Figure 1.10b*, for instance, the four prism faces make a zone.

The crystal system favoured by a substance is to some extent dependent on the atomic or molecular complexity of the substance. More than 80 per cent of the crystalline elements and very simple inorganic compounds belong to the regular and hexagonal systems. As the constituent molecules become more complex, the orthorhombic and monoclinic systems are favoured; about 80 per cent of the known crystalline organic substances and 60 per cent of the natural minerals belong to these systems.

1.5 Miller indices

All the faces of a crystal can be described and numbered in terms of their axial intercepts. The axes referred to here are the crystallographic axes (usually three) which are chosen to fit the symmetry; one or more of these axes may be axes of symmetry or parallel to them, but three convenient crystal edges can be used if desired. It is best if the three axes are mutually perpendicular, but this cannot always be arranged. On the other hand, crystals of the hexagonal system are often allotted four axes for indexing purposes.

If, for example, three crystallographic axes have been decided upon, a plane that is inclined to all three axes is chosen as the standard or *parametral plane*. It is sometimes possible to choose one of the crystal faces to act as the parametral plane. The intercepts X , Y and Z of this plane on the axes x , y and z are called parameters a , b and c . The ratios of the parameters $a:b$ and $b:c$ are called the axial ratios, and by convention the values of the parameters are reduced so that the value of b is unity.

W. H. Miller suggested, in 1839, that each face of a crystal could be represented by the indices h , k and l , defined by

$$h = \frac{a}{X}, \quad k = \frac{b}{Y} \quad \text{and} \quad l = \frac{c}{Z}$$

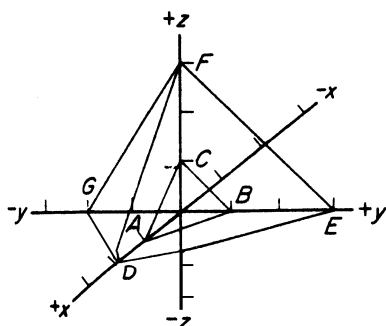


Figure 1.11. Intercepts of planes on the crystallographic axes

For the parametral plane, the axial intercepts X , Y and Z are the parameters a , b and c , so the indices h , k and l are a/a , b/b and c/c , i.e. 1, 1 and 1. This is usually written (111). The indices for the other faces of the crystal are calculated from the values of their respective intercepts X , Y and Z , and these intercepts can always be represented by ma , nb and pc , where m , n and p are small whole numbers or infinity (Häüy's Law of Rational Intercepts).

The procedure for allotting face indices is indicated in *Figure 1.11*, where equal divisions are made on the x , y and z axes. The parametral plane ABC , with axial intercepts of $OA = a$, $OB = b$ and $OC = c$, respectively, is indexed (111), as described above. Plane DEF has axial intercepts $X = OD = 2a$, $Y = OE = 3b$ and $Z = OF = 3c$; so the indices for this face can be calculated as

$$h = a/X = a/2a = \frac{1}{2}$$

$$k = b/Y = b/3b = \frac{1}{3}$$

$$l = c/Z = c/3c = \frac{1}{3}$$

Hence $h:k:l = \frac{1}{2} : \frac{1}{3} : \frac{1}{3}$, and multiplying through by six, $h:k:l = 3:2:2$. Face DEF , therefore, is indexed (322). Similarly, face DFG , which has axial intercepts of $X = 2a$, $Y = -2b$ and $Z = 3c$, gives $h:k:l = \frac{1}{2} : -\frac{1}{2} : \frac{1}{3} = 3 : -3 : 2$ or (332). Thus the Miller indices of a face are inversely proportional to its axial intercepts.

The generally accepted notation for Miller indices is that (hkl) represents a crystal face or lattice plane, while $\{hkl\}$ represents a crystallographic form comprising all faces that can be derived from hkl by symmetry operations of the crystal.

Figure 1.12 shows two simple crystals belonging to the regular system. As there is no inclined face in the cube, no face can be chosen as the parametral plane (111). The intercepts Y and Z of face A on the axes y and z are at infinity,

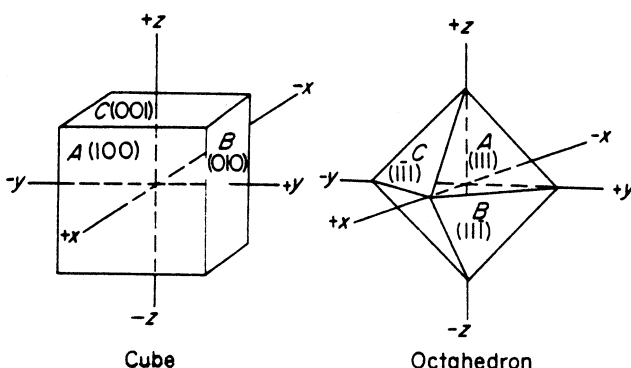


Figure 1.12. Two simple crystals belonging to the regular system, showing the use of Miller indices

so the indices h , k and l for this face will be a/a , b/∞ and c/∞ , or (100). Similarly, faces B and C are designated (010) and (001), respectively. For the octahedron, face A is chosen arbitrarily as the parametral plane, so it is designated (111). As the crystal belongs to the regular system, the axial intercepts made by the other faces are all equal in magnitude, but not in sign, to the parametral intercepts a , b and c . For instance, the intercepts of face B on the z axis is negative, so this face is designated (111). Similarly, face C is designated (111), and the unmarked D face is (111).

Figure 1.13 shows some geometrical figures representing the seven crystal systems, and *Figure 1.14* indicates a few characteristic forms exhibited by crystals of some common substances.

Occasionally, after careful goniometric measurement, crystals may be found to exhibit plane surfaces which appear to be crystallographic planes, being symmetrical in accordance with the symmetry of the crystal, but which cannot be described by simple indices. These are called *vicinal faces*. A simple method for determining the existence of these faces is to observe the reflection of a spot of light on the face: four spot reflections, for example, would indicate four vicinal faces.

The number of vicinal faces corresponds to the symmetry of the face, and this property may often be used as an aid to the classification of the crystal. For example, a cube face (fourfold axis of symmetry) may appear to be made up of an extremely flat four-sided pyramid with its base being the true (100) plane but its apex need not necessarily be at the centre of the face. An octahedral face (threefold symmetry) may show a three-sided pyramid. These vicinal faces most probably arise from the mode of layer growth on the individual faces commencing at point sources (see section 6.1).

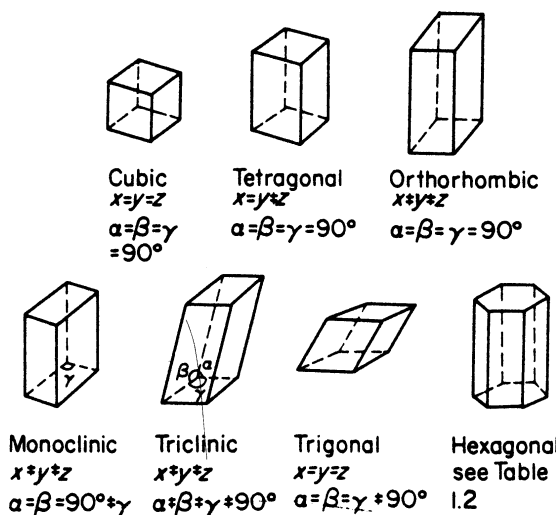


Figure 1.13. The seven crystal systems

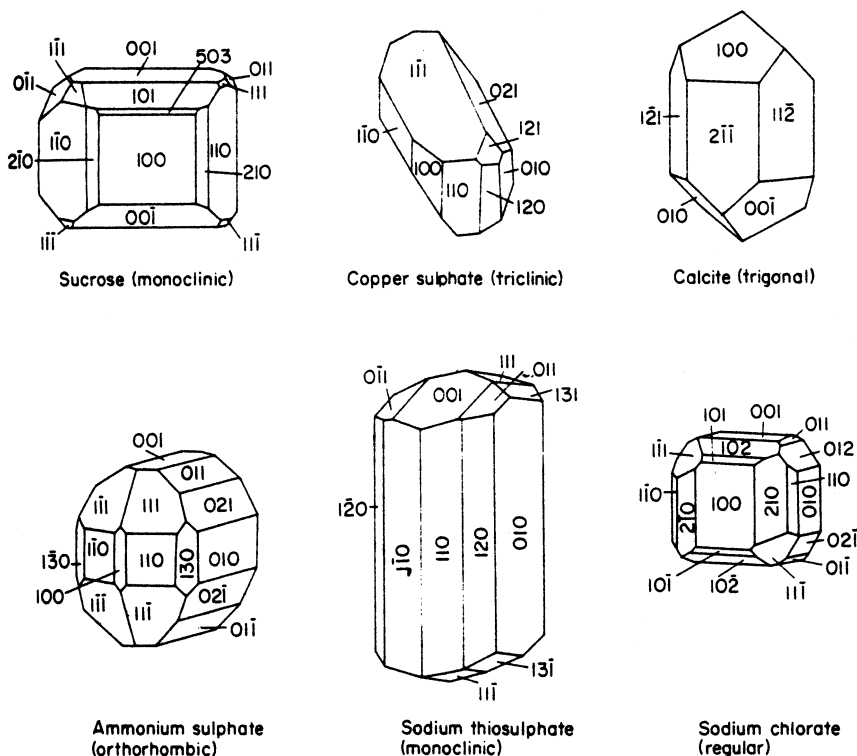


Figure 1.14. Some characteristic crystal forms

1.6 Space lattices

The external development of smooth faces on a crystal arises from some regularity in the internal arrangement of the constituent ions, atoms or molecules. Any account of the crystalline state, therefore, should include some reference to the internal structure of crystals. It is beyond the scope of this book to deal in any detail with this large topic, but a brief description will be given of the concept of the space lattice. For further information reference should be made to the specialized works listed in the Bibliography.

It is well known that some crystals can be split by cleavage into smaller crystals which bear a distinct resemblance in shape to the parent body. While there is clearly a mechanical limit to the number of times that this process can be repeated, eighteenth century investigators, Hooke and Haüy in particular, were led to the conclusion that all crystals are built up from a large number of minute units, each shaped like the larger crystal. This hypothesis constituted a very important step forward in the science of crystallography because its logical extension led to the modern concept of the space lattice.

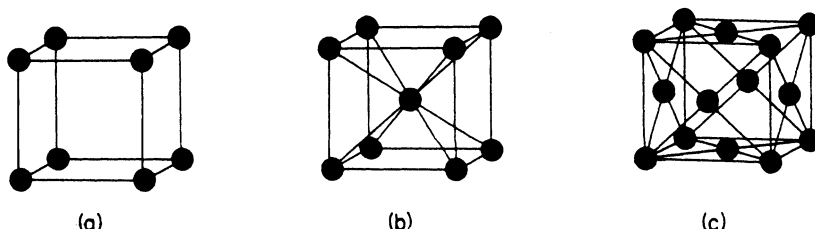
A space lattice is a regular arrangement of points in three dimensions, each point representing a structural unit, e.g. an ion, atom or a molecule. The whole

Table 1.3. The fourteen Bravais lattices

Type of symmetry	Lattice	Corresponding crystal system
Cubic	Cube	Regular
	Body-centred cube	
	Face-centred cube	
Tetragonal	Square prism	Tetragonal
	Body-centred square prism	
Orthorhombic	Rectangular prism	Orthorhombic
	Body-centred rectangular prism	
	Rhombic prism	
	Body-centred rhombic prism	
Monoclinic	Monoclinic parallelepiped	Monoclinic
	Clinorhombic prism	
Triclinic	Triclinic parallelepiped	Triclinic
Rhombohedral	Rhombohedron	Trigonal
Hexagonal	Hexagonal prism	Hexagonal

structure is homogeneous, i.e. every point in the lattice has an environment identical with every other point's. For instance, if a line is drawn between any two points, it will, when produced in both directions, pass through other points in the lattice whose spacing is identical with that of the chosen pair. Another way in which this homogeneity can be visualized is to imagine an observer located within the structure; he would get the same view of his surroundings from any of the points in the lattice.

By geometrical reasoning, Bravais postulated in 1848 that there were only 14 possible basic types of lattice that could give the above environmental identity. These 14 lattices can be classified into seven groups based on their symmetry, which correspond to the seven crystal systems listed in *Table 1.2*. The 14 Bravais lattices are given in *Table 1.3*. The three cubic lattices are illustrated in *Figure 1.15*; the first comprises eight structural units arranged at the corners of a cube, the second consists of a cubic structure with a ninth unit located at the centre of the cube, and the third of a cube with six extra units each located on a face of the cube.

**Figure 1.15.** The three cubic lattices: (a) cube; (b) body-centred cube; (c) face-centred cube

The points in any lattice can be arranged to lie on a larger number of different planes, called lattice planes, some of which will contain more points per unit area than others. The external faces of a crystal are parallel to lattice planes, and the most commonly occurring faces will be those which correspond to planes containing a high density of points, usually referred to as a high reticular density (Law of Bravais). Cleavage also occurs along lattice planes. Bravais suggested that the surface energies, and hence the rates of growth, should be inversely proportional to the reticular densities, so that the planes of highest density will grow at the slowest rate and the low-density planes, by their high growth rate, may soon disappear. For these reasons, the shape of a grown crystal may not always reflect the symmetry expected from its basic unit cell (see section 6.4).

Although there are only 14 basic lattices, interpenetration of lattices can occur in actual crystals, and it has been deduced that 230 combinations are possible which still result in the identity of environment of any given point. These combinations are the 230 space groups, which are divided into the 32 point groups, or classes, mentioned above in connection with the seven crystal systems. The law of Bravais has been extended by Donnay and Harker in 1937 into a more generalized form (the Bravais–Donnay–Harker Principle) by consideration of the space groups rather than the lattice types.

1.7 Solid state bonding

Four main types of crystalline solid may be specified according to the method of bonding in the solid state, viz. ionic, covalent, molecular and metallic. There are materials intermediate between these classes, but most crystalline solids can be classified as predominantly one of the basic types.

The *ionic crystals* (e.g. sodium chloride) are composed of charged ions held in place in the lattice by electrostatic forces, and separated from the oppositely charged ions by regions of negligible electron density. In *covalent crystals* (e.g. diamond) the constituent atoms do not carry effective charges; they are connected by a framework of covalent bonds, the atoms sharing their outer electrons. *Molecular crystals* (e.g. organic compounds) are composed of discrete molecules held together by weak attractive forces (e.g. π -bonds or hydrogen bonds).

Metallic crystals (e.g. copper) comprise ordered arrays of identical cations. The constituent atoms share their outer electrons, but these are so loosely held that they are free to move through the crystal lattice and confer ‘metallic’ properties on the solid. For example, ionic, covalent and molecular crystals are essentially non-conductors of electricity, because the electrons are all locked into fixed quantum states. Metals are good conductors because of the presence of mobile electrons.

Semiconducting crystals (e.g. germanium) are usually covalent solids with some ionic characteristics, although a few molecular solids (e.g. some polycyclic aromatic hydrocarbons such as anthracene) are known in which under certain conditions a small fraction of the valency electrons are free to move in the

crystal. The electrical conductivity of semiconductors is electronic in nature, but it differs from that in metals. Metallic conductivity decreases when the temperature is raised, because thermal agitation exerts an impeding effect. On the other hand, the conductivity of a semiconductor increases with heating, because the number of electron–‘hole’ pairs, the electricity carriers in semiconductors, increases greatly with temperature. Metals have electrical resistivities in the ranges 10^{-8} to $10^{-6}\text{ S}^{-1}\text{ m}$. Insulators cover the range 10^8 to 10^{20} (diamond) and semiconductors 10 to $10^7\text{ S}^{-1}\text{ m}$.

The electrical conductivity of a semiconductor can be profoundly affected by the presence of impurities. For example, if x silicon atoms in the lattice of a silicon crystal are replaced by x phosphorus atoms, the lattice will gain x electrons and a negative (n-type) semiconductor results. On the other hand, if x silicon atoms are replaced by x boron atoms, the lattice will lose x electrons and a positive (p-type) semiconductor is formed. The impurity atoms are called ‘donors’ or ‘acceptors’ according to whether they give or take electrons to or from the lattice.

1.8 Isomorphs and polymorphs

Two or more substances that crystallize in almost identical forms are said to be *isomorphous* (Greek: ‘of equal form’). This is not a contradiction of Haüy’s law, because these crystals do show small, but quite definite, differences in their respective interfacial angles. Isomorphs are often chemically similar and can then be represented by similar chemical formulae; this statement is one form of Mitscherlich’s Law of Isomorphism, which is now recognized only as a broad generalization. One group of compounds which obey and illustrate Mitscherlich’s law is represented by the formula $M'_2\text{SO}_4 \cdot M''_2(\text{SO}_4)_3 \cdot 24\text{H}_2\text{O}$ (the alums), where M' represents a univalent radical (e.g. K or NH_4) and M''' represents a trivalent radical (e.g. Al, Cr or Fe). Many phosphates and arsenates, sulphates and selenates are also isomorphous.

Sometimes isomorphous substances can crystallize together out of a solution to form ‘mixed crystals’ or, as they are better termed, crystalline ‘solid solutions’. In such cases the composition of the homogeneous solid phase that is deposited follows no fixed pattern; it depends largely on the relative concentrations and solubilities of the substances in the original solvent. For instance, chrome alum, $\text{K}_2\text{SO}_4 \cdot \text{Cr}_2(\text{SO}_4)_3 \cdot 24\text{H}_2\text{O}$ (purple), and potash alum, $\text{K}_2\text{SO}_4 \cdot \text{Al}_2(\text{SO}_4)_3 \cdot 24\text{H}_2\text{O}$ (colourless), crystallize from their respective aqueous solutions as regular octahedra. When an aqueous solution containing both salts is crystallized, regular octahedra are again formed, but the colour of the crystals (which are now homogeneous solid solutions) can vary from almost colourless to deep purple, depending on the proportions of the two alums in the crystallizing solution.

Another phenomenon often shown by isomorphs is the formation of overgrowth crystals. For example, if a crystal of chrome alum (octahedral) is placed in a saturated solution of potash alum, it will grow in a regular manner such that the purple core is covered with a continuous colourless overgrowth. In

a similar manner an overgrowth crystal of nickel sulphate, $\text{NiSO}_4 \cdot 7\text{H}_2\text{O}$ (green), and zinc sulphate, $\text{ZnSO}_4 \cdot 7\text{H}_2\text{O}$ (colourless), can be prepared.

There have been many ‘rules’ and ‘tests’ proposed for the phenomenon of isomorphism, but in view of the large number of known exceptions to these it is now recognized that the only general property of isomorphism is that crystals of the different substances shall show very close similarity. All the other properties, including those mentioned above, are merely confirmatory and not necessarily shown by all isomorphs.

A substance capable of crystallizing into different, but chemically identical, crystalline forms is said to exhibit *polymorphism*. Different polymorphs of a given substance are chemically identical but will exhibit different physical properties. Dimorphous and trimorphous substances are commonly known, e.g.

Calcium carbonate: calcite (trigonal-rhombohedral)

 aragonite (orthorhombic)

 vaterite (hexagonal)

Carbon: graphite (hexagonal)

 diamond (regular)

Silicon dioxide: cristobalite (regular)

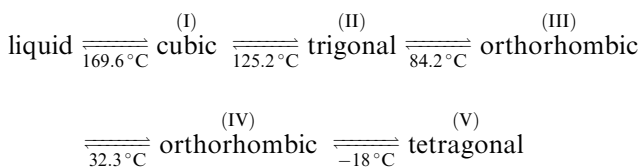
 tridymite (hexagonal)

 quartz (trigonal)

The term *allotropy* instead of polymorphism is often used when the substance is an element.

The different crystalline forms exhibited by one substance may result from a variation in the crystallization temperature or a change of solvent. Sulphur, for instance, crystallizes in the form of orthorhombic crystals (α -S) from a carbon disulphide solution, and of monoclinic crystals (β -S) from the melt. In this particular case the two crystalline forms are interconvertible: β -sulphur cooled below 95.5°C changes to the α form. This interconversion between two crystal forms at a definite transition temperature is called *enantiotropy* (Greek: ‘change into opposite’) and is accompanied by a change in volume.

Ammonium nitrate (melting point 169.6°C) exhibits five polymorphs and four enantiotropic changes between -18 and 125°C , as shown below:



The transitions from forms II to III and IV to V result in volume increases: the changes from I to II and III to IV are accompanied by a decrease in volume. These volume changes frequently cause difficulty in the processing and storage of ammonium nitrate. The salt can readily burst a metal container into which it has been cast when change II to III occurs. The drying of ammonium nitrate crystals must be carried out within fixed temperature limits, e.g. 40 – 80°C ,

otherwise the crystals can disintegrate when a transition temperature is reached.

Crystals of polymorphic substances sometimes undergo transformation without a change of external form, the result being an aggregate of very small crystals of the stable modification confined within the boundaries of the original unstable form. For example, an unstable rhombohedral form of potassium nitrate can crystallize from a warm aqueous solution, but when these crystals come into contact with a crystal of the stable modification, transformation sweeps rapidly through the rhombohedra which retain their shape. The crystals lose much of their transparency and acquire a finely granular appearance and their original mechanical strength is greatly reduced. Such *pseudomorphs* as they are called exhibit confused optical properties which cannot be correlated with the external symmetry (Hartshorne and Stuart, 1969).

When polymorphs are not interconvertible, the crystal forms are said to be *monotropic*: graphite and diamond are monotropic forms of carbon. The term *isopolymorphism* is used when each of the polymorphous forms of one substance is isomorphous with the respective polymorphous form of another substance. For instance, the regular and orthorhombic polymorphs of arsenious oxide, As_2O_3 , are respectively isomorphous with the regular and orthorhombic polymorphs of antimony trioxide, Sb_2O_3 . These two oxides are thus said to be isodimorphous.

Polytypism is a form of polymorphism in which the crystal lattice arrangements differ only in the manner in which identical two-dimensional arrays are stacked (Verma and Krishna, 1966).

1.9 Enantiomorphs and chirality

Isomeric substances, different compounds having the same formula, may be divided into two main groups:

- (a) *constitutional isomers*, which differ because their constituent atoms are connected in a different order, e.g., ethanol $\text{CH}_3\text{CH}_2\text{OH}$ and dimethylether CH_3OCH_3 ,
- (b) *stereoisomers*, which differ only in the spacial arrangement of their constituent atoms. Stereoisomers can also be divided into two groups:
 - (i) *enantiomers*, molecules that are mirror images of one another, and
 - (ii) *diastereomers*, which are not.

Diastereomers can have quite different properties, e.g., the cis- and trans-compounds maleic and fumaric acids which have different melting points, 130 °C and 270 °C respectively. On the other hand, enantiomers have identical properties with one exception, viz., that of *optical activity*, the ability to rotate the plane of polarization of plane-polarized light. One form will rotate to the right (*dextrorotatory*) and the other to the left (*laevorotatory*). The direction and magnitude of rotation are measured with a polarimeter.

Molecules and substances that exhibit optical activity are generally described as *chiral* (Greek *cheir* ‘hand’). Two crystals of the same substance that are

mirror images of each other are said to be *enantiomorphous* (Greek ‘of opposite form’). These crystals have neither planes of symmetry nor a centre of symmetry. Enantiomorphous crystals are not necessarily optically active, but all known optically active substances are capable of being crystallized into enantiomorphous forms. In many cases the solution or melt of an optically active crystal is also optically active. However, if dissolution or melting destroys the optical activity, this is an indication that the molecular structure was not enantiomeric.

Tartaric acid (*Figure 1.16*) and certain sugars are well-known examples of optically active substances. Optical activity is generally associated with compounds that possess one or more atoms around which different elements or groups are arranged asymmetrically, i.e., a *stereocentre*, so that the molecule can exist in mirror image forms. The most common stereocentre in organic compounds is an asymmetric carbon atom, and tartaric acid offers a good example. Three possible arrangements of the tartaric acid molecule are shown in *Figure 1.17*. The (a) and (b) forms are mirror images of each other; both contain asymmetric carbon atoms and both are optically active; one will be the dextro-form and the other the laevo-form. Although there are two asymmetric carbon atoms in formula (c), this particular form (*meso-tartaric acid*) is optically inactive; the potential optical activity of one-half of the molecule is compensated by the opposite potential optical activity of the other.

Dextro- and laevo-forms are now designated in all modern texts as (+) and (−) respectively. The optically inactive *racemate*, a true double compound

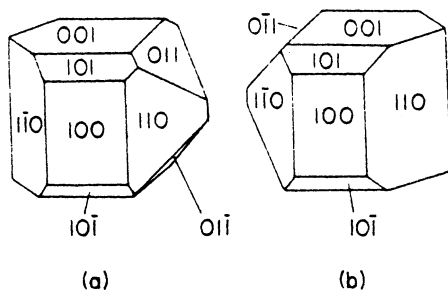


Figure 1.16. (a) Dextro- and (b) laevo-tartaric acid crystals (monoclinic system)

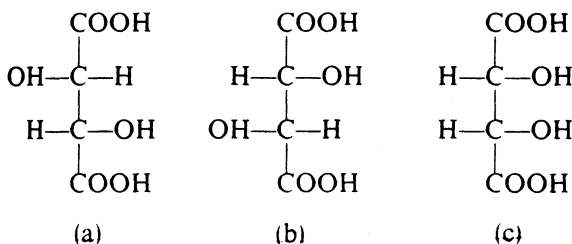
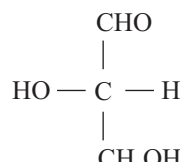
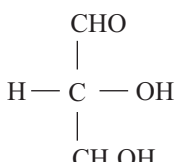


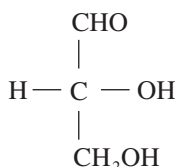
Figure 1.17. The tartaric acid molecule: (a) and (b) optically active forms; (c) meso-tartaric acid, optically inactive

(section 4.3.2), comprising an equimolar mixture of (+) and (−) forms, is designated (\pm). The symbols d- and l-, commonly found in older literature to designate optically active dextro- and laevo-forms, were abandoned to avoid confusion with the capital letters D and L which are still commonly used to designate molecular configuration, but *not* the direction of rotation of plane-polarized light. It is important to note, therefore, that not all D series compounds are necessarily dextrorotatory (+) nor are all L series compounds laevorotatory (−).

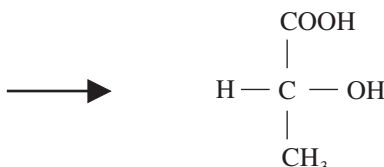
The D, L system, was arbitrarily based on the configuration of the enantiomeric glyceraldehyde molecules: the (+)-isomer was taken to have the structure implied by formula 1 and this arrangement of atoms was called the D configuration. Conversely, formula 2 was designated as representing the L configuration:



Lactic acid provides a simple example of how the D, L system could be applied to other compounds. The relative configuration of lactic acid is determined by the fact that it can be synthesized from (D)-(+)-glyceraldehyde without breaking any bonds to the asymmetric carbon atom:



(D)-(+)-glyceraldehyde

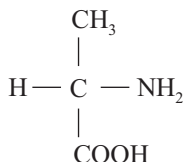


(D)-(-)-lacticacid

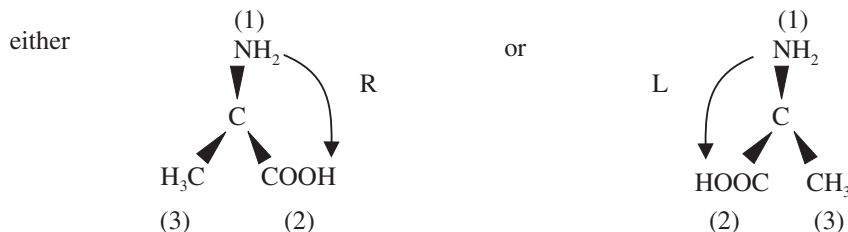
The lactic acid produced by this reaction, however, is laevorotatory not dextrorotatory like the starting material, thus illustrating the above warning that there is no essential link between optical rotation and molecular configuration.

The D, L system becomes ambiguous for all but the simplest of molecules and is now increasingly being replaced with the more logically based and adaptable R, S system, which has been internationally adopted by IUPAC for classifying absolute molecular configuration. Comprehensive accounts of the R, S convention and its application are given in most modern textbooks on organic chemistry, but the following short introduction may serve as a brief guide to the procedure for classifying a compound with a single asymmetric carbon atom as the stereocentre.

First, the four different groups attached to the stereocentre are identified and each is assigned a priority number, 1 to 4, using the Cahn–Ingold–Prelog ‘sequence rules’ according to which the highest priority (1) is given to the group with the atom directly attached to the stereocentre that has the highest atomic number. If by this rule two or more groups would at first appear to have identical priorities, the atomic numbers of the second atoms in each group are compared, continuing with the subsequent atoms until a difference is identified. For example, for α -aminopropionic acid (*alanine*)



the following priorities would be assigned: $\text{NH}_2 = 1$, $\text{COOH} = 2$, $\text{CH}_3 = 3$ and $\text{H} = 4$. The model of the molecule is then oriented in space so that the stereocentre is observed from the side opposite the lowest priority group. So observing the stereocentre with the lowest priority group ($\text{H} = 4$) to the rear, the view would be



According to the Cahn–Ingold–Prelog rules, if the path from 1 to 2 to 3 runs clockwise the stereocentre is designated by the letter **R** (Latin: *rectus*, right). If the path runs anticlockwise it is designated by the letter **s** (Latin: *sinister*, left). If the structure has only one stereocentre, (**R**) or (**s**) is used as the first prefix to the name, e.g., (**s**)-aminopropionic acid. The optical rotation of the compound is indicated by a second prefix, e.g., (**s**)-(+)aminopropionic acid, noting again as mentioned above for the **D**, **L** system, there is no necessary connection between (**s**) left and (**R**) right configurations and the (–) left and (+) right directions of optical rotation. If the molecule has more than one stereocentre their designations and positions are identified in the prefix, e.g., (2**R**, 3**R**)-dibromopentane.

1.9.1 Racemism

The case of tartaric acid serves to illustrate the property known as *racemism*. An equimolar mixture of crystalline **D** and **L** tartaric acids dissolved in water will produce an optically inactive solution. Crystallization of this solution will

yield crystals of optically inactive racemic acid which are different in form from the **D** and **L** crystals. There is, however, a difference between a racemate and a *meso*-form of a substance; the former can be resolved into **D** and **L** forms but the latter cannot.

Crystalline racemates are normally considered to belong to one of two basic classes:

1. Conglomerate: an equimolar mechanical mixture of two pure enantiomorphs.
2. Racemic compound: an equimolar mixture of two enantiomers homogeneously distributed throughout the crystal lattice.

A racemate can be resolved in a number of ways. In 1848 Pasteur found that crystals of the sodium ammonium tartrate (racemate)



deposited from aqueous solution, consisted of two clearly different types, one being the mirror image of the other. The **D** and **L** forms were easily separated by hand picking. Although widely quoted, however, this example of manual resolution through visual observation is in fact a very rare occurrence.

Bacterial attack was also shown by Pasteur to be effective in the resolution of racemic acid. *Penicillium glaucum* allowed to grow in a dilute solution of sodium ammonium racemate destroys the **D** form but, apart from being a rather wasteful process, the attack is not always completely selective.

A racemate may also be resolved by forming a salt or ester with an optically active base (usually an amine) or alcohol. For example, a racemate of an acidic substance *A* with, say, the dextro form of an optically active base *B* will give



and the two salts **D***A* · **D***B* and **L***A* · **D***B* can then be separated by fractional crystallization.

A comprehensive account of the resolution of racemates is given by Jacques, Collet and Wilen (1981). This topic is further discussed in section 7.2.

1.10 Crystal habit

Although crystals can be classified according to the seven general systems (*Table 1.1*), the relative sizes of the faces of a particular crystal can vary considerably. This variation is called a modification of habit. The crystals may grow more rapidly, or be stunted, in one direction; thus an elongated growth of the prismatic habit gives a needle-shaped crystal (acicular habit) and a stunted growth gives a flat plate-like crystal (tabular, platy or flaky habit). Nearly all manufactured and natural crystals are distorted to some degree, and this fact frequently leads to a misunderstanding of the term ‘symmetry’. Perfect geometric symmetry is rarely observed in crystals, but crystallographic symmetry is readily detected by means of a goniometer.

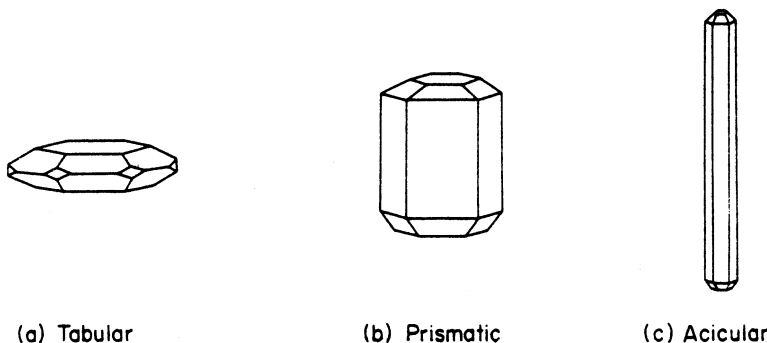


Figure 1.18. Crystal habit illustrated on a hexagonal crystal

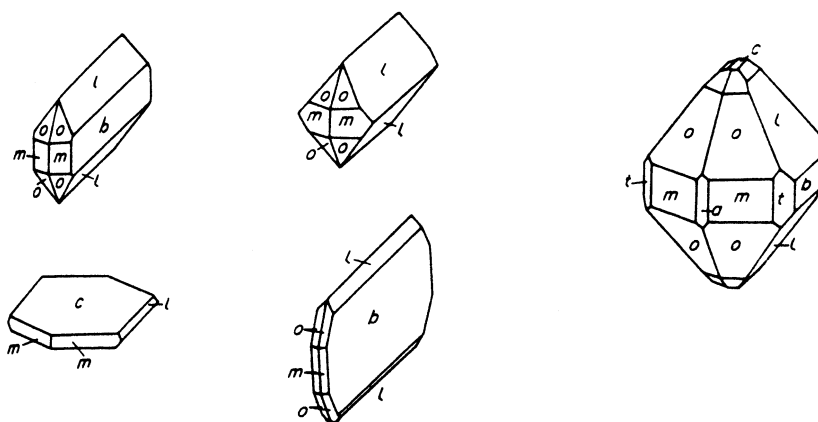


Figure 1.19. Some common habits of potassium sulphate crystals (orthorhombic system): $a = \{100\}$, $b = \{010\}$, $c = \{011\}$, $l = \{021\}$, $m = \{110\}$, $o = \{111\}$, $t = \{130\}$

Figure 1.18 shows three different habits of a crystal belonging to the hexagonal system. The centre diagram (b) shows a crystal with a predominant prismatic habit. This combination-form crystal is terminated by hexagonal pyramids and two flat faces perpendicular to the vertical axis; these flat parallel faces cutting one axis are called *pinacoids*. A stunted growth in the vertical direction (or elongated growth in the directions of the other axes) results in a tabular crystal (a); excessively flattened crystals are usually called plates or flakes. An elongated growth in the vertical direction yields a needle or acicular crystal (c); flattened needle crystals are often called blades.

Figure 1.19 shows some of the habits exhibited by potassium sulphate crystals grown from aqueous solution and Figure 1.20 shows four different habits of sodium chloride crystals.

The relative growths of the faces of a crystal can be altered, and often controlled, by a number of factors. Rapid crystallization, such as that produced by the sudden cooling or seeding of a supersaturated solution, may result in the formation of needle crystals; impurities in the crystallizing solution can stunt

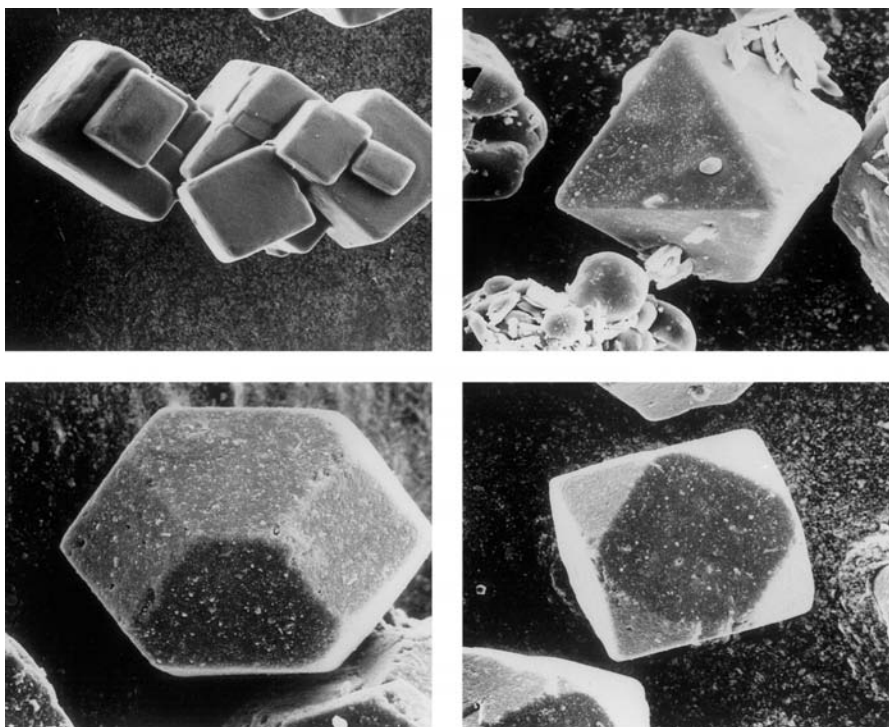


Figure 1.20. Four different habits of sodium chloride (regular system) crystals (Courtesy of ICI Ltd, Mond Division)

the growth of a crystal in certain directions; and crystallization from solutions of the given substance in different solvents generally results in a change of habit. The degree of supersaturation or supercooling of a solution or melt often exerts a considerable influence on the crystal habit, and so can the state of agitation of the system. These and other factors affecting the control of crystal habit are discussed in section 6.4.

1.11 Dendrites

Rapid crystallization from supercooled melts, supersaturated solutions and vapours frequently produces tree-like formations called dendrites, the growth of which is indicated in *Figure 1.21*. The main crystal stem grows quite rapidly in a supercooled system that has been seeded, and at a later stage primary branches grow at a slower rate out of the stem, often at right angles to it. In certain cases, small secondary branches may grow slowly out of the primaries. Eventually branching ceases and the pattern becomes filled in with crystalline material.

Most metals crystallize from the molten state in this manner, but because of the filling-in process the final crystalline mass may show little outward appear-

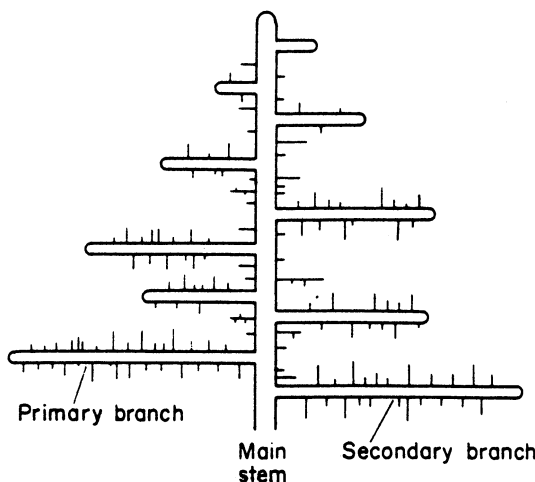


Figure 1.21. Dendritic growth

ance of dendrite formation. The fascinating patterns of snow crystals are good examples of dendritic growth, and the frosting of windows often affords a visual observation of this phenomenon occurring in two dimensions. The growth of a dendrite can be observed quite easily under a microscope by seeding a drop of a supersaturated solution on the slide.

Dendrites form most commonly during the early stages of crystallization; at later stages a more normal uniform growth takes place and the pattern may be obliterated. Dendritic growth occurs quite readily in thin liquid layers, probably because of the high rate of evaporative cooling, whereas agitation tends to suppress this type of growth. Dendrite formation tends to be favoured by substances that have a high enthalpy of crystallization and a low thermal conductivity.

1.12 Composite crystals and twins

Most crystalline natural minerals, and many crystals produced industrially, exhibit some form of aggregation or intergrowth, and prevention of the formation of these composite crystals is one of the problems of large-scale crystallization. The presence of aggregates in a crystalline mass spoils the appearance of the product and interferes with its free-flowing nature. More important, however, aggregation is often indicative of impurity because crystal clusters readily retain impure mother liquor and resist efficient washing (section 9.7.2).

Composite crystals may occur in simple symmetrical forms or in random clusters. The simplest form of aggregate results from the phenomenon known as *parallel growth*; individual forms of the same substance grow on the top of one another in such a manner that all corresponding faces and edges of the individuals are parallel. Potash alum, $K_2SO_4 \cdot Al_2(SO_4)_3 \cdot 24H_2O$, exhibits this type of growth; *Figure 1.22* shows a typical structure in which regular octahedra

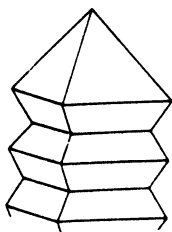


Figure 1.22. Parallel growth on a crystal of potash alum

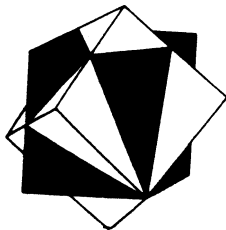


Figure 1.23. Interpenetrant twin of two cubes (e.g. fluorspar)

are piled on top of one another in a column symmetrical about the vertical axis. Parallel growth is often associated with isomorphs; for instance, parallel growths of one alum can be formed on the crystals of another, but this property is no longer regarded as an infallible test for isomorphism.

Another composite crystal frequently encountered is known as a *twin* or a *macle*; it appears to be composed of two intergrown individuals, similar in form, joined symmetrically about an axis (a twin axis) or a plane (a twin plane). A twin axis is a possible crystal edge and a twin plane is a possible crystal face. Many types of twins may be formed in simple shapes such as a V, +, L and so forth, or they may show an interpenetration giving the appearance of one individual having passed completely through the other (*Figure 1.23*). Partial interpenetration (*Figure 1.24*) can also occur. In some cases, a twin crystal may present the outward appearance of a form that possesses a higher degree of symmetry than that of the individuals, and this is known as *mimetic twinning*. A typical example of this behaviour is orthorhombic potassium sulphate, which can form a twin looking almost identical with a hexagonal bipyramid.

Parallel growth and twinning (or even triplet formation) are usually encountered when crystallization has been allowed to take place in an undisturbed medium. Although twins of individuals belonging to most of the seven crystal systems are known, twinning occurs most frequently when the crystals belong to the orthorhombic or monoclinic systems. Certain impurities in the crystallizing medium can cause twin formation even under vigorously agitated conditions: this is one of the problems encountered in the commercial crystallization of sugar.

The formation of crystal clusters, aggregates or conglomerates which possess no symmetrical properties is probably more frequently encountered in large-scale crystallization than the formation of twins. Relatively little is still known

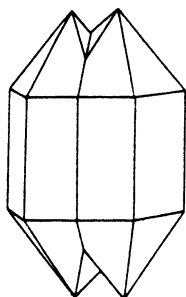


Figure 1.24. Partial interpenetrant twin (e.g. quartz)

about the growth of these irregular crystal masses, but among the factors that generally favour their formation are poor agitation, the presence of certain impurities in the crystallizing solution, seeding at high degrees of supersaturation and the presence of too many seed crystals, leading to conditions of overcrowding in the crystallizer.

1.13 Imperfections in crystals

Very few crystals are perfect. Indeed, in many cases they are not required to be, since lattice imperfections and other defects can confer some important chemical and mechanical properties on crystalline materials. Surface defects can also greatly influence the process of crystal growth. There are three main types of lattice imperfection: point (zero-dimensional), line (one-dimensional) and surface (two-dimensional).

1.13.1 Point defects

The common point defects are indicated in *Figure 1.25*. *Vacancies* are lattice sites from which units are missing, leaving ‘holes’ in the structure. These units may be atoms, e.g. in metallic crystals, molecules (molecular crystals) or ions (ionic crystals). The *interstitials* are foreign atoms that occupy positions in the interstices between the matrix atoms of the crystal. In most cases the occurrence of interstitials leads to a distortion of the lattice.

More complex point defects can occur in ionic crystals. For example, a cation can leave its site and become relocated interstitially near a neighbouring cation. This combination of defects (a cation vacancy and an interstitial cation) is called a *Frenkel imperfection*. A cation vacancy combined with an anion vacancy is called a *Schottky imperfection*.

A foreign atom that occupies the site of a matrix atom is called a *substitutional impurity*. Many types of semiconductor crystals contain controlled quantities of substitutional impurities. Germanium crystals, for example, can be grown containing minute quantities of aluminium (p-type semiconductors) or phosphorus (n-type).

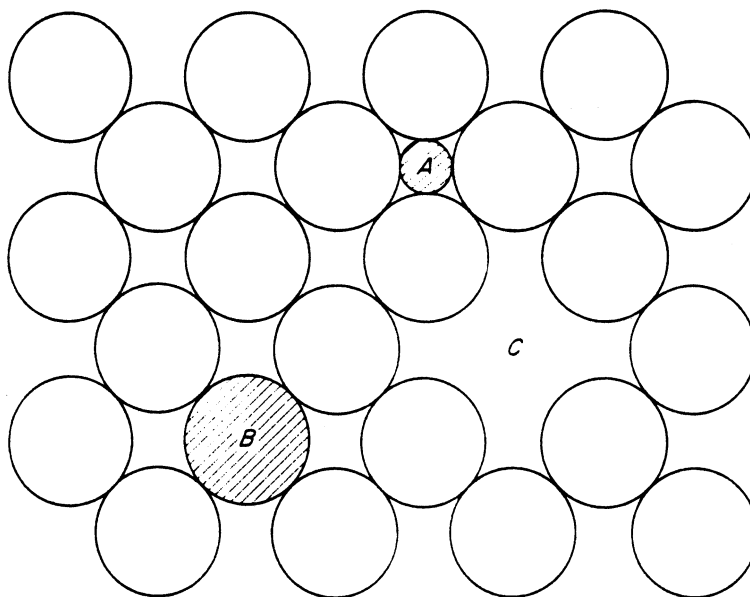


Figure 1.25. Representation of some common point defects: *A*, interstitial impurity; *B*, substitutional impurity; *C*, vacancy

1.13.2 Line defects

The two main types of line defect which can play an important role in the model of crystal growth are the *edge* and *screw dislocations*. Both of these are responsible for slip or shearing in crystals. Large numbers of dislocations occur in most crystals; they form readily during the growth process under the influence of surface and internal stresses.

Figure 1.26 shows in diagrammatic form the cross-sectional view of a crystal lattice in which the lower part of a vertical row of atoms is missing. The position of the dislocation is marked by the symbol \perp ; the vertical stroke of this symbol indicates the extra plane of atoms and the horizontal stroke indicates the slip plane. The line passing through all the points \perp , i.e. drawn vertical to the plane of the diagram, is called the edge dislocation line. In an edge dislocation, therefore, the atoms are displaced at right angles to the dislocation line.

The process of slip under the action of a shearing force may be explained as follows (see *Figure 1.26*). The application of a shear stress to a crystal causes atom *A* to move further away from atom *B* and closer to atom *C*. The bond between *A* and *B*, which is already strained, breaks and a new bond is formed between *A* and *C*. The dislocation thus moves one atomic distance to the right, and if this process is continued the dislocation will eventually reach the edge of the crystal. The direction and magnitude of slip are indicated by the *Burgers vector*, which may be one or more atomic spacings. In the above example, where the displacement is one lattice spacing, the Burgers vector is equal to 1.

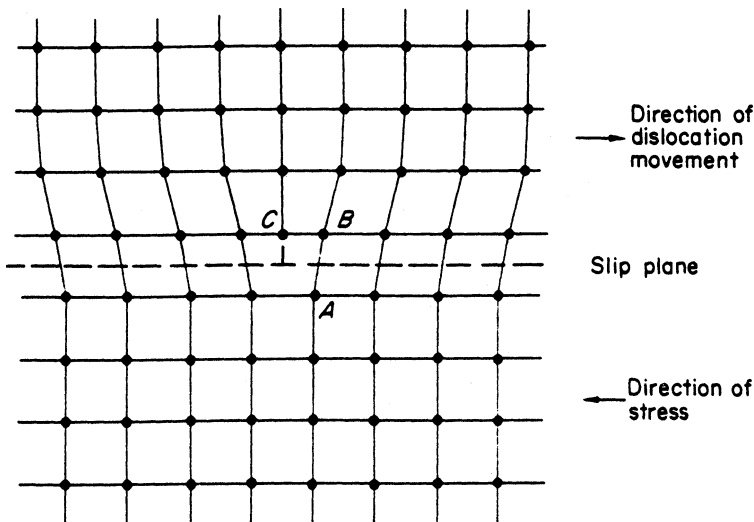


Figure 1.26. Movement of an edge dislocation through a crystal

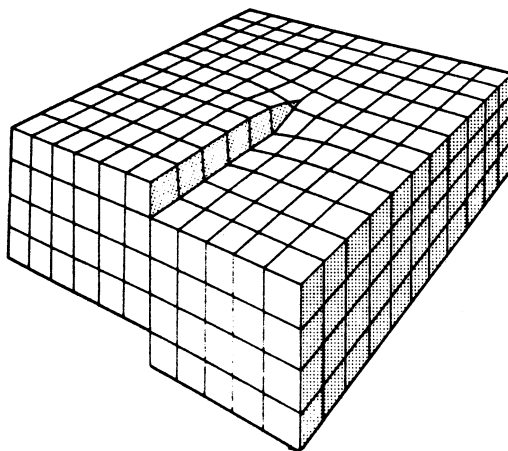


Figure 1.27. A screw dislocation

A screw dislocation forms when the atoms are displaced along the dislocation line, rather than at right angles to it as in the case of the edge dislocation. *Figure 1.27* indicates this type of lattice distortion. In this example the Burgers vector is 1 (unit step height), but its magnitude may be any integral number.

Screw dislocations give rise to a particular mode of growth in which the attachment of growth units to the face of the dislocation results in the development of a spiral growth pattern over the crystal face (see section 6.1.2).

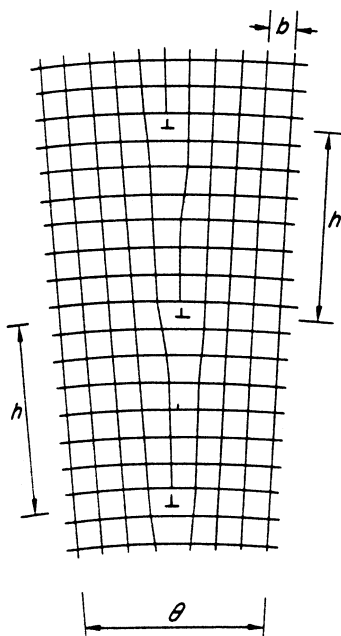


Figure 1.28. A simple tilt boundary

1.13.3 Surface defects

A variety of surface imperfections, or mismatch boundaries, can be produced in crystalline materials as a result of mechanical or thermal stresses or irregular growth. Grain boundaries, for example, can be created between individual crystals of different orientation in a polycrystalline aggregate.

When the degree of mismatching is small, the boundary can be considered to be composed of a line of dislocations. A low-angle *tilt boundary* is equivalent to a line of edge dislocations, and the angle of tilt is given by $\theta = b/h$ where b is the Burgers vector and h the average vertical distance between the dislocations (*Figure 1.28*). A *twist boundary* can be considered, when the degree of twist is small, as a succession of parallel screw dislocations. For a full account of this subject reference should be made to the specialized works (see Bibliography).

Bibliography

- Buckley, H. E. (1952) *Crystal Growth*. London: Wiley
- Bunn, C. W. (1961) *Chemical Crystallography*, 2nd edn. Oxford: Clarendon Press
- Chandrasekhar, S. (1992) *Liquid Crystals*, 2nd edn. Cambridge: University Press
- Hartshorne, N. H. and Stuart, A. (1969) *Practical Optical Crystallography*, 2nd edn. London: Arnold
- Hirth, J. P. and Loethe, J. (1968) *Theory of Dislocations*. New York: McGraw-Hill
- Kelly, A. and Groves, G. (2000) *Crystallography and Crystal Defects*. Chichester: Wiley

- McKie, D. and McKie, C. (1974) *Crystalline Solids*, 3rd edn. London: Nelson
- Phillips, F. C. (1980) *Introduction to Crystallography*, 4th edn. London: Longmans Green
- Rosenberg, H. M. (1978) *The Solid State*. Oxford: Clarendon Press
- Vainshtein, B. K., Chernov, A. A. and Shuvalov, L. A. (1984) (eds.) *Modern Crystallography*, vol. 1 *Symmetry of Crystals*; vol. 2 *Structure of Crystals*; vol. 3 ; vol. 4 *Physical Properties of Crystals*. Berlin: Springer
- Van Bueren, H. G. (1960) *Imperfections in Crystals*. New York: Interscience
- Wells, A. F. (1962) *Structural Inorganic Chemistry*, 3rd edn. Oxford: Clarendon Press
- Wright, J. D. (1987) *Molecular Crystals*. Cambridge: University Press

2 Physical and thermal properties

2.1 Density

2.1.1 Solids

The densities of most pure solid substances are readily available in the standard physical property handbooks. The densities of actual crystallized substances, however, may differ from the literature values on account of the presence of vapour or liquid inclusions (see section 6.6) or adhering surface moisture. For example, recorded values of ‘commercially pure’ sucrose crystals have ranged from 1580 to 1610 kg m⁻³ compared with an expected value of 1587 kg m⁻³.

The theoretical density, ρ_c^* , of a crystal may be calculated from the lattice parameters (section 1.6) by means of the relationship:

$$\rho_c^* = \frac{nM}{VN} \quad (2.1)$$

Where n is the number of formula units in the unit cell, V is the volume of the unit cell, M is the molar mass of the substance and N is the Avogadro number (6.023×10^{26} kmol⁻¹). For sucrose, the lengths of the a , b and c axes of this monoclinic crystal are 10.9, 8.70 and 7.75×10^{-10} m, respectively, with the angle $\beta = 103^\circ$ ($\sin \beta = 0.9744$). Hence the volume $V = 716.1 \times 10^{-30}$ m³. Further, $M = 342.3$ kg kmol⁻¹ and $n = 2$. Substituting these values in equation 2.1 gives a value of $\rho_c^* = 1587$ kg m⁻³.

The actual density of a solid substance, even of a relatively small individual crystal, may be measured by determining the density of an inert liquid mixture in which the crystal remains just suspended. Examples of a convenient group of miscible organic liquids for many inorganic salts include chloroform (1492 kg m⁻³ at 20 °C), carbon tetrachloride (1594), ethyl iodide (1930), ethylene dibromide (2180), bromoform (2890) and methylene iodide (3325).

For example, a crystal of sodium nitrate (2260 kg m⁻³) could be floated in about 50 mL of bromoform in a suitable flask, taking care that no air bubbles are attached, and then caused to achieve the ‘just suspended’ state by slowly adding chloroform from a burette. At this point the crystal density may be assumed to be equal to that of the liquid mixture, which can readily be estimated.

Solid densities have a very small temperature dependence, but this can be ignored for industrial crystallization purposes. For example the density of sodium chloride decreases by about 0.7 per cent when the temperature increases from 10 to 80 °C. The calculation needs a knowledge of the coefficient of thermal expansion.

The densities of bulk particulate solids and slurries are discussed in section 2.1.3.

2.1.2 Liquids

The density of a liquid is significantly temperature dependent. The ratio of the density of a given liquid at one temperature to the density of water at the same, or another, temperature is known as the specific gravity of the liquid. Thus, a specific gravity quoted at say 20 °C/4 °C is numerically equal to the density of the liquid at 20 °C expressed in g cm⁻³ since water exhibits its maximum density (1 g cm⁻³) at 4 °C.

The simplest instrument for measuring liquid density is the hydrometer, a float with a graduated stem. To approach reasonable accuracy, however, it is essential to make the measurement at the particular calibration temperature marked on the hydrometer. Densities may be determined more accurately by the specific gravity bottle method, or with a pyknometer (BS 733, 1983) or Westphal balance, details of which may be found in most textbooks of practical physics.

In recent years, several high-precision instruments have become available, the most noteworthy of which are those based on an oscillating sample holder. A glass U-tube is filled with the sample and caused to oscillate at its natural frequency, which is dependent on the total mass of the system. Since the tube has a constant mass and sample volume, the measured frequency of oscillation can be related to the liquid sample density. Precisions of up to ±10⁻⁶ g cm⁻³ have been claimed for some instruments.

It is often possible to estimate to ±5% the density of a solution from a knowledge of the solute and solvent densities by means of the equation

$$\rho_{\text{soln}} = \frac{\frac{L + S}{L} \cdot \frac{S}{\rho_L + \frac{S}{\rho_S}}}{(2.2)}$$

where L and S are the masses of the solvent (liquid) and solute (solid), respectively, and ρ_L and ρ_S are the densities of the respective components. It has to be acknowledged, of course, that the volume of a solution is not exactly equal to the volumes of the solvent and added solute, but the error incurred in making this assumption is often insignificant, particularly for industrial purposes, as the following examples show:

1. An aqueous solution of potassium sulphate at 80 °C containing 0.214 kg K₂SO₄/kg water ($\rho_L = 971.8 \text{ kg m}^{-3}$ at 80 °C, $\rho_S = 2660 \text{ kg m}^{-3}$).

$$\rho_{\text{soln}} = (1 + 0.214)/[(1/971.8) + (0.214/2660)] = 1095 \text{ kg m}^{-3}.$$

Experimental value: 1117 kg m⁻³.

2. An aqueous solution of sodium sulphate at 15 °C containing 0.429 kg Na₂SO₄ · 10H₂O/kg 'free' water ($\rho_L = 999.1 \text{ kg m}^{-3}$ at 15 °C, $\rho_S = 1460 \text{ kg m}^{-3}$).

$$\rho_{\text{soln}} = (1 + 0.429)/[(1/999.1) + (0.429/1460)] = 1103 \text{ kg m}^{-3}$$

Experimental value: 1125 kg m⁻³.

3. An aqueous solution of sucrose at 80 °C containing 3.62 kg C₆H₁₂O₆/kg water ($\rho_L = 971.8 \text{ kg m}^{-3}$ at 80 °C, $\rho_S = 1590 \text{ kg m}^{-3}$).

$$\rho_{\text{soln}} = (1 + 3.62)/[(1/971.8) + (3.62/1590)] = 1397 \text{ kg m}^{-3}$$

Experimental value: 1350 kg m⁻³.

For more reliable estimations of solution density, reference should be made to the procedures described in the book by Söhnel and Novotný (1985) which also contains detailed density data for a large number of inorganic salt solutions. In a later publication (Novotný and Söhnel, 1988) densities of some 300 inorganic salt solutions are recorded.

The densities of some aqueous solutions are recorded in the Appendix (*Table A.9*).

2.1.3 Bulk solids and slurries

The bulk density of a quantity of particulate solids is not a fixed property of the system since the bulk volume occupied contains significant amounts of void space, normally filled with air. The relationship between the density of the solid particles, ρ_S , and the bulk solids density, ρ_{BS} , is

$$\rho_{\text{BS}} = \rho_S(1 - \varepsilon) \quad (2.3)$$

where ε is the voidage, the volume fraction of voids, which is considerably dependent on particle shape, particle size distribution and the packing of the particles. Further, ε can vary considerably depending on how the particulate material has been processed or handled. For example, it can be increased by aeration, as in freshly poured solids, and decreased by vibration, e.g. after transportation in packaged form.

Expression of slurry densities

Many different terms are used for specifying the solids content of slurries and each has its own particular use.

Slurry concentrations are not usually simple to measure experimentally since it is not always convenient to filter-off, wash, dry and weigh the solids content. So other more convenient, but less precise methods, are often adopted. For example, it is common practice to take a sample of slurry in a graduated cylinder, allow the solids to settle and to measure the volume percentage of *settled* solids. Although this is often a rapid and quite satisfactory way of assessing the slurry concentration, particularly for routine testing under industrial plant conditions, it does not directly give the actual quantity of *suspended* solids, because the settled volume (the overall volume occupied by the settled solids) contains a significant proportion of liquid. Settled spheres of uniform size, for example, enclose a void space of about 40 per cent, but considerable deviations from this value can occur for multisized particles of irregular shape.

The relationship between system voidages and the settled solids fraction is given by equation 2.4. Other useful relationships are given in equations 2.5 to 2.9.

$$\varepsilon = 1 - S(1 - \varepsilon_S) \quad (2.4)$$

$$= 1 - (M_T / \rho_S) \quad (2.5)$$

$$= (\bar{\rho} - \rho_S) / (\rho_S - \rho_L) \quad (2.6)$$

$$M_T = (1 - \varepsilon) \rho_S \quad (2.7)$$

$$= X \bar{\rho} \quad (2.8)$$

$$= X [\rho_S - \varepsilon(\rho_S - \rho_L)] \quad (2.9)$$

where S = settled solids fraction (m^3 of settled solids plus associated liquor in the voids/ m^3 of total sample taken)

X = mass fraction of solids (kg of suspended solids/kg of total suspension)

M_T = slurry density (kg of suspended solids/ m^3 of total suspension)

ε = voidage of the slurry (m^3 of liquid/ m^3 of total suspension)

$1 - \varepsilon$ = volume fraction of solids (m^3 of solids/ m^3 of total suspension)

ε_S = voidage of the settled solids

$\bar{\rho}$ = overall mean density of the suspension (kg m^{-3})

ρ_S = density of solid (kg m^{-3})

ρ_L = density of liquid (kg m^{-3})

For the special case of an industrial crystallizer, it is sometimes possible to assess the slurry (magma) density by chemical analysis, measuring (a) the total overall concentration of solute (crystals plus dissolved solute) in the suspension and (b) the concentration of dissolved solute in the supernatant liquor. Thus,

$$C = M_T + \varepsilon C^* \quad (2.10)$$

and

$$M_T = \rho_S(C - C^*) / (\rho_S - C^*) \quad (2.11)$$

where C = kg of crystallizing substance (suspended and dissolved)/ m^3 of total suspension, and C^* = kg of dissolved crystallizing substance / m^3 of supernatant liquor.

2.2 Viscosity

The once common units of absolute viscosity, the poise (P) ($1 \text{ g cm}^{-1} \text{ s}^{-1}$) and its useful sub-multiple the centipoise (cP), have now been replaced by the SI unit ($\text{kg m}^{-1} \text{ s}^{-1}$) which is generally written as Pa s and sometimes as N s m^{-2} . The following relationships hold:

$$\begin{aligned} 1 \text{ cP} &= 0.01 \text{ P} = 1 \text{ mPa s} = 1 \text{ mN s m}^{-2} = 10^{-3} \text{ kg m}^{-1} \text{ s}^{-1} \\ &= 2.42 \text{ lb ft}^{-1} \text{ h}^{-1} \end{aligned}$$

Similarly, the once common units of kinematic viscosity (= absolute viscosity/density), the stokes (St) ($1 \text{ cm}^2 \text{ s}^{-1}$) and its sub-multiple the centistokes (cSt), have been replaced by the SI unit ($\text{m}^2 \text{ s}^{-1}$). The following relationships hold:

$$1 \text{ cSt} = 0.01 \text{ St} = 10^{-6} \text{ m}^2 \text{ s}^{-1} = 0.0388 \text{ ft}^2 \text{ h}^{-1}$$

The viscosity of a liquid decreases with increasing temperature, and for many liquids the relationship

$$\eta = A \exp(-B/T) \quad (2.12)$$

holds reasonably well. A and B are constants and the temperature T is expressed in kelvins. Plots of $\log \eta$ versus T^{-1} or $\log \eta$ versus $\log T$ usually yield fairly straight lines and this property may be used for interpolating viscosities at temperatures within the range covered.

In general, dissolved solids increase the viscosity of water, although a few exceptions to this rule are known. Occasionally, the increase in viscosity is considerable, as in the case of the system sucrose–water where, for example, the viscosity increases from around 2 to 60 mPa s for a concentration increase from 20 to 60 g/100 g of solution at 20 °C.

Figure 2.1a shows an example of a solute that decreases the viscosity of the solvent; in this system (KI–water) a minimum viscosity is exhibited. Several other potassium and ammonium salts also exhibit a similar behaviour. Figure 2.1b shows the effect of concentration and temperature on the ethanol–water system which exhibits a maximum viscosity.

A comprehensive survey of the viscosity characteristics of aqueous solutions of electrolytes has been made by Stokes and Mills (1965) who also give experimental data on a considerable number of systems. Viscosities of some aqueous solutions are recorded in the Appendix (Table A.10).

Unfortunately, no completely reliable method is available for the prediction of the viscosities of solutions or liquid mixtures. A general survey is made by

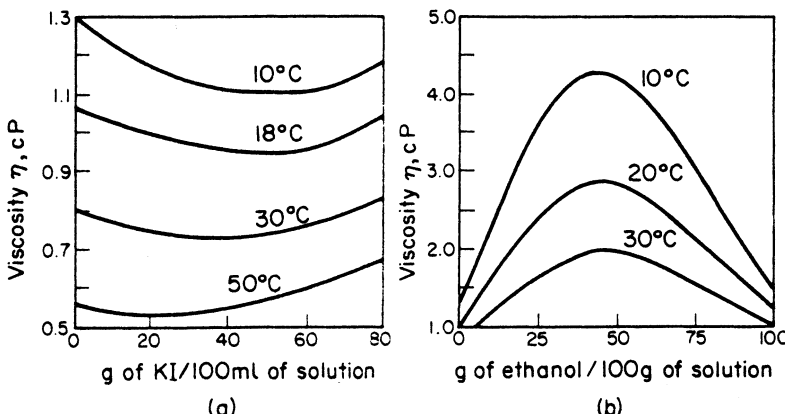


Figure 2.1. Aqueous solutions exhibiting (a) minimum, (b) maximum viscosities. (After Hatschek, 1928)

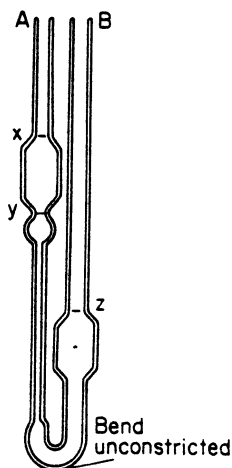


Figure 2.2. Simple U-tube viscometer

Reid, Prausnitz and Poling (1987) and some indication of the complexities involved in making estimates of the viscosities of mixed salt solutions may be gained from the survey made by Nowlan, Thi and Sangster (1980).

Numerous instruments have been devised for the measurement of liquid viscosity, many of which are based on the flow of a fluid through a capillary tube and the application of Poiseuille's law in the form

$$\eta = \frac{\pi r^4 \Delta P}{8lV} \quad (2.13)$$

where ΔP = the pressure drop across the capillary of length l and radius r , and V = volume of fluid flowing in unit time. One simple type of *U-tube viscometer* is shown in *Figure 2.2*. The liquid under test is sucked into leg B until the level in this leg reaches mark z. The tube is arranged truly vertical, and the temperature of the liquid is measured and kept constant. The liquid is then sucked up into leg A to a point above x and the time t for the meniscus to fall from x to y is recorded. The kinematic viscosity of the liquid v can be calculated from

$$v = kt \quad (2.14)$$

where k is a constant for the apparatus, determined by measurements on a liquid of known viscosity, e.g. water.

The falling-sphere method of viscosity determination also has many applications, and Stokes' law may be applied in the form

$$\eta = \frac{(\rho_s - \rho_1)d^2g}{18u} \quad (2.15)$$

where d , ρ and u are the diameter, density and terminal velocity, respectively, of a solid sphere falling in the liquid of density ρ_1 . A simple *falling-sphere viscometer* is shown in *Figure 2.3*. The liquid under test is contained in the inner

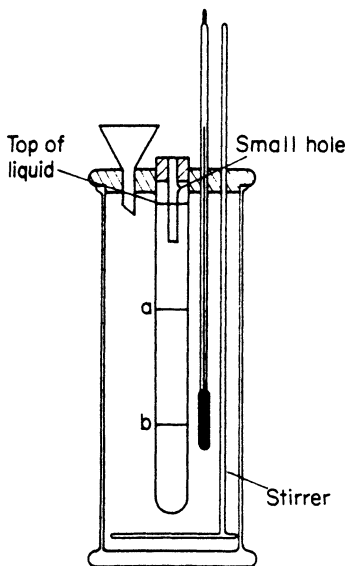


Figure 2.3. Falling-sphere viscometer

tube of 30 mm diameter and about 300 mm length. The central portion of the tube contains two reference marks a and b, 150 mm apart. The tube is held truly vertical, and the temperature of the liquid is measured and kept constant. A 1.5 mm diameter steel ball, previously warmed to the test temperature, is inserted through a small guide tube and its time of passage between the two reference marks is measured. A mean of several measurements should be taken. The viscosity of the liquid can then be calculated from equation 2.15. Modern instrumental versions of the falling-sphere technique are claimed to measure viscosities in the range 0.5–500 mPa with high precision at controlled temperatures using sample volumes as low as 0.5 mL.

Several high-precision viscometers are based on the concentric-cylinder method. The liquid under test is contained in the annulus between two vertical coaxial cylinders; one cylinder can be made to rotate at a constant speed, and the couple required to prevent the other cylinder rotating can be measured. For more detailed information on practical viscometry reference should be made to specialized publications (Dinsdale and Moore 1962, BS 188, 1993).

2.2.1 Solid–liquid systems

The viscosity characteristics of liquids can be altered considerably by the presence of finely dispersed solid particles, especially of colloidal size. The viscosity of a suspension of rigid spherical particles in a liquid, when the distance between the spheres is much greater than their diameter, may be expressed by the Einstein equation:

$$\eta_s = \eta_0(1 + 2.5\phi) \quad (2.16)$$

where η_s is the effective viscosity of the disperse system, η_0 the viscosity of the pure dispersion medium, and ϕ the ratio of the volume of the dispersed particles to the total volume of the disperse system. In other words, $\phi = 1 - \varepsilon$, where ε is the voidage of the system. Equation 2.16 applies reasonably well to lyophobic sols and very dilute suspensions, but for moderately concentrated suspensions and lyophilic sols the Guth–Simha modification is preferred:

$$\eta_s = \eta_0(1 + 2.5\phi + 14.1\phi^2) \quad (2.17)$$

For concentrated suspensions of solid particles, the Frankel–Acrivos (1967) relationship

$$\eta_s = \frac{9}{8}\eta_0 \left(\frac{(\phi/\phi_m)^{1/3}}{(1 - \phi/\phi_m)^{1/3}} \right) \quad (2.18)$$

can be applied for values of $\phi/\phi_m \rightarrow 1$, where ϕ_m is the maximum attainable volumetric concentration of solids in the system (usually about 0.6 for packed monosize spherical particles). Equation 2.18 has met with experimental support in the region $(\phi/\phi_m) > 0.7$. However, for solids concentrations such as those normally encountered in industrial crystallizers (say $\varepsilon \sim 0.8$, $\phi \sim 0.2$ and $\phi/\phi_m \sim 0.3$ for granular crystals) the much simpler equation 2.17 predicts the order of magnitude of apparent viscosity reasonably well.

2.3 Surface tension

Of the many methods available for measuring the surface tension of liquids (Findlay, 1973), the capillary rise and ring techniques are probably the most useful for general applications.

In the capillary rise method, the surface tension, γ , of a liquid can be determined from the height, h , of the liquid column in a capillary tube of radius r . If the liquid completely wets the tube (zero contact angle),

$$\gamma = \frac{1}{2}rh\Delta\rho g \quad (2.19)$$

where $\Delta\rho$ is the difference in density between the liquid and the gaseous atmosphere above it. The height, h , can be accurately measured with a cathetometer from the base of the liquid meniscus to the flat surface of the free liquid surface in a containing vessel. However, to minimize errors, this reference to a flat surface can be eliminated by measuring the difference in capillary rise in two tubes of different bore (*Figure 2.4*). Then

$$\gamma = \frac{1}{2}r_1h_1\Delta\rho g = \frac{1}{2}r_2h_2\Delta\rho g$$

From which it follows that

$$\gamma = \frac{\Delta h \Delta \rho r_1 r_2 g}{2(r_1 - r_2)} \quad (2.20)$$

The differential height Δh can be measured with precision.

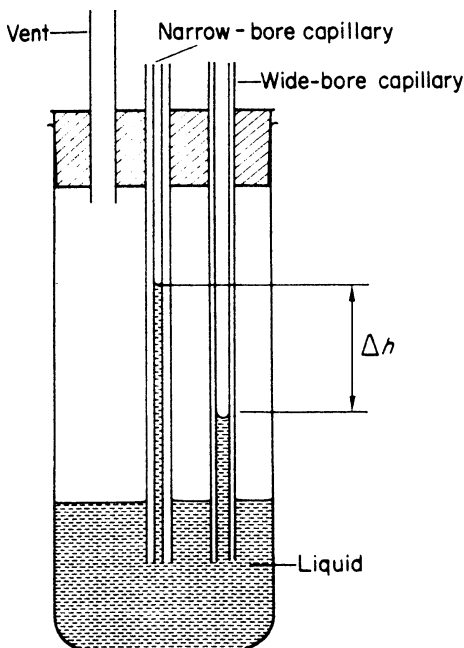


Figure 2.4. Measurement of surface tension by the differential capillary rise method

The ring technique, and its many variations, is widely used in industrial laboratories. Several kinds of commercial apparatus incorporating a torsion balance are available under the name du Noüy tensiometer. The method is simple and rapid, and is capable of measuring the surface tension of a pure liquid to a precision of 0.3% or better.

The force necessary to pull a ring (usually of platinum or platinum–iridium wire) from the surface of the liquid is measured. The surface tension is calculated from the pull and the dimensions of the ring after the appropriate correction factors have been applied.

It is often possible to predict the surface tension of non-aqueous mixtures of solvents by assuming a linear dependence with mole fraction. Aqueous solutions, however, generally show a pronounced non-linear behaviour and prediction is not recommended.

The surface tension of a liquid decreases with an increase in temperature, but the decrease is not always linear (*Table 2.1*).

The addition of an electrolyte to water generally increases the surface tension very slightly, although an initial decrease is usually observed at very low concentrations ($< 0.002 \text{ mol L}^{-1}$) (Harned and Owen, 1958). Non-electrolytes generally decrease the surface tension of water. For example, saturated aqueous solutions of α -naphthol, adipic acid and benzoic acid at 22°C are 48, 55 and 60 mN m^{-1} , respectively, whereas a saturated solution of potassium sulphate at the same temperature has a surface tension of 73 mN m^{-1} .

Table 2.1. Surface tensions of some common solvents at different temperatures

Solvent	Surface tension, mN m ⁻¹					
	0°	10°	20°	30°	40°	50 °C
Water	76.0	73.5	72.8	71.2	69.6	67.9
Benzene	31.6	30.2	28.9	27.2	26.3	25.0
Toluene	30.8	29.7	28.5	27.4	26.2	25.1
CCl ₄	29.5	28.0	26.8	25.5	24.4	23.1
Acetone	25.5	24.4	23.3	22.3	21.2	—
Methanol	24.3	23.4	22.6	21.7	20.8	—
Ethanol	24.1	23.1	22.3	21.4	20.6	19.8

1 mN m⁻¹ = 1 mJ m⁻² = 1 dyn cm⁻¹

2.3.1 Interfacial tension

The surface tension of a liquid, as normally measured, is the interfacial tension between a liquid surface and air saturated with the relevant vapour.

The interfacial tension of a crystalline solid in contact with a solution of the dissolved solid is a quantity of considerable importance in crystal nucleation and growth processes. It is also sometimes referred to as the ‘surface energy’. This subject is dealt with in section 5.6.

2.4 Diffusivity

Two examples of a theoretical approach to the problem of the prediction of diffusion coefficients in fluid media are the equations postulated in 1905 by Einstein and in 1936 by Eyring. The former is based on kinetic theory and a modification of Stokes’ law for the movement of a particle in a fluid, and is most conveniently expressed in the form

$$D = \frac{\mathbf{k}T}{\phi r\eta} \quad (2.21)$$

where D = diffusivity ($\text{m}^2 \text{s}^{-1}$), T = absolute temperature (K), η = viscosity ($\text{kg s}^{-1} \text{m}^{-1}$), r = molecular radius (m), \mathbf{k} = Boltzmann’s constant and the dimensionless factor ϕ has a numerical value between 4π and 6π depending on the solute : solvent molecular size ratio. Eyring’s approach, based on reaction rate theory, treats a liquid as a disordered lattice structure with vacant sites into which molecules move, i.e. diffuse. For low solute concentration Eyring’s equation may be expressed in a form identical with that of equation 2.21 but a different value of ϕ applies.

The usefulness of these equations, however, is strictly limited because they both contain a term, r , which denotes the radius of the solute molecule. Values of this quantity are difficult to obtain. Consequently, the most directly useful relationship that emerges is

$$D\eta/T = \text{constant} \quad (2.22)$$

which is of considerable value in predicting, for a given system, the effect of temperature and viscosity on the diffusion coefficient. This simple relation is often referred to as the Stokes–Einstein equation.

The very limited success of the theoretical equations has led to the development of many empirical and semi-empirical relationships for the prediction of diffusion coefficients. Amongst those devised for diffusion in liquids the following may be mentioned. For diffusion in aqueous solutions Othmer and Thakar (1953) proposed the correlation

$$D = \frac{14 \times 10^{-5}}{\eta^{1.1} v^{0.6}} \quad (2.23)$$

where v is the molar volume of the solute ($\text{cm}^3 \text{ mol}^{-1}$) and η is the viscosity in cP, giving the diffusivity D in $\text{cm}^2 \text{ s}^{-1}$. By correlating a large number of published experimental diffusivities Wilke and Chang (1955) arrived at the relationship

$$D = 7.4 \times 10^{-8} \frac{(\gamma M) T^{1/2}}{\eta v^{0.6}} \quad (2.24)$$

where M is the molar mass (kg kmol^{-1}), v is the molal volume ($\text{cm}^3 \text{ mol}^{-1}$) and T is in kelvins, giving D in $\text{cm}^2 \text{ s}^{-1}$. For unassociated solvents, e.g. benzene, ether and heptane, the so-called association parameter $\gamma = 1$. For water, methanol and ethanol, $\gamma = 2.6, 1.9$ and 1.5 , respectively.

Despite the widespread use of these and many other similar correlations, however, they are notoriously unreliable; deviations from experimental values as high as 30% are not unusual (Mullin and Cook, 1965). Furthermore, these empirical relationships were devised from diffusion data predominantly on liquid–liquid systems, and there is little evidence to suggest that they are reliable for the prediction of the diffusion of solid solutes in liquid solutions, although an ‘order of magnitude’ estimation is sometimes possible. For example, the diffusivity of sodium chloride in water at 25°C is $1.3 \times 10^{-9} \text{ m}^2 \text{ s}^{-1}$, while values calculated from equations 2.23 and 2.24 range from 1.7 to $2.6 \times 10^{-9} \text{ m}^2 \text{ s}^{-1}$. Similarly, for sucrose in water at 25°C , $D = 5.2 \times 10^{-10} \text{ m}^2 \text{ s}^{-1}$, while the predicted values range from 3.6 to $4.2 \times 10^{-10} \text{ m}^2 \text{ s}^{-1}$.

It is also important to note that these empirical correlations are meant to apply only to dilute solutions. Despite the fact that they all contain a term relating to viscosity which is a function of concentration, they usually fail to predict the rate of diffusion from a concentrated solution to a less concentrated one. For example, the diffusion coefficient for sucrose diffusing from a 1% aqueous solution into water at 25°C is approximately five times the value for the diffusion between 61.5 and 60.5% solutions, whereas over the concentration range 1 to 60%, the viscosity exhibits a fortyfold increase.

These empirical equations also fail to discriminate between isomers as was pointed out by Mullin and Cook (1965), who measured the diffusivities of *o*-, *m*- and *p*-hydroxybenzoic acid in water. The data measured at 20°C are

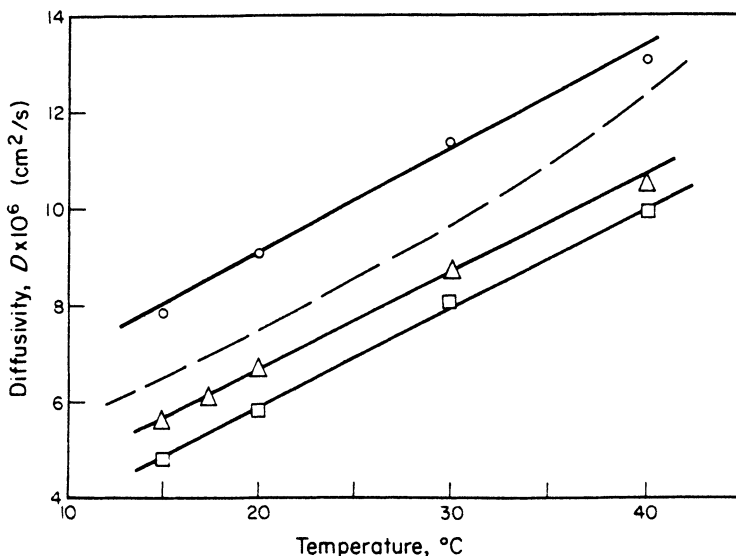


Figure 2.5. Diffusivities of saturated aqueous solutions of the hydroxybenzoic acids into water: \circ = *ortho*-, \square = *meta*-, \triangle = *para*-, — = predicted from equation 2.24 (after Mullin and Cook, 1965)

compared with values predicted by equation 2.24 in *Figure 2.5*, where the deviation is about $\pm 30\%$ between the estimated values and those measured for the *m*- and *p*-isomers, with a difference of about 60% between the *o*- and *m*-.

Clearly equation 2.24 and other empirical relationships, fail to take some property of the system into account, and it is likely that this quantity is the ‘size’ of the diffusing component. For the case of the hydroxybenzoic acids the differences in diffusivity can be accounted for by considering the different hydrogen bonding tendencies of the three isomers, which in turn would influence both the size and shape of the diffusing species.

2.4.1 Experimental measurements

In a diffusion cell, where two liquids are brought into contact at a sharp boundary, three different states of diffusion may be recognized. In the case of ‘free’ diffusion, concentrations change progressively away from the interface; when concentrations begin to change at the ends of the cell, ‘restricted’ diffusion is said to occur. If the concentration at a given point in the cell remains constant with respect to time, ‘steady-state’ diffusion is taking place, and, as in all other steady-state processes, a constant supply of material to and removal from the system is required. Several comprehensive accounts have been given of the methods used for measuring diffusion coefficients under these three conditions (Tyrrell, 1961; Stokes and Mills, 1965; Robinson and Stokes, 1970).

The techniques used for restricted and steady-state diffusion generally involve the use of a diaphragm cell. This method has the disadvantage that the cell has first to be calibrated with a system with a known diffusion coefficient, and for systems with relatively slow diffusivities each run may require an inconveniently long time.

The diffusion coefficient under free-diffusion conditions can be measured by analysis at the termination of the experiment or by continuous or intermittent analysis while diffusion continues. Care has to be taken not to disturb the system, and the most widely employed methods for measuring diffusion coefficients in liquids are interferometric, resulting from the original work of Gouy in the 19th century.

Two kinds of diffusivity can be recorded, viz. the *differential*, D , and the *integral*, \bar{D} . The differential diffusivity is a value for one particular concentration, c , and driving force, $c_1 - c_2$, where $c = (c_1 + c_2)/2$ and $c_1 - c_2$ is sufficiently small for D to remain unchanged over the concentration range. However, the diffusion coefficient is usually concentration dependent, and in most cases it is the integral diffusivity that is normally measured. This is an average value over the concentration range c_1 to c_2 .

The differential diffusivity is of considerable theoretical importance, and it is only through this quantity that experimental measurements by different techniques can be compared. On the other hand, it is the integral coefficient that is generally required for mass transfer assessment, since this coefficient represents the true ‘average’ diffusivity over the concentration range involved in the mass transfer process.

For example, in the dissolution of a solid into a liquid, the solute diffuses from the saturated solution at the interface to the bulk solution. In crystallization the solute diffuses from the supersaturated bulk solution to the saturated solution at the interface. The relevant diffusivity that should be used in an analysis of these two processes, therefore, is the integral diffusivity, which covers the range of concentration from equilibrium saturation to that in the bulk solution.

Integral diffusivities may be measured directly by the diaphragm cell technique (Dullien and Shemilt, 1961), but unless the concentration on both sides of the diaphragm (see *Figure 2.6*) is maintained constant throughout the experiment, the diffusivity measured is the rather complex double-average known as the ‘diaphragm cell integral diffusivity’. \bar{D}_d , defined by an integrated form of Fick’s law of diffusion:

$$\bar{D}_d = \frac{1}{\beta t} \ln \left(\frac{c_{1_0} - c_{2_0}}{c_{1_t} - c_{2_t}} \right) \quad (2.25)$$

where c_0 and c_t are the initial and final (at time t) concentrations, 1 and 2 refer to the lower and upper cells, and β is the cell constant (m^{-2}), which can be calculated from the cell dimensions:

$$\beta = \frac{A}{L} \left(\frac{1}{V_1} + \frac{1}{V_2} \right) \quad (2.26)$$

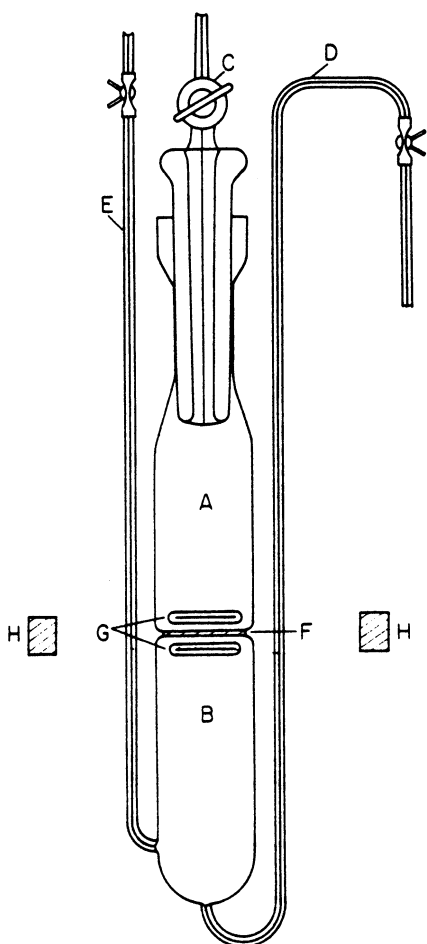


Figure 2.6. Diaphragm diffusion cell (after Dullien and Shemilt, 1961). *A*, light liquid compartment; *B*, heavy liquid compartment; *C*, stop-cock; *D*, *E*, capillaries; *F*, sintered glass diaphragm; *G* = polythene-coated iron stirrers; *H*, rotating magnets

where A and L = area and thickness of diaphragm, and V_1 and V_2 = volume of the cell compartments.

The above method is extremely time-consuming and the process of converting integral to differential values is both tedious and inaccurate. It is more practicable, therefore, to measure the differential diffusivity, D , at intervals over the whole concentration range and to calculate the required integral diffusivity, \bar{D} , by means of the relationship

$$\bar{D} = \frac{1}{c_1 - c_2} \int_{c_2}^{c_1} Ddc \quad (2.27)$$

Figure 2.7 shows the measured differential and calculated integral diffusivities for the systems KCl–H₂O and NH₄Cl–H₂O (Nienow, Unahabkhokha and

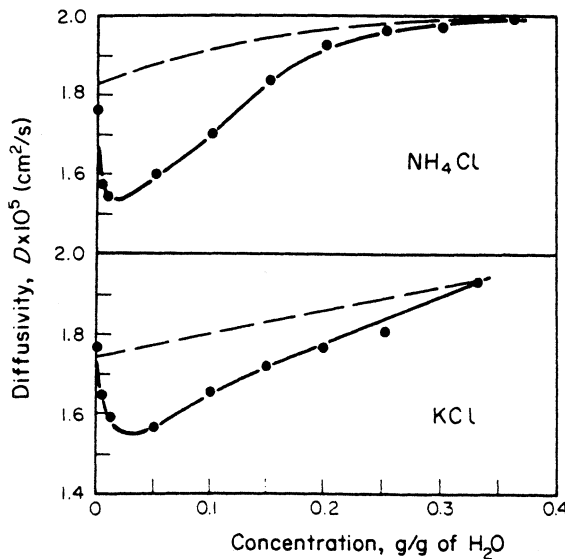


Figure 2.7. Measured differential (●) and calculated integral (broken line) diffusivities for the systems NH₄Cl–H₂O and KCl–H₂O at 20°C (after Nienow, Unahabokha and Mullin, 1968)

Mullin, 1968). Diffusivities for a number of common electrolyte systems are given in the Appendix (Table A.11).

The diffusivity of a strong electrolyte at infinite dilution is called the *Nernst limiting value* of the diffusion coefficient, D^0 , which can be calculated from

$$D^0 = \frac{\mathbf{R}T(\nu_1 - \nu_2)}{\mathbf{F}^2\nu_1|z_1|} \cdot \frac{\Lambda_{01}\Lambda_{02}}{\Lambda_{01} + \Lambda_{02}} \quad (2.28)$$

where Λ_{01} and Λ_{02} are the limiting conductivities, and ν_1 and ν_2 are the number of cations and anions of valency z_1 and z_2 , respectively. Using the conditions of neutrality:

$$\nu_1z_1 + \nu_2z_2 = 0$$

so equation 2.28 may also be written

$$D^0 = \frac{\mathbf{R}T}{\mathbf{F}^2} \cdot \frac{|z_1| + |z_2|}{|z_1z_2|} \cdot \frac{\Lambda_{01}\Lambda_{02}}{\Lambda_{01} + \Lambda_{02}} \quad (2.29)$$

where \mathbf{F} is the Faraday constant ($9.6487 \times 10^4 \text{ C mol}^{-1}$), \mathbf{R} is the gas constant ($8.3143 \text{ J K}^{-1} \text{ mol}^{-1}$), giving values of RT/\mathbf{F}^2 of 2.4381, 2.6166 and $2.7951 \times 10^{-2} \text{ S}^{-1} \text{ mol}^{-1} \text{ s}^{-1}$ at 0, 20 and 40°C, respectively. These may be used with the values of Λ_0 ($\text{S m}^2 \text{ mol}^{-1}$) in the Appendix (Table A.13) to give values of D^0 in $\text{m}^2 \text{ s}^{-1}$.

By the application of reaction rate theory to both viscosity and diffusion it can be shown that

$$\eta = A \exp(-E_V/\mathbf{R}T) \quad (2.30)$$

and

$$D = B \exp(-E_D/\mathbf{R}T) \quad (2.31)$$

A plot of $\log \eta$ against $1/T$ should yield a straight line, and similarly a linear relationship should exist between $\log D$ and $1/T$. The slopes of these plots give the respective energies of activation E_V (viscosity) and E_D (diffusion).

2.5 Refractive index

Refractometric measurements can often be used for the rapid measurement of solution concentration. Several standard instruments (Abbe, Pulfrich, etc.) are available commercially. A sodium lamp source is most usually used for illumination, and an instrument reading to the fourth decimal place is normally adequate for crystallization work. It is advisable that calibration curves be measured, in terms of temperature and concentration, prior to the study with the actual system.

If a dipping-type refractometer is used, a semi-continuous measurement may be made of the change in concentration as the system crystallizes. However, if nucleation is heavy or if large numbers of crystals are present, it may be difficult to provide sufficient illumination for the prism because of the light scattering. One solution to this problem (Leci and Mullin, 1968) is to use a fibre optic (a light wire) fitted into a collar around the prism illuminated from an external source (*Figure 2.8*). In this way undue heating of the solution is also avoided.

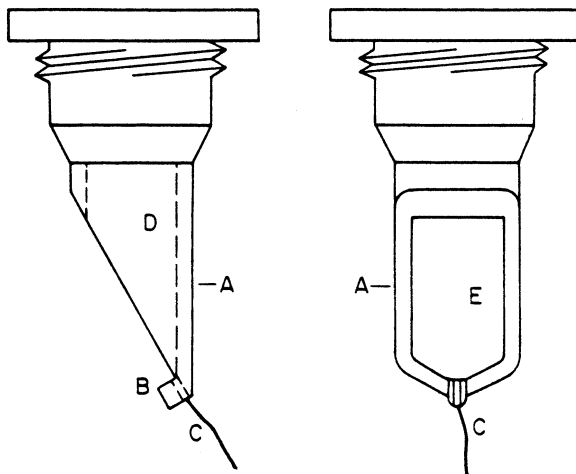


Figure 2.8. A technique for illuminating the prism of a dipping-type refractometer in an opaque solution: A, Perspex collar; B, fibre optic holder; C, fibre optic; D, refractometer prism; E, polished face of prism

2.6 Electrolytic conductivity

The electrolytic conductance of dilute aqueous solutions can often be measured with high precision and thus afford a useful means of determining concentration (see section 3.6.3). A detailed account of the methods used in this area is given by Robinson and Stokes (1970).

In the author's experience, however, conductivity measurements are of limited use in crystallization work because of the unreliability of measurement in near-saturated or supersaturated solutions. The temperature dependence of electrical conductivity usually demands a very high precision of temperature control. Torgesen and Horton (1963) successfully operated conductance cells for the control of ADP crystallization, but they had to control the temperature to $\pm 0.002^\circ\text{C}$.

2.7 Crystal hardness

Crystals vary in hardness not only from substance to substance but also from face to face on a given crystal (Brookes, O'Neill and Redfern, 1971). One of the standard tests for hardness in non-metallic compounds and minerals is the scratch test, which gave rise to the Mohs scale. Ten 'degrees' of hardness are designated by common minerals in such an order that a given mineral will scratch the surface of any of the preceding members of the scale (see *Table 2.2*).

The hardness of metals is generally expressed in terms of their resistance to indentation. A hard indenter is pressed into the surface under the influence of a known load and the size of the resulting indentation is measured. A widely used instrument is the Vickers indenter, which gives a pyramidal indentation, and the results are expressed as a Vickers hardness number (kgf mm^{-2}). Other

Table 2.2. *Mohs scale of hardness*

Mohs hardness number <i>M</i>	Reference substance	Formula	Vickers hardness number <i>V</i>
1	talc	$3\text{MgO} \cdot 4\text{SiO}_2 \cdot \text{H}_2\text{O}$	50
2	gypsum	$\text{CaSO}_4 \cdot 2\text{H}_2\text{O}$	80
3	calcite	CaCO_3	130
4	fluorite	CaF_2	200
5	apatite	$\text{CaF}_2 \cdot 3\text{Ca}_3(\text{PO}_4)_2$	320
6	orthoclase	$\text{K}_2\text{O} \cdot \text{Al}_2\text{O}_3 \cdot 6\text{SiO}_2$	500
7	quartz	SiO_2	800
8	topaz	$(\text{AlF})_2 \cdot \text{SiO}_4$	1 300
9	corundum	Al_2O_3	2 000
10	diamond	C	10 000

tests include the Rockwell, which uses a conical indenter and the Brinell, which uses a hard steel ball (Bowden and Tabor, 1964).

The relation between Mohs hardness, M , and the Vickers hardness, V , is not a clear one. However, if diamond ($M = 10$) is omitted from the Mohs scale, the relationship

$$\log V = 0.2 M + 1.5 \quad (2.32)$$

may be used for rough approximation purposes for values of $M < 9$.

A few typical surface hardnesses (Mohs) of some common substances are:

sodium	0.5	aluminium	2–3
potassium	0.5	gold	2.5–3
lead	1.5	brass	3–4
magnesium	2	glass	3–4

The scratch test is not really suitable for specifying the hardness of substances commonly crystallized from aqueous solutions, because their Mohs values lie in a very short range, frequently between 1 and 3 for inorganic salts and below 1 for organic substances. For a reliable measurement of hardness of these soft crystals the indentation test is preferred. Ridgway (1970) has measured mean values of the Vickers hardness for several crystalline substances:

sodium thiosulphate	(Na ₂ S ₂ O ₃ · 5H ₂ O)	:	18
potassium alum	(KAl(SO ₄) ₂ · 12H ₂ O)	:	56
ammonium alum	(NH ₄ Al(SO ₄) ₂ · 12H ₂ O)	:	58
potassium dihydrogen phosphate	(KH ₂ PO ₄)	:	150
sucrose	(C ₁₂ H ₂₂ O ₁₁)	:	64

He has also determined the hardnesses of different faces of the same crystal:

ammonium dihydrogen phosphate	(NH ₄ H ₂ PO ₄)	(100)	:	69
		(110)	:	73
potassium sulphate	(K ₂ SO ₄)	(100)	:	95
		(110)	:	100
		(210)	:	130

Hardness appears to be closely related to density (proportional to) and to atomic or molecular volume (inversely proportional), but few reliable data are available. In a recent study, Ulrich and Kruse (1989) made some interesting comments on these relationships and confirmed the need for more experimental data before any acceptable prediction method can be developed.

2.8 Units of heat

The SI heat energy unit is the joule (J), but four other units still commonly encountered are the calorie (cal), kilocalorie (kcal), British thermal unit (Btu) and the centigrade heat unit (chu). The old definitions of these four units are

Table 2.3. Equivalent values of the common heat energy units

<i>cal</i>	<i>kcal</i>	<i>Btu</i>	<i>chu</i>	<i>J</i>
1	0.001	0.00397	0.00221	4.187
1000	1	3.97	2.21	4187
252	0.252	1	0.556	1.055
453.6	0.4536	1.8	1	1.898
0.2388	2.388×10^{-4}	9.478×10^{-4}	5.275×10^{-4}	1

based on the heat energy required to raise the temperature of a unit mass of water by one degree:

1 cal = 1 g of water raised through 1 °C (or K)

1 kcal = 1 kg of water raised through 1 °C (or K)

1 chu = 1 lb of water raised through 1 °C (or K)

1 Btu = 1 lb of water raised through 1 °F

The definitions of these units are linked to the basic SI unit, the joule:

$$1 \text{ J} = 1 \text{ Ws} = 1 \text{ N m}$$

Table 2.3 indicates the equivalent values of these various heat units.

2.9 Heat capacity

The amount of heat energy associated with a given temperature change in a given system is a function of the chemical and physical states of the system. A measure of this heat energy can be quantified in terms of the quantity known as the heat capacity which may be expressed on a mass or molar basis. The former is designated the specific heat capacity ($\text{J kg}^{-1} \text{ K}^{-1}$) and the latter the molar heat capacity ($\text{J mol}^{-1} \text{ K}^{-1}$). The relationships between some commonly used heat capacity units are:

specific heat capacity, C

$$\begin{aligned} 1 \text{ cal g}^{-1} \text{ °C}^{-1} (\text{or } \text{K}^{-1}) &= 1 \text{ Btu lb}^{-1} \text{ °F}^{-1} \\ &= 1 \text{ chu lb}^{-1} \text{ °C}^{-1} (\text{or } \text{K}^{-1}) \\ &= 4.187 \text{ kJ kg}^{-1} \text{ K}^{-1} \end{aligned}$$

molar heat capacity, C

$$\begin{aligned} 1 \text{ cal mol}^{-1} \text{ °C}^{-1} (\text{or } \text{K}^{-1}) &= 1 \text{ Btu lb-mol}^{-1} \text{ °F}^{-1} \\ &= 1 \text{ chu lb-mol}^{-1} \text{ °C}^{-1} (\text{or } \text{K}^{-1}) \\ &= 4.187 \text{ J mol}^{-1} \text{ K}^{-1} \end{aligned}$$

For gases two heat capacities have to be considered, at constant pressure, C_p , and at constant volume, C_v . The value of the ratio of these two quantities, $C_p/C_v = \gamma$, varies from about 1.67 for monatomic gases (e.g. He) to about 1.3

for triatomic gases (e.g. CO₂). For liquids and solids there is little difference between C_p and C_v , i.e. $\gamma \sim 1$, and it is usual to find C_p values only quoted in the literature.

2.9.1 Solids

Specific heat capacities of solid substances near normal atmospheric temperature can be estimated with a reasonable degree of accuracy by combining two empirical rules.

The first of these, due to Dulong and Petit, expresses a term called the ‘atomic heat’ which is defined as the product of the relative atomic mass and the specific heat capacity. For all solid elemental substances, the atomic heat is assumed to be roughly constant:

$$\text{atomic heat} \simeq 6.2 \text{ cal mol}^{-1} \text{ }^{\circ}\text{C}^{-1}$$

which in SI units is equivalent to approximately 26 J mol⁻¹ K⁻¹. However, since virtually all the data available in the literature are recorded in calorie units, these will be retained in this section for all the examples.

The second rule, due to Kopp, applies to solid compounds and may be expressed by

molar heat capacity = sum of the atomic heats of the constituent atoms

In applying these rules, the following exceptions to the approximation ‘atomic heat $\simeq 6.2$ ’ must be noted:

$$\begin{array}{llll} \text{C} = 1.8 & \text{H} = 2.3 & \text{B} = 2.7 & \text{Si} = 3.8 \\ \text{O} = 4.0 & \text{F} = 5.0 & \text{S} = 5.4 & [\text{H}_2\text{O}] = 9.8 \end{array}$$

The substance [H₂O] refers to water as ice or as water of crystallization in solid substances. Obviously a reliable measured value of a heat capacity is preferable to an estimated value, but in the absence of measured values, Kopp’s rule can prove extremely useful. A few calculated and observed values of the molar heat capacity are compared in *Table 2.4*.

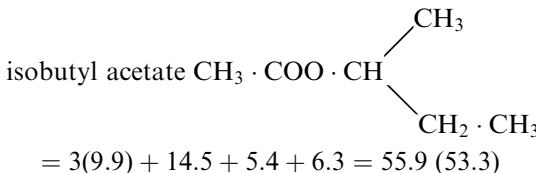
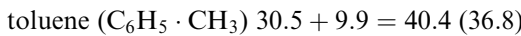
Table 2.4. Estimated (Kopp’s rule) and observed values of molar heat capacity of several solid substances at room temperature

Solid	Formula	Calculation	$C \text{ cal mol}^{-1} \text{ }^{\circ}\text{C}^{-1}$	
			<i>Calc.</i>	<i>Obs.</i>
Sodium chloride	NaCl	$6.2 + 6.2$	12.4	12.4
Magnesium sulphate	MgSO ₄ · 7H ₂ O	$6.2 + 5.4 + 4(4.0) + 7(9.8)$	96.2	89.5
Iodobenzene	C ₆ H ₅ I	$6(1.8) + 5(2.3) + 6.2$	28.5	24.6
Naphthalene	C ₁₀ H ₈	$10(1.8) + 8(2.3)$	36.4	37.6
Potassium sulphate	K ₂ SO ₄	$2(6.2) + 5.4 + 4(4.0)$	33.8	30.6
Oxalic acid	C ₂ H ₂ O ₄ · 2H ₂ O	$2(1.8) + 2(2.3) + 4(4.0)$ + 2(9.8)	43.8	43.5

Many inorganic solids have values of specific heat capacity, c_p , in the range 0.1–0.3 cal g⁻¹ °C⁻¹ (0.4–1.3 kJ kmol⁻¹ K⁻¹) and many organic solids have values in the range 0.2–0.5 (0.8–2.1). In general, the heat capacity increases slightly with an increase in temperature. For example, the values of c_p at 0 and 100 °C for sodium chloride are 0.21 and 0.22 cal g⁻¹ °C⁻¹ (8.8 and 9.2 kJ kmol⁻¹ K⁻¹) respectively, and the corresponding values for anthracene are 0.30 and 0.35 (approximately 13 and 15 kJ kmol⁻¹ K⁻¹).

2.9.2 Pure liquids

A useful method for estimating the molar heat capacity of an organic liquid is based on the additivity of the heat capacity contributions [C] of the various atomic groupings in the molecules (Johnson and Huang, 1955). *Table 2.5* lists some [C] values, and the following examples illustrate the use of the method – the molar capacity values (cal mol⁻¹ °C⁻¹) in parentheses denote values obtained experimentally at 20 °C:



The heat capacity of a substance in the liquid state is generally higher than that of a substance in the solid state. A large number of organic liquids have specific heat capacity c values in the range 0.4–0.6 cal g⁻¹ °C⁻¹ (1.7–2.5 kJ kg⁻¹ K⁻¹) at about room temperature. The heat capacity of a liquid usually increases with increasing temperature: for example, the values of c for ethyl alcohol at 0, 20

Table 2.5. Contributions of various atomic groups to the molar heat capacity (cal mol⁻¹ °C⁻¹) of organic liquids at 20 °C (after A. I. Johnson and C. J. Huang, 1955)

Group	[C]	Group	[C]
C ₆ H ₅ —	30.5	—OH	11.0
CH ₃ —	9.9	—NO ₂	15.3
—CH ₂ —	6.3	—NH ₂	15.2
—CH	5.4	—CN	13.9
—COOH	19.1	—Cl	8.6
—COO— (esters)	14.5	—Br	3.7
C=O (ketones)	14.7	—S—	10.6
—H (formates)	3.6	—O— (ethers)	8.4

and 60 °C are 0.54, 0.56 and 0.68 cal g⁻¹ °C⁻¹ (2.3, 2.3 and 2.9 kJ kg⁻¹ K⁻¹) and those for benzene at 20, 40 and 60 °C are 0.40, 0.42 and 0.45 (1.7, 1.8 and 2.1 kJ kg⁻¹ K⁻¹). Water is an exceptional case; it has a very high heat capacity and exhibits a minimum value at 30 °C. The values for water at 0, 15, 30 and 100 °C are 1.008, 1.000, 0.9987 and 1.007 cal g⁻¹ °C⁻¹, respectively.

2.9.3 Liquid mixtures and solutions

Although not entirely reliable, the following relationship may be used to predict the molar heat capacity C of a mixture of two or more liquids:

$$C_{\text{mixt}} = x_A C_A + x_B C_B + \dots \quad (2.33)$$

where x denotes the mole fraction of the given component in the mixture. A similar relationship may be used to give a rough estimate of the specific heat capacity c :

$$c_{\text{mixt}} = X_A c_A + X_B c_B + \dots \quad (2.34)$$

where X is a mass fraction.

For example, the value of c for methanol at 20 °C is 2.4 kJ kg⁻¹ K⁻¹. From equation 2.34 it can be calculated that an aqueous solution containing 75 mass per cent of methanol has a specific heat capacity of 2.9 kJ kg⁻¹ K⁻¹, which coincides closely with measured values.

For dilute aqueous solutions of inorganic salts, a rough estimate of the specific heat capacity can be made by ignoring the heat capacity contribution of the dissolved substance, i.e.

$$|c| = |1 - Y| \quad (2.35)$$

where Y = mass of solute/mass of water, and $c = \text{cal g}^{-1} \text{ } ^\circ\text{C}^{-1}$. Thus, solutions containing 5 g NaCl, 10 g KCl and 15 g CuSO₄ per 100 g of solution would by this method be estimated to have specific heat capacities of 0.95, 0.89 and 0.82 cal g⁻¹ °C⁻¹, respectively. Measured values (25 °C) for these solutions are 0.94, 0.91 and 0.83 cal g⁻¹ °C⁻¹ (3.9, 3.8 and 3.5 kJ kg⁻¹ K⁻¹), respectively. This estimation method cannot be applied to aqueous solutions of non-electrolytes or acids.

Another rough estimation method for the specific heat capacity of aqueous solutions is based on the empirical relationship

$$|c| = |\rho^{-1}| \quad (2.36)$$

where ρ = density of the solution in g cm⁻³. For example, at 30 °C a 2 per cent aqueous solution of sodium carbonate by mass has a density of 1.016 g cm⁻³ and a specific heat capacity of 0.98 cal g⁻¹ °C⁻¹ ($1/\rho = 0.98$), while a 20 per cent solution has a density of 1.210 and a specific heat capacity of 0.86 ($1/\rho = 0.83$).

2.9.4 Experimental measurement

The specific heat capacity of a liquid may be measured by comparing its cooling rate with that of water. This is most conveniently done in a calorimeter, a copper vessel fitted with a copper lid and heavy copper wire stirrer, supported in a draught-free space kept at constant temperature. The vessel is filled almost to the top with a known mass of water at about 70 °C and its temperature is recorded every 2 minutes as it cools to, say, 30 °C. Significant errors may be incurred if the starting temperature exceeds about 70 °C because evaporation greatly increases the rate of cooling. The water is then replaced by the same volume of the liquid or solution under test and its cooling curve is determined over the same temperature range.

Taking the specific heat capacities of copper and water to be 385 and 4185 J kg⁻¹ K⁻¹ respectively, a balance of the heat losses gives

$$(4185m_w + 385m_c)(d\theta/dt)_w = (c_1 m_1 + 385m_c)(d\theta/dt)_1$$

where m_c = mass of the copper calorimeter, lid and stirrer, m_w = mass of water and m_1 = mass of liquid. The cooling rates ($d\theta/dt$) are taken from the slopes of the cooling curves at the chosen temperature θ , and the specific heat capacity c_1 of the liquid under test can thus be evaluated.

2.10 Thermal conductivity

The thermal conductivity, κ , of a substance is defined as the rate of heat transfer by conduction across a unit area, through a layer of unit thickness, under the influence of a unit temperature difference, the direction of heat transmission being normal to the reference area. Fourier's equation for steady conduction may be written as

$$\frac{dq}{dt} = -\kappa A \frac{d\theta}{dx} \quad (2.37)$$

where q , t , A , θ and x are units of heat, time, area, temperature and length (thickness), respectively.

The SI unit for thermal conductivity is W m⁻¹ K⁻¹ although other units such as cal s⁻¹ cm⁻¹ °C⁻¹ and Btu h⁻¹ ft⁻¹ °F⁻¹ are still commonly encountered. The conversion factors are:

$$1 \text{ cal s}^{-1} \text{ cm}^{-1} \text{ }^{\circ}\text{C}^{-1} = 418.7 \text{ W m}^{-1} \text{ K}^{-1} = 241.9 \text{ Btu h}^{-1} \text{ ft}^{-1} \text{ }^{\circ}\text{F}^{-1}$$

The thermal conductivity of a crystalline solid can vary considerably according to the crystallographic direction, but very few directional values are available in the literature. Some overall values (W m⁻¹ K⁻¹) for polycrystalline or non-crystalline substances include KCl (9.0), NaCl (7.5), KBr (3.8), NaBr (2.5), MgSO₄ · 7H₂O (2.5), ice (2.2), K₂Cr₂O₇ (1.9), borosilicate glass (1.0), soda glass (0.7) and chalk (0.7).

Table 2.6. Thermal conductivities of some pure liquids

Temperature, °C	Thermal conductivity, κ (W m ⁻¹ K ⁻¹)					
	Water	Acetone	Benzene	Methanol	Ethanol	CCl ₄
10	0.59	0.16	0.14	0.21	0.18	0.11
40	0.62	0.15	0.15	0.19	0.17	0.099
95	0.67	—	—	—	—	—

An increase in the temperature of a liquid usually results in a slight decrease in thermal conductivity, but water is a notable exception to this generalization. Furthermore, water has a particularly high thermal conductivity compared with other pure liquids (*Table 2.6*). There are relatively few values of thermal conductivity for solutions recorded in the literature and regrettably they are frequently conflicting. There is no generally reliable method of estimation.

The thermal conductivity of an aqueous solution of a salt is generally slightly lower than that of pure water at the same temperature. For example, the values at 25 °C for water, and saturated solutions of sodium chloride and calcium chloride are 0.60, 0.57 and 0.54 W m⁻¹ K⁻¹, respectively.

The thermal conductivity κ (W m⁻¹ K⁻¹) of pure liquids between about 0 and 70 °C may be roughly estimated by the equation

$$\kappa = 3.6 \times 10^{-8} c\rho(\rho/M)^{1/3} \quad (2.38)$$

where c is the specific heat capacity (J kg⁻¹ K⁻¹), ρ is the density (kg m⁻³) and M is the molar mass (kg kmol⁻¹).

2.11 Boiling, freezing and melting points

When a non-volatile solute is dissolved in a solvent, the vapour pressure of the solvent is lowered. Consequently, at any given pressure, the boiling point of a solution is higher and the freezing point lower than those of the pure solvent. For dilute ideal solutions, i.e. such as obey Raoult's law, the boiling point elevation and freezing point depression can be calculated by an equation of the form

$$\Delta T = \frac{mK}{M} \quad (2.39)$$

where m = mass of solute dissolved in a given mass of pure solvent and M = molar mass of the solute. When ΔT refers to the freezing point depression, $K = K_f$, the cryoscopic constant; when ΔT refers to the boiling point elevation, $K = K_b$, the ebullioscopic constant. Values of K_f and K_b for several common solvents are given in *Table 2.7*; these, in effect, give the depression in freezing point, or elevation in boiling point, in °C when 1 mol of solute is dissolved, without dissociation or association, in 1 kg of solvent.

Table 2.7. Cryoscopic and ebullioscopic constants for some common solvents

Solvent	Freezing point, °C	Boiling point, °C	K_f K kg mol ⁻¹	K_b K kg mol ⁻¹
Acetic acid	16.7	118.1	3.9	3.1
Acetone	-95.5	56.3	2.7	1.7
Aniline	-6.2	184.5	5.9	3.2
Benzene	5.5	80.1	5.1	2.7
Carbon disulphide	-108.5	46.3	3.8	2.4
Carbon tetrachloride	-22.6	76.8	32.0	4.9
Chloroform	-63.5	61.2	4.8	3.8
Cyclohexane	6.2	80	20.0	2.8
Nitrobenzene	5.7	211	7.0	5.3
Methyl alcohol	-97.8	64.7	2.6	0.8
Phenol	42.0	181	7.3	3.0
Water	0.0	100.0	1.86	0.52

The cryoscopic and ebullioscopic constants can be calculated from values of the enthalpies of fusion and vaporization, respectively, by the equation

$$K = \frac{\mathbf{R}T^2}{\Delta H} \quad (2.40)$$

When $K = K_f$, T refers to the freezing point T_f (K) and ΔH to the enthalpy of fusion, ΔH_f (J kg⁻¹). When $K = K_b$, T refers to the boiling point T_b and $\Delta H = \Delta H_{vb}$, the enthalpy of vaporization at the boiling point. The gas constant $\mathbf{R} = 8.314 \text{ J mol}^{-1} \text{ K}^{-1}$.

Boiling points and freezing points are both frequently used as criteria for the estimation of the purity of near-pure liquids. Detailed specifications of standard methods for their determination are given, for example, in the British Pharmacopoeia (2000).

Equation 2.40 cannot be applied to concentrated solutions or to aqueous solutions of electrolytes. In these cases the freezing point depression cannot readily be estimated. The boiling point elevation, however, can be predicted with a reasonable degree of accuracy by means of the empirical Dühring rule: the boiling point of a solution is a linear function of the boiling point of the pure solvent. Therefore, if the boiling points of solutions of different concentrations are plotted against those of the solvent at different pressures, a family of straight lines (not necessarily parallel) will be obtained. A typical Dühring plot, for aqueous solutions of sodium hydroxide, is given in *Figure 2.9* from which it can be estimated, for example, that at a pressure at which water boils at 80 °C, a solution containing 50 per cent by mass of NaOH would boil at about 120 °C, i.e. a boiling point elevation of about 40 °C.

The boiling point elevation (BPE) of some 40 saturated aqueous solutions of inorganic salts have been reported by Meranda and Furter (1977) who proposed the correlating relationship

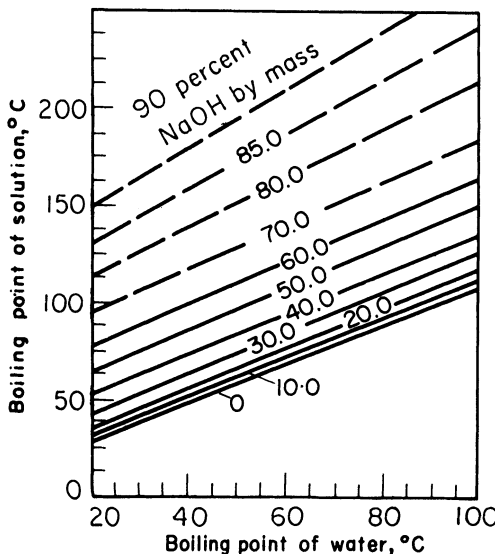


Figure 2.9. Dühring plot for aqueous solutions of sodium hydroxide

$$\text{BPE } (\text{°C}) = 104.9 x_S^{1.14} \quad (2.41)$$

where x_S is the mole fraction of salt in the solution.

The practical difficulties of measuring boiling point elevations have been discussed by Nicol (1969).

2.11.1 Melting points

The melting point of a solid organic substance is frequently adopted as a criterion of purity, but before any reliance can be placed on the test, it is necessary for the experimental procedure to be standardized. Several types of melting point apparatus are available commercially, but the most widely used method consists of heating a powdered sample of the material in a glass capillary tube located close to the bulb of a thermometer in an agitated bath of liquid.

The best type of glass tube is about 1 mm internal diameter, about 70 mm long, with walls about 0.1 mm thick. The tube is heat-sealed at one end, and the powdered sample is scraped into the tube and knocked or vibrated down to the closed end to give a compacted layer about 5 mm deep. It is then inserted into the liquid bath at about 10 °C below the expected melting point and attached close to the thermometer bulb. The bath is agitated and temperature is raised steadily at about 3 °C/min. The melting point of the substance is taken as the temperature at which a definite meniscus is formed in the tube. For pure substances the melting point can be readily and accurately reproduced; for impure substances it is better to record a melting range of temperature.

Table 2.8. *Melting points of pure organic compounds useful for calibrating thermometers*

Substance	Melting point, °C
Phenyl salicylate (salol)	42
<i>p</i> -Dichlorbenzene	53
Naphthalene	81
<i>m</i> -Dinitrobenzene	90
Acetamide	114
Benzoic acid	123
Urea	133
Salicylic acid	160
Succinic acid	183
Anthracene	217
<i>p</i> -Nitrobenzene acid	242
Anthraquinone	286

Some organic substances are extremely sensitive to the presence of traces of alkali in soft soda-glass capillary tubes, giving unduly low melting points. In these cases, borosilicate glass tubes are recommended. Traces of moisture in the tube will also lower the melting point so the capillary tubes should always be stored in a desiccator.

Some organic substances begin to decompose near their melting point, so that it is important not to keep the sample at an elevated temperature for prolonged periods. The insertion of the capillary into the bath at 10 °C below the melting point, allowing the temperature to rise at 3 °C/min, usually eliminates any difficulties. For reproducible results to be obtained, the sample should be in a finely divided state (<100 µm). The thermometer, preferably graduated in increments of 0.1 °C, should be accurately calibrated over its whole range and, if in constant use, should be checked regularly. The well-known standardization temperatures are the freezing and boiling points of water, but other standards that can be used are the melting points of pure organic substances, such as those indicated in *Table 2.8*.

The liquid used in the heating bath depends on the working temperature; water is quite suitable for melting points from about room temperature to about 70 °C and liquid paraffin and a range of silicone fluids are widely used for more elevated temperatures.

Specifications of methods for determining melting points are given in the British Pharmacopoeia (2000). See also section 4.5.1.

2.12 Enthalpies of phase change

When a substance undergoes a phase change, a quantity of heat is transferred between the substance and its surrounding medium. Several types of enthalpy

change, still often referred to as the latent heat, and the following types may be distinguished:

- | | |
|---------------------------------------|---|
| solid I \rightleftharpoons solid II | (enthalpy of transition, ΔH_t) |
| solid \rightleftharpoons liquid | (enthalpy of fusion, ΔH_f) |
| solid \rightleftharpoons gas | (enthalpy of sublimation, ΔH_s) |
| liquid \rightleftharpoons gas | (enthalpy of vaporization, ΔH_v) |

Only the last three of these represent significant quantities of heat energy: enthalpies of transition can for most industrial purposes be ignored. For example, the transformation of monoclinic to orthorhombic sulphur is accompanied by an enthalpy change of about 2 kJ kg^{-1} , whereas the fusion of orthorhombic sulphur is accompanied by an enthalpy change of about 70 kJ kg^{-1} .

Enthalpy changes, like the other thermal properties, can be expressed on a mass or molar basis, but to avoid confusion, all in this section will be expressed on a molar basis. The relationship between some commonly used units are:

$$1 \text{ cal g}^{-1} = 1 \text{ chu 1b}^{-1} = 1.8 \text{ Btu 1b}^{-1} = 4.187 \text{ kJ kg}^{-1}$$

$$1 \text{ cal mol}^{-1} = 1 \text{ chu 1b-mol}^{-1} = 1.8 \text{ Btu 1b-mol}^{-1} = 4.187 \text{ J mol}^{-1}$$

The relationship between any enthalpy change ΔH and the pressure–volume–temperature conditions of a system is given by the Clapeyron equation

$$\frac{dp}{dT} = \frac{\Delta H}{T\Delta v} \quad (2.42)$$

where dp/dT = rate of change of vapour pressure with absolute temperature and Δv = volume change accompanying the phase change.

A typical temperature–pressure phase diagram for a one-component system is shown in *Figure 2.10*. The sublimation curve AX indicates the increase of the vapour pressure of the solid with an increase in temperature. This is expressed quantitatively by the Clapeyron equation written as

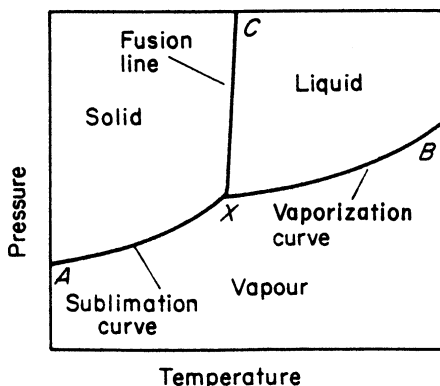


Figure 2.10. Temperature–pressure diagram for a single-component system

$$\left(\frac{dp}{dT}\right)_s = \frac{\Delta H_s}{T(v_g - v_s)} \quad (2.43)$$

where v_g and v_s = the molar volumes of the vapour and solid, respectively, and ΔH_s = enthalpy of sublimation. The vaporization curve XB indicates the increase of the vapour pressure of the liquid with an increase in temperature:

$$\left(\frac{dp}{dT}\right)_v = \frac{\Delta H_v}{T(v_g - v_l)} \quad (2.44)$$

where v_l = the molar volume of the liquid, and ΔH_v = latent heat of vaporization. Curve XB is not a continuation of curve AX ; this fact can be confirmed by calculating their slopes dp/dT from equations 2.43 and 2.44 at point X .

The fusion line XC indicates the effect of pressure on the melting point of the solid; it can either increase or decrease with an increase in pressure, but the effect is so small that line XC deviates only slightly from the vertical. When the fusion line deviates to the right, as in *Figure 2.10*, the melting point increases with an increase in pressure, and the substance contracts on freezing. Most substances behave in this manner. When the line deviates to the left, the melting point decreases with increasing pressure, and the substance expands on freezing. Water (see section 4.4) and type metals (Pb–Bi alloys) are among the few examples of this behaviour that can be quoted. The equation for the fusion line is

$$\left(\frac{dp}{dT}\right)_t = \frac{\Delta H_f}{T(v_l - v_s)} \quad (2.45)$$

where ΔH_f is the enthalpy of fusion.

The enthalpies of sublimation, vaporization and fusion are related by

$$\Delta H_s = \Delta H_f + \Delta H_v \quad (2.46)$$

but this additivity is applicable only at one specific temperature. The variation of an enthalpy change with temperature can be calculated from the Clausius equation

$$\frac{d\Delta H}{dT} - \frac{\Delta H}{T} = c_2 - c_1 \quad (2.47)$$

When $\Delta H = \Delta H_v$, c_1 and c_2 are the molar heat capacities of the liquid, just on the point of vaporization, and of the saturated vapour, respectively. Equation 2.47 can also be used for calculating ΔH_f and ΔH_s the appropriate values of c being inserted.

The specific volumes v_l and v_s are much smaller than v_g ; equations 2.43 and 2.44 can therefore be simplified to

$$\frac{dp}{dT} = \frac{\Delta H}{Tv_g} \quad (2.48)$$

where $\Delta H = \Delta H_v$ or ΔH_s . From the ideal gas laws $v_g = \mathbf{R}T/p$, so that equation 2.48 may be written

$$\frac{dp}{p} = \frac{\Delta H}{\mathbf{R}T^2} dT \quad (2.49)$$

This is the Clausius–Clapeyron equation. If the enthalpy change is considered to be constant over a small temperature range, T_1 to T_2 , equation 2.49 may be integrated to give

$$\ln \frac{p_2}{p_1} = \frac{\Delta H(T_2 - T_1)}{\mathbf{R}T_1 T_2} \quad (2.50)$$

Equation 2.50 can be used to estimate enthalpies of vaporization and sublimation if vapour pressure data are available, or to estimate vapour pressures from a value of the enthalpy change. Analysis of sublimation problems (see section 7.4), is frequently difficult owing to the scarcity of published vapour pressure and enthalpy data. If two values of vapour pressure are available, however, a considerable amount of information can be derived from equation 2.50 as illustrated by the following example.

Suppose that the only data available on solid anthracene are that its vapour pressure at 210° and 145°C are 40 and 1.3 mbar, respectively; the vapour pressure at 100°C is required. Equation 2.50 can be used twice – first to calculate a value of ΔH_s then that of the required pressure:

$$\begin{aligned} \ln \left(\frac{40}{1.3} \right) &= \frac{\Delta H_s(483 - 418)}{8.314 \times 483 \times 418} \\ \Delta H_s &= 88.5 \text{ kJ mol}^{-1} \end{aligned}$$

Substituting this value of ΔH_s in equation 2.50 again,

$$\ln \left(\frac{40}{p_{100^\circ\text{C}}} \right) = \frac{88.5 (483 - 373)}{8.314 \times 483 \times 373}$$

therefore,

$$p_{100^\circ\text{C}} = 0.04 \text{ mbar}$$

2.12.1 Enthalpy of vaporization

There are several methods available for the estimation of enthalpies of vaporization at the atmospheric boiling point of the liquid. Trouton's rule, for example, is only suitable for non-polar liquids, but the Giacalone equation is fairly reliable for both polar and non-polar liquids:

$$\Delta H_{vb} = 88T_b \quad (\text{Trouton}) \quad (2.51)$$

$$\Delta H_{vb} = \left(\frac{\mathbf{R}T_c T_b}{T_c - T_b} \right) \ln P_c \quad (\text{Giacalone}) \quad (2.52)$$

where ΔH_{vb} = enthalpy of vaporization (J mol^{-1}) at the boiling point, T_b = boiling point (K) of the liquid at 760 mm Hg, T_c = critical temperature (K) of the liquid, and P_c = critical pressure (atm) of the liquid. (1 atm = 760 mm Hg = $1.013 \times 10^5 \text{ N/m}^2$.)

The enthalpy of vaporization of a liquid at some temperature T_1 can be calculated from its value at another temperature T_2 by means of the Watson equation:

$$\Delta H_{v1} = \Delta H_{v2} \left(\frac{T_c - T_1}{T_c - T_2} \right)^{0.38} \quad (2.53)$$

For example, the enthalpy of vaporization of benzene at its boiling point (353 K) is 30.8 J mol⁻¹, its critical temperature 563 K. From equation 2.44 the corresponding value at 25 °C (298 K) can be calculated as 33.6 J mol⁻¹, which compares with an experimental result of 33.7 J mol⁻¹.

A critical account of these and other more recent methods is given by Reid, Prauznitz and Poling (1987).

2.13 Heats of solution and crystallization

When a solute dissolves in a solvent without reaction, heat is usually absorbed from the surrounding medium (still commonly referred to as the heat of solution), i.e. if the dissolution occurs adiabatically the solution temperature falls. When a solute crystallizes out of its solution, heat is usually liberated (still commonly referred to as the heat of crystallization) and the solution temperature rises. The reverse cases, viz. heat evolution on dissolution and heat absorption on crystallization, may be encountered with solutes that exhibit an inverted solubility characteristic, e.g. anhydrous sodium sulphate in water.

The dissolution of an anhydrous salt in water at a temperature at which the hydrated salt is the stable crystalline form frequently leads to the release of heat energy, owing to the exothermic nature of the hydration process:

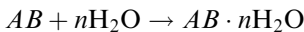


Table 2.9 lists the heats of solution of anhydrous and hydrated magnesium sulphate and sodium carbonate in water to illustrate the effect of water of crystallization.

The enthalpy changes associated with dissolution (ΔH_{sol}) and crystallization (ΔH_{crys}) are generally recorded as the number of heat units liberated by the system when the process takes place isothermally. According to this system of nomenclature, if an adiabatic operation is considered, the expression $\Delta H_{\text{sol}} = +q$ (heat units per unit mass of solute) means that the solution temperature will increase; $\Delta H_{\text{sol}} = -q$ means that it will fall.

The magnitude of the heat effect accompanying the dissolution of solute in a given solvent or undersaturated solution depends on the quantities of solute and solvent involved, the initial and final concentrations and the temperature at

Table 2.9. Heats of solution of anhydrous and hydrated salts in water at 18 °C and infinite dilution

Salt	Formula	Heat of solution, kJ mol ⁻¹
Magnesium sulphate	MgSO ₄	+88.3
	MgSO ₄ · H ₂ O	+58.6
	MgSO ₄ · 2H ₂ O	+49.0
	MgSO ₄ · 4H ₂ O	+20.5
	MgSO ₄ · 6H ₂ O	+2.3
	MgSO ₄ · 7H ₂ O	-13.3
Sodium carbonate	Na ₂ CO ₃	+23.3
	Na ₂ CO ₃ · H ₂ O	+9.2
	Na ₂ CO ₃ · 7H ₂ O	-42.6
	Na ₂ CO ₃ · 10H ₂ O	-67.9

which the dissolution occurs. The standard reference temperature is nowadays generally taken as 25 °C.

The first differential heat of solution (heat of solution at infinite dilution), $\Delta H_{\text{sol}}^{\infty}$, may be regarded as the heat liberated or absorbed when 1 mole of solute dissolves in a large amount of pure solvent. This is the value most generally recorded in the data handbooks. For inorganic salts in water, it normally lies between about 5 and 15 kcal mol⁻¹, i.e. about 20 to 60 kJ mol⁻¹. For organic substances in organic solvents, it normally lies between 1 and 5 kcal mol⁻¹ (about 5 to 20 kJ mol⁻¹). The last differential heat of solution $\Delta H_{\text{sol}}^{\text{d}}$ is the amount of heat liberated or absorbed, when 1 mole of the solute dissolves in a large amount of virtually saturated solution. This is numerically equal to the heat of crystallization, ΔH_{crys} , but of opposite sign. The relationship between these quantities is

$$-\Delta H_{\text{crys}} = \Delta H_{\text{sol}}^{\infty} + \Delta H_{\text{dil}} = \Delta H_{\text{sol}}^{\text{d}} \quad (2.54)$$

In crystallization practice, however, it is usual to take the heat of crystallization as being equal in magnitude, but opposite in sign, to the heat of solution at infinite dilution, since this is the quantity most commonly available in the handbooks, i.e.

$$\Delta H_{\text{crys}} \simeq -\Delta H_{\text{sol}}^{\infty} \quad (2.55)$$

Few values of heats of dilution are available in the literature, especially for the higher concentration ranges usually associated with industrial practice, but this quantity is usually only a small fraction of the heat of solution. Furthermore, as the dilution of most aqueous salt solutions is exothermic, i.e. the concentration is endothermic, the true value of the heat of crystallization will be slightly less than that obtained by taking the negative value of the heat of solution alone. Therefore the calculated quantity of heat to be removed from a crystallizing solution will be slightly greater than the true value, and this small error can serve as a factor of safety in the design of cooling heat transfer equipment.

An alternative way to evaluate the heat of solution, and hence to estimate the heat of crystallization, is to consider the effect of temperature on the solubility: the greater the effect the higher is the heat of solution of the solute as quantified by the relationship

$$\frac{d \ln c^*}{dT} \simeq \frac{\Delta H_{\text{sol}}^{\text{d}}}{RT^2} \quad (2.56)$$

where $\Delta H_{\text{sol}}^{\text{d}}$ is the final differential heat of solution.

2.14 Size classification of crystals

The most widely employed physical test applied to a crystalline product is the one by means of which an estimate may be made of the particle size distribution. Product specifications invariably incorporate a clause that defines, often quite stringently, the degree of fineness or coarseness of the material. For many industrial purposes the demand is for a narrow range of particle size; regularity results in the crystals having good storage and transportation properties, a free-flowing nature and, above all, a pleasant appearance. Terms such as 'fine' and 'coarse' are frequently used, although usually without definition, to describe crystalline and powdered materials. For pharmaceutical products, however, some guidance is available from recommendations in the British Pharmacopoeia (2000), based on sieve gradings.

Coarse	all passes 1700 µm	≥40% passes 355 µm
Moderately coarse	all passes 710 µm	≥40% passes 250 µm
Moderately fine	all passes 355 µm	≥40% passes 180 µm
Fine	all passes 180 µm	≥40% passes 125 µm
Very fine	all passes 125 µm	≥40% passes 45 µm
Microfine	≤90% passes 45 µm	

Some of the more important procedures associated with the characterization of particulate solids are outlined below.

2.14.1 Sampling

The physical and chemical characteristics of a bulk quantity of crystalline material are determined by means of tests on small samples. These test samples must be truly representative of the bulk quantity; otherwise any results obtained will be grossly misleading or completely useless. Inefficient sampling followed by careful analysis in the laboratory constitutes a waste of everyone's time and effort. Sampling, which is a highly specialized skill, should be carried out by conscientious, well-trained personnel who are fully aware of the tests that are to be made on the sample, without having any direct interest in the outcome of the analyses.

The actual technique employed for sampling will depend on the nature of the bulk quantity of material, its location, the properties to be tested, the accuracy

required in the test, and so on. Difficulties may be encountered in the sampling of solids in containers after transportation, owing to the partial segregation of fine and coarse particles; the fines tend to migrate towards the bottom of the container, and thorough remixing may be the only answer. Similar problems caused by segregation may be met in the sampling of solids flowing down chutes or through outlets.

Hand sampling, widely employed for batch-produced or stored materials, is time-consuming and prone to error, but its use cannot always be avoided. One common method involves the use of a sample 'thief', a piece of pipe with a sharp bottom edge which is plunged into the full depth of the material. It is then withdrawn and the sample removed. This operation can be performed at fixed or random intervals in the bulk quantity. Sampling at intervals by means of scoops or shovels, known as grab sampling, is also widely used, but serious errors can be encountered when dealing with non-homogeneous materials.

Automatic sampling is preferred to sampling by hand, and is also better suited to continuous processes. Ideally, the sample should be taken from a moving stream of solids or slurry. To eliminate segregation effects, samples should be taken by collecting the whole of the flowing stream for short periods. Isokinetic sampling is recommended for crystal suspensions in agitated vessels and pipelines (section 9.2).

Bulk samples, which may range up to several hundred kilograms for large tonnage lots, have to be reduced to a smaller laboratory sample which, in turn, will have to be divided into several smaller test samples for subsequent analysis. These operations may be carried out by hand or with the aid of a sample divider.

The best-known hand method is that of coning and quartering. The sequence of operations, carried out on a clean, smooth surface, or on glossy paper for small quantities in the laboratory, is shown in *Figure 2.11*. The bulk sample is thoroughly mixed and piled into a conical heap. The pile is then flattened and the truncated cone divided into four equal quarters (*Figure 2.11c*). This may be done, for example, with a sharp-edged wooden or sheet metal cross pressed into the heap. One pair of opposite quarters are rejected, the other pair are thoroughly mixed together and piled into a conical heap, the procedure being repeated until the required laboratory sample is obtained.

A simple sample divider is the riffle which usually takes the form of a box divided into a number of compartments with bottoms sloping about 60° to the horizontal, the slopes of alternate chutes being directed towards opposite sides of the box. Thus, when the bulk sample is poured through the riffle, it is divided

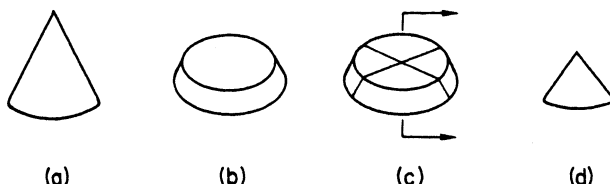


Figure 2.11. Method of coning and quartering: (a) bulk sample in a conical heap; (b) flattened heap; (c) flattened heap quartered; (d) two opposite quarters mixed together and piled into a conical heap

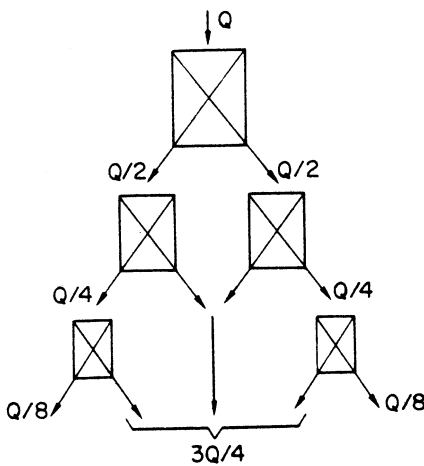


Figure 2.12. Battery of riffles used for reduction of a large quantity of material

into two equal portions. The dimensions of a riffle depend on the size of the particles and the quantity of material – an even flow of solids must be spread over the whole inlet area. When very large bulk samples have to be reduced to small test quantities, a battery of riffles decreasing in size may be employed, as shown diagrammatically in *Figure 2.12*. This arrangement is also suitable for the continuous or intermittent sampling of materials flowing out of hoppers or other items of process plant.

The rotary sample divider, or spinning riffle, is less prone to operator error than is the static riffle. Basically it consists of a hopper which allows particulate material to flow on to a vibrating chute which then discharges into a number of sample boxes located in a rotating ring. Several units of this type are available commercially.

The statistical theories of sampling are discussed by Allen (1990) who also describes, in considerable detail, a large number of sampling methods. BS 3406/1 (1986) also gives guidance on sampling, the sub-division of laboratory samples and the reporting of results.

2.14.2 Particle size and surface area

A large number of methods are now available for measuring particle size, some of which are listed in *Table 2.10* together with their approximate ranges of application. The book by Allen (1990) and a series of British Standards (BS 3406, 1986; BS 4359, 1984) give excellent coverage of the subject. Only a short review will be given here.

It is not possible to measure or define absolutely the size of an irregular particle, and perfectly regular crystalline solids are rarely, if ever, encountered. The terms length, breadth, thickness or diameter applied to irregular particles are meaningless unless accompanied by further definition, because so many different values of these quantities can be measured. The only meaningful properties that can be defined for a single solid particle are the volume and surface area, but even the

Table 2.10. Some methods of particle size measurement and their approximate useful size ranges

Method	Size range (μm)
Sieving (woven wire)	125 000–20
Sieving (electroformed)	120–5
Sieving (perforated plate)	125 000–1000
Microscopy (optical)	150–0.5
Microscopy (electron)	5–0.001
Sedimentation (gravity)	50–1
Sedimentation (centrifugal)	5–0.1
Electrical sensing zone (Coulter)	200–1
Laser light scattering (Fraunhofer)	1000–0.1
Permeametry } Gas adsorption } about 50 μm	Surface area measurement: useful for particle sizes smaller than about 50 μm

measurement of these quantities may present insuperable experimental difficulties. All particle size measurements are made by indirect methods: some property of the solid body which can be related to size is measured.

Despite these difficulties of definition and measurement it is most convenient for classification purposes, if a single-length parameter can be ascribed to an irregular solid particle. The most frequent expression used in connection with particle size is the ‘equivalent diameter’, i.e. the diameter of a sphere that behaves exactly like the given particle when submitted to the same experimental procedure. Several of these equivalent diameters are defined below.

Sieving

Woven wire test sieves were formerly designated by a mesh number (the number of wires per inch) but as the important sieve characteristic is the size of its apertures all standard test sieves are now designed, by international agreement, by their aperture size in millimetres or micrometres. The aperture sizes in a standard series are related to one another, e.g. following a fourth root of two (1.189) or a tenth root of ten (1.259) progression. The two most widely used standard sieve scales are the American (ASTM E11, 1995) and British (BS 410, 2000) both of which are compatible with the international scale (ISO 3310, 2000) (*Table 2.11*).

The range of aperture sizes in most standard series extends from 125 mm to 20 μm . At the top end of the range particles must be carefully hand-placed on the sieve. At the lower end, sieving with the aid of a liquid is often needed to assist the flow of particles through the mesh. Particles that pass through a sieve are characterized by an equivalent sieve aperture diameter, $d_{\text{s.a.}}$, the diameter of a sphere that would just pass through. Care needs to be taken to interpret this quantity, however, as explained in section 2.14.3 (see *Figure 2.14*).

Perforated plate sieves are available, with round (125 to 1 mm) or square (125 to 4 mm) apertures, for coarse particle sizing. Microsieves with electroformed

Table 2.11. Comparison between the British and US standard wire mesh sieve scales* showing the danger of using the ‘mesh number’ as a sieve designation

Mesh number† (obsolete)	Aperture width (µm)		Mesh number† (obsolete)	Aperture width (µm)	
	BS 410	ASTM E11		BS 410	ASTM E11
3	5600		50		300
3½	4750	5600	52	300	
4	4000	4750	60	250	250
5	3350	4000	70		212
6	2800	3350	72	212	
7	2360	2800	80		180
8	2000	2360	85	180	
10	1700	2000	100	150	150
12	1400	1700	120	125	125
14	1180	1400	140		106
16	1000	1180	150	106	
18	850	1000	170	90	90
20		850	200	75	75
22	710		230		63
25	600	710	240	63	
30	500	600	270		53
35		500	300	53	
36	425		325		45
40		425	350	45	
44	355		400	38	38
45		355	450	32	32

*Both standard test sieve scales BS 410 and ASTM E11 are compatible with the international (ISO 3310) scale.

†The definition of ‘mesh number’ is the number of apertures per inch in the sieve mesh. This obsolete designation leads to confusion because different standards specify different wire diameters.

round or square apertures (120 to 5 µm) in nickel plate are available for very fine particle sizing.

Sieving is basically a very simple and justifiably popular particle sizing technique, but the precautions necessary to produce reliable data do not appear to be widely appreciated. Some of the more important points to note about the use of standard test sieves for particle size analysis are as follows.

1. Particles must not be forced through the sieve apertures.
2. Sieving should be continued to an end-point, i.e. until the amount of material passing through ceases to affect the result significantly. When using a mechanical shaker, it is recommended that each sieve removed from the stack should be given a brief brisk tapping and shaking by hand to ensure that the end-point has been reached. If it has not, sieving must be continued.
3. It should be clearly understood that the aperture size marked on the sieve is only a nominal size. The actual value can vary from this value, within

specified tolerances. For accurate work, it is advisable to calibrate the sieve, e.g. by sieving a reference sample of known size distribution.

Procedures for test sieving, both wet and dry, are prescribed in standard specifications (ISO 2591, 1989; BS 1796, 1990). Methods for the analysis of sieve test data are described in section 2.14.4.

Microscopy

Microscopy is commonly used as a basic reference method for particle sizing since individual particles may be observed while measuring or assessing their size, shape and composition. Particle images may be viewed directly in an optical microscope or by projection. The particle size may be recorded as the projected area diameter $d_{\text{p.a.}}$, the diameter of a circle that has the same area as the projected image of the particle viewed in a direction perpendicular to its plane of maximum stability. This may be assessed by comparison with graduated circles on an eyepiece graticule. The microscopic method can be tedious and time-consuming, although automatic counting devices are now available. Photographic methods are popular, but can introduce further errors into the system (BS 3406/4, 1990; ISO 13322, 2001). The problems of preparing a microscope slide containing a well-dispersed representative sample of small crystals can be very considerable (Allen, 1990).

Sedimentation

A simple sedimentation technique, which readily lends itself to the determination of crystal size distribution in the range 1–50 µm, is the Andreasen pipette method. Although it is generally better to prepare a fresh suspension of the crystals under test in a suitable inert liquid, it is possible to classify crystals suspended in their own mother liquor. If the difference in density between the particles and suspending liquid is $< 0.5 \text{ g cm}^{-3}$ special care must be taken to avoid convection currents. The method, briefly, is as follows (BS 3406/2, 1986).

A homogeneous suspension of the crystalline material in a suitable liquid is prepared in the graduated sedimentation cylinder of capacity $\sim 600 \text{ cm}^3$ (Figure 2.13). Small samples (e.g. 10 cm^3) of the suspension are withdrawn through the fixed pipette, at a known depth, h , below the liquid level, at chosen time intervals. The samples, including the one taken at zero time, are analysed for total *suspended solids* content by a suitable method. Ideally the suspension should be dilute (< 3 per cent) and a dispersion agent may be needed to prevent agglomeration: for particles in insoluble water a 0.1 per cent solution of sodium pyrophosphate is generally suitable.

A sample taken at time t will contain no particles larger than size d_{St} calculated from Stokes' law which may be written

$$d_{\text{St}} = \left[\frac{18h\eta}{(\rho_s - \rho_f)gt} \right]^{1/2} \quad (2.57)$$

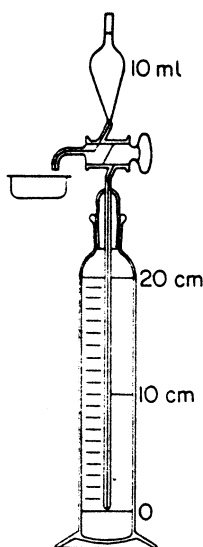


Figure 2.13. Andreasen fixed pipette method

Thus by taking samples at suitable intervals, e.g. 0, 5, 10, 20, 40, 80... min, the size distribution of the original suspension may be evaluated. For routine analysis only one or two samples may be needed to characterize the particles. If t is measured in minutes, h in cm, ρ in g cm^{-3} and η in centipoise, then the particle size d , in μm , is given by

$$d_{\text{St}} = 17.5 \left[\frac{h\eta}{(\rho_s - \rho_f)t} \right]^{1/2} \quad (2.58)$$

For a given sample, n , the cumulative mass percentage, P_n , of particles smaller than the limiting Stokes' diameter for the time interval, t_n , may be calculated from the mass W_n , of the suspended solids in the fraction by

$$P_n = 100 \left[\frac{W_n}{W} \cdot \frac{V}{V_n} \right] \quad (2.59)$$

where W = mass (g) of solids originally suspended in the apparatus, V = original volume of the suspension (cm^3) and V_n = volume of sample taken via pipette (cm^3).

A typical analysis is given in *Table 2.12*, where the size distribution of precipitated calcium carbonate ($\rho_s = 2.7 \text{ g cm}^{-3}$) is measured by sedimentation at 20°C in water containing 0.1 per cent sodium pyrophosphate as dispersant ($\rho_f = 1.0 \text{ g cm}^{-3}$ and $\eta = 1.0 \text{ cP}$, i.e. 10^{-3} N s/m^2). In this test the CaCO_3 was determined volumetrically by adding 0.2 M HCl to each sample, boiling to remove CO_2 and back-titrating with 0.1 M NaOH. A 'blank' was run on the suspending liquid. Alternatively, in this case, a gravimetric method could have been used, i.e. by evaporation to dryness.

Descriptions of other gravitational sedimentation techniques are outlined in a recent international standard (BS ISO 13317, 2000) for particles in the size

Table 2.12. Measurement of the particle size distribution of a sample of precipitated calcium carbonate by the Andreasen pipette method

Time, <i>t</i> (min)	Pipette depth, <i>h</i> (cm)	Stokes' diameter, <i>d</i> (μm)	CaCO ₃ in fraction* <i>W_n</i> (g)	Cumulative percentage undersize
0	20.0	—	0.231†	—
5	19.6	28	0.147	64
10	19.2	19	0.108	47
20	18.7	13	0.0763	33
40	18.3	9.1	0.0508	22
80	17.9	6.4	0.0299	13
160	17.4	4.4	0.0184	8
320	17.0	3.1	0.00924	4

*Sample volume $V_n = 10 \text{ cm}^3$.† Test sample mass $W = 14.3 \text{ g}$ in suspension volume $V = 620 \text{ cm}^3$.

range 1–100 μm . For particles smaller than about 5 μm , however, problems can arise from convection effects and Brownian motion, but these difficulties may be reduced by speeding up the settling process by centrifuging the suspension. A number of procedural methods and commercial equipment for centrifugal sedimentation are now available for determining particle size in the 0.1–5 μm range (Allen, 1990; ISO 13318, 2000).

Electrical sensing zone (Coulter) methods

In the Coulter technique, particles have to be suspended in an electrolyte solution and then induced to pass through a small orifice, with surrounding electrodes, located in the measurement cell. Changes in electrical impedance in the orifice channel for each particle passage are measured and counted. The result is a number-size (volume) distribution of particles (BS ISO 13319, 2000). The method has found applicability in a wide range of industries. For application to crystallizing systems, however, it is important to choose a unit in which the voltage between the inner and the outer electrode is automatically adjusted so as to maintain a constant current. This renders the calibration, and hence the actual counting, insensitive to the type of electrolyte used as well as to concentration and temperature changes within the electrolyte. This precaution is of paramount importance for crystallization studies where changes in electrolyte properties due to phase transitions are inevitable (Jančić and Grootscholten, 1984).

Laser light scattering (Fraunhofer) methods

Another widely used particle size analyser is based on the forward scattering of laser light through a dilute (<1% by volume) suspension of crystals retained in a small ($\sim 10 \text{ mL}$) agitated cell. The resulting Fraunhofer diffraction pattern is detected and translated, by means of the instrument software, into a particle size distribution (BS ISO 13320, 2000).

Specific surface area measurement

In many cases, particularly for very small particles, surface area is a more appropriate characteristic to assess than some size based on an equivalent diameter. Particle surface area is important, for example, in paints and pigments or when chemical reactivity is an important property, as in the setting of cement. Precipitated materials are often characterized in this manner. Amongst the several techniques available, those based on permeability and gas adsorption are probably the most popular.

In the permeability methods a known quantity of air is forced through a small bed of the fine solids under a constant pressure drop, and the flow time is recorded. The theory is based on the laminar flow of fluids through porous beds, and the specific surface area S ($\text{m}^2 \text{ g}^{-1}$) of the material is calculated from the Kozeny equation

$$S^2 = \frac{\Delta P}{ku\eta L\rho^2} \cdot \frac{\varepsilon^3}{(1-\varepsilon)^2} \quad (2.60)$$

where ΔP = pressure drop across the bed; ε = voidage of the bed; L = depth of the bed; η = viscosity of the air; u = empty-tube velocity; ρ = density of the solid material; k is a constant (Kozeny's constant), which has a value equal to about 5.0 for granular solids. Several different types of permeability cell are available (BS 4359/2, 1982; Allen, 1990).

A solid particle exposed to a gas will adsorb gas molecules on to its exposed surfaces. The derivation of a multilayer adsorption theory for gases on solid surfaces by Brunauer, Emmett and Teller in 1938 led to the development of the so-called BET adsorption methods for measuring the specific surface area of particulate solids. Several techniques are available (BS 4359/1, 1982; Lowell and Shields, 1984; Allen, 1990).

Dry tests like the BET adsorption method can often give misleading information when used to characterize precipitated materials because the sample preparation operations of filtering, washing and drying can result in considerable damage and distortion to the particles. For this reason, a dye adsorption technique has been found to give a more realistic measurement of the specific area of precipitates while still suspended in their original mother liquor (Mullin *et al.*, 1989a). A sample of the precipitate suspension is pipetted into a small flask containing a known quantity of a concentrated solution of a suitable dye, the selection of which depends on the chemical nature of the precipitate. After shaking to allow the mixture to come to equilibrium it is clarified in a laboratory centrifuge and the clear liquid analysed with a UV spectrophotometer. Knowing the mass of dye adsorbed on a given mass of precipitate, and the 'coverage' value of the dye (the so-called Paneth value), it is a straightforward matter to calculate a specific surface area of the precipitate in, for example, $\text{m}^2 \text{ g}^{-1}$.

It should also be noted that size data produced by the many different electronic techniques and instruments now available are dependent on the particular analysis algorithm incorporated into the instrument by the manufacturer. Significant differences in sizing results can therefore be recorded by

commercial equipment of basically the same type. Indeed, for precise work, *repeatability* tests should be carried out to determine the closeness of agreement between independent tests made with the same method on identical test material in the same laboratory by the same operator using the same equipment. For inter-laboratory investigations *reproducibility* tests should be made to determine the closeness of agreement between tests made with the same method on identical test material in different laboratories with different operators using different equipment. Recommended procedures for repeatability and reproducibility tests are described in ISO 5725 (1992).

Comparison of data

From the above brief descriptions of a few commonly used particle sizing techniques it can be seen that the different methods arrive at an expression of particle 'size' after measuring quite different particle properties. It is not surprising, therefore, that for a given sample of particulate material the different techniques will give different, often very different, sizes.

It is advisable to use, if at all possible, only one sizing technique over the whole particle size range encountered in any one analysis. Even in sieving, only one type of sieving medium should be used throughout (woven wire, perforated or electroformed plate, round or square aperture) because of their individual sieving characteristics. When it is necessary, because of a very wide size distribution, to apply two different sizing techniques it is advisable that the data from both methods overlap over a significant part of the range to enable all the data to be converted to a common basis. Examples of overlap studies have been reported for sieve/zone sensing (Mullin and Ang, 1974; Jančić and Grootscholten, 1984) and for sieve/laser light scattering (Brečević and Garside, 1981).

2.14.3 Shape factors

A precise calculation of the volume or surface area of a solid body of regular geometric shape can only be made when its length, breadth and thickness are known. For particulate solids in general, these three dimensions can never be precisely measured. Therefore, before a brief account is given of some of the methods of calculation available, a word of warning is necessary. It must be fully appreciated that the precision of calculation is always far greater than that of measurement of the various quantities used in the mathematical expressions. An equation, especially a complex one, always has a look of absolute dependability, but in this particular connection it most certainly leads to a false sense of security. All calculated volume or surface area data must be used with caution.

Most calculation methods are based on one dimension of the particle, usually the equivalent diameter. If this dimension is obtained from a sieve analysis, it will be the sieve aperture diameter, $d_{s.a.}$; but as crystals are never true spheres, this diameter will normally be the second largest dimension of the particle. *Figure 2.14* demonstrates some particle shapes that would, in a sieve analysis, all yield the same value for $d_{s.a.}$. One potential source of error is thus clearly seen.

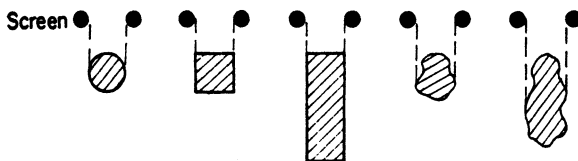


Figure 2.14. Various particle shapes that would all be classified under the same sieve-aperture diameter

For a single particle, the size of which is defined by some length parameter or equivalent diameter, d , and density, ρ the following relationships can be applied:

$$\text{volume} \quad v = f_v d^3 \quad (2.61)$$

$$\text{mass} \quad m = f_v \rho d^3 \quad (2.62)$$

$$\text{surface area} \quad s = f_s d^2 \quad (2.63)$$

The constants f_v and f_s may be called volume and surface shape factors, respectively. In the expressions for crystal growth rate in section 6.2.1, f_v and f_s are given the symbols α and β , respectively. These latter symbols are also used in Chapter 8.

For spherical (diameter = d) and cubic (length of side = d) particles

$$\alpha = f_v = \frac{\pi}{6} \text{ (sphere) and } 1 \text{ (cube)}$$

$$\beta = f_s = \pi \text{ (sphere) and } 6 \text{ (cube)}$$

The shape factors are readily calculated for other regular geometrical solids. For an octahedron, for example, with d representing the length of an edge, $v = \sqrt{2}d^3/3$ and $s = 2\sqrt{3}d^2$, therefore

$$\alpha = f_v = v/d^3 = \sqrt{2}/3 = 0.471$$

$$\beta = f_s = s/d^2 = 2\sqrt{3} = 3.46$$

From equations 2.61–2.63 two basic ratios may be defined:

$$\text{surface : volume } \frac{s}{v} = \frac{f_s d^2}{f_v d^3} = \frac{F}{d} \quad (2.64)$$

$$\text{surface : mass } \frac{s}{m} = \frac{f_s d^2}{f_v \rho d^3} = \frac{F}{\rho d} \quad (2.65)$$

Equation 2.65 defines the useful quantity known as the specific surface area, i.e. the surface area per unit mass of solid. The constant $F (= f_s/f_v = \beta/\alpha)$ may be called the overall, surface-volume or specific surface shape factor. For spheres and cubes, $F = 6$. For other shapes $F > 6$. For an octahedron $f_v = \sqrt{2}/3$, $f_s = 2\sqrt{3}$ and $F = 7.35$. Values of $F \sim 10$ are frequently encountered in comminuted solids, and much higher values may be found for flakes and plate-like crystals. If the particles are elongated or needle-shaped, their volume and surface area may be calculated on the assumption that they are

cylindrical; length and diameter may be measured microscopically, or the diameter can be taken as the equivalent sieve aperture diameter.

For example, a crystal with a length : breadth : thickness ratio of 5:2:1 would be characterized in sieving by its second largest dimension, i.e. $d = 2$. Therefore $f_v = v/d^3 = 10/8 = 1.25$, $f_s = s/d^2 = 34/4 = 8.5$ and $F = f_s/f_v = 6.8$.

Volume shape factors may be measured by weighing a known number of particles from a close-sieve fraction, the number depending on the size of the particles and the accuracy with which the total mass can be weighed. The need for a close-sieve fraction arises from the fact that the shape factor of crystals can vary greatly with size (Garside, Mullin and Das, 1973).

The determination of volume shape factors for particles smaller than about 500 μm becomes extremely difficult, since it may be necessary to count and weigh several thousand particles. However, the following method may be used to simplify the procedure. Prepare a sample of the particles by sieving between two close sieves. Clean the finer of the two sieves (the retaining sieve) and attach a strip of adhesive tape of known mass and dimensions, to its underside. Place a quantity of the particles on the sieve and shake the sieve for several minutes. Peel off the adhesive tape, which will now have hundreds or thousands of particles in a regular matrix (more or less one per sieve aperture). The approximate number of particles per unit area can be determined from the designation of the sieve mesh. For example, a 150 μm aperture sieve with 100 μm diameter wires contains about 1600 apertures per cm^2 . The adhesive strip can then be weighed and the average mass of one particle determined.

Surface shape factors are much more difficult to measure than volume shape factors and they are subject to greater uncertainty. One method is as follows. A few individual crystals are observed through a low-power microscope fitted with a calibrated eyepiece, and sufficient measurements taken to allow a sketch to be made of a representative geometric shape, e.g. a parallelepipedon, ellipsoid, oblate spheroid, etc. The surface area of the representative solid body may then be calculated. It should be appreciated, of course, that the result of such a calculation will be prone to significant error.

Another quantity that has been used to characterize crystal shape is the sphericity, ψ , defined as the ratio of the surface area of a sphere having the same volume as the particle to the apparent estimated surface area of the particle. This can be rewritten (Nývlt, 1990) as

$$\psi = \frac{(6f_v/\pi)^{2/3}}{f_s/\pi} \quad (2.66)$$

For isometric particles ψ is close to 1 while for needles or platelets its value is much lower. Evaluation of ψ is useful for checking the values of f_v and f_s since $0 < \psi < 1$.

When three mutually perpendicular dimensions of a particle may be determined, Heywood's ratios may help to characterize shape (Allen, 1990):

elongation ratio $n = L/B$

flakiness ratio $m = B/T$

The thickness T is the minimum distance between two parallel planes which are tangential to opposite surfaces of the particle, one plane being the plane of maximum stability. The breadth B is the minimum distance between two parallel planes which are perpendicular to the planes defining the thickness and are tangential to opposite sides of the particle. The length L is the distance between two parallel planes which are perpendicular to the planes defining thickness and breadth and are tangential to opposite sides of the particle.

When using shape factors, it is important to remember that they depend on the dimension chosen to characterize the particle. For example, a geometrical shape such as regular parallelepipedon with a length : breadth : thickness ratio, $L:B:T$, of 5:2:1 the following shape factors may be calculated:

	f_v	f_s	F
using $L = 5$	0.08	1.4	17
$B = 2$	1.25	8.5	6.8
$T = 1$	10	34	3.4

Different answers again would result if measured values of the different equivalent diameters, such as $d_{\text{s.a.}}$, $d_{\text{p.a.}}$, d_{St} , etc. were used. An example of apparent shape factor change caused by the use of different sieves (woven wire, round or square hole, perforated plate) to measure the particle size is reported by Garside, Mullin and Das (1973).

2.14.4 Size data analysis

Mean particle size

In a total mass, M , of uniform particles, each of mass m and equivalent diameter d , the number of particles, n , is given by

$$n = \frac{M}{m} = \frac{M}{f_v \rho d^3} \quad (2.67)$$

and the total surface area, Σs , by

$$\Sigma s = ns = \frac{f_s M d^2}{f_v \rho d^3} = \frac{FM}{\rho d} \quad (2.68)$$

Equations 2.67 and 2.68 can be applied to masses of non-uniform particles if a suitable average or mean value of d can be chosen. This becomes an intractable problem, however, since there are so many possible choices that could be made.

The simplest of all average diameters is the arithmetic mean. For example, if sieving has been carried out between two sieves of aperture a_1 and a_2 , the average particle equivalent diameter is given by

$$\bar{d}_a = (a_1 + a_2)/2 \quad (2.69)$$

This description may be quite adequate for two close sieves in a $\sqrt[4]{2}$ series, but it can be absolutely meaningless for two sieves at extreme ends of the mesh range.

Another simple average diameter is the geometric mean, defined by

$$\bar{d}_g = \sqrt{(a_1 a_2)} \quad (2.70)$$

Values of \bar{d} calculated from equation 2.70 are smaller than those given by equation 2.67, but for two close sieves the difference is not great.

The volume mean diameter (or mass mean if the particle density is constant) is widely used:

$$\bar{d}_v = \frac{\Sigma n d^3}{\Sigma n d^3} = \frac{\Sigma (Md)}{\Sigma M} \quad (2.71)$$

When the surface area of the particles is an important property the surface mean diameter can be employed, defined by

$$\bar{d}_s = \frac{\Sigma n d^3}{\Sigma n d^2} = \frac{\Sigma M}{\Sigma (M/d)} \quad (2.72)$$

where n and M are the number and mass, respectively, of all particles of equivalent diameter d .

The root mean square diameter is also frequently used when surface properties are important. This statistical quantity is defined by

$$\bar{d}_{rms} = \sqrt{\left(\frac{\Sigma n d^2}{\Sigma n} \right)} = \sqrt{\left[\frac{\Sigma (M/d)}{\Sigma (M/d^3)} \right]} \quad (2.73)$$

Values of the overall mean diameters calculated from equations 2.71–2.73 can differ considerably (see *Table 2.13*), yet for a mass of particles with a wide size distribution there is no general agreement as to the preferred method.

Two other statistical diameters are often encountered, viz. the modal and median diameters; both are determined from frequency plots (size interval versus number of particles in each interval). The modal diameter is the diameter at the peak of the frequency curve, whereas the median diameter defines a mid-point in the distribution – half the total number of particles are smaller than the median, half are larger. If the distribution curve obeys the Gaussian or Normal Error law, the median and modal diameters coincide.

Table 2.13. Calculation of overall ‘mean’ diameters

Size range (μm)	Mean size of fraction, d (μm)	Mass of fraction, M (g)	Md	M/d	M/d^3
850–600	725	11.8	8550	0.0163	0.031×10^{-6}
600–425	512	18.6	9520	0.0363	0.139×10^{-6}
425–300	362	38.5	13 900	0.1064	0.812×10^{-6}
300–212	256	22.7	5810	0.0887	1.353×10^{-6}
212–150	181	8.4	1520	0.0464	1.417×10^{-6}
		100.0	39 300	0.2941	3.752×10^{-6}

$$\bar{d}_v = 39 300/100 = 393 \text{ μm.}$$

$$\bar{d}_s = 100/0.2941 = 340 \text{ μm.}$$

$$\bar{d}_{rms} = (0.2941/3.75 \times 10^{-6})^{1/2} = 280 \text{ μm.}$$

In connection with particle size measurement more than 20 different ‘mean’ diameters have been proposed at one time or another; and while several have certain points in their favour in special cases, none has yet been found to be generally satisfactory. Therefore all calculations based on an average diameter are prone to appreciable error, and it is recommended that such calculated quantities be clearly annotated with the method of calculation so that the results of different workers can be compared.

Graphical analysis

Once a size analysis has been performed and the results recorded, there remains the task of assessing the size characteristics of the tested material and of extracting the maximum amount of information from the data. While a table may record all the measured quantities, this form of expression is not always the best one; the magnitudes of the various quantities may be readily visualized, but certain trends may be completely obscured in a mass of figures. The real significance of a sizing test can most readily be judged when the data are expressed graphically. From such a pictorial representation trends in the data are easily detected, and the prediction of the expected behaviour of the material on sieves other than those used in the test can often be made with a reasonable degree of accuracy.

Many different forms of graphical expression may be employed, and the use and applicability of some of these methods are demonstrated below with reference to the results of a sieve test. The graphical procedures described, however, are applicable, with suitable nomenclature changes, to all methods of particle size analysis. The sieve test data in *Table 2.14* are recorded in three different ways, viz. the percentage by mass of the fractions retained on each sieve, and the cumulative mass percentages of oversize and undersize material.

Four types of graph paper are commonly used for plotting particle size distributions, depending on the sort of information that is required: (a) ordinary

Table 2.14. Sieve test data used for the construction of Figures 2.15 to 2.18

Sieve aperture, μm	Fractional mass per cent retained	Cumulative mass per cent oversize	Cumulative mass per cent undersize
2360	1.2	1.2	98.8
1700	2.9	4.1	95.9
1180	18.8	22.9	77.1
850	28.8	51.7	48.3
600	22.0	73.7	26.3
425	11.1	84.8	15.2
300	6.0	90.8	9.2
212	3.9	94.7	5.3
150	1.8	96.5	3.5
106	1.3	97.8	2.2
—	2.2	—	—

squared or arithmetic, (b) log-linear or semi-log, where one of the axes is marked off on a log scale and the other on an arithmetic scale, (c) log-log where both axes are marked off on a logarithmic scale, and (d) arithmetic-probability, where one axis is marked off on a probability scale, the intervals being based on the probability integral. Log-probability and double-logarithmic (RRS) grids also find use in special cases.

In *Figure 2.15a* the mass percentages of the fractions retained on each successive sieve used in the test are plotted against the widths of the sieve apertures (in microns). The lines joining the points have no significance; they merely complete the frequency polygon. The sharp peak in the distribution curve occurs at 850 µm. This point, however, represents the fraction that passes the 1180 µm sieve and is retained on the 850 µm, so it could be plotted at the 'mean' size of 1015 µm. Alternatively, the results may be represented in the form of a frequency histogram (*Figure 2.15b*) depicting the size range of each collected fraction. From both diagrams the general picture of the overall spread of particle size can be seen quite clearly, but the simple arithmetic method of plotting suffers from the disadvantage of producing a congested picture in the regions of the fine mesh sieves.

When the data are plotted on semi-log paper (*Figure 2.16a*), with the aperture widths recorded on the logarithmic scale, the points in the coarse sieve region are brought closer together, and those in the fine sieve region located further apart than in the corresponding simple arithmetic plot. In fact, the successive points are more or less equally spaced along the horizontal scale. The frequency histogram (*Figure 2.16b*) is composed of columns of approximately equal widths.

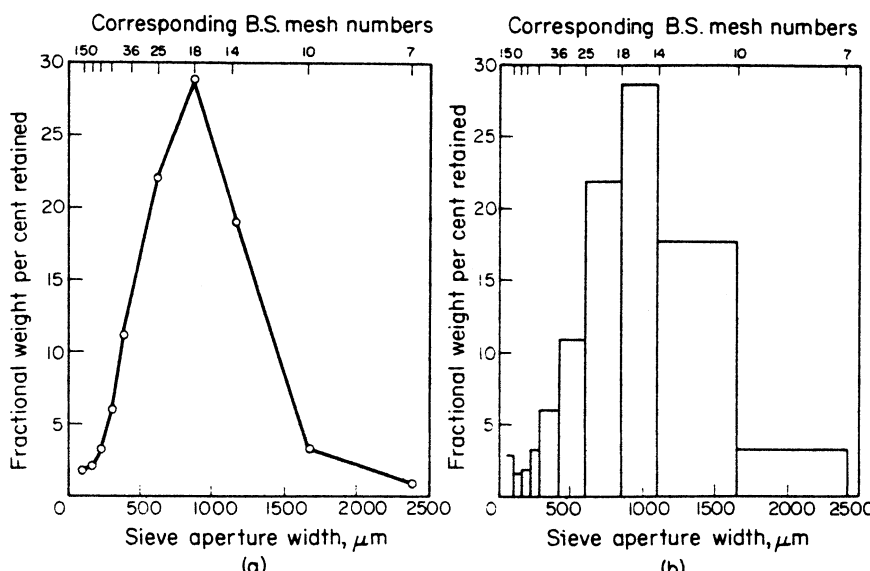


Figure 2.15. Sieve test data plotted on arithmetic graph paper – percentage by weight of the fractions retained between two given sieves in the B.S. series: (a) the frequency polygon; (b) the frequency histogram

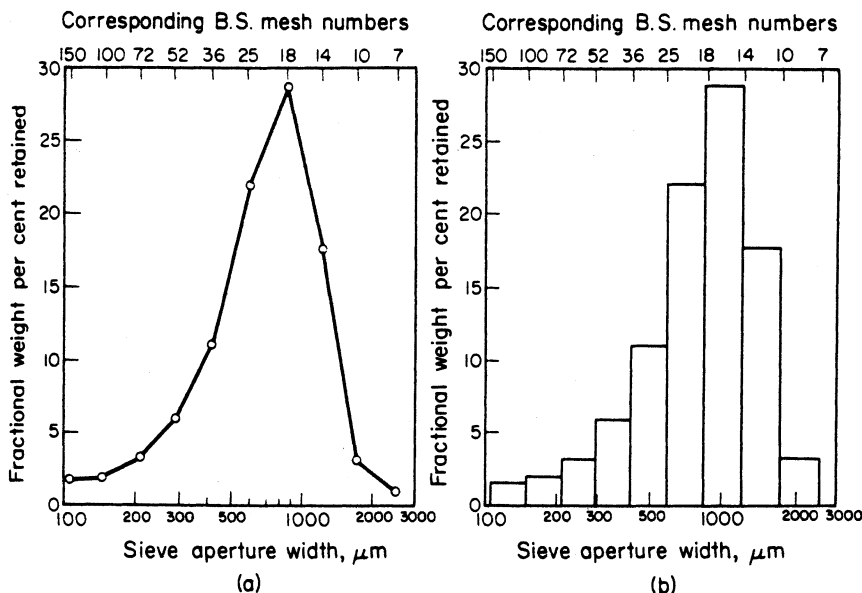


Figure 2.16. Sieve test data plotted on semi-log graph paper – percentage by weight of fractions retained between two sieves in the B.S. series: (a) the frequency polygon; (b) the frequency histogram

The semi-log graphs of the cumulative oversize and undersize percentages (*Figure 2.17a*) show that the curves are mirror images of each other. In practice only one need be plotted. The two curves cross over at the *median size* (50 per cent is larger than the median, and 50 per cent is smaller). In this case the median size is 870 μm. Interpolation is facilitated by the even spread of the plotted points. It can be estimated, for instance, that about 87 per cent of the original material would be retained on a 355 μm sieve or that about 7 per cent would pass through a 250 μm sieve.

The cumulative percentages of oversize and undersize particles may also be plotted against aperture size on a log–log basis (*Figure 2.17b*). In this type of plot the cumulative undersize data tend to lie on a straight line over a wide range of particle size, about 100 to 1200 μm in this case. The undersize and oversize curves are clearly not mirror images, and oversize data are rarely correlated on this basis.

The log–log method of plotting of undersize data is extremely useful because rough checks may be made on the size distribution by the use of only two, or possibly three, test sieves. Material of the type considered in *Table 2.11* could be size-checked with 1000, 500 and 250 μm sieves, for example.

Coefficient of variation (CV)

Probability plots have often been suggested for particle size analysis, particularly in connection with the assessment of comminution processes.

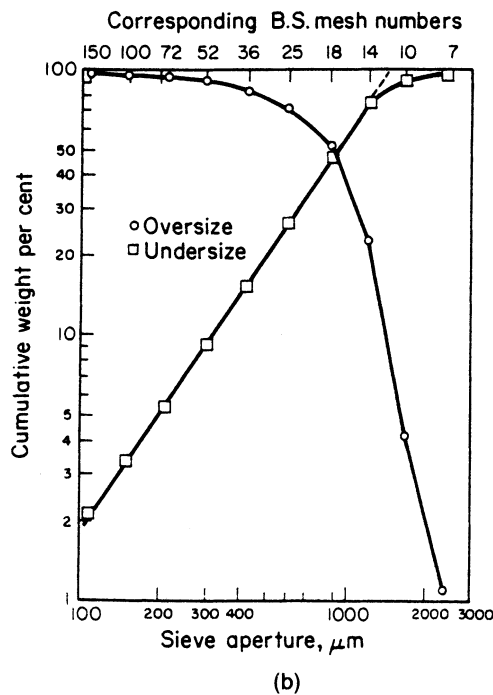
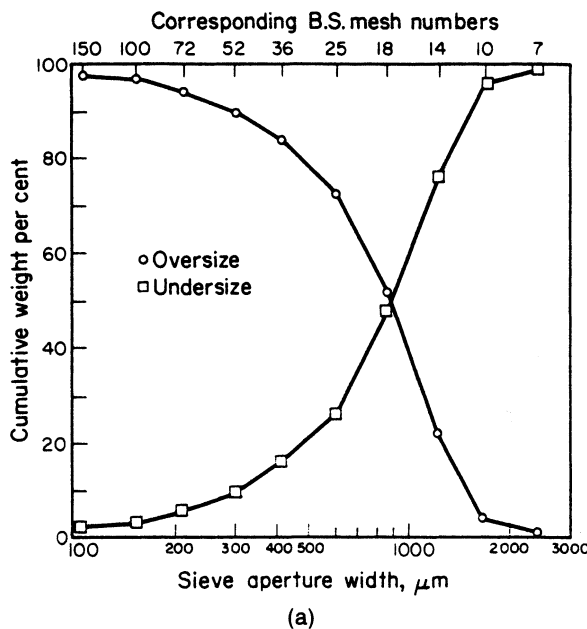


Figure 2.17. Sieve test data plotted on (a) semi-log graph paper, (b) on log-log graph paper—cumulative oversize and undersize percentages

The following method, proposed by Powers (1948) for use in the sugar industry, has much to be said in its favour for the size specification of crystalline products. This method employs arithmetic-probability graph paper (one scale divided into equal intervals, the other marked off according to the probability integral) and provides a simple means of recording the crystal size distribution in terms of two numbers only – the *median size* (MS), and a statistical quantity the *coefficient of variation* (CV) expressed as a percentage.

The evaluation of MS/CV is demonstrated in *Figure 2.18a* with the sieve analysis data from *Table 2.13*. The cumulative undersizes (or oversizes if preferred) are plotted on the probability scale, the sieve aperture sizes on the arithmetic scale. If the data between about 10 and 90 per cent lie on a straight line, the MS/CV method can be applied. The data in *Figure 2.18a* comply with this requirement. Thus the median size is 870 µm. The coefficient of variation can be deduced as follows.

The equation for the normal probability (Gaussian) curve may be expressed as

$$f(d) = \frac{1}{\sigma\sqrt{(2\pi)}} \exp\left[-\frac{(d - \bar{d})^2}{2\sigma^2}\right] \quad (2.74)$$

where d is an equivalent particle diameter, in this case based on sieve aperture size, and σ is the standard deviation. If the area enclosed under the normal curve between sieve apertures $d = 0$ to ∞ is taken as unity, the area enclosed between $d = 0$ and $d = \bar{d} + \sigma$, where \bar{d} is the median (50 per cent) size MS, is 0.8413. This value is obtained from tables of the normal probability function. Therefore the area enclosed between $d = \bar{d} + \sigma$ and $d = \infty$ is $1 - 0.8413 = 0.1587$. The value of σ , the standard deviation, can be obtained from the arithmetic probability diagram by reading the value of d at 84.13 per cent (84 per cent is accurate enough for this purpose) and subtracting the value of \bar{d} . Alternatively, the value of d at 15.87 (or 16) per cent can be subtracted from \bar{d} , i.e.

$$\sigma = d_{84\%} - \bar{d} = \bar{d} - d_{16\%}$$

These two values of σ may not coincide, so a mean value can be taken as

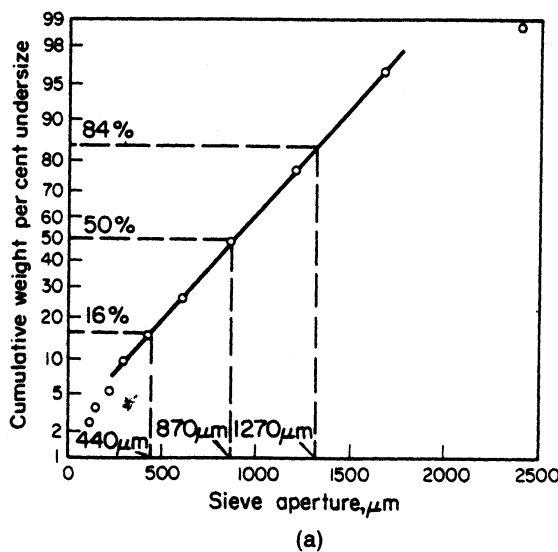
$$\sigma = \frac{d_{84\%} - d_{16\%}}{2}$$

The coefficient of variation, as a percentage, is given by

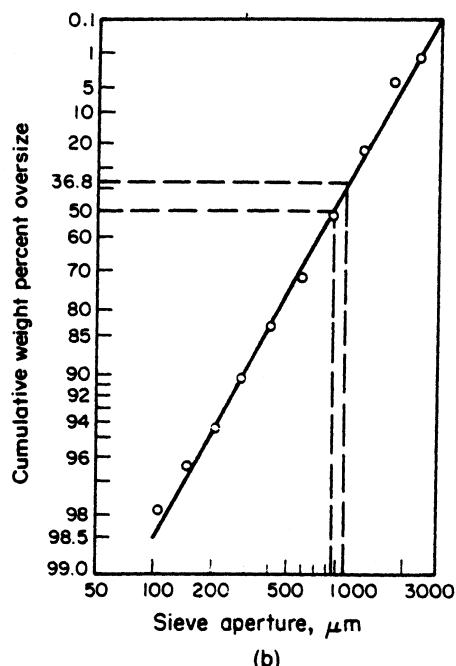
$$CV = \frac{100\sigma}{\bar{d}} = \frac{100\sigma}{d_{50\%}} \quad (2.75)$$

or

$$CV = \frac{100(d_{84\%} - d_{16\%})}{2d_{50\%}} \quad (2.76)$$



(a)



(b)

Figure 2.18. Sieve test data plotted on (a) arithmetic/probability graph paper (cumulative undersize percentages) illustrating the use of the MS/CV method of analysis, (b) on Rosin–Rammler–Sperling (RRS) double logarithmic graph paper

From *Figure 2.18a*

$$CV = \frac{100(1270 - 440)}{2(870)} = 48 \text{ per cent}$$

and the size distribution can be specified, in terms of MS/CV, as 870/48.

The size distribution does not have to be Gaussian for the MS/CV method to be applied. Many skew distributions also give the necessary linear relationship between about 10 and 90 per cent, although in these cases MS will not coincide with the *modal* diameter at the peak of the distribution curve.

For skew distributions that are not approximately Gaussian over the 10–90 per cent region, plotting on log-probability paper (one scale logarithmic, the other marked off according to the logarithmic probability function) may give a better correlation. The equation of the logarithmic normal curve is

$$f(\log d) = \frac{1}{\log \sigma' \sqrt{2\pi}} \exp \left[-\frac{(\log d - \log \bar{d}')^2}{2 \log^2 \sigma'} \right] \quad (2.77)$$

where \bar{d}' is the geometric mean size and σ' is the geometric standard deviation.

The log-normal distribution gives a curve skewed towards the larger sizes, and it frequently gives a good representation of particle size distributions from precipitation and comminution processes. Furthermore, the log-normal distribution is often used because it overcomes the objection to the normal (Gaussian) distribution function which implies the existence of particles of negative size.

Another distribution function gaining popularity for characterizing crystal size distributions is the gamma function, expressed as

$$f(d) = d^x \exp(dx/y)\Gamma(x+1)(y/x)^{x+1} \quad (2.78)$$

The parameters x and y , which give measures of the ‘skewness’ and ‘size’ of the distribution respectively, can be related to the crystallization process. The median size MS ($= \bar{d}$) and standard deviation, σ , may be calculated from

$$\bar{d} = y(x+1)/x \quad \text{and} \quad \sigma = y(x+1)^{1/2}/x$$

Therefore from equation 2.75 the coefficient of variation is given by

$$CV = 100(x+1)^{-1/2} \quad (2.79)$$

Some skew distributions, particularly those of comminuted materials can be fitted by the Rosin–Rammller–Sperling (RRS) function. This relationship, based on one originally derived from probability considerations, may be written

$$P = 100 \exp[-(d/d')^n] \quad (2.80)$$

where P = cumulative percentage oversize, d = particle size, and d' is a statistical mean size corresponding to $P = 36.8\%$ ($100/e$, where $e = 2.718$, the base of natural logarithms). Equation 2.80 indicates a linear relationship between

$\log \log(100/P)$ and $\log d$. The slope of the line, n , has been called a ‘uniformity factor’, i.e. $n = \tan \theta$, where θ is the angle between the RRS line and the horizontal. As the size distribution narrows towards a mono-sized dispersion, $n \rightarrow \infty$; as it broadens, $n \rightarrow 0$.

Special double logarithmic graph paper suitable for this type of plotting is available and the data from *Table 2.14* are shown on such a plot in *Figure 2.18b*. From this plot it is possible to determine the 16, 50 and 84% cumulative percentages needed to calculate the MS/CV, as described above. Alternatively, the distribution can be characterized by the uniformity factor, n . In the example shown the median size $d_{50\%} = 870 \mu\text{m}$ (the same as determined in *Figure 2.18a*), the statistical mean size $d' = 1000 \mu\text{m}$, and the uniformity factor $n = 1.8$.

3 *Solutions and solubility*

3.1 Solutions and melts

A solution (gaseous, liquid or solid) is a homogeneous mixture of two or more substances. The constituents of liquid solutions are frequently called solvents and solutes, but despite common usage there is no fundamental reason why any one particular component of a solution should be termed the solvent, and considerable confusion can arise from adhering to rigid definitions. For example, a salt such as potassium nitrate fuses in the presence of small amounts of water at a much lower temperature than the pure salt does. The use of the term ‘solvent’ for water would hardly seem to be justified in this case, and although it may seem strange to refer to ‘a solution of water in potassium nitrate’, this would be an equally acceptable description. Fusion is nothing more than an extreme case of liquefaction by solution, so it may be said that when a salt dissolves in water the salt, in fact, melts.

Owing to the widespread and often indiscriminate use of the word ‘melt’, it is difficult to give a precise definition of the term. Strictly speaking, a melt is a liquid close to its freezing point, but in its general application the term also includes homogeneous liquid mixtures of two or more substances that would individually solidify on cooling to ambient temperatures. Thus α -naphthol heated above its melting point ($96\text{ }^\circ\text{C}$) would be regarded as a melt, and so would a liquid mixture of α -naphthol and β -naphthol (m.p. $122\text{ }^\circ\text{C}$). On the other hand, a liquid mixture of α -naphthol and methanol would normally be classified as a solution. However, no rigid definition is possible. The $\text{KNO}_3-\text{H}_2\text{O}$ system quoted above, and the many well-known cases of hydrated salts dissolving in their own water of crystallization at elevated temperatures, would in all probability be considered to be melts.

3.2 Solvent selection

Water is almost exclusively used as the solvent for the industrial crystallization of inorganic substances from solution. This fact is quite understandable because, apart from the relative ease with which a very large number of chemical compounds dissolve in it, water is readily available, cheap and innocuous. For these reasons water is used whenever possible even for the industrial crystallization of organic compounds, although for a variety of reasons other solvents may have to be used in this particular field.

The selection of the ‘best’ solvent for a given crystallization operation is not always an easy matter. Many factors must be considered and some compromise must inevitably be made; several undesirable characteristics may have to be accepted to secure the aid of one important solvent property. There are several

hundred organic liquids that are potentially capable of acting as crystallization solvents, but outside the laboratory the list can be shortened to a few dozen selected from the following groups: acetic acid and its esters, lower alcohols and ketones, ethers, chlorinated hydrocarbons, benzene homologues, and light petroleum fractions. In many cases, of course, the solvent may already have been selected by the prevailing process conditions. In others, the cost of solvent recovery may override other considerations.

A mixture of two or more solvents will occasionally be found to possess the best properties for a particular crystallization purpose. Common binary solvent mixtures that have proved useful include alcohols with water, ketones, ethers, chlorinated hydrocarbons or benzene homologues, etc. and normal alkanes with chlorinated hydrocarbons or aromatic hydrocarbons.

A second liquid is sometimes added to a solution to reduce the solubility of the solute, cause its precipitation/crystallization and maximize the yield of product. It is necessary, of course, for the two liquids (the original solvent and the added precipitant) to be completely miscible with one another in all proportions. The process is commonly encountered, for instance, in the crystallization of organic substances from water-miscible organic solvents by the controlled addition of water. The term 'watering-out' is often used in this connection. This approach is also used to reduce the solubility of an inorganic salt in aqueous solution by the addition of a water-miscible organic solvent in salting-out precipitation processes (section 7.2.5).

Some of the main points that should be considered when choosing a solvent for a crystallization process include the following. The solute to be crystallized should be readily soluble in the solvent. It should also be easily deposited from the solution in the desired crystalline form after cooling, evaporation, salting-out with an additive, etc. There are many exceptions to the frequently quoted rule that 'like dissolves like', but this rough empiricism can serve as a useful guide. Solvents may be classified as being polar or non-polar; the former description is given to liquids which have high dielectric constants, e.g. water, acids, alcohols, and the latter refers to liquids of low dielectric constant, e.g. aromatic hydrocarbons. A non-polar solute (e.g. anthracene) is usually more soluble in a non-polar solvent (e.g. benzene) than in a polar solvent (e.g. water). However, close chemical similarity between solute and solvent should be avoided, because their mutual solubility will in all probability be high, and crystallization may prove difficult or uneconomical. It should be noted that the crystal habit can often be changed by changing the solvent (section 6.4).

Based on the nature of their intermolecular bonding interactions solvents may be conveniently divided into three main classes:

1. polar protic, e.g. water, methanol, acetic acid;
2. dipolar aprotic, e.g. nitrobenzene, acetonitrile, furfural;
3. non-polar aprotic, e.g. hexane, benzene, ethyl ether.

In polar protic solvents the solvent molecules interact by forming strong hydrogen bonds. In order to dissolve, the solute must break these bonds and replace them with bonds of similar strength. To have a reasonable solubility, therefore, the solute must be capable of forming hydrogen bonds, either

because the solute itself is hydrogen bonded or because it is sufficiently basic to accept a donated hydrogen atom to form a hydrogen bond. If the solute is aprotic and not basic it cannot form strong bonds with the solvent molecules and therefore will have a very low solubility.

In dipolar aprotic solvents, characterized by high dielectric constants, the solvent molecules interact by dipole–dipole interactions. If the solute is also dipolar and aprotic it can interact readily with the solvent molecules forming similar dipole–dipole interactions. If the solute is non-polar it cannot interact with the dipoles of the solvent molecules and so cannot dissolve. Protic solutes are found to be soluble in basic dipolar aprotic solvents because strong hydrogen bonds are formed, replacing the hydrogen bonds between the solute molecules in the solid state. If a dipolar aprotic solvent is not basic, however, a protic solute will have a low solubility because the strong hydrogen bonds in the solid phase can only be replaced by weaker dipole–dipole interactions between solvent and solute molecules.

In non-polar aprotic solvents, characterized by low dielectric constants, molecules interact by weak van der Waals forces. Non-polar solutes are readily soluble as the van der Waals forces between solute molecules in the solid phase are replaced by similar interactions with solvent molecules. Dipolar and polar protic solutes are generally found to have very low solubilities in these solvents except in cases where non-polar complexes are formed.

Solvent power

The ‘power’ of a solvent is usually expressed as the mass of solute that can be dissolved in a given mass of pure solvent at one specified temperature. Water, for example, is a more powerful solvent at 20 °C for calcium chloride than *n*-propanol (75 and 16 g/100 g solvent, respectively). At the same temperature *n*-propanol is a more powerful solvent than water for benzoic acid (42.5 and 0.29 g/100 g solvent, respectively).

The temperature coefficient of solubility is another important factor to be considered. For example, at 20 °C water is a more powerful solvent for potassium sulphate (11 g/100 g water) than for potassium chlorate (7 g/100 g), but the converse is true at 80 °C (K_2SO_4 , 21 g/100 g; $KClO_3$, 39 g/100 g). Thus, on cooling the respective saturated solutions from 80 to 20 °C, more than 80% of the dissolved $KClO_3$ would be deposited compared with less than 50% of the K_2SO_4 .

Both the solvent power and the temperature coefficient of solubility must be considered when choosing a solvent for a cooling crystallization process; the former quantity influences the volume of the crystallizer, and the latter determines the crystal yield. It frequently happens, especially in aqueous organic systems, that a low solubility is combined with a high temperature coefficient of solubility. For example, the solubilities of salicylic acid in water at 20 and 80 °C are 0.20 and 2.26 g/100 g, respectively. Therefore, on cooling from 80 to 20 °C, most of the dissolved solute (91%) is deposited, and consequently the solute yield is high. However, on account of the low solubility, even at the higher temperature, an excessively large crystallizer would be required to

give a reasonable production rate and consequently water could not be considered as a suitable solvent for salicylic acid crystallization.

Potassium chromate is an example of a solute with a reasonably high solubility in water and a low temperature coefficient of solubility (61.7 and 72.1 g/100 g at 20 and 80 °C, respectively). The low yield on cooling (about 14 per cent) makes it necessary to effect crystallization in some other manner, such as a combination of cooling and evaporation, thus increasing the cost of the operation. An algorithm for the prediction of an optimal solvent or solvent mixture for cooling crystallization has been proposed by Nass (1994).

Solvent hazards

A few words on the subjects of purity and hazards might not be entirely out of place at this point, because their consideration is inevitable when choosing a solvent for a crystallization process. No deleterious impurity, dissolved or suspended, should be introduced into a crystallizing system. The solvent, therefore, should be as clean and as pure as possible. No colouring matter should be permitted to affect the appearance of the final crystals. No residual odours should remain in the product after drying, a problem often encountered after crystallization from organic solvents with distinctive odours. If no previous experience has been obtained with a potential solvent, simple laboratory trials should be made, but due caution should be exercised in interpreting the results because laboratory filtration, washing and drying techniques generally prove to be much more efficient than the corresponding large-scale operations.

The solvent should be stable under all foreseeable operating conditions: it should neither decompose nor oxidize, and it must not attack any of the materials of construction of the plant. When organic solvents are being used, care must be taken in choosing the correct gasket materials; most common types of rubber and many synthetic elastomers, for example, swell and disintegrate after prolonged contact with chlorinated hydrocarbons.

The solute and solvent should not be capable of reacting together chemically, although solvate formation may be permitted under certain circumstances. Hydrated crystals are frequently desired as end-products, but should the anhydrous substance be required the necessary drying process may prove difficult and expensive. Methanol, ethanol, benzene and acetic acid are also known to form solvates with certain substances, and the loss of solvent on drying imposes an additional cost on the process.

Highly viscous solvents are not usually conducive to efficient crystallization, filtration and washing operations. In general, therefore, solvents of low viscosity are preferred. If the solvent recovery process involves distillation, a reasonably volatile solvent is desirable. On the other hand, the loss of a solvent with a high vapour pressure from filters and other processing equipment can be considerable and may prove both costly and hazardous. Solvents with freezing points above about -5°C present wintertime storage and transportation difficulties. Benzene (f.p. 5°C) and acetic acid (f.p. 17°C) are good examples.

Most organic solvents employed in crystallization processes are flammable, and their use necessitates stringent operating conditions. Two of the most

important properties of a flammable solvent are the flash point and explosive limits; the former is the temperature at which the mixture of air and vapour above the liquid can be ignited by means of a spark, and the latter refers to the percentages by volume in air between which the vapour mixture will, if ignited, explode in a confined space. Diethyl ether is an example of a solvent with a very low flash-point (-30°C) and wide range of explosive limits (1 to 50%).

All organic solvents are toxic to a greater or lesser degree: the prolonged inhalation of almost any vapour will produce some harmful effect on a human being. Some solvents are acute poisons, some have a cumulative poisoning effect, and others produce narcosis or intoxication on inhalation, or dermatitis on contact with the skin. Information on these aspects and on the maximum vapour concentrations permitted in working areas can be obtained from specialized reference books. The handbooks by Sax (1992) and Bretherick (1999) deal comprehensively with solvent properties and hazards. Health risks in the use of common solvents are dealt with in RSC/CEC (1986, 1988).

3.3 Expression of solution composition

The composition of a solution, or melt, may be expressed in many different ways, e.g. mass per unit mass of solvent, mass per unit mass of solution, mass per unit volume of solvent, and so on. The mass unit may refer to the dissolved species itself or to a solvated form, e.g. a hydrate.

For the expression of crystallization kinetics there is some theoretical justification for recording compositions on a molar basis, e.g. as kmol m^{-3} (i.e. mol L^{-1}), while mole fractions are most frequently used for thermodynamic calculations. Mass fractions are commonly used in the construction of phase diagrams, although the use of mole fractions is recommended for the representation of reciprocal salt pair systems (section 4.7.2).

For the purpose of expressing a mass balance on an item of process plant, there is considerable merit in expressing solution composition as mass of unsolvated solute per unit mass of solvent, particularly when temperature changes are expected. This avoids the need for further calculation to account for density changes.

In view of the frequent need to make interconversions of composition units it is recommended that, whenever solution concentration measurements are made, the density of the solution at the relevant temperature is also measured and recorded (see section 3.9).

Many of the above methods of solubility expression can lead to the use of the potentially misleading term ‘percentage concentration’. For instance, an expression such as ‘a 10 per cent aqueous solution of sodium sulphate’ could be taken to mean, without further definition, any one of the following:

- 10 g of Na_2SO_4 in 100 g of water
- 10 g of Na_2SO_4 in 100 g of solution
- 10 g of $\text{Na}_2\text{SO}_4 \cdot 10\text{H}_2\text{O}$ in 100 g of water
- 10 g of $\text{Na}_2\text{SO}_4 \cdot 10\text{H}_2\text{O}$ in 100 g of solution

If 10 g of anhydrous Na_2SO_4 in 100 g of water were the intended description of the solution concentration, this would then be equivalent to

- 9.1 g of Na_2SO_4 in 100 g of solution
- 20.6 g of $\text{Na}_2\text{SO}_4 \cdot 10\text{H}_2\text{O}$ in 100 g of solution
- 26.0 g of $\text{Na}_2\text{SO}_4 \cdot 10\text{H}_2\text{O}$ in 100 g of water

which gives some measure of the magnitude of the possible misinterpretation. To make matters even worse, the term ‘percentage concentration’ is often applied on a volume basis, e.g. 10 g of Na_2SO_4 in 100 mL of water, of solution, and so on.

Table 3.1 lists the interconversions between a number of the common expressions of solution composition. For convenience, the expressions are drafted in terms of aqueous systems, but the relationships are completely general if the terms ‘unsolvated substance’, ‘solvate’ and ‘solvent’ are substituted for ‘anhydrous substance’, ‘hydrate’, and ‘water’, respectively.

Table 3.1. Conversion factors for solution concentration units

Concentration	Equivalent expressions					
C_1	$\frac{C_2}{1 - C_2}$	$\frac{C_3}{R - C_3}$	$\frac{C_4}{R + (R - 1)C_4}$	$\frac{C_5}{\rho - C_5}$	$\frac{C_6}{\rho R - C_6}$	$\frac{M_A C_7}{\rho - M_A C_7}$
C_2	$\frac{C_1}{1 + C_1}$	$\frac{C_3}{R}$	$\frac{C_4}{R(1 + C_4)}$	$\frac{C_5}{\rho}$	$\frac{C_6}{\rho R}$	$\frac{M_A C_7}{\rho}$
C_3	$\frac{RC_1}{1 + C_1}$	RC_2	$\frac{C_4}{1 + C_4}$	$\frac{RC_5}{\rho}$	$\frac{C_6}{\rho}$	$\frac{M_H C_7}{\rho}$
C_4	$\frac{RC_1}{1 - (R - 1)C_2}$	$\frac{RC_2}{1 - RC_2}$	$\frac{C_3}{1 - C_3}$	$\frac{RC_5}{\rho - RC_5}$	$\frac{C_6}{\rho - C_6}$	$\frac{M_H C_7}{\rho - M_H C_7}$
C_5	$\frac{\rho C_1}{1 + C_1}$	ρC_2	$\frac{\rho C_3}{R}$	$\frac{\rho C_4}{R(1 + C_4)}$	$\frac{C_6}{R}$	$M_A C_7$
C_6	$\frac{\rho RC_1}{1 + C_1}$	ρRC_2	ρC_3	$\frac{\rho C_4}{1 + C_4}$	RC_5	$M_H C_7$
C_7 and C_8	$\frac{\rho C_1}{M_A(1 + C_1)}$	$\frac{\rho C_2}{M_A}$	$\frac{\rho C_3}{M_H}$	$\frac{\rho C_4}{M_H(1 + C_4)}$	$\frac{C_5}{M_A}$	$\frac{C_6}{M_H}$

C_1 = kg of anhydrous substance/kg of water

C_2 = kg of anhydrous substance/kg of solution

C_3 = kg of hydrate/kg of solution

C_4 = kg of hydrate/kg of ‘free’ water

C_5 = kg of anhydrous substance/ m^3 of solution

C_6 = kg of hydrate/ m^3 of solution

C_7 = kmol of anhydrous substance/ m^3 of solution

C_8 = kmol of hydrate/ m^3 of solution

C_9 = mole fraction of anhydrous substance

C_{10} = mole fraction of hydrate

M_A = molar mass of anhydrous substance

M_H = molar mass of hydrate

M_W = molar mass of water

R = M_H/M_A

ρ = density of solution (kg m^{-3})

Interconversions between mass or molar units and those based on mole fractions are a little more complex than those in *Table 3.1*. The mole fraction x of a particular component in a mixture of several substances is given by

$$x_1 = \frac{m_1/M_1}{m_1/M_1 + m_2/M_2 + m_3/M_3 + \dots} \quad (3.1)$$

where m is the mass of a particular component, and M its molar mass.

The relationship between compositions expressed in mole fractions and in other units is given by

$$C_9 = \frac{M_W C_1}{M_W C_1 + M_A} = \frac{M_W C_4}{M_H + (M_H + M_W - M_A) C_4} \quad (3.2)$$

and

$$C_{10} = \frac{M_W C_1}{M_A - (M_H - M_A - M_W) C_1} = \frac{M_W C_4}{M_W C_4 + M_H} \quad (3.3)$$

A large number of terms have been used to express the relative solubility of a solute in a given solvent. The following, together with some examples of solubility (g L^{-1}) at around ambient temperature, are the most frequently encountered:

Practically insoluble	BaSO_4	0.002
Slightly soluble	$\text{Ca}(\text{OH})_2$	1.5
Sparingly soluble	PbCl_2	10
Soluble	NaCl	350
Very soluble	Sucrose	2000

3.4 Solubility correlations

In the majority of cases the solubility of a solute in a solvent increases with temperature, but there are a few well-known exceptions to this rule. Some typical solubilities for various salts in water are shown in *Figure 3.1*, where all concentrations are expressed as kg of anhydrous substance per 100 kg of water. In *Figure 3.1a* sodium chloride is a good example of a salt whose solubility increases only slightly with an increase in temperature, whereas sodium acetate shows a fairly rapid increase.

The solubility characteristics of a solute in a given solvent have a considerable influence on the choice of a method of crystallization. It would be useless, for instance, to cool a hot saturated solution of sodium chloride in the hope of depositing crystals in any quantity. A reasonable yield could only be achieved by removing some of the water by evaporation, and this is what is done in practice. On the other hand, a direct cooling crystallization operation would be adequate for a salt such as copper sulphate: cooling from 90 to 20 °C would produce about 44 kg of CuSO_4 for every 100 kg of water present in the original solution. As the stable phase of copper sulphate at 20 °C is the pentahydrate the

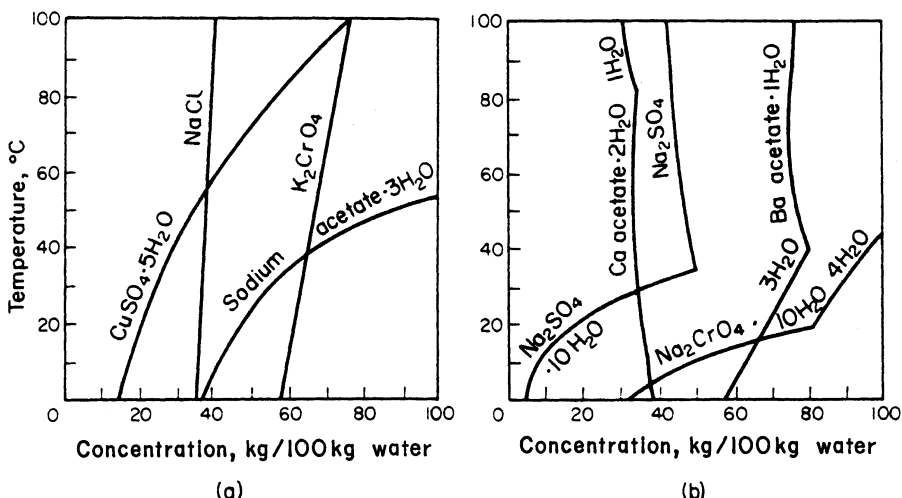


Figure 3.1. Solubility curves for some salts in water: (a) smooth curves, (b) indicating occurrence of phase changes

actual crystal yield would be about 69 kg of $\text{CuSO}_4 \cdot 5\text{H}_2\text{O}$ for every 100 kg of water present initially.

Not all solubility curves are smooth, as can be seen in Figure 3.1b. A discontinuity in the solubility curve denotes a phase change. For example, the solid phase deposited from an aqueous solution of sodium sulphate below 32.4°C will consist of the decahydrate, whereas the solid deposited above this temperature will consist of the anhydrous salt. The solubility of anhydrous sodium sulphate decreases with an increase in temperature. This negative solubility effect, or inverted solubility as it is sometimes called, is also exhibited by substances such as calcium sulphate (gypsum), calcium, barium and strontium acetates, calcium hydroxide, etc. These substances can cause trouble in certain types of crystallizer by causing a deposition of scale on heat-transfer surfaces.

The solubility curves for two different phases meet at the transition point, and a system may show a number of these points. For instance, three forms of ferrous sulphate may be deposited from aqueous solution depending upon the temperature: $\text{FeSO}_4 \cdot 7\text{H}_2\text{O}$ up to 56°C , $\text{FeSO}_4 \cdot 4\text{H}_2\text{O}$ from 56 to 64°C and $\text{FeSO}_4 \cdot \text{H}_2\text{O}$ above 64°C .

The general trend of a solubility curve can be predicted from Le Chatelier's Principle which, for the present purpose, can be stated: when a system in equilibrium is subjected to a change in temperature or pressure, the system will adjust itself to a new equilibrium state in order to relieve the effect of the change. Most solutes dissolve in their near-saturated solutions with an absorption of heat (endothermic heat of solution) and an increase in temperature results in an increase in the solubility. An inverted solubility effect occurs when the solute dissolves in its near-saturated solution with an evolution of heat (exothermic heat of solution).

Strictly speaking, solubility is also a function of pressure, but the effect is generally negligible in the systems normally encountered in crystallization from solution. In the purification of melt systems, however, pressure manipulation can be utilized for separating organic isomers (section 7.3.2).

Many equations have been proposed for the correlation and prediction of solubility data. Some are better than others, but none has been found to be of general applicability. In any case, an experimentally determined solubility is undoubtedly preferred to an estimated value, particularly in systems that may contain impurities. Nevertheless, there is frequently a need for a simple mathematical expression of solubility to assist the recording and correlation of data.

One of the most commonly used expressions of the influence of temperature on solubility is the polynomial

$$c = A + Bt + Ct^2 + \dots \quad (3.4)$$

where t is the temperature, e.g. in °C, and c is the solution composition, expressed in any convenient units. A , B , C , etc. are constants that depend on the units used. There is rarely any need to resort to higher-order polynomials for this empirical relationship.

In addition to equation 3.4, a number of semi-empirical equations have been proposed for solubility correlation purposes, some of which are based on thermodynamic relationships relating to phase equilibria. Examples of some of the expressions that have found favour, at one time or another, are

$$\log x = A + BT \quad (3.5)$$

$$\log x = A + BT + CT^2 \quad (3.6)$$

$$\log x = A + BT^{-1} \quad (3.7)$$

$$\log x = A + BT^{-1} + CT^{-2} \quad (3.8)$$

$$\log x = A + BT^{-1} + C \log T \quad (3.9)$$

In all these relationships the solution composition x is expressed as mole fraction of solute and the temperature T is expressed in kelvins (K). The constants A , B and C in equations 3.4 to 3.9, of course, are not related to one another.

Broul, Nývlt and Söhnel (1981) came to the conclusion that, when tested against solubility data from 70 inorganic salts in water, the accuracy of the two-constant equations was consistently lower than that of the three-constant equations. However, they found that there was little to choose between individual equations in these two groups, but they did select equation 3.9 as being the most reliable.

There is still considerable merit, however, in favour of equation 3.7 because of its simple form and its usefulness in the graphical estimation of transition points. Conventional solubility plots, such as those shown in *Figure 3.1*, can prove unreliable for this purpose when only a few data points are available, especially when the points lie on one or more different curves. Solubilities plotted in accordance with equation 3.7 are shown in *Figure 3.2*. Mole fraction concentrations x are recorded on the logarithmic abscissa and values of $10^3 T^{-1}$

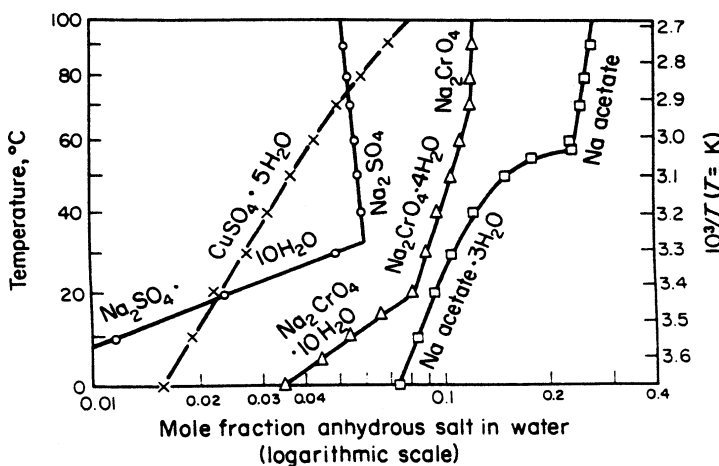


Figure 3.2. Alternative method for the graphical representation of solubility data

(because T^{-1} in the range 273–373 K is a very small quantity) are recorded on the right-hand linear ordinate scale. Alternatively, log–reciprocal graph paper can be used on which the temperature in degrees Celcius can be plotted directly, as on the left-hand ordinate in *Figure 3.2*.

In *Figure 3.1* the solubility of CuSO_4 over the temperature range 0–100 °C is represented by a smooth curve, and the solubilities of Na_2SO_4 and Na_2CrO_4 are represented by smooth curves that intersect at transition points. Several advantages of the $\log x$ versus T^{-1} plot shown in *Figure 3.2* immediately become apparent. For example, the data for the above three salts lie on a series of straight lines, which greatly assists interpolation and allows transition points to be identified with some precision. It is easier, for example, to produce the two straight lines for sodium sulphate in *Figure 3.2*, to meet at 32.4 °C than it is to extend the two corresponding curves in *Figure 3.1*. The two straight lines for CuSO_4 intersect at about 67 °C, which indicates a phase transition at this temperature; this transition between two different crystalline forms of the pentahydrate is not detected in *Figure 3.1*. Incidentally, the transition $\text{CuSO}_4 \cdot 5\text{H}_2\text{O} \rightleftharpoons \text{CuSO}_4 \cdot 3\text{H}_2\text{O}$ occurs at 95.9 °C. Only two of the transitions for the sodium chromate system are indicated in *Figure 3.2*. There are actually three transition points in this system: $10\text{H}_2\text{O} \rightleftharpoons 6\text{H}_2\text{O}$ (19.6 °C), $6\text{H}_2\text{O} \rightleftharpoons 4\text{H}_2\text{O}$ (26.6 °C) and $4\text{H}_2\text{O} \rightleftharpoons \text{anhydrous}$ (64.8 °C).

The solubility data for sodium acetate are included in *Figure 3.2* to illustrate the fact that straight lines do not always result from this method of plotting. Curved lines are often obtained for highly soluble substances, or in regions where the temperature coefficient of solubility is high, or in cases where several hydrates can exist over a narrow range of temperature. It is possible, of course, that the curved portion of the sodium acetate line in the region of about 40–58 °C could be a series of straight lines representing hydrates other than the trihydrate, but there is no evidence to support this view.

3.5 Theoretical crystal yield

If the solubility data for a substance in a particular solvent are known, it is a simple matter to calculate the maximum yield of pure crystals that could be obtained by cooling or evaporating a given solution. The calculated yield will be a maximum, because the assumption has to be made that the final mother liquor in contact with the deposited crystals will be just saturated. Generally, some degree of supersaturation may be expected, but this cannot be estimated. The yield will refer only to the quantity of pure crystals deposited from the solution, but the actual yield of solid material may be slightly higher than that calculated, because crystal masses invariably retain some mother liquor even after filtration. When the crystals are dried they become coated with a layer of material that is frequently of a lower grade than that in the bulk of the crystals. Impure dry crystal masses produced commercially are very often the result of inadequate mother liquor removal.

Washing on a filter helps to reduce the amount of mother liquor retained by a mass of crystals, but there is always the danger of reducing the final yield by dissolution during the washing operation. If the crystals are readily soluble in the working solvent, another liquid in which the substance is relatively insoluble may be used. Alternatively, a wash consisting of a cold, near-saturated solution of the pure substance in the working solvent may be employed. The efficiency of washing depends largely on the shape and size of the crystals (see section 8.6.1).

The calculation of the yield for the case of crystallization by cooling is quite straightforward if the initial concentration and the solubility of the substance at the lower temperature are known. The calculation can be complicated slightly if some of the solvent is lost, deliberately or accidentally, during the cooling process, or if the substance itself removes some of the solvent, e.g. by taking up water of crystallization. All these possibilities are taken into account in the following equations, which may be used to calculate the maximum yields of pure crystals under a variety of conditions.

Let C_1 = initial solution concentration (kg anhydrous salt/kg solvent)

C_2 = final solution concentration (kg anhydrous salt/kg solvent)

W = initial mass of solvent (kg)

V = solvent lost by evaporation (kg per kg of original solvent)

R = ratio of molar masses of hydrate and anhydrous salt

Y = crystal yield (kg)

Substance crystallizes unsolvated (e.g. anhydrous salt)

$$\text{Total loss of solvent: } Y = WC_1 \quad (3.10)$$

$$\text{No loss of solvent: } Y = W(C_1 - C_2) \quad (3.11)$$

$$\text{Partial loss of solvent: } Y = W[C_1 - C_2(1 - V)] \quad (3.12)$$

Substance crystallizes as a solvate

$$\text{Total loss of free solvent: } Y = WRC_1 \quad (3.13)$$

$$\text{No loss of solvent: } Y = \frac{WR(C_1 - C_2)}{1 - C_2(R - 1)} \quad (3.14)$$

$$\text{Partial loss of solvent: } Y = \frac{WR[C_1 - C_2(1 - V)]}{1 - C_2(R - 1)} \quad (3.15)$$

Equation 3.15 can, of course, be used as the general equation for all cases.

Example 1

Calculate the theoretical yield of pure crystals that could be obtained from a solution containing 100 kg of sodium sulphate (mol. wt. = 142) in 500 kg of water by cooling to 10 °C. The solubility of sodium sulphate at 10 °C is 9 kg of anhydrous salt per 100 kg of water, and the deposited crystals will consist of the decahydrate (mol. wt. = 322). Assume that 2 per cent of the water will be lost by evaporation during the cooling process.

$$R = 322/142 = 2.27$$

$$C_1 = 0.2 \text{ kg Na}_2\text{SO}_4 \text{ per kg of water}$$

$$C_2 = 0.09 \text{ kg Na}_2\text{SO}_4 \text{ per kg of water}$$

$$W = 500 \text{ kg of water}$$

$$V = 0.02 \text{ kg per kg of water present initially}$$

Substituting these values in equation 3.15 gives

$$Y = \frac{500 \times 2.27[0.2 - 0.09(1 - 0.02)]}{1 - 0.09(2.27 - 1)}$$

$$\text{Yield} = 143 \text{ kg Na}_2\text{SO}_4 \cdot 10\text{H}_2\text{O}$$

To determine the crystal yield from a vacuum crystallizer (section 7.5.3) it is necessary to estimate the amount of solvent evaporated, V . This depends on the heat made available during the operation of the crystallizer, i.e. the sum of the sensible heat drop of the solution, which cools from the feed temperature to the equilibrium temperature in the vessel, and the heat of crystallization liberated. The heat balance, therefore, will be

$$VW\lambda_v = c(t_1 - t_2)W(1 + C_1) + \lambda_c Y \quad (3.16)$$

where, in addition to the symbols defined for equation 3.15,

λ_v = enthalpy of vaporization of solvent (kJ kg^{-1})

λ_c = heat of crystallization of product (kJ kg^{-1})

t_1 = initial temperature of solution ($^\circ\text{C}$)

t_2 = final temperature of solution ($^\circ\text{C}$)

c = mean specific heat capacity of solution ($\text{kJ kg}^{-1} \text{ K}^{-1}$)

Substituting for the value of Y from equation 3.15 and simplifying

$$V = \frac{\lambda_c R(C_1 - C_2) + c(t_1 - t_2)(1 + C_1)[1 - C_2(R - 1)]}{\lambda_v[1 - C_2(R - 1)] - \lambda_c RC_2} \quad (3.17)$$

Example 2

Estimate the yield of sodium acetate crystals ($\text{CH}_3\text{COONa} \cdot 3\text{H}_2\text{O}$) from a continuous vacuum crystallizer operating with an internal pressure of 15 mbar when it is supplied with 2000 kg h^{-1} of a 40 per cent aqueous solution of sodium acetate (0.4 kg of anhydrous salt in 0.6 kg water) at 80°C . The boiling point elevation of the solution may be taken as 11.5°C .

Heat of crystallization of $\text{CH}_3\text{COONa} \cdot 3\text{H}_2\text{O}$, λ_c	$= 144 \text{ kJ kg}^{-1}$
Specific heat capacity of the solution, c	$= 3.5 \text{ kJ kg}^{-1} \text{ K}^{-1}$
Latent heat of vaporization of water at 15 mbar, λ_v	$= 2.46 \text{ MJ kg}^{-1}$
Boiling point of water at 15 mbar	$= 17.5^\circ\text{C}$
Operating temperature $= 17.5^\circ\text{C} + 11.5^\circ\text{C}$	$= 29^\circ\text{C}$
Solubility at 29°C , C_2	$= 0.539 \text{ kg kg}^{-1}$
Initial concentration, $C_1 = 0.4/0.6$	$= 0.667 \text{ kg kg}^{-1}$
Initial mass of water in feed, $W = 0.6 \times 2000$	$= 1200 \text{ kg h}^{-1}$
Ratio of molar masses, $R = 136/82$	$= 1.66$

The quantity of water vaporized is calculated from equation 3.17: $V = 0.153 \text{ kg/kg}$ of water present originally which, when substituted in equation 3.15, gives the crystal yield as $Y = 660 \text{ kg h}^{-1}$ of sodium acetate trihydrate.

3.6 Ideal and non-ideal solutions

An ideal solution is one in which the interaction between solute and solvent molecules is identical with that between the solute molecules and the solvent molecules themselves. From this definition alone it is clear that a truly ideal solution is most unlikely to exist, but the concept is still very useful as a reference condition. For instance, if the solute and solvent did form an ideal solution, the solubility could be predicted from the van't Hoff equation:

$$\ln x = \frac{\Delta H_f}{R} \left[\frac{1}{T_f} - \frac{1}{T} \right] \quad (3.18)$$

where x is the mole fraction of the solute in the solution, T is the solution temperature (K), T_f is the fusion temperature (melting point) of the solute (K), ΔH_f is the molal enthalpy of fusion of the solute (J mol^{-1}) and R is the gas constant ($8.314 \text{ J mol}^{-1} \text{ K}^{-1}$).

For example, the solubility of naphthalene at 20°C in an ideal solution may be calculated from its melting point (80°C) and enthalpy of fusion (18.8 kJ mol^{-1}) to give $x = 0.269$. In principle, therefore, by performing such calculations over a range of temperatures, an 'ideal' solubility curve may be constructed, but it is important to note that any such calculated solubility is expressed without reference to any particular solvent. Furthermore, the assumption of ideality for most real solutions is generally unjustified.

The potential unreliability of equation 3.18 in predicting solubility can be demonstrated by comparing the above calculated ideal solubility ($x = 0.269$) of naphthalene with measured solubilities in a few common solvents:

benzene 0.241 toluene 0.224 CC₁₄ 0.205 hexane 0.090

Even in the case of benzene, with its chemical similarity to naphthalene, ideality is barely approached (the predicted solubility is some 12% too high). The solution in hexane, however, is highly non-ideal (the prediction is 200% too high).

The van't Hoff equation can also be written in the form:

$$\ln x = -\frac{\Delta H_f}{RT} + \frac{\Delta S_f}{R} \quad (3.18a)$$

since $\Delta H_f = T_f \Delta S_f$. ΔS_f is the molal entropy of fusion. It should be understood, however, that even though a plot of $\ln x$ versus T^{-1} may give a straight line, its slope may differ from $-\Delta H_f/R$ if the solution exhibits non-ideal behaviour. In such cases, the enthalpy and entropy of mixing must be taken into account by replacing ΔH_f with ΔH_d (of dissolution) and ΔS_f by ΔS_d (Beiny and Mullin, 1987), i.e., using:

$$\ln x = -\frac{\Delta H_d}{RT} + \frac{\Delta S_d}{R} \quad (3.18b)$$

Another approach stems from a consideration of the Gibbs free energy change ΔG for a dissolution process, which in general may be expressed in terms of the enthalpy and entropy changes associated with the mixing process:

$$\Delta G = \Delta H - T\Delta S \quad (3.19)$$

For the formation of an ideal solution, e.g. by mixing two liquids, the Gibbs free energy may also be expressed as

$$\Delta G = RT \ln x \quad (3.20)$$

where x is the solution composition expressed as a mole fraction of one of the components. The entropy change accompanying this dissolution process, from equation 3.19, is

$$\Delta S = -R \ln x \quad (3.21)$$

since the enthalpy of mixing, ΔH , is zero for an ideal solution.

The overall free energy change may also be expressed in terms of the activity, a , of one of the components:

$$\Delta G = RT \ln a \quad (3.22)$$

In other words, if the solution is ideal,

$$a = x \quad (3.23)$$

For non-ideal solutions, however, equation 3.23 has to be modified by the appropriate activity coefficient, γ , i.e.

$$a = \gamma x \quad (3.24)$$

Similarly, equation 3.18 should be expressed as

$$\ln(x\gamma) = \frac{\Delta H_f}{R} \left[\frac{1}{T_f} - \frac{1}{T} \right] \quad (3.25)$$

The key to the use of equation 3.25 for the prediction of solubilities in non-ideal systems is a reliable estimation of the activity coefficient γ . For organic solutes in organic solvents, this may be achieved (Gmehling, Anderson and Prausnitz, 1978) by the UNIFAC group contribution method which is discussed, together with other techniques for the prediction of solubility data, in section 3.10.

3.6.1 Activity and ionic strength

The colligative properties of solutions, e.g. osmotic pressure, boiling point elevations, freezing point depression and vapour pressure reduction, depend on the effect of solute concentration on the solvent activity. The chemical potential, μ , of a non-electrolyte in dilute solution may be expressed by

$$\mu = \mu_{oc} + RT \ln c \quad (3.26)$$

where c is the solute molar concentration (mol L^{-1}) and μ_{oc} is the standard chemical potential also expressed on a molar basis (J mol^{-1}).

Equation 3.26 is unsatisfactory for non-electrolyte solute concentrations in excess of about 0.1 molar, and it cannot be applied to solutions of electrolytes for concentrations greater than about 10^{-3} molar. For such cases an expression based on activity rather than concentration should be applied, e.g.

$$\mu = \mu_{oc} + RT \ln a_c \quad (3.27)$$

where a_c is the solute activity expressed on a molar basis, which is related to composition c through the corresponding activity coefficient, γ_c , by

$$a_c = c\gamma_c \quad (3.28)$$

The activity coefficient becomes unity at infinite dilution, i.e. when ideality may be assumed.

For electrolyte solutions it is more appropriate to use the mean ionic activity, a_{\pm} , defined with respect to the mean ionic concentration and mean ionic activity coefficient by

$$a_c = a_{\pm c}^{\nu} = (c \gamma_{\pm c})^{\nu} = (Q c \gamma_{\pm c})^{\nu} \quad (3.29)$$

where ν is the number of moles of ions in 1 mole of electrolyte, i.e.

$$\nu = \nu_+ + \nu_- \quad (3.30)$$

and

$$Q = (\nu_+^{\nu_+} \nu_-^{\nu_-})^{1/\nu} \quad (3.31)$$

For non-electrolytes, $\nu = 1$.

From the Debye–Hückel theory of electrolytes, the limiting (infinite dilution) law gives the mean activity coefficient of the ion as

$$\log \gamma_{\pm} = -A|z_+ z_-|I^{1/2} \quad (3.32)$$

where the ionic strength, I , expressed as mol L⁻¹, is defined by

$$I = \frac{1}{2} \sum c_i z_i^2 \quad (3.33)$$

where c_i is the concentration (mol L⁻¹) of the i th ionic species and z_i the valency, and z_+ and z_- are the valencies of the cation and anion, respectively. The Debye–Hückel constant, A , has values of 0.493, 0.499, 0.509 and 0.519 at 5, 15, 25 and 35 °C, respectively.

Similar relationships to those of equations 3.26 to 3.33 may be written for solution compositions expressed as molality, m (mol/kg of solvent), and mole fraction, x , respectively. For example, equation 3.26 could be written as either

$$\mu = \mu_{\text{om}} + \mathbf{R}T \ln m \quad (3.26a)$$

or

$$\mu = \mu_{\text{ox}} + \mathbf{R}T \ln x \quad (3.26b)$$

and equation 3.33 as either

$$I_m = \frac{1}{2} \sum m_i z_i^2 \quad (3.33a)$$

or

$$I_x = \frac{1}{2} \sum x_i z_i^2 \quad (3.33b)$$

For simplicity, however, only the molar-based ionic strength ($I = I_c$) will be used subsequently in this section.

The Debye–Hückel limiting law (equation 3.32) has to be modified for all but the most dilute solutions, and many modifications have been proposed. For example, the Güntelberg equation:

$$\log \gamma_{\pm} = -A|z_+ z_-| \left[\frac{I^{1/2}}{I + I^{1/2}} \right] \quad (3.34)$$

is useful for solutions of sparingly soluble electrolytes, and the Davies equation:

$$\log \gamma_{\pm} = -A|z_+ z_-| \left\{ \left[\frac{I^{1/2}}{I + I^{1/2}} \right] - 0.3I \right\} \quad (3.35)$$

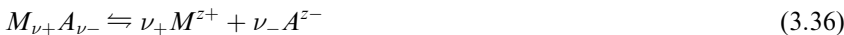
is generally quite satisfactory for values of I up to about 0.2 mol L⁻¹ (Davies, 1962; Nancollas, 1966). For concentrated mixed electrolyte solutions, more complex relationships have to be employed (see section 3.10).

The calculation of the ionic strength of a mixed solution of electrolytes may be illustrated, using equation 3.33, for a mixture of equal volumes of 0.1 mol L⁻¹ NaCl and CaCl₂ solutions, assuming complete dissociation:

$$\begin{aligned} I &= \frac{1}{2}([(\text{Na}^+) \times 1^2] + [(\text{Ca}^{2+}) \times 2^2] + [(\text{Cl}^-) \times 1^2]) \\ &= \frac{1}{2}(0.1 \times 1 + 0.1 \times 4 + 3 \times 0.1 \times 1) \\ &= 0.4 \text{ mol L}^{-1} \end{aligned}$$

3.6.2 Association and dissociation

For incompletely dissociated electrolytes, it is generally convenient to define another activity coefficient, the mean activity coefficient of ions in solution, γ'_{\pm} . For a binary electrolyte which dissociates according to



the concentration of free ions in a solution of molar concentration, c , is αc , where α is the degree of dissociation, and the activity coefficients are related by

$$c\gamma_{\pm c} = \alpha c\gamma'_{\pm c} \quad (3.37)$$

i.e.

$$\alpha = \gamma_{\pm c}/\gamma'_{\pm c} \quad (3.38)$$

The degree of dissociation, α , of dissolved electrolyte was first expressed by Arrhenius in 1887 as the ratio of the molar conductivity (see section 3.6.3) of the solution, Λ , to that of a solution at its most extreme dilution, Λ_0 , i.e.

$$\alpha = \Lambda/\Lambda_0 \quad (3.39)$$

The degree of dissociation can also be expressed in terms of the van't Hoff factor, i , and the number of moles of ions, ν , in one mole of solute:

$$i = 1 - \alpha + \nu\alpha \quad (3.40)$$

i.e.

$$\alpha = \frac{i - 1}{\nu - 1} \quad (3.41)$$

For strong electrolytes (virtually complete dissociation, $\alpha \rightarrow 1$)

$$i = \nu \quad (3.42)$$

The dissociation of an electrolyte molecule in solution into oppositely charged ions, however, is by no means a simple matter. The ionic association theory, first developed by Bjerrum in 1926, indicates that some kind of association will still exist between oppositely charged ions even when they are several molecular diameters apart. The rates of dissociation and reformation, of molecules or other complexes, are extremely fast and it is doubtful if the ions can

ever truly be considered to be ‘free’. Ion association should be taken into account in any complete treatment of aqueous electrolyte solutions since it reduces the value of the ionic activity coefficients.

3.6.3 Conductance and conductivity

The current flowing through an electrolyte solution is proportional to the reciprocal of its *resistance*, R (Ohm’s law). This quantity, $1/R$, is called the *conductance* of the solution, which formerly was expressed as reciprocal ohms (mhos, Ω^{-1}), but now bears the SI unit name of the siemens, S. Thus, a solution with a resistance of $10\ \Omega$ has a conductance of 0.1 S .

The resistances of different solutions can be compared through the quantity known as the *resistivity*, ρ , defined by the relationship

$$\rho = Ra/l \quad (3.43)$$

where l is the length of the conductivity path in the solution and a is its cross-sectional area. The units of ρ are the ohm metre, $\Omega\text{ m}$, or in SI units, siemens $^{-1}$ metre, $\text{S}^{-1}\text{ m}$.

In a similar manner to resistances, the conductances can be compared through the quantity known as the *conductivity*, κ ($\Omega^{-1}\text{ m}^{-1}$ or S m^{-1}), which is the reciprocal of the resistivity, i.e.

$$\kappa = \frac{1}{\rho} \quad (3.44)$$

For electrolyte solutions the molar conductivity, Λ (the conductivity per mole of electrolyte), is a useful characteristic since it allows comparisons to be made between solutions of different substances. Λ is defined by

$$\Lambda = \kappa/c \quad (3.45)$$

where c is the solution concentration, expressed as mol m^{-3} , giving Λ the units of $\Omega^{-1}\text{ m}^2\text{ mol}^{-1}$, i.e. $\text{S m}^2\text{ mol}^{-1}$. According to Kohlrauch’s law, the value of Λ at infinite dilution, Λ_0 , is the sum of the corresponding molar ionic conductivities, also at infinite dilution (see *Tables 3.2 and A.13*), i.e.

$$\Lambda_0 = \Lambda_0^+ + \Lambda_0^- \quad (3.46)$$

The utility of the above relationships in estimating the solubility of sparingly soluble salts is discussed in section 3.9.3.

Furthermore, in addition to its straightforward application, equation 3.46 can be used to calculate Λ_0 for weak electrolytes, e.g. organic acids, from Λ_0 values for their strong electrolyte salts. For example, Λ_0 for acetic acid can be calculated (Moore, 1972) from values of sodium acetate, HCl and sodium chloride. At 25°C :

$$\begin{aligned} \Lambda_0(\text{HAc}) &= \Lambda_0(\text{NaAc}) + \Lambda_0(\text{HCl}) - \Lambda_0(\text{NaCl}) \\ &= (91 + 425 - 128) \times 10^{-4} \\ &= 388 \times 10^{-4} \text{ S m}^2\text{ mol}^{-1} \end{aligned}$$

Table 3.2. Some molar ionic conductivities at infinite dilution at 25 °C

Cation	$10^4 \Lambda_0^+$ ($\text{S m}^2 \text{ mol}^{-1}$)	Anion	$10^4 \Lambda_0^-$ ($\text{S m}^2 \text{ mol}^{-1}$)
H^+	349.8	OH^-	198.5
K^+	73.5	Br^-	78.4
NH_4^+	73.4	I^-	76.8
Ag^+	61.9	Cl^-	76.3
Na^+	50.1	F^-	55.0
Li^+	38.7	NO_3^-	71.4
$\frac{1}{2}\text{Mg}^{2+}$	53.1	ClO_4^-	68.0
$\frac{1}{2}\text{Ca}^{2+}$	59.5	CH_3CO_2^-	40.9
$\frac{1}{2}\text{Sr}^{2+}$	59.5	$\frac{1}{2}\text{CO}_3^{2-}$	74.0
$\frac{1}{2}\text{Ba}^{2+}$	63.6	$\frac{1}{2}\text{SO}_4^{2-}$	78.8
$\frac{1}{2}\text{Pb}^{2+}$	65.0	$\frac{1}{2}\text{CrO}_4^{2-}$	83.0

The values of Λ_0 expressed here as $\times 10^{-4} \text{ S m}^2 \text{ mol}^{-1}$ are equivalent to the former common units of $\Omega^{-1} \text{ cm}^2 \text{ mol}^{-1}$.

3.6.4 Solubility products

The solubility of a sparingly soluble electrolyte in water is often expressed in terms of the *concentration solubility product*, K_c . To take the simplest case, if one molecule of such an electrolyte dissociates in solution into x cations and y anions according to the equation



where z^+ and z^- are the valencies of the ions, then for a saturated solution

$$(c_+)^x(c_-)^y = \text{constant} = K_c \quad (3.48)$$

where c_+ and c_- are the ionic concentrations expressed as mol L^{-1} .

Solubility products are often recorded, for convenience, as $\text{p}K$ values where $\text{p}K_c = -\log K_c$. Thus a value of $K_c = 3.9 \times 10^{-6}$ would be reported as $\text{p}K_c = 5.4$.

For a salt which produces two ions per molecule (1–1, 2–2, etc. electrolytes, i.e. for $x = y = 1$) $c_+ = c_- = c^*$, where c^* is the equilibrium solubility (mol L^{-1}).

Therefore, equation 3.48 becomes

$$c^* = (K_c)^{1/2} \quad (3.49)$$

In general

$$c^* = (K_c/x^x y^y)^{1/(x+y)} \quad (3.50)$$

Therefore, for a 2–1 electrolyte

$$c^* = (K_c/4)^{1/3} \quad (3.51)$$

and for a 3–1 electrolyte

$$c^* = (K_c/27)^{1/4} \quad (3.52)$$

For example, the solubility products of silver bromide, lead iodide and aluminium hydroxide at 18 °C are 4.1×10^{-13} , 9.3×10^{-9} and 1.1×10^{-15} respectively, so their solubilities in water at this temperature may be expressed as:

AgBr (equation 3.49):

$$c^* = (4.1 \times 10^{-13})^{1/2} = 6.4 \times 10^{-7} \text{ mol L}^{-1}$$

PbI_2 (equation 3.51):

$$c^* = [(7.5 \times 10^{-9})/4]^{1/3} = 1.2 \times 10^{-3} \text{ mol L}^{-1}$$

Al(OH)_3 (equation 3.52):

$$c^* = [(1.1 \times 10^{-15})/27]^{1/4} = 8.0 \times 10^{-5} \text{ mol L}^{-1}$$

However, the simple solubility product principle has extremely limited use. It should, for example, be restricted to solutions of very sparingly soluble salts ($< 10^{-3} \text{ mol L}^{-1}$). For more concentrated solutions it is necessary to adopt a more fundamental approach involving the use of activity concepts.

The *activity solubility product*, K_a , is defined

$$(a_+)^x(a_-)^y = \text{constant} = K_a \quad (3.53)$$

where a_+ and a_- are the ionic activities. As the activity of an ion may be expressed in terms of the ionic concentration, c , and the ionic activity coefficient, γ , equation 3.53 may be written

$$(c_+\gamma_+)^x(c_-\gamma_-)^y = K_a \quad (3.54)$$

i.e.

$$K_a = K_c(\gamma_{\pm})^\nu \quad (3.55)$$

where γ_{\pm} is the mean ionic activity coefficient and ν ($=x + y$) is the number of moles of ions produced by one mole of electrolyte.

So the concentration solubility product is equal to the activity solubility only when $\gamma_{\pm} = 1$, i.e. at infinite dilution. In practice, K_a and K_c may be assumed approximately equal for concentrations up to about $10^{-3} \text{ mol L}^{-1}$, but above this concentration significant deviations can occur. The activity of an ion depends on the concentration of all the other ions in solution, so the presence of a dissolved foreign electrolyte can greatly influence the value of γ_{\pm} of a sparingly soluble salt.

A number of cases which appear anomalous when the simple solubility product is used can be explained when activity coefficients are taken into account. For instance, the addition of a common ion generally decreases the solubility of a salt, but cases are known where additions of a salt with a common ion result in increase in solubility. The reason for this is that a large

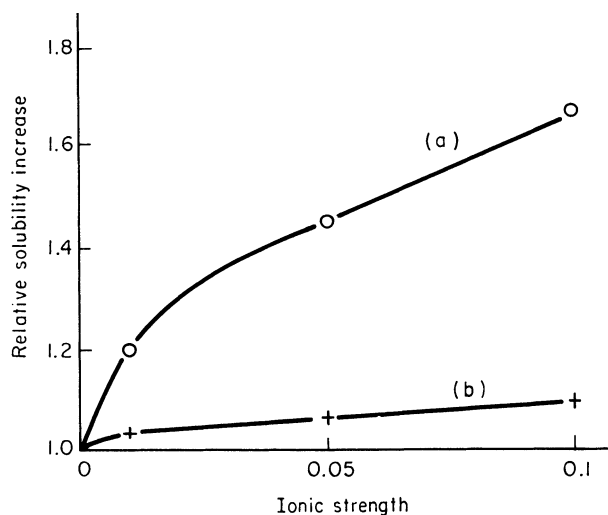
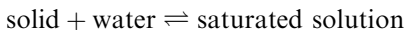


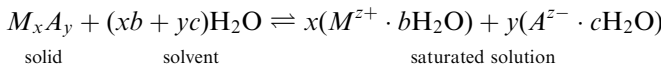
Figure 3.3. Relative increase in solubility with increase in ionic strength: (a) BaSO₄ in KNO₃ solution, (b) AgCl in KNO₃ solution. (After Lewin, 1960)

increase in ionic concentration can cause a reduction in the activity coefficients. Thus from equation 3.54 an increase in c_- will result in a decrease in c_+ , i.e. precipitation of the sparingly soluble salt, if γ_+ and γ_- remain fairly constant, but an increase in c_- to a value which reduces both γ_+ and γ_- must result in an increase in c_+ if K_a is to remain constant. The addition of a salt without a common ion often increases the solubility; this again is the result of the increased ionic concentration reducing the activity coefficients (*Figure 3.3*).

Lewin (1960) has pointed out that even equation 3.54 does not represent the true situation since a saturated aqueous solution in equilibrium with the solid phase involves the reversible reaction



so at constant temperature and pressure



where b and c are the numbers of water molecules associated with the cation and anion respectively. Consequently, under equilibrium conditions, by the Law of Mass Action:

$$\frac{(a_+)^x (a_-)^y}{(a_{\text{solid}})(a_{\text{water}})^{(xb+yc)}} = K \quad (3.56)$$

which Lewin called the *comprehensive activity solubility product*. The use of this thermodynamically rigorous form of the solubility product can resolve most apparently anomalous problems.

Common and diverse ion effects

The addition of an electrolyte to a saturated solution of a sparingly soluble salt with a common ion depresses the solubility of the latter (the common ion effect) and leads to its precipitation. For example, the solubility product of AgCl at 25 °C is 1.56×10^{-10} ($K_a = K_c$ at this dilution), i.e.

$$[\text{Ag}^+][\text{Cl}^-] = 1.56 \times 10^{-10}$$

giving, from equation 3.49, a solubility of

$$c^* = 1.25 \times 10^{-5} \text{ mol L}^{-1}$$

If a small quantity of a more soluble chloride, e.g. NaCl, is added to a saturated solution of AgCl the Cl^- concentration will temporarily exceed $1.25 \times 10^{-5} \text{ mol L}^{-1}$, i.e.

$$[\text{Ag}^+][\text{Cl}^-] > 1.56 \times 10^{-10}$$

This unstable condition cannot persist so the system readjusts itself until the new ionic product equals the solubility product and this results in the precipitation of some of the AgCl.

The solubility product principle can only be strictly applied to equilibrium conditions, although it has often been used to explain such precipitations as those encountered in qualitative analysis by the traditional wet-test methods. However, these sudden precipitations do not take place under anything like equilibrium conditions and the fact that reasonably successful predictions can usually be made is mainly due to the enormous excess ionic concentrations (supersaturations) generated compared with those required by the corresponding solubility products. Errors of magnitude of 10^5 – 10^7 per cent have been estimated (Lewin, 1960) for such calculations and these clearly swamp other variations such as neglect of solute activity coefficients, complex ion formation, etc.

Whereas the presence in solution of an ion in common with a sparingly soluble salt can significantly decrease the salt solubility, the presence of an ion not in common with any of those of the solute can increase the solute solubility on account of the increase in ionic strength. For example, the solubility of silver bromide in water is increased by around 30% in a 0.1 mol L⁻¹ sodium nitrate aqueous solution, as can be seen in the following rough calculation.

The solubility of silver bromide in water at 15 °C is about $6 \times 10^{-7} \text{ mol L}^{-1}$. At this low concentration the ‘activity’ and ‘concentration’ solubility products may be assumed to be equal (see equation 3.55), i.e.

$$K_c = (c^*)^2 = 3.6 \times 10^{-13} = K_a$$

For a 0.1 molar solution of sodium nitrate, using equations 3.35 with a value of $A = 0.499$ appropriate for 15 °C, the calculated ionic activity coefficient γ_+ is 0.783, from which it may be estimated that

$$K_c = 3.6 \times 10^{-13}/(0.783)^2 = 5.87 \times 10^{-13}$$

giving the solubility

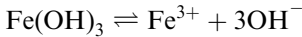
$$c^* = K_c^{1/2} = 7.7 \times 10^{-7} \text{ mol L}^{-1}$$

Temperature effects

The ionic product of water

$$K_w = [\text{H}^+][\text{OH}^-] \quad (3.57)$$

is temperature dependent, rising from about 10^{-15} at 0°C , to 10^{-14} at 25°C and 10^{-13} at 60°C . Such a large variation is of considerable significance in the precipitation of sparingly soluble metal hydroxides, and its neglect can lead to gross errors. Fe(III) hydroxide, for example, dissociates according to:



and the solubility product

$$K_c = [\text{Fe}^{3+}][\text{OH}^-]^3$$

i.e.

$$[\text{Fe}^{3+}] = \frac{K_c}{[\text{OH}^-]^3} = \frac{K_c[\text{H}^+]^3}{[K_w]^3}$$

Thus at a given pH the Fe^{3+} concentration above which precipitation may be considered possible is

$$[\text{Fe}^{3+}] \propto K_w^{-3}$$

A value of $K_w = 10^{-14}$ is commonly used in rough calculations, but this is only correct at 25°C . If it were to be used for conditions at 15°C , where the correct value of K_w is 0.45×10^{-14} , an error of about $(1/0.45)^{-3} \times 100$, i.e. > 1000 per cent, would be incurred.

3.7 Particle size and solubility

The relationship between particle size and solubility, originally derived for vapour pressures in liquid-vapour systems by Thomson (who became Lord Kelvin in 1892) in 1871, utilized later by Gibbs, and applied to solid-liquid systems by Ostwald (1900) and Freundlich (1926) may be expressed in the form

$$\ln \left[\frac{c(r)}{c^*} \right] = \frac{2M\gamma}{\nu \mathbf{R} T \rho r} \quad (3.58)$$

where $c(r)$ is the solubility of particles of size (radius) r , c^* is the normal equilibrium solubility of the substance, \mathbf{R} is the gas constant, T is absolute temperature, ρ is the density of the solid, M is the molar mass of the solid in solution and γ is the interfacial tension of the solid in contact with the solution.

The quantity ν represents the number of moles of ions formed from one mole of electrolyte (equation 3.30). For a non-electrolyte, $\nu = 1$.

Confusingly, but for understandable reasons, equation 3.58 is referred to in the literature by a variety of names such as the Gibbs–Thomson, Gibbs–Kelvin and Ostwald–Freundlich relation. For consistency, however, the designation ‘Gibbs–Thomson’ will be used throughout this work.

As a result of the particle size solubility effect, solution compositions may exceed greatly the normal equilibrium saturation value if the excess solute particles dispersed in the solution are very small. For most solutes in water, however, the solubility increase only starts to become significant for particle sizes smaller than about 1 μm .

For example, for barium sulphate at 25 °C: $T = 298 \text{ K}$, $M = 233 \text{ kg kmol}^{-1}$, $\nu = 2$, $\rho = 4500 \text{ kg m}^{-3}$, $\gamma = 0.13 \text{ J m}^{-2}$, $\mathbf{R} = 8.3 \times 10^3 \text{ J kmol}^{-1} \text{ K}^{-1}$. Thus for a 1 μm , crystal ($r = 5 \times 10^{-7} \text{ m}$), $c/c^* = 1.005$ (i.e. 0.5% increase). For 0.1 μm , $c/c^* = 1.06$ (i.e. 6% increase) and for 0.01 μm , $c/c^* = 1.72$ (i.e. 72% increase).

For a very soluble organic compound such as sucrose ($M = 342 \text{ kg kmol}^{-1}$, $\nu = 1$, $\rho = 1590 \text{ kg m}^{-3}$, $\gamma = 10^{-2} \text{ J m}^{-2}$) the effect is similar: 1 μm (0.4% increase), 0.1 μm (4%), 0.01 μm (40%). All such calculated values, however, should be treated with caution, not only because of the unreliability of γ values but also because the Gibbs–Thomson effect may cease to be influential at extremely small crystal sizes (see *Figure 3.4*).

For practical application to crystals, equation 3.58 could be more usefully redrafted in terms of particle size expressed as a convenient length parameter, L , coupled with an approximate overall shape factor, F :

$$\ln \left[\frac{c(L)}{c^*} \right] = \frac{2FM\gamma}{3\nu\mathbf{R}T\rho L} \quad (3.59)$$

For spheres and cubes $F = 6$ (L = diameter or length of side). For other shapes $F > 6$, e.g. for an octahedron $F = 7.35$ (section 2.14.3).

Strictly speaking, equation 3.58 should be expressed in terms of solution activities rather than concentrations (Enüstün and Turkevich, 1960). Furthermore, it involves a number of assumptions that may not always be valid. For example, the solid–liquid interfacial tension (section 5.6) is implicitly assumed to be independent of particle size, and no account is taken of any ionization or

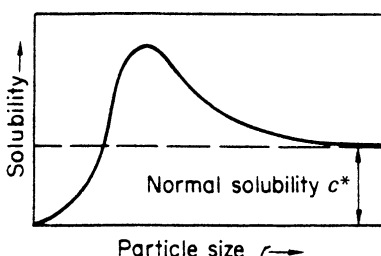


Figure 3.4. The effect of particle size on solubility

dissociation of the solute in solution. This latter effect, discussed in detail by Jones and Partington (1915), leads to the relationship

$$\ln \left[\frac{c(r)}{c^*} \right] = \frac{2M\gamma}{(1 - \alpha + \nu\alpha)\mathbf{R}T\rho r} \quad (3.60)$$

where α is the degree of dissociation. For the case of complete dissociation ($\alpha = 1$) equation 3.60 reduces to equation 3.58.

Another fault of equation 3.58 is that it postulates an exponential increase in solubility to infinity with a reduction in particle size to zero:

$$c(r) = c^* \exp(2M\gamma/\nu\mathbf{R}T\rho r) \quad (3.61)$$

To overcome this anomaly, Knapp (1922) considered that the total surface energy (interfacial tension) of very small solid particles should be regarded as the sum of their ‘normal’ surface energy plus the surface electrical charge that such particles would carry. From these considerations he derived for the case of isolated charged spheres an equation of the form

$$c(r) = c^* \exp(Ar^{-1} - Br^{-4}) \quad (3.62)$$

where $A = 2\gamma M/\mathbf{R}T\rho$ and $B = q^2 M/8\pi\kappa\mathbf{R}T\rho$, q being the electrical charge on the particle of radius r and κ its dielectric constant. Equation 3.62 gives a curve of the type shown in *Figure 3.4*. Subsequent work has tended to lend support to Knapp’s postulation and measurements made by Harbury (1946) indicated maximum:equilibrium solubility ratios of 3, 6 and 13 for salts KNO_3 , KClO_3 , $\text{K}_2\text{Cr}_2\text{O}_7$ and $\text{Na}_2\text{SO}_4 \cdot 10\text{H}_2\text{O}$ in water.

3.8 Effect of impurities on solubility

So-called pure solutions are rarely encountered outside the analytical laboratory, and even then the impurity levels are usually well within detectable limits. Industrial solutions, on the other hand, are almost invariably impure, by any definition of the term, and the impurities present can often have a considerable effect on the solubility characteristics of the main solute.

If to a saturated binary solution of A (a solid solute) and B (a liquid solvent) a small amount of the third component C (also soluble in B) is added, one of four conditions can result. First, nothing may happen, although this is comparatively rare, in which case the system remains in its original saturated state. Second, component C may react or otherwise combine or react chemically with A by forming a complex or compound, thus altering the whole nature of the system. In the third case, the presence of component C may make the solution super-saturated with respect to solute A , which would then be precipitated. In the fourth case, the solution may become unsaturated with respect to A . The terms ‘salting-out’ and ‘salting-in’ are commonly used to describe these last two cases, particularly when electrolytes are involved.

The salting-out effect of an electrolyte added to an aqueous solution of a non-electrolyte, can often be represented by the empirical equation

$$\log \frac{c^{*'}}{c^*} = kC + \beta \quad (3.63)$$

where c^* and $c^{*'}$ are the equilibrium saturation concentrations (mol L^{-1}) of the non-electrolyte in pure water and in a salt solution of concentration C (mol L^{-1}), respectively. The constants k , called the salting parameter, and β refer to one particular electrolyte and its effect on one particular non-electrolyte at a given temperature. This type of relationship, which often applies with a reasonable accuracy for low non-electrolyte concentrations and electrolyte concentrations up to 4 or 5 mol L^{-1} , is commonly employed to characterize the precipitation of proteins from aqueous solution using inorganic electrolytes (Bell, Hoare and Dunnill, 1983).

Occasionally the presence of an electrolyte increases the solubility of a non-electrolyte (negative value of k) and this salting-in effect is exhibited by several salts, with large anions and cations, which themselves are very soluble in water. Sodium benzoate and sodium *p*-toluenesulphonate are good examples of these *hydrotropic* salts and the phenomenon of salting-in is sometime referred to as *hydrotropism*. Values of the salting parameter for three salts applied to benzoic acid are NaCl (0.17), KCl (0.14) and sodium benzoate (-0.22). Long and McDevit (1952) have made a comprehensive review of salting-in and salting-out phenomena.

Halstead (1970) reported that potassium sulphate once dissolved would not recrystallize from aqueous solutions contaminated with traces of chromium(III) or iron(III) and suggested that these impurities prevented the nucleation of K_2SO_4 crystals. Trace impurities can sometimes have highly unexpected effects on equilibrium solubility measurements. For example, the solubility of potassium sulphate is significantly lowered when measured by dissolving K_2SO_4 crystals in water containing ppm traces of Cr(III) (Kubota *et al.*, 1988). A measured value obtained under these circumstances, however, is only an apparent or pseudo-solubility, the value of which is determined by two competing rate processes, viz., the adsorption of Cr(III) species on the K_2SO_4 crystals and the dissolution of the crystals. Interestingly, a false solubility measurement is also obtained when, instead of approaching equilibrium from the undersaturated state, it is approached from the supersaturated condition, e.g., by cooling a solution to deposit excess solute. In this case, the recorded pseudo-solubility is higher than the true equilibrium value because the Cr(III) species in solution adsorb on the depositing K_2SO_4 crystals, retard their growth and prevent complete desupersaturation of the solution. The actual species adsorbed, one of the many possible hydroxo-Cr(III) complexes, depends on the particular salt added as impurity and the pH of the solution (Kubota *et al.*, 1994). The magnitude of the decrease in the measured pseudo-solubilities depends on pH, impurity concentration and the particular salt of the impurity added. Similar patterns of behaviour are seen when traces of Fe(III) salts are used as the added impurity (Kubota *et al.*, 1999). An account of the effects of trace impurities on crystal growth and dissolution processes is given in section 6.2.8.

When considerable quantities of a soluble impurity are present in, or deliberately added to, a binary solution, the system may be assessed better in terms of three components, expressing the data on a triangular ternary equilibrium diagram (see section 4.6).

3.9 Measurement of solubility

Innumerable techniques, of almost infinite variety, have been proposed at one time or another for the measurement of the solubility of solids in liquids. No single method can be identified, however, as being generally applicable to all possible types of system. The choice of the most appropriate method for a given case has to be made in the light of the system properties, the availability of apparatus and analytical techniques, the skill and experience of the operators, the precision required, and so on.

The accuracy required of a solubility measurement depends greatly on the use that is to be made of the information. Requirements vary enormously. In some cases, a simple assessment of whether a substance is highly, moderately or sparingly soluble in a given solvent, with some rough quantification, may be quite sufficient. In others, very high precisions may be demanded. For most work, however, a precision of $< 1\%$ should be aimed for, and usually this is not too difficult to attain.

Extensive reviews of the literature on the subject of experimental solubility determination have been made by Vold and Vold (1949) and Zimmerman (1952). Purdon and Slater (1946) give an excellent account of the determination of solubility in aqueous salt systems. The monographs of Blasdale (1927) and Teeple (1929) give comprehensive accounts of the problems encountered in measuring equilibria in complex multicomponent aqueous salt systems.

Temperature control

Constant temperature control is essential during all the experimental procedures for solubility determination, not only during equilibration, but also during the sampling of saturated solution for analysis. The allowable limits of temperature variation depend on the system under investigation and the required precision of the solubility measurement. Much greater care has to be taken when the solubility changes appreciably with a change in temperature. In the determination of the solubility at 25 °C of, say, sodium chloride in water (*Figure 3.1a*), a variation of ± 0.1 °C in the experimental temperature would allow for a potential precision of less than 0.01 per cent in the solubility, but the same temperature variation would allow for more than 1 per cent in the case of sodium sulphate (*Figure 3.1b*). For most general purposes, a thermostat precision of better than ± 0.1 °C is normally adequate.

It is essential that any thermometers, thermocouples, thermistors, etc. used in the thermostat bath and equilibrium cell are accurately calibrated with reference to a standard thermometer. This point cannot be emphasized too strongly.

Agitation of solutions

Agitation is generally necessary to bring liquid and solid phases into intimate contact and facilitate equilibration. Agitation with a stirrer in an open vessel is not normally recommended, on account of the potential loss of solvent by evaporation, but sealed-agitated vessels are commonly used. Agitation in tightly stoppered vessels, that are rocked, rotated or shaken whilst immersed in a thermostat bath, is also quite a popular method, particularly when many samples have to be tested at the same time.

Sampling

Once equilibrium has been attained, i.e. when the originally over- and under-saturated solutions are of equal composition, the mixture is allowed to stand for an hour or more, at the relevant constant temperature, to enable any finely dispersed solid particles to settle. The withdrawal of a sample of clear supernatant liquid for analysis can be effected in a number of ways, depending on the characteristics of the system. For example, a suitably warmed pipette, with the tip protected by a piece of cotton wool, glass wool or similar substance, is often quite adequate. The pipette may be warmed to the appropriate temperature by leaving it standing in a stoppered tube immersed in the thermostat bath. Alternatively, a variety of sintered glass filters can be utilized (*Figure 3.5*) (Nývlt, 1977). In all cases, several portions of solution should first be withdrawn and discarded to satisfy any possible capacity of the filter to adsorb solute from the saturated solution (Vold and Vold, 1949). The sample of saturated solution may then be analysed by any convenient technique (section 3.9.2).

It is important to note that a weighed quantity, not a measured volume, of solution should be taken for analysis. Weighing should be carried out to ± 0.0005 g if possible, depending on the required precision.

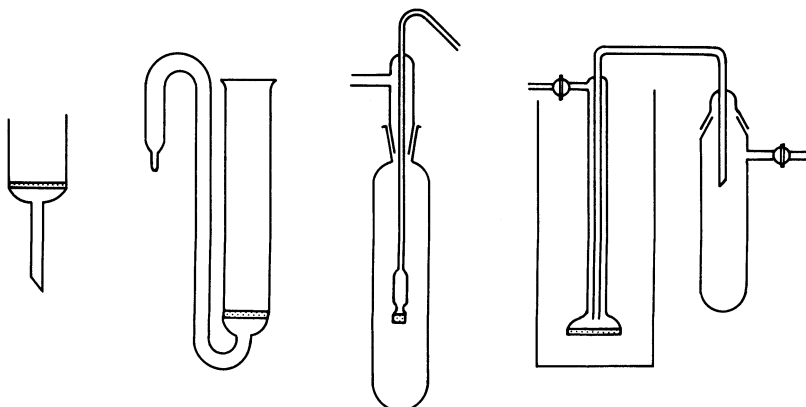


Figure 3.5. Some sintered glass filters for separating an equilibrium solid phase from a saturated solution. (After Nývlt, 1977)

Achievement of equilibrium

The achievement of equilibrium presents one of the major experimental difficulties in solubility determination. Prolonged agitated contact is required between excess solid solute and solution at a constant temperature, usually for several hours. In some cases, however, contact for days or even weeks may be necessary. Viscous solutions and systems at relatively low temperatures often require long contact times and so do substances of low solubility.

A check should always be made, if possible, on the accuracy of a solubility determination at a given temperature, by approaching equilibrium from both the under-saturated and over-saturated states. In the first method a quantity of solid, in excess of the amount required to saturate the solvent at the given temperature, is added to the solvent and the two are agitated until apparent equilibrium is reached, i.e. when the solution attains a constant composition. In the second method the same quantities of solute and solvent are mixed, but the system is then heated for about 20 minutes above the required temperature, if the solubility increases with temperature, so that most but not all of the solid is dissolved. The solution is then cooled and agitated for a long period at the given temperature while the excess solid is deposited and an apparent equilibrium is reached. If the two solubility determinations agree, it can be reasonably assumed that the result represents the true equilibrium saturation concentration at the given temperature. If they do not, more time has to be allowed. This important point always has to be borne in mind when solubility measurements have to be made in solutions containing impurities (section 3.8).

Unless solubility data for specific industrial substances are required, both the solute and solvent should be of the highest purity possible. The solute particles should be reasonably small to facilitate rapid dissolution, but not too small that the excess particles will not settle readily in the saturated solution. Settling is generally desirable to allow solid and liquid phase samples to be taken, after equilibration, for separate analysis. In practice, a close-sieved crystal fraction in the 100–300 µm size range is generally suitable for most purposes.

3.9.1 Solution and solid phase analysis

Tremendous advances have been made in the past few decades in both the range and sensitivity of the analytical methods now available. For the purpose of solubility measurement, solution compositions can be measured by any convenient analytical technique, among which may be listed: liquid chromatography (HPLC), spectroscopy (UV, IR, NMR and mass), differential scanning calorimetry (DSC), differential thermal analysis (DTA), thermogravimetric analysis (TGA), refractometry, polarimetry, and most recently capillary electrophoresis (Altria, 2000).

For the identification of crystalline polymorphs, IR spectroscopy and X-ray diffraction are the most commonly used techniques, while a combination of DSC–TGA or DTA–TGA are useful for analysing solvates.

Descriptions of these techniques will be found in most handbooks of chemical and physical analysis (e.g. Findlay, 1973; Matthews, 1985). Comprehensive

accounts of modern instrumental methods of analysis is given by Willard, Merritt, Dean and Settle (1988) and Ewing (1997).

When the dissolved substance is stable to heat, the mass present in a known mass of solution may often be determined by gentle evaporation to dryness, followed by heating to constant mass in an air oven at around 100 °C. Great care must be taken in this procedure to avoid solids loss by spattering. Another problem is that of solution creeping up the sides of the evaporating dish and over the edge. Gentle evaporation on a water bath may be used with aqueous solutions, covering the evaporating dish with a large funnel to prevent dust contamination.

For substances that are not stable on heating to dryness, e.g. hydrates, their concentration in solution may be determined in some cases by chemical analysis and in others by measuring some concentration-dependent physical property. The latter is often convenient when a large number of determinations have to be made. Solution density and refractive index are probably the two properties most commonly measured for this purpose and the many well-established techniques available are fully described in standard textbooks of practical physical chemistry.

In all cases, however, it is necessary to prepare a calibration chart. The first step, therefore, is to make up a series of solutions of known strength and measure the physical property in question for these solutions. This may be done for a range of temperatures, so that a series of calibration curves can be constructed. The composition of an unknown solution may then be determined by measuring the property in question at a given temperature, usually a few degrees above the saturation temperature to avoid the possibility of crystallization. Alternatively, a weighed quantity of the unknown solution is diluted with a known mass of solvent before measurement.

It is always advisable, incidentally, to measure the density of a saturated solution at the same time that the equilibrium saturation concentration is being measured, for the simple practical reason that density is the mass–volume conversion factor, and this quantity is frequently required in process calculations. Söhnel and Novotný (1985) have published an extensive compilation of concentration–density data for aqueous solutions of inorganic salts.

The final step that has to be taken in a solubility determination, in order to complete the information, is to determine the composition of the solid phase that was in equilibrium with the solution at the given temperature, remembering that the stable phase can change appreciably over quite a short range of temperature, especially in hydrated systems. For example, in the determination of the solubility of sodium carbonate in water over the temperature range 10–50 °C, it would be found that the stable solid phase is $\text{Na}_2\text{CO}_3 \cdot 10\text{H}_2\text{O}$ up to 32.0 °C, $\text{Na}_2\text{CO}_3 \cdot 7\text{H}_2\text{O}$ between 32.0 and 35.4 °C and $\text{Na}_2\text{CO}_3 \cdot \text{H}_2\text{O}$ above 35.4 °C.

A sample of the equilibrium solid phase may be separated from its saturated solution by means of sintered glass filters like those depicted in *Figure 3.5*. It is necessary to ensure that the separation is made at the appropriate temperature, e.g. by carrying out the operation with the filter immersed in the thermostat bath itself. No matter how efficiently the filtration is made, however, the

recovered solid particles will always be wet with adhering mother liquor and this must be accounted for in any subsequent analysis. First, it is essential to separate the wet solid sample as quickly as possible and transfer it immediately to a weighing bottle which can be closed to minimize loss of solvent.

For simple binary systems, i.e. one solute and one solvent, correction for adhering mother liquor may be made in the following manner. The damp solid is weighed (mass m_1) and then dried to constant mass, m_2 , at an appropriate temperature, taking care to avoid decomposition, dehydration of hydrates, etc. The amount of solvent present in the mother liquor, s (e.g. grams of solvent per gram of solution) is determined from the saturated solution analysis described above. The mass of mother liquor, m_3 , originally retained in the damp solid sample may then be calculated from

$$m_3 = (m_1 - m_2)/s \quad (3.64)$$

The actual composition of the equilibrium solid phase may then be calculated from a simple mass balance, using the respective compositions of the damp solid and the equilibrium mother liquor.

For multi-component systems the composition of the equilibrium solid phase may be determined indirectly by the so-called ‘wet residues’ method first proposed by Schreinemakers (1893) in which the need for solid–liquid separation by filtration, etc. is avoided. The experimental procedures, together with those of the alternative ‘synthetic complex’ method, are fully described in section 4.6.5.

3.9.2 Measurement techniques

The so-called ‘synthesis’ methods of solubility determination involve the preparation of a solvent–solute mixture of known composition, initially containing excess solute. The complete dissolution of the solid phase is then observed, either when the mixture is subjected to slow controlled heating (the ‘polythermal’ methods) or at constant temperature when small quantities of fresh solvent are sequentially added over a period of time (the ‘isothermal’ methods). The disappearance of the solid phase can be observed visually or monitored by recording some appropriate physical or physicochemical property of the system.

Polythermal methods

Solute and solvent are weighed into a small (50–100 mL) glass vessel in proportions corresponding approximately to the composition of a saturated solution in the middle of the proposed operating temperature range. The objective is to have some solid phase in excess at the lowest temperature used and all in solution at the highest.

The closed vessel is fitted with a calibrated thermometer graduated in increments of 0.1 °C and a suitable stirrer, and the contents are heated gently until all the crystals have been dissolved. The clear solution is first cooled until it is nucleated. Then, under controlled conditions, the temperature is increased

slowly ($\sim 0.2^\circ\text{C}/\text{min}$) until the last crystal dissolves. At this point the equilibrium saturation temperature θ^* has been achieved. Repeat runs will enable θ^* for a given solution composition to be determined with a precision of $\pm 0.1^\circ\text{C}$ for solutions with a moderate to high temperature coefficient of solubility (section 3.2).

An apparatus in which the controlled heating and cooling sequences demanded in the above technique is depicted in *Figure 5.9* and described in section 5.3. Determination of the instant at which all the crystals have finally dissolved in a solution is most commonly made by visual observation. In principle, however, the monitoring of any concentration-sensitive physical or physicochemical property (refractive index, conductivity, density, vapour pressure, particle size distribution, etc.) can offer alternative procedures.

Nývlt (1977), for example, has described how refractive index measurements may be used for this purpose, where the sequence of events is as drawn in *Figure 3.6a*. As the solution containing suspended crystals is heated, the refractive index of the solution increases as the crystals dissolve. At point A the last crystal dissolves, at the equilibrium saturation temperature θ^* . Further increases in temperature lead to a slow decrease in refractive index. The reverse curve traces the cooling sequence, with nucleation occurring at point B, when the refractive index suddenly falls to point C and subsequently follows the equilibrium saturation curve. The corresponding solution composition-temperature graph is also included in *Figure 3.6b*. The refractive index may be monitored with a dipping-type refractometer.

The property of refractive index may be utilized in another way. A novel technique was devised by Dauncy and Still (1952) for the direct and rapid measurement of solution saturation temperatures. This method is based on an optical effect caused by the slight change in concentration, and therefore in refractive index, occurring in a layer of solution immediately in contact with a crystal that is either growing or dissolving.

The saturation cell is a small Perspex container fitted with a stirrer (alternatively, the solution may be passed continuously through the cell), a calibrated

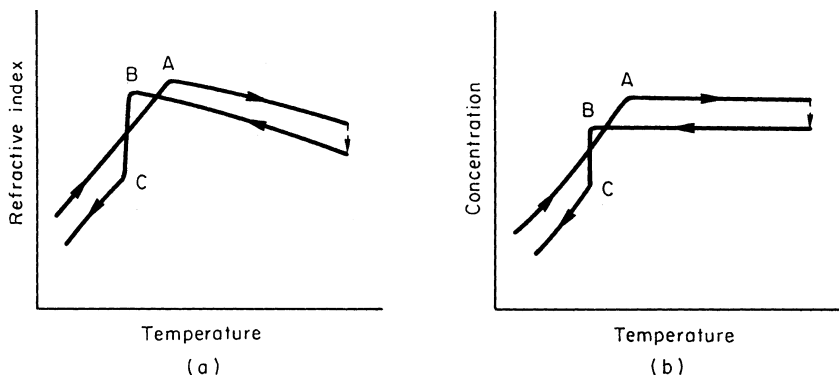


Figure 3.6. Refractive index (a) and composition (b) changes during solubility measurement by the polythermal method. (After Nývlt, 1977)

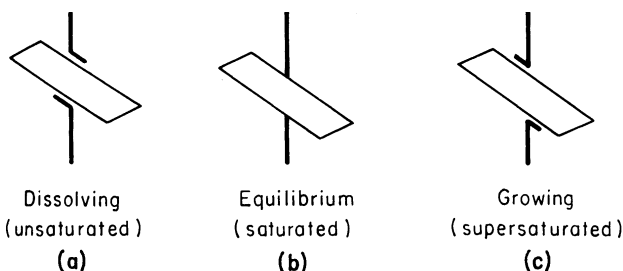


Figure 3.7. *An optical method of solubility measurement*

thermometer and a holder for a medium-sized crystal. The cell is placed in a thermostatically-controlled water bath also made of Perspex. A beam of light from an optical slit is directed on to an edge of the crystal, and the appearance of the slit when viewed from behind the crystal will take the form of one of the three sketches shown in *Figure 3.7*. The light is bent into an obtuse angle when the solution is unsaturated (*a*), and into an acute angle when it is supersaturated (*c*). As soon as it is determined that the solution near the crystal face is unsaturated or supersaturated, the temperature is raised or lowered until view (*b*) is obtained. The temperature at this point is the equilibrium saturation temperature. It was reported that, with ethylenediamine hydrogen tartrate and ammonium dihydrogen phosphate, points on the respective solubility curves could be plotted at the rate of 8–10 per hour. Wise and Nicholson (1955) adapted the method and applied it successfully in the determination of sucrose solubilities.

Isothermal methods

The disappearance of the solid phase in a solubility cell can be observed under isothermal conditions while adding small portions of fresh solvent to a solution–suspension of known composition. Mullin and Šipek (1982) have described one use of this technique for solubility measurements in the three-phase system potash-alum–water–ethanol.

The apparatus used for the solubility determinations (*Figure 3.8*) was a small glass vessel (~50 mL) fitted with a four-blade glass stirrer with a glycerol shaft seal. The cell was immersed in a thermostat water bath controlled to $\pm 0.02^\circ\text{C}$. Weighed quantities of potash alum and alcohol, together with predetermined amounts of water, were charged to the cell and agitated for ~1 h. At the end of this time, as predicted, only a small amount of crystalline material was left undissolved. Small quantities of water (starting with 1 mL and reducing) were then added to the mixture at hourly intervals until all traces of crystalline material (observed under a strong back-light) had disappeared. Towards the end-point, water was added dropwise. This method, when carefully performed, could reproducibly determine the solubility to a precision of at least $\pm 0.5\%$.

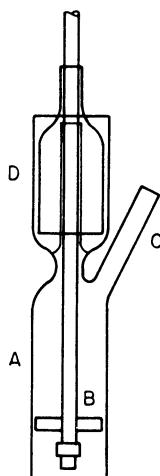


Figure 3.8. Solubility apparatus: (a) 50 mL glass cell; (b) four-bladed glass stirrer; (c) charging port; (d) glycerol seal for stirrer shaft. (After Mullin and Šipek, 1982)

Measurement under pressure

An equilibrium cell for use under pressure is described by Brosheer and Anderson (1946). Although originally devised specifically for solubility measurements of monoammonium and diammonium phosphates in the system $\text{NH}_3\text{--H}_2\text{O--H}_3\text{PO}_4$, it is clearly of more general applicability. For a detailed account of this method, reference should be made to the original paper. A simple apparatus for the measurement of solubility under pressure was earlier described by Gibson (1934) who also made an interesting analysis of the pressure effect and demonstrated the possibility of estimating the solubility of certain salts in water under pressures up to 10 kbar using data obtained at lower pressures.

Thermal and dilatometric methods

A phase reaction is generally accompanied by significant enthalpy and volume changes. The detection and quantification of these effects form the basis of several useful methods for determining solubilities and phase equilibria. Some of these techniques are discussed in section 4.5.

Sparingly soluble salts

The solubility of sparingly soluble electrolytes in water, with the exception of the salts of weak acids or bases, may be determined from conductivity measurements on their saturated solutions. A variety of commercial instruments are now available for this purpose and experimental details may be found in handbooks of practical physical chemistry, e.g. Findlay, 1973; Matthews, 1985.

If the equilibrium saturation concentration, c^* , of the salt is expressed in mol m^{-3} , the molar conductivity, Λ , ($\text{S m}^2 \text{ mol}^{-1}$) of the solution may be expressed (see equation 3.45) as

$$\Lambda = \kappa/c^* \quad (3.65)$$

where κ is the conductivity (S m^{-1}). Even a saturated solution of sparingly soluble salt is still very dilute, so it may be assumed that $\Lambda \simeq \Lambda_0$ where Λ_0 is the molar conductivity at infinite dilution. If, therefore, the value of Λ_0 is known, or can be calculated since it is the sum of the ionic conductivities (equation 3.46), the saturation concentration of salt may be calculated from

$$c^* = \kappa/\Lambda_0 \quad (3.66)$$

where κ is the measured conductivity of the saturated solution.

For example, the conductivity of a saturated solution of barium sulphate in water at 25°C has been experimentally determined as $1.66 \times 10^{-4} \text{ S m}^{-1}$. If the conductivity of the water used in the determination ($2.5 \times 10^{-5} \text{ S m}^{-1}$) is deducted from the measured solution conductivity, the value attributable to BaSO_4 is $\kappa = 1.41 \times 10^{-4} \text{ S m}^{-1}$. From *Table 3.2*, the relevant molar ionic conductivities at 25°C at infinite dilution are $\Lambda_{1/2\text{Ba}^{2+}} = 63.6 \times 10^{-4} \text{ S m}^2 \text{ mol}^{-1}$ and $\Lambda_{1/2\text{SO}_4^{2-}} = 78.8 \times 10^{-4} \text{ S m}^2 \text{ mol}^{-1}$ giving $\Lambda_0 = 143.4 \times 10^{-4} \text{ S m}^2 \text{ mol}^{-1}$. From equation 3.66,

$$\begin{aligned} c^* &= 1.41 \times 10^{-4} / 143.4 \times 10^{-4} \\ &= 9.83 \times 10^{-3} \text{ mol m}^{-3} \\ &= 9.83 \times 10^{-6} \text{ mol L}^{-1} \end{aligned}$$

The corresponding solubility product K_c may be calculated from equation 3.49 (since BaSO_4 is a 2–2 electrolyte), i.e.

$$K_c = (c^*)^2 = 9.66 \times 10^{-11} \text{ mol}^2 \text{ L}^{-2}$$

3.10 Prediction of solubility

A measured value of solubility, even when roughly determined, generally gives more confidence than an estimated one. Accurate solubility measurements, however, demand laboratory facilities and experimental skills (section 3.9) and can be very time-consuming on account of the need to achieve equilibrium and the fact that large numbers of individual measurements may be necessary to cover adequately all the ranges of variables. There will always be a need, therefore, for methods of solubility prediction that can avoid these difficulties, but it has to be pointed out that in employing such methods some other more serious problems may well be incurred in return. A good number of solubility correlation and prediction methods are available ranging from simple techniques of interpolation and extrapolation to some quite complex procedures, based on thermodynamic reasoning, that have considerable computational requirements.

The success of any given method can vary enormously from system to system. Some can only be used for rough assessment while others can occasionally yield data of comparable precision to those attained by careful experimental measurement. Each system must be considered independently.

For binary solutions (one solute, one solvent) data correlations of the type indicated by equations 3.4 and 3.9 are commonly used for predicting, by interpolation, values that were not otherwise measured. If the correlating equation is based on adequate data, interpolation can be carried out with reasonable confidence (e.g. see *Figure 3.2*). Extrapolation, on the other hand, is generally inadvisable and should never be attempted if there is any suspicion that a phase change is possible in the unknown region.

Prediction methods using theoretical relationships based on the assumption of solution ideality can be very unreliable, as shown by the example in section 3.6 which indicates that an assumption of ideality for the ‘simple’ case of naphthalene dissolved in an organic solvent can result in an error of up to 200% in estimating the solubility.

The number of solubility measurements necessary for the construction of a multicomponent phase diagram increases enormously as the number of components is increased. It is in this area, therefore, that the demand for prediction method most often lies. The methods range from the entirely empirical, generally based on geometrical concepts, to the semi-theoretical, i.e. partly based on thermodynamic descriptions. A comprehensive account of some of these methods, together with several detailed worked examples, is given by Nývlt (1977).

Several thermodynamic approaches have been made to the problem of solubility predictions in multicomponent aqueous salt solutions over the past 30 years or so, with varying degrees of success. Most methods are based to some extent on modified Debye–Hückel equations (section 3.6.1) and require the prediction of activity coefficients, enthalpies and entropies of solution, and specific heat capacities. Within the confines of this chapter, however, it is not possible to give more than a flavour of the relevant literature in this area.

For example, Marshall and Slusher (1966) made a detailed evaluation of the solubility of calcium sulphate in aqueous sodium chloride solution, and suggested that variations in the ion solubility product could be described, for ionic strengths up to around 2 M at temperatures from 0 to 100 °C, by adding another term in an extended Debye–Hückel expression. Above 2 M and below 25 °C, however, further correction factors had to be applied, the abnormal behaviour being attributed to an increase in the complexity of the structure of water under these circumstances. Enthalpies and entropies of solution and specific heat capacity were also reported as functions of ionic strength and temperature.

A thermodynamic model developed by Barba, Brandani and di Giacomo (1982) described the solubility of calcium sulphate in saline water. A system of equations based on Debye–Hückel and other models was used to describe isothermal activity coefficients of partially or completely dissociated electrolytes. Using binary parameters, good agreement was claimed between experimental and predicted values of calcium sulphate solubility in sea water and brackish brines including those with a magnesium content.

The solubilities of the scale-forming salts barium and strontium sulphates in aqueous solutions of sodium chloride have been reviewed by Raju and Atkinson (1988, 1989). Equations were proposed for the prediction of specific heat capacity, enthalpy and entropy of dissolution, etc., for all the species in the solubility equilibrium, and the major thermodynamic quantities and equilibrium constraints expressed as a function of temperature. Activity coefficients were calculated for given temperatures and NaCl concentrations and a computer program was used to predict the solubility of BaSO₄ up to 300 °C and SrSO₄ up to 125 °C.

A group contribution method called UNIFAC, an acronym which stands for the UNIQUAC Functional Group Activity Coefficient (UNIQUAC stands for the Universal Quasi-chemical Activity Coefficient), has been developed for estimating liquid-phase activity coefficients in non-electrolyte mixtures. The UNIFAC method is fully described by Fredenslund, Jones and Prausnitz (1975) and Skold-Jorgensen, Rasmussen and Fredenslund (1982).

To estimate the solubility of an organic solid solute in a solvent it is only necessary to know its melting point, enthalpy of fusion and relevant activity coefficient. Gmehling, Anderson and Prausnitz (1978) have shown that this activity coefficient can be estimated by the UNIFAC group contribution method, and they report a number of cases where the solubilities of a variety of organic solids in single and mixed solvents are accurately predicted. Even eutectic temperatures and compositions may be estimated for some binary systems.

Gupta and Heidemann (1990) used a modified UNIFAC model to predict the effects of temperature and pH on the solubility of amino acids in water. They also made a similar approach to the modelling of the solubility of several antibiotic substances in mixed non-aqueous solvents. Macedo, Skovborg and Rasmussen (1990) used a modified UNIFAC model to calculate phase equilibria for aqueous solutions of strong electrolytes.

As explained in section 3.6.1, many modifications have been proposed for the Debye-Hückel relationship for estimating the mean ionic activity coefficient γ_{\pm} of an electrolyte in solution and the Davies equation (equation 3.35) was identified as one of the most reliable for concentrations up to about 0.2 molar. More complex modifications of the Debye-Hückel equation (Robinson and Stokes, 1970) can greatly extend the range of γ_{\pm} estimation, and the Bromley (1973) equation appears to be effective up to about 6 molar. The difficulty with all these extended equations, however, is the need for a large number of interacting parameters to be taken into account for which reliable data are not always available.

A more simple, but purely empirical, approach to the estimation of γ_{\pm} was suggested by Meissner and Tester (1972) who claimed applicability up to saturation or 20 molar. They noted that for over a 100 electrolytes a plot of a 'reduced' activity coefficient versus the ionic strength, I, formed a family of non-intersecting curves. They proposed methods of interpolation and extrapolation working from the basis of at least one known value of γ_{\pm} for a concentrated solution of the chosen electrolyte. A survey of the use of this method, and its subsequent development for computer-assisted calculations (Meissner and

Manning, 1983), has been made by Demopoulos, Kondos and Papangelakis (1988).

Vega and Funk (1974) presented a thermodynamic correlation for solid–liquid equilibria in concentrated aqueous salt solutions and applied the correlation to the six-component system containing Na^+ , K^+ , Mg^{2+} , NO_3^- , SO_4^{2-} from 0 to 50 °C. In their correlation they define an activity coefficient as if the given salt were a non-electrolyte, although this new quantity is easily related to the mean ionic activity coefficient γ_{\pm} . The derived parameters are claimed to enable correlation of equilibria for ternary and quaternary systems with errors in liquid phase composition of less than 2 g salt per 100 g water.

3.11 Solubility data sources

The main primary sources of solid–liquid solubility data, i.e. those which report experimental measurements together with the full literature source references, are those of Stephen and Stephen (1963), Seidell (1958) and the continuing multivolume IUPAC Solubility Data Series (1980–91) which by the end of 1991 had reached its 48th volume. The series covers gas–liquid, liquid–liquid and solid–liquid equilibria, but up to the present time fewer than one quarter of the published volumes are devoted to solid–liquid systems. In all these publications, ternary as well as binary data are reported and solvents other than water are considered. Blasdale (1927) and Teeple (1929) give extensive data on equilibria in aqueous salt solutions relevant to natural brines and natural salt deposits, ranging from binary to quinary complex systems. The compilation by Wisniak and Herskowitz (1984) is an excellent literature source reference, but no actual data are recorded.

Among the secondary sources of data available, i.e. summaries assembled from several sources, sometimes ‘smoothed’, include the compilations of Nývlt (1977), and Broul, Nývlt and Söhnel (1981) and Appendices A4 and A5 in this book.

3.12 Supersolubility

A saturated solution is in thermodynamic equilibrium with the solid phase, at a specified temperature. It is often easy, however, e.g. by cooling a hot concentrated solution slowly without agitation, to prepare solutions containing more dissolved solid than that represented by equilibrium saturation. Such solutions are said to be supersaturated.

The state of supersaturation is an essential requirement for all crystallization operations. Ostwald (1897) first introduced the terms ‘labile’ and ‘metastable’ supersaturation to classify supersaturated solutions in which spontaneous (primary) nucleation (see section 5.1) would or would not occur, respectively. The work of Miers and Isaac (1906, 1907) on the relationship between supersaturation and spontaneous crystallization led to a diagrammatic representation of the metastable zone on a solubility–supersolubility diagram (*Figure 3.9*). The

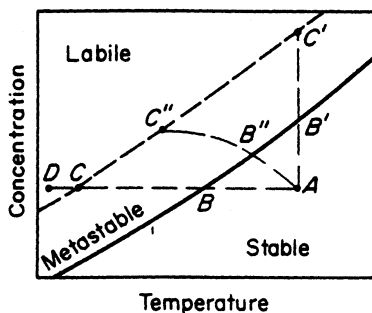


Figure 3.9. The solubility–supersolubility diagram

lower continuous solubility curve, determined by one of the appropriate techniques described in section 3.9, can be located with precision. The upper broken supersolubility curve, which represents temperatures and concentrations at which uncontrolled spontaneous crystallization occurs, is not as well defined as that of the solubility curve. Its position in the diagram is considerably affected by, amongst other things, the rate at which supersaturation is generated, the intensity of agitation, the presence of trace impurities and the thermal history of the solution (sections 5.3 and 5.4).

In spite of the fact that the supersolubility curve is ill-defined, there is no doubt that a region of metastability exists in the supersaturated region above the solubility curve. The diagram is therefore divided into three zones, one well-defined and the other two variable to some degree:

1. The stable (unsaturated) zone, where crystallization is impossible.
2. The metastable (supersaturated) zone, between the solubility and supersolubility curves, where spontaneous crystallization is improbable. However, if a crystal seed were placed in such a metastable solution, growth would occur on it.
3. The unstable or labile (supersaturated) zone, where spontaneous crystallization is probable, but not inevitable.

If a solution represented by point *A* in *Figure 3.9* is cooled without loss of solvent (line *ABC*), spontaneous crystallization cannot occur until conditions represented by point *C* are reached. At this point, crystallization may be spontaneous or it may be induced by seeding, agitation or mechanical shock. Further cooling to some point *D* may be necessary before crystallization can be induced, especially with very soluble substances such as sodium thiosulphate. Although the tendency to crystallize increases once the labile zone is penetrated, the solution may have become so highly viscous as to prevent crystallization and could even set to a glass.

Supersaturation can also be achieved by removing some of the solvent from the solution by evaporation. Line *AB'C'* represents such an operation carried out at constant temperature. Penetration beyond the supersolubility curve into the labile zone rarely happens, as the surface from which evaporation takes place is usually supersaturated to a greater degree than the bulk of the solution.

Crystals which appear on this surface eventually fall into the solution and seed it, often before conditions represented by point C' are reached in the bulk of the solution. In practice, a combination of cooling and evaporation is employed, and such an operation is represented by the line $AB''C''$ in *Figure 3.9*.

Experimental techniques for determining the metastable zone width, the amount of undercooling that a solution will tolerate before nucleating, are described in section 5.3. The significance of the metastable zone and the interpretation of metastable zone width measurements are somewhat contentious subjects. Experimental values depend very strongly on the method of detection of the onset of nucleation, but it is still possible to extract kinetic information on the nucleation process as well as on the growth behaviour of very small crystals. These topics are discussed in some detail in section 5.3.

3.12.1 Expressions of supersaturation

The supersaturation, or supercooling, of a system may be expressed in a number of different ways, and considerable confusion can be caused if the basic units of concentration are not clearly defined. The temperature must also be specified.

Among the most common expressions of supersaturation are the concentration driving force, Δc , the supersaturation ratio, S , and a quantity sometimes referred to as the absolute or relative supersaturation, σ , or percentage supersaturation, 100σ . These quantities are defined by

$$\Delta c = c - c^* \quad (3.67)$$

$$S = \frac{c}{c^*} \quad (3.68)$$

$$\sigma = \frac{\Delta c}{c^*} = S - 1 \quad (3.69)$$

where c is the solution concentration, and c^* is the equilibrium saturation at the given temperature.

The term supercooling, defined by

$$\Delta\theta = \theta^* - \theta \quad (3.70)$$

is occasionally used as an alternative to the supersaturation, Δc , the two quantities being related through the local slope of the solubility curve, $dc^*/d\theta$, by

$$\Delta c = (dc^*/d\theta)\Delta\theta \quad (3.71)$$

Of the above three expressions for supersaturation (equations 3.67 to 3.69) only Δc is dimensional, unless the solution composition is expressed in mole fractions or mass fractions. The magnitudes of these quantities depend on the units used to express concentration, as the following examples show.

Example 1

Potassium sulphate (mol. mass = 174) at 20 °C. The equilibrium saturation $c^* = 109 \text{ g}$ of $\text{K}_2\text{SO}_4/\text{kg}$ of water, which gives a solution density of 1080 kg m^{-3} .

Let the concentration of a supersaturated solution $c = 116 \text{ g/kg}$, giving a solution density of 1090 kg m^{-3} at 20 °C. Then the following quantities may be calculated:

Solution composition	c	c^*	Δc	S	σ
g/kg water	116	109	7.0	1.06	0.06
g/kg solution	104	98.3	5.7	1.06	0.06
g/L solution ($= \text{kg m}^{-3}$)	113.3	106.1	7.2	1.07	0.07
mol/L solution ($= \text{kmol m}^{-3}$)	0.650	0.608	0.042	1.07	0.07
mol fraction of K_2SO_4	0.0119	0.0112	0.0007	1.06	0.06

It is essential to quote the temperature when expressing the supersaturation of a system, since the equilibrium saturation concentration is temperature dependent. In the above case of potassium sulphate, for example, $S = 1.06$ means a concentration driving force $\Delta c = 7 \text{ g/kg}$ of water at 20 °C and 13 g/kg at 80 °C.

The quantity that changes most in example 1 is Δc ; neither S nor σ is very greatly affected. However, with very soluble substances considerable changes can occur in all expressions of supersaturation depending on the concentration units used, as seen in example 2 where σ varies from 0.08 to 0.20.

Example 2

Sucrose (mol. mass = 342) at 20 °C, $c^* = 2040 \text{ g/kg}$ of water (solution density = 1330 kg m^{-3}). Let $c = 2450 \text{ g/kg}$ of water (density = 1360 kg m^{-3}). Thus:

Solution composition	c	c^*	Δc	S	σ
g/kg water	2450	2040	410	1.20	0.20
g/kg solution	710	671	39	1.06	0.06
g/L solution ($= \text{kg m}^{-3}$)	966	893	73	1.08	0.08
mol/L solution ($= \text{kmol m}^{-3}$)	2.82	2.61	0.21	1.08	0.08
mole fraction of sucrose	0.114	0.097	0.017	1.18	0.18

The situation becomes even more confused than that hinted at in examples 1 and 2 if the substance crystallizes as a hydrate, because in these cases solution compositions can be expressed in terms of the hydrate or the anhydrate, thus further increasing the number of possible definitions of supersaturation.

Interconversion of solution composition units, as discussed in section 3.3, is facilitated by the formulae listed in *Table 3.1*. Interconversion of solution supersaturation values, based on seven different solution composition units, is facilitated by the formulae listed in *Table 3.3* (Mullin, 1973). It should be clearly

Table 3.3. Conversion factors for supersaturation units (Mullin, 1973)

Super-saturation	Equivalent expressions						
S_1	$\frac{C_1}{C_1^*}$	$S_2 \left(\frac{1 - C_2^*}{1 - C_2} \right)$	$S_3 \left(\frac{R - C_3^*}{R - C_3} \right)$	$S_4 \left[\frac{R + C_4^*(R - 1)}{R + C_4(R - 1)} \right]$	$S_5 \left(\frac{\rho^* - C_5^*}{\rho - C_5} \right)$	$S_6 \left(\frac{\rho^* R - C_6^*}{\rho R - C_6} \right)$	$S_7 \left(\frac{\rho^* - M_A C_7^*}{\rho - M_A C_7} \right)$
S_2	$S_1 \left(\frac{1 + C_1^*}{1 + C_1} \right)$	$\frac{C_2}{C_2^*}$	S_3	$S_4 \left(\frac{1 + C_4^*}{1 + C_4} \right)$	$\frac{S_5}{r}$	$\frac{S_6}{r}$	$\frac{S_7}{r}$
S_4	$S_1 \left[\frac{1 - C_1^*(R - 1)}{1 - C_1(R - 1)} \right]$	$S_2 \left(\frac{1 - RC_3^*}{1 - RC_3} \right)$	$S_3 \left(\frac{1 - C_3^*}{1 - C_3} \right)$	$\frac{C_4}{C_4^*}$	$S_5 \left(\frac{\rho^* - RC_5^*}{\rho - RC_5} \right)$	$S_6 \left(\frac{\rho^* R - C_6^*}{\rho R - C_6} \right)$	$S_7 \left(\frac{\rho^* - M_A C_7^*}{\rho - M_A C_7} \right)$
S_5	$rS_1 \left(\frac{1 + C_1^*}{1 + C_1} \right)$	rS_2	rS_3	$rS_4 \left(\frac{1 + C_4^*}{1 + C_4} \right)$	$\frac{C_5}{C_5^*}$	S_6	S_7

C_1 = kg of anhydrous substance/kg of water

C_2 = kg of anhydrous substance/kg of solution

C_3 = kg of hydrate/kg of solution

C_4 = kg of hydrate/kg of 'free' water

C_5 = kg of anhydrous substance/m³ of solution

C_6 = kg of hydrate/m³ of solution

C_7 = kmol of anhydrous substance/m³ of solution

M_A = molar mass of anhydrous substance

M_H = molar mass of hydrate

M_W = molar mass of water

$R = M_H/M_A$

ρ = density of supersaturated solution (kg/m³)

ρ^* = density of saturated solution (kg/m³)

$r = \rho/\rho^*$

Note: $S_3 = \frac{C_3}{C_3^*} = S_2$ and $S_6 = \frac{C_6}{C_6^*} = S_7 = \frac{C_7}{C_7^*} = S_5$

appreciated, however, that none of these different supersaturations coincides exactly with the true thermodynamic supersaturation.

The fundamental driving force for crystallization is the difference between the chemical potential of the given substance in the transferring and transferred states, e.g. in solution (state 1) and in the crystal (state 2). This may be written, for the case of an unsolvated solute crystallizing from a binary solution, as

$$\Delta\mu = \mu_1 - \mu_2 \quad (3.72)$$

The chemical potential, μ , is defined in terms of the standard potential, μ_0 , and the activity, a , by

$$\mu = \mu_0 + \mathbf{R}T \ln a \quad (3.73)$$

where \mathbf{R} is the gas constant and T is the absolute temperature.

The fundamental dimensionless driving force for crystallization may therefore be expressed as

$$\frac{\Delta\mu}{\mathbf{R}T} = \ln(a/a^*) = \ln S \quad (3.74)$$

where a^* is the activity of a saturated solution and S is the fundamental supersaturation, i.e.

$$S = \exp(\Delta\mu/\mathbf{R}T) \quad (3.75)$$

For electrolyte solutions it is more appropriate to use the mean ionic activity, a_{\pm} , defined by

$$a = a_{\pm}^{\nu} \quad (3.76)$$

where $\nu (= \nu_+ + \nu_-)$ is the number of moles of ions in 1 mole of solute (equation 3.30). Therefore,

$$\Delta\mu/\mathbf{R}T = \nu \ln S_a \quad (3.77)$$

where

$$S_a = a_{\pm}/a_{\pm}^* \quad (3.78)$$

Alternatively, the supersaturation may be expressed as

$$\sigma_a = S_a - 1 \quad (3.79)$$

and equation 3.77 as

$$\Delta\mu/\mathbf{R}T = \nu \ln(1 + \sigma_a) \quad (3.80)$$

For low supersaturations ($\sigma_a < 0.1$)

$$\Delta\mu/\mathbf{R}T \approx \nu\sigma_a \quad (3.81)$$

is a valid approximation.

However, for practical purposes, supersaturations are generally expressed directly in terms of solution concentrations, e.g.

$$S_c = \frac{c}{c^*}, \quad S_m = \frac{m}{m^*} \quad \text{and} \quad S_x = \frac{x}{x^*} \quad (3.82)$$

where c = molarity (mol/litre of solution), m = molality (mol/kg of solvent) and x = mole fraction. The asterisks denote equilibrium saturation.

The relationship between these concentration-based supersaturations and the fundamental (activity-based) supersaturation may be expressed through the relevant concentration-dependent activity coefficient ratio, $A = \gamma/\gamma^*$, i.e.

$$S_a = S_c A_c = S_m A_m = S_x A_x \quad (3.83)$$

where $A_c = \gamma_c/\gamma_c^*$, $A_m = \gamma_m/\gamma_m^*$ and $A_x = \gamma_x/\gamma_x^*$.

If the relevant activity coefficients can be evaluated, it is possible to establish how the different supersaturations differ from one another and, more importantly, from the fundamental supersaturation, S_a . The decisive factor is the activity coefficient ratio, A . The more it deviates from unity, the greater is the incurred inaccuracy. In general, when $A_m > 1$, m -based concentration units are preferred, but when $A_m < 1$, x - or c -based units are better than m -based. The choice between x - and c -based units in this case again depends on the activity coefficient ratio: if $A_x > A_c$, the x -based units are preferred and vice versa.

For example, the mean ionic activity coefficients (see section 3.6.2) for a saturated solution of KCl in water at 25 °C ($m^* = 4.761$ mol KCl/kg water) (Robinson and Stokes, 1970) are

$$\gamma_{\pm c}^* = 0.6938; \quad \gamma_{\pm m}^* = 0.5923; \quad \gamma_{\pm x}^* = 1.013$$

and those corresponding to a solution at the same temperature of concentration $m = 5.237$ mol KCl/kg water, i.e. of supersaturation $S_m = 1.1$ (Mullin and Söhnel, 1977) are

$$\gamma_{\pm c} = 0.7157; \quad \gamma_{\pm m} = 0.6019; \quad \gamma_{\pm x} = 1.030$$

The respective activity coefficient ratios ($A = \gamma/\gamma^*$) are, therefore,

$$A_c = 1.032; \quad A_m = 1.016; \quad A_x = 1.017$$

so from equation 3.83

$$S_c = 0.969 S_a; \quad S_m = 0.984 S_a; \quad S_x = 0.983 S_a$$

which indicates that in this case the supersaturation expressed on a molar basis is the least reliable.

In general, in the absence of any information on the activity coefficient ratio, preference should be given to supersaturations based on molal units because of their more practical utility compared with mole fractions and their temperature independence compared with molar units. In other words, a concentration scale based on mass of solvent is generally preferred to one based on volume of solution.

An extension of the above analysis to more complex cases (Söhnel and Mullin, 1978a) leads to the conclusion that the dimensionless driving force for crystallization of a hydrate should always be expressed in terms of the hydrate and not of the anhydrous salt, i.e.

$$(\Delta\mu/RT)_H = \nu \ln S_H A_H \quad (3.84)$$

where the solution concentrations and activity coefficients and their ratio A_H both relate to the hydrate. The difference between the hydrate (H) and anhydrous (A) quantities, $(\Delta\mu/RT)_H$ and $(\Delta\mu/RT)_A$, can be very considerable. When, for lack of information, the quantity A_H cannot be evaluated, the approximation

$$(\Delta\mu/RT)_H \approx \nu \ln S_H \quad (3.85)$$

may be used. No general rules have yet been derived about the preference for c -, m - or x -based concentration units for the expression of the supersaturation S_H in these cases, although the subject is further discussed by Söhnel and Garside (1992).

Sparingly soluble electrolytes

Supersaturations in aqueous solutions of sparingly soluble electrolytes are best expressed in terms of the solubility product, e.g.

$$S = (IAP/K_a)^{1/\nu} \quad (3.86)$$

where IAP is the ion activity product of the lattice ions in solution, K_a is the activity solubility product of the salt, i.e., the value of IAP at equilibrium as defined in section 3.6.4, and ν is the number of ions in a formula unit of the salt.

When applying equation 3.86 to express the level of supersaturation created before the onset of precipitation, it is important to recognize that the values of IAP and K_a used should be those appropriate to the conditions existing in the actual mother liquor at the completion of the precipitation reaction, and not to those relating to equilibria between the pure precipitate and pure solvent (water) which is the basis on which solubility products are normally listed, as in *Table A.3*.

A simple example of the magnitude of the error that can be incurred using the incorrect solubility values is demonstrated by the precipitation of BaSO_4 after mixing equal volumes of 1 molar aqueous solutions of BaCl_2 and H_2SO_4 at 10°C , thus producing an initial mixture containing 0.5 mol L^{-1} BaSO_4 and 1 mol L^{-1} HCl. The equilibrium solubility of BaSO_4 at 10°C in water is $8.56 \times 10^{-6} \text{ mol L}^{-1}$, but in aqueous 1 molar HCl it is $2.36 \times 10^{-4} \text{ mol L}^{-1}$. So the initial supersaturation (equation 3.68) of BaSO_4 with respect to water is $(0.5/8.56) \times 10^{-6} = 58400$, whereas that expressed, more correctly, with respect to solution in 1 molar HCl is $(0.5/2.36) \times 10^{-4} = 2120$ (Söhnel and Garside, 1992).

A further difficulty in establishing the correct supersaturation with some systems is the necessity to determine the extent of any ion association, complex formation and hydration in the supersaturated solution. For example, in system such as $\text{CaCO}_3\text{-H}_2\text{O}$, in addition to the presence of Ca^{2+} and CO_3^{2-} ions, others such as HCO_3^- and CaHCO_3^+ must also be taken into consideration. The

calcium phosphate systems show even greater complexity. Good examples of the iterative calculations necessary to identify the correct value of *IAP* to be employed in equation 3.86 are given by Nancollas and Gardner (1974) and Barone and Nancollas (1977).

Mixed salt systems

It is not easy to quantify precisely the supersaturation levels of given species generated in mixed salt systems or in solutions in which ion association occurs. Relationships such as equations 3.67–3.69 cannot be simply applied because of the difficulty of expressing the true reference condition of equilibrium saturation. It is first necessary to identify all the possible single species, ion pairs and solid–liquid phase equilibria that can occur in the system. The relevant thermodynamic association/dissociation constants (*K* values) must be known. The activity coefficients for the various ionic species must be calculated, e.g. by means of Debye–Hückel type equations (section 3.6.2). Equilibrium concentrations of all the possible species present are then evaluated by iterative procedures.

Examples of these complex computing procedures are given in several publications, e.g., for calcium carbonate (Wiechers, Sturrock and Marias, 1975), calcium phosphate (Barone and Nancollas, 1977), calcium oxalate (Nancollas and Gardner, 1974) and magnesium hydroxide (Liu and Nancollas, 1973), in a variety of electrolyte solutions.

3.12.2 Measurement of supersaturation

If the concentration of a solution can be measured at a given temperature, and the corresponding equilibrium saturation concentration is known, then it is a simple matter to calculate the supersaturation (equations 3.67–3.69). Just as there are many methods of measuring concentration (section 3.9.2) so there are also many ways of measuring supersaturation, but not all of these are readily applicable to industrial crystallization practice.

Solution concentration may be determined directly by analysis, or indirectly by measuring some property of the system that is a sensitive function of solute concentration. The properties most frequently chosen for this purpose are density and refractive index which can often be measured with high precision, especially if the actual measurement is made under carefully controlled conditions in the laboratory.

For the operation of a crystallizer under laboratory or pilot plant conditions the demand is usually for an *in situ* method, preferable one capable of continuous operation. In these circumstances problems may arise from the temperature dependence of the property being measured. Nevertheless, the above properties can be measured, more or less continuously, with sufficient accuracy for supersaturation determination.

The supersaturation of a concentrated solution may be determined from a knowledge of its boiling point elevation. Holven (1942) applied the principle of Dühring's rule (the boiling point of a solution is a linear function of the boiling point of the pure solvent at the same pressure) to sucrose solutions over the

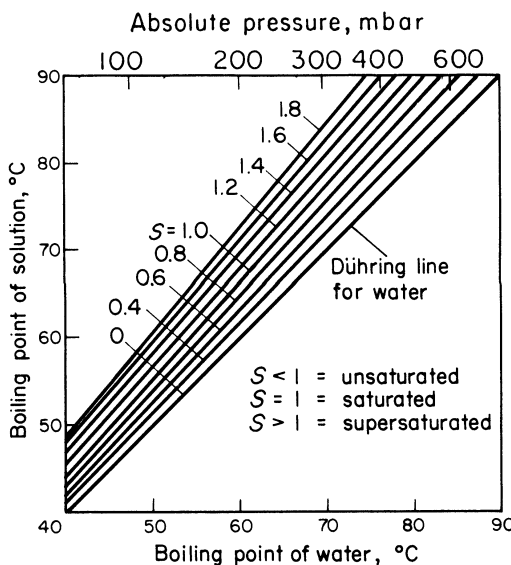


Figure 3.10. Dühring-type plot showing constant supersaturation lines (range $S = 0$ to 1.8) for aqueous solutions of sucrose. (After Holven, 1942)

range of pressures normally encountered in sugar boiling practice (Figure 3.10) and developed an automatic method for recording and controlling the degree of supersaturation in sugar crystallizers.

3.13 Solution structure

Water is a unique liquid. It is also the most abundant compound on earth ($\sim 10^{21}$ kg in the oceans with perhaps a similar quantity bound up as water of crystallization in rocks and minerals) and it is an essential constituent of all living organisms. Its unusual properties, such as a high boiling point compared with its related hydrides, a high thermal conductivity, dielectric constant and surface tension, a low enthalpy of fusion, the phenomenon of maximum density (at 4°C), etc., are usually explained by assuming that liquid water has a structure.

It is not possible at the present time to decide conclusively between the various structural models that have been proposed, but there is no doubt that liquid water does retain a loose local structure for short periods maintained by hydrogen bonds disposed tetrahedrally around each oxygen atom. Hydrogen bonded clusters readily form, but their lifetime is short (probably $\sim 10^{-11}$ s); and the name ‘flickering clusters’ is particularly apt.

The presence of a solute in water alters the liquid properties profoundly. In aqueous solutions of electrolytes, for example, the coulombic forces exerted by the ions lead to a local disruption of the hydrogen bonded structure. Each ion is surrounded by dipole orientated water molecules firmly bonded in what is known as the ‘primary hydration sphere’. For monatomic and monovalent ions, four molecules of water most probably exist in the firmly fixed layer. For

polyvalent ions such as Cr^{3+} , Fe^{3+} and Al^{3+} , six is a common number. The hydrated proton H_3O^+ most probably exists as $\text{H}_3\text{O}(\text{H}_2\text{O})_3^+$.

The electrostatic effects of an ion, however, can extend far beyond the primary hydration sphere. This accounts for the very large so-called hydration numbers that have been reported for some ions (up to 700 for Na^+ , for example). There is clearly a much larger region around the ion which contains loosely bound, but probably non-orientated, water. This assembly constitutes the 'secondary hydration sphere'.

Some interesting comments have been made by Wojciechowski (1981) on evidence for structure in saturated aqueous solutions. An analysis of the solubilities of a number of inorganic salts in water, together with views on the structure of water, suggested a statistical concentration of phase transitions near certain temperatures, e.g. 30, 45 and 60°C, giving a possible explanation for changes in the number of waters of crystallization in hydrates crystallizing around these temperatures.

Detailed accounts of current theories of liquid structure are given by Samoilov (1965), Franks and Ives (1966), Franks (1972–82) and in Faraday Discussions (1967, 1978).

Solute clustering

The structure of a supersaturated solution is probably more complex than that of an unsaturated or saturated solution. As reported by Khamskii (1969) a number of attempts have been made to find the distinguishing features of supersaturated solutions by investigating the dependences of various physical properties on concentration. In most cases, however, no evidence of discontinuity of the property-concentration curves at the equilibrium saturation point has been found, although an observation that light transmittancy could decrease sharply in the supersaturated region was regarded as evidence for solute clustering.

Table 3.4. Concentration gradients developed in quiescent aqueous citric acid solutions kept under isothermal conditions (Mullin and Leci, 1969a)

Initial concentration on all three positions	Concentration after time <i>t</i>								Solution temp. °C	Time <i>t</i> h	
	Top [†]		Middle [†]		Bottom [†]		<i>c</i>	<i>S</i>			
	<i>c</i>	<i>S</i>	<i>c</i>	<i>S</i>	<i>c</i>	<i>S</i>					
2.247	1.055	2.244	1.053	2.253	1.057	2.263	1.061	28.2	70		
2.568	1.393	2.531	1.372	2.546	1.381	2.604	1.412	22.6	71		
2.624	1.173	2.500	1.131	2.616	1.169	2.652	1.182	30.0	92		
2.336	1.185	2.303	1.168	2.333	1.183	2.336	1.185	25.2	336		
‡1.553	0.714	1.553	0.714	1.553	0.714	1.553	0.714	28.5	158		

c = solution concentration (g of citric acid monohydrate/g of 'free' water).

*c** = equilibrium saturation concentration (g of citric acid monohydrate/g of 'free' water).

S = supersaturation ratio = c/c^* .

† = vertical distance between the sample points = 20 cm.

‡ = unsaturated solution (one of many similar runs).

Mullin and Leci (1969a) reported that supersaturated aqueous solutions of citric acid, kept quiescent at constant temperature, develop concentration gradients with the highest concentrations in the lower regions (*Table 3.4*). This unusual behaviour was taken as a strong indication of the existence of molecular clusters in such solutions, which is perhaps not unexpected in this case because citric molecules by virtue of their —OH and —COOH groups are capable of extensive hydrogen bonding between themselves and with the solvent water molecules. Using a similar technique, Allen *et al.* (1972) observed concentration gradients in supersaturated solutions of sucrose and developed a ‘settling’ equation based on thermodynamic considerations.

Larson and Garside (1986) reported on work with several supersaturated aqueous solutions, including citric acid, urea and sodium nitrate. Treating the cluster concentration as the solute concentration in excess of saturation, they developed a relationship which was in some respects similar to that used by Allen *et al.* (1972) from which cluster size estimates were made between 4 and 10 nm, containing up to 7000 molecules. In analysis based on non-equilibrium thermodynamics, Veverká, Söhnel, Bennema and Garside (1991) have suggested that concentration gradients could be expected to develop in quiescent columns of supersaturated solutions whether or not clustering occurs. The phenomenon of solute clustering, however, is still fully compatible with their proposed theory.

Several attempts have been made to use Raman spectroscopy to estimate the degree of ionic and/or molecular association in supersaturated aqueous salt solutions. From the Raman spectra of ammonium dihydrogen phosphate solutions, Cerrata and Berglund (1987) concluded that whilst low-order (monomers and dimers) and high-order species were present, none of the clusters exhibited crystalline properties. A similar conclusion was reached by Rusli, Schrader and Larson (1989) in a study on supersaturated solutions of sodium nitrate. In fact, the concentrated solution spectra were found to be very similar to those of sodium nitrate melts.

The diffusivity of electrolytes and non-electrolytes in aqueous solution increases steadily with increasing concentration up to near the equilibrium saturation point, as shown by the data for NH₄Cl and KCl in *Figure 2.7*. However, Myerson and his co-workers have demonstrated that above the saturation limit the diffusivity declines very rapidly. This is to be expected since supersaturated solutions are metastable and the diffusivity falls to zero at the spinodal, i.e., at the limit of the metastable zone (section 5.1.1). Diffusivity was also shown to decrease with solution age. All these observations are compatible with cluster theory, and analyses by Lo and Myerson (1990) and Ginde and Myerson (1992) suggest that clusters in supersaturated aqueous solutions of glycine are mainly in the form of dimers and trimers, although a few up to 100 molecules can exist. Mohan, Kaytancioglu and Myerson (2000) also found trimer clusters in highly supersaturated solutions of ammonium sulphate and observed that the true metastable zone was much wider than had previously been thought, suggesting that virtually all bulk experiments involve heterogeneous rather than homogeneous nucleation. Further comments on clusters and their role as nucleation precursors are made in section 5.1.

4 Phase equilibria

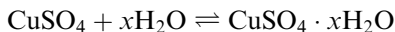
4.1 The phase rule

The amount of information which the simple solubility diagram can yield is strictly limited. For a more complete picture of the behaviour of a given system over a wide range of temperature, pressure and concentration, a phase diagram must be employed. This type of diagram represents graphically, in two or three dimensions, the equilibria between the various phases of a system. The Phase Rule, developed by J. Willard Gibbs in 1876, relates the number of components, C , phases, P , and degrees of freedom, F , of a system by means of the equation

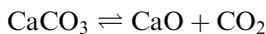
$$P + F = C + 2$$

These three terms are defined as follows.

The number of *components* of a system is the minimum number of chemical compounds required to express the composition of any phase. In the system water–copper sulphate, for instance, five different chemical compounds can exist, viz. $\text{CuSO}_4 \cdot 5\text{H}_2\text{O}$, $\text{CuSO}_4 \cdot 3\text{H}_2\text{O}$, $\text{CuSO}_4 \cdot \text{H}_2\text{O}$, CuSO_4 and H_2O ; but for the purpose of applying the Phase Rule there are considered to be only two components, CuSO_4 and H_2O , because the composition of each phase can be expressed by the equation



Again, in the system represented by the equation



three different chemical compounds can exist, but there are only two components because the composition of any phase can be expressed in terms of the compounds CaO and CO_2 .

A *phase* is a homogeneous part of a system. Thus any heterogeneous system comprises two or more phases. Any mixture of gases or vapours is a one-phase system. Mixtures of two or more completely miscible liquids or solids are also one-phase systems, but mixtures of two partially miscible liquids or a heterogeneous mixture of two solids are two-phase systems, and so on.

The three variables that can be considered in a system are temperature, pressure and concentration. The number of these variables that may be changed in magnitude without changing the number of phases present is called the number of *degrees of freedom*. In the equilibrium system water–ice–water vapour $C = 1$, $P = 3$, and from the Phase Rule, $F = 0$. Therefore in this system there are no degrees of freedom: no alteration may be made in either temperature or pressure (concentration is obviously not a variable in a one-component system) without a change in the number of phases. Such a system is called ‘invariant’.

For the system water–water vapour $C = 1$, $P = 2$ and $F = 1$: thus only one variable, pressure or temperature, may be altered independently without changing the number of phases. Such a system is called ‘univariant’. The one-phase water vapour system has two degrees of freedom; thus both temperature and pressure may be altered independently without changing the number of phases. Such a system is called ‘bivariant’.

Summarizing, it may be said that the physical nature of a system can be expressed in terms of phases, and that the number of phases can be changed by altering one or more of three variables: temperature, pressure or concentration. The chemical nature of a system can be expressed in terms of components, and the number of components is fixed for any given system.

Comprehensive accounts of the phase rule and its applications have been given by Bowden (1950), Findlay and Campbell (1951), Ricci (1966), Haase and Schönert (1969) and Nývlt (1979).

4.2 One-component systems

The two variables that can affect the phase equilibria in a one-component, or unary, system are temperature and pressure. The phase diagram for such a system is therefore a temperature–pressure equilibrium diagram.

Figure 4.1 illustrates the equilibria between the vapour, liquid and solid phases of water. Curve AB , often referred to as the sublimation curve, traces the effect of temperature on the vapour pressure of ice. Curve BC is the vapour pressure curve for liquid water, and line BD indicates the effect of pressure on the melting point of ice, i.e. the freezing point of water. Water is an unusual substance in that it expands on freezing, indicated by the slope of line BD towards the left of the diagram, i.e. pressure decreases the melting point. The

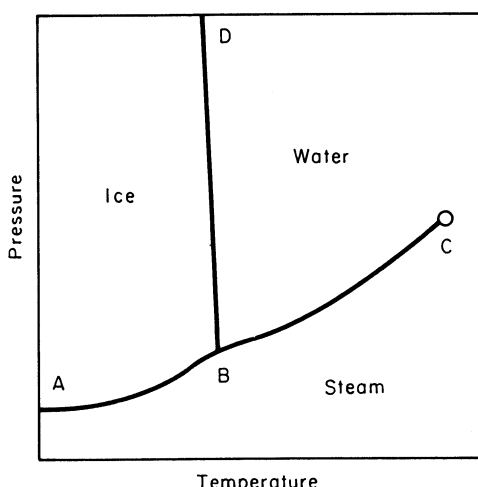


Figure 4.1. Phase diagram for water (not to scale)

vast majority of other substances behave in the opposite manner (see *Figure 4.10*). The three curves meet at the triple point *B* ($0.01\text{ }^{\circ}\text{C}$, 6.1 mbar (610 Pa)) where ice, liquid water and water vapour can coexist in equilibrium. At the critical point *C* ($374\text{ }^{\circ}\text{C}$, 220 bar (22 MPa)) liquid and vapour phases become indistinguishable. Above the critical point water is referred to as a supercritical fluid.

The solvent properties of supercritical fluids are particularly interesting. Liquid water, for example, has a dielectric constant of around 80, whereas the value for supercritical water is around 2. At this low value it no longer acts as a polar solvent and many organic compounds can be dissolved in and crystallized from it. The potential exploitation of supercritical fluids, especially H_2O and CO_2 , in crystallization processes is discussed in section 7.1.4.

4.2.1 Polymorphs

Figure 4.2 illustrates the case of sulphur, a system that exhibits two crystalline polymorphs. The area above the curve *ABEF* is the region in which orthorhombic sulphur is the stable solid form. The areas bounded by curves *ABCD* and *FECD* indicate the existence of vapour and liquid sulphur, respectively. The ‘triangular’ area *BEC* represents the region in which monoclinic sulphur is the stable solid form. Curves *AB* and *BC* are the vapour pressure curves for orthorhombic and monoclinic sulphur, respectively, and these curves intersect at the transition point *B*.

Curve *BE* indicates the effect of pressure on the transition temperature for orthorhombic $\text{S} \rightleftharpoons$ monoclinic S . Point *B*, therefore, is a triple point representing the temperature and pressure ($95.5\text{ }^{\circ}\text{C}$ and 0.51 N m^{-2}) at which orthorhombic sulphur and sulphur vapour can coexist in stable equilibrium. Curve *EF* indicates the effect of pressure on the melting point of orthorhombic sulphur;

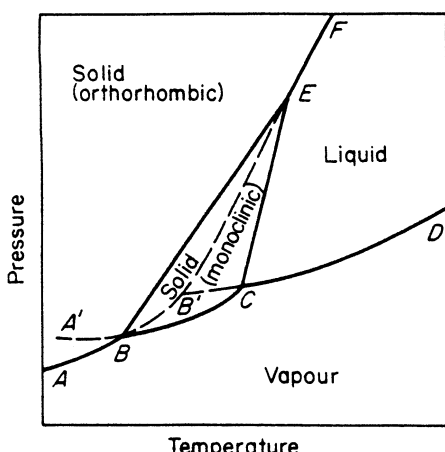


Figure 4.2. Phase diagram for sulphur (not to scale)

point *E* is a triple point representing the temperature and pressure (151°C and $1.31 \times 10^8 \text{ N m}^{-2}$) at which orthorhombic and monoclinic sulphur and liquid sulphur are in stable equilibrium. Curve *CD* is the vapour pressure curve for liquid sulphur, and curve *CE* indicates the effect of pressure on the melting point of monoclinic sulphur. Point *C*, therefore, is another triple point (115°C and 2.4 N m^{-2}) representing the equilibrium between monoclinic and liquid sulphur and sulphur vapour.

The broken lines in *Figure 4.2* represent metastable conditions. If orthorhombic sulphur is heated rapidly beyond 95.5°C , the change to the monoclinic form does not occur until a certain time has elapsed; curve *BB'*, a continuation of curve *AB*, is the vapour pressure curve for metastable orthorhombic sulphur above the transition point. Similarly, if monoclinic sulphur is cooled rapidly below 95.5°C , the change to the orthorhombic form does not take place immediately, and curve *BA'* is the vapour pressure curve for metastable monoclinic sulphur below the transition point. Likewise, curve *CB'* is the vapour pressure curve for metastable liquid sulphur below the 115°C transition point, and curve *B'E* the melting point curve for metastable orthorhombic sulphur. Point *B'*, therefore, is a fourth triple point (110°C and 1.7 N m^{-2}) of the system.

Only three of the four possible phases orthorhombic (solid), monoclinic (solid), liquid and vapour can coexist in stable equilibrium at any one time, and then only at one of the three 'stable' triple points.

Transformations

The transformation from one polymorph to another can be reversible or irreversible; in the former case the two crystalline forms are said to be enantiotropic; in the latter, monotropic. These phenomena, already described in section 1.8, can be demonstrated with reference to the pressure–temperature phase diagram.

Figure 4.3a shows the phase reactions exhibited by two enantiotropic solids, α and β . *AB* is the vapour pressure curve for the α form, *BC* that for the β form, and *CD* that for the liquid. Point *B*, where the vapour pressure curves of the two solids intersect, is the transition point; the two forms can coexist in equilibrium under these conditions of temperature and pressure. Point *C* is a triple point at which vapour, liquid and β solid can coexist. This point can be considered to be the melting point of the β form.

If the α solid is heated slowly, it changes into the β solid and finally melts. The vapour pressure curve *ABC* is followed. Conversely, if the liquid is cooled slowly, the β form crystallizes out first and then changes into the α form. Rapid heating or cooling, however, can result in a different behaviour. The vapour pressure of the α form can increase along curve *BB'*, a continuation of *AB*, the α form now being metastable. Similarly, the liquid vapour pressure can fall along curve *CB'*, a continuation of *DC*, the liquid being metastable. Point *B'*, therefore, is a metastable triple point at which the liquid, vapour and α solid can coexist in metastable equilibrium.

The type of behaviour described above is well illustrated by the case of sulphur (*Figure 4.2*), where the orthorhombic and monoclinic forms are

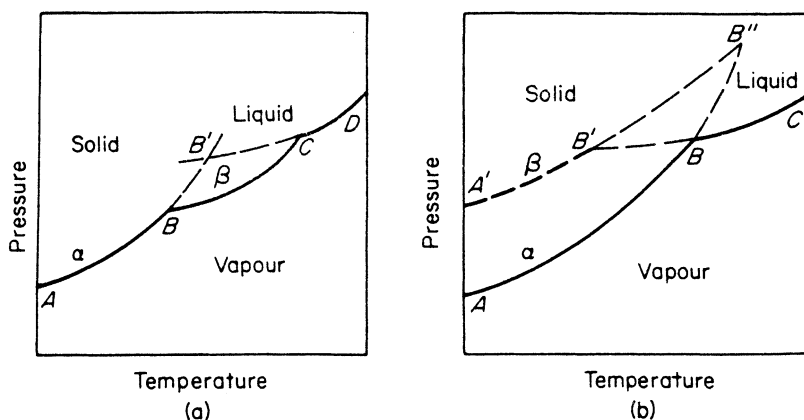


Figure 4.3. Pressure–temperature diagrams for dimorphous substances: (a) enantiotropy; (b) monotropy

enantiotropic; the transition point occurs at a lower temperature than does the triple point.

Figure 4.3b shows the pressure–temperature curves for a monotropic substance. AB and BC are the vapour pressure curves for the α solid and liquid, respectively, and $A'B'$ is that for the β solid. In this case the vapour pressure curves of the α and β forms do not intersect, so there is no transition point within this range of temperature and pressure. The solid form with the higher vapour pressure at any given temperature (β in this case) is the metastable form. Curves BB' and BB'' are the vapour pressure curves for the liquid and metastable α solid, so B' is a metastable triple point. If this system did exhibit a true transition point, it would lie at point B'' ; but as this represents a temperature higher than the melting point of the solid, it cannot exist.

A typical case of monotropy is the change from white to red phosphorus. Benzophenone is another example of a monotropic substance: the stable melting point is $49\text{ }^\circ\text{C}$, whereas the metastable form melts at $29\text{ }^\circ\text{C}$.

The kinetics of polymorphic transformations in melts and solutions are discussed in section 6.5.

4.3 Two-component systems

The three variables that can affect the phase equilibria of a binary system are temperature, pressure and concentration. The behaviour of such a system should, therefore, be represented by a space model with three mutually perpendicular axes of pressure, temperature and concentration. Alternatively, three diagrams with pressure–temperature, pressure–concentration and temperature–concentration axes, respectively, can be employed. However, in most crystallization processes the main interest lies in the liquid and solid phases of a system; a knowledge of the behaviour of the vapour phase is only required

when considering sublimation processes. Because pressure has little effect on the equilibria between liquids and solids, the phase changes can be represented on a temperature-concentration diagram; the pressure, usually atmospheric, is ignored. Such a system is said to be 'condensed', and a 'reduced' phase rule can be formulated excluding the pressure variable:

$$P + F' = C + 1$$

where F' is the number of degrees of freedom, not including pressure.

Four different types of two-component system will now be considered. Detailed attention is paid to the first type solely to illustrate the information that can be deduced from a phase diagram. It will be noted that the concentration of a solution on a phase diagram is normally given as a mass fraction or mass percentage and not as 'mass of solute per unit mass of solvent', as recommended for the solubility diagram (section 3.3). Mole fractions and mole percentages are also suitable concentration units for use in phase diagrams.

4.3.1 Simple eutectic

A typical example of a system in which the components do not combine to form a chemical compound is shown in *Figure 4.4*. Curves *AB* and *BC* represent the temperatures at which homogeneous liquid solutions of naphthalene in benzene begin to freeze or to crystallize. The curves also represent, therefore, the temperatures above which mixtures of these two components are completely liquid. The name 'liquidus' is generally given to this type of curve. In aqueous systems of this type one liquidus is the freezing point curve, the other the normal solubility curve. Line *DBE* represents the temperature at which solid mixtures

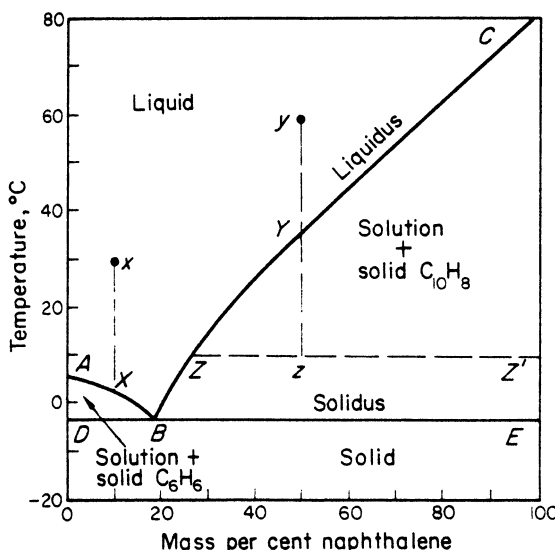


Figure 4.4. Phase diagram for the simple eutectic system naphthalene–benzene

of benzene and naphthalene begin to melt, or the temperature below which mixtures of these two components are completely solid. The name ‘solidus’ is generally given to this type of line. The melting or freezing points of pure benzene and naphthalene are given by points *A* (5.5 °C) and *C* (80.2 °C), respectively. The upper area enclosed by the liquidus, *ABC*, represents the homogeneous liquid phase, i.e. a solution of naphthalene in benzene; that enclosed by the solidus, *DBE*, indicates solid mixtures of benzene and naphthalene. The small and large ‘triangular’ areas *ABD* and *BCE* represent mixtures of solid benzene and solid naphthalene, respectively, and benzene–naphthalene solution.

If a solution represented by point *x* is cooled, pure solid benzene is deposited when the temperature of the solution reaches point *X* on curve *AB*. As solid benzene separates out, the solution becomes more concentrated in naphthalene and the equilibrium temperature of the system falls, following curve *AB*. If a solution represented by point *y* is cooled, pure solid naphthalene is deposited when the temperature reaches point *Y* on the solubility curve; the solution becomes more concentrated in benzene and the equilibrium temperature follows curve *CB*. Point *B*, common to both curves, is the eutectic point (−3.5 °C and 0.189 mass fraction of naphthalene), and this is the lowest freezing point in the whole system. At this point a completely solidified mixture of benzene and naphthalene of fixed composition is formed: it is important to note that the eutectic is a physical mixture, not a chemical compound. Below the eutectic temperature all mixtures are solid.

If the solution *y* is cooled below the temperature represented by point *Y* on curve *BC* to some temperature represented by point *z*, the composition of the system as a whole remains unchanged. The physical state of the system has been altered, however; it now consists of a solution of benzene and naphthalene containing solid naphthalene. The composition of the solution, or mother liquor, is given by point *z* on the solubility curve, and the proportions of solid naphthalene and solution are given, by the so-called ‘mixture rule’, by the ratio of the lengths *zZ* and *zZ'*, i.e.

$$\frac{\text{mass of solid C}_{10}\text{H}_8}{\text{mass of solution}} = \frac{zZ}{zZ'}$$

A process involving both cooling and evaporation can be analysed in two steps. The first is as described above, i.e. the location of points *z*, *Z* and *Z'*; this represents the cooling operation. If benzene is evaporated from the system, *z* no longer represents the composition; thus the new composition point *z'* (not shown in the diagram) is located along line *ZZ'* between points *z* and *Z*. Then the ratio *z'Z/z'Z'* gives the proportions of solid and solution.

The systems KCl–H₂O and (NH₄)₂SO₄–H₂O are good examples of aqueous salt solutions that exhibit simple eutectic formation. In aqueous systems the eutectic mixture is sometimes referred to as a *cryohydrate*, and the eutectic point a ‘cryohydric point’.

It should be understood that the term ‘pure’ when commonly used, as in this chapter, does not mean absolute 100% purity. In industrial crystallization practice this is neither necessary nor indeed achievable, and for many bulk-produced chemicals a purity of >95% is often accepted as justifying the

designation ‘pure’. In any case, a single crystallization step cannot produce 100% pure crystals for a variety of reasons, e.g., they can be contaminated with residual solvent or other impurities that have not been removed by washing, or have been incorporated into the crystal interstitially or as liquid inclusions, and so on. Furthermore, contamination commonly results from the existence of *terminal solid solutions*, which inevitably accompany both eutectic and chemical compound systems, as described in section 7.2.

4.3.2 Compound formation

The solute and solvent of a binary system may, and frequently do, combine to form one or more different compounds. In aqueous solutions these compounds are called ‘hydrates’; for non-aqueous systems the term ‘solvate’ is sometimes used. Two types of compound can be considered: one can coexist in stable equilibrium with a liquid of the same composition, and the other cannot behave in this manner. In the former case the compound is said to have a *congruent melting point*; in the latter, to have an *incongruent melting point*.

Figure 4.5 illustrates the phase reactions in the manganese nitrate–water system. Curve *AB* is the freezing point curve. The solubility curve *BCDEFG* for $\text{Mn}(\text{NO}_3)_2$ in water is not continuous owing to the formation of several different hydrates. The area above curve *ABCDEF* represents homogeneous liquid solutions. Mixtures of the hexahydrate and solution exist in areas *BCH* and *ICD*. The tetrahydrate is the stable phase in region *DEJ* and the dihydrate in *EKF*. The rectangular areas under *FH*, *IJ* and *KL* represent completely

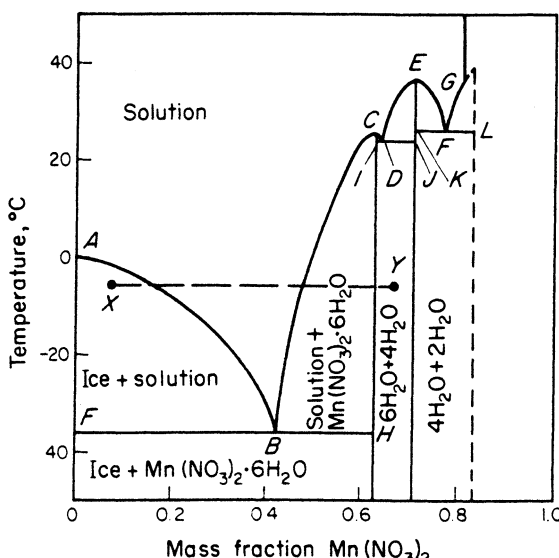


Figure 4.5. Phase diagram for the system $\text{Mn}(\text{NO}_3)_2-\text{H}_2\text{O}$

solidified systems (ice and hexahydrate, hexa- and tetrahydrates, and tetra- and dihydrates, respectively). Point *B* is a eutectic or cryohydric point with the co-ordinates -36°C and 0.405 mass fraction of $\text{Mn}(\text{NO}_3)_2$.

Point *C* in *Figure 4.5* indicates the melting point (25.8°C) and composition (0.624 mass fraction) of the hexahydrate. Thus when a solution of this composition is cooled to 25.8°C it solidifies to the hexahydrate, i.e. no change in composition occurs. Point *C*, therefore, is a congruent point. Similarly, point *E* is the congruent point for the tetrahydrate (melting point 37.1°C , composition 0.713). Points *D* and *F* are the other two eutectic points of the system. Point *G* is the transition point at which the dihydrates decomposes into the monohydrate and water, i.e. it is the incongruent melting point of the dihydrate. The vertical broken line at 0.834 mass fraction represents the composition of the dihydrate.

The behaviour of manganese nitrate solutions on cooling can be traced in the same manner as that described above for simple eutectic systems. The solution concentrations and the proportions of solid and solution can similarly be deduced graphically. The process of isothermal evaporation in congruent melting systems presents an interesting phenomenon. For example, the mixture represented by point *X* in *Figure 4.5* represents a slurry of ice and solution; but when sufficient water is removed to bring the system composition into the region to the right of curve *AB*, it becomes a homogeneous liquid solution. When more water is removed, so that region *BCG* is entered, the system partially solidifies again, depositing crystals of the hexahydrate. On further evaporation, once the composition exceeds 62.4 per cent of $\text{Mn}(\text{NO}_3)_2$, e.g. at point *Y*, the system solidifies completely to a mixture of the hexa- and tetrahydrates. The reverse order of behaviour occurs on isothermal hydration.

The formation of eutectics and solvates with congruent points is observed in many organic, aqueous inorganic and metallic systems. The case illustrated above is a rather simple example. Some systems form a large number of solvates and their phase diagrams can become rather complex. Ferric chloride, for example, forms four hydrates, and the $\text{FeCl}_3-\text{H}_2\text{O}$ phase diagram exhibits five-cryohydric points and four congruent points.

A solvate that is unstable in the presence of a liquid of the same composition is said to have an incongruent melting point. Such a solvate melts to form a solution and another compound, which may or may not be a solvate. For instance, the hydrate $\text{Na}_2\text{SO}_4 \cdot 10\text{H}_2\text{O}$ melts at 32.4°C to give a saturated solution of sodium sulphate containing a suspension of the anhydrous salt; hence, this temperature is the incongruent melting point of the decahydrate. The terms ‘meritectic point’ and ‘transition point’ are also used instead of the expression ‘incongruent melting point’.

Figure 4.6 illustrates the behaviour of the system sodium chloride–water. The various areas are marked on the diagram. *AB* is the freezing point curve and *BC* is the solubility curve for the dihydrate. Point *B* (-21°C) is a eutectic or cryohydric point at which a solid mixture of ice and $\text{NaCl} \cdot 2\text{H}_2\text{O}$ of fixed composition (0.29 mass fraction of NaCl) is deposited. At point *C* (0.15°C) the dihydrate decomposes into the anhydrous salt and water; this is, therefore, the incongruent melting point, or transition point, of $\text{NaCl} \cdot 2\text{H}_2\text{O}$. The vertical line commencing at 0.619 mass fraction of NaCl represents the composition of

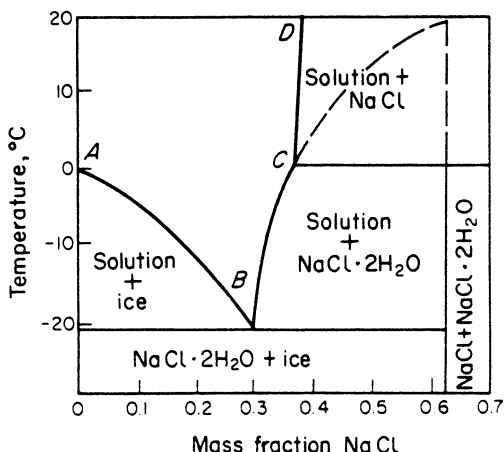


Figure 4.6. Phase diagram for the system NaCl–H₂O

the dihydrate. If this system had a congruent melting point, which it does not have, this line would meet the peak of the extension of curve BC (e.g. see Figure 4.5).

Many aqueous and organic systems exhibit eutectic and incongruent points. Several cases are known of an inverted solubility effect after the transition point (see Figure 3.1b); the systems Na₂SO₄–H₂O and Na₂CO₃–H₂O are particularly well-known examples of this behaviour.

Salt hydrates for energy storage

There has been a growing interest in recent years in the use of salt hydrates as heat storage materials, e.g. solar heat for space-heating purposes or in small heat parks for personal uses. The hydrates are melted in the energy absorbing stage and they subsequently release heat at the phase transition temperature when they recrystallize. Ideally the hydrates should have a congruent melting point so that the phase transition crystal ⇌ melt ⇌ crystal can be repeated indefinitely. In practice, however, many otherwise acceptable hydrates exhibit slightly incongruent behaviour and have to be used in admixture with other substances.

Examples of hydrates that have been considered for domestic application include CaCl₂ · 6H₂O, Na₂SO₄ · 10H₂O, Na₂S₂O₃ · 5H₂O, Na₂HPO₄ · 12H₂O and CH₃COONa · 3H₂O (Kimura, 1980; Grønvold and Meisingset, 1982; Feilchenfeld and Sarig, 1985; Kimura and Kai, 1985; Tamme, 1987).

4.3.3 Solid solutions

Many binary systems when submitted to a cooling operation do not at any stage deposit one of the components in the pure state: both components are deposited simultaneously. The deposited solid phase is, in fact, a solid solution.

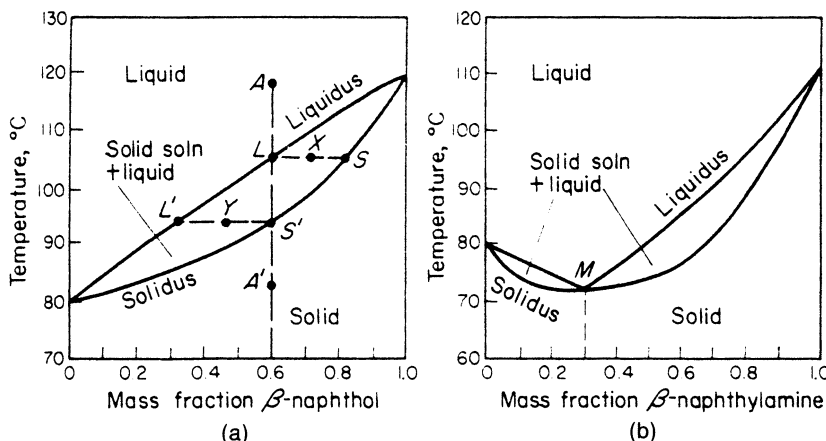


Figure 4.7. Solid solutions: (a) continuous series (naphthalene- β -naphthol; (b) minimum melting point (naphthalene- β -naphthylamine)

Only two phases can exist in such a system: a homogeneous liquid solution and a solid solution. Therefore, from the reduced phase rule, $F' = 1$, so an invariant system cannot result. One of three possible types of equilibrium diagram can be exhibited by systems of this kind. In the first type, illustrated in Figure 4.7a, all mixtures of the two components have freezing or melting points intermediate between the melting points of the pure components. In the second type shown in Figure 4.7b, a minimum is produced in the freezing and melting point curves. In the third, rare, type of diagram, a maximum is exhibited in the curves.

Figure 4.7a shows the temperature-concentration phase diagram for the system naphthalene- β -naphthol, which forms a continuous series of solid solutions. The melting points of pure naphthalene and β -naphthol are 80 and 120 °C, respectively. The upper curve is the liquidus or freezing point curve, the lower the solidus or melting point curve. Any system represented by a point above the liquidus is completely molten, and any point below the solidus represents a completely solidified mass. A point within the area enclosed by the liquidus and solidus curves indicates an equilibrium mixture of liquid and solid solution. Point X, for instance, denotes a liquid of composition L in equilibrium with a solid solution of composition S, and point Y a liquid L' in equilibrium with a solid S'.

The phase reactions occurring on the cooling of a given mixture can be traced as follows. If a homogeneous liquid represented by point A (60 per cent β -naphthol) is cooled slowly, it starts to crystallize when point L (105 °C) is reached. The composition of the first crystals is given by point S (82 per cent β -naphthol). As the temperature is lowered further, more crystals are deposited but their composition changes successively along curve SS', and the liquid composition changes along curve LL'. When the temperature is reduced to 94 °C (points L' and S'), the system solidifies completely. The over-all composition of the solid system at some temperature represented by, say, point A' is the same as that of the original homogeneous melt, assuming that no crystals have

been removed during the cooling process, but the system is no longer homogeneous because of the successive depositions of crystals of varying composition. The changes occurring when a solid mixture A' is heated can be traced in a manner similar to the cooling operation.

Figure 4.7b shows the relatively uncommon, but not rare, type of binary system in which a common minimum temperature is reached by both the upper liquidus and lower solidus curves. These two curves approach and touch at point M . The example shown in *Figure 4.7b* is the system naphthalene– β -naphthylamine. Freezing and melting points of mixtures of this system do not necessarily lie between the melting points of the pure components. Three sharp melting points are observed: 80 °C (pure naphthalene), 110 °C (pure β -naphthylamine) and 72.5 °C (mixture M , 0.3 mass fraction β -naphthylamine). Although the solid solution deposited at point M has a definite composition, it is not a chemical compound. The components of such a minimum melting point mixture are rarely, if ever, present in stoichiometric proportions. Point M , therefore, is not a eutectic point: the liquidus curve is completely continuous; it only approaches and touches the solidus at M . The phase reactions occurring when mixtures of this system are cooled can be traced in the same manner as that described for the continuous series solid solutions.

4.4 Enthalpy–composition diagrams

The heat effects accompanying a crystallization operation may be determined by making heat balances over the system, although many calculations may be necessary, involving knowledge of specific heat capacities, heats of crystallization, heats of dilution, heats of vaporization, and so on. Much of the calculation burden can be eased, however, by the use of a graphical technique in which enthalpy data, solubilities and phase equilibria are represented on an enthalpy–composition (H – x) diagram, sometimes known as a Merkel chart.

The use of the H – x diagram for the analysis of chemical engineering unit operations such as distillation, evaporation and refrigeration processes, is now quite common, and the procedures are well described in textbooks, e.g. Coulson and Richardson (1991), McCabe, Smith and Harriott (1985). These charts are less frequently applied to crystallization processes, however, because not many H – x diagrams are available.

Among the few enthalpy–composition charts for solid–liquid systems published in the open literature (all for aqueous solutions) are:

- ammonium nitrate (Othmer and Frohlich, 1960)
- calcium chloride (Hougen, Watson and Ragatz, 1943)
- calcium nitrate (Scholle and Brunclíková, 1968)
- magnesium sulphate (McCabe, 1935)
- sodium tetraborate (borax) (Scholle and Szmigierská, 1965)
- sodium carbonate (Tyner, 1955)
- sodium hydroxide (McCabe, 1935)
- sodium sulphate (Foust *et al.*, 1960)

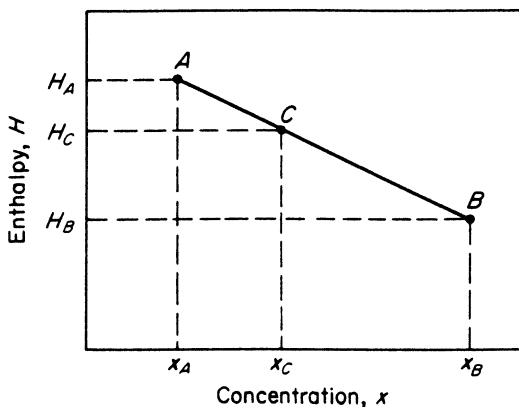


Figure 4.8. An adiabatic mixing process represented on an H - x diagram

boric acid (Scholle and Szmigielská, 1965)

hydrazine (Tyner, 1955)

urea (Banerjee and Doraiswamy, 1960)

The construction of an H - x diagram is laborious (McCabe, 1935) and would normally be undertaken only if many calculations were to be performed, e.g. on a system of commercial importance. Nevertheless, once an H - x chart is available its use is simple, and a great deal of information can be obtained rapidly. If the concentration x of one component of a binary mixture is expressed as a mass fraction, the enthalpy is expressed as a number of heat units per unit mass of mixture, e.g. Btu lb^{-1} or J kg^{-1} . Molar units are less frequently used in crystallizer design practice.

The basic rule governing the use of an H - x chart is that an adiabatic mixing, or separation, process is represented by a straight line. In *Figure 4.8* points A and B represent the concentrations and enthalpies x_A , H_A and x_B , H_B of two mixtures of the same system. If A is mixed adiabatically with B , the enthalpy and concentration of the resulting mixture is given by point C on the straight line AB . The exact location of point C , which depends on the masses m_A and m_B of the two initial mixtures, can be determined by the *mixture rule* or lever-arm principle:

$$m_A(x_C - x_A) = m_B(x_B - x_C) \quad (4.1)$$

or

$$x_C = \frac{m_B x_B + m_A x_A}{m_A + m_B} \quad (4.2)$$

Similarly, if mixture A were to be removed adiabatically from mixture C , the enthalpy and composition of residue B can be located on the straight line through points A and C by means of the equation

$$x_B = \frac{m_C x_C - m_A x_A}{m_C - m_A} \quad (4.3)$$

$H-x$ charts in SI units for aqueous solutions of sodium carbonate and sodium sulphate (both recalculated from original data) are given in Figures 4.9 and 4.10, respectively, and a chart for magnesium sulphate, retained in its original Imperial units, is given in Figure 4.11.

In Figure 4.11, for example, the isotherms in the region above curve $pabcdq$ represent enthalpies and concentrations of unsaturated aqueous solutions of MgSO_4 , and the very slight curvature of these isotherms indicates that the heat of dilution of MgSO_4 solutions is very small. Point p (zero enthalpy) represents pure water at 32°F , point n the enthalpy of pure ice at the same temperature. The portion of the diagram below curve $pabcdq$, which represents liquid–solid systems, can be divided into five polythermal regions:

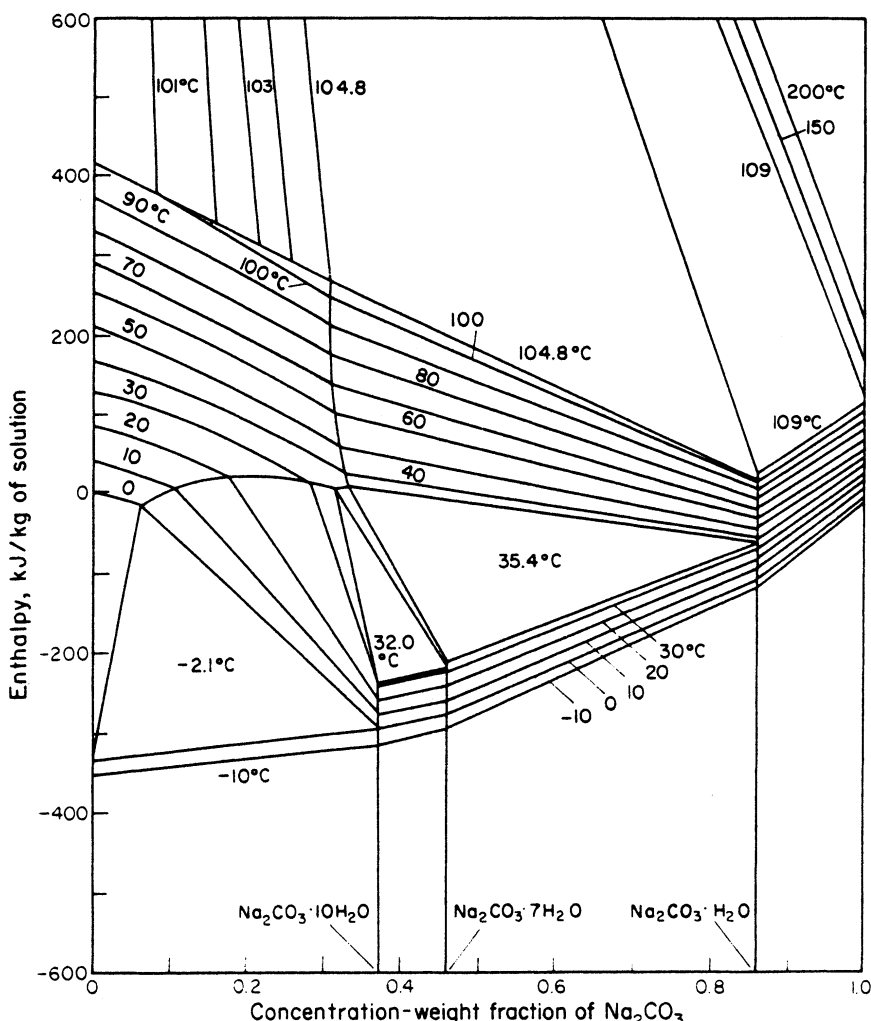


Figure 4.9. Enthalpy–concentration diagram for the system $\text{Na}_2\text{CO}_3\text{--H}_2\text{O}$

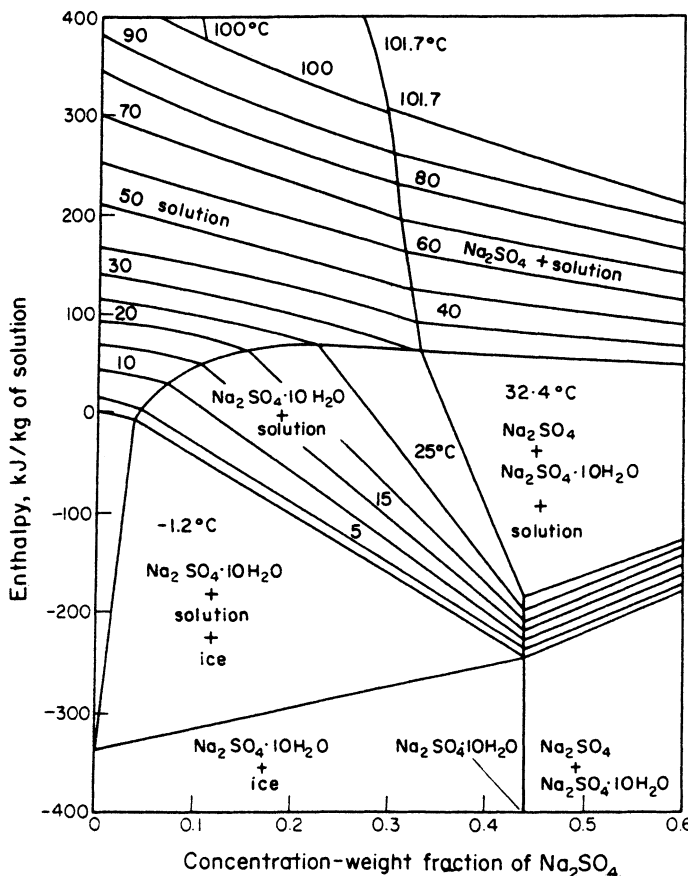


Figure 4.10. Enthalpy-concentration diagram for the system $\text{Na}_2\text{SO}_4\text{-H}_2\text{O}$

- pae solutions of MgSO_4 in equilibrium with pure ice
- abfg equilibrium mixtures of $\text{MgSO}_4 \cdot 12\text{H}_2\text{O}$ and saturated solution
- bcih equilibrium mixtures of $\text{MgSO}_4 \cdot 7\text{H}_2\text{O}$ and saturated solution
- cdlj equilibrium mixtures of $\text{MgSO}_4 \cdot 6\text{H}_2\text{O}$ and saturated solution
- dqrk equilibrium mixtures of $\text{MgSO}_4 \cdot \text{H}_2\text{O}$ and saturated solution

In between these five regions lie four isothermal triangular areas, which represent the following conditions:

- aef (25°F) mixtures of ice, cryohydrate *a* and $\text{MgSO}_4 \cdot 12\text{H}_2\text{O}$
- bfh (37.5°F) mixtures of solid $\text{MgSO}_4 \cdot 12\text{H}_2\text{O}$ and $\text{MgSO}_4 \cdot 7\text{H}_2\text{O}$ in a 21 per cent MgSO_4 solution
- cji (118.8°F) mixtures of solid $\text{MgSO}_4 \cdot 7\text{H}_2\text{O}$ and $\text{MgSO}_4 \cdot 6\text{H}_2\text{O}$ in a 33 per cent MgSO_4 solution
- dkl (154.4°F) mixtures of solid $\text{MgSO}_4 \cdot 6\text{H}_2\text{O}$ and $\text{MgSO}_4 \cdot \text{H}_2\text{O}$ in a 37 per cent MgSO_4 solution

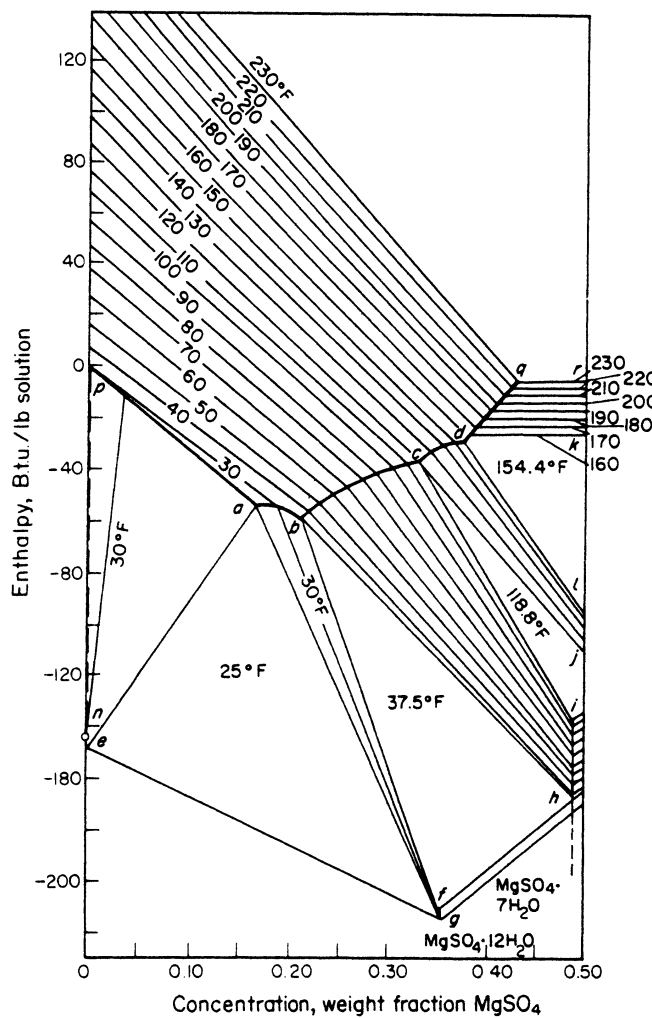


Figure 4.11. Enthalpy-concentration diagram for the system $\text{MgSO}_4\text{-H}_2\text{O}$. (From McCabe, 1963, by courtesy of McGraw-Hill)

The short vertical lines *fg* and *ih* represent the compositions of solid $\text{MgSO}_4 \cdot 12\text{H}_2\text{O}$ (0.359 mass fraction MgSO_4) and $\text{MgSO}_4 \cdot 7\text{H}_2\text{O}$ (0.49 mass fraction). The following example demonstrates the use of Figure 4.11.

Example

Calculate (a) the quantity of heat to be removed and (b) the theoretical crystal yield when 5000 lb of a 30 per cent solution of MgSO_4 by mass at 110°F is cooled to 70°F . Evaporation and radiation losses may be neglected.

Figure 4.12 indicates the relevant section – not to scale – of the $H\text{-}x$ diagram in Figure 4.11.

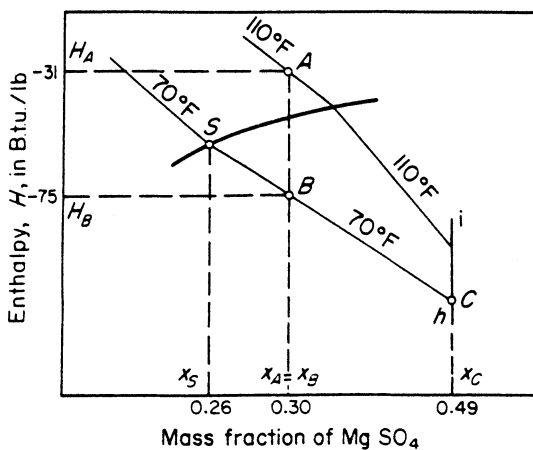


Figure 4.12. Graphical solution of Example (enlarged portion of Figure 4.11 – not to scale)

- (a) Initial solution, *A* $x_A = 0.30, H_A = -31 \text{ Btu/lb}$
 Cooled system, *B* $x_B = 0.30, H_B = -75 \text{ Btu/lb}$
 Enthalpy change $\Delta H = -44 \text{ Btu/lb}$
 Heat to be removed $44 \times 5000 = -220\,000 \text{ Btu}$

(b) The cooled system *B*, located in the region *bcih* in Figure 4.11, comprises $\text{MgSO}_4 \cdot 7\text{H}_2\text{O}$ crystals in equilibrium with solution *S* on curve *bc*. The actual proportions of solid and solution can be calculated by the mixture rule.

$$\begin{array}{ll} \text{Solution composition} & x_S = 0.26 \\ \text{Crystalline phase composition} & x_C = 0.49 \end{array}$$

4.5 Phase change detection

4.5.1 Thermal analysis

A phase reaction is always accompanied by an enthalpy change (section 2.12), and this heat effect can readily be observed if a cooling curve is plotted for the system. In many cases a very simple apparatus can be used. A large glass test-tube, fitted with a stirrer and a thermometer graduated in increments of 0.1°C and held in a temperature-controlled environment, will often suffice. The temperature of the system is recorded at regular intervals of say 1 min.

A smooth cooling curve is followed until a phase reaction takes place, when the accompanying heat effect causes an arrest or change in slope. Figure 4.13a shows a typical example for a pure substance. *AB* is the cooling curve for the homogeneous liquid phase. At point *B* the substance starts to freeze and the system remains at constant temperature, the freezing point, until solidification is complete at point *C*. The solid then cools at a rate indicated by curve *CD*. It is possible, of course, for the liquid phase to cool below the freezing point, and

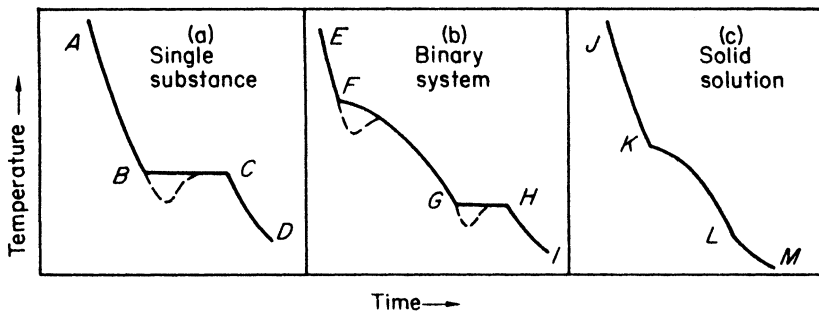


Figure 4.13. Some typical cooling curves

some systems may withstand appreciable degrees of supercooling. The dotted curve in *Figure 4.13a* denotes the sort of path followed if supercooling occurs. Seeding of the system will minimize these effects.

Figure 4.13b shows the type of cooling curve obtained for a binary system in which eutectic or compound formation occurs. The temperature of the homogeneous liquid phase falls steadily along curve *EF* until, at point *F*, deposition of the solid phase commences. The rate of cooling changes along curve *FG* as more solid is deposited. The composition of the remaining solution changes until the composition of the eutectic is reached, then crystallization or freezing continues at constant temperature (line *GH*), i.e. the eutectic behaves as a single pure substance. The completely solidified system cools along curve *HL*. Supercooling, denoted by the dotted lines, may be encountered at both arrest points if the system is not seeded.

Figure 4.13c shows a typical cooling curve for a binary mixture that forms a series of solid solutions. The first arrest, *K*, in the curve corresponds to the onset of freezing, and this represents a point on the liquidus. The second arrest, *L*, occurs on the completion of freezing and represents a point on the solidus. It will be noted that no constant-temperature freezing point occurs in such a system.

The discontinuities may not always be clearly defined on a cooling curve (temperature θ versus time t plot). In such cases, the arrest points can often be greatly exaggerated by plotting an inverse rate curve (θ versus $dt/d\theta$, i.e. the inverse of the cooling rate). A typical plot is shown in *Figure 4.14*.

Equilibria in solid solutions are better studied by a heating than by a cooling process. This is the basis of the thaw–melt method. An intimate mixture of known composition of the two pure components is prepared by melting, solidifying and then crushing to a fine powder. A small sample of the powder is placed in a melting-point tube, attached close to the bulb of a thermometer graduated in increments of 0.1°C , and immersed in a stirred bath. The temperature is raised slowly and regularly at a rate of about 1°C in 5 min. The ‘thaw point’ is the temperature at which liquid first appears in the tube; this is a point on the solidus. The ‘melt point’ is the temperature at which the last solid particle melts; this is a point on the liquidus. Only pure substances and eutectic mixtures have sharp melting points. The thaw–melt method is particularly

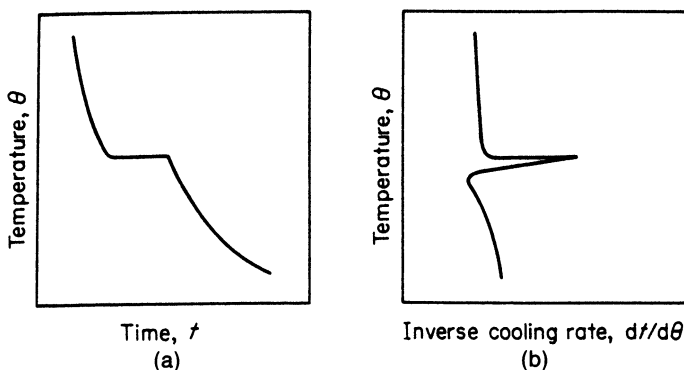


Figure 4.14. Detection of the arrest point for a single substance: (a) on a temperature–time curve, (b) on an inverse rate curve

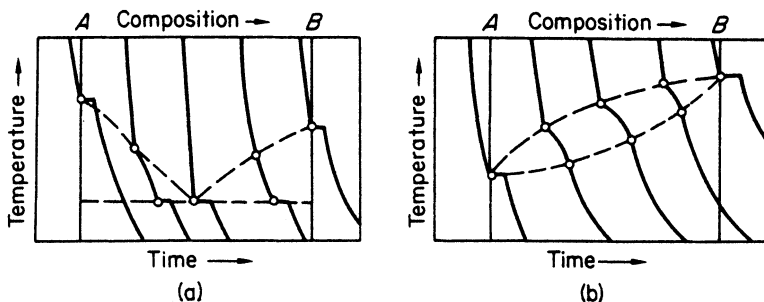


Figure 4.15. Construction of equilibrium diagrams from ‘thaw–melt’ data: (a) eutectic system; (b) solid solution

useful if the system is prone to supercooling, and it has the added advantage of requiring only small quantities of test material.

The construction of equilibrium diagrams from cooling or thaw–melt data is indicated in *Figure 4.15*. In practice, however, a large number of different mixtures of the two components *A* and *B*, covering the complete range from pure *A* to pure *B*, would be tested. The liquidus curves are drawn through the first-arrest points, the solidus curves through the second-arrest points. Only at 100 per cent *A*, 100 per cent *B* and the eutectic point do the liquidus and solidus meet.

Differential thermal analysis (DTA)

Differential thermal analysis is a method used for observing phase changes and measuring the associated changes in enthalpy. A small test sample, often only a few milligrams, is heated in close proximity to a sample of reference material in an identical container. The reference material, chosen for its similarity to the test sample, must not exhibit any phase change over the temperature range under consideration.

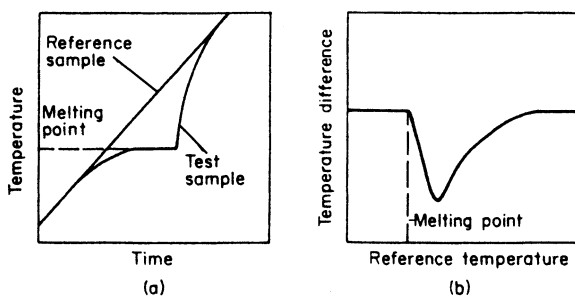


Figure 4.16. Differential thermal analysis: (a) comparative heating curves, (b) differential temperature curve for a single substance

When the test sample undergoes a phase change, there will be heat release or absorption. For example, if it melts it will absorb heat and its temperature will lag behind that of the reference material (*Figure 4.16a*). The difference in temperature between the two samples is detected by a pair of matched thermocouples and recorded as a function of time. The area between the differential curve (*Figure 4.16b*) and the base line is a function of the enthalpy associated with the phase change.

Differential scanning calorimetry (DSC)

Differential scanning calorimetry is another calorimetric technique for observing solid–liquid phase changes. Two independently controlled heaters allow the sample and reference pans to be heated at a fixed rate. The instrument detects the temperature difference ΔT between the sample and reference, during heating or cooling, and records the amount of heat added to or removed from the sample at the sample temperature to compensate for the temperature difference. The melting point and enthalpy of fusion of the sample material can thus be determined simultaneously from the DSC curve. An exothermic reaction in the sample results in a positive peak in the DSC curve. An endothermic reaction gives a negative peak.

Some typical DSC curves are shown in *Figure 4.17*. The negative peaks indicate endothermic melting. The height of the peak quantifies the enthalpy of fusion. A pure sample gives a sharp peak (*Figure 4.17a*) while an impure sample would show a broader peak, an indefinite start and a blunt maximum. Different types of DSC curve will be obtained for different types of phase equilibria. For example, *Figure 4.17b* indicates, for a binary system, the behaviour for a simple eutectic and *Figure 4.17c* shows the behaviour for the formation of a series of solid solutions.

A good introductory account of the basic principles and practical requirements of a range of modern techniques of thermal analysis is given by Brown (1988). The development of a differential scanning calorimeter, coupled with a personal computer, for the measurement of solid–liquid equilibria, has been described by Matsuoka and Ozawa (1989).

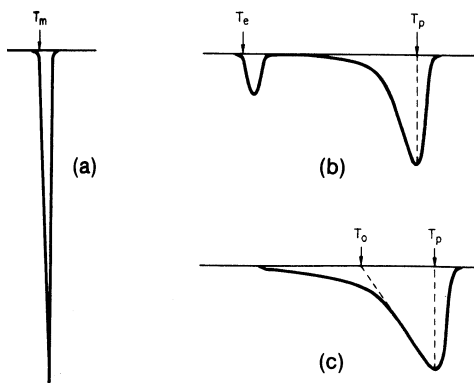


Figure 4.17. DSC curves: (a) pure component, (b) eutectic mixture, (c) solid solution (T_m melting point, T_e eutectic point, T_0 onset temperature, T_p peak temperature)

4.5.2 Dilatometry

The dilatometric methods for detecting phase changes utilize volume changes in the same way as the calorimetric methods utilize thermal effects. Dilatometry is widely used in the analysis of melts and particularly of fats and waxes (Bailey, 1950; Swern, 1979). The techniques and equipment are usually quite simple.

Solids absorb heat on melting and, with the notable exception of ice, expand. They evolve heat when they undergo polymorphic transformation to a more stable polymorphic and contract. Consequently, dilatometric (specific volume–temperature) curves bear a close resemblance to calorimetric (enthalpy–temperature) curves. The melting dilation corresponds to the heat of fusion, and the coefficient of cubical expansion, a , corresponds to the specific heat capacity, c . The ratio c/a is virtually a constant independent of temperature.

A dilatometer used for fats and waxes is shown in *Figure 4.18*. Mercury, or some other suitable liquid, is used as the confining fluid and the liquid thread in

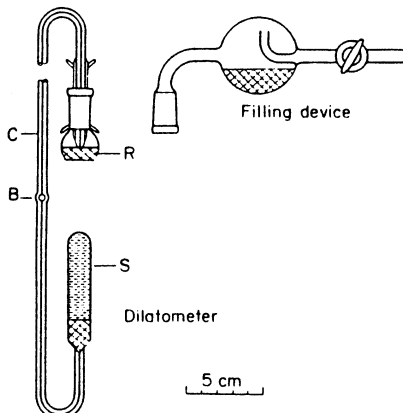


Figure 4.18. Gravimetric dilatometer and filling device. (After Bailey, 1950)

the capillary, *C*, communicates with the reservoir, *R*. Volume changes in the sample, *S*, are measured by weighing the liquid in the reservoir before and after. The small expansion bulb, *B*, is warmed to expel any air that enters the end of the capillary when the flask is detached. Owing to the high density of mercury and the accuracy with which weighings can be made, volume changes as small as $10^{-5}\text{cm}^3\text{ g}^{-1}$ have been detected.

Melting points can be determined with great precision by dilatometry. A plot of dilation versus temperature usually gives two straight lines – one for the solid dilation, which generally has a steep slope, and one for the liquid, with a low slope. The point of intersection of these two lines give the melting point, which may often be estimated to $\pm 0.01\text{ }^\circ\text{C}$.

4.6 Three-component systems

4.6.1 Construction of ternary diagrams

The phase equilibria in ternary systems can be affected by four variables, viz. temperature, pressure and the concentration of any two of the three components. This fact can be deduced from the phase rule:

$$P + F = 3 + 2$$

which indicates that a one-phase ternary system will have four degrees of freedom. It is impossible to represent the effects of the four possible variables in a ternary system on a two-dimensional graph. For solid–liquid systems, however, the pressure variable may be neglected, and the effect of temperature will be considered later.

The composition of a ternary system can be represented graphically on a triangular diagram. Two methods are in common use. The first utilizes the equilateral triangle, and the method of construction is shown in *Figure 4.19a*. The apexes of the triangle represent the pure components *A*, *B* and *C*. A point on a side of the triangle stands for a binary system, *AB*, *BC* or *AC*; a point within the triangle represents a ternary system *ABC*. The scales may be constructed in any convenient units, e.g. weight or mole percent, weight or mole fraction, etc., and any point on the diagram must satisfy the equation $A + B + C = 1$ or 100. The quantities of the components *A*, *B* and *C* in a given mixture *M* are represented by the perpendicular distance from the sides of the triangle.

Special triangular graph paper is required if the equilateral diagram is to be used, and for this reason many workers prefer to employ the right-angled triangular diagram which can be drawn on ordinary squared graph paper. The construction of the right-angled isosceles triangle is shown in *Figure 4.19b*. Again, as in the case of the equilateral triangle, each apex represents a pure component *A*, *B* or *C*, a point on a side a binary system, and a point within the triangle a ternary system; in all cases $A + B + C = 1$ or 100. The quantities of *A*, *B* and *C* in a given mixture *M* are represented by the perpendicular

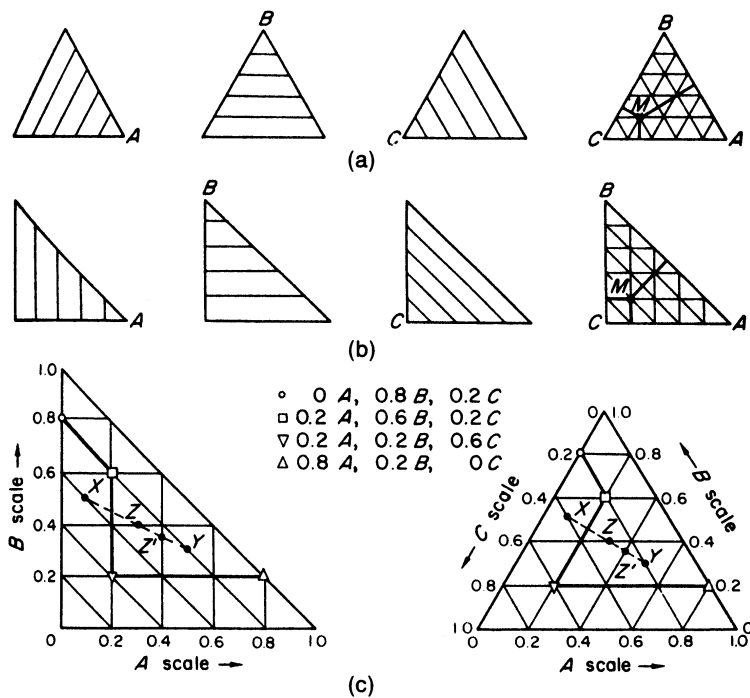


Figure 4.19. Construction of equilateral triangular diagrams

distances to the sides of the triangle. If two compositions, A and B , B and C , or A and C are known, the composition of the third component is fixed on both triangular diagrams.

Two actual plots are shown in *Figure 4.19c* to illustrate the interpretation of these diagrams. For clarity the C scale has been omitted from the right-angled diagram; the C values can be obtained from the expression $C = 1 - (A + B)$. The ‘mixture rule’ is also illustrated in *Figure 4.19c*. When any two mixtures X and Y are mixed together, the composition of the final mixture Z is represented by a point on the diagram located on a straight line drawn between the points representing the initial mixtures. The position of Z is located by the expression

$$\frac{\text{mass of mixture } X}{\text{mass of mixture } Y} = \frac{\text{distance } YZ}{\text{distance } XZ}$$

For example, if one part of a mixture X ($0.1A, 0.5B, 0.4C$) is mixed with one part of a mixture Y ($0.5A, 0.3B, 0.2C$), the composition of the final mixture Z ($0.3A, 0.4B, 0.3C$) is found on the line XY where $XZ = YZ$. Again, if 3 parts of Y are mixed with 1 part of X , the mixture composition Z' ($0.4A, 0.35B, 0.25C$) is found on the line XY where $XZ' = 3(YZ')$. The mixture rule also applies to the removal of one or more constituents from a system. Thus, one part of a mixture X removed from 2 parts of a mixture Z would yield one part of a mixture Y given by:

$$\frac{\text{mass of original } Z}{\text{mass of } X \text{ removed}} = \frac{YX}{YZ} = \frac{2}{1}$$

Similarly, one part of X removed from 4 parts of Z' would yield 3 parts of a mixture Y given by

$$\frac{\text{mass of original } Z'}{\text{mass of } X \text{ removed}} = \frac{YX}{YZ'} = \frac{4}{1}$$

The principle of the mixture rule is the same as that employed in the operation of lever-arm problems, i.e. $m_1l_1 = m_2l_2$, where m is a mass and l is the distance between the line of action of the mass and the fulcrum. For this reason, the mixture rule is often referred to as the lever-arm or centre of gravity principle.

Although ternary equilibrium data are most frequently plotted on equilateral diagrams, the use of the right-angled diagram has several advantages. Apart from the fact that special graph paper is not required, it is claimed that information may be plotted more rapidly on it, and some people find it easier to read. In this section the conventional equilateral diagram will mostly be employed, but one or two illustrations of the use of the right-angled diagram will be given.

4.6.2 Eutectic formation

Equilibrium relationships in three-component systems can be represented on a temperature–concentration space model as shown in *Figure 4.20*. The ternary system *ortho*-, *meta*- and *para*-nitrophenol, in which no compound formation occurs, is chosen for illustration purposes. The three components will be referred to as O , M and P , respectively. Points O' , M' and P' on the vertical

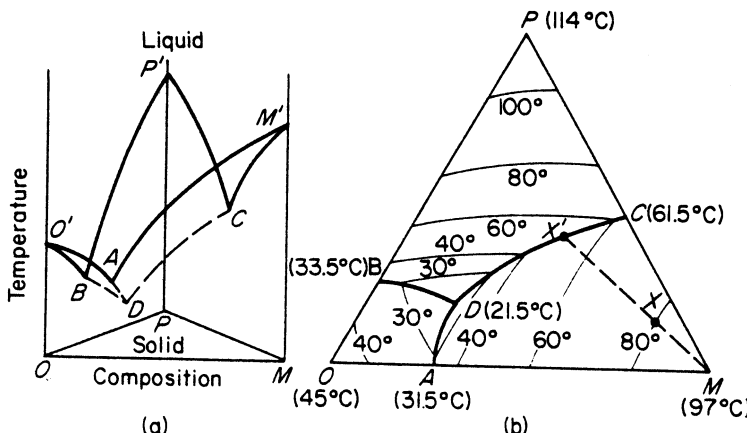


Figure 4.20. Eutectic formation in the three-component system o-, m- and p-nitrophenol: (a) temperature–concentration space model; (b) projection on a triangular diagram

edges of the model represent the melting points of the pure components *ortho*- (45 °C), *meta*- (97 °C) and *para*- (114 °C). The vertical faces of the prism represent the temperature-concentration diagrams for the three binary systems *O*-*M*, *O*-*P* and *M*-*P*. These diagrams are each similar to that shown in *Figure 4.4* described in the section on binary eutectic systems. In this case, however, the solidus lines have been omitted for clarity.

The binary eutectics are represented by points *A* (31.5 °C; 72.5 per cent *O*, 27.5 per cent *M*), *B* (33.5 °C; 75.5 per cent *O*, 24.5 per cent *M*) and *C* (61.5 °C; 54.8 per cent *M*, 45.2 per cent *P*). Curve *AD* within the prism represents the effect of the addition of the component *P* to the *O*-*M* binary eutectic *A*. Similarly, curves *BD* and *CD* denote the lowering of the freezing points of the binary eutectics *B* and *C*, respectively, on the addition of the third component. Point *D*, which indicates the lowest temperature at which solid and liquid phases can coexist in equilibrium in this system, is a ternary eutectic point (21.5 °C; 57.7 per cent *O*, 23.2 per cent *M*, 19.1 per cent *P*). At this temperature and concentration the liquid freezes invariantly to form a solid mixture of the three components. The section of the space model above the freezing point surfaces formed by the liquidus curves represents the homogeneous liquid phase. The section below these surfaces down to a temperature represented by point *D* denotes solid and liquid phases in equilibrium. Below this temperature the section of the model represents a completely solidified system.

Figure 4.20b is the projection of the curves *AD*, *BD* and *CD* in *Figure 4.20a* on to the triangular base. The apexes of the triangle represent the pure components *O*, *M* and *P* and their melting points. Points *A*, *B* and *C* on the sides of the triangle indicate the three binary eutectic points, point *D* the ternary eutectic point. The projection diagram is divided by curves *AD*, *BD* and *CD* into three regions which denote the three liquidus surfaces in the space model. The temperature falls from the apexes and sides of the triangle towards the eutectic point *D*, and several isotherms showing points on the liquidus surfaces are drawn on the diagrams. The phase reactions occurring when a given ternary mixture is cooled can now be traced.

A molten mixture with a composition as in point *X* starts to solidify when the temperature is reduced to 80 °C. Point *X* lies in the region *ADCM*, so pure *meta*- is deposited on decreasing temperature. The composition of the remaining melt changes along line *MXX'* in the direction away from point *M* representing the deposited solid phase (the mixture rule). At *X'*, where line *MXX'* meets curve *CD*, the temperature is about 50 °C, and at this point a second component (*para*-) also starts to crystallize out. On further cooling, *meta*- and *para*- are deposited and the liquid phase composition changes in the direction *X'D*. When melt composition and temperature reach point *D*, the third component (*ortho*-) crystallizes out, and the system solidifies without any further change in composition. A similar reasoning may be applied to the cooling, or melting, of systems represented by points in the other regions of the diagrams.

An example of the use of a ternary eutectic diagram for the assessment of a melt recrystallization process (for nitrotoluene isomers) is given in section 8.2.1.

4.6.3 Two salts and water

There are many different types of phase behaviour encountered in ternary systems consisting of water and two solid solutes. Only a few of the simpler cases will be considered here; attention will be devoted to a brief survey of systems in which there is (a) no chemical reaction, (b) formation of a solvate, e.g. a hydrate, (c) formation of a double salt, and (d) formation of a hydrated double salt.

At one given temperature the composition of, and phase equilibria in, a ternary aqueous solution can be represented on an isothermal triangular diagram. The construction of these diagrams has already been described. Polythermal diagrams can also be constructed, but in the case of complex systems the charts tend to become congested and rather difficult to interpret.

No compound formed

This simplest case is illustrated in *Figure 4.21* for the system $\text{KNO}_3\text{--NaNO}_3\text{--H}_2\text{O}$ at 50°C . Neither salt forms a hydrate, nor do they combine chemically. Point *A* represents the solubility of KNO_3 in water at the stated temperature (46.2 g/100 g of solution) and point *C* the solubility of NaNO_3 (53.2 g/100 g). Curve *AB* indicates the composition of saturated ternary solutions that are in equilibrium with solid KNO_3 , curve *BC* those in equilibrium with solid NaNO_3 . The upper area enclosed by *ABC* represents the region of unsaturated homogeneous solutions. The three ‘triangular’ areas are constructed by drawing straight lines from point *B* to the two apexes of the triangle; the compositions of the phases within these regions are marked on the diagram. At point *B* the solution is saturated with respect to both KNO_3 and NaNO_3 , and from the reduced phase rule $F' = 1$. This means that point *B*, generally referred to as a *eutonic point*, is univariant, i.e. invariant when the temperature is fixed.

The effect of isothermal evaporation on such a system can be shown as follows. If water is evaporated from an unsaturated solution represented by

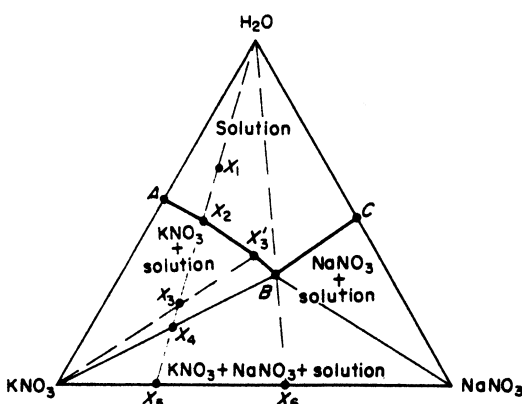


Figure 4.21. Phase diagram for the system $\text{KNO}_3\text{--NaNO}_3\text{--H}_2\text{O}$ at 50°C

point X_1 in the diagram, the solution concentration will increase, following line X_1X_2 . Pure KNO_3 will be deposited when the concentration reaches point X_2 . If more water is evaporated to give a system of composition X_3 , the composition of the solution will be represented by point X'_3 on the saturation curve AB ; and when composition X_4 is reached, by point B : any further removal of water will cause the deposition of NaNO_3 as well as KNO_3 . All solutions in contact with solid will thereafter have a constant composition B . For this reason the eutonic point B is sometimes referred to as the *drying-up point* of the system. After the complete evaporation of water the composition of the solid residue is indicated by point X_5 on the base line.

Similarly, if an unsaturated solution, represented by a point located to the right of B in the diagram, were evaporated isothermally, only NaNO_3 would be deposited until the solution composition reached the drying-up point B , when KNO_3 would also be deposited. The solution composition would thereafter remain constant until evaporation was completed. If water is removed isothermally from a solution of composition B , the composition of the deposited solid is given by point X_6 on the base line, and it remains unchanged throughout the remainder of the evaporation process.

The effect of the addition of one of the salts to the system $\text{KNO}_3\text{--NaNO}_3\text{--H}_2\text{O}$ at 50°C is shown in *Figure 4.22a*. This time the equilibria are plotted on a right-angled triangular diagram simply to demonstrate the use of this type of chart. Points A and C , as in *Figure 4.21*, refer to the solubilities at 50°C of KNO_3 and NaNO_3 , respectively. Curves AB and BC indicate the saturated ternary solutions in equilibrium with solid KNO_3 or NaNO_3 , and show, for instance, that the solubility of KNO_3 in water is depressed when NaNO_3 is present in the system, and vice versa.

Take, for example, a binary system $\text{NaNO}_3\text{--H}_2\text{O}$ represented by point Y_1 (0.7 mass fraction of NaNO_3 and 0.3 H_2O). As this point lies in the 'triangular'

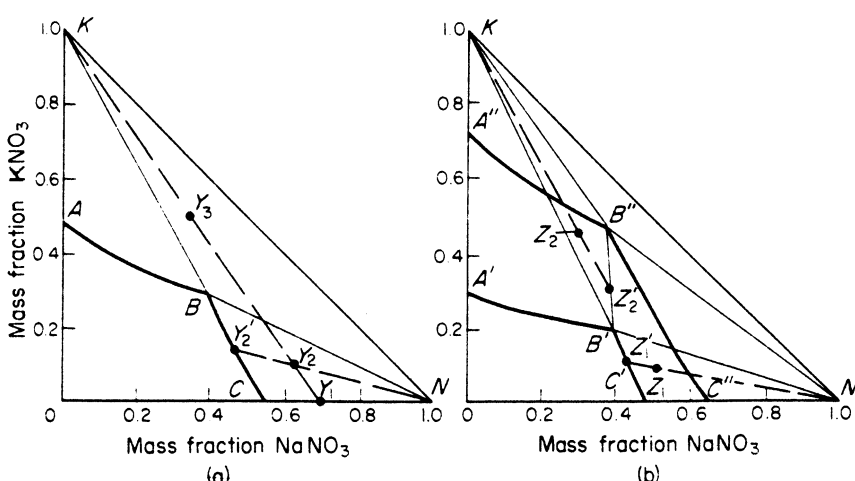


Figure 4.22. Phase diagrams for the system $\text{KNO}_3\text{--NaNO}_3\text{--H}_2\text{O}$: (a) at 50°C ; (b) at 24 and 100°C

region to the right of curve BC , the system consists of a saturated solution of NaNO_3 , with a composition given by point C , and excess solid NaNO_3 . If a quantity of KNO_3 is added to this binary system, the temperature being kept constant at 50°C so that the new composition is represented by point Y_2 ($0.64 \text{ NaNO}_3, 0.1 \text{ KNO}_3, 0.26 \text{ H}_2\text{O}$), the composition of the ternary saturated solution in contact with the excess solid NaNO_3 present is given by Y'_2 ($0.46 \text{ NaNO}_3, 0.15 \text{ KNO}_3, 0.39 \text{ H}_2\text{O}$) on the line drawn from the apex N through Y_2 to meet curve BC . As more KNO_3 is added, the solution concentration alters, following curve CB . At point B the solution becomes saturated with respect to both NaNO_3 and KNO_3 ; its concentration is $0.4 \text{ NaNO}_3, 0.29 \text{ KNO}_3, 0.31 \text{ H}_2\text{O}$. If after this point further quantities of KNO_3 are added to bring the system concentration up to some point Y_3 , no more KNO_3 dissolves, the solution composition remains at point B .

The interpretation of these phase diagrams is aided by remembering the rule of mixtures – i.e. on the removal or addition of any component from or to a system, the composition of the system changes along a straight line drawn from the original composition point to the apex representing the pure given component. In *Figure 4.22a* the right-angled apex represents pure water, the top apex K pure KNO_3 and the other acute apex N pure NaNO_3 .

The effect of temperature on the system $\text{KNO}_3\text{--NaNO}_3\text{--H}_2\text{O}$ is shown in *Figure 4.22b*. Two isotherms, $A'B'C'$ and $A''B''C''$, for 25 and 100°C , respectively, are drawn on this diagram. The lower left-hand area enclosed by $A'B'C$ represents homogeneous unsaturated solutions at 25°C , the larger area enclosed by $A''B''C''$ unsaturated solutions at 100°C . The line $B'B''$ shows the locus of the drying-up points between 25 and 100°C . To illustrate the effect of temperature changes in the system, let point Z_1 refer to the composition ($0.5 \text{ NaNO}_3, 0.1 \text{ KNO}_3, 0.4 \text{ H}_2\text{O}$) of a certain quantity of the ternary mixture. From the position of Z_1 in the diagram it can be seen that at 100°C the system would be a homogeneous unsaturated solution, but at 25°C it would consist of pure undissolved NaNO_3 in a saturated aqueous solution of NaNO_3 and KNO_3 . Thus pure NaNO_3 would crystallize out of the solution Z_1 on cooling from, say, 100 to 25°C , in fact at about 50°C . Despite the phase changes, of course, the overall system composition remains at Z_1 until one or more components are removed. At 25°C the composition of the solution in contact with the crystals of NaNO_3 is given by the intersection of the line from N through Z_1 with curve $B'C'$, i.e. at point Z'_1 ($0.43 \text{ NaNO}_3, 0.11 \text{ KNO}_3, 0.46 \text{ H}_2\text{O}$). The quantity of NaNO_3 which would crystallize out at 25°C is given by the mixture rule

$$\frac{\text{mass of crystals deposited}}{\text{mass of saturated solution}} = \frac{\text{length } Z_1Z'_1}{\text{length } Z_1N}$$

where N represents the NaNO_3 apex of the triangle.

When a ‘pure’ solute is to be crystallized from a ternary two-solute system by cooling, there is usually a temperature limit below which the desired solute becomes ‘contaminated’ with the other solute. This can be demonstrated by considering a system represented by point Z_2 in *Figure 4.22b*. The composition at Z_2 is $0.3 \text{ NaNO}_3, 0.45 \text{ KNO}_3, 0.25 \text{ H}_2\text{O}$; at 100°C the system is a homogeneous

unsaturated solution. At 25 °C, however, this point lies in the region where both solid NaNO₃ and KNO₃ are in equilibrium with a saturated solution of both salts, its composition being given by point B'. If it is desired to cool solution Z₂ in order to yield only KNO₃ crystals, then the temperature limitation is found by drawing a straight line from the KNO₃ apex K through point Z₂ and producing it to meet the drying-up line B'B'' at Z'_2. Point Z'_2 occupies the position of an invariant point on an isotherm; by referring to Figure 4.22a it can be seen that it corresponds approximately to point B on the 50 °C isotherm. Thus solution Z₂ must not be cooled below 50 °C if only KNO₃ crystals are to be deposited.

Solvate formation

When one of the solutes in a ternary system is capable of forming a compound, with the solvent, the phase diagram will contain more regions to consider than in the simple case described above. A common example of solvate formation is the production of a hydrated salt in a ternary aqueous system. Figure 4.23 shows the isothermal diagrams for the system NaCl–Na₂SO₄–H₂O at two temperatures, 17.5 and 25 °C, at which different phase equilibria are exhibited. Sodium sulphate combines with water, under certain conditions, to form Na₂SO₄ · 10H₂O. Sodium chloride, however, does not form a hydrate at the temperature being considered. Figure 4.23a shows the case where the decahydrate is stable in the presence of NaCl, and Figure 4.23b that of the decahydrate being dehydrated by the NaCl under certain conditions.

Points A and C in Figure 4.23a represent the solubilities of NaCl (26.5 mass per cent) and Na₂SO₄ (13.8 per cent) in water at 17.5 °C, curves AB and BC the ternary solutions in equilibrium with solid NaCl and Na₂SO₄ · 10H₂O, respectively. Point D shows the composition of the hydrate Na₂SO₄ · 10H₂O. For convenience, the following symbols are used on the diagram to mark the phase

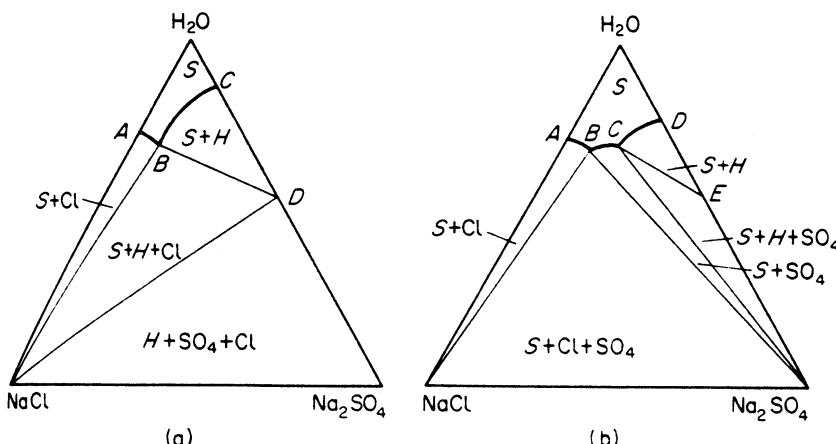


Figure 4.23. Phase diagrams for the system NaCl–Na₂SO₄–H₂O: (a) at 17.5 °C; (b) at 25 °C

regions: S = solution; H = hydrate $\text{Na}_2\text{SO}_4 \cdot 10\text{H}_2\text{O}$; SO_4 = Na_2SO_4 and $\text{Cl} = \text{NaCl}$. The solution above curve ABC is unsaturated. The lowest triangular region represents a solid mixture of Na_2SO_4 , $\text{Na}_2\text{SO}_4 \cdot 10\text{H}_2\text{O}$ and NaCl . Point B is the eutonic or drying-up point of the system.

In Figure 4.23b, points A and D denote the solubilities of NaCl (26.6 mass per cent) and Na_2SO_4 (21.6 per cent) in water at 25°C , point E the composition of $\text{Na}_2\text{SO}_4 \cdot 10\text{H}_2\text{O}$. In this diagram there are three curves, AB , BC and CD , which give the composition of the ternary solutions in equilibrium with NaCl , Na_2SO_4 and $\text{Na}_2\text{SO}_4 \cdot 10\text{H}_2\text{O}$. The various phase regions are indicated on the diagram. If NaCl is added to a system in the region CDE , i.e. to an equilibrium mixture of solid $\text{Na}_2\text{SO}_4 \cdot 10\text{H}_2\text{O}$ in a solution of NaCl and Na_2SO_4 , the solution concentration will change along curve DC . When point C is reached, the NaCl can only dissolve by dehydrating the $\text{Na}_2\text{SO}_4 \cdot 10\text{H}_2\text{O}$, and anhydrous Na_2SO_4 is deposited. Further addition of NaCl will result in the complete removal of the decahydrate from the system, the solution concentration following curve CB ; under these conditions the excess solid phase consists of anhydrous Na_2SO_4 . At the eutonic point B the solution is saturated with respect to both NaCl and Na_2SO_4 .

The effects of isothermal evaporation, salt additions and cooling can be traced from Figure 4.23 in a manner similar to that outlined for Figures 4.21 and 4.22.

Double salt formation

Cases are encountered in ternary systems where the two dissolved solutes combine in fixed proportions to form a definite double compound. Figure 4.24 shows two possible cases for a hypothetical aqueous solution of two salts A and B . Point C on the AB side of each triangle represents the composition of the double salt; points L and O show the solubilities of salts A and B in water at the given temperature. Curves LM and NO denote ternary solutions saturated

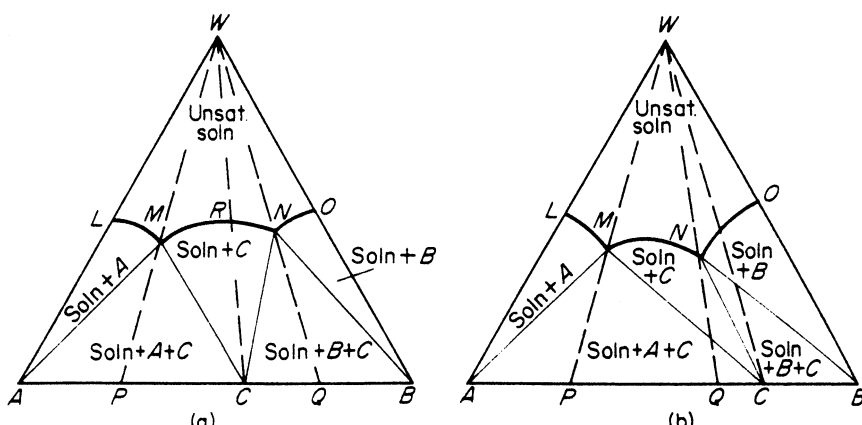


Figure 4.24. Formation of a double salt: (a) stable in water; (b) decomposed by water

with salts *A* and *B*, respectively, curve *MN* ternary solutions in equilibrium with the double salt *C*. The significance of the various areas is marked on the diagrams.

The isothermal dehydration of solutions in *Figure 4.24a* can be traced in the manner described for *Figures 4.21* and *4.22*. Point *M* is the eutonic or drying-up point for solutions located to the left of broken line *WR*, point *N* that for solutions to the right of this line. A solution on line *WM* behaves as a solution of a single salt in water; when its composition reaches point *M*, a mixture of salt *A* and double salt *C* crystallizes out in the fixed ratio of the lengths *PC/AP*. Similarly, a solution on line *WN* yields a mixture of *B* and *C*, in the ratio *CQ/QB*, when its composition reaches point *N*. A solution represented by a point on line *WR* also behaves as a solution of a single salt; when its composition reaches point *R*, the double compound *C* crystallizes out and neither of salts *A* and *B* is deposited at any stage. Point *R*, therefore, is the third drying-up point of the system. An example of this type of system is ammonium and silver nitrates in water, giving the double salt $\text{NH}_4\text{NO}_3 \cdot \text{AgNO}_3$.

The phase diagram in *Figure 4.24b* shows a different case. There are only two drying-up points, *M* and *N*, in this system, the first for solutions located to the left, the second for solutions to the right of line *WN*. Each solution on lines *WM* and *WN* behaves as a solution of single salt in water. The line *WC* does not cross the saturation curve *MN* of the double salt but cuts the saturation curve for salt *B*, indicating that the double salt is not stable in water; it is decomposed and salt *B* is deposited. An example of this type of system is glaserite, a non-stoichiometric double salt of potassium and sodium sulphates with the formula $\text{K}_3\text{Na}(\text{SO}_4)_2$.

Hydrated double salt

Figure 4.25a shows the phase diagram for the case of a hydrated double salt that is stable in water. The best-known examples of this type of system are the

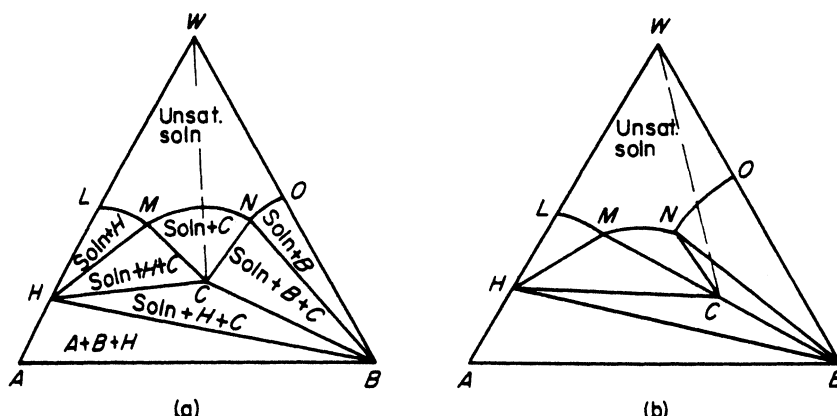


Figure 4.25. Formation of a hydrated double salt: (a) stable in water, (b) decomposed by water

alums ($M_2^I SO_4 \cdot M_2^{III} (SO_4)_3 \cdot 24H_2O$, where M^I and M^{III} represent mono- and trivalent cations, e.g. $M^I = Na, K, NH_4, Cs, Rb, Tl$ or hydroxylamine; $M^{III} = Al, Ti, V, Cr, Mn, Fe, Co$ or Ga ; the sulphate radical may be replaced by selenate) and the Tutton salts ($M_2^I M^{II} (SO_4)_2 \cdot 6H_2O$, where M^I and M^{II} represent mono- and bivalent ions, respectively, e.g. $M^I = NH_4, K, Rb, Cs$ or Te ; $M^{III} = Ni, Mn, Mg, Fe, Co, Zn$ or Cu).

In the case depicted salt A forms a hydrate of composition H . Its saturation curve is LM . Salt B is anhydrous and its saturation curve is ON . Point W represents water. Salts A and B combine together to form a hydrated double salt of composition denoted by point C within the triangular diagram. MN is the saturation curve for the hydrated double salt. The compositions of the phases in the eight separate regions are indicated in the diagram. The only region in which the pure hydrated double salt will crystallize out of solution, at the temperature for which the particular phase diagram is drawn, is the area bounded by MNC .

In Figure 4.25a line WC cuts the saturation curve MN of the hydrated double salt, which indicates that the salt is stable in the presence of water. In Figure 4.25b line WC does not cross curve MN , which indicates that the hydrated double salt decomposes in the presence of water. This is a comparatively rare behaviour, but an example is the case of $MgSO_4 \cdot Na_2SO_4 \cdot 4H_2O$ (astrakanite) at $25^\circ C$.

4.6.4 Solid solutions

Ternary systems comprising water and two electrolytes containing a common ion often yield solid solutions. Such a system can be represented in the manner indicated in Figure 4.26: an isothermal diagram for salts A and B and solvent water W . Points a and b represent the solubilities of salts A and B at the given

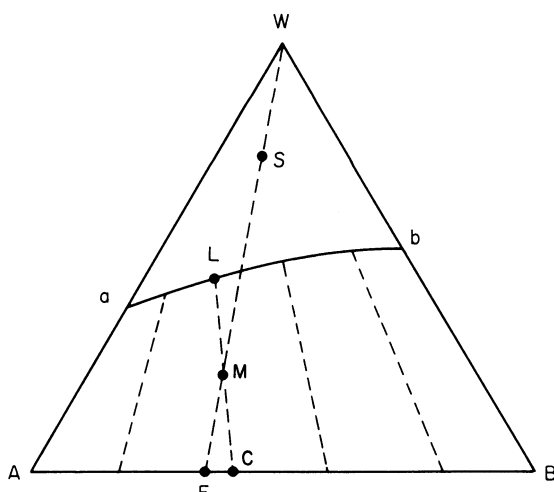


Figure 4.26. Solid solution formation in a ternary system, e.g. two salts in water

temperature. The curve ab represents the equilibrium solubilities of mixtures of salts A and B . The sector abW represents unsaturated solutions, and sector $AabB$ represents mixture of AB solid solutions (crystals) in equilibrium with aqueous solutions saturated with salts A and B . The broken tie lines connect equilibrium mixtures of liquid solutions (curve ab) and solid solutions (base line AB).

For example, a solution S , isothermally evaporated to a condition represented by point M would yield a mixture of crystals (solid solution) of overall composition C at one end of the tie line suspended in a solution of composition represented by point L at the other end. If evaporation were to be continued to dryness, the overall composition of the solid solution would be represented by point F on line AB . The deposited crystals would not be homogeneous, however, since they would have successively grown from a whole range of solution compositions and would tend to reflect these conditions by their outer layers being of slightly different composition from their insides.

An alternative method of representing ternary solid solution systems graphically is to plot the concentration of one component in the solid phase against its composition in the liquid phase. On this basis, Roozeboom in 1891 showed that five different types of system were possible. Only two of these will be mentioned here, however, but a good account of all five types of behaviour is given by Blasdale (1927).

Type I behaviour is characterized by complete miscibility, with the concentration of one of the salts in the liquid phase exceeding that in the solid phase for all concentrations (Figure 4.27a). Examples of type I systems include $\text{K}_2\text{SO}_4-(\text{NH}_4)_2\text{SO}_4-\text{H}_2\text{O}$, $\text{KH}_2\text{AsO}_4-\text{H}_2\text{O}$ and $\text{K}-\text{alum}-\text{NH}_4\text{-alum}-\text{H}_2\text{O}$.

Type II behaviour is also characterized by complete miscibility, but while the concentration of one of the salts in the liquid phase exceeds that in the solid phase for a certain rate of concentrations, it is less for the remaining concentrations. In other words, at one particular concentration the $A:B$ salt ratios in the solid and liquid phases are identical (Figure 4.27b). An example of this less-common type II behaviour is the system $\text{KCl}-\text{KBr}-\text{H}_2\text{O}$.

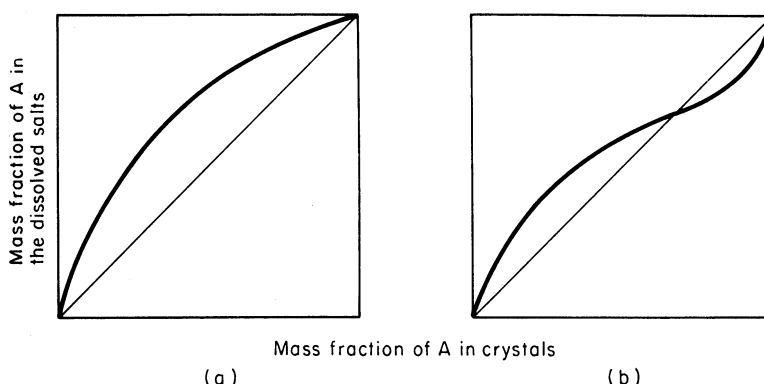


Figure 4.27. Solid solution formation in a ternary system: (a) Type 1; (b) Type 2

Solid solutions with a eutectic

Not all solid solution systems form continuous series; some exhibit partial miscibility, i.e. one solid solution being partially miscible with another, and, as in the case of partially miscible liquids, the phase region between the two homogeneous phases is referred to as the miscibility gap. Partially miscible solid solution systems can exhibit a number of different types of behaviour, but only one simple case will be described here for illustration purposes.

Figure 4.28 shows an example of two solid solutions that form a eutectic, a fairly common occurrence in organic melts. Curve AE indicates how increasing amounts of component B lower the freezing point of AB liquid mixtures. Curve BE shows the effect of component A on B . All systems above curve AEB (the liquidus) are homogeneous liquid and all systems below curve $ACEDB$ (the solidus) are solid. In the sectors to the left of ACF and to the right of BDG , the solid phases are homogeneous solid solutions α and β , respectively. The sector $FCEDG$, the miscibility gap, encloses heterogeneous mixtures of the two solid solutions α and β . The sectors ACE and BDE contain mixtures of $\alpha +$ liquid and $\beta +$ liquid respectively. Point E represents the temperature and composition of the eutectic, a conglomerate of solid solutions α and β . The cooling of a liquid mixture X to some temperature Y may be traced as follows. Point Y , which lies in sector BDE , represents a suspension of solid solution β , of composition S , in equilibrium with a liquid of composition L . The proportion of solid to liquid is represented by the distance ratio $LY: SY$ (the mixture rule).

When the miscibility gap extends close to the pure component compositions, it can be difficult to distinguish between this type of system and that of the simple eutectic described in section 4.3.1. The problem of *terminal solid solutions* is discussed in section 7.2.

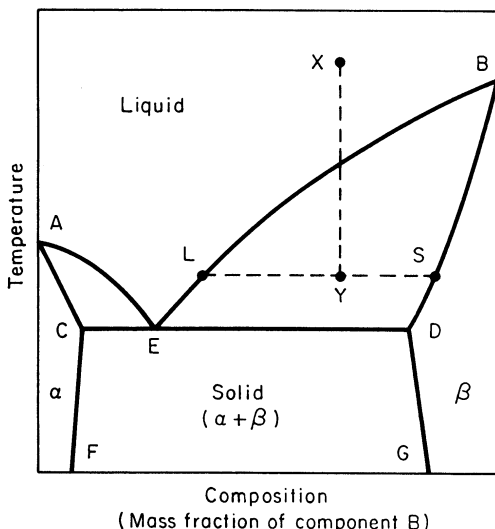


Figure 4.28. Two solid solutions that form a eutectic

4.6.5 Equilibrium determinations

For multicomponent systems the composition of the equilibrium solid phase can be determined indirectly by the so-called *wet-residues* method, first proposed by Schreinemakers (1893), in which the need for solid–liquid separation before analysis is avoided. In practice, the equilibrium system is allowed to settle and then most of the saturated supernatant solution is decanted off the sedimented solids. A sample of the wet solids is then scooped out and quickly weighed in a closed weighing bottle, to avoid solvent loss, and subsequently analysed by the most convenient analytical technique.

The method of wet residues is based on the application of the straight-line mixture rule on a phase diagram. For a ternary system, the solid–liquid phase equilibria can be represented on a triangular diagram, with the equilibrium solution composition being represented by a point on the solubility curve and the wet-residue composition by a point within the triangle. By virtue of the properties of a triangular phase diagram, the three points representing the compositions of equilibrium solubility, wet-residue and the equilibrium solid phase, must lie on a straight line (section 4.6.1). The point at which a line drawn through the solubility and wet-residue points and extended to meet the side of the triangle therefore gives the composition of the equilibrium solid phase.

Although extrapolations are commonly made graphically on phase diagrams, algebraic extrapolation is less subjective, more accurate, and lends itself to the application of statistical methods which minimize errors. Mathematical extrapolation procedures for the method of wet residues have been described by Ricci (1966) and Schott (1961).

The *synthetic complex* method of solid–liquid equilibrium determination in multicomponent systems offers an alternative procedure to that of the wet-residue method, and is capable of yielding more rapid results. The procedure is as follows. Several mixtures of the solutes are prepared, covering a range of compositions, and known amounts of solvent are added to each sample. Thus a number of ‘synthetic complexes’ of known composition are obtained and their composition points can be plotted within a phase diagram. The samples are then shaken or agitated to equilibrate at constant temperature, using any convenient method, after which the clear supernatant saturated solution is analysed. Again, as in the wet-residues method, a line is drawn through the ‘solution’ point, its corresponding ‘complex’ point, and then extended to one side of the phase diagram (triangular for a ternary system) to give the composition of the solid phase.

Purdon and Slater (1946) give good accounts of the practical difficulties that may be encountered in applying both the wet-residues and synthetic complex methods of solid phase analysis.

4.7 Four-component systems

A one-phase, four-component or quaternary system has five degrees of freedom. Therefore the phase equilibria in these systems may be affected by the five

variables: pressure, temperature and the concentrations of any three of the four components. To represent quaternary systems graphically, one or more of the above variables must be excluded. The effect of pressure on solid–liquid systems may be ignored, and if only one temperature is considered an isothermal space model can be constructed. If the concentration of one of the components is excluded, usually the liquid solvent, a two-dimensional graph can be drawn, but this simplification will be described later.

4.7.1 Three salts and water

The first, simple, type of quaternary system to be considered here consists of three solid solutes, *A*, *B* and *C*, and a liquid solvent, *S*. No chemical reaction takes place between any of the components, e.g. water and three salts with a common ion. The isothermal space model for this type of system can be constructed in the form of a tetrahedron (*Figure 4.29a*) with the solvent at the top apex and the three solid solutes on the base triangle. The four triangular faces of the tetrahedron represent the four ternary systems *A–B–C*, *A–B–S*, *A–C–S* and *B–C–S*. The three faces, excluding the base, have the appearance of the ‘two salts and water’ diagram shown in *Figure 4.21*.

A point on an edge of the tetrahedron represents a binary system, a point within it a quaternary. On the faces *ABS*, *BCS* and *ACS* the solubility curves meet at points *L*, *M* and *N*, respectively, which represent the solvent saturated with two solutes. They are the starting points for the three curves *LO*, *MO* and *NO*, which denote solutions of three solutes in the solvent; point *O* represents the solution which, at the given temperature, is saturated with respect to all three solutes. All these curves form three curved surfaces within the space model. The section between these surfaces and the apex of the tetrahedron indicates unsaturated solution, that between the surfaces and the triangular base complex mixtures of liquid and solid.

Figure 14.29b shows another way in which systems of this type can be represented as a space model. Here it takes the form of a triangular prism where the apexes of the triangular base represent the three solid components

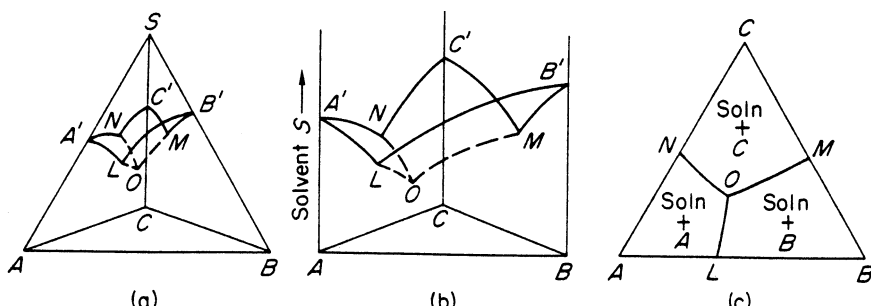


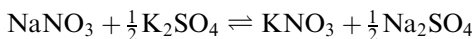
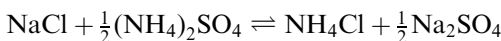
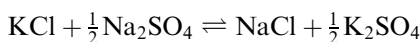
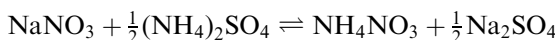
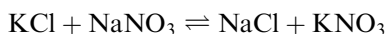
Figure 4.29. Isothermal representation of a quaternary system of the ‘three salts with a common ion in water’ type: (a) tetrahedral space model; (b) triangular prism space model; (c) Jänecke projection

and the vertical scale the liquid solvent. The interpretation of this model is similar to that just described for the tetrahedron; the same symbols have been used.

For a complete picture of the phase behaviour of quaternary systems a space model is essential; yet, because of its time-consuming construction, a two-dimensional ‘projection’ is frequently employed. Such a projection, named after E. Jänecke, is shown in *Figure 4.29c*. In this type of isothermal diagram the solvent is excluded. The curved surfaces *A'LON*, *B'MOL* and *C'NOM* in *Figures 4.29a* and *4.29b*, which represent solutions in equilibrium with solutes *A*, *B* and *C*, respectively, are projected on to the triangular base and become areas *ALON*, *BMOL* and *CNOM* in *Figure 4.29c*. Curves *LO*, *MO* and *NO* denote solutions in equilibrium with two solutes, viz. *A* and *B*, *B* and *C*, *A* and *C*, respectively, while point *O* represents a solution in equilibrium with the three solutes. For this type of system the projection diagram can be plotted in terms of mass or mole fractions or percentages.

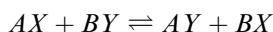
4.7.2 Reciprocal salt pairs

The second, and more important, type of quaternary system that will be considered is one consisting of two solutes and a liquid solvent where the two solutes inter-react and undergo double decomposition (metathesis). This behaviour is frequently encountered in aqueous solutions of two salts that do not have a common ion. Typical examples of double decomposition reactions of commercial importance are



The four salts in each of the above systems form what is known as a ‘reciprocal salt pair’. Although all four may be present in aqueous solution, the composition of any mixture can be expressed in terms of three salts and water. Thus, from the phase rule point of view, an aqueous reciprocal salt pair system is considered to be a four-component system.

Reciprocal salt pair solutions may be represented on an isothermal space model, in the form of either a square-based pyramid or a square prism. *Figure 4.30a* indicates the pyramidal model: the four equilateral triangular faces stand for the four ternary systems *AX-AY-W*, *AY-BY-W*, *BY-BX-W* and *4X-BX-W* (*W* = water) for the salt pair represented by the equation



The apex of the pyramid denotes pure water, its base the anhydrous quaternary system *AX-AY-BX-BY*. Points *L*, *M*, *N* and *O* on the four triangular faces of

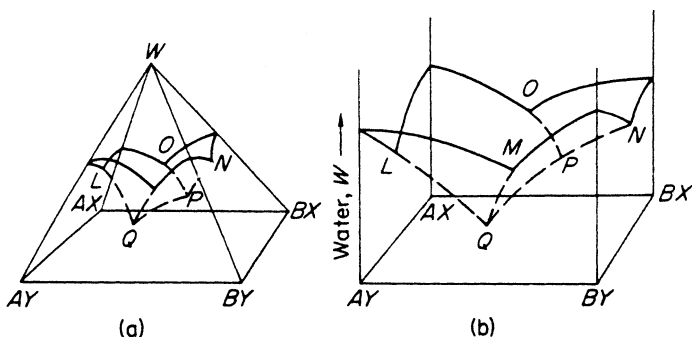


Figure 4.30. Isothermal representation of a quaternary system of the ‘reciprocal salt pair’ type: (a) square-based pyramid; (b) square prism

the pyramid indicate the equilibria between two salts and water. Point P , which represents a solution of three salts AX , BX and BY in water saturated with all three salts, is a quaternary invariant point. So is Q , which shows the equilibrium between salts AX , AY and BY and water. Curves OP , NP and LQ , MQ , which join these quaternary invariant points P and Q to the corresponding ternary invariant points on the triangular faces of the pyramid, represent solutions of three salts in water saturated with two salts, and so does curve PQ , joining the two quaternary invariant points.

The square-prism space model (*Figure 4.30b*) illustrates another way in which a quaternary system of the reciprocal salt pair type may be represented. The vertical axis stands for the water content, and the points on the diagram are the same as those marked on *Figure 4.30a*. In both diagrams all surfaces formed between the internal curves represent solutions of three salts in water saturated with one salt, all internal curves solutions of three salts in water saturated with two salts, and the two points P and Q solutions of three salts in water saturated with the three salts. The section above the internal curved surfaces denotes unsaturated solutions, the section below them mixtures of liquid and solid.

4.7.3 Jänecke diagrams

In order to simplify the interpretation of the phase equilibria in reciprocal salt pair systems, the water content may be excluded. The curves of the space model can then be projected on to the square base to give a two-dimensional graph, called a Jänecke diagram as described in section 4.7.1. A typical projection is shown in *Figure 4.31a*; the lettering is that used in *Figure 4.30*. The enclosed areas, which represent saturation surfaces, indicate solutions in equilibrium with one salt, the curves solutions in equilibrium with two salts, points P and Q solutions in equilibrium with three salts.

Molar or ionic bases must be used in this type of diagram for reciprocal salt pairs. The four corners of the square represent 100 mol of the pure salts AX , BX , BY and AY . Any point inside the square denotes 100 mol of a mixture of these salts; its composition can always be expressed in terms of three salts. The

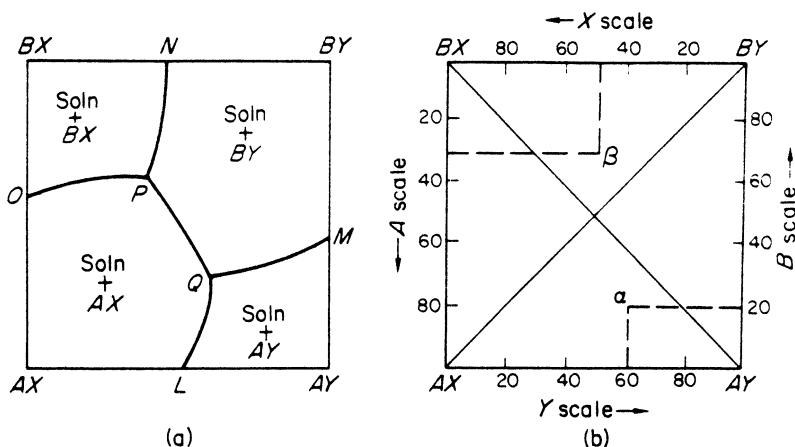


Figure 4.31. Interpretation of the Jänecke diagram for reciprocal salt pairs: (a) projection of the surfaces of saturation on to the base; (b) method of plotting

scales in Figure 4.31b are marked in ionic percentages of A , B , X and Y . Take, for example, 100 mol of a mixture expressed as

Salt	moles of compounds	moles of ions			
		A	B	X	Y
AX	20	20		20	
AY	60		60		60
BX	20			20	20
	100	80	20	40	60

The totals of the $A + B$ ions (e.g. the basic radicals) and the $X + Y$ ions (e.g. the acidic radicals) must always equal 100. Thus point α , indicating this mixture can be plotted: the square is divided by the two diagonals into four right-angled triangles, and point α lies in triangles $AX.AY.BX$ and $AX.AY.BY$. Therefore the composition of the above mixture could also have been expressed in terms of salts AX (40 mol), AY (40 mol) and BX (20 mol). In a similar manner, it can be shown that point β which lies within the two triangles $AX.BX.BY$ and $BX.BY.AY$ represents 100 mol of a mixture with a composition expressed either by 50 BY , 30 AX and 20 BX , or by 50 BX , 30 AY and 20 BY .

Although it is usually more convenient to plot ionic percentages on the square, it is quite in order to plot mole percentages of the salts direct. The numerical scales marked on Figure 4.31b must now be ignored. If point α is considered to lie in triangle $AX.AY.BX$, representing a mixture 20 AX , 60 AY and 20 BX , the compositions of the two salts at opposite ends of the diagonal AY and BX are used for plotting purposes. Thus point α is located by 60 along the horizontal AY scale and 20 up the vertical BX scale. If α is taken to lie in triangle $AX.AY.BY$, the composition is represented by 40 AX , 20 BY , 40 AY ,

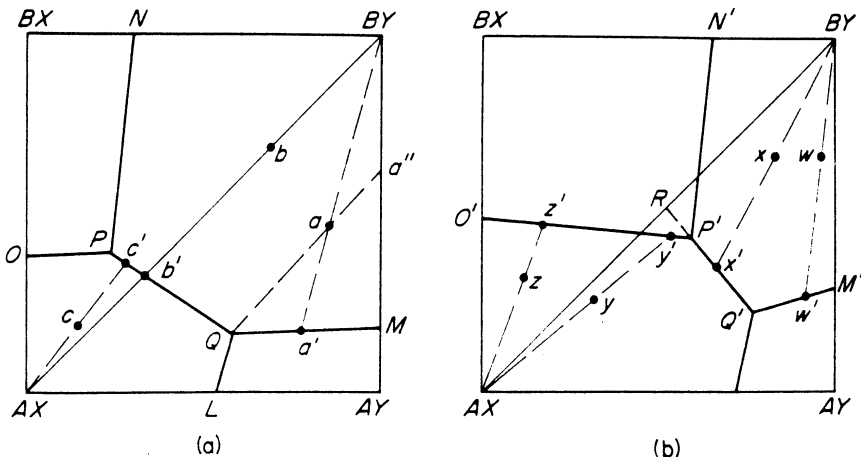


Figure 4.32. Jänecke projections for aqueous solutions of a reciprocal salt pair, showing (a) two congruent points, (b) congruent and incongruent points

and the AY and BX compositions are used for plotting. A similar reasoning may be applied to the plotting of point β in triangles AX , BX , BY and AY , BY , BX .

Figure 4.32 shows Jänecke diagrams for solutions of a given reciprocal salt pair at different temperatures. These two simple cases will be used to demonstrate some of the phase reactions that can be encountered in such systems. Both diagrams are divided by the saturation curves into four areas which are actually the projections of the surfaces of saturation (e.g., see Figure 4.32b). Salts AX and BY can coexist in solution in stable equilibrium: the solutions are given by points along curve PQ . Salts BX and AY , however, cannot coexist in solution because their saturation surfaces are separated from each other by curve PQ . Thus AX and BY are called the *stable salt pair*, or the *compatible salts*, BX and AY the *unstable salt pair*, or the *incompatible salts*. In Figure 4.32a the AX - BY diagonal cuts curve PQ which joins the two quaternary invariant points, while in Figure 4.32b curve $P'Q'$ is not cut by either diagonal. These are two different cases to consider.

Point P represents a solution saturated with salts AX , BX and BY , Q one saturated with salts AX , BY and AY . In Figure 4.32a both P and Q lie in their ‘correct’ triangles, i.e. $AX \cdot BX \cdot BY$ and $AX \cdot BY \cdot AY$, respectively, and solutions represented by P and Q are said to be congruently saturated. In Figure 4.32b point Q' lies in its ‘correct’ triangle, $AX \cdot BY \cdot AY$, but P' lies in the ‘wrong’ triangle, the same as Q' . Point Q' , therefore, is *congruent* and point P' is *incongruent*.

Isothermal evaporation

The phase reactions occurring on the removal of water from a reciprocal salt pair system will first be described with reference to *Figure 4.32a*. Point *a* which lies on the *BY* saturation surface represents a solution saturated with salt *BY*. When water is removed isothermally from this solution, the pure salt *BY* is

deposited and the solution composition (i.e. the composition of the salts in solution, the water content being ignored) moves from a towards a' along the straight line drawn from BY through a to meet curve QM . When a sufficient quantity of water has been removed, the solution composition reaches point a' and here the solution is saturated with two salts, BY and AY .

Further evaporation results in the deposition of AY as well as BY ; the composition of the solid phase being deposited is given by point M . The overall composition of deposited solid therefore moves from BY towards a'' on the line $BY . AY$. The solution composition, being depleted in solid M , moves away from point M towards Q . On reaching point Q , three salts AX , AY and BY are deposited. The composition of the solid phase deposited is also given by point Q ; the overall composition of the solid phase, assuming that none has been removed from the system, by point a'' . The solution composition, the water content being ignored, and the composition of the deposited solid phase remain constant at point Q for the rest of the evaporation process, and the overall solids content changes along line $a''a$, composition a representing the completely dry complex. Point Q is a quaternary drying-up point for all solutions represented by points within triangle $AX . AY . BY$.

The isothermal evaporation of solution b on the diagonal can be traced as follows. If point b lies on the saturation surface, it represents a solution saturated with salt BY . While salt BY is being deposited, the solution composition changes along the diagonal from b towards b' . At b' the solution becomes saturated with salts AX and BY . This ternary system ($AX-BY-H_2O$) thereafter dries up, without change in composition, at point b' . Point b' , therefore, is a ternary drying-up point.

If point c lies on the saturation surface, it represents a solution saturated with salt AX . When this solution is evaporated isothermally, AX is deposited and the solution composition changes along line cc' . At c' salt BY also crystallizes out and the composition of the solid phase deposited is given by b' , the point at which the diagonal crosses line PQ . The solution composition, therefore, changes along line $c'P$, and at P the three salts AX , BY and BX are co-deposited: point P is the quaternary drying-up point for all solutions represented by points within triangle $AX . BX . BY$.

The isothermal evaporation of a solution denoted by point w in *Figure 4.32b* can be traced in the same manner as that described for point a in *Figure 4.32a*. Q' is the drying-up point. The evaporation of solution x can be traced as follows. At x the solution is saturated with salt BY , and this salt is deposited until the solution composition reaches x' , where the solution is saturated with the two salts AX and BY . The composition of the solid phase being deposited at this stage is given by point R on the diagonal. As evaporation proceeds, the solution composition changes from point x' along line $x'Q'$, i.e. in a direction away from point R , and at Q' the solution is saturated with the three salts AX , AY and BY . Both solution and deposited solids thereafter have a constant composition until evaporation is complete: Q' is the quaternary drying-up point.

Point Q' is also the drying-up point for a solution represented by point y . The solution composition changes along line yy' while salt AX crystallizes out, and

then from y' towards P' while the two salts AX and BY of composition O' are deposited. At P' the solution is saturated with the three salts AX , BX and BY , the composition of the solid phase deposited at this point being given by R . On further evaporation, the solution composition remains constant at P' while salts AX and BY are deposited and salt BX is dissolved. When all BX has dissolved, the solution composition changes from P' towards Q' , and the solution finally dries up at Q' .

Point P' , therefore, is incongruent. It is not a true drying-up point except for the case where the original complex lies within the triangle representing the three salts of which it is the saturation point, i.e. AX , BY and BX . Point z may be taken as an example of this case. On evaporation, the solution composition changes from z to z' while salt AX is deposited, from z' towards P' while salts AX and BX are deposited. The composition of the solid phase at this latter stage is given by point O' . At P' this solution is saturated with salts AX , BX and BY . Further evaporation results in the deposition of AX and BY and the dissolution of BX . The solution dries up at point P' .

Representation of water content

So far in the discussion of Jänecke projections for reciprocal salt pair systems the water content has been ignored. This is not too serious, because much information can be obtained from the projection before consideration of the quantity of water present. One way in which the water content can be represented is shown in *Figure 4.33a*; the plan shows the projection of the saturation surfaces, the elevation indicates the water contents. To avoid unnecessary complication, the elevation only shows the horizontal view of the particular saturation curve concerned in the problem.

The isothermal evaporation of water from a complex a was considered in *Figure 4.32a*, where point a , representing the composition of the given complex, was taken to lie on the saturation surface. In *Figure 4.33a* the isothermal dehydration of an unsaturated solution S is considered, the dissolved salt having the same composition a as that in *Figure 4.32a*. Point S , therefore, is located on the elevation vertically above point a in the plan. The exact position of S is determined by the water content of the given solution, i.e. distance Sa_3 on the water scale denotes the moles of water per 100 mol of salt content. Line Sa_3 , called the *water line*, represents the course of the isothermal dehydration. Points Q and M are similarly located on the elevation, according to their corresponding water contents, vertically above points Q and M on the plan. Point a' lies on curve QM vertically above a' in the plan. Point T on the elevation represents the water content of a saturated solution of pure salt BY , the salt to be deposited.

Three construction lines can now be drawn on the elevation. Line Ta' cuts the water line at point a . The BY saturation surface is assumed for simplicity to be plane, so Taa' is a line on this surface. The Y corner of the elevation represents pure salts AY and BY and all their mixtures. The line drawn from a' to Y (BY on plan) cuts the water line at a_1 , that from Q to Y (a'' on plan) at a_2 .

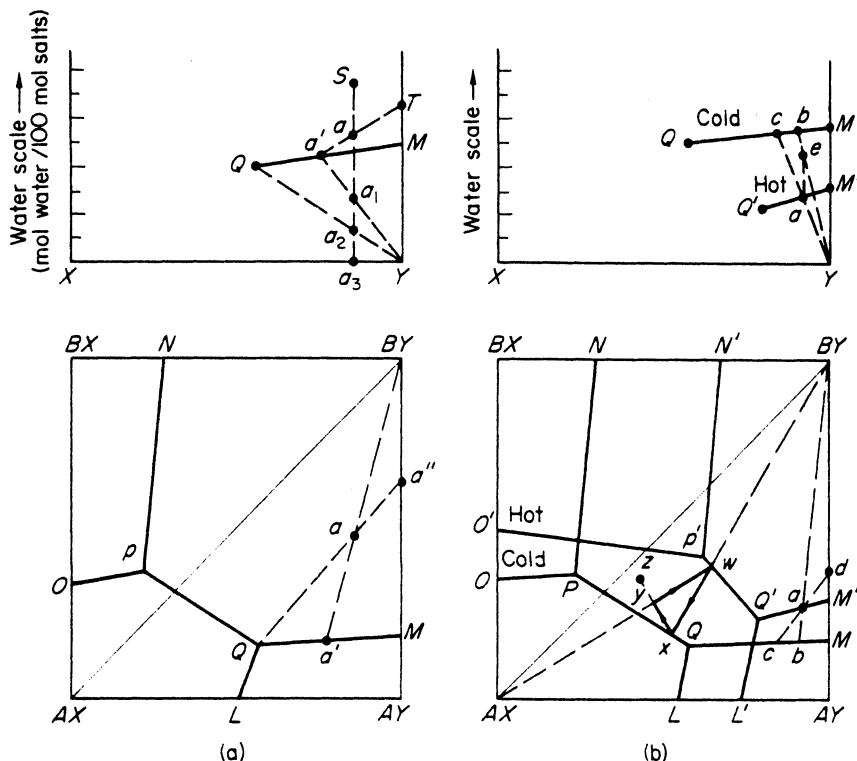


Figure 4.33. Representation of water content: (a) isothermal evaporation; (b) crystallization by cooling

When water is removed isothermally from the unsaturated solution S , the water content falls along the water line Sa_3 . When point a is reached, the solution is saturated with salt BY , and pure BY starts to crystallize out. The quantity of water to be removed to achieve this condition is determined from the water scale readings on the elevation diagram, i.e. Sa mol of water has to be removed from a system containing 100 mol of salts dissolved in Sa_3 mol of water. Salt BY is deposited while the water content falls from a to a_1 , and at point a_1 the solution (of composition a') becomes saturated with salts BY and AY . Both salts are deposited while the water content falls from a_1 to a_2 , and the overall deposited solids content changes along line BY/a'' on the plan. At point a_2 the solution (composition Q) is saturated with respect to the three salts AX , AY and BY , and further evaporation from a_2 to a_3 proceeds at constant solution composition Q . The solids composition changes along line $a''a$ on the plan.

Crystallization by cooling

The graphical procedure described above, viz. the drawing of a plan and elevation, provides a simple pictorial representation of the phase reactions

occurring in a given system at two different temperatures. *Figure 4.33b* shows two isotherms labelled ‘hot’ and ‘cold’, respectively; they are in fact the curves from *Figure 4.32*, plotted on one diagram, and the same lettering is used. By way of example, two different cooling operations will be considered.

Point *a* on curve $Q'M'$ represents a hot solution saturated with the two salts AY and BY . When it is cooled to the lower temperature point *a* lies in the BY field of the projection. Line BY/a is drawn on the plan to meet curve QM at *b*, but point *b* represents the solution composition only if point *a* lies on the BY saturation surface in the ‘cold’ projection, i.e. if pure BY was crystallizing out. To find the actual solution composition and the composition of the deposited solid phase, point *b* is projected from the plan onto curve QM in the elevation.

Point *Y* on the elevation diagram represents salts AY or BY or any mixture of them. Line Ya is drawn on the elevation and then produced to meet curve QM at *c*. It can be seen that in this case points *b* and *c* do not coincide. This means that the deposited solid phase is not pure salt BY but some mixture of BY and AY . Point *c* is projected from the elevation onto the plan, and line cad is drawn. Thus the final solution composition is given by point *c*, and the overall solid phase composition by point *d*.

If pure salt BY was required to be produced during the cooling operation, the water content of the system would have to be adjusted accordingly. Solution point *c* has to move to become coincident with point *d*, and solid point *d* has to move to BY on the plan. In this case, therefore, water has to be added to the system, e.g. to the hot solution before cooling. The quantity of water required per 100 mol of salts is given by the vertical distance ae on the elevation.

A different sequence of operations is shown in another section of *Figure 4.33b*. Point *w* on curve $P'Q'$ represents a solution saturated with salts AX and BY at the higher temperature. At the lower temperature, however, point *w* lies in the BY field of the diagram. If the correct amount of water is present in the system, pure BY crystallizes out on cooling, and the solution composition is given by point *x* located on line BY/w produced to meet curve PQ . A cyclic process can now be planned.

The pure salt BY is filtered off and a quantity of solid mixture, e.g. of composition *z*, is added to solution *x*. The quantity of solid *z* to be added, calculated by the mixture rule, must be the amount necessary to give complex *y*, the composition of which is chosen so that, on being heated to the higher temperature, it lies in the AX field, yields the original solution *w* and deposits the pure salt AX . Thus the sequence of operations is

1. Cool solution *w* to the lower temperature
2. Filter off solid BY
3. Add solid mixture *z* to the mother liquor *x* to give complex *y*
4. Heat the complex to the higher temperature
5. Filter off solid AX
6. Cool mother liquor *w* to the lower temperature, and so on

Of course, the water contents at each stage in the cycle must be adjusted so that the solutions deposit only one pure salt at a time. The quantities of water to be

added or removed can be estimated graphically on the elevation diagram in the manner described above for solution *a*.

Only the simplest type of reciprocal salt pair diagram has been considered here. Many systems form hydrates or double salts: in others the stable salt pair at one temperature may become the unstable pair at another. For information on these more complicated systems reference should be made to specialized works on the phase rule. The monographs by Blasdale (1927) and Purdon and Slater (1946) are particularly noteworthy in this respect; graphical solutions of problems of commercial importance are given, and five-component aqueous systems are analysed. Teeple (1929) and Fitch (1970) also give accounts of the use of multicomponent phase diagrams for the design of industrial fractional crystallization processes.

The phase diagrams described in this section are by no means limited to ‘salts in water’ systems, as a comparison between *Figures 4.20* and *4.29* will clearly show. A worked example of the use of a diagram similar to both *Figures 4.20b* and *4.29c* is given in section 8.2.1 to demonstrate the recovery of one pure component from a ternary organic eutectic system by cooling melt crystallization. The use of multicomponent phase diagrams for selecting appropriate crystallization methods for a wide range of separation procedures including cooling, evaporating, salting-out, adduct formation, etc. with both organic and inorganic systems has been extensively demonstrated by Chang and Ng (1998), Cesar and Ng (1999) and Wibowo and Ng (2000).

4.8 ‘Dynamic’ phase diagrams

One of the problems of trying to establish reliable phase equilibria in multicomponent solid–liquid systems is that very long periods of contact between crystals and solution are often necessary before the equilibrium state is approached. In fact, some systems can appear to be unable to achieve a stable equilibrium, in which case a meaningful phase diagram cannot be constructed.

Not only are reliable multicomponent phase equilibria difficult to measure in the laboratory, the measured data may be found to be inapplicable to certain industrial procedures where, for example, contact times between solid and liquid phases can be quite short and true equilibrium state conditions are not achieved.

It has long been appreciated that phase equilibria of complex salt systems measured under laboratory conditions may have limited industrial use. It was first noted by van’t Hoff (1903), when crystallizing salts from seawater, that certain thermodynamically expected stable salts never crystallized. Even exceedingly slow crystallization together with deliberate seeding by the salts themselves did not help. Yet the salts in question all occupied clearly defined zones on the appropriate stable phase diagrams.

Studies on similar systems were made in the USSR by Kurnakov in the 1920s and Valyashka in the 1940s (see Hadzeriga, 1967), in Germany by Autenrieth (1953) and in the USA by Hadzeriga (1967). Attempts to reproduce in the laboratory conditions of natural saline lake evaporation appropriate to the

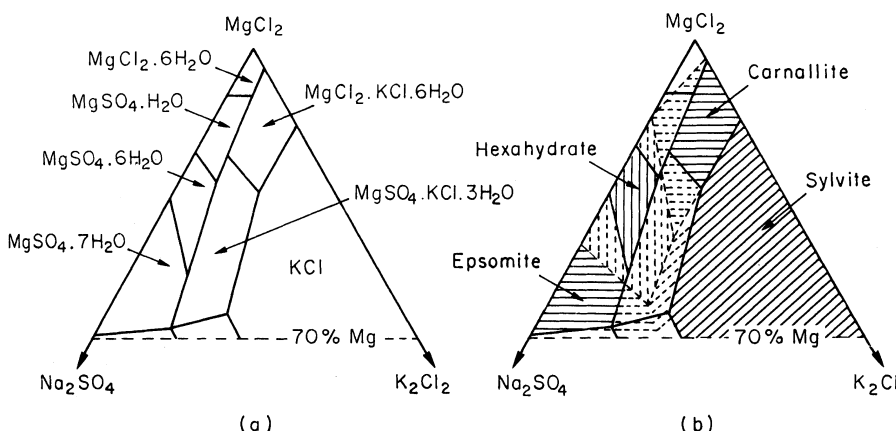


Figure 4.34. A 'dynamic' phase diagram superimposed on a conventional equilibrium diagram for the quinary system Na, K, Mg, Cl, SO₄ in water at 25°C

solar evaporation of natural brines have led to proposals for the use of 'dynamic' as opposed to conventional 'equilibrium' phase diagrams. Figure 4.34 is such a diagram for the quinary aqueous system Na⁺, K⁺, Mg²⁺, Cl⁻ and SO₄²⁻ saturated with NaCl, using a Jänecke projection. The particular area of interest represents only the upper third of the full phase diagram.

Although there is a large central field of kainite (MgSO₄ · KCl · 3H₂O) on the 'equilibrium' diagram (zones bounded by bold lines in Figure 4.34a) kainite does not crystallize out when brines in this region are evaporated in solar ponds. In fact, under these operating conditions, all the phase boundaries are changed; the sylvite (KCl) field, for example, is slightly enlarged; carnallite (KCl · MgSO₄ · 6H₂O) and hexahydrate (MgSO₄ · 6H₂O) are greatly expanded; kainite disappears altogether; epsomite (MgSO₄ · 7H₂O) is slightly reduced, and so on (Figure 4.34b).

When crystallizing from multicomponent systems, kinetic factors often override thermodynamic considerations (the so-called Ostwald rule of stages – section 5.7). The phase which crystallizes is not necessarily the one which is thermodynamically most stable, but the one which crystallizes the fastest. Numerous examples of this sort of behaviour are available.

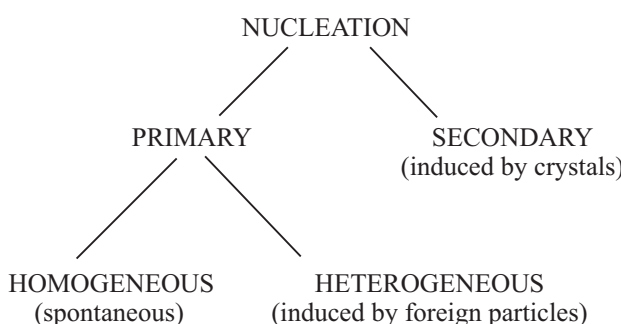
5 Nucleation

The condition of supersaturation or supercooling alone is not sufficient cause for a system to begin to crystallize. Before crystals can develop there must exist in the solution a number of minute solid bodies, embryos, nuclei or seeds, that act as centres of crystallization. Nucleation may occur spontaneously or it may be induced artificially. It is not always possible, however, to decide whether a system has nucleated of its own accord or whether it has done so under the influence of some external stimulus.

Nucleation can often be induced by agitation, mechanical shock, friction and extreme pressures within solutions and melts, as shown by the early experiments of Young (1911) and Berkeley (1912). The erratic effects of external influences such as electric and magnetic fields, spark discharges, ultra-violet light, X-rays, γ -rays, sonic and ultrasonic irradiation have also been studied over many years (Khamskii, 1969) but so far none of these methods has found any significant application in large-scale crystallization practice.

Cavitation in an under-cooled liquid can cause nucleation, and this probably accounts for a number of the above reported effects. Hunt and Jackson (1966) demonstrated, by a novel experimental technique, that nucleation occurs when a cavity collapses rather than when it expands. Very high pressures ($\sim 10^5$ bar) can be generated by the collapse of a cavity; the change in pressure lowers the crystallization temperature of the liquid and nucleation results. It is even suggested that nucleation caused by scratching the side of the containing vessel could be the result of cavitation effects.

At the present time there is no general agreement on nucleation nomenclature so to avoid confusion the terminology to be used in this and subsequent chapters will be defined here. The term 'primary' will be reserved for all cases of nucleation in systems that do not contain crystalline matter. On the other hand, nuclei are often generated in the vicinity of crystals present in a supersaturated system; this behaviour will be referred to as 'secondary' nucleation. Thus we may consider a simple scheme:

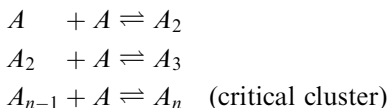


5.1 Primary nucleation

5.1.1 Homogeneous nucleation

Exactly how a stable crystal nucleus is formed within a homogeneous fluid is not known with any degree of certainty. To take a simple example, the condensation of a supersaturated vapour to the liquid phase is only possible after the appearance of microscopic droplets, called condensation nuclei, on the condensing surface. However, as the vapour pressure at the surface of these minute droplets is exceedingly high, they evaporate rapidly even though the surrounding vapour is supersaturated. New nuclei form while old ones evaporate, until eventually stable droplets are formed either by coagulation or under conditions of very high vapour supersaturation.

The formation of crystal nuclei is an even more difficult process to envisage. Not only have the constituent molecules to coagulate, resisting the tendency to redissolve (section 3.7), but they also have to become orientated into a fixed lattice. The number of molecules in a stable crystal nucleus can vary from about ten to several thousand: water (ice) nuclei, for instance, may contain about 100 molecules. However, a stable nucleus could hardly result from the simultaneous collision of the required number of molecules since this would constitute an extremely rare event. More likely, it could arise from a sequence of bimolecular additions according to the scheme:



Further molecular additions to the critical cluster would result in nucleation and subsequent growth of the nucleus. Similarly, ions or molecules in a solution can interact to form short-lived clusters. Short chains may be formed initially, or flat monolayers, and eventually a crystalline lattice structure is built up. The construction process, which occurs very rapidly, can only continue in local regions of very high supersaturation, and many of the embryos or ‘sub-nuclei’ fail to achieve maturity; they simply redissolve because they are extremely unstable. If, however, the nucleus grows beyond a certain critical size, as explained below, it becomes stable under the average conditions of supersaturation obtaining in the bulk of the fluid.

The structure of the assembly of molecules or ions which we call a critical nucleus is not known, and it is too small to observe directly. It could be a miniature crystal, nearly perfect in form. On the other hand, it could be a rather diffuse body with molecules or solvated ions in a state not too different from that in the bulk fluid, with no clearly defined surface. The morphology of very small atomic clusters has been discussed by Hoare and McInnes (1976).

The classical theory of nucleation, stemming from the work of Gibbs (1948), Volmer (1939), Becker and Döring (1935) and others, is based on the condensation of a vapour to a liquid, and this treatment may be extended to

crystallization from melts and solutions. The free energy changes associated with the process of homogeneous nucleation may be considered as follows.

The overall excess free energy, ΔG , between a small solid particle of solute (assumed here, for simplicity, to be a sphere of radius r) and the solute in solution is equal to the sum of the surface excess free energy, ΔG_S , i.e. the excess free energy between the surface of the particle and the bulk of the particle, and the volume excess free energy, ΔG_V , i.e. the excess free energy between a very large particle ($r = \infty$) and the solute in solution. ΔG_S is a positive quantity, the magnitude of which is proportional to r^2 . In a supersaturated solution G_V is a negative quantity proportional to r^3 . Thus

$$\begin{aligned}\Delta G &= \Delta G_S + \Delta G_V \\ &= 4\pi r^2 \gamma + \frac{4}{3} \pi r^3 \Delta G_v\end{aligned}\quad (5.1)$$

where ΔG_v is the free energy change of the transformation per unit volume and γ is the interfacial tension, i.e., between the developing crystalline surface and the supersaturated solution in which it is located. The term ‘surface energy’ is often used as an alternative to interfacial tension, but the latter term will be used throughout here for consistency. The two terms on the right-hand side of equation 5.1 are of opposite sign and depend differently on r , so the free energy of formation, ΔG , passes through a maximum (see Figure 5.1). This maximum value, ΔG_{crit} , corresponds to the critical nucleus, r_c , and for a spherical cluster is obtained by maximizing equation 5.1, setting $d\Delta G/dr = 0$:

$$\frac{d\Delta G}{dr} = 8\pi r\gamma + 4\pi r^2 \Delta G_v = 0 \quad (5.2)$$

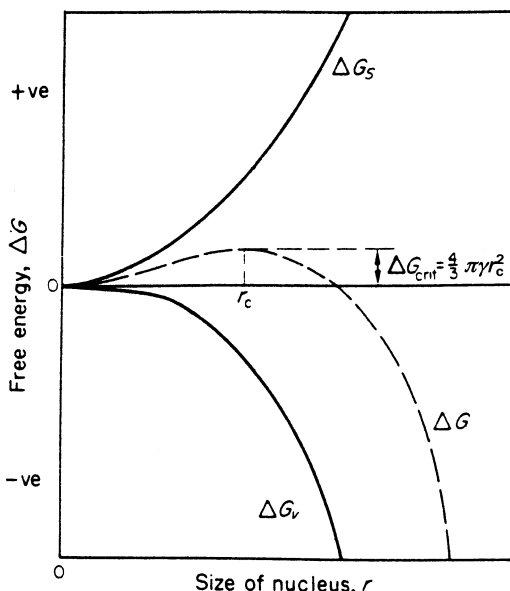


Figure 5.1. Free energy diagram for nucleation explaining the existence of a ‘critical nucleus’

therefore

$$r_c = \frac{-2\gamma}{\Delta G_v} \quad (5.3)$$

where ΔG_v is a negative quantity. From equations 5.1 and 5.3 we get

$$\Delta G_{\text{crit}} = \frac{16\pi\gamma^3}{3(\Delta G_v)^2} = \frac{4\pi\gamma r_c^2}{3} \quad (5.4)$$

The behaviour of a newly created crystalline lattice structure in a supersaturated solution depends on its size; it can either grow or redissolve, but the process which it undergoes should result in the decrease in the free energy of the particle. The critical size r_c , therefore, represents the minimum size of a stable nucleus. Particles smaller than r_c will dissolve, or evaporate if the particle is a liquid in a supersaturated vapour, because only in this way can the particle achieve a reduction in its free energy. Similarly, particles larger than r_c will continue to grow.

Although it can be seen from the free energy diagram why a particle of size greater than the critical size is stable, it does not explain the amount of energy, ΔG_{crit} , necessary to form a stable nucleus is produced. This may be explained as follows. The energy of a fluid system at constant temperature and pressure is constant, but this does not mean that the energy level is the same in all parts of the fluid. There will be fluctuations in the energy about the constant mean value, i.e. there will be a statistical distribution of energy, or molecular velocity, in the molecules constituting the system, and in those supersaturated regions where the energy level rises temporarily to a high value nucleation will be favoured.

The rate of nucleation, J , e.g. the number of nuclei formed per unit time per unit volume, can be expressed in the form of the Arrhenius reaction velocity equation commonly used for the rate of a thermally activated process:

$$J = A \exp(-\Delta G/kT) \quad (5.5)$$

where k is the Boltzmann constant, the gas constant per molecule ($1.3805 \times 10^{-23} \text{ J K}^{-1}$), R/N , where R is the gas constant = $8.314 \text{ J K}^{-1} \text{ mol}^{-1}$ and N = the Avogadro number = $6.023 \times 10^{23} \text{ mol}^{-1}$).

The basic Gibbs–Thomson relationship (section 3.7) for a non-electrolyte may be written

$$\ln S = \frac{2\gamma v}{kTr} \quad (5.6)$$

where S is defined by equation 3.68 and v is the molecular volume; this gives

$$-\Delta G_v = \frac{2\gamma}{r} = \frac{kT \ln S}{v} \quad (5.7)$$

Hence, from equation 5.4

$$\Delta G_{\text{crit}} = \frac{16\pi\gamma^3 v^2}{3(kT \ln S)^2} \quad (5.8)$$

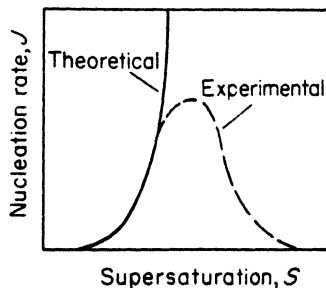


Figure 5.2. Effect of supersaturation on the nucleation rate

and from equation 5.5

$$J = A \exp \left[-\frac{16\pi\gamma^3 v^2}{3k^3 T^3 (\ln S)^2} \right] \quad (5.9)$$

This equation indicates that three main variables govern the rate of nucleation: temperature, T ; degree of supersaturation, S ; and interfacial tension, γ .

A plot of equation 5.9, as shown by the solid curve in *Figure 5.2*, indicates the extremely rapid increase in the rate of nucleation once some critical level of supersaturation is exceeded.

The dominant effect of the degree of supersaturation on the time required for the spontaneous appearance of nuclei in supercooled water vapour was calculated by Volmer (1925) as

Supersaturation, S	Time
1.0	∞
2.0	10^{62} years
3.0	10^3 years
4.0	0.1 s
5.0	10^{-13} s

In this case, a ‘critical’ supersaturation could be said to exist in the region of $S \sim 4.0$, but it is also clear that nucleation would have occurred at *any* value of $S > 1$ if sufficient time had been allowed to elapse.

Equation 5.9 may be rearranged to give

$$\ln S = \left[\frac{16\pi\gamma^3 v^2}{3k^3 T^3 \ln(A/J)} \right]^{1/2} \quad (5.10)$$

and if, arbitrarily, the critical supersaturation, S_{crit} , is chosen to correspond to a nucleation rate, J , of say, one nucleus per second per unit volume, then equation 5.10 becomes

$$\ln S_{\text{crit}} = \left[\frac{16\pi\gamma^3 v^2}{3k^3 T^3 \ln A} \right]^{1/2} \quad (5.10a)$$

From equations 5.3 and 5.7 the radius of a spherical critical nucleus at a given supersaturation can be expressed as

$$r_c = 2\gamma v / kT \ln S \quad (5.11)$$

For the case of non-spherical nuclei, the geometrical factor $16\pi/3$ in equations 5.4 and 5.8–5.10a must be replaced by an appropriate value (e.g. 32 for a cube).

Similar expressions to the above may be derived for homogeneous nucleation from the melt in terms of supercooling. The volume free energy ΔG_v is given by

$$\Delta G_v = \frac{\Delta H_f \Delta T}{T^*} \quad (5.12)$$

where T^* is the solid–liquid equilibrium temperature expressed in kelvins, $\Delta T = T^* - T$ is the supercooling and ΔH_f is the latent heat of fusion. The radius of a critical nucleus is given by

$$r_c = \frac{2\gamma T^*}{\Delta H_f \Delta T} \quad (5.13)$$

and the rate of nucleation, from equation 5.9, may be expressed by

$$J = A \exp \left[-\frac{16\pi\gamma^3}{3kT^*\Delta H_f^2 T_r (\Delta T_r)^2} \right] \quad (5.14)$$

where T_r is the reduced temperature defined by $T_r = T/T^*$ and $\Delta T_r = \Delta T/T^*$, i.e. $\Delta T_r = 1 - T_r$. Equation 5.14, like equation 5.9, indicates the dominant effect of supercooling on the nucleation rate.

For a wide range of substances, including organic melts, the critical homogeneous nucleation temperature expressed in kelvins is approximately 0.8–0.85 T^* , although for hydrocarbons $>C_{15}$ it may approach 0.95 T^* .

The size of the critical nucleus is dependent on temperature, since the volume free energy, ΔG_v , is a function of the supercooling, ΔT , (equations 5.12 and 5.13) giving

$$r_c \propto (\Delta T)^{-1} \quad (5.15)$$

and from equation 5.4

$$\Delta G_{\text{crit}} \propto (\Delta T)^{-2} \quad (5.16)$$

These relationships are shown in *Figure 5.3*, where it can be seen that the size of a critical nucleus increases with temperature.

Melts frequently demonstrate abnormal nucleation characteristics, as noted in the early work of Tamman (1925). The rate of nucleation usually follows an exponential curve (solid curve in *Figure 5.2*) as the supercooling is increased, but reaches a maximum and subsequently decreases (broken curve in *Figure 5.2*). Tamman suggested that this behaviour was caused by the sharp increase in viscosity with supercooling which restricted molecular movement and inhibited the formation of ordered crystal structures. Turnbull and Fisher (1949) quantified this behaviour with a modified form of equation 5.9:

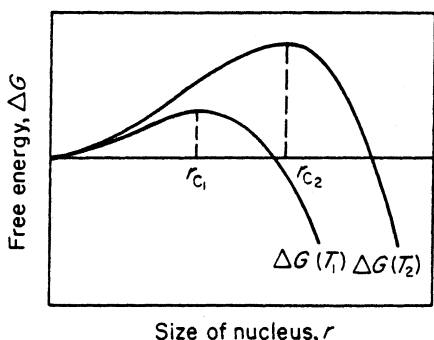


Figure 5.3. Effect of temperature on the size and free energy of formation of a critical nucleus ($T_1 < T_2$)

$$J = A' \exp \left[-\frac{16\pi\gamma^3 v^2}{3k^3 T^3 (\ln S)^2} + \frac{\Delta G'}{kT} \right] \quad (5.17)$$

which includes a ‘viscosity’ term. When $\Delta G'$, the activation energy for molecular motion across the embryo-matrix interface, is exceptionally large (e.g. for highly viscous liquids and glasses) the other exponential term is small because under these circumstances S is generally very large. $\Delta G'$ then becomes the dominant factor in this rate equation and a decrease in nucleation rate is predicted.

The formation of the glassy state is by no means uncommon; Tamman (1925) reported that out of some 150 selected organic compounds, all capable of being crystallized fairly easily, over 30 per cent yielded the glassy state on cooling their melts slowly.

Although most reported experimental observations of this reversal of the nucleation rate have been confined to melts, it is interesting to note that this behaviour has also been observed in highly viscous aqueous solutions of citric acid (*Figure 5.4*) (Mullin and Leci, 1969b).

Excessive supercooling does not aid nucleation. There is an optimum temperature for nucleation of a given system (see *Figures 5.2* and *5.4*) and any reduction below this value decreases the tendency to nucleate. As indicated by the classical relationship (equation 5.9) nucleation can theoretically occur at any temperature, provided that the system is supercooled, but under normal conditions the temperature range over which massive nucleation occurs may be quite restricted. Therefore, if a system has set to a highly viscous or glass-like state, further cooling will not cause crystallization. To induce nucleation the temperature would have to be increased to a value in the optimum region.

The nucleation process has been discussed above in terms of the so-called classical theories stemming from the thermodynamic approach of Gibbs and Volmer, with the modifications of Becker, Döring and later workers. The main criticism of these theories is their dependence on the interfacial tension (surface energy), γ , e.g. in the Gibbs-Thomson equation, and this term is probably meaningless when applied to clusters of near critical nucleus size.

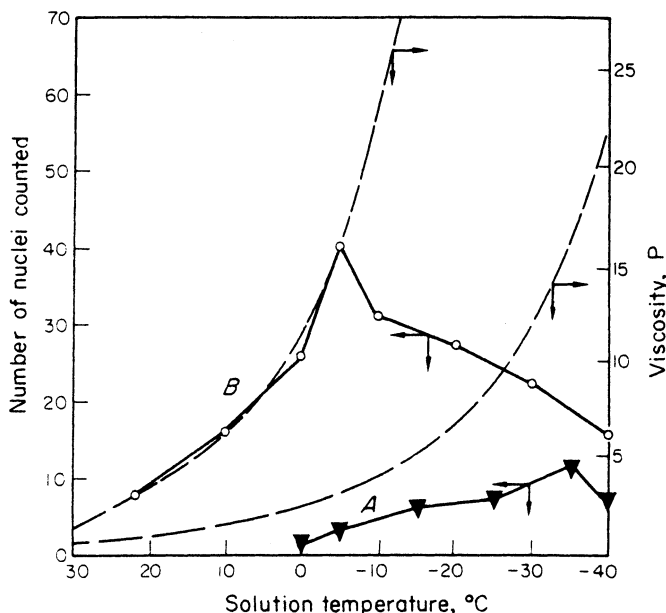


Figure 5.4. Spontaneous nucleation in supercooled citric acid solutions: A, 4.6 kg of citric acid monohydrate per kg of 'free' water ($T^* = 62^\circ\text{C}$); B, 7.0 kg/kg ($T^* = 85^\circ\text{C}$). (After Mullin and Leci, 1969b)

An empirical approach to the nucleation process is described by Nielsen (1964), expressing a relationship between the induction period, t_{ind} (the time interval between mixing two reacting solutions and the appearance of crystals) and the initial concentration, c , of the supersaturated solution:

$$t_{\text{ind}} = kc^{1-p} \quad (5.18)$$

where k is a constant and p is the number of molecules in a critical nucleus. It was suggested that the induction period, which may range from microseconds to days depending on the supersaturation, represents the time needed for the assembly of a critical nucleus, although this is an over-simplification (see section 5.5).

The so-called classical theories of homogeneous nucleation and the above empirical theory all utilize the concept of a clustering mechanism of reacting molecules or ions, but they do not agree on the effect of supersaturation on the size of a critical nucleus. The former theories indicate that the size is dependent on the supersaturation, whereas the latter theory indicates a smaller but constant nucleus size. So far these differences have not been resolved, largely owing to the fact that the experimental investigation of true homogenous nucleation is fraught with difficulty since the production of an impurity-free system is virtually impossible.

Critical reviews of nucleation mechanisms have been made by, for example, Nancollas and Purdie (1964), Nielsen (1964), Walton (1967),

Strickland-Constable (1968), Zettlemoyer (1969), Nývlt *et al.* (1985) and Söhnel and Garside (1992). The recent publication by Kashchiev (2000) is noteworthy for its in-depth analyses of the thermodynamics and kinetics of homogeneous and heterogeneous nucleation.

Measurement techniques

It is only in recent years that suitable techniques have been devised for studying the kinetics of homogeneous nucleation. The main difficulties have been the preparation of systems free from impurities, which might act as nucleation catalysts, and the elimination of the effects of retaining vessel walls which frequently catalyse nucleation.

An early attempt to study homogeneous nucleation was made by Vonnegut (1948) who dispersed a liquid system into a large number of discrete droplets, exceeding the number of heteronuclei present. A significant number of droplets were therefore entirely mote-free and could be used for the study of true homogeneous nucleation. The dispersed droplet method, however, has many attendant experimental difficulties: concentrations and temperatures must be measured with some precision for critical supersaturations to be determined; the tiny droplets ($< 1 \text{ mm}$) must be dispersed into an inert medium, e.g. an oil, which will not act as a nucleation catalyst; and any nuclei that form in the droplets have to be observed microscopically.

Variations of the droplet method have since been developed to overcome the above difficulties (White and Frost, 1959; Melia and Moffitt, 1964; Komarov, Garside and Mullin, 1976), but the reliability of homogeneous nucleation studies is still difficult to judge. For example, experimental values of the ‘collision factor’ (the pre-exponential factor A in equation 5.9) have frequently been reported in the range 10^3 to $10^5 \text{ cm}^{-3} \text{ s}^{-1}$, but as these are well outside the range predicted from the Gibbs–Volmer theory ($\sim 10^{25}$) it is probable that true homogeneous nucleation was not being observed in these cases. Another point to note is that the interfacial energy term γ , which appears in equation 5.14 to the third power, cannot be assumed to be independent of temperature (see section 5.6).

An interesting technique was reported by Garten and Head (1963, 1966) who showed that crystalloluminescence occurs during the formation of a three-dimensional nucleus in solution, and that each pulse of light emitted lasting less than 10^{-7} s corresponds to a single nucleation event. Nucleation rates thus measured were close to those predicted from classical theory, with collision factors in the range 10^{25} to $10^{30} \text{ cm}^{-3} \text{ s}^{-1}$. In their work on the precipitation of sodium chloride in the presence of lead impurities, true homogeneous nucleation occurred only at very high supersaturations ($S > 14$). The nucleation process was envisaged as the development in the solution of a molecular cluster, as a disordered quasi-liquid, which after attaining critical size suddenly ‘clicks’ into crystalline form. As a result of this high-speed rearrangement, the surface of the newly formed crystalline particle may be expected to contain large numbers of imperfections that would encourage further rapid crystalline growth. As a nucleus appears to be generated in $< 10^{-7} \text{ s}$, its steady build-up

as a crystalline body by diffusion is ruled out (a diffusion coefficient for NaCl of $10^{-5} \text{ cm}^2 \text{ s}^{-1}$ gives a formation time more than ten times greater than the pulse period). These observations, therefore, may be taken as strong evidence for the existence and development of molecular clusters in supersaturated solutions.

From their work with sodium chloride Garten and Head suggested that a critical nucleus can be as small as about 10 molecules. A different order of magnitude was proposed by Otpushchennikov (1962), who estimated the sizes of critical nuclei by observing the behaviour of ultrasonic waves in melts kept just above their freezing point. For phenol, naphthalene and azobenzene, for example, he suggested that fewer than 1000 molecules constitute a stable nucleus. In contrast to this, the work of Adamski (1963) with relatively insoluble barium salts led to the conclusion that a critical nucleus was about 10^{-15} g , and as small as this mass may appear it still represents several million molecules. It is obvious, therefore, that there are still some widely diverging views on the question of the size of a critical nucleus, but this is not surprising as the critical size is supersaturation-dependent (equation 5.11) and no consideration is given to this important variable by any of the above authors.

Agitation is frequently used to induce crystallization. Stirred water, for example, will allow only about $\frac{1}{2}^\circ\text{C}$ of supercooling before spontaneous nucleation occurs, whereas undisturbed water will allow over 5°C . Actually, very pure water, free from all extraneous matter, has been supercooled some 40°C . Most agitated solutions nucleate spontaneously at lower degrees of supercooling than quiescent ones. In other words, the supersolubility curve (*Figure 3.9*) tends to approach the solubility curve more closely in agitated solutions, i.e. the width of the metastable zone is reduced.

However, the influence of agitation on the nucleation process is probably very complex. It is generally agreed that mechanical disturbances can enhance nucleation, but it has been shown by Mullin and Raven (1961, 1962) that an increase in the intensity of agitation does not always lead to an increase in nucleation. In other words, gentle agitation causes nucleation in solutions that are otherwise stable, and vigorous agitation considerably enhances nucleation, but the transition between the two conditions may not be continuous; a portion of the curve (see *Figure 5.5*) may have a reverse slope indicating a region where an increase in agitation actually *reduces* the tendency to nucleate. This phenomenon, observed with aqueous solutions of ammonium dihydrogen phosphate, magnesium sulphate and sodium nitrate, might be explained by assuming that agitation effects can lead to the disruption of sub-nuclei or molecular clusters in the solution (section 3.13).

There has long been an interest in the potential effects on the nucleation process of externally applied electrostatic or magnetic fields. There is evidence that both homogeneous nucleation and the duration of the nucleation induction period (section 5.5) can be influenced. However, the relevance of experimental data, obtained from small-scale investigations under controlled laboratory conditions, to bulk solutions in flow or agitated conditions normally encountered in industrial practice (section 9.5) is still the subject of considerable controversy (Söhnel and Mullin, 1988c). A detailed account of recent theor-

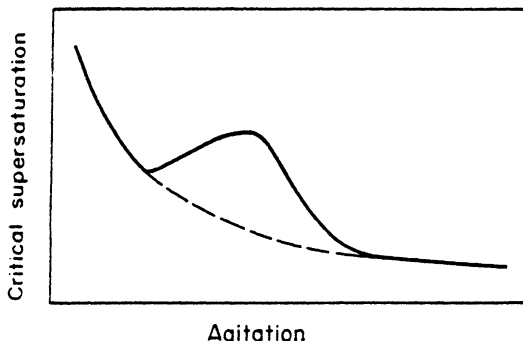


Figure 5.5. Influence of agitation on nucleation, showing a region where increased agitation can reduce the tendency to nucleate. (After Mullin and Raven, 1962)

etical studies on the effect of electric fields on nucleation has been given by Kashchiev (2000).

Spinodal decomposition

The existence of concentration fluctuations in a multicomponent fluid system is an implicit assumption in the Gibbs theory of homogeneous nucleation. Two types of phase transition (nucleation) have been postulated, viz. composition fluctuations large in degree and infinitesimal in spatial extent (e.g. an infinitesimal droplet with properties approaching those of the bulk supercooled phase) or infinitesimal in degree and large in extent (e.g. continuous changes of phase). Classical nucleation theory, based on the former postulate, requires the further assumption that a sharp interface exists between the nucleating (stable) and supercooled (unstable) phases. The latter mode of transition, known as *spinodal decomposition*, does not require this assumption; a diffuse interface may be considered to exist between the phases.

The underlying theory for spinodal decomposition rests on Gibbs' derivation for the limit of stability of a fluid phase with respect to continuous changes of phase, represented by

$$\left. \frac{\partial^2 G}{\partial c^2} \right|_{T,P} = 0 \quad (5.19)$$

where G is the Gibbs free energy per mole of solution and c is the solution concentration. On a phase diagram the locus of such points, representing the limit of stability, is referred to as the *spinodal* (see Figure 5.6). Thus, for spinodal decomposition to occur, a spontaneous phase transition is necessary and the condition

$$(\partial^2 G / \partial c^2) \leq 0 \quad (5.20)$$

should apply. Within the spinodal region any phase separation can lower the free energy of the system and no nucleation step is required. Outside

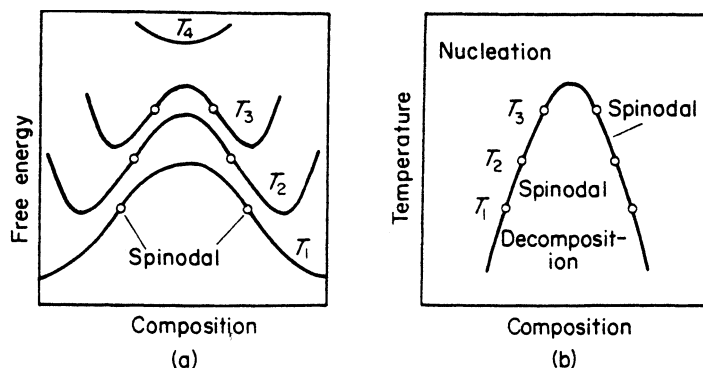


Figure 5.6. (a) Free energy–composition–temperature surface, showing the location of the spinodal; (b) temperature–composition graph of the spinodal

this boundary, nucleation is essential to effect a phase change. The spinodal curve represents the limit of the metastable zone (sections 3.12 and 5.3) and is characterized by the condition of zero diffusivity (Myerson and Senol, 1984).

5.1.2 Heterogeneous nucleation

The rate of nucleation of a solution or melt can be affected considerably by the presence of mere traces of impurities in the system. However, an impurity that acts as a nucleation inhibitor in one case may not necessarily be effective in another; indeed it may even act as an accelerator. No general rule applies and each case must be considered separately.

Many reported cases of spontaneous (homogeneous) nucleation are found on careful examination to have been induced in some way. Indeed, it is generally accepted that true homogeneous nucleation is not a common event. For example, a supercooled system can be seeded unknowingly by the presence of atmospheric dust which may contain ‘active’ particles (heteronuclei). Aqueous solutions as normally prepared in the laboratory may contain $>10^6$ solid particles per cm^3 of sizes $<1\ \mu\text{m}$. It is virtually impossible to achieve a solution completely free of foreign bodies, although careful filtration can reduce the numbers to $<10^3\ \text{cm}^{-3}$ and may render the solution more or less immune to spontaneous nucleation.

Cases are often reported of large volumes of a given system nucleating spontaneously at smaller degrees of supercooling than small volumes. A plausible explanation is that the larger samples stand a greater chance of being contaminated with active heteronuclei. The size of the solid foreign bodies is important and there is evidence to suggest that the most active heteronuclei in liquid solutions lie in the range 0.1 to $1\ \mu\text{m}$.

Heteronuclei play an important role in atmospheric water condensation or ice formation (Mason, 1957). Atmospheric nuclei have been classified as ‘giant’ (10 to $1\ \mu\text{m}$) which remain airborne for limited periods only, ‘large’ (1 to

0.2 µm) and ‘Aitken’ (0.2 to 0.005 µm). Particles smaller than about 10^{-3} µm are not normally found in air because they readily aggregate. Aitken nuclei are so called because they are active at the supersaturations produced in an Aitken counter, an apparatus in which a known volume of air is rapidly expanded; water droplets, formed on the particles, settle and are counted microscopically. Aitken nuclei, which occur $\sim 10^4$ to 10^5 cm⁻³ in the atmosphere, result from industrial smokes and vapours, ocean salts arising from spindrift, land dusts, particles from volcanic eruptions and even from outer space (Faraday Discussions, 1998).

As the presence of a suitable foreign body or ‘sympathetic’ surface can induce nucleation at degrees of supercooling lower than those required for spontaneous nucleation, the overall free energy change associated with the formation of a critical nucleus under heterogeneous conditions $\Delta G'_{\text{crit}}$, must be less than the corresponding free energy change, ΔG_{crit} , associated with homogeneous nucleation, i.e.

$$\Delta G'_{\text{crit}} = \phi \Delta G_{\text{crit}} \quad (5.21)$$

where the factor ϕ is less than unity.

It has been indicated above, e.g. equation 5.9, that the interfacial tension, γ , is one of the important factors controlling the nucleation process. Figure 5.7 shows an interfacial energy diagram for three phases in contact; in this case, however, the three phases are not the more familiar solid, liquid and gas, but two solids and a liquid. The three interfacial tensions are denoted by γ_{cl} (between the solid crystalline phase, c, and the liquid l), γ_{sl} (between another foreign solid surface, s, and the liquid) and γ_{cs} (between the solid crystalline phase and the foreign solid surface). Resolving these forces in a horizontal direction

$$\gamma_{\text{sl}} = \gamma_{\text{cs}} + \gamma_{\text{cl}} \cos \theta \quad (5.22)$$

or

$$\cos \theta = \frac{\gamma_{\text{sl}} - \gamma_{\text{cs}}}{\gamma_{\text{cl}}} \quad (5.23)$$

The angle θ , the angle of contact between the crystalline deposit and the foreign solid surface, corresponds to the angle of wetting in liquid–solid systems.

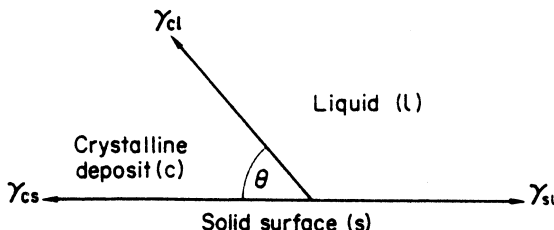


Figure 5.7. Interfacial tensions at the boundaries between three phases (two solids, one liquid)

The factor ϕ in equation 5.21 can be expressed (Volmer, 1939) as

$$\phi = \frac{(2 + \cos \theta)(1 - \cos \theta)^2}{4} \quad (5.24)$$

Thus, when $\theta = 180^\circ$, $\cos \theta = -1$ and $\phi = 1$, equation 5.21 becomes

$$\Delta G'_{\text{crit}} = \Delta G_{\text{crit}} \quad (5.25)$$

When θ lies between 0 and 180° , $\phi < 1$; therefore

$$\Delta G'_{\text{crit}} < \Delta G_{\text{crit}} \quad (5.26)$$

When $\theta = 0$, $\phi = 0$, and

$$\Delta G'_{\text{crit}} = 0 \quad (5.27)$$

The three cases represented by equations 5.25–5.27 can be interpreted as follows. For the case of complete non-affinity between the crystalline solid and the foreign solid surface (corresponding to that of complete non-wetting in liquid–solid systems), $\theta = 180^\circ$, and equation 5.25 applies, i.e. the overall free energy of nucleation is the same as that required for homogeneous or spontaneous nucleation. For the case of partial affinity (cf. the partial wetting of a solid with a liquid), $0 < \theta < 180^\circ$, and equation 5.26 applies, which indicates that nucleation is easier to achieve because the overall excess free energy required is less than that for homogeneous nucleation. For the case of complete affinity (cf. complete wetting) $\theta = 0$, and the free energy of nucleation of zero. This case corresponds to the seeding of a supersaturated solution with crystals of the required crystalline product, i.e. no nuclei have to be formed in the solution. Figure 5.8 indicates the relationship between ϕ and θ .

As mentioned above, the heterogeneous nucleation of a solution can occur by seeding from embryos retained in cavities, e.g. in foreign bodies or the walls

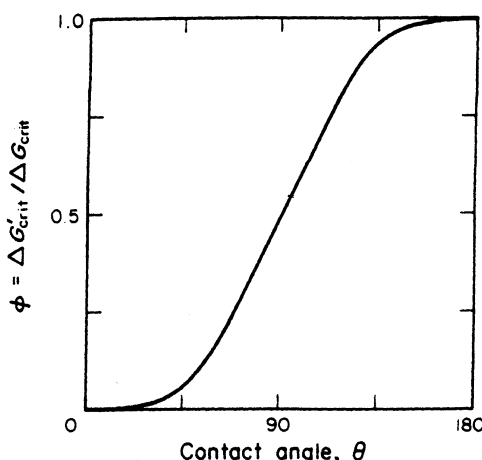


Figure 5.8. Ratio of free energies of homogeneous and heterogeneous nucleation as a function of the contact angle

of the retaining vessel, under conditions in which the embryos would normally be unstable on a flat surface. This problem has been analysed by Turnbull (1950) for different types of cavity. The maximum diameter of a cylindrical cavity which will retain a stable embryo is given by

$$d_{\max} = \frac{4\gamma_{\text{cl}} \cos \theta}{\Delta G_v} \quad (5.28)$$

where ΔG_v is the volume free energy for the phase transformation. If the system is heated, this reducing the supersaturation or supercooling and eliminating all embryos in cavities larger than d_{\max} , and subsequently cooled, the embryos retained in the cavities smaller than d_{\max} will grow to the mouth of the cavity. They will then act as nuclei only if the cavity size $d_{\max} \geq 2r_c$, where r_c is the size of a critical nucleus (equation 5.3 or 5.13).

5.2 Secondary nucleation

A supersaturated solution nucleates much more readily, i.e. at a lower supersaturation, when crystals of the solute are already present or deliberately added. The term *secondary* nucleation will be used here for this particular pattern of behaviour to distinguish it from so-called *primary* nucleation (no crystals initially present) discussed in section 5.1. There have been several comprehensive reviews of the literature on secondary nucleation (Strickland-Constable, 1968; Botsaris, 1976; de Jong, 1979; Garside and Davey, 1980; Garside, 1985; Nývlt *et al.*, 1985).

Among the early papers on this subject may be mentioned the work of Ting and McCabe (1934) who demonstrated that solutions of magnesium sulphate nucleated in a more reproducible manner at moderate supersaturations in the presence of seed crystals. Similar observations were made in studies with copper sulphate (McCabe and Stevens, 1951).

A particular type of secondary nucleation in KBr solutions was interpreted by Gyulai (1948) as evidence for a ‘transitional boundary layer’ of partially integrated units which could be stripped off the crystal surfaces by fluid motion. This behaviour was demonstrated by Powers (1963), in a series of simple experiments, showing that the movement of a sucrose crystal in a supersaturated solution, or the movement of the solution past a stationary crystal, produced nuclei. Inert replicas of the crystals did not produce nuclei under the same conditions. These results tended to suggest that a fluid mechanical shearing of weak outgrowths or loosely bonded units from the crystal-solution interface was responsible. Sung, Estrin and Youngquist (1973) have also invoked the concept of fluid shear in an agitated vessel as a mechanism for generating embryos (sub-nuclei) which develop into stable nuclei when swept into regions of high supersaturation.

Strickland-Constable (1968) described several possible mechanisms of secondary nucleation, such as ‘initial’ breeding (crystalline dust swept off a newly introduced seed crystal), ‘needle’ breeding (the detachment of weak outgrowths), ‘polycrystalline’ breeding (the fragmentation of a weak polycrystalline

mass) and ‘collision’ breeding (a complex process resulting from the interaction of crystals with one another or with parts of the crystallization vessel).

5.2.1 Contact nucleation

Clontz and McCabe (1971) showed that at moderate levels of supersaturation, crystal contacts readily caused secondary nucleation of $\text{MgSO}_4 \cdot 7\text{H}_2\text{O}$, but crystal–crystal contacts gave up to five times as many nuclei as did crystal–metal rod contacts. Furthermore, the faster growing faces produced fewer nuclei than did the slower growing faces (Johnson, Rousseau and McCabe, 1972) indicating a connection between secondary nucleation and the crystal growth process.

Collisions in a liquid medium can initiate complex behaviours. Fracture may occur at the point of contact, but substantial hydrodynamic forces can operate over the surfaces in the vicinity of the point of contact, giving rise to plastic and elastic deformation in the parent crystal. Due to energy absorption, a small fragment broken off a crystal by collision could be in a considerably disordered state, with many dislocations and mismatch surfaces: in fact, it may be nearer to an amorphous glassy condition than to a crystal (Strickland-Constable, 1979). It is not surprising, therefore, that these small crystalline fragments often grow much more slowly than macrocrystals. Indeed, cases have been recorded where they do not grow at all (Bujac, 1976; van’t Land and Wienk, 1976). Ristic, Sherwood and Shripathi (1991) suggest that the formation of varying numbers of dislocations and the development of elastic strain in the new interface are the two main reasons for growth rate dispersion (section 6.2.7) in attrition fragments smaller than about 150 µm.

Crystal–agitator contacts are prime suspects for causing secondary nucleation in crystallizers, although only those crystals that manage to penetrate the fluid boundary layer around the blade will actually be hit. The probability of such an impact is directly proportional to the rotational speed of the agitator (Nienow, 1976). The relative hardness of the contacting bodies is also a factor to consider: a metal impeller gives a much higher nucleation rate than one coated with a soft material such as polyethylene (Shah, McCabe and Rousseau, 1973; Randolph and Sikdar, 1974; Ness and White, 1976; Toyokura, Yamazoe and Mogi, 1976).

Energy–impact models have been developed from the results of attrition and breakage studies in agitated vessels using crystals suspended in inert liquids (Fasoli and Conti, 1976; Nienow and Conti, 1978). A generalized model to quantify nucleation by mechanical attrition, based on Rittinger’s law for the energy required for producing new surface and the additivity of two attrition processes due to crystal–crystal and crystal–impeller collisions, has been proposed by Kuboi, Nienow and Conti (1984).

Several hydrodynamic models of secondary nucleation in agitated crystallizers were applied to experimental data obtained from a 6-L agitated batch crystallizer using potassium sulphate by Shamloo, Jones and Djamarani (1990). They concluded that the secondary nuclei were produced by an attrition process with a turbulent fluid-induced mechanism with critical eddies in the

viscous dissipation subrange of the turbulent energy spectrum. An empirical attrition model, which relates crystal attrition to crystal size and hold-up, was developed by Jager *et al.* (1991) from data obtained with a 20-L continuous evaporative crystallizer using ammonium sulphate.

Direct observation of impact-induced microattrition at the surfaces of potash alum crystals immersed in supersaturated solution (Garside, Rusli and Larson, 1979) indicated that the majority of the fragments produced were in the 1–10 µm size range and had a supersaturation-dependent size distribution. Impact energy and the frequency of impact also have an important influence on the number of crystals resulting from contact secondary nucleation (Larson, 1982).

Crystalline fragments smaller than about 1 µm probably do not survive in an agitated crystallizer where fluctuations of both temperature and supersaturation commonly occur. The so-called ‘survival theory’ (Garabedian and Strickland-Constable, 1972) is based on the Gibbs–Thomson effect (section 3.7) which suggests that microcrystals can dissolve in solutions that are supersaturated with respect to macrocrystals.

The production of breakage fragments, i.e. secondary nuclei, may not always be a direct result of crystal interactions or collisions. Chernov, Zaitseva and Rashkovich (1990) have shown that growing crystals containing dislocations, defects or inclusions are prone to secondary nucleation through the development of internal stresses which lead to crack formation and the subsequent production of breakage fragments, i.e. secondary nuclei. Crack propagation initiated by the adsorption of impurity species at defects on crystal surface was earlier suggested by Sarig and Mullin (1980) as a possible explanation of an observed phenomenon of crystal breakdown in a gently agitated suspension in a just-saturated solution that also contained a trace amount of a substance that was known to be an active habit modifier.

5.2.2 Seeding

Probably the best method for inducing crystallization is to inoculate or seed a supersaturated solution with small particles of the material to be crystallized. Deliberate seeding is frequently employed in industrial crystallization to effect a control over the product size and size distribution (section 7.5.5).

Atmospheric dust frequently contains particles of the crystalline product itself, especially in industrial plants or in laboratories where quantities of the material have been handled. Fortuitous seeding from this source can serve to prevent the crystallization of thermodynamic unstable phases, e.g., hydrates or polymorphs, that might otherwise appear (Ostwald’s rule of stages, section 5.7).

Seed crystals, however, do not necessarily have to consist of the material being crystallized in order to be effective; isomorphous substances will frequently induce crystallization. For example, phosphates will often nucleate solutions of arsenates; sodium tetraborate decahydrate (borax) can nucleate sodium sulphate decahydrate; phenol can nucleate *m*-cresol; and so on. The success of silver iodide, as an artificial rain-maker, is generally attributed to the striking similarity of the AgI and ice crystal lattices. However, there are many

cases where lattice similarity does not exist and undoubtedly other factors have to be considered. Micro-organisms like *Pseudomonas syringae*, for example, have been used commercially as ice nucleators in the snow-making process (Liao and Ng, 1990).

In laboratory and large-scale crystallizations the first sign of nucleation often appears in one given region of the vessel, usually where there is a local high degree of supersaturation, such as near a cooling surface or at the surface of the liquid. On the other hand, it is not uncommon to find some particular spot on the vessel wall or on the stirrer acting as a crystallization centre. The most reasonable explanation of this phenomenon is that minute cracks and crevices in the surface retain tiny crystals from a previous batch which seed the system when it becomes supercooled. It is possible, of course, for some part of a metal or glass surface to be in a condition in which it acts as a catalyst for nucleation.

Melia and Moffitt (1964) studied secondary nucleation in aqueous solutions of KCl and reported that the nucleation rate was independent of the number of seeds added. At a constant cooling rate a time-lag or induction period (section 5.5) was recorded before secondary nucleation commenced. Cayey and Estrin (1967) also observed an induction period with seeded solutions of MgSO₄ in a 2-L agitated crystallizer and reported a strange effect of the quantity of seeds added: one seed (~1 mm, <2 mg) was more effective in inducing nucleation than 50 mg, but less effective than 500 mg. This anomaly, however, was not pursued. They also reported that a crystal was not capable of giving rise to fresh nuclei until it had reached a critical size of around 220 µm. Rousseau, Li and McCabe (1976) suggested a critical size of about 200 µm. Toyokura, Mogi and Hirasawa (1977) reported that crystals smaller than about 100 µm did not produce secondary nuclei in a fluidized bed with solutions of K alum supercooled by 3 °C. Using the same system at a lower supercooling (2 °C) in an agitated vessel, Kubota and Fujiwara (1990) demonstrated that the critical size could vary between about 200 and 500 µm depending on the agitator speed and its material of construction.

There are several reasons why the seed crystal size may be influential in secondary nucleation. For example, large seeds generate more secondary nuclei in agitated systems than do small seeds because of their greater contact probabilities and collision energies. Indeed, very small crystals can follow the streamlines within the turbulence eddies in vigorously agitated solutions, behaving essentially as if they were suspended in a stagnant fluid, rarely coming into contact with the agitator or other crystals. Other factors to consider are that crystals smaller than about 10 µm probably grow much more slowly than do macrocrystals (section 6.2.7) and, as mentioned above, some damaged crystal fragments may not be capable of growing at all.

Secondary nucleation was observed to occur in a series of pulses, mainly during the latent period (section 5.4), when citric acid solutions were seeded in an agitated vessel (Mullin and Leci, 1972). The secondary nucleation rate decreased with an increase in the seed size or in the number of seeds of a given size. The latent period was drastically reduced by decreasing the seed size, but was relatively unaffected by the number of seeds added. Increased supersatura-

tion increased secondary nucleation and decreased the latent period. Increased agitation increased the desupersaturation rate to a maximum and decreased the latent period to a minimum. No evidence of fluid mechanical shearing was found, and a mechanism of secondary nucleation based on molecular cluster formation in solution was proposed.

Belyustin and Rogacheva (1966) studied the nucleation of $\text{MgSO}_4 \cdot 7\text{H}_2\text{O}$ which crystallizes in enantiomorphic forms (section 1.9) at room temperature. When this salt nucleated spontaneously (unseeded), the product crystals were mostly left-handed. When the solution was seeded with right-handed crystals, the number of product crystals increased and the percentage of left-handed crystals in the total product decreased. Increases in solution velocity and supersaturation in the presence of a right-handed seed both led to decreases in the percentage of right-handed crystals in the product. They concluded, however, that secondary nucleation in these cases was not caused by fragmentation. Because filtration of the solution retarded both seeded and unseeded nucleation they proposed that foreign particles (heteronuclei) coming into contact with the seed crystals became activated and initiated nucleation.

In a similar study, Denk and Botsaris (1972) studied the seeded nucleation of sodium chlorate enantiomorphs in non-agitated solution and attempted to distinguish between nuclei originating from either the solution or a fixed single crystal suspended in the solution. At high supercoolings ($>12^\circ\text{C}$) when primary nucleation was considered to be the dominant mode, the crystals that developed were found to be roughly 50:50 D- and L-forms. At supercoolings between 12 and 4°C , however, virtually 100% of the developed crystals were of the same form as the suspended seed, indicating that the nuclei were derived directly from the parent crystal. At supercoolings below about 4°C the proportion fell to around 60% (*Figure 5.9*).

The use of selective seeding as a method for separating solutes in solutions supersaturated with two salts was proposed by Rousseau and O'Dell (1980). Supersaturated aqueous solutions of potassium sulphate together with either potassium chloride or dichromate were seeded with one of the solutes to cause secondary nucleation of that substance. After recovering the developed crystals by filtration, the filtrate was seeded with the second solute to complete the separation.

Unintentional seeding

The deliberate use of seed crystals is common practice in both research laboratory, e.g., to encourage the crystallization of a 'difficult' substance, and in industrial plant to exert control over the crystal size distribution of the final product (section 8.4.5). On the other hand, unintentional seeding, also frequently encountered in both laboratory and industry, is an uncontrolled event which can often cause considerable frustration and trouble.

The technical literature abounds with tales, some dating back over 150 years, of problems caused by the perverse behaviour of crystallizing systems (e.g., Buckley, 1952; Woodward and McCrone, 1975; Dunitz and Bernstein, 1995). Xylitol, for example, first prepared in 1891 was considered to be a liquid until

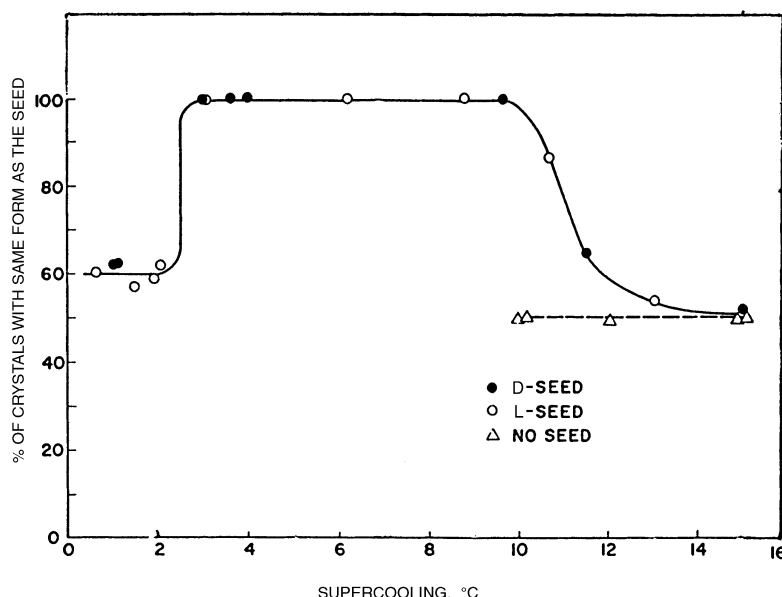


Figure 5.9. Seeded nucleation of sodium chlorate enantiomorphs in non-agitated solution.
(After Denk and Botsaris, 1972)

1941 when a solid form melting at 61 °C unexpectedly crystallized. Two years later, another form melting at 94 °C appeared, after which subsequent attempts to prepare the lower melting (less stable) polymorph have been unsuccessful. Benzophenone and the sugars melibiose, levulose and turanose are all examples of former liquids that are now regularly produced in crystalline form. Single piezoelectric crystals of anhydrous ethylene diamine tartrate were manufactured on the industrial scale for many years until suddenly at one plant a monohydrate nucleated and grew preferentially. Within weeks the affliction spread to a second plant many miles away. In another case, ampicillin, a broad-spectrum penicillin, could be readily crystallized as either an anhydrate or a trihydrate. Several years later a monohydrate made its appearance, since when the anhydrate has never been prepared. The secure patenting of pharmaceutical products, usually done at a relatively early stage of the laboratory investigations, long before industrial production, has become a complex and difficult matter.

Undoubtedly, many of the above and other examples have been caused by unintentional seeding. Reference has already been made in section 5.1.2 to the role atmospheric dust can play as a nucleating agent, noting that even foreign bodies in the dust can also act as nucleation promoters. Once a certain crystalline form has been prepared in a laboratory or plant, the working atmosphere inevitably becomes contaminated with seeds of the particular material. If later a thermodynamically more stable polymorph or hydrate (pseudopolymorph) appears, then seeds of this too will enter the atmosphere and play a dominant role. However, it is the speed with which another laboratory or plant, often some large distance apart, sometimes even in another country, also become

contaminated that has led to suggestions of ‘world-wide seeding’, a phenomenon which cannot be justified. Seeding is essentially a *local* problem. There are innumerable ways in which seeds can be transferred from one location to another without assuming that every spot on the earth has become inoculated. For example, personnel travel widely and inadvertently carry contaminating seeds with them. Samples of the material are frequently passed from one location to another, and so on. As Dunitz and Bernstein (1995) say in their entertaining and highly informative paper: ‘We believe that once a particular polymorph has been crystallized it is always possible to obtain it again; it is only a matter of finding the right experimental conditions’.

5.3 Metastable zone widths

The lack of success of the classical nucleation theories in explaining the behaviour of real systems has led a number of authors to suggest that most primary nucleation in industrial crystallizers is heterogeneous rather than homogeneous and that empirical relationships such as

$$J = k_n \Delta c_{\max}^n \quad (5.29)$$

are the only ones that can be justified. J is the nucleation rate, k_n the nucleation rate constant and Δc_{\max} the maximum allowable supersaturation (or metastable zone width). The exponent n , which is frequently referred to as the apparent order of nucleation, has no fundamental significance. It does not give an indication of the number of elementary species involved in the nucleation process.

However, equation 5.29 is not entirely empirical since it can be derived from the classical nucleation relationship (equation 5.9) (Nielsen, 1964; Nývlt, 1968). The nucleation rate may be expressed in terms of the rate at which supersaturation is created by cooling, viz.

$$J = q \dot{\theta} \quad (5.30)$$

where $\dot{\theta} = -d\theta/dt$ and q is the mass of crystalline substance deposited per unit mass of ‘free’ solvent present when the solution is cooled by 1°C . q is a function of the concentration change and of the crystallizing species. In general,

$$q = \varepsilon \frac{dc^*}{d\theta} \quad (5.31)$$

where $\varepsilon = R/[1 - c(R - 1)]^2$. R is the ratio of the molecular weights of hydrate: anhydrous salt and c is the solution concentration expressed as mass of anhydrous solute per unit mass of solvent at a given temperature.

The maximum allowable supersaturation, Δc_{\max} , may be expressed in terms of the maximum allowable undercooling, $\Delta\theta_{\max}$:

$$\Delta c_{\max} = \left(\frac{dc^*}{d\theta} \right) \Delta\theta_{\max} \quad (5.32)$$

so equation 5.29 can be rewritten as

$$\varepsilon \left(\frac{dc^*}{d\theta} \right) \dot{\theta} = k_n \left[\left(\frac{dc^*}{d\theta} \right) \Delta\theta_{\max} \right]^n \quad (5.33)$$

or, taking logarithms,

$$\log \dot{\theta} = (n - 1) \log \left(\frac{dc^*}{d\theta} \right) - \log \varepsilon + \log k_n + n \log \Delta\theta_{\max} \quad (5.34)$$

which indicates that the dependence of $\log \dot{\theta}$ on $\log \Delta\theta_{\max}$ is linear with a line of slope n .

Although equation 5.34 can be useful for characterizing the metastability of crystallizing systems, as will be described below, it is no longer regarded as a reliable indicator of the nucleation kinetics alone. The over-simplification in the above analysis is that it assumes that at the moment when nuclei are first detected the rate of supersaturation is equal to the rate of nucleation, but the true situation is rather more complex. The created supersaturation is dissipated in two ways, partly by growth on existing crystalline particles and partly by the formation of new nuclei. Further, in the experimental determination of the metastable limit, nuclei are not detected at the moment of their creation but at some later time when they have grown to visible size (at say about $10 \mu\text{m}$). In other words, the results of such measurements are dependent not only on nucleation but also on the subsequent crystal growth process.

Recognizing this fact, Nývt (1983) proposed a refinement of the theoretical analysis and concluded that for unseeded solutions the slope of the

$$\log \Delta\theta_{\max} \text{ versus } \log \dot{\theta}$$

line is not equal to n but to $(3g + 4 + n)/4$ where g is the apparent ‘order’ of the growth process (equation 6.18).

Janse and de Jong (1978) have warned that attempts to evaluate crystallization kinetics from metastable zone width evidence should be treated with caution, while Kubota, Kawakami and Tadaki (1986) have suggested that the cooling rate dependence of $\Delta\theta_{\max}$ can reasonably be explained by a random nucleation model. Other detailed analyses of metastable zone width measurements and their relationship to nucleation and growth kinetics have been made by Mullin and Jančić (1979) and Söhnle and Mullin (1988b).

The simple apparatus shown in *Figure 5.10* (Mullin, Chakraborty and Mehta, 1970), based on an earlier one devised by Nývt (1968), can be used to determine equilibrium solubilities (section 3.9) as well as metastable zone widths (section 3.12). About 40 mL of nearly saturated solution of known concentration is placed in the 50-mL flask and rapidly cooled until nucleation commences. The contents of the flask are then slowly heated. The cooling and heating sequences may be effected by means of the water jacket, as shown, or by an externally operated cold/hot air blower. On approaching the saturation temperature the heating rate is reduced to about $0.2^\circ\text{C}/\text{min}$. The temperature at which the last crystalline particle disappears is taken as the saturation temperature, θ^* .

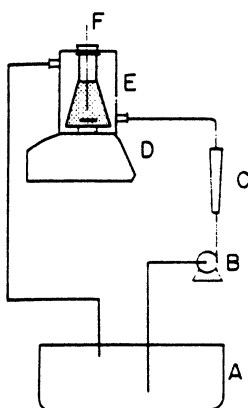


Figure 5.10. Apparatus for measuring metastable limits in agitated solutions: A, cooling water-bath; B, pump; C, flow meter; D, magnetic stirrer; E, Perspex water jacket; F, thermometer

The nucleation temperature is measured in a similar way. The flask containing the solution of known concentration is warmed to about 4 or 5° higher than the saturation temperature. A steady rate of cooling is maintained and the temperature at which nuclei first appear is recorded. The difference between the saturation and nucleation temperatures is the maximum allowable undercooling, $\Delta\theta_{\max}$, corresponding to a particular cooling rate $\dot{\theta}$.

Nucleation temperatures in the presence of crystalline materials can be determined by a procedure similar to that for the measurement of unseeded data by introducing two small crystals (~2 mm in size) into the flask when the solution has cooled to its predetermined saturation temperature.

The variation of the maximum allowable undercooling $\Delta\theta_{\max}$ with the cooling rate $\dot{\theta}$ for aqueous solutions of ammonium sulphate (Mullin, Chakraborty and Mehta, 1970) is shown in *Figure 5.11*. The lines for seeded and unseeded solutions are not parallel; the seeded points lie approximately 1.5–2 °C below the unseeded. The slopes of the lines for seeded and unseeded solutions are approximately 2.6 and 6.4, respectively, which indicates that the mechanisms of primary and secondary nucleation are different. The best straight lines through the data yield the relationships

$$\dot{\theta} = (1.38 \pm 0.9) \Delta\theta^{2.64 \pm 0.92} \quad \text{seeded (secondary)}$$

and

$$\dot{\theta} = (1.28 \pm 0.91) \times 10^{-2} \Delta\theta^{6.43 \pm 1.62} \quad \text{unseeded (primary)}$$

which give a measure of the scatter of the data. The maximum allowable undercoolings for seeded and unseeded solutions are more or less independent of the saturation temperature over the range 20–40 °C, but do depend on the rate of cooling. At low rates of cooling (~5 °C/h) the values are about 1.8 and 3.8 °C for seeded and unseeded solutions, respectively, of ammonium sulphate compared with 3.5 and 5 °C for a cooling rate of 30 °C/h.

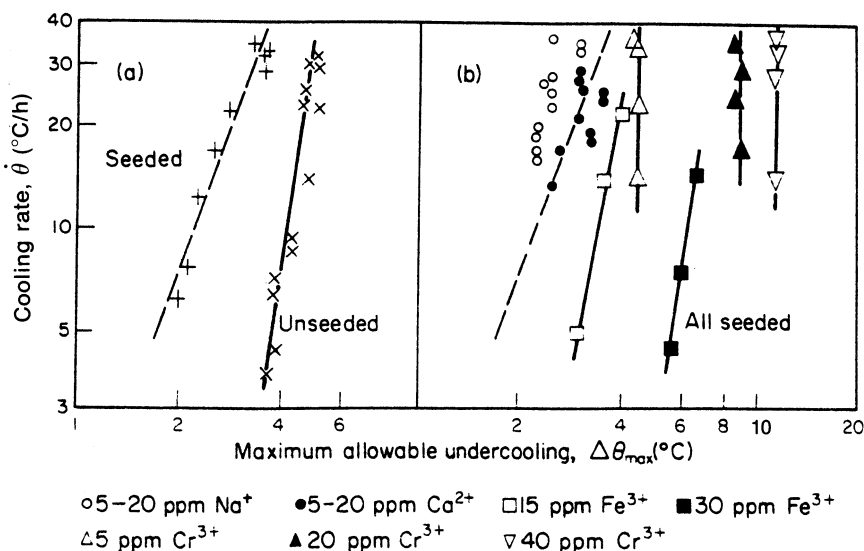


Figure 5.11. Nucleation characteristics of ammonium sulphate aqueous solution: (a) pure solutions, seeded and unseeded; (b) effect of impurities in seeded solutions. The broken line represents data from (a). (After Mullin, Chakraborty and Mehta, 1970)

Undercooling data obtained from unseeded solutions have little or no industrial relevance. In fact it is often impossible to obtain consistent ‘unseeded’ values for many aqueous solutions, e.g. sodium acetate, sodium thiosulphate and citric acid. For crystallizer design purposes, the lowest ‘seeded’ value should be taken as the maximum allowable undercooling, and the working value of the undercooling should be kept well below this.

Some typical maximum allowable undercoolings in seeded solutions are given in Table 5.1. It should be noted that although the values of $\Delta\theta_{\max}$ for any two substances may be similar, the values of the supersaturation, Δc_{\max} and S , may be very different. The relationship between the two quantities is

Table 5.1. Maximum allowable undercooling*, $\Delta\theta_{\max}$, for some common aqueous salt solutions at 25°C (measurements made in the presence of crystals under conditions of slow cooling ($\sim 5^{\circ}\text{C}/\text{h}$) and moderate agitation)

Substance	°C	Substance	°C	Substance	°C	Substance	°C
NH ₄ alum	3.0	MgSO ₄ · 7H ₂ O	1.0	NaI	1.0	KBr	1.1
NH ₄ Cl	0.7	NiSO ₄ · 7H ₂ O	4.0	NaHPO ₄ · 12H ₂ O	0.4	KCl	1.1
NH ₄ NO ₂	0.6	NaBr · 2H ₂ O	0.9	NaNO ₃	0.9	KI	0.6
(NH ₄) ₂ SO ₄	1.8	Na ₂ CO ₃ · 10H ₂ O	0.6	NaNO ₂	0.9	KH ₂ PO ₄	9.0
NH ₄ H ₂ PO ₄	2.5	Na ₂ CrO ₄ · 10H ₂ O	1.6	Na ₂ SO ₄ · 10H ₂ O	0.3	KNO ₃	0.4
CuSO ₄ · 5H ₂ O	1.4	NaCl	1.0	Na ₂ S ₂ O ₃ · 5H ₂ O	1.0	KNO ₂	0.8
FeSO ₄ · 7H ₂ O	0.5	Na ₂ B ₄ O ₇ · 10H ₂ O	4.0	K alum	4.0	K ₂ SO ₄	6.0

*The working value for normal crystallizer operation may be 50% of these values, or lower. The relation between $\Delta\theta_{\max}$ and Δc_{\max} is given by equation 5.32.

given by equation 5.32. For example, $\Delta\theta_{\max} = 1^\circ\text{C}$ for both sodium chloride and sodium thiosulphate, but the corresponding values of Δc_{\max} are 0.25 and 18 g of crystallizing substance per kg of solution and $S \sim 1.01$ and 1.4, respectively.

It has long been known that the metastable zone width can be greatly affected by the thermal history of the solution. A solution that has been kept for an hour or so at a temperature sufficiently higher than the saturation temperature will be found to have a wider metastable zone than if it had been kept only slightly above the saturation temperature. The higher the preheating and the longer the solution is maintained at that temperature, the higher the supersaturation at which nucleation commences. Preheating also increases the induction period (section 5.5) and decreases the number of crystals formed (Söhnle and Garside, 1992). The influence of thermal history has often been attributed to the deactivation of heteronuclei in the solution, but an alternative view is that preheating changes the solution structure and influences the sub-critical cluster sizes (Nývlt *et al.*, 1985).

The experimental measurement of industrially meaningful metastable zone widths can be very time consuming. For this reason Mersmann and Bartosch (1998) have proposed a theoretical model claimed to be able to predict working values for the design of seeded batch crystallizers. A number of basic assumptions are made. First, that the secondary nucleation is not caused by attrition between seed crystals, but by surface nucleation on the seeds which develop into outgrowths and later detach. This mode of behaviour was first analysed by Nielsen (1964) and given the name ‘needle breeding’ by Strickland-Constable (1979). It is further assumed that the development of the outgrowths is controlled by the integration step (section 6.1.4) and that the shower of detectable nuclei that marks the onset of secondary nucleation occurs when the volumetric hold-up of crystals in the vessel is between 10^{-4} and 10^{-3} (m^3 crystals/ m^3 suspension) corresponding to a detectable size of $\sim 10\,\mu\text{m}$.

5.4 Effect of impurities

The presence of impurities in a system can affect nucleation behaviour very considerably. It has long been known, for example, that the presence of small amounts of colloidal substances such as gelatin can suppress nucleation in aqueous solution, and certain surface-active agents also exert a strong inhibiting effect. Traces of foreign ions, especially Cr^{3+} and Fe^{3+} , can have a similar action on inorganic salts, as can be seen from the data recorded in *Figure 5.11b*.

It would be unwise to attempt a general explanation of the phenomenon of nucleation suppression by added impurities with so little quantitative evidence yet available, but certain patterns of behaviour are beginning to emerge. For example, the higher the charge on the cation the more powerful the inhibiting effect, e.g. $\text{Cr}^{3+} > \text{Fe}^{3+} > \text{Al}^{3+} > \text{Ni}^{2+} > \text{Na}^+$. Furthermore there often appears to be a ‘threshold’ concentration of impurity above which the inhibiting effect may actually diminish (Mullin, Chakraborty and Mehta, 1970). The modes of action of high molecular weight substances and cations are probably

quite different. The former may have their main action on the heteronuclei, rendering them inactive by adsorbing on their surfaces, whereas the latter may act as structure-breakers in the solution phase.

Other suggestions have been made for the action of impurities. For example, Botsaris, Denk and Chua (1972) suggested that if the impurity suppresses primary nucleation, secondary nucleation can occur if the uptake of impurity by the growing crystals is significant; the seed crystal creates an impurity concentration gradient about itself; the concentration of impurity near the crystal surface becomes lower than that in the bulk solution; and if it is reduced low enough, nucleation can occur. Another possibility is that certain impurities could enhance secondary nucleation by adsorbing at defects on existing crystal surfaces and, by initiating crack propagation, render the crystals prone to disintegration (Sarig and Mullin, 1980). Kubota, Ito and Shimizu (1986), on the other hand, have interpreted the effects of ionic impurities on contact secondary nucleation by a random nucleation model.

The presence of soluble impurities can also affect the induction period, t_{ind} (section 5.5), but it is virtually impossible to predict the effect. Ionic impurities, especially Fe^{3+} and Cr^{3+} , may increase the induction period in aqueous solutions of inorganic salts. Some substances, such as sodium carboxymethyl-cellulose or polyacrylamide, can also increase t_{ind} , whereas others may have no effect at all. The effects of soluble impurities may be caused by changing the equilibrium solubility or the solution structure, by adsorption or chemisorption on nuclei or heteronuclei, by chemical reaction or complex formation in the solution, and so on. The effects of insoluble impurities are also unpredictable.

The effects of soluble impurities on crystal growth and crystallization processes in general are discussed in more detail in sections 6.2.8 and 6.4, respectively.

5.5 Induction and latent periods

A period of time usually elapses between the achievement of supersaturation and the appearance of crystals. This time lag, generally referred to as an 'induction period', is considerably influenced by the level of supersaturation, state of agitation, presence of impurities, viscosity, etc.

The existence of an induction period in a supersaturated system is contrary to expectations from the classical theory of homogeneous nucleation (section 5.1.1), which assumes ideal steady-state conditions and predicts immediate nucleation once supersaturation is achieved. The induction period may therefore be considered as being made up of several parts. For example, a certain 'relaxation time', t_r , is required for this system to achieve a quasi-steady-state distribution of molecular clusters. Time is also required for the formation of a stable nucleus, t_n , and then for the nucleus to grow to a detectable size, t_g . So the induction period, t_{ind} , may be written.

$$t_{\text{ind}} = t_r + t_n + t_g \quad (5.35)$$

It is difficult, if not impossible, to isolate these separate quantities. The relaxation time depends to a great extent on the system viscosity and, hence, diffusivity. Nielsen (1964) has suggested that $t_r \sim 10^{-17} D^{-1}$, where D = diffusivity ($\text{m}^2 \text{s}^{-1}$). In an aqueous solution of an electrolyte, with $D \sim 10^{-9} \text{ m}^2 \text{s}^{-1}$, the relaxation time would be about 10^{-8} s . In highly viscous systems, however, values of D can be extremely low and t_r accordingly very high. Indeed, some systems can set to a glass before nucleation occurs. The nucleation time depends on the supersaturation which affects the size of the critical nucleus (section 5.1.1), but its estimation is the subject of speculation (Söhnle and Mullin, 1988a). The growth time depends on the size at which 'nuclei' are detectable and the growth rate applicable to this early stage of development. This latter quantity is difficult to predict since the rate of growth of a nucleus cannot be assumed to have the same order of magnitude as that of a macrocrystal: the mechanism and rate may well be quite different (section 6.2.7).

In some systems, particularly at low supersaturation, another time lag may be observed. To distinguish it from the induction period, defined above as the point at which crystals are first detected in the system, the term 'latent period' will be used, and is defined here as the onset of a significant change in the system, e.g. the occurrence of massive nucleation or some clear evidence of substantial solution desupersaturation.

Figure 5.12 indicates some of these events diagrammatically on a typical desupersaturation curve. Supersaturation is created at zero time (point *A*) and a certain induction time t_{ind} elapses before crystals are first detected (*B*). This point, of course, is not the nucleation time $t_n(B')$ since critical-sized nuclei cannot be detected; they need a certain time ($t_{\text{ind}} - t_n$) to grow into crystals of detectable size. However, at point *B*, and often for a considerable time afterwards, no significant changes in the solution may be detected until, at point *C*, sometimes referred to as the end of the latent period, t_{lp} , rapid desupersaturation occurs (*D*). Crystal growth predominates during the desupersaturation region. Towards the end of the gradual approach to equilibrium, *E*, which may take hours or days, an ageing process may occur (section 7.2.2). At very high supersaturations, the induction time and latent period can be extremely short and virtually indistinguishable.

The presence of seed crystals generally reduces the induction period, but does not necessarily eliminate it. Even if the system is seeded at time $t = 0$, a measurable induction period t_{ind} may elapse before new crystals are detected. By definition, these are 'secondary' nuclei and they may appear in several bursts throughout the latent period, making it difficult to attach any real significance to the induction time itself. For these reasons it may be preferable to record the latent period as the more practical characteristic of the system. Factors that can influence the induction and latent periods and the rate of desupersaturation are temperature, agitation, heat effects during crystallization, seed size, seed surface area and the presence of impurities.

Induction periods are often measured visually, but a different result can be recorded if new crystalline matter in the system is detected by more sensitive means, e.g. by laser light scattering or electric zone sensing methods

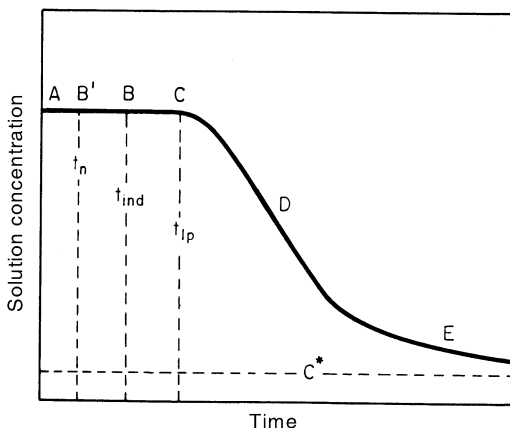


Figure 5.12. A desupersaturation curve (diagrammatic): c^* = equilibrium saturation, t_n = nucleation time, t_{ind} = induction time, t_{lp} = latent period

(section 2.14.2). This variability serves to emphasize the fact that an experimentally determined t_{ind} is not, by itself, a fundamental characteristic of a crystallizing system.

In practice, the determination of t_{ind} by conventional methods presents few problems so long as it exceeds about 10 s. For example, reacting solutions may be quickly mixed in an agitated vessel and the time recorded when the first physical property change or the first crystals are detected (Mullin and Osman, 1973). Serious complications can arise, however, when t_{ind} is less than about 5 s because the mixing time in a simple vessel could be comparable with or even exceed the measured induction period. For the successful measurement of short induction periods, therefore, two things are essential: (1) very rapid mixing and (2) a fast sensitive method for the detection of the appropriate system changes.

A useful technique for the precipitation of relatively insoluble electrolytes is the stopped-flow method (Söhnel and Mullin, 1978b). If two stable solutions, which react to form a supersaturated solution of the reactant, are mixed together instantaneously, no detectable changes occur for some time. However, as soon as the reactant starts to precipitate the concentration of the electrically conductive species begins to decrease and this causes the solution conductivity to diminish. The period of conductivity steadiness is inversely proportional to the supersaturation, and for highly supersaturated solutions it can be less than a millisecond.

A precipitation cell made of Perspex (overall dimensions $100 \times 60 \times 40$ mm) is shown in *Figure 5.13*. The two reactant solutions (5 mL each) are placed in the separate 10-mm diameter chambers, *A*, from where they are displaced by the twin piston, *B*, into the mixing chamber, *C*. The twin piston is rapidly plunged by hand, an operation that takes less than 0.1 s, and a microswitch, situated at the lowest position of the piston, is triggered when the piston stops at the bottom of the feedstock chambers. Two platinum electrodes, *D*, are located in the 4-mm diameter outlet channel, *E*, at a distance of 15 mm from

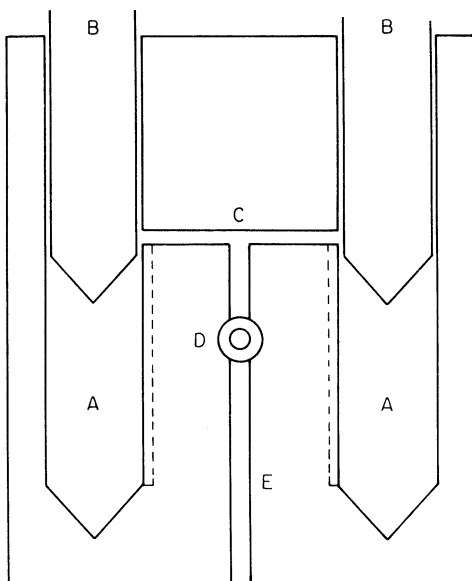


Figure 5.13. Precipitation cell. (A) reactant solution chambers; (B) twin pistons; (C) mixing chamber; (D) disc electrodes; (E) outlet channel. (After Söhnel and Mullin, 1978b)

the mixing chamber in such a way that they do not obstruct the liquid flow. The detection equipment includes a storage oscilloscope which permits time measurements from 10 s to 1 μ s. A microswitch triggers the oscilloscope sweep.

The sensitivity of the method may be estimated as follows. Two solutions are forced into the mixing chamber where they react to form a supersaturated solution of the reactant. The supersaturated solution then travels down the outlet channel. At some distance, l , from the mixing chamber, the first detectable change in conductivity occurs. The distance, l , which depends on both the liquid velocity and the level of supersaturation achieved, is a constant while liquid is flowing in the channel, assuming steady-state conditions. However, when the flow stops, i.e. when the mixing process is completed, the 'detection boundary' in the liquid phase travels back up the channel, towards the mixing chamber, with a velocity l/t_{ind} and it reaches the measuring point, located at a distance, d , from the mixing chamber, in a time t_{exp} after the cessation of liquid flow where

$$t_{\text{exp}} = t_{\text{ind}}(l - d)/l \quad (5.36)$$

If $l \gg d$ then $t_{\text{exp}} \sim t_{\text{ind}}$, i.e. the experimentally measured time can be regarded as being equivalent to the induction period. The limit of application may be estimated to lie at $l \sim 3d$, where t_{exp} may still be regarded as approximately equal to t_{ind} if experimental errors are taken into account.

A typical curve recorded on the oscilloscope display is shown in *Figure 5.14*. From point A (where liquid movement had stopped and the oscilloscope sweep was initiated by the microswitch) to point B, the solution conductivity does not change detectably. Then the conductivity suddenly decreases (B to C) and

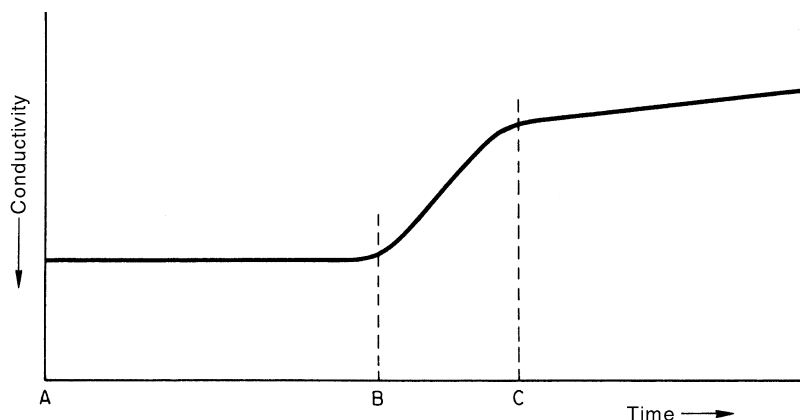


Figure 5.14. A typical oscilloscope record indicating the induction period *AB*

continues to decrease slowly over a long period. The time corresponding to the interval *AB* is taken as the induction period of precipitation. The interval *BC*, the length of which is a function of the initial solution supersaturation, is caused by the sudden creation of nuclei and their subsequent growth. The last period, beyond point *C*, reflects the final slow growth of the crystals in a solution with a near-depleted supersaturation.

5.6 Interfacial tension (surface energy)

As the induction period can be affected profoundly by so many external influences, it cannot be regarded as a fundamental property of a system. Nor can it be relied upon to yield basic information on the process of nucleation. Nevertheless, despite its complexity and uncertain composition, the induction period has frequently been used as a measure of the nucleation event, making the simplifying assumption that it can be considered to be inversely proportional to the rate of nucleation:

$$t_{\text{ind}} \propto J^{-1} \quad (5.37)$$

The classical nucleation relationship (equation 5.9) may therefore be written

$$\log t_{\text{ind}} \propto \left[\frac{\gamma^3}{T^3(\log S)^2} \right] \quad (5.38)$$

which suggests that, for a given temperature, a plot of $\log t_{\text{ind}}$ versus $(\log S)^{-2}$ should yield a straight line, the slope of which should allow a value of the interfacial tension, γ , to be calculated. *This can only be justified, however, if the data relate to true homogeneous nucleation.* In a similar manner, the Arrhenius reaction velocity relationship (equation 5.5) written in terms of the induction period:

$$t_{\text{ind}} = A \exp(\Delta G/kT) \quad (5.39)$$

will allow evaluation of the activation energy of homogeneous nucleation from the slope of a linear plot of $\log t_{\text{ind}}$ versus T^{-1} .

An experimentally determined linear relationship between $\log t_{\text{ind}}$ and $(\log S)^{-2}$ is no guarantee that homogeneous nucleation has occurred, as can be seen from stopped-flow precipitation data for CaCO_3 plotted in *Figure 5.14* (Söhnel and Mullin, 1978b) where two different straight lines can be drawn through the experimental points. The change of slope at $(\log S)^{-2} \sim 0.55$, i.e. $S \sim 20$, marks a division between homogeneous and heterogeneous nucleation. The slope of the line in the higher supersaturation region to the left of the diagram gives a value of $\gamma \sim 80 \text{ mJ m}^{-2}$. Data for SrCO_3 , an even less soluble salt, does not show a transition to heterogeneous nucleation in the supersaturation range studied ($S = 50\text{--}70$) and a value of $\gamma \sim 100 \text{ mJ m}^{-2}$ is calculated from the slope of this line.

Much lower values of γ are expected for soluble salts. The data in *Figure 5.16* for nickel ammonium sulphate, where t_{ind} was determined visually (Mullin and Osman, 1973; Mullin and Ang, 1976), again show a homogeneous/heterogeneous division, this time at a value of $S \sim 1.8$, and a value of $\gamma \sim 4 \text{ mJ m}^{-2}$ is calculated from data in the left hand region for $S > 2$.

The temperature dependence of interfacial tension has been demonstrated using induction period data for nickel ammonium sulphate recorded over a short temperature range. The salt was precipitated by quickly mixing equimolar solutions of nickel and ammonium sulphates after which the system was allowed to remain static until nucleation occurred. Plots of $\log t_{\text{ind}}$ versus $T^{-3}(\log S)^{-2}$, in accordance with equation 5.38, gave a family of straight lines

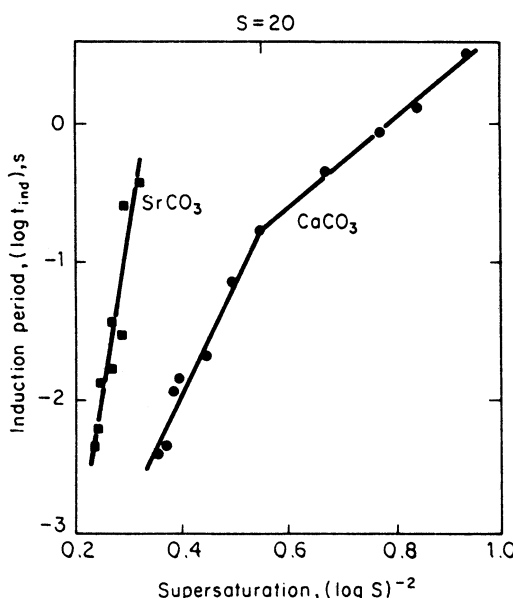


Figure 5.15. Induction period as a function of initial supersaturation for calcium and strontium carbonates. The data for CaCO_3 indicate a transition between homogeneous and heterogeneous nucleation. (After Söhnel and Mullin, 1978b)

of different slope indicating that γ increased from 3.9 mJ m^{-2} at 20°C to 4.6 mJ m^{-2} at 0°C (Mullin and Osman, 1973).

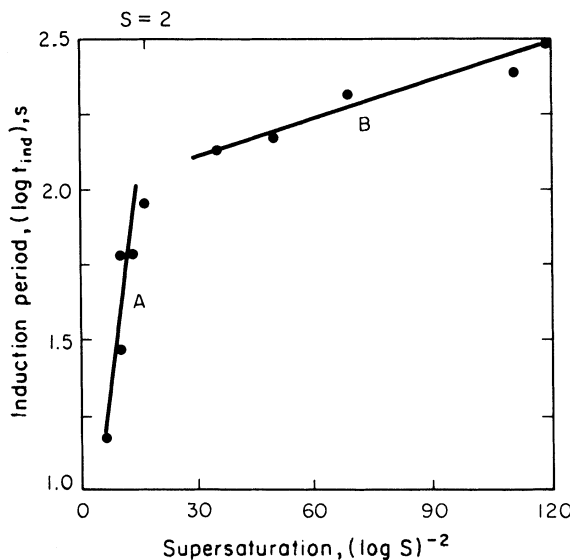


Figure 5.16. Induction period as a function of initial supersaturation for nickel ammonium sulphate. A = homogeneous, B = heterogeneous nucleation. (After Mullin and Ang, 1976)

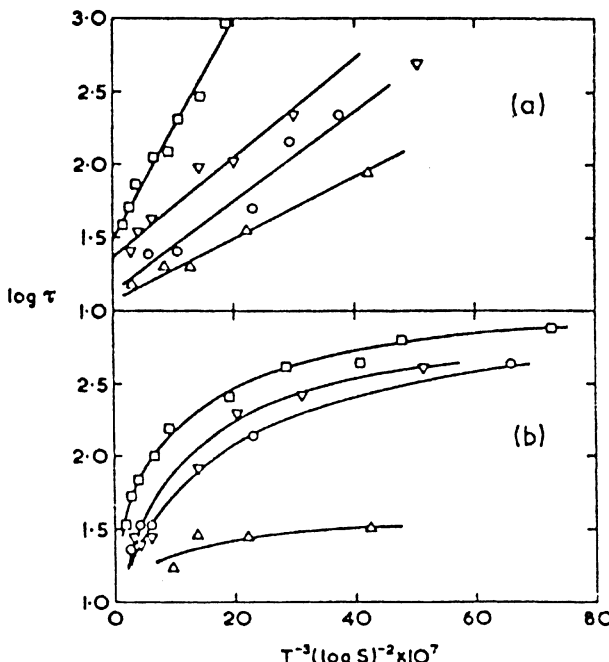


Figure 5.17. Plot of $\log \tau$ versus $T^{-3}(\log S)^{-2}$ for (a) non-agitated and (b) agitated systems: (□) 15, (▽) 20, (○) 25, and (△) 35°C. (After Mullin and Žáček, 1981)

Another example is shown in *Figure 5.17* for the precipitation of potassium alum. The data points for the static system (*Figure 5.17a*) lie on three straight lines giving γ values, calculated from equation 5.38, ranging from 2.03 mJ m^{-2} at 35°C to 3.14 mJ m^{-2} at 15°C . A different picture emerges from precipitation in agitated solution (*Figure 5.17b*) when the relationship between $\log \tau$ and $T^{-3}(\log S)^{-2}$ is non-linear suggesting a heterogeneous or even a secondary mode of nucleation (Mullin and Žáček, 1981). A value of γ around 37 mJ m^{-2} has been reported (Lancia, Musmarra and Prisciandaro, 1999) for the sparingly soluble $\text{CaSO}_4 \cdot 2\text{H}_2\text{O}$ and no significant variation was found over the temperature range 25 – 90°C .

A graph (*Figure 5.18*) attempting to relate interfacial tension γ with equilibrium solubility c^* was constructed by Nielsen and Söhnel (1971) after assessing a wide variety of experimental data. The link between γ and c^* can be substantiated on the basis of regular solution theory (Bennema and Söhnel, 1990). Following similar lines, Mersmann (1990) proposed the equation

$$\gamma = 0.414 kT \left[\frac{\rho_c N}{M} \right]^{2/3} \ln \left[\frac{c_s}{c_L} \right] \quad (5.40)$$

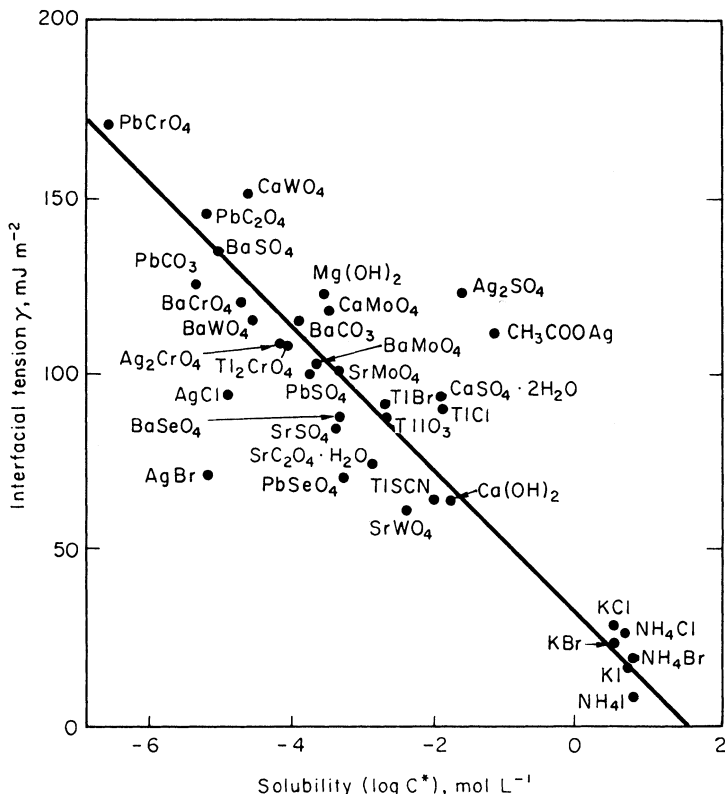


Figure 5.18. Interfacial tension as a function of solubility. (After Nielsen and Söhnel, 1971)

derived from fundamental relationships, for predicting interfacial tension $\gamma (\text{J m}^{-2})$; $k = \text{Boltzmann constant } (1.38 \times 10^{-23} \text{ J K}^{-1})$, $N = \text{Avogadro constant } (6.02 \times 10^{26} \text{ kmol}^{-1})$, $M = \text{molar mass } (\text{kg kmol}^{-1})$, $\rho_c = \text{crystal density } (\text{kg m}^{-3})$, c_s and c_L are the solute concentrations (kmol m^{-3}) in the solid and liquid phases, respectively. Equation 5.39 appears to be compatible with published data on more than 50 anhydrous salts in aqueous solution. For example, for BaSO_4 at 18°C in saturated aqueous solution $T = 291 \text{ K}$, $\rho_c = 4500 \text{ kg m}^{-3}$, $M = 233 \text{ kg kmol}^{-1}$, $c_s = 4500/233 = 19.3 \text{ kmol m}^{-3}$, solubility product $K_c = 0.87 \times 10^{-10}$, $c_L = (K_c)^{1/2} = 0.93 \times 10^{-5} \text{ kmol m}^{-3}$, and the value of γ may be calculated as approximately 0.12 J m^{-2} .

A comprehensive review of the general subject of solid material surface energy has been made by Linford (1972).

5.7 Ostwald's rule of stages

In the early part of the 19th century several workers made the experimental observation that some aqueous solutions of inorganic salts, when cooled rapidly, first deposited crystals of a less stable form than that which normally crystallizes. A frequently quoted example is that of sodium sulphate solution which can precipitate heptahydrate crystals at around room temperature before the thermodynamically stable decahydrate appears. Another is the crystallization of an unstable polymorph of potassium nitrate in advance of the more stable rhombic form.

Ostwald (1896, 1897) attempted to generalize this sort of behaviour by propounding a ‘rule of stages’ which he stated as: an unstable system does not necessarily transform directly into the most stable state, but into one which most closely resembles its own, i.e. into another transient state whose formation from the original is accompanied by the smallest loss of free energy. Ostwald recognized that there were many exceptions to this ‘rule’ and countless others have since been recorded. Thermodynamic explanations alone do not offer any theoretical support (Dufor and Defay, 1963; Dunning, 1969), but a combined thermodynamics-kinetics approach (Cardew and Davey, 1982) does appear to offer some justification, although the conclusion is that the rule has no general proof. A more recent proposal, based on the assumption of structural changes taking place in crystallizing solutions, has been offered as an alternative explanation by Nývlt (1995) together with experimental evidence from aqueous solutions of citric acid, ferrous sulphate and sodium hydrogen phosphate. Some support for this has been given by a computer simulation of crystallization from solution (Anwar and Boateng, 1998) which demonstrated the development of a diffuse precursor phase, with some elements of crystallinity, eventually transforming into a stable crystalline structure.

Despite the lack of definitive theoretical proof, some form of the rule of stages does seem to operate often enough for it to be regarded as important to bear in mind when, for example, operating large-scale precipitation processes (section 7.2.6). The most probable explanation of the phenomenon lies in the kinetics of the transformation, the deciding factor being the relative rates of

crystal nucleation and growth of the more-stable and less-stable forms. It is in fact, a good example of the behaviour where, if more than one reaction is thermodynamically possible, the resulting reaction is not the one that is thermodynamically most likely, but the one that has the fastest rate. In other words, kinetics are often more important than thermodynamics, and this should always be borne in mind when dealing with industrial (non-equilibrium) precipitating systems.

6 Crystal growth

6.1 Crystal growth theories

As soon as stable nuclei, i.e. particles larger than the critical size (section 5.1.1), have been formed in a supersaturated or supercooled system, they begin to grow into crystals of visible size. The many proposed mechanisms of crystal growth may broadly be discussed under a few general headings.

The surface energy theories are based on the postulation that the shape a growing crystal assumes is that which has a minimum surface energy. This approach, although not completely abandoned, has largely fallen into disuse. The diffusion theories presume that matter is deposited continuously on a crystal face at a rate proportional to the difference in concentration between the point of deposition and the bulk of the solution. The mathematical analysis of the operation is similar to that used for other diffusional and mass transfer processes. The suggestion by Volmer (1939) that crystal growth was a discontinuation process, taking place by adsorption, layer by layer, on the crystal surface led to the adsorption-layer theories, several notable modifications of which have been proposed in recent years.

For a comprehensive account of the historical development of the many crystal growth theories, reference should be made to the critical reviews by Wells (1946), Buckley (1952), Strickland-Constable (1968), Lewis (1980), Chernov (1980, 1989) and Nývlt *et al.* (1985).

6.1.1 Surface energy theories

An isolated droplet of a fluid is most stable when its surface free energy, and thus its area, is a minimum. In 1878 Gibbs (1948) suggested that the growth of a crystal could be considered as a special case of this principle: the total free energy of a crystal in equilibrium with its surroundings at constant temperature and pressure would be a minimum for a given volume. If the volume free energy per unit volume is assumed to be constant throughout the crystal, then

$$\sum_1^n a_i g_i = \text{minimum} \quad (6.1)$$

where a_i is the area of the i th face of a crystal bounded by n faces, and g_i the surface free energy per unit area of the i th face. Therefore, if a crystal is allowed to grow in a supersaturated medium, it should develop into an ‘equilibrium’ shape, i.e. the development of the various faces should be in such a manner as to ensure that the whole crystal has a minimum total surface free energy for a given volume.

Of course, a liquid droplet is very different from a crystalline particle; in the former the constituent atoms or molecules are randomly dispersed, whereas in

the latter they are regularly located in a lattice structure. Gibbs was fully aware of the limitations of his simple analogy, but in 1885 Curie found it a useful starting point for an attempt to evolve a general theory of crystal growth and in 1901 Wulff showed that the equilibrium shape of a crystal is related to the free energies of the faces; he suggested that the crystal faces would grow at rates proportional to their respective surface energies.

The surface energy and the rate of growth of a face, however, should be inversely proportional to the reticular or lattice density of the respective lattice plane, so that faces having low reticular densities would grow rapidly and eventually disappear. In other words, high index faces grow faster than low.

The velocity of growth of a crystal face is measured by the outward rate of movement in a direction perpendicular to that face. In fact to maintain constant interfacial angles in the crystal (Haüy's law), the successive displacements of a face during growth or dissolution must be parallel to each other. Except for the special case of a geometrically regular crystal, the velocity of growth will vary from face to face. *Figure 6.1a* shows the ideal case of a crystal that maintains its geometric pattern as it grows. Such a crystal is called 'invariant'. The three equal *A* faces grow at an equal rate; the smaller *B* faces grow faster; while the smallest face *C* grows fastest of all. A similar, but reverse, behaviour may be observed when a crystal of this type dissolves in a solvent; the *C* face dissolves at a faster rate than the other faces, but the sharp outlines of the crystal are soon lost once dissolution commences.

In practice, a crystal does not always maintain geometric similarity during growth; the smaller, faster-growing faces are often eliminated, and this mode of crystal growth is known as 'overlapping'. *Figure 6.1b* shows the various stages of growth of such a crystal. The smaller *B* faces, which grow much faster than the *A* faces, gradually disappear from the pattern.

So far there is no general acceptance of the surface energy theories of crystal growth, since there is little quantitative evidence to support them. These theories, however, still continue to attract attention, but their main defect is their failure to explain the well-known effects of supersaturation and solution movement on the crystal growth rate.

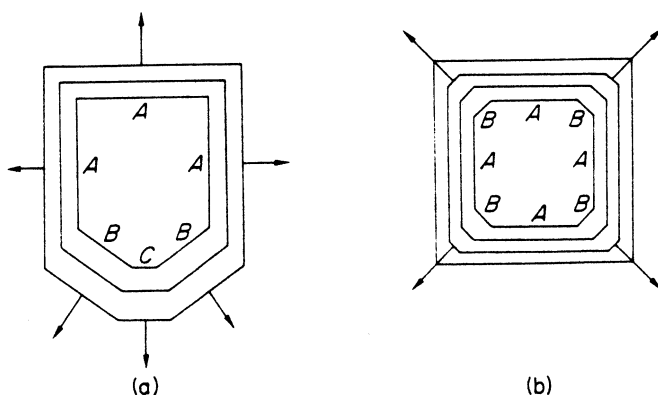


Figure 6.1. Velocities of crystal growth faces: (a) invariant crystal; (b) overlapping

6.1.2 Adsorption layer theories

The concept of a crystal growth mechanism based on the existence of an adsorbed layer of solute atoms or molecules on a crystal face was first suggested by Volmer (1939). Many other workers have contributed to, and modified Volmer's original postulation. The brief account of this subsequent development given below will serve merely to indicate the important features of layer growth and the role of crystal imperfections in the growth process.

Volmer's theory, or as some prefer to call it, the Gibbs–Volmer theory, is based on thermodynamic reasoning. When units of the crystallizing substance arrive at the crystal face they are not immediately integrated into the lattice, but merely lose one degree of freedom and are free to migrate over the crystal face (surface diffusion). There will, therefore, be a loosely adsorbed layer of integrating units at the interface, and a dynamic equilibrium is established between this layer and the bulk solution. The adsorption layer, or 'third phase', as it is sometimes called, plays an important role in crystal growth and secondary nucleation (section 5.3). The thickness of the adsorption layer probably does not exceed 10 nm, and may even be nearer 1 nm.

Atoms, ions or molecules will link into the lattice in positions where the attractive forces are greatest, i.e. at the 'active centres', and under ideal conditions this step-wise build-up will continue until the whole plane face is completed (*Figure 6.2a* and *b*). Before the crystal face can continue to grow, i.e. before a further layer can commence, a 'centre of crystallization' must come into existence on the plane surface, and in the Gibbs–Volmer theory it is

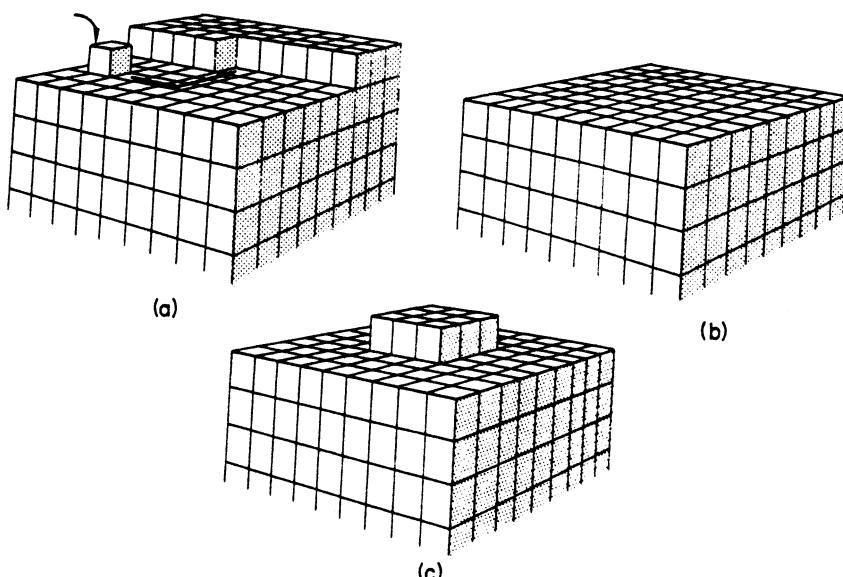


Figure 6.2. *A mode of crystal growth without dislocations: (a) migration towards desired location; (b) completed layer; (c) surface nucleation*

suggested that a monolayer island nucleus, usually called a two-dimensional nucleus, is created (*Figure 6.2c*).

Expressions for the energy requirement of two-dimensional nucleation and the critical size of a two-dimensional nucleus may be derived in a similar manner to those for homogeneous three-dimensional nucleation (section 5.1.1). The overall excess free energy of nucleation may be written

$$\Delta G = a\gamma + v\Delta G_v \quad (6.2)$$

where a and v are the area and volume of the nucleus, and if this is a circular disc of radius r and height h , then

$$\Delta G = 2\pi rh\gamma + \pi r^2 h\Delta G_v \quad (6.3)$$

and, maximizing to find the critical size, r_c ,

$$\frac{d\Delta G}{dr} = 2\pi h\gamma + 2\pi rh\Delta G_v = 0 \quad (6.4)$$

whence

$$r_c = -\frac{\gamma}{\Delta G_v} \quad (6.5)$$

In other words, the critical radius of a two-dimensional nucleus is half that of a three-dimensional nucleus (equation 5.3) formed under similar environmental conditions.

Similarly,

$$\Delta G_{\text{crit}} = -\frac{\pi h\gamma^2}{\Delta G_v} \quad (6.6)$$

where ΔG_v is a negative quantity; so from equation (5.7)

$$\Delta G_{\text{crit}} = \frac{\pi h\gamma^2 v}{kT \ln S} \quad (6.7)$$

In a similar manner to that described earlier, the rate of two-dimensional nucleation, J' , can be expressed in the form of the Arrhenius reaction velocity equation:

$$J' = B \cdot \exp(-\Delta G_{\text{crit}}/kT) \quad (6.8)$$

or

$$J = B \cdot \exp\left[-\frac{\pi h\gamma^2 v}{k^2 T^2 \ln S}\right] \quad (6.9)$$

Comparing equations 5.8 and 6.7 it can be seen that the ratio of the energy requirements of three- to two-dimensional nucleation (sphere:disc) is $16\gamma v/3h kT \ln S$. By inserting some typical values, e.g. $\gamma = 10^{-1} \text{ J m}^{-2}$, $v = 2 \times 10^{-29} \text{ m}^3$, $h = 5 \times 10^{-10} \text{ m}$, $kT = 4 \times 10^{-21} \text{ J}$, it can be calculated that the ratio is about 50:1 for a supersaturation of $S = 1.1$ and about 1.2:1 for $S = 10$. In general, therefore, it may be said that a reasonably high degree of

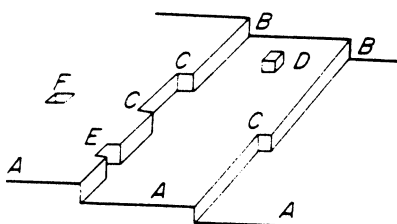


Figure 6.3. Kossel's model of a growing crystal surface showing flat surfaces (A), steps (B), kinks (C), surface-adsorbed growth units (D), edge vacancies (E) and surface vacancies (F)

local supersaturation is necessary for two-dimensional nucleation to occur, but lower than that required for the formation of three-dimensional nuclei under equivalent conditions.

The Kossel (1934) model of a growing crystal face is depicted in *Figure 6.3*. It envisages that an apparently flat crystal surface is in fact made up of moving layers (*steps*) of monatomic height, which may contain one or more *kinks*. In addition, there will be loosely adsorbed growth units (atoms, molecules or ions) on the crystal surface and vacancies in the surfaces and steps. Growth units are most easily incorporated into the crystal at a kink; the kink moves along the step and the face is eventually completed. A fresh step could be created by surface nucleation, and this frequently commences at the corners.

A crystal should grow fastest when its faces are entirely covered with kinks, and the theoretical maximum growth rate can be estimated (equation 6.37). It is unlikely, however, that the number of kinks would remain at this high value for any length of time; it is well known, for example, that broken crystal surfaces rapidly 'heal' and then proceed to grow at a much slower rate. However, many crystal faces readily grow at quite fast rates at relatively low supersaturation, far below those needed to induce surface nucleation. Crystals of iodine, for example, can be grown from the vapour at 1 per cent supersaturation at rates some 10^{1000} times greater than those predicted by classical theory (Volmer and Schultz, 1931)! So it must be concluded that the Kossel model, and its dependence on surface nucleation, is unreasonable for growth at moderate to low supersaturation.

A solution to the dilemma came when Frank (1949) postulated that few crystals ever grow in the ideal layer-by-layer fashion without some imperfection occurring in the pattern. Most crystals contain dislocations (see section 1.13) which cause steps to be formed on the faces and promote growth. Of these the screw dislocation (section 1.13.2) is considered to be important for crystal growth, since it obviates the necessity for surface nucleation. Once a screw dislocation has been formed, the crystal face can grow perpetually 'up a spiral staircase'. *Figure 6.4a–c* indicates the successive stages in the development of a growth spiral starting from a screw dislocation. The curvature of the spiral cannot exceed a certain maximum value, determined by the critical radius for a two-dimensional nucleus under the conditions of supersaturation in the medium in which the crystal is growing.

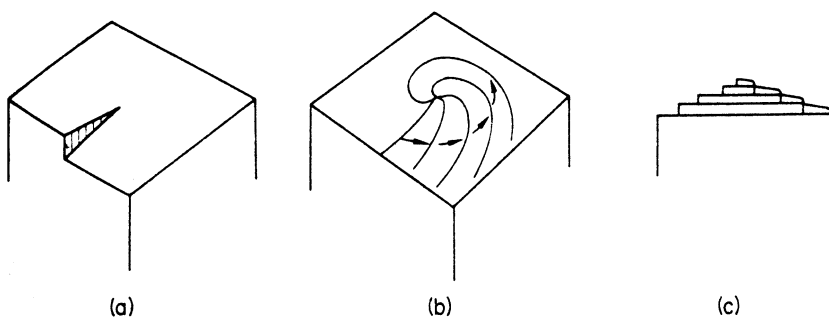


Figure 6.4. Development of a growth spiral starting from a screw dislocation

An example of a circular growth spiral on a silicon carbide crystal is shown in *Figure 6.5*. The major and minor axes of the elliptical spirals on the (100) face of an ammonium dihydrogen phosphate crystal growing in aqueous solution (*Figure 6.6*) point in the [010] and [001] directions respectively, indicating that surface diffusion is faster in the former direction (Davey and Mullin, 1974). The polygonized spiral on the C₃₆ hydrocarbon crystal (*Figure 6.7*) is probably only a few long-chain molecules in height. Quite often very complex spirals develop, especially when several screw dislocations grow together. Many examples of these are shown in the books by Verma (1953) and Read (1953).

As a completely smooth face never appears under conditions of spiral growth, surface nucleation is not necessary and the crystal grows as if the surface were covered with kinks. Growth continues uninterrupted at near the maximum theoretical rate for the given level of supersaturation. The behaviour of a crystal face with many dislocations is practically the same as that of a crystal face containing just one. Burton, Cabrera and Frank (1951) developed

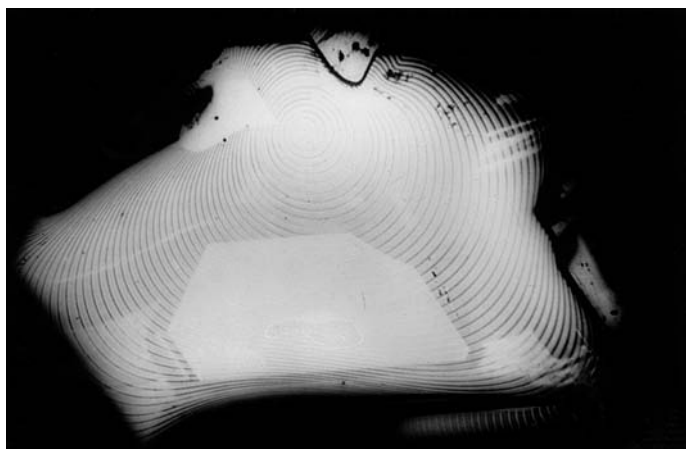


Figure 6.5. A circular spiral on a silicon carbide crystal. (Courtesy of the Westinghouse Corporation)

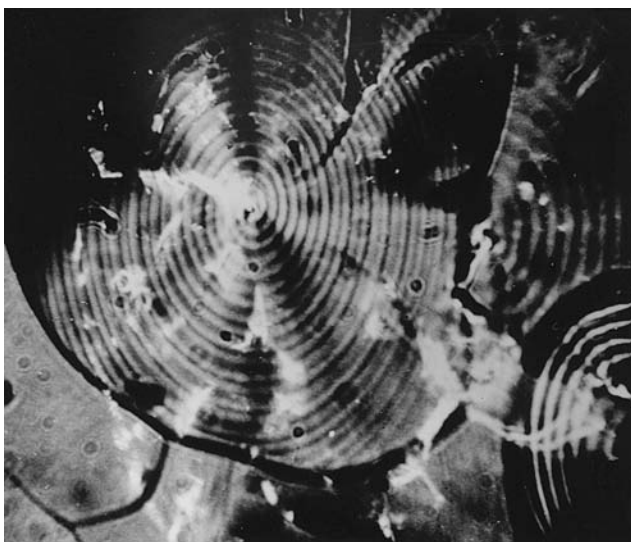


Figure 6.6. An elliptical spiral on the (100) face of an ammonium dihydrogen phosphate crystal growing in aqueous solution (Davey and Mullin, 1974)

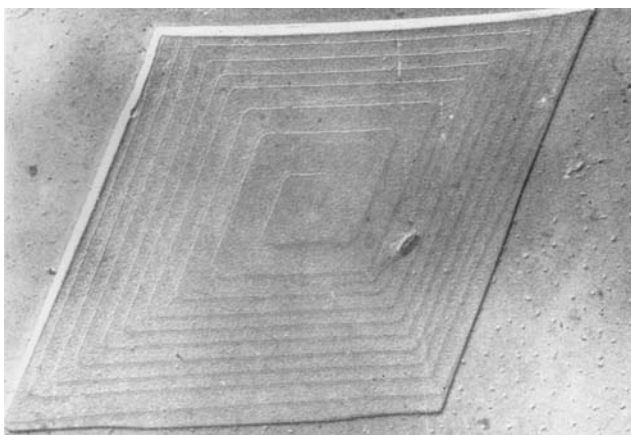


Figure 6.7. A polygonized spiral on the face of a C₃₆ normal alkane crystal. (Courtesy of R. Boistelle)

a kinetic theory of growth in which the curvature of the spiral near its origin was related to the spacing of successive turns and the level of supersaturation. By the application of Boltzmann statistics they predicted kink populations, and by assuming that surface diffusion is an essential step in the process they were able to calculate the growth rate at any supersaturation.

The Burton–Cabrera–Frank (BCF) relationship may be written

$$R = A\sigma^2 \tanh(B/\sigma) \quad (6.10)$$

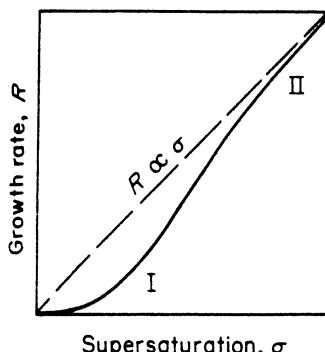


Figure 6.8. The Burton–Cabrera–Frank (BCF) supersaturation–growth relationship (I, $R \propto \sigma^2$; II, an approach to $R \propto \sigma$)

where R = crystal growth rate. The supersaturation $\sigma = S - 1$ where $S = c/c^*$ (see section 3.12.1). A and B are complex temperature-dependent constants which include parameters depending on step spacings.

At low supersaturations the BCF equation approximates to $R \propto \sigma^2$, but at high supersaturations $R \propto \sigma$. In other words, it changes from a parabolic to a linear growth law as the supersaturation increases. The volume diffusion model proposed by Chernov (1961) gives the same result. The general form of these expressions is shown in *Figure 6.8*.

It should be pointed out that the BCF theory was derived for crystal growth from the vapour; and while it should also apply to growth from solutions (and melts), it is difficult to quantify the relationships because of the more complex nature of these systems. Viscosities, for example, are higher and diffusivities lower in solutions ($\sim 10^{-3} \text{ N s m}^{-2}$ (1 cP) and $10^{-9} \text{ m}^2 \text{ s}^{-1}$) than in vapours ($\sim 10^{-5} \text{ N s m}^{-2}$ and $10^{-4} \text{ m}^2 \text{ s}^{-1}$). In addition, the dependence of diffusivity on solute concentration can be complex (section 2.4). Transport phenomena in ionic solutions can be complicated, especially if the different ions exhibit complex hydration characteristics. Furthermore, little is known about surface diffusion in adsorbed layers, and ion dehydration in or near these layers must present additional complicating factors.

For a comprehensive account of the relationships between the various surface and bulk diffusion models of crystal growth, and their relevance to crystal growth, reference may be made to the reviews by Bennema (1968, 1969, 1984) and Chernov (1980, 1989, 1993).

6.1.3 Kinematic theories

Two processes are involved in the layer growth of crystals, viz. the generation of steps at some source on the crystal face followed by the movement of layers across the face. Consideration of the movement of macrosteps of unequal distance apart (BCF theory considers a regular distribution of monoatomic steps) led Frank (1958) to develop a ‘kinematic’ theory of crystal growth. The

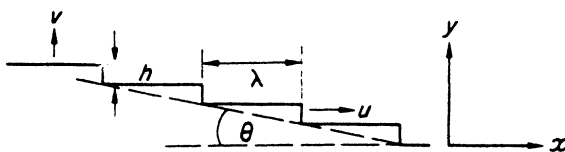


Figure 6.9. Two-dimensional diagrammatic representation of steps on a crystal face

step velocity, u , depends on the proximity of the other steps since all steps are competing units (Figure 6.9). Thus

$$u = q/n \quad (6.11)$$

where q is the step flux (the number of steps passing a given point per unit time) and n is the step density (the number of steps per unit length in a given region). The distance between steps, $\lambda = n^{-1}$. The slope of the surface, p , with reference to the close packed surfaces, i.e. the flat ledges, is given by

$$p = \tan \theta = hn \quad (6.12)$$

and the face growth rate, v , normal to the reference surface by

$$v = hq = hnu \quad (6.13)$$

where h is the step height.

If the steps are far apart ($\theta \rightarrow 0$), and the diffusion fields do not interfere with one another, the velocity of each step, u , will be a maximum. As the step spacings decrease and the slope increases, u decreases to a minimum at $hn = 1$ ($\theta = 45^\circ$). Looking at it another way: as the slope θ increases, the face growth velocity v ($= u \tan \theta$) increases, approaches a flat maximum and then decreases to zero. The shape of this $v(p)$ curve, which is affected by the presence of impurities, is an important characteristic of the growth process.

For the two-dimensional case depicted in Figure 6.9 another velocity, $c = dx/dt$, may be defined which represents the motion of 'kinematic waves' (regions on the crystal surface with a constant slope p and velocity v). These waves do not contain the same monomolecular steps all the time, as the step velocity $u = v/p$ can be greater or less than c . When two kinematic waves of different slope meet, a discontinuity in slope occurs, giving rise to 'shock waves' across the surface.

Another problem that can be treated on the basis of the kinematic theory is that of step bunching. The steps that flow across a face are usually randomly spaced and of different height and velocity. Consequently they pile-up or bunch. Growth, and dissolution, can be characterized by the relationship between the step flux, q , and step density, n . Two general forms of this relationship can be considered depending upon whether $d^2q/dn^2 < 0$ (Type I) or $d^2q/dn^2 > 0$ (Type II). The former is analogous to the flow of traffic along a straight road and the latter to flood water on a river (see Figure 6.10).

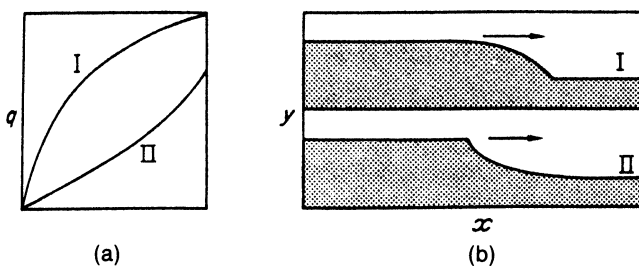


Figure 6.10. (a) Step flux density curves: type I, $d^2q/dn^2 < 0$; type II, $d^2q/dn^2 > 0$. (b) Surface profiles arising from bunches with type I and type II kinetics, respectively

6.1.4 Diffusion-reaction theories

The origin of the diffusion theories dates back to the work of Noyes and Whitney (1897) who considered that the deposition of solid on the face of a growing crystal was essentially a diffusional process. They also assumed that crystallization was the reverse of dissolution, and that the rates of both processes were governed by the difference between concentration at the solid surface and in the bulk of the solution. An equation for crystallization was proposed in the form

$$\frac{dm}{dt} = k_m A(c - c^*) \quad (6.14)$$

where m = mass of solid deposited in time t ; A = surface area of the crystal; c = solute concentration in the solution (supersaturated); c^* = equilibrium saturation concentration; and k_m = coefficient of mass transfer.

On the assumption that there would be a thin stagnant film of liquid adjacent to the growing crystal face, through which molecules of the solute would have to diffuse, Nernst (1904) modified equation 6.14 to the form

$$\frac{dm}{dt} = \frac{D}{\delta} A(c - c^*) \quad (6.15)$$

where D = coefficient of diffusion of the solute, and δ = length of the diffusion path.

The thickness δ of the stagnant film would obviously depend on the relative solid-liquid velocity, i.e. on the degree of agitation of the system. Film thicknesses up to $150\text{ }\mu\text{m}$ have been measured on stationary crystals in stagnant aqueous solution, but values rapidly drop to virtually zero in vigorously agitated systems. As this could imply an almost infinite rate of growth in agitated systems, it is obvious that the concept of film diffusion alone is not sufficient to explain the mechanism of crystal growth. Furthermore, crystallization is not necessarily the reverse of dissolution. A substance generally dissolves at a faster rate than it crystallizes at, under the same conditions of temperature and concentration.

Another important finding was made by Miers (1904), who determined, by refractive index measurements, the solution concentrations near the faces of

crystals of sodium chlorate growing in aqueous solution; he showed that the solution in contact with a growing crystal face is not saturated but supersaturated.

In the light of these facts, a considerable modification was made to the diffusion theory of crystal growth by Berthoud (1912) and Vleton (1924), who suggested that there were two steps in the mass deposition, viz. a diffusion process, whereby solute molecules are transported from the bulk of the fluid phase to the solid surface, followed by a first-order 'reaction' when the solute molecules arrange themselves into the crystal lattice. These two stages, occurring under the influence of different concentration driving forces, can be represented by the equations

$$\frac{dm}{dt} = k_d A(c - c_i) \quad (\text{diffusion}) \quad (6.16)$$

and

$$\frac{dm}{dt} = k_r A(c_i - c^*) \quad (\text{reaction}) \quad (6.17)$$

where k_d = a coefficient of mass transfer by diffusion; k_r = a rate constant for the surface reaction (integration) process; and c_i = solute concentration in the solution at the crystal-solution interface.

A pictorial representation of these two stages is shown in *Figure 6.11* where the various concentration driving forces can be seen. It must be clearly understood, however, that this is only diagrammatic: the driving forces will rarely be of equal magnitude, and the concentration drop across the stagnant film is not necessarily linear. Furthermore, there appears to be some confusion in recent crystallization literature between this hypothetical film and the more fundamental 'boundary layers' (see section 6.3.2).

Equations 6.16 and 6.17 are not easy to apply in practice because they involve interfacial concentrations that are difficult to measure. It is usually more convenient to eliminate the term c_i by considering an 'overall' concentration driving force, $c - c^*$, which is quite easily measured. A general equation for crystallization based on this overall driving force can be written as

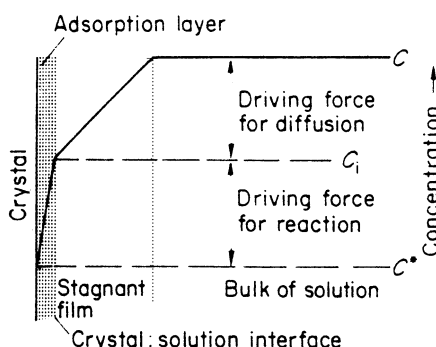


Figure 6.11. Concentration driving forces in crystallization from solution according to the simple diffusion-reaction model

$$\frac{dm}{dt} = K_G A(c - c^*)^g \quad (6.18)$$

where K_G is an overall crystal growth coefficient. The exponent g is usually referred to as the ‘order’ of the overall crystal growth process, but the use of this term should not be confused with its more conventional use in chemical kinetics, where the order always refers to the power to which a *concentration* should be raised to give a factor proportional to the rate of an elementary reaction. In crystallization work the exponent, which is applied to a *concentration difference*, has no fundamental significance and cannot give any indication of the number of elementary species involved in the growth process.

If $g = 1$ and the surface reaction (equation 6.17) is also first-order, the interfacial concentration, c_i , may be eliminated from equations 6.16 and 6.17 to give

$$\frac{dm}{dt} = \frac{A(c - c^*)}{1/k_d + 1/k_r} \quad (6.19)$$

i.e.

$$\frac{1}{K_G} = \frac{1}{k_d} + \frac{1}{k_r} \quad (6.20)$$

or

$$K_G = \frac{k_d k_r}{k_d + k_r} \quad (6.21)$$

For cases of extremely rapid reaction, i.e. large k_r , $K_G \approx k_d$ and the crystallization process is controlled by the diffusional operation. Similarly, if the value of k_d is large, i.e. if the diffusional resistance is low, $K_G \approx k_r$, and the process is controlled by the surface integration. It is worth pointing out that whatever the relative magnitude of k_d and k_r they will always contribute to K_G .

The diffusional step (equation 6.16) is generally considered to be linearly dependent on the concentration driving force, but the validity of the assumption of a first-order surface reaction (equation 6.17) is highly questionable. Many inorganic salts crystallizing from aqueous solution give an overall growth rate order, g , in the range 1 to 2. The rate equations, therefore, may be written

$$R_G = \frac{1}{A} \cdot \frac{dm}{dt} = k_d(c - c_i) \quad (\text{diffusion}) \quad (6.22)$$

$$= k_r(c_i - c^*)^r \quad (\text{reaction}) \quad (6.23)$$

$$= K_G(c - c^*)^g \quad (\text{overall}) \quad (6.24)$$

The reverse process of dissolution may be represented by the overall relationship

$$R_D = K_D(c^* - c)^d \quad (6.25)$$

where d is generally, but not necessarily, unity. From equation

$$c_i = c - R_G/k_d \quad (6.26)$$

so equation 6.23 representing the surface integration step, may be written

$$R_G = k_r \left(\Delta c - \frac{R_G}{k_d} \right)^r \quad (6.27)$$

where $\Delta c = c - c^*$ and $r \geq 1$. If $r = 1$,

$$R_G = \left[\frac{k_d k_r}{k_d + k_r} \right] \Delta c \quad (6.28)$$

as in equation 6.21. However, if $r \neq 1$, the surface integration step is dependent on the concentration driving force in non-linear manner. For example, if $r = 2$, equation 6.27 can be solved to give

$$R_G = k_d \left[\left(1 + \frac{k_d}{2k_r \Delta c} \right) - \sqrt{\left\{ \left(1 + \frac{k_d}{2k_r \Delta c} \right)^2 - 1 \right\}} \right] \Delta c \quad (6.29)$$

However, apart from such simple cases, equation 6.27 cannot be solved explicitly for R_G and the relationship between the coefficients K_G , k_d and k_r remains obscure. Recently, however, Sobczak (1990) has proposed an integral method, based on a linearization of equation 6.27, which allows reasonable values of k_d and k_r to be estimated.

Effectiveness factors

A quantitative measure of the degree of diffusion or surface integration control may be made through the concept of effectiveness factors. A crystal growth rate effectiveness factor, η_c , may be defined (Garside, 1971; Garside and Tavare, 1981) as the ratio of the growth rate at the interface conditions to the growth rate expected if the interface were exposed to the bulk solution conditions, or

$$\eta_c = (1 - \eta_c Da)^r \quad (6.30)$$

where r is the ‘order’ of the surface integration process, and Da is the Damköhler number for crystal growth, which represents the ratio of the pseudo-first-order rate coefficient at the bulk conditions to the mass transfer coefficient, defined by

$$Da = k_r(c - c^*)^{r-1}(1 - \omega)k_d^{-1} \quad (6.31)$$

where ω is the mass fraction of solute in solution. The plot of equation 6.30 in *Figure 6.12* shows that when Da is large, the growth is diffusion controlled ($\eta_c \rightarrow Da^{-1}$) and when Da is small, the growth is surface integration controlled ($\eta_c \rightarrow 1$).

Other contributing steps

It might be thought possible that the diffusional and surface reaction coefficients could be quantified by making certain assumptions. For example, if it is assumed that the diffusional mass transfer coefficient, k_d , in the crystallization

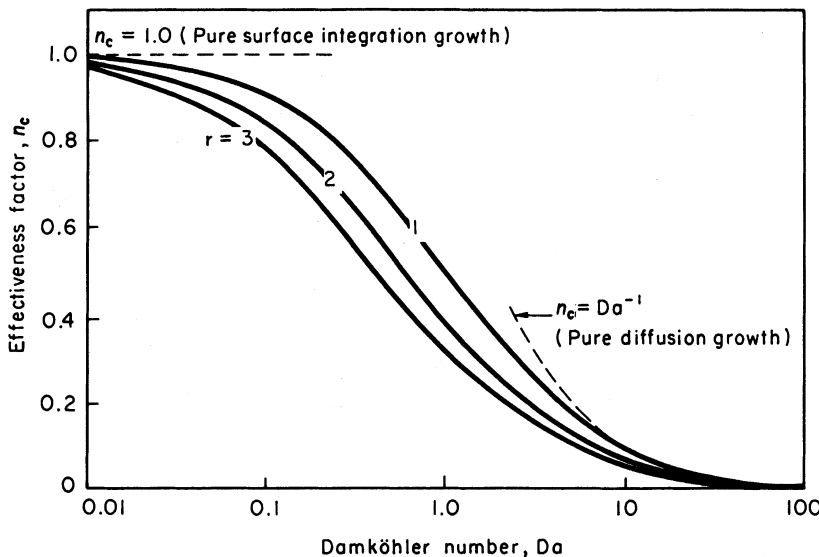


Figure 6.12. The effectiveness factor for crystal growth (equation 6.30). (After Garside and Tavare, 1981)

process is the same as that measured for crystal dissolution in near-saturated solutions under the same concentration driving force, temperature, etc., then values of k_r can be predicted.

Such calculations have been made (Garside and Mullin, 1968; Mullin and Gaska, 1969), but the assumption that the diffusion step in crystal growth can be related to the diffusion step in dissolution may not always be valid. It is possible, for example, that even dissolution is not a simple one-step process. Indeed some form of surface reaction (disintegration) step has been measured for the dissolution of lead sulphate in water (Bovington and Jones, 1970).

In any case, the growth process is undoubtedly much more complex than the simple two-step process envisaged above. For an electrolyte crystallizing from aqueous solution, for example, the following processes may all be taking place simultaneously:

1. Bulk diffusion of hydrated ions through the diffusion boundary layer
2. Bulk diffusion of hydrated ions through the adsorption layer
3. Surface diffusion of hydrated or dehydrated ions
4. Partial or total dehydration of ions
5. Integration of ions into the lattice
6. Counter-diffusion of released water through the adsorption layer
7. Counter-diffusion of water through the boundary layer

The potential importance of the ion dehydration step in the crystallization of electrolytes from aqueous solution has been discussed by several authors (Reich and Kahlweit, 1968; Nielsen, 1984), and there is evidence that an allowance for these effects could account substantially for discrepancies between theoretical

and actual growth rates. However, any one of the above processes could become rate-controlling, and a rigorous solution of the problem is virtually unattainable. Furthermore, the thicknesses of the different layers and films cannot be known with any certainty. Adsorbed molecular layers probably do not exceed $10^{-2}\text{ }\mu\text{m}$; partially disordered solution near the interface may account for another $10^{-1}\text{ }\mu\text{m}$; and the diffusion boundary layer is probably not much thicker than about $10\text{ }\mu\text{m}$ (see section 6.3.2).

The individual constants k_d and k_r are not only difficult if not impossible to determine, but can vary from face to face on the same crystal. It is even possible for k_d to vary over one given face: although it is true that the solution in contact with growing crystal face is always supersaturated, the degree of supersaturation can vary at different points over the face. In general, the supersaturation is highest at the corners and lowest at the centre of the face (Berg, 1938; Bunn, 1949).

The diffusion theories of crystal growth cannot yet be reconciled with the adsorption layer and dislocation theories. It is acknowledged that the diffusion theories have grave deficiencies (they cannot explain layer growth or the faceting of crystals, for example), yet crystal growth rates are conveniently measured and reported in diffusional terms. The utilization of the mathematics of mass transfer processes makes this the preferred approach, from the chemical engineer's point of view at any rate, despite its many limitations.

If a crystallization process were entirely diffusion-controlled or surface reaction controlled, it should be possible to predict the growth rate by fundamental reasoning. In the case of diffusion-controlled growth, for example, the molecular flux, F ($\text{mol s}^{-1}\text{ cm}^{-2}$) is related to the concentration gradient, dc/dx , by

$$F = D(dc/dx) \quad (6.32)$$

where x is the length of the diffusion path and D is the diffusion coefficient. Therefore the rate of diffusion, dn/dt (mol s^{-1}), to a spherical surface, distance r from the centre, is given by

$$\frac{dn}{dt} = 4\pi r^2 D \frac{dc}{dr} \quad (6.33)$$

At any instant dn/dt is a constant, so equation 6.33 may be integrated to give

$$4\pi D \int_{c_1}^{c_2} dc = \frac{dn}{dt} \int_{r_1}^{r_2} \frac{dr}{r^2} \quad (6.34)$$

i.e.

$$\frac{dn}{dt} = \frac{4\pi D(c_2 - c_1)}{\frac{1}{r_1} - \frac{1}{r_2}} \quad (6.35)$$

If $c_1 = c^*$ (equilibrium saturation) at $r_1 = r$ (the surface of the sphere) and $c_2 = c$ (the bulk liquid concentration) at $r_2 = \infty$ (i.e. $r_2 \gg r_1$), then

$$\frac{dn}{dt} = 4\pi r D(c - c^*) = \frac{dr}{dt} \cdot \frac{4\pi r^2}{v} \quad (6.36)$$

So the general equation for the diffusion-controlled linear growth rate may be expressed as

$$\frac{dr}{dt} = \frac{Dv(c - c^*)}{r} \quad (6.37)$$

The same relationship may be used for the reverse process of dissolution. For dissolution into a pure solvent ($c = 0$) integration of equation 6.37 gives

$$r^2 = r_0^2 - 2Dvc^*t \quad (6.38)$$

where r_0 is the initial size at time $t = 0$. The time for complete dissolution ($r = 0$) is thus given by

$$t = \frac{r_0^2}{2Dvc^*} \quad (6.39)$$

Substitution of typical values into equation 6.39 leads to some interesting observations. Small crystals of reasonably soluble salts may dissolve in fractions of a second, but those of sparingly soluble substances can take very long periods of time. For example, a $1\text{ }\mu\text{m}$ crystal ($r = 5 \times 10^{-7}\text{ m}$) of lead chromate ($D \approx 10^{-9}\text{ m}^2\text{ s}^{-1}$, $v \approx 5 \times 10^{-5}\text{ m}^3\text{ mol}^{-1}$, $c^* \approx 10^{-4}\text{ mol m}^{-3}$) would take about 7 h to dissolve in water at room temperature. A $10\text{ }\mu\text{m}$ crystal would take about 30 days. Tiny crystalline fragments of relatively insoluble substances may therefore remain undissolved in unsaturated solutions and act as nuclei in subsequent crystallization operations. The behaviour of precipitates attributed to the past history of the system may well be associated with this behaviour.

6.1.5 Birth and spread models

Several growth models based on crystal surface (two-dimensional) nucleation, followed by the spread of the monolayers have been developed in recent years (O'Hara and Reid, 1973; van der Eerden, Bennema and Cherepanova, 1978). The term 'birth and spread' (B + S) model will be used here, but other names such as 'nuclei on nuclei' (NON) and 'polynuclear growth' may also be seen in the literature to describe virtually the same behaviour. As depicted in *Figure 6.13*, growth develops from surface nucleation that can occur at the edges, corners and on the faces of a crystal. Further surface nuclei can develop on the monolayer nuclei as they spread across the crystal face.

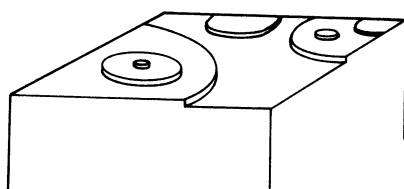


Figure 6.13. Development of polynuclear growth by the birth and spread (B + S) mechanism

The B + S model results in a face growth velocity–supersaturation relationship of the form

$$v = A_1 \sigma^{5/6} \exp(A_2/\sigma) \quad (6.40)$$

where A_1 and A_2 are system-related constants. Equation 6.40 is interesting in that it describes the only growth model that allows a growth order, g , greater than 2.

6.1.6 Combinations of effects

Pure diffusion-controlled growth for all sizes in a crystal population is unlikely. From diffusional considerations Turnbull (1953) derived the mass flux, N , to a growing particle of radius r as

$$N = K \left(\frac{dr}{dt} \right) = \frac{D\kappa c}{D + \kappa} \quad (6.41)$$

where D = diffusivity, K is a constant and κ is an interface transfer coefficient defined by $N = \kappa(c_r - c^*)$. Concentrations c , c_r and c^* refer to the bulk solution, particle surface and equilibrium saturation, respectively. Integration of equation 6.41 gives

$$\frac{r^2}{2D} + \frac{r}{\kappa} = Ktc \quad (6.42)$$

For $r \rightarrow 0$ this becomes

$$r \approx \kappa Ktc \quad (6.43)$$

indicating that the growth of very small nuclei should be interface-controlled.

For large values of r

$$r \rightarrow \sqrt{(2DKtc)} \quad (6.44)$$

indicating diffusion control.

A further complicating factor in using diffusion-controlled growth rate expressions such as equation 6.37 is the fact that very small crystals can have solubilities significantly higher than those of macrocrystals (Gibbs–Thomson effect, section 3.7). In any complete analysis of the growth process, therefore, the combined effects of diffusion, surface integration and size-solubility may have to be considered together. An analysis along these lines by Matz (1970) provided results that appeared to be consistent with experimental data for the growth of sodium chloride crystals from aqueous solution. In another approach, Leubner (1987) developed a combination model for crystal formation by the precipitation of sparingly soluble compounds, e.g. the silver halides, which relates the number of stable crystals formed to the precipitation conditions and to the crystal growth mechanism.

It is quite possible for more than one basic growth mechanism to influence the crystal growth rate simultaneously. When two mechanisms act in parallel, e.g. BCF and B + S, the individual rates are additive, and the one that gives

faster rate is rate-determining. When the two mechanisms act consecutively, e.g. bulk diffusion followed by BCF growth, they have to share the driving force and the slower one (at equal driving force) will be rate determining (Nielsen, 1984).

The combined effects of nucleation and growth on the development of crystal populations in crystallizers are discussed in section 6.9.4.

6.1.7 Crystal surface structure

The structure of a growing crystal surface at its interface with the growth medium, e.g. a supersaturated solution, has an important bearing on the particular mode of crystal growth adopted. This property has been characterized by a quantity variously designated as a surface roughness or surface entropy factor, or more frequently nowadays simply as the alpha factor (Jackson, 1958; Tempkin, 1964; Bennema and van der Eerden, 1977) which may be defined by

$$\alpha = \xi \Delta H / \mathbf{k}T \quad (6.45)$$

where ξ is an anisotropy factor related to the bonding energies in the crystal surface layers, ΔH is the enthalpy of fusion and \mathbf{k} is the Boltzmann constant.

Although reliable α values are not easy to calculate, it is possible, making certain simplifying assumptions (Davey, 1982), to make estimates from solubility data. Values of $\alpha < 2$ are taken to be indicative of a rough (i.e. at the molecular level) crystal surface which will allow continuous growth to proceed. The growth will be diffusion-controlled and the face growth rates, v , will be linear with respect to the supersaturation, σ , i.e.

$$v \propto \sigma \quad (6.46)$$

For $\alpha > 5$, a smooth surface is indicated and, as the high energy barrier discourages surface nucleation at low supersaturation, growth generally proceeds by the screw dislocation (BCF) mechanism (equation 6.10) in which case the face growth rate, v , is given by

$$v \propto \sigma^2 \tanh(B'/\sigma) \quad (6.47)$$

which, at low supersaturation, reduces to

$$v \propto \sigma^2 \quad (6.48)$$

and at high supersaturation, to equation 6.46.

For α values between about 2 and 5, the most probable mode of growth is the generation and spreading of surface nuclei, i.e. by the B + S model (section 6.15), when equation 6.40 applies.

For practical correlations of experimental data, however, the simple power law

$$v \propto \sigma^r \quad (6.49)$$

is commonly used. This represents the two limiting cases of the BCF equation ($r = 1$ and 2 , respectively) and is also a good approximation for the intermediate regime $1 < r < 2$. It also makes a satisfactory approximation for the B + S model over a limited range of supersaturation (Garside, 1985).

6.1.8 Crystallization from melts

The rate of crystallization from a melt depends on the rate of heat transfer from the crystal face to the bulk of the liquid. As the process is generally accompanied by the liberation of heat of crystallization, the surface of the crystal will have a slightly higher temperature than the supercooled melt. These conditions are shown in *Figure 6.14* where the melting point of the substance is denoted by T^* and the temperature of the bulk of the supercooled melt by T . The overall degree of supercooling, therefore, is $T^* - T$. The temperature at the surface of the crystal, the solid–liquid interface, is denoted by T_i , so the driving force for heat transfer across the ‘stagnant’ or ‘effective’ film of liquid close to the crystal face is $T_i - T$. The rate of heat transfer, dq/dt , can be expressed in the form of the equation

$$\frac{dq}{dt} = hA(T_i - T) \quad (6.50)$$

where A is the area of the growing solid surface and h is a film coefficient of heat transfer defined by

$$h = \frac{\kappa}{\delta'} \quad (6.51)$$

where κ is the thermal conductivity and δ' is the effective film thickness for heat transfer. There is a distinct similarity between the form of equation 6.50 for heat transfer and equation 6.16 for mass transfer by diffusion. Agitation of the system will reduce the effective film thickness, increase the film coefficient of heat transfer and tend to increase the interfacial temperature, T_i , to a value near to that of the melting point, T^* .

The rate of crystallization of a supercooled melt achieves a maximum value at a lower degree of supercooling, i.e. at a temperature higher than that

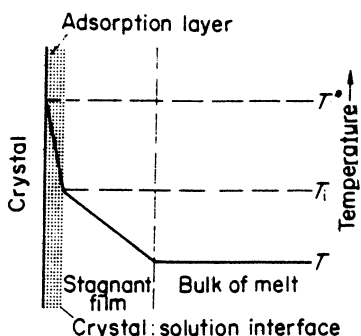


Figure 6.14. Temperature gradients near the face of a crystal growing in a melt

required for maximum nucleation. The nucleation and crystallization rate curves are dissimilar: the former has a relatively sharp peak (*Figure 5.2*), the latter usually a rather flat one. Tamman (1925) suggested that the maximum rate of crystallization would occur at a melt temperature, T , given by

$$T = T^* - \left(\frac{\Delta H_{\text{cryst}}}{c_m} \right) \quad (6.52)$$

where ΔH_{cryst} is the heat of crystallization and c_m is the mean specific heat capacity of the melt.

The crystal growth rate (e.g. mass per unit time) may be expressed as a function of the overall temperature driving force (cf. equation 6.18), by

$$\frac{dm}{dt} = K'_G A (T^* - T)^{g'} \quad (6.53)$$

where A is the crystal surface area, K'_G is an overall mass transfer coefficient for growth and exponent g' generally has a value in the range 1.5 to 2.5. The reverse process of melting, like that of dissolution, is often assumed to be first-order with respect to the temperature driving force, but this is not always the case (Palermo, 1967; Strickland-Constable, 1968; Kirwan and Pigford, 1969), i.e.

$$-\frac{dm}{dt} = K_M A (T - T^*)^x \quad (6.54)$$

where $x \geq 1$, K_M is an overall mass transfer coefficient for melting.

Melting is a simultaneous heat and mass transfer process, i.e.

$$\frac{dq}{dt} = U_M A \Delta T = -\frac{dm}{dt} \Delta H_f \quad (6.55)$$

therefore

$$-\frac{dm}{dt} = \frac{U_M A \Delta T}{\Delta H_f} \quad (6.56)$$

where $\Delta T = T - T^*$, q is a heat quantity, ΔH_f is the enthalpy of fusion and U_M is an overall heat transfer coefficient for melting.

The surface area of the melting solid ($A = \beta L^2$) is related to the mass ($m = \alpha \rho L^3$) by

$$A = \beta \left(\frac{m}{\alpha \rho} \right)^{2/3} \quad (6.57)$$

where L is a linear dimension, ρ = density, and α and β = volume and surface shape factors, respectively (see section 2.14.3). Hence, equation 6.56 becomes

$$-\frac{dm}{dt} = \beta \left(\frac{m}{\alpha \rho} \right)^{2/3} \frac{U_M \Delta T}{\Delta H_f} \quad (6.58)$$

and, assuming the U_M , ΔT , α and β remain constant,

$$\int m^{-2/3} dm = -\frac{\beta U_M \Delta T}{(\alpha \rho)^{2/3} \Delta H_f} \int dt$$

or

$$\Delta(m^{1/3}) = -\gamma t \quad (6.59)$$

where $\gamma = \beta U_M \Delta T / 3 \Delta H_f (\alpha \rho)^{2/3}$, or in terms of the change in particle size, ΔL ,

$$\Delta L = -\gamma' t \quad (6.60)$$

where $\gamma' = \beta U_M \Delta T / 3 \Delta H_f \alpha \rho$.

For an account of the basic theories of melting and crystal growth from the melt, reference should be made to the monographs by Brice (1965) and Ubbelohde (1965). Good accounts of dendritic growth from the melt are given by Gill (1989) and Ananth and Gill (1991).

6.2 Growth rate measurements

Many different experimental techniques have been employed to facilitate crystal growth rate measurements. The single crystal growth techniques, which can focus on individual face growth rates, are predominantly used for fundamental studies relating to growth mechanisms. Measurements made on populations of crystals are useful for determining overall mass transfer rates under controlled conditions and for observing size-dependent growth or growth rate dispersion. Additionally, the population methods can provide useful information for crystallizer design (Chapter 9).

6.2.1 Crystal growth rate expressions

There is no simple or generally accepted method of expressing the rate of growth of a crystal, since it has a complex dependence on temperature, supersaturation, size, habit, system turbulence, and so on. However, for carefully defined conditions crystal growth rates may be expressed as a mass deposition rate R_G ($\text{kg m}^{-2} \text{s}^{-1}$), a mean linear velocity \bar{v} (m s^{-1}) or an overall linear growth rate G (m s^{-1}). The relationships between these quantities are

$$\begin{aligned} R_G &= K_G \Delta c^g = \frac{1}{A} \cdot \frac{dm}{dt} = \frac{3\alpha}{\beta} \cdot \rho_c G \\ &= \frac{3\alpha}{\beta} \rho_c \frac{dL}{dt} = \frac{6\alpha}{\beta} \cdot \rho_c \frac{dr}{dt} = \frac{6\alpha}{\beta} \cdot \rho_c \bar{v} \end{aligned} \quad (6.61)$$

where L is some characteristic size of the crystal, e.g. the equivalent sieve aperture size, r is the radius corresponding to the equivalent sphere, and ρ_c is the crystal density. The volume and surface shape factors, α and β , respectively, are defined (see section 2.14.3) by $m = \alpha \rho_c L^3$ (i.e. $dm = 3\alpha \rho_c L^2 dL$) and $A = \beta L^2$, where m and A are the particle mass and area. For spheres and cubes $6\alpha/\beta = 1$. For octahedra $6\alpha/\beta = 0.816$.

The utility of the overall linear growth rate, G , in the design of crystallizers is demonstrated in section 8.3.2. Some typical values of the mean linear growth velocity \bar{v} ($= \frac{1}{2}G$) are given in *Table 6.1*.

Table 6.1. Some mean overall crystal growth rates expressed as a linear velocity[†]

Crystallizing substance	°C	S	\bar{v} (m s^{-1})
$(\text{NH}_4)_2\text{SO}_4 \cdot \text{Al}_2(\text{SO}_4)_3 \cdot 24\text{H}_2\text{O}$	15	1.03	$1.1 \times 10^{-8*}$
	30	1.03	$1.3 \times 10^{-8*}$
	30	1.09	$1.0 \times 10^{-7*}$
	40	1.08	$1.2 \times 10^{-7*}$
NH_4NO_3	40	1.05	8.5×10^{-7}
$(\text{NH}_4)_2\text{SO}_4$	30	1.05	$2.5 \times 10^{-7*}$
	60	1.05	4.0×10^{-7}
	90	1.01	3.0×10^{-8}
$\text{NH}_4\text{H}_2\text{PO}_4$	20	1.06	6.5×10^{-8}
	30	1.02	3.0×10^{-8}
	30	1.05	1.1×10^{-7}
	40	1.02	7.0×10^{-8}
$\text{MgSO}_4 \cdot 7\text{H}_2\text{O}$	20	1.02	$4.5 \times 10^{-8*}$
	30	1.01	$8.0 \times 10^{-8*}$
	30	1.02	$1.5 \times 10^{-7*}$
$\text{NiSO}_4 \cdot (\text{NH}_4)_2\text{SO}_4 \cdot 6\text{H}_2\text{O}$	25	1.03	5.2×10^{-9}
	25	1.09	2.6×10^{-8}
	25	1.20	4.0×10^{-8}
$\text{K}_2\text{SO}_4 \cdot \text{Al}_2(\text{SO}_4)_3 \cdot 24\text{H}_2\text{O}$	15	1.04	$1.4 \times 10^{-8*}$
	30	1.04	$2.8 \times 10^{-8*}$
	30	1.09	$1.4 \times 10^{-7*}$
	40	1.03	$5.6 \times 10^{-8*}$
KCl	20	1.02	2.0×10^{-7}
	40	1.01	6.0×10^{-7}
KNO_3	20	1.05	4.5×10^{-8}
	40	1.05	1.5×10^{-7}
K_2SO_4	20	1.09	$2.8 \times 10^{-8*}$
	20	1.18	$1.4 \times 10^{-7*}$
	30	1.07	$4.2 \times 10^{-8*}$
	50	1.06	$7.0 \times 10^{-8*}$
	50	1.12	$3.2 \times 10^{-7*}$
KH_2PO_4	30	1.07	3.0×10^{-8}
	30	1.21	2.9×10^{-7}
	40	1.06	5.0×10^{-8}
	40	1.18	4.8×10^{-7}
NaCl	50	1.002	2.5×10^{-8}
	50	1.003	6.5×10^{-8}
	70	1.002	9.0×10^{-8}
	70	1.003	1.5×10^{-7}
$\text{Na}_2\text{S}_2\text{O}_3 \cdot 5\text{H}_2\text{O}$	30	1.02	1.1×10^{-7}
	30	1.08	5.0×10^{-7}
Citric acid monohydrate	25	1.05	3.0×10^{-8}
	30	1.01	1.0×10^{-8}
	30	1.05	4.0×10^{-8}

Table 6.1. (Continued)

Crystallizing substance	$^{\circ}\text{C}$	S	$\bar{v} (\text{m s}^{-1})$
Sucrose	30	1.13	$1.1 \times 10^{-8*}$
	30	1.27	$2.1 \times 10^{-8*}$
	70	1.09	9.5×10^{-8}
	70	1.15	1.5×10^{-7}

[†]The supersaturation is expressed by $S = c/c^*$ with c and c^* as kg of crystallizing substance per kg of free water. The significance of the mean linear growth velocity, \bar{v} ($= \frac{1}{2}G$), is explained by equation 6.61 and the values recorded here refer to crystals in the approximate size range 0.5–1 mm growing in the presence of other crystals. An asterisk (*) denotes that the growth rate is probably size dependent.

6.2.2 Face growth rates

The different faces of a crystal grow at different rates under identical environmental conditions, as first demonstrated by Bentivoglio (1927). In general, the high index faces grow faster than the low. A fundamental assessment of the growth kinetics, therefore, must involve a study of the individual face growth rates.

An apparatus that permits precise measurement of crystal growth rates is shown in *Figure 6.15* (Mullin and Amatavivadhana, 1967; Mullin and Garside, 1967). Briefly, the technique is as follows. A small crystal (2–5 mm) is mounted on a 1 mm tungsten wire in a chosen orientation. Solution of known temperature ($\pm 0.05^{\circ}\text{C}$), supersaturation and velocity is pumped through the cell, and the rate of advance of the chosen crystal face is observed through a travelling microscope. Several glass cells have been used ranging in internal diameter from 10 to 30 mm, permitting a wide range of solution velocities to be used.

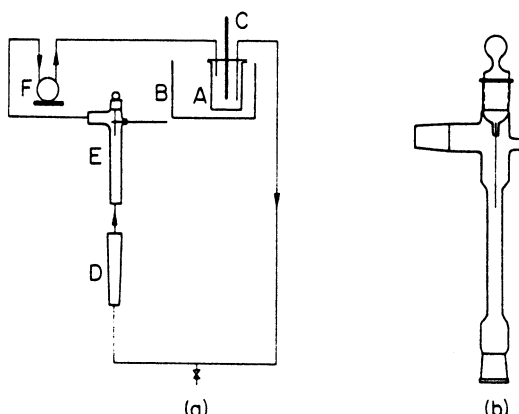


Figure 6.15. Single-crystal growth cell: (a) complete circuit, (b) the cell. A, solution reservoir; B, thermostat bath; C, thermometer; D, flow meter; E, cell; F, pump. (After Mullin and Amatavivadhana, 1967; Mullin and Garside, 1967)

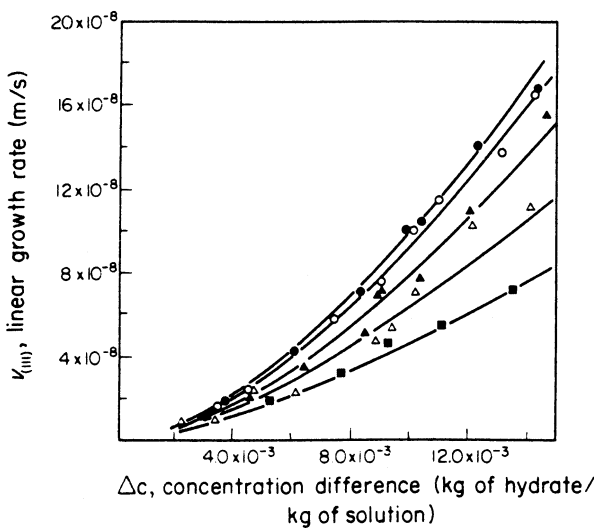


Figure 6.16. Face growth rates of single crystals of potash alum at 32°C. Solution velocities: ● = 0.127, ○ = 0.120, ▲ = 0.064, △ = 0.022, ■ = 0.006 m s⁻¹. (After Mullin and Garside, 1967)

The results in *Figure 6.16* show the effects of both solution supersaturation and velocity on the linear growth rates of the (111) faces of potash alum crystals at 32 °C. This hydrated salt [K₂SO₄ · Al₂(SO₄)₃ · 24H₂O] grows as almost perfect octahedra, i.e. eight (111) faces.

Three interesting points may be noted. First, the growth rate is not first-order with respect to the supersaturation (concentration driving force, Δc). If the data are plotted on logarithmic co-ordinates (not given here) straight line correlations are obtained giving

$$v_{(111)} = K\Delta c^g \quad (6.62)$$

where g varies from about 1.4 to 1.6. For v expressed in m s⁻¹ and Δc in kg of hydrate per kg of solution, K varies from about 3×10^{-5} to 2×10^{-4} as the solution velocity increases from 6 to 22 cm s⁻¹. Second, the solution velocity has a significant effect on the growth rate. Third, significant crystal growth does not appear to commence until a certain level of supersaturation is exceeded.

The effect of solution velocity can be seen more clearly in *Figure 6.17*. The points on this graph have been taken from the smoothed curves in *Figure 6.16*. For a given supersaturation the growth rate increases with solution velocity, the effect being more pronounced at the higher values of Δc .

If the solution velocity is sufficiently high, the overall growth rate should be determined by the rate of integration of the solute molecules into the crystal lattice. If the crystal is grown in a stagnant solution ($u = 0$), then the rate of the diffusion step will be at a minimum. The growth curves in *Figure 6.17* have therefore been extrapolated to $u = 0$ and ∞ to obtain an estimate of the growth rates when the rate-controlling process is one of natural convection ($u = 0$) and

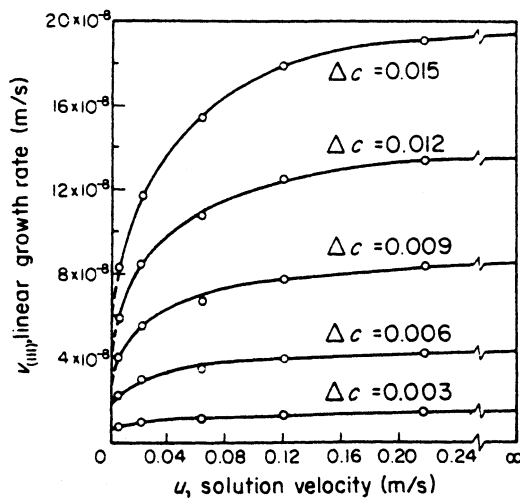


Figure 6.17. Effect of solution velocity on the (111) face growth rate of potash alum crystals at 32°C. (After Mullin and Garside, 1967)

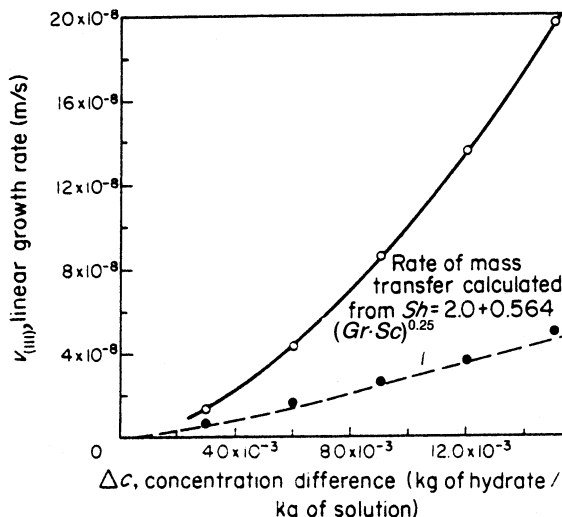


Figure 6.18. Extrapolated growth rates of potash alum crystals at limiting velocities ($\circ = u \rightarrow \infty$, $\bullet = u \rightarrow 0$) (After Mullin and Garside, 1967)

surface reaction ($u \rightarrow \infty$). It is, of course, unlikely that the growth curves would change in a smooth continuous manner when the rate-controlling mechanism changes from surface reaction control to natural convective diffusion control, and it is by no means certain that these curves can be extrapolated, with any precision, to the point where the growth rate becomes constant. However, the derived curves in *Figure 6.18* give an indication of the possible limits of the growth curves.

Rates of mass transfer by natural convection are usually correlated by a semi-theoretical equation of the form

$$Sh = 2 + \alpha(Gr \cdot Sc)^{0.25} \quad (6.63)$$

where the Sherwood number $Sh = kL/D$, Schmidt number $Sc = \eta/\rho_s D$ and Grashof number $Gr = L^3 \rho_s \Delta \rho_s g / \eta^2$, ρ_s = solution density, $\Delta \rho_s$ = difference between solution density at the interface and in the bulk solution, η = viscosity ($\text{kg m}^{-1} \text{s}^{-1}$), L = crystal size (m), D = diffusivity ($\text{m}^2 \text{s}^{-1}$) and k = a mass transfer coefficient (m s^{-1}). The mean value of the constant α based on the results of a number of workers is 0.56. Growth rates, calculated from equation 6.63 lie very close to the experimental points and this tends to confirm that the growth process in stagnant solution is controlled by natural convection. It is of interest to note in this connection that the Grashof number contains a term $\Delta \rho_s$, which is directly proportional to the concentration difference, Δc , so the mass transfer rate under conditions of *natural convection* depends on $\Delta c^{1.25}$. When *forced convection* is the rate-controlling process, the mass transfer rate is directly proportional to Δc .

Diffusional mass transfer rates under conditions of forced convection may be correlated by an equation of the form

$$Sh = 2 + \phi Re_p^a Sc^b \quad (6.64)$$

where Re_p is the particle Reynolds number ($\rho_s u L / \eta$). Equation 6.64 is frequently referred to as the Frössling equation. However, for reasonably high values of Sh (say > 100) it is common practice to ignore the constant 2 (the limiting value of Sh as $Re_p \rightarrow 0$, i.e. mass transfer in the absence of natural convection) and use the simpler expression

$$Sh = \phi Re_p^a Sc^b \quad (6.65)$$

Dissolution rate data, for example, are conveniently expressed in this way. The mass transfer coefficient, in the Sherwood number, depends on the solution velocity, u , raised to the power a . It is possible, therefore, that the effect of solution velocity on crystal growth may also be represented by an equation of this type in the region where diffusion influences the growth rate.

The effect of the two variables, Δc and u , on crystal face growth rates may thus be represented by

$$v_{hkl} = Cu^a \Delta c^g \quad (6.66)$$

where c is a constant, and a and g are both functions of the solution velocity. For the growth of potash alum at 32 °C, as $u \rightarrow \infty$, $u \rightarrow 0$ and $g \rightarrow 1.62$, while as $u \rightarrow 0$, $g \rightarrow 1.25$.

It is of interest at this point to refer back to the consequences of the BCF growth theory (equation 6.10). At low supersaturation, S , the growth rate is expected to be proportional to $(S - 1)^2$, but at high supersaturation the rate tends to become a linear function of $S - 1$. For growth from solution Chernov (1961) showed that for the range $1.01 < S < 1.2$ (which corresponds to

$0.0015 < \Delta c < 0.03 \text{ kg/kg}$ in the present case of potash alum) the growth rate can be represented by

$$v_{hkl} = K(S - 1)^g \quad (6.67)$$

where values of K and g are determined by the parameters in the theoretical relationship. Now $S = c/c^*$, i.e. $S - 1 = \Delta c/c^*$, so equations 6.62 and 6.67 are of the same form and the value of the exponent g , measured experimentally, is within the range predicted theoretically.

The velocity of the solution past the crystal face is thus capable of influencing the growth rate, and this velocity effect manifests itself as a crystal size effect when freely suspended crystals are grown in a crystallizer. The reason, of course, is that large crystals have higher settling velocities than small crystals, i.e. higher relative solid–liquid velocities are needed to keep the larger crystals suspended. This important effect, which has not often been appreciated in the past, can rapidly be detected and quantified in the growth cell described above.

Salts that have been established as having solution velocity dependent growth rates include ammonium and potassium alums, nickel ammonium sulphate, sodium thiosulphate and potassium sulphate. Ammonium sulphate, ammonium and potassium dihydrogen phosphates, for example, do not.

6.2.3 Layer growth rates

The movement of growth layers on the face of a crystal growing in solution can often be detected and measured by observing the particular face microscopically, using reflected light. An apparatus that permits this to be done is shown in *Figure 6.19*. Small crystals are nucleated and grown on the lower non-reflecting surface of the observation cell.

The arrangement consists of a central portion, 20 mm in diameter and 4 mm deep, in which the crystals are growing, enclosed in a water jacket which controls the cell temperature to within $\pm 0.05^\circ\text{C}$. Solution is circulated through the cell under controlled conditions of temperature, supersaturation, flow rate and purity. The solution velocity across the central portion of the cell may be varied between about 1 and 20 mm s^{-1} . The crystals growing in the cell are illuminated with a highly collimated, intense light beam from a 24-V, 150-W tungsten–halogen lamp. Angular adjustment of the cell in the horizontal and vertical planes allows light reflected from the crystal surface to be diverted into the microscope objective. The growth layer velocities are measured with the aid of a micrometer eyepiece.

Extensive use of this type of cell for the measurement of layer velocities on crystal faces has been reported by Davey and Mullin (1974). The moving layer fronts observed by this technique are not elementary (monomolecular) steps but macrosteps, often several hundred or thousand molecules in height, which build-up from the bunching of smaller layers with velocities a hundred times faster than the macrosteps (Phillips and Mullin, 1976). These fast moving layers are generally difficult to monitor, but velocity measurements of near-elementary

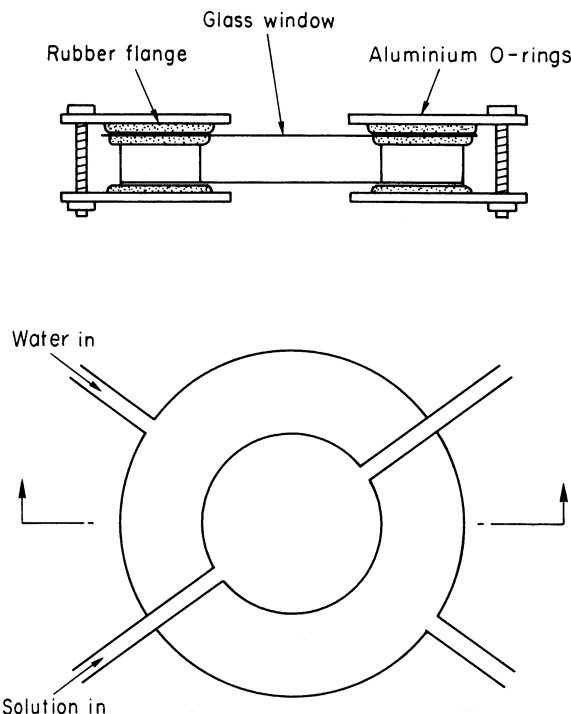


Figure 6.19. A cell for making layer growth observations by reflection microscopy. (After Davey and Mullin, 1974)

layers have recently been made using atomic force microscopy, a powerful tool that promises to cast new light on the fundamental mechanisms of crystal growth (Land *et al.*, 1999).

6.2.4 Overall growth rates

It is often much more convenient, and more useful for crystallizer design purposes, to measure crystal growth rates in terms of mass deposited per unit time per unit area of crystal surface rather than as individual face growth rates. This may be done in agitated vessels or fluidized beds, e.g. by measuring the mass deposition on a known mass of sized seed crystals under carefully controlled conditions.

The overall linear growth rate, G , (m s^{-1}) may then be evaluated from

$$G = \frac{M_i^{1/3} - M_f^{1/3}}{(\alpha\rho N)^{1/3} t} \quad (6.68)$$

where M_i and M_f are the initial and final crystal masses (kg), respectively. N is the number of individual crystals, α is their volume shape factor, ρ is their density (kg m^{-3}) and t is time (s).

Alternatively, expressing the overall mass deposition rate R_G ($\text{kg m}^{-2} \text{s}^{-1}$) as in equations 6.14 and 6.61 the overall linear growth rate G may be expressed as

$$G = \frac{\beta}{3\alpha\rho} K_G \Delta c^g \quad (6.69)$$

where β is the crystal surface shape factor and Δc is the mean supersaturation over the run ($\text{kg solute/kg solvent}$). The value of exponent g is given by the slope of the linear plot of $\log G$ versus $\log \Delta c$, and the overall mass transfer coefficient K_G ($\text{kg m}^{-2} \text{s}^{-1}$) can then be evaluated.

Experimental precautions

A number of precautions need to be taken when attempting to measure reliable crystal growth rates by gravimetric measurement and subsequent calculation (Phillips, 1974). The seed crystals should be carefully selected, both for size and surface quality. The crystal surface area is often required and this is most commonly calculated on the assumption that the crystals have a definite geometrical form and plane faces. The seeds ought to have faces that, macroscopically at least, are smooth. The volume and surface shape factors of the seeds and the grown crystals should be determined (section 2.14.3) so that any changes may be taken into account in subsequent calculations, e.g. when using equations 6.68 or 6.69. The volume shape factor of potassium sulphate crystals, for example, changes from about 1 to 0.6 as the crystals grow from about $300 \mu\text{m}$ to 2 mm (Mullin and Gaska, 1969; Garside, Mullin and Das, 1973).

At the end of a growth run, the crystals must be cleanly and qualitatively separated from the mother liquor so that their final dry mass can be measured. Filtration is commonly followed by washing to recover residual mother liquor. These operations should be carried out rapidly to minimize any chance of the crystals undergoing change. Ideally the wash liquid should be completely miscible with the mother liquor, and the crystals should be practically insoluble in the wash liquid. Further, to assist rapid drying, the wash liquid should be reasonably volatile. Methanol, ethanol and acetone, for example, are often chosen for inorganic salts that have crystallized from aqueous solution. Filtration should remove a very high proportion of the mother liquor so that the chance of salting-out and consequent surface contamination is minimized. Further comments on the problems associated with crystal washing under industrial conditions are made in section 9.7.1.

Fluidized beds

A laboratory-scale fluidized bed crystallizer capable of yielding useful growth rate information is shown in *Figure 6.20*. It is constructed mainly of glass (total capacity 10–13 L) with growth zones 5–8 cm diam. and 75 cm long. A combination of heating tapes and water cooler enables the temperature of the solution to be maintained to $\pm 0.03^\circ\text{C}$. Solution concentration can be measured at intervals or continuously. A typical run would consist of adding about

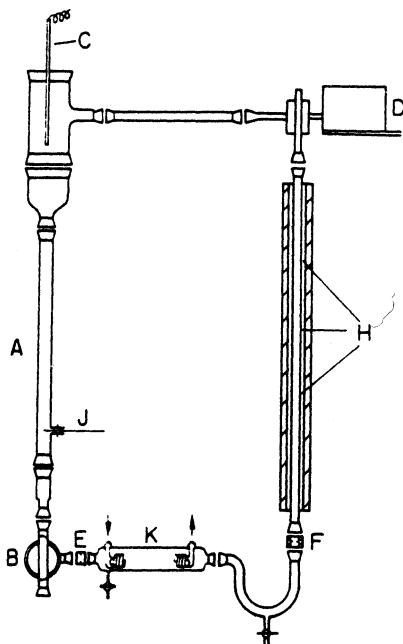


Figure 6.20. A laboratory-scale fluidized bed crystallizer: A, growth zone; B, outlet cock; C, resistance thermometer; E, F, orifice plates; H, heating tapes; J, thermometer; K, water cooler. (After Mullin and Garside, 1967)

5 g ± 1 mg of carefully sized seed crystals and controlling the solution velocity so that the crystals are uniformly suspended in the growth zone until their mass has increased to, say, 15 g. This mass increase would allow 600 µm crystals of potassium sulphate, for example, to grow to about 800 µm. The duration of a run varies from about $\frac{1}{4}$ to 3 h, depending on the working level of supersaturation. At the end of a run the crystals are removed, dried, weighed and sieved. Some typical results are shown in *Figure 6.21* for potash alum crystals grown at 32 °C. These results may be compared with those shown in *Figure 6.16*. Here, again, the effect of supersaturation can be seen and so can the effect of crystal size. As explained above, solution velocity dependent growth shows up as crystal size dependent growth when freely suspended crystals are grown in a crystallizer. In this case large crystals grow faster than small.

For potash alum it has been shown that

$$R_G = K_G \Delta c^g \quad (6.70)$$

For R_G expressed as $\text{kg m}^{-2} \text{s}^{-1}$ and Δc as kg hydrate/kg solution K_G varies from 0.115 to 0.218 and g from 1.54 to 1.6 for crystals ranging from 0.5 to 1.5 mm. Or, since it has already been shown that $v_{hkl} = Cu^a \Delta c^g$ for single crystals (equation 6.66), then

$$R_G = C' \bar{L}^m \Delta c^g \quad (6.71)$$

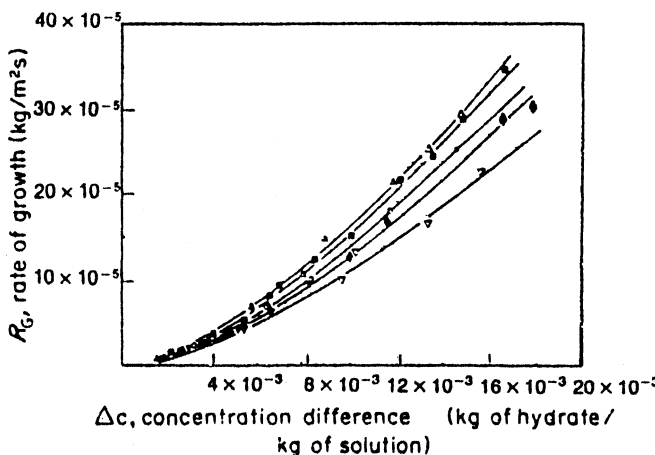


Figure 6.21. Overall growth rates of potash alum crystals at 32°C (mean crystal sizes: $\triangle = 1.96$, $\blacksquare = 1.4$, $\circ = 0.99$, $\blacktriangle = 0.75$, $\triangledown = 0.53$ mm. (After Mullin and Garside, 1967)

which is similar to the equation used by Bransom (1960) as the starting point for a theoretical analysis of crystal size distribution. In the above case of potash alum

$$R_G = 16\bar{L}^{0.63}\Delta c^g \quad (6.72)$$

Overall growth rates for potash alum measured in the fluidized bed crystallizer coincide very well with those predicted from face growth rates measured in the single crystal cell (*Figure 6.22*). The alums grow as almost perfect octahedra, i.e. eight (111) faces, so it is a simple matter, using the crystal density, ρ_c , to convert linear face velocities to overall mass deposition rates ($R_G = \rho_c v_{(111)}$).

Agitated vessels

It is possible to determine overall crystal growth rates by adding a known mass of sized seeds to a supersaturated solution in an agitated vessel, following a similar procedure to that outlined above for the fluidized bed method. To correlate the data, however, it is necessary to estimate the particle–fluid slip velocity as a function of impeller speed in the agitated vessel using relationships of the type described in section 9.4.1.

An example of the comparison of growth rate data obtained in both fluidized bed and agitated vessel crystallizers, using ammonium alum, has been reported by Nienow, Bujac and Mullin (1972).

Measurement from desupersaturation rates

A rapid method for overall crystal growth rate estimation may be made by suspending a batch of seed crystals in a supersaturated solution kept at constant temperature, and following the decay of supersaturation over a period of time. A mass of seed crystals of known size and surface area is added to the solution in a closed system, e.g. in a fluidized bed or an agitated vessel.

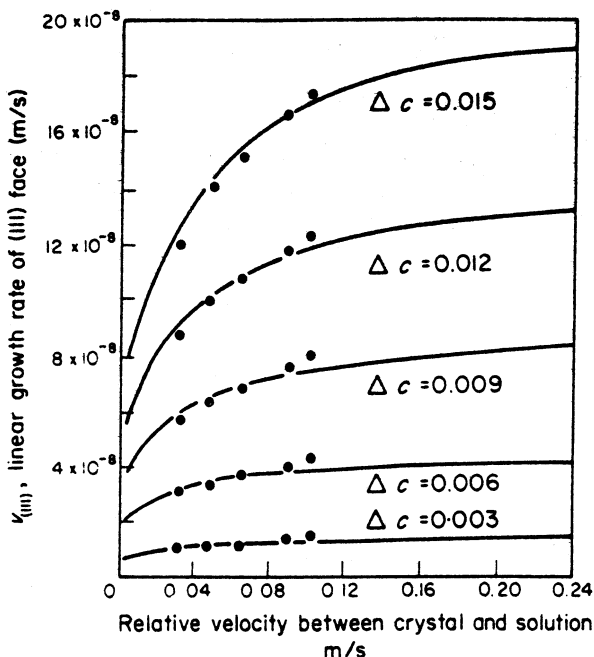


Figure 6.22. Comparison between face (smooth curve) and overall (points) growth rates of potash alum crystals at 32°C. (After Mullin and Garside, 1967)

The initial supersaturation is recorded and the desupersaturation decay is monitored by continuous or frequent intermittent solution analysis, e.g. by measuring some relevant physical property such as density, refractive index, conductivity, etc. The same procedure may be used, with appropriate nomenclature changes, to determine overall dissolution rates by measuring the increase in solution concentration.

Assuming that negligible nucleation occurs after the seeds are added, the change in solution concentration dc at any instant is proportional to the mass deposition dm on existing crystals, i.e.,

$$dm = -Wdc \quad (6.73)$$

W is the mass of 'free water' present. If the crystallizing substance is hydrate, the solution concentration c should be expressed as kg of hydrate per kg of free water.

The overall crystal growth rate, R_G (the mass rate of deposition, dm/dt , per unit crystal surface area, A , see equation 6.61) may thus be expressed as

$$R_G = \frac{1}{A} \cdot \frac{dm}{dt} = \frac{-W}{A} \cdot \frac{dc}{dt} \quad (6.74)$$

Values of dc/dt may be obtained from the measured desupersaturation curve. W is a constant for a given run and the surface area, A , of the added seeds can be estimated from their total mass, M , and characteristic size, L :

$$A = \beta M / \alpha \rho_c L \quad (6.75)$$

where α and β are the volume and surface shape factors, respectively, and ρ_c is the crystal density. It is advisable to use seed crystals as near uniform as possible, in both size and shape, to minimize errors.

If the surface area change cannot be neglected, a mean value \bar{A} may be used in equation 6.75, based on the initial and final areas, and calculated from (Ang and Mullin, 1979)

$$\bar{A} = \frac{1}{L_t - L_0} \int_{L_0}^{L_t} A\left(\frac{L}{L_0}\right) dL \quad (6.76)$$

$$= \frac{A_0}{3} \left[1 + \left(\frac{M_t}{M_0}\right)^{1/3} + \left(\frac{M_t}{M_0}\right)^{2/3} \right] \quad (6.77)$$

where M_0 and M_t are the initial and final crystal masses.

Desupersaturation methods for crystal growth rate measurements have been reported for ammonium alum (Bujac and Mullin, 1969), potassium sulphate (Jones and Mullin, 1973a), nickel ammonium sulphate (Ang and Mullin, 1979), potassium chloride (Nývlt, 1989) and succinic acid (Qui and Rasmuson, 1990).

A different approach was adopted by Garside, Gibilaro and Tavare (1982) who suggested that crystal growth rates could be evaluated from a knowledge of the first two zero-time derivatives of a desupersaturation curve which had been approximated by an n th order polynomial. The analytical procedures adopted are fully described in the above paper, together with an example of the application of the approach to the growth of potassium sulphate crystals in a fluidized bed crystallizer.

Measurement on a rotating disc

The rotating disc method may be used to study the separate roles of diffusion and integration in crystal growth since it enables the mass transfer (diffusion) step to be isolated. A uniform hydrodynamic boundary layer of thickness

$$\delta_h = 2.8(\nu/\omega)^{1/2} \quad (6.78)$$

is produced over the smooth surface of a small disc rotated in a horizontal plane about its axis; ν is the kinematic viscosity of the liquid and ω is the angular velocity of the disc. For example, a disc rotating at $N = 200$ rev/min ($\omega = 2\pi N \simeq 21$ radians/s), and taking $\nu = 10^{-6} \text{ m}^2 \text{ s}^{-1}$, gives the value of $\delta_h \simeq 600 \mu\text{m}$. The mass transfer (diffusion) boundary layer thickness δ_m would only be a small fraction of this (see section 6.3.2).

The disc, impregnated with the crystalline material, is rotated in a relatively large volume of solution so that the solution concentration remains virtually unchanged during a run.

The technique may be used to study both growth and dissolution using solutions of the appropriate solute concentrations. It has been used to measure individual face growth rates by mounting a well-formed crystal in the disc with one face only exposed, but it is more commonly employed for measuring overall growth or dissolution rates of a multicrystalline compact compressed

into a recess in the disc surface, thus exposing a random orientation of faces to the solution.

Flow over the disc must be laminar, so the disc Reynolds number ($Re = \omega r^2/\nu$) should be kept between 10^3 and 10^5 . For example, for a 50-mm diameter disc, these limits correspond to rotational speeds of around 15 and 1500 rev/min, respectively. Turbulent flow starts at a Reynolds number of about 2×10^5 and below about 10^2 natural convection can interfere with the mass transfer process. The disc is weighed before and after a run during which a loss, or gain, of around 0.2 g in mass has occurred, depending on whether growth or dissolution is being studied. It is essential, of course, to standardize the disc-drying procedure in such studies.

Descriptive accounts of the construction and use of rotating disc units have been given by Bourne *et al.* (1976), Karel and Nývlt (1989) and Garside, Mersmann and Nývlt (1990).

6.2.5 Growth and nucleation rates

The processes of growth and nucleation interact in a crystallizer, and both contribute to the crystal size distribution (CSD) of the product (see section 9.1). Kinetic data needed for crystallizer design purposes (effective growth and nucleation rates) can be conveniently measured on the laboratory scale in a mixed-suspension, mixed-product removal (MSMPR) crystallizer operated continuously in the steady state (*Figure 9.3*). The assumptions made are that no crystals are present in the feed stream, that all crystals are of the same shape, that crystals do not break down by attrition, and that crystal growth rate is independent of crystal size.

The relationship between crystal size, L , and population density, n (number of crystals per unit size per unit volume of the system), derived directly from the population balance (Randolph and Larson, 1988) (section 9.1.1) is

$$n = n_0 \exp(-L/G\tau) \quad (6.79)$$

where n_0 is the population density of nuclei (zero-sized crystals) and τ is the residence time. Equation 6.79 describes the crystal size distribution for steady-state operation. Rates of nucleation B and growth $G (= dL/dt)$ are conventionally written in terms of supersaturation as

$$B = k_1 \Delta c^b \quad (6.80)$$

and

$$G = k_2 \Delta c^g \quad (6.81)$$

These empirical expressions can be combined to give

$$B = k_3 G^i \quad (6.82)$$

where

$$i = b/g \quad (6.83)$$

in which b and g are the kinetic orders of nucleation and growth, respectively, and i is the relative kinetic order. The relationship between nucleation and growth may be expressed as

$$B = n_0 G \quad (6.84)$$

or

$$n_0 = k_4 G^{i-1} \quad (6.85)$$

Experimental measurement of crystal size distribution (recorded on a number basis) in a steady-state MSMPR crystallizer can thus be used to quantify nucleation and growth rates. A plot of $\log n$ vs. L should give a straight line of slope $-(G\tau)^{-1}$ with an intercept at $L = 0$ equal to n_0 (equation 6.79 and *Figure 6.23a*); if the residence time τ is known, the crystal growth rate G can be calculated. Similarly, a plot of $\log n_0$ vs. $\log G$ should give a straight line of slope $i - 1$ (equation 6.85 and *Figure 6.23b*); if the order g of the growth process is known, the order of nucleation b can be calculated from equation 6.83.

A typical laboratory MSMPR crystallizer suitable for measuring kinetic data is shown in *Figure 6.24*. Such a unit would typically be operated for around ten residence times to achieve the steady-state conditions necessary before taking a sample of the magma to assess the crystal size distribution. The solenoid-operated discharge mechanism is based on the one described by Žáček *et al.* (1982). Normally only one feed system would be required, e.g. for cooling crystallization, but two independent feed systems as illustrated, would be necessary for reaction crystallization or precipitation studies. With suitable modification to the crystallization vessel, the unit can be adapted for reduced-pressure evaporation.

MSMPR units with crystallizer working volumes as small as 250 mL have been operated successfully, but if the kinetic data are to be used for industrial design purposes, the working volume should not be less than about 4 L, and sizes up to 20 L have been recommended (Garside, Mersmann and Nývlt,

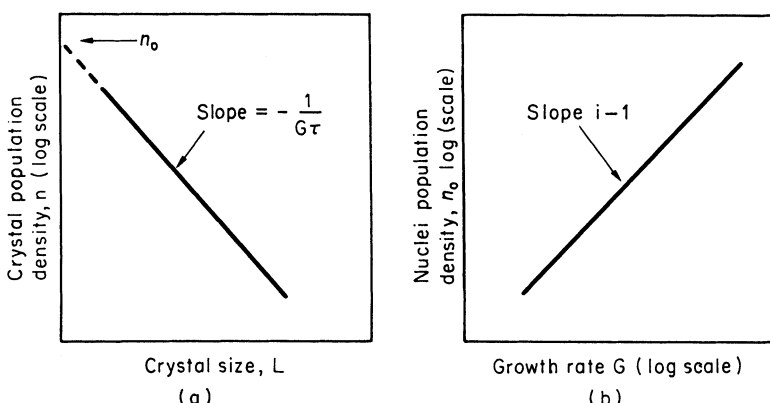


Figure 6.23. Population plots characterizing (a) the crystal size distribution and (b) the nucleation and growth kinetics for a continuous MSMPR crystallizer

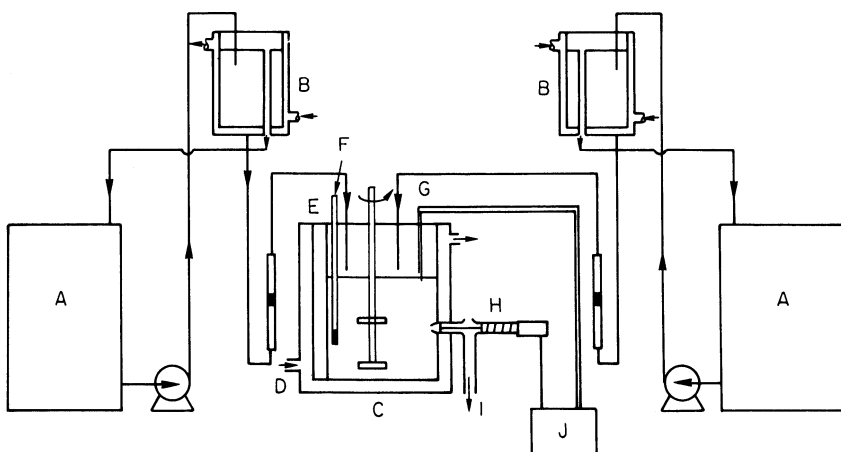


Figure 6.24. A laboratory-scale MSMPR crystallizer: A, thermostatted feedstock tank; B, constant-head tank; C, MSMPR crystallizer; D, water inlet to jacket; E, baffle; F, thermometer; G, level detector; H, solenoid-operated discharge valve; I, magma outlet; J, control unit

1990). The larger the working volume, the more meaningful will be the nucleation data, particularly for scale-up purposes, but the more difficult it will be to achieve good mixing and MSMPR conditions in the vessel. Further, because of the large quantities of feedstock solution to be handled, more expensive ancillary equipment will be required. Conversely, although it is much easier to achieve MSMPR operation in small volume units and to operate with much simpler equipment, the consequent low feedstock solution flowrates in narrow supply lines can cause severe problems arising from crystallization blockage. A detailed example of the evaluation of kinetic information from MSMPR data is given in section 9.2.

Mersmann and Kind (1988) have surveyed data reported in the literature on 17 different inorganic substances crystallizing or precipitating from aqueous solution in MSMPR crystallizers. One of the interesting compilations is shown in *Figure 6.25* where some orders of magnitude of potential growth and nucleation rate are indicated. Below a relative supersaturation, $\sigma (= \Delta c/c^*)$, of about 1, the processes could be described as crystallization (by cooling, evaporation, salting out, etc.) coupled with secondary nucleation. For $\sigma > 1$ the processes are more appropriately described as precipitation coupled with primary nucleation.

6.2.6 Effect of temperature

The relationship between a reaction rate constant, k , and the absolute temperature, T , is given by the Arrhenius equation

$$\frac{d \ln k}{dT} = \frac{E}{RT^2} \quad (6.86)$$

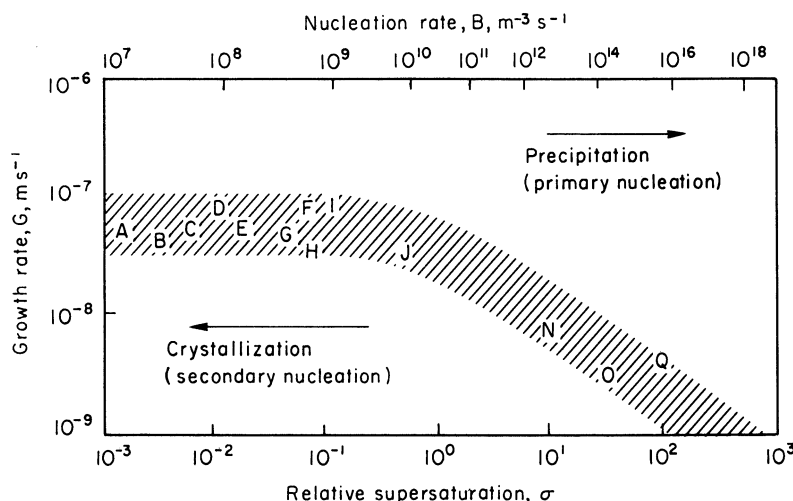


Figure 6.25. Growth and nucleation rates in an MSMPR crystallizer: A, KCl; B, NaCl; C, $(\text{NH}_2)_2\text{CS}$; D, $(\text{NH}_4)_2\text{SO}_4$; E, KNO₃; F, Na₂SO₄; G, K₂SO₄; H, $\text{NH}_4\text{Al}(\text{SO}_4)_2$; I, K₂Cr₂O₇; J, KAl(SO₄)₂; N, CaCO₃; O, TiO₂; Q, BaSO₄. (After Mersmann and Kind, 1988)

where E is the energy of activation for the particular reaction. On integration equation 6.86 gives

$$k = A \cdot \exp(-E/\mathbf{R}T) \quad (6.87)$$

or, taking logarithms,

$$\ln k = \ln A - \frac{E}{\mathbf{R}T} \quad (6.88)$$

Therefore, if the Arrhenius equation applies, a plot of $\log k$ against T^{-1} should give a straight line of slope $-E/\mathbf{R}$ and intercept $\log k$.

Alternatively, if only two measurements of the rate constant are available, k_1 at T_1 and k_2 at T_2 , the following equation may be used:

$$E = \frac{\mathbf{R}T_1 T_2}{T_2 - T_1} \ln \frac{k_2}{k_1} \quad (6.89)$$

Equation 6.89 is obtained by integrating equation 6.86 between the limits T_1 and T_2 assuming that E remains constant over this temperature range.

The above equations may be applied to diffusion, dissolution or crystallization processes; k can be taken as the relevant rate constant. For example, a plot of $\log K_G$ versus T^{-1} would give a so-called activation energy for crystal growth, E_{cryst} ; $\log K_D$ versus T^{-1} gives E_{diss} ; $\log D$ versus T^{-1} , where D = diffusivity, gives E_{diff} ; and $\log \eta$ versus T^{-1} , where η = viscosity, gives a value of E_{visc} ; and so on.

Activation energies for diffusion are usually $\sim 10\text{--}20 \text{ kJ mol}^{-1}$ and for surface integration $\sim 40\text{--}60 \text{ kJ mol}^{-1}$. As the rate of integration increases more

rapidly with temperature than does the rate of diffusion, crystal growth rates tend to become diffusion controlled at high temperature and integration controlled at low temperature. For example, sucrose is reported to be diffusion controlled above 40 °C (Smythe, 1967) and sodium chloride above 50 °C (Rumford and Bain, 1960). Over a significant intermediate range of temperature, however, both processes can be influential, and accordingly Arrhenius plots of crystal growth data often give curves rather than straight lines, indicating that the apparent activation energy of the overall growth process is temperature dependent.

6.2.7 Effect of crystal size

It is probably true to say that all crystal growth rates are particle size dependent; it all depends on the size and size range under consideration. The effect of size may be quite insignificant for macrocrystals, but the situation can change dramatically for crystals of microscopic or sub-microscopic size.

Size-dependent growth

One effect of crystal size on the overall growth rates of macrocrystals has already been mentioned in section 6.2.4 (see *Figure 6.21*). Not all substances exhibit this type of size-growth effect, but in cases where they do, an overall growth rate expression of the form of equation 6.71 can be useful. Because of the limitations imposed by traditional experimental techniques, the crystals normally studied do not extend much outside the range 200 µm to 2 mm. In this range any effect of size would appear to be closely linked with the effect of solution velocity: large particles have higher terminal velocities than those of small particles and, in cases where diffusion plays a dominant role in the growth process, the larger the crystals the higher their growth rate.

A different effect may be considered for crystals smaller than about 10 µm. Because of their very small terminal velocity, and sizes smaller than that of turbulent eddies, they may be growing in a virtually stagnant medium, even in an apparently well-agitated system.

Another, and often more powerful, effect of crystal size may be exhibited at sizes smaller than a few micrometres, and is caused by the Gibbs-Thomson effect (section 3.7). Crystals of near-nucleic size may grow at extremely slow rates because of the lower supersaturation they experience owing to their higher solubility. Hence the smaller the crystals, in the size range below say 1 or 2 µm, the lower their growth rate.

A third factor to be considered in connection with the crystal size-growth rate effect is the possibility of the surface integration kinetics being size dependent. The number of dislocations in a crystal increases with size due to mechanical stresses, incorporation of impurity species into the lattice, etc. In addition, the larger the crystals the more energetically will they collide in agitated suspensions and the greater is the potential for surface damage. Both of these effects favour faster surface integration kinetics and lead to higher growth rates with increasing crystal size (Garside and Davey, 1980).

Some comments are made in section 9.1.1 on attempts to develop appropriate empirical formulae to relate crystal growth rate with crystal size, particularly for the assessment of MSMPR crystallizer data.

Growth rate dispersion

The above size-dependent effects are all concerned with the growth rate change of a crystal solely on account of its size, i.e. a genuine size–growth effect. In contrast, the behaviour now generally known as ‘growth rate dispersion’ refers to the fact that individual crystals, all initially of the same size, each apparently subjected to identical growth environments (temperature, supersaturation, hydrodynamics, etc.), can grow at different rates. White and Wright (1971) first identified this phenomenon in the batch crystallization of sucrose, and this is now a generally accepted behaviour in all crystallizers. It has also been demonstrated for the growth of secondary nuclei (Garside, Rusli and Larson, 1979; Berglund, Kaufman and Larson, 1983). Reviews of the subject have been made by Ulrich (1989) and Tavare (1991).

Growth rate dispersion stems mainly from different interferences with the surface integration kinetics on different crystals. Random surface adsorption or physical incorporation of impurity species, leading to the development of different crystallographic faces, may account for some cases, but there is evidence to suggest that the prime causes could be the varying degrees of lattice strain and deformation in individual crystals and their dislocation structure (Ristic, Sherwood and Shripathi, 1991; Jones *et al.*, 2000). Lattice strain can be caused by mechanical stresses imparted to crystals in a crystallizer by fluid shear, or physical contact with other crystals, the agitator or other internal parts of the equipment. The less ductile the crystals the more likely they are to be prone to growth rate dispersion.

6.2.8 Effect of impurities

The presence of impurities in a system can have a profound effect on the growth of a crystal. Some impurities can suppress growth entirely; some may enhance growth, while others may exert a highly selective effect, acting only on certain crystallographic faces and thus modifying the crystal habit (see section 6.4). Some impurities can exert an influence at very low concentrations, less than 1 part per million, whereas others need to be present in fairly large amounts before having any effect. The influence of impurities on nucleation has been discussed in section 5.4.

Any substance other than the material being crystallized can be considered an ‘impurity’, so even the solvent from which the crystals are grown is in the strictest sense an impurity, and it is well known that a change of solvent frequently results in a change of crystal habit (see section 6.4.2).

Impurities can influence crystal growth rates in a variety of ways. They can change the properties of the solution (structural or otherwise) or the equilibrium saturation concentration and hence the supersaturation. They can alter the characteristics of the adsorption layer at the crystal–solution interface and

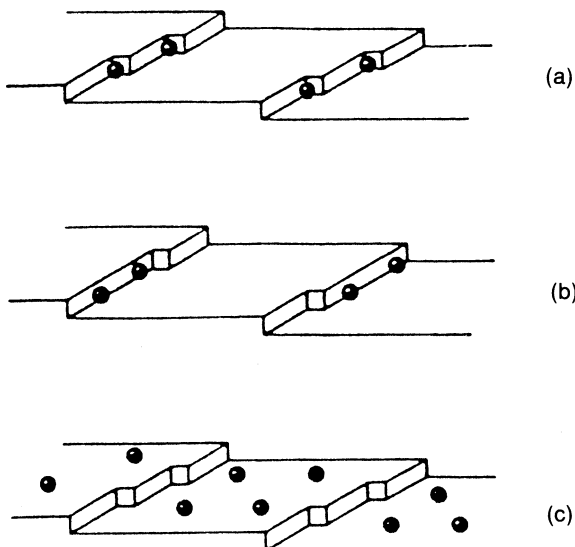


Figure 6.26. Sites for impurity adsorption on a growing crystal, based on the Kossel model: (a) kink; (b) step; (c) ledge (face). (After Davey and Mullin, 1974)

influence the integration of growth units. They may be built into the crystal, especially if there is some degree of lattice similarity.

Impurities are often adsorbed selectively on to different crystal faces and retard their growth rates. To effect retardation, however, it is not necessary for the impurity to achieve total face coverage. As seen in *Figure 6.26*, utilizing the Kossel model (section 6.2), three sites may be considered at which impurity species may become adsorbed and disrupt the flow of growth layers across the faces, viz. at a kink, at a step or on a ledge (face) between steps. Considering the theoretical implications of adsorption at each of these sites in relation to experimental observations, it is possible to assess which of the adsorption sites are important in reducing layer velocities (Davey and Mullin, 1976). Briefly, if kink site adsorption is possible, growth retardation may be affected at very low impurity levels in the solution. More impurity would be needed if step site adsorption is the preferred mode while much higher levels may be required if adsorption only occurs on a ledge or face site.

The use of single-crystal growth-rate measurements in the quantitative prediction of crystal habit was first demonstrated by Michaels and Colville (1960) who grew adipic acid crystals from aqueous solution in the presence of trace surfactants. Sodium dodecylbenzenesulphonate (SDBS) (anionic) caused a much greater reduction in the growth rate of the (010) and (110) faces than of the (001) face, leading to the formation of prisms or needles. Trimethyl dodecyl-ammonium chloride (TMDAC) (cationic) had the opposite effect, favouring the formation of plates or flakes.

A similar study was made by Mullin and Amatavivadhana (1967) and Mullin, Amatavivadhana and Chakraborty (1970) on the face growth rates of ammonium and potassium dihydrogenphosphates which are affected by trace

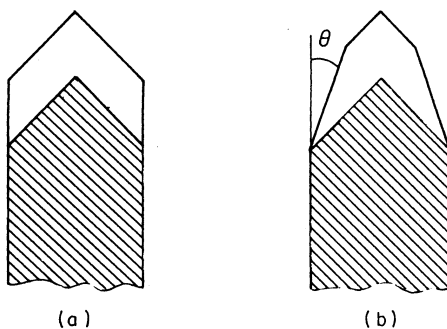


Figure 6.27. (a) Perfect ‘capping’ of an ADP crystal; (b) tapered growth caused by traces of Fe^{3+} (θ = angle of taper). (After Mullin, Amatavivadhana and Chakraborty, 1970)

quantities of Cr^{3+} or Fe^{3+} and also by solution pH changes. The most visual effect is a tapering of the prism faces (Figure 6.27), the angle of taper increasing with increase in impurity cation concentration. The overall effect, which was confirmed in a fluidizing bed crystallizer, is that growth at pH 4 gives thin needles, at pH 5 gives squat prisms and at pH 4 with 5 ppm Fe^{3+} in the solution gives tapered needles. Possible mechanisms for the complex action of these trivalent cations, and the effect of pH, have been proposed by Davey and Mullin (1976) and Kubota *et al.* (1994, 1999). This topic is considered further in section 6.4.

Theoretical analyses of the effects of impurities on crystal growth have been made by Bunn (1933), Lacmann and Stranski (1958), Chernov (1965), Davey (1976) and Boistelle (1982). Cabrera and Vermilyea (1958) visualized a general impurity effect in terms of a ‘pinning’ mechanism whereby the progress of growth layers on a crystal surface is blocked by individually adsorbed impurity species. They proposed that complete stoppage of growth would occur when the distance between the adsorbed impurity species was $< 2r_c$, where r_c represented the radius of a critical two-dimensional nucleus (equation 6.5). For spacings $> 2r_c$ the elementary growth layers could squeeze through the gaps between the impurity species and crystal growth would continue, although at a lower rate than that without any impurities present.

The blockage of active sites by impurities can be related to the impurity concentration in solution through the Langmuir adsorption isotherm, and a number of models utilizing this concept have been proposed (Davey and Mullin, 1974; Black *et al.*, 1986; Klug, 1993). A recent refinement, which incorporates the concept of an impurity effectiveness factor (Kubota and Mullin, 1995), offers an opportunity to explain several hitherto anomalous patterns of behaviour and may be summarized as follows.

The growth layer velocity v in the presence of an impurity relative to the velocity v_0 in pure solution may be represented by

$$\frac{v}{v_0} = 1 - \alpha \theta_{\text{eq}} \quad (6.90)$$

where θ_{eq} is the fractional surface coverage by adsorbed impurities at equilibrium, and α is an impurity effectiveness factor. Thus when $\alpha = 1$ and $\theta_{\text{eq}} = 1$,

the step velocity $v = 0$, i.e., complete stoppage of growth at complete coverage. However, when $\alpha > 1$ and $\theta_{\text{eq}} < 1$ (incomplete coverage) $v \rightarrow 0$, but when $\alpha < 1$, v never approaches zero, even for $\theta_{\text{eq}} = 1$.

Assuming the Langmuir adsorption isotherm to apply,

$$\theta_{\text{eq}} = Kc/(1 + Kc) \quad (6.91)$$

where K is the Langmuir constant and c is the impurity concentration. The relative step velocity can be expressed as

$$v/v_0 = 1 - [\alpha Kc/(1 + Kc)] \quad (6.92)$$

and assuming that the crystal face growth rate G is proportional to the step velocity

$$G/G_0 = 1 - [\alpha Kc/(1 + Kc)] \quad (6.93)$$

Relative step velocities calculated from equation 6.92 are shown in *Figure 6.28* for several different effectiveness factors as a function of the dimensionless impurity concentration Kc . When $\alpha > 1$, the relative velocity decreases very rapidly with increasing impurity concentration, reaching zero at a small value of Kc . For $\alpha = 1$, the step velocity approaches zero asymptotically. For $\alpha < 1$, however, the step velocity never approaches a non-zero value as the impurity concentration is increased. These three types of behaviour in the step velocity-impurity relationship can be found in many reports in the literature. For example, the case of $\alpha > 1$ is illustrated by the effect of raffinose on the step velocities on the {100} faces of sucrose (Albon and Dunning, 1962). The effects of FeCl_3 and AlCl_3 on the step velocities on the {100} faces of ammonium dihydrogen phosphate (Davey and Mullin, 1974) are good examples of $\alpha = 1$,

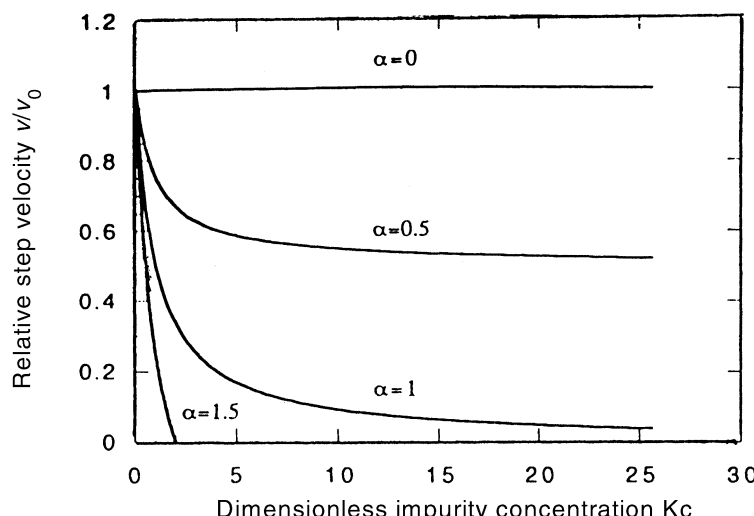


Figure 6.28. Relationship between the relative step velocity v/v_0 and the dimensionless impurity concentration Kc for different values of the impurity effectiveness factor α . (After Kubota and Mullin, 1995)

and the effect of aliphatic carboxylic acids on the {100} face growth rates of KBr (Bliznakov and Nikolaeva, 1967) neatly illustrates the case of $\alpha < 1$.

The impurity effectiveness factor α is related to the critical radius of a two-dimensional nucleus at low supersaturation ($\sigma \ll 1$) Mullin and Kubota (1995) as

$$\alpha = \gamma a / kT\sigma L \quad (6.94)$$

where a is the size of a growth unit, γ the edge free energy, σ the supersaturation (equation 3.69), L the separation of sites available for impurity adsorption, T the absolute temperature and k the Boltzman constant.

Equilibrium adsorption, however, is neither necessary for impurity action, nor is it the most commonly encountered condition. Impurities can still retard growth rate under non-equilibrium adsorption conditions so long as sufficient surface coverage is attained. To consider non-steady-state impurity action θ_{eq} in equation 6.90 is replaced by θ , the surface coverage at time t :

$$v/v_0 = 1 - \alpha\theta \quad (6.95)$$

and, assuming the Langmuir mechanism to apply, the net adsorption rate can be expressed as

$$d\theta/dt = k_1(1 - \theta)c - k_2\theta \quad (6.96)$$

where k_1 and k_2 are constants and c is the impurity concentration, also assumed to be constant. Integrating equation 6.96 with the initial condition of $\theta = 0$ at $t = 0$ for a given impurity concentration c gives the surface coverage θ as a function of time:

$$\theta = \theta_{eq}[1 - \exp(-t/\tau)] \quad (6.97)$$

where the adsorption process time constant $\tau = (k_1 + k_2)^{-1}$. The final equilibrium coverage θ_{eq} is given by equation 6.91 and from equations 6.95 and 6.97

$$v/v_0 = 1 - \alpha\theta_{eq}[1 - \exp(-t/\tau)] \quad (6.98)$$

or in terms of face growth rates

$$G/G_0 = 1 - \alpha\theta_{eq}[1 - \exp(-t/\tau)] \quad (6.99)$$

Equations 6.98 and 6.99 are valid for all values of t for weak impurities ($\alpha \leq 1$) and up to a characteristic time t_c , when the face growth rate G becomes zero, for strong impurities ($\alpha > 1$) where

$$t_c = \ln [\alpha\theta_{eq}/(\alpha\theta_{eq} - 1)]\tau \quad (6.100)$$

The combined influence of supersaturation and impurity concentration on crystal growth can be quite complex, but two basic cases may be considered (Kubota, Yokota and Mullin, 2000): (i) growth is only suppressed in the low range of supersaturation while at higher supersaturations the impurity effect disappears completely and (ii) growth rate suppression occurs throughout a very wide range of supersaturation. The first case may be explained by

assuming slow unsteady-state adsorption of impurity at high supersaturation. The second is actually a special case of the first, where the adsorption time constant becomes very small even at higher supersaturations.

For the simple case in which adsorption equilibrium is established instantaneously ($\tau = 0$) regardless of the supersaturation, equation 6.99 reduces to the equilibrium adsorption model equation

$$G/G_0 = 1 - \alpha\theta_{eq} \quad \text{for } \alpha\theta_{eq} \ll 1 \quad (6.101)$$

which, using equations 6.91 and 6.94, becomes

$$G/G_0 = 1 - [(\text{Kc}/1 + \text{Kc})(\gamma a/\text{kT}\sigma L)] \quad (6.102)$$

Equation 6.102 can be modified to describe the relative growth rate as a function of supersaturation σ at a given temperature under the influence of a given impurity concentration

$$G/G_0 = 1 - (\sigma/\sigma_c)^{-1} \quad \text{for } \sigma_c < \sigma \ll 1 \quad (6.103)$$

where σ_c , the critical supersaturation below which $G = 0$, is defined by

$$\sigma_c = \gamma a \text{Kc} / \text{kT}L(1 + \text{Kc}) \quad (6.104)$$

Any growth model can be used for G_0 in equations 6.102 and 6.103, but if a linear model ($G_0 = k_G\sigma$) is assumed, equation 6.103 becomes

$$G = k_G(\sigma - \sigma_c) \quad \text{for } \sigma_c < \sigma \ll 1 \quad (6.105)$$

Equation 6.105 is represented by the dotted line in *Figure 6.29a* showing that for instantaneous adsorption ($\tau = 0$) growth rate suppression occurs over a wide range of supersaturation. For the case of very slow adsorption ($\tau = \infty$), no impurity effect would be expected, i.e., growth in the presence of impurity would be the same as if no impurity were present, i.e. $G = G_0$. This is represented by the continuous line in *Figure 6.29a*.

In most cases the impurity adsorption rate decreases as the supersaturation is increased. The time constant τ increases from zero at some critical supersaturation σ_0 , below which adsorption occurs instantaneously. The time-averaged growth rate would change gradually from G for $\tau = 0$ (instantaneous adsorption) to G_0 (the growth rate in pure solution) for $\tau = \infty$ (very slow adsorption)

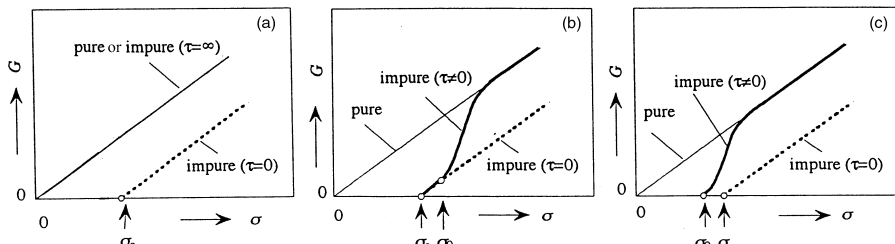


Figure 6.29. Face growth rate G as a function of supersaturation σ : (a) for instantaneous ($\tau = 0$) and very slow ($\tau = \infty$) adsorption, (b) and (c) for a continuous increase of τ from 0 to ∞ , (b) for $\sigma_0 > \sigma_c$ and (c) for $\sigma_0 < \sigma_c$. (After Kubota, Yokota and Mullin, 2000)

in the manner shown schematically in *Figures 6.29b* and *6.29c* as thick solid lines for the cases of $\sigma_c < \sigma_0$ and $\sigma_c \geq \sigma_0$.

Another interesting behaviour, often exhibited in the presence of impurities, is growth rate hysteresis where a crystal growing in a high supersaturation solution can continue to grow, at appropriate reduced rates, down to a low supersaturation, if the supersaturation is lowered continuously from the higher level. Yet the reverse does not occur, i.e., a crystal which has ceased to grow at a low supersaturation is unable to grow even when the supersaturation is continuously raised to a very much higher level. The hysteresis effect is an indication of unsteady-state growth behaviour and can be explained by assuming a slow impurity adsorption at higher supersaturations as discussed above. If the supersaturation is lowered from a high value the crystal can continue to grow before impurity species block the active sites, whereas if the supersaturation is raised from a low value, impurities quickly block the sites and stop the growth. Several cases of growth rate hysteresis are described by Kubota, Yokota and Mullin (1997).

6.3 Crystal growth and dissolution

If both crystallization and dissolution processes were purely diffusion controlled in nature, they should exhibit a true reciprocity; the rate of crystallization should equal the rate of dissolution at a given temperature and under equal concentration driving forces, i.e. at equal displacements away from the equilibrium saturation conditions. In addition, all faces of a crystal would grow and dissolve at the same rate. These conditions rarely, if ever, occur in practice.

Crystals usually dissolve much faster than they grow, and up to fivefold differences are not uncommon. Different crystallographic faces grow at different rates; they may even dissolve at different rates, but few reliable measurements of this behaviour have yet been reported. These facts have led most investigators to support the view that the crystallization process can be considered on the basis of a simple two-step process: bulk diffusion being followed by a surface ‘reaction’ at the growing crystal face (section 6.1.4). There have, however, been other suggestions put forward. Some authors have suggested that crystals dissolve faster than they grow because the exposed surface is not the same in each case; etch pits rapidly form on the faces of a dissolving crystal (these occur either at random point defects or points where line defects break the surface) as seen in *Figure 6.30a*. Dissolution then proceeds by a pitting and layer-stripping process. It is well known that a broken or etched crystal grows initially at a much faster rate than that when the faces are smooth, but as Van Hook (1961) has pointed out, even an overgenerous allowance of extra surface area due to pitting cannot possibly explain the greater rates of dissolution compared with the rate of crystallization of sucrose under comparable conditions. Other workers have expressed similar views, and it has been shown that some dissolution processes may also involve a slow ‘reaction’ step at the crystal surface (Bovington and Jones, 1970; Zhang and Nancollas, 1991).

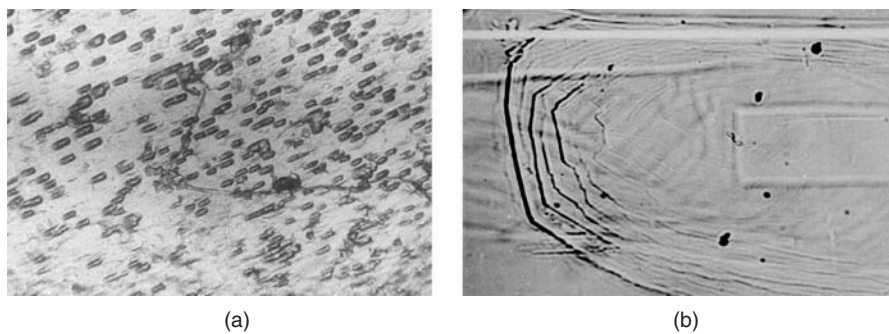


Figure 6.30. Growth and dissolution of a sucrose crystal: (a) etch pits appearing at the onset of dissolution; (b) growth layers moving over a crystal surface

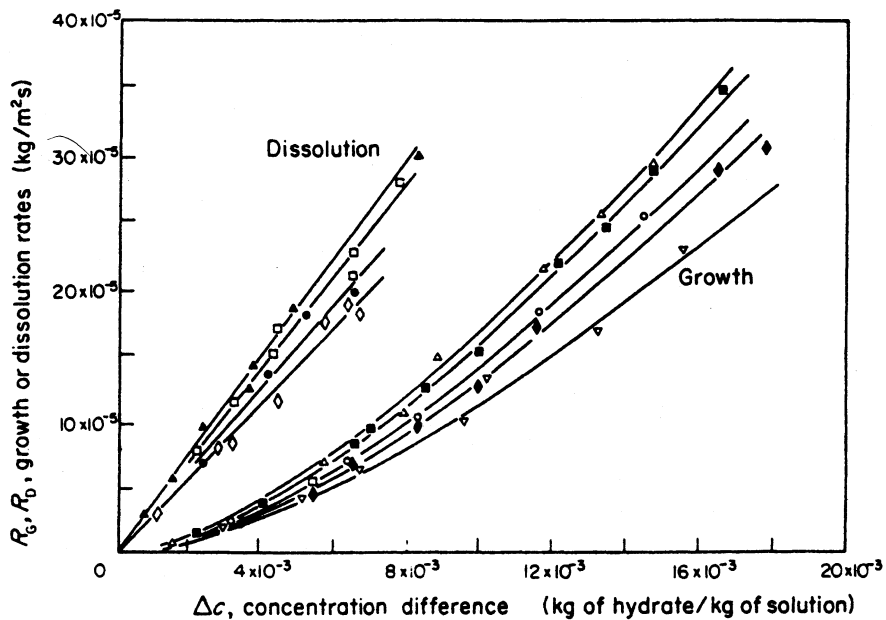


Figure 6.31. Growth and dissolution for potash alum crystals at 32°C . Mean crystal sizes: $\blacktriangle = 1.75$, $\square = 1.02$, $\bullet = 0.73$, $\diamond = 0.51$, $\triangle = 1.69$, $\blacksquare = 1.4$, $\circ = 0.99$, $\blacklozenge = 0.75$, $\triangledown = 0.53$ mm. (After Garside and Mullin, 1968)

Growth and dissolution rates of crystals can be measured conveniently in the laboratory fluidized bed crystallizer described above (Figure 6.20). Some typical results for potash alum are shown in Figure 6.31, where it can be seen that dissolution rates are very much greater than growth rates under equal driving forces (Δc). Similar results have been reported for potassium sulphate (Mullin

and Gaska, 1969). However, whilst in both cases the dissolution rates are first-order with respect to supersaturation, i.e.

$$R_D = K_D \Delta c \quad (6.106)$$

the growth processes are not, i.e. $R_G = K_G \Delta c^g$ (equation 6.70) where $g \simeq 1.6$ for potash alum at 32 °C and $g \simeq 2$ for potassium sulphate at all temperatures from 10 to 50 °C. In equations 6.70 and 6.90 K_D and K_G are the overall dissolution and growth mass transfer coefficients, respectively.

Crystal growth retardants do not necessarily have an influence on the dissolution process, but many such cases have been reported. Sears (1958) showed that complex inorganic ions such as FeF_6^{3-} can retard both the growth and dissolution of lithium fluoride at concentrations of $< 10^{-5} \text{ mol L}^{-1}$. Nancollas and Zawacki (1984) commented on the growth and dissolution retardation of sparingly soluble salts using, for example, chelating anions that adsorb at cationic sites. Kubota *et al.* (1988) demonstrated that ppm traces of Cr^{3+} in solution can prevent potassium sulphate crystals dissolving, with the effect that solubilities of this salt measured under these conditions are always lower than the true equilibrium solubility (section 2.8).

An example of the effect of trace impurities on both dissolution and growth is shown in *Figure 6.32* for the case of Fe(III) and a single crystal of potassium sulphate (Kubota *et al.*, 1999). The effect of temperature on both growth and dissolution processes has been considered in section 6.2.6.

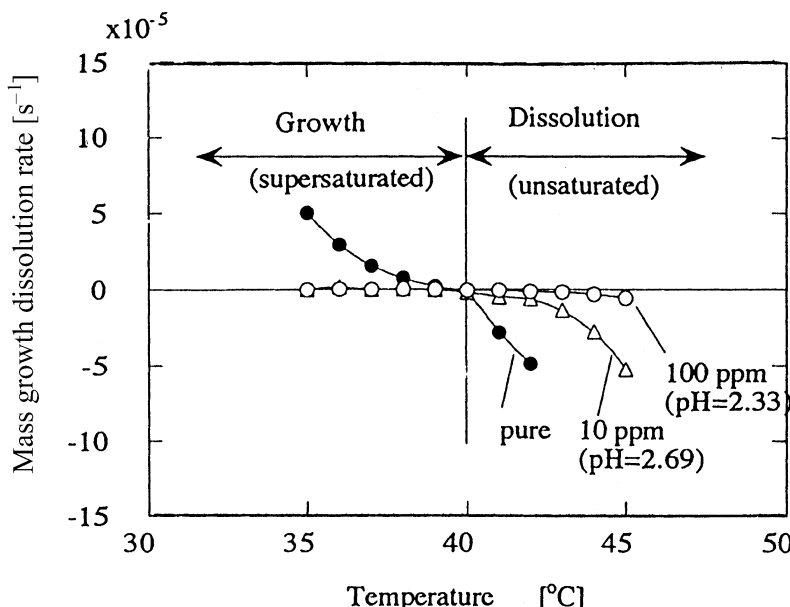


Figure 6.32. Dissolution and growth rates (expressed as a mass increase or decrease, normalized with the initial seed crystal mass) of a single potassium sulphate crystal in the presence of Fe(III) as trace impurity added as $\text{FeNH}_4(\text{SO}_4)_2 \cdot 2\text{H}_2\text{O}$. (After Kubota *et al.*, 1999)

6.3.1 Mass transfer correlations

Dissolution rate data obtained under forced convection conditions can be correlated by means of equation 6.64 or 6.65. As described in section 6.2.2, equation 6.64 is the preferred relationship on theoretical grounds, since $Sh = 2$ for mass transfer by convection in stagnant solution ($Re = 0$), whereas equation 6.65 incorrectly predicts a zero mass transfer rate ($Sh = 0$) for this condition. However, at reasonably high values of Sh (>100) the use of the simpler equation 6.65 is quite justified. The exponent of the Schmidt number b is usually taken to be $\frac{1}{3}$ and for mass transfer from spheres the exponent of the Reynolds number $a = \frac{1}{2}$.

Data plotted in accordance with equation 6.65 for the dissolution of potash alum crystals yield the relationship (Garside and Mullin, 1968)

$$Sh = 0.37 Re_p^{0.62} Sc^{0.33} \quad (6.107)$$

where the particle Reynolds number, Re_p , is based on a mean crystal size and its relative velocity when suspended in the solution.

Rowe and Claxton (1965) have shown that heat and mass transfer from a single sphere in an assembly of spheres when water is the fluidizing medium can be described by

$$Sh = A + B Re_s^m Sc^{1/3} \quad (6.108)$$

where $A = 2[1 - (1 - \varepsilon)^{1/3}]$, $B = 2/3\varepsilon$ and $(2 - 3m)/(3m - 1) = 4.65 Re_s^{-0.28}$. The solution Reynolds number, Re_s , is based on the superficial fluid velocity, u_s , and ε = voidage.

Another correlation used for predicting rates of mass transfer in fixed and fluidized beds is that of Chu, Kalil and Wetteroth (1953). The j -factor for diffusional mass transfer given by

$$j_d = \left(\frac{K_D}{u_s \rho_s} \right) Sc^{2/3} \quad (6.109)$$

is plotted against the modified solution Reynolds number $Re'_s(1 - \varepsilon)$, where Re'_s contains \bar{L}' , the diameter of a sphere with the same surface area as the crystal under consideration. The recommended expressions for calculating the mass transfer coefficients are:

$$1 < Re'_s/(1 - \varepsilon) < 30: \quad j_d = 5.7 Re'_s/(1 - \varepsilon)^{-0.78} \quad (6.110)$$

$$30 < Re'_s/(1 - \varepsilon) < 5000: \quad j_d = 1.77 Re'_s/(1 - \varepsilon)^{-0.44} \quad (6.111)$$

Dissolution rate data for potash alum are plotted in accordance with equations 6.108 and 6.110 with $\varepsilon = 0.95$, in *Figure 6.33*, where it can be seen that the results lie reasonably close ($\pm 20\%$) to the predicted values. However, it should be noted that equation 6.110 is very sensitive to values of ε as $\varepsilon \rightarrow 1$, so it cannot be applied with any reliability to very lean beds of dissolving particles and certainly not to the dissolution of single particles.

For the dissolution of crystals smaller than about 60 µm, a rough estimate of the diffusional mass transfer rate may be made because as $Re_p \rightarrow 0$ Sh reduces

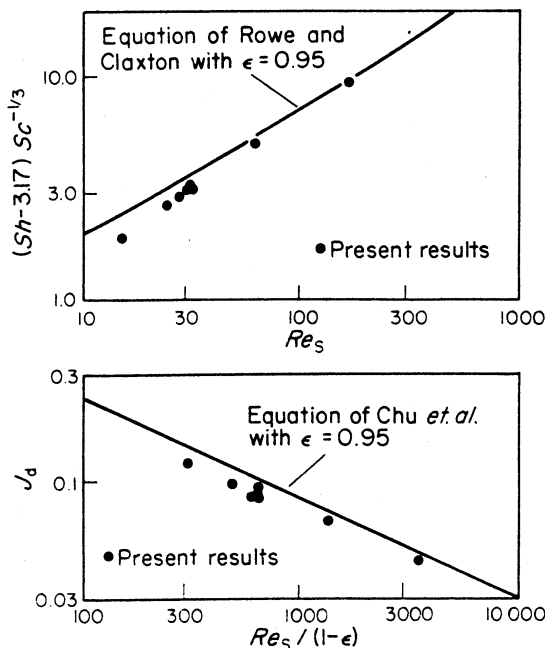


Figure 6.33. Comparison of dissolution data for potash alum at 32°C with the mass transfer correlations of Rowe and Claxton and Chu et al. (After Rowe and Claxton, 1965; Chu, Kalil and Wetteroth, 1953)

to its limiting value of 2 (equation 6.64), i.e., $K_D = 2D/L$ where D is the diffusivity ($\text{m}^2 \text{s}^{-1}$), L the crystal size (m) and K_D the mass transfer coefficient for dissolution (m s^{-1}). The dissolution time, t_D , of fine crystals of size L may therefore be expressed as $t_D = \rho L^2 / 8D\Delta c$, where ρ is the crystal density and $\Delta c = c^* - c$ is the undersaturation, the driving force for dissolution, the reverse of equation 3.67.

For crystals larger than about 60 µm in agitated vessels, it is difficult to estimate the relative crystal–solution velocity (section 9.4.1), and hence Re_p , but an order of magnitude estimate of the dissolution mass transfer coefficient may be made from the Levins and Glastonbury (1972) equation:

$$Sh = 2 + 0.47 \left(\frac{\rho_s \epsilon^{1/3} L^{4/3}}{\eta} \right)^{0.62} \left(\frac{d_S}{d_V} \right)^{0.17} \left(\frac{\eta}{\rho_s D} \right)^{0.36} \quad (6.112)$$

where d_S and d_V are the diameters of the stirrer and vessel, respectively and ϵ is the stirrer energy dissipation rate (W kg^{-1}) in the vessel.

6.3.2 Films and boundary layers

When a fluid flows past a solid surface there is a thin region near the solid–liquid interface where the velocity becomes reduced owing to the influence of the surface. This region, called the ‘hydrodynamic boundary layer’ δ_h , may be

partially turbulent or entirely laminar in nature, but in the case of crystals suspended in their liquor the latter is most probable.

For mass transfer processes another boundary layer may be defined, viz. the 'mass-transfer or diffusion boundary layer', δ_m . This is a thinner region close to the interface across which, in the case of a laminar hydrodynamic boundary layer around the crystal, mass transfer proceeds by molecular diffusion. Under these conditions the relative magnitudes of the two boundary layers may be roughly estimated from

$$\frac{\delta_h}{\delta_m} \approx Sc^{1/3} \quad (6.113)$$

where $Sc = \eta/\rho_s D$ is the dimensionless Schmidt number (η = viscosity, ρ_s = solution density, D = diffusivity).

The ratio of the thicknesses of the two layers depends considerably on the solution viscosity and diffusivity. For example, for ammonium alum crystals in near-saturated aqueous solution at 25°C , $\eta = 1.2 \times 10^{-3} \text{ kg m}^{-1} \text{ s}^{-1}$, $D = 4 \times 10^{-10} \text{ m}^2 \text{ s}^{-1}$, $\rho_s = 1.06 \times 10^3 \text{ kg m}^{-3}$. Therefore, $Sc = 2.8 \times 10^3$ and $\delta_h/\delta_m \approx 14$. However, for sucrose at 25°C , $\eta = 10^{-1}$, $D = 9 \times 10^{-11}$ and $\rho_s = 1.5 \times 10^3$, giving $Sc = 7.4 \times 10^5$ and $\delta_h/\delta_m \approx 90$.

In the description of mass transfer processes another fluid layer is frequently postulated, viz. the 'stagnant film' (see *Figure 6.8*) or, as it is sometimes called, the 'effective film for mass transfer', δ . This hypothetical film is not the same thing as the more fundamental diffusion boundary layer δ_m , but it may be considered to be of the same order of magnitude.

The thickness of the effective film for mass transfer, δ , is defined by

$$\delta = \frac{D}{k} \quad (6.114)$$

where ρ_s = solution density, D = diffusivity and k is a mass transfer coefficient expressed as m s^{-1} . As described earlier, mass transfer data are frequently correlated by relationships such as equation 6.65 in which the Sherwood number $Sh = kL/D$ and particle Reynolds number $Re_p = \rho_s u L / \eta$. L = particle size and u = relative particle solution velocity. Exponent b of the Schmidt number is generally taken as $\frac{1}{3}$, and in the case of a laminar boundary layer it can be shown theoretically that exponent a of the Reynolds number is $\frac{1}{2}$. However, a can vary from about 0.5 to 0.8 if the boundary layer is not truly laminar. Values of the constant ϕ for granular solids may range from about 0.3 to 0.9. So, writing a simple, arbitrary form of equation 6.65 as

$$Sh = \frac{2}{3} Re_p^{1/2} Sc^{1/3} \quad (6.115)$$

and expressing $Sh = L/\delta$ (using equation 6.114), we get

$$\delta = \frac{3L}{2} \left(\frac{\rho_s u L}{\eta} \right)^{-1/2} \left(\frac{\eta}{\rho_s D} \right)^{-1/3} \quad (6.116)$$

and this equation has often been used to give a rough estimate of the value of δ . It should be noted, however, that equation 6.116 depends on the mass transfer

process being first-order with respect to the concentration driving force, otherwise Sh is not dimensionless and equation 6.115 is invalid. A further complication (Paterson and Hayhurst, 2000) is that equation 6.114 only strictly applies to the case of a planar film of thickness δ whereas the appropriate relationship for a spherical shell film should be expressed in terms of a characteristic distance for mass transfer l where

$$l = D/k = L/(2 + L/\delta) \quad (6.117)$$

which leads to the statement that

$$Sh = 2 + L/\delta = 2 + f(Re, Sc) \quad (6.118)$$

This equation encompasses two asymptotic results for (i) the stagnant case: $\delta/L \rightarrow \infty$, $Sh \rightarrow 2$ and (ii) the planar case: $\delta/L \rightarrow 0$, $l \rightarrow \delta$.

It is thus possible to estimate a value for the thickness of the so-called stagnant film, δ , but it is perhaps worthwhile at this point to question the meaning and utility of this quantity. The concept of a stagnant film at an interface is undoubtedly useful in providing a simple pictorial representation of the mass transfer process, but in the case of crystals growing or dissolving in multi-particle suspensions the actual existence of stable films, of the magnitude normally calculated as shown above, around each small particle is debatable, to say the least. Further, the value of δ can only be deduced indirectly from the mass transfer coefficient and diffusivity (equation 6.114), and it is difficult to select the appropriate value of D to use in any given situation. The question arises, therefore, as to whether or not δ is a meaningful quantity to calculate in these circumstances. In any case, the hypothetical nature of the stagnant film should be clearly appreciated, and calculated values of its thickness should be used with considerable caution.

6.3.3 Driving forces for mass transfer

There is a wide choice of possible driving forces for a mass transfer process, but provided that the driving force is clearly defined the selection is generally of little importance. However, in certain cases, e.g. under conditions of high mass flux, the choice becomes critical.

For low mass flux mass transfer from a single sphere to an extensive fluid, the general correlation

$$Sh = 2 + 0.72Re_p^{1/2}Sc^{1/3} \quad (6.119)$$

may be used over the range $20 < Re_p < 2000$.

The mass transfer coefficient in the Sherwood number may be defined by

$$R = k_c(c_0 - c_\infty) \quad (6.120)$$

$$= k_c(\rho_0\omega_0 - \rho_\infty\omega_\infty) \quad (6.121)$$

$$= \rho_s k_c(\omega_0 - \omega_\infty) \quad (6.122)$$

since for low mass flux $\rho_0 \simeq \rho_\infty \simeq \rho_s$. Other definitions of the mass transfer coefficient include

$$R = k_\omega(\omega_0 - \omega_\infty) \quad (6.123)$$

$$= k_y(Y_0 - Y_\infty) \quad (6.124)$$

$$= k_b B \quad (6.125)$$

In equations 6.120–6.125 R = mass flux ($\text{kg m}^{-2} \text{s}^{-1}$), c = solution concentration (kg m^{-3}), k = mass transfer coefficient ($k_c = \text{m s}^{-1}$, $k_\omega = \text{kg m}^{-2} \text{s}^{-1} \Delta\omega^{-1}$, $k_y = \text{kg m}^{-2} \text{s}^{-1} \Delta Y^{-1}$ and $k_b = \text{kg m}^{-2} \text{s}^{-1} B^{-1}$), ρ_s = solution density (kg m^{-3}), ω = mass fraction of solute in solution (dimensionless) and Y is the mass ratio of solute to solvent in the solution (dimensionless). The subscripts 0 and ∞ refer to the interfacial and bulk solution conditions, respectively.

The dimensionless mass transfer driving force B is defined by

$$B = \frac{\omega_0 - \omega_\infty}{\omega_t - \omega_0} \quad (6.126)$$

where ω_t is the mass fraction of the solute in the transferred solid substance, i.e. $\omega_t = 1$ for a single component. If the solute is a hydrate, then $\omega_t = 1$ only if the mass fractions are expressed as mass of hydrate per unit mass of solution.

Equation 6.119 should describe the dissolution of a solid solute into a solvent or its own solution, and either k_c or k_ω can be used, as $Sh = k_c d/D = k_\omega d/\rho_s D$. However, complications can arise if the solute solubility is high. First, the concentration dependence of the physical properties become significant and, since $\rho_0 \neq \rho_\infty$, the Sherwood numbers based on k_c and k_ω will not be equal. Second, the mass flux from the surface of the solid alters the concentration gradient at the surface compared with that obtained under otherwise identical conditions of low mass flux.

Diffusion coefficients of electrolytes in water are greatly dependent on concentration; variations of $\pm 100\%$ from infinite dilution to near-saturation are not uncommon. Moreover the change is often non-linear and accurate prediction of its effect is extremely difficult. Other physical properties, such as viscosity and density, change over this concentration range but not to such an extent.

The effects of concentration dependent physical properties on the correlation of dissolution mass transfer data have been reported in some detail by Nienow, Unahabhoka and Mullin (1966, 1968). ‘Mean’ solution properties should be used for the Sherwood and Schmidt groups in equation 6.119 if the mass transfer data for moderately soluble substances are to be correlated effectively. The arithmetic mean will suffice for viscosity and density, but the integral value must be used for the diffusivity (equation 2.27). Bulk solution properties are used for the Reynolds number.

For low to moderate mass flux mass transfer studies, therefore, provided that the physical property changes are taken into account, mass transfer coefficients k_c or k_ω may be used. The dimensionless mass ratio driving force, ΔY , has been used quite successfully in crystallization and dissolution studies (Garside and

Mullin, 1968; Mullin and Gaska, 1969), but this has the disadvantage that each value of ω_∞ yields a different value of ϕ , even if the physical property variations are allowed for.

However, if the dimensionless driving force, B , is used, together with the appropriate physical properties, the value of ϕ in equations 6.64 and 6.65 remains substantially constant at about 0.7–0.8 for a wide range of systems. There is little doubt that B is the best driving force to use for high mass flux studies.

A comprehensive account of the role of transport processes in crystallization has been given by Garside (1991).

6.3.4 Mass transfer in agitated vessels

Crystallization and dissolution data obtained from agitated vessel studies may be analysed by the methods discussed above, but a survey of the literature related to the subject of solid–liquid mass transfer in agitated vessels shows that there is an extremely wide divergence of results, correlations and theories. The difficulty is the extremely large number of variables that can affect transfer rates, the physical properties and geometry of the system and the complex liquid–solid–agitator interactions.

Relationships such as equations 6.64 and 6.65 are commonly used for correlating solid–liquid mass transfer data. However, the Reynolds number should not be based on the agitator dimensions and speed, because this cannot take into account one of the most important factors, viz. the state of particle suspension. The mass transfer coefficient increases sharply with agitator speed until the particles become fully suspended in the liquid, after which the rate of increase with further increases in speed is reduced considerably. A maximum rate of mass transfer occurs when substantial aeration of the liquid occurs at high agitator speeds. From the ‘just-suspended’ to ‘severe aeration’ conditions the mass transfer coefficient may be enhanced by 40–50% while the agitator power input may be increased tenfold. There is little justification, therefore, for using agitator speeds much higher than those needed to suspend the particles in the system.

The appropriate velocity term for the particle Reynolds number in equations 6.64 and 6.65 is the slip velocity, i.e. the relative velocity between particle and fluid. The slip velocity is usually assumed to be the free fall velocity of the particle, but this quantity is not easy to predict.

The critical mass transfer rate, for particles just suspended in a liquid, can be estimated from equation 6.119, the ‘mean’ solution properties being used as explained above. The terminal velocity, u_t , for use in the Reynolds number may be calculated from the empirical equations

$$u_t = 0.153 g^{0.71} L^{1.14} \Delta\rho^{0.71} \rho_s^{-0.29} \eta^{-0.43} \quad (6.127)$$

for particles smaller than 500 µm, and from

$$u_t = (4gL\Delta\rho/3\rho_s)^{1/2} \quad (6.128)$$

for particles larger than 1500 µm (Nienow, 1969). For particles of intermediate size, u_t should be predicted from both relationships, and the smaller value used in the Re_p as a conservative estimate. In equations 6.127 and 6.128, $u_t = \text{cm s}^{-1}$, $g = 981 \text{ cm s}^{-2}$, $L = \text{cm}$, $\rho = \text{g cm}^{-3}$ and $\eta = \text{poise} (\text{g s}^{-1} \text{ cm}^{-1})$ where ρ_s and η refer to the bulk solution. $\Delta\rho$ is the solid–liquid density difference.

The expected mass transfer coefficient can be predicted from the critical value by multiplying by an enhancement factor ranging from about 1.1 for particles $\sim 200 \mu\text{m}$ to about 1.4 for particles $\sim 5 \text{ mm}$. Particle density also influences the rate of mass transfer. The reason for this enhancement is the increased level of turbulence at which larger and denser particles become suspended in the liquid.

Another model for mass transfer is based on the Kolmogoroff theory of homogeneous isotropic turbulence adapted to solid–liquid systems (Kolař, 1958, 1959; Middleman, 1965; Hughmark, 1969). The energy put into the system by the agitator is considered to be transferred first to large-scale eddies and then to larger numbers of smaller isotropic eddies from which it is dissipated by viscous forces in the form of heat. For a given system the mass transfer coefficient, k , can be related to the energy input, e , to the system by $k \propto e^{0.25}$.

The Kolmogoroff theory can account for the increase in mass transfer rate with increasing system turbulence and power input, but it does not take into consideration the important effects of the system physical properties. The weakness of the slip velocity theory is the fact that the relationship between terminal velocity and the actual slip velocity in a turbulent system is really unknown. Nevertheless, on balance, the slip velocity theory appears to be the more successful for solid–liquid mass transfer in agitated vessels.

6.4 Crystal habit modification

6.4.1 Crystal morphology and structure

The morphology of a crystal depends on the growth rates of the different crystallographic faces. Some faces grow very fast and have little or no effect on the growth form; the ones that have most influence are the slow-growing faces. The growth of a given face is governed by the crystal structure and defects on the one hand, and by the environmental conditions on the other.

A number of attempts have been made to predict the equilibrium form of a crystal. According to the Bravais rule (chapter 1), the important faces governing the crystal morphology are those with the highest reticular densities and the greatest interplanar distances, d_{hkl} . Or, in simpler terms, the slowest-growing and most influential faces are the closest-packed and have the lowest Miller indices. The surface energy theories of crystal growth (section 6.1.1) suggest that the equilibrium form should be such that the crystal has a minimum total surface free energy per unit volume.

The morphological theory of Hartman and Perdok (1955) considers the bond energies involved in the integration of growth units into the lattice. In this

theory crystal growth is considered to be controlled by the formation of strong bonds between crystallizing particles. A strong bond is defined as a bond in the first co-ordination sphere of a particle. The two-dimensional crystal shown in *Figure 6.34a* is bounded by straight edges that are parallel to uninterrupted chains of strong bonds. Such a straight edge is formed when the probability of a particle being integrated is greater for site *A* than site *B*. In the case illustrated the particle at site *A* is bonded to the crystal with one strong bond more than at site *B*. The uninterrupted chains of strong bonds have been called *periodic bond chains* (PBC); and as the number of strong bonds per unit cell is limited, there exists a maximum length for the period of a PBC and, hence, a limited number of PBCs.

The minimum thickness of a growth layer is the elementary ‘slice’, d_{hkl} , and faces that grow slice after slice are called flat or F-faces. The condition for a slice to exist is that two neighbouring parallel periodic bond chains be bonded together with strong bonds (*Figure 6.34b*). If this is not so, no slice exists, i.e. no layer growth can occur. Such faces are called stepped or S-faces (*Figure 6.34c*).

If no PBC exists within a layer, d_{hkl} , the face is called a kinked or K-face, which needs no nucleation for growth since it corresponds to a generalized type

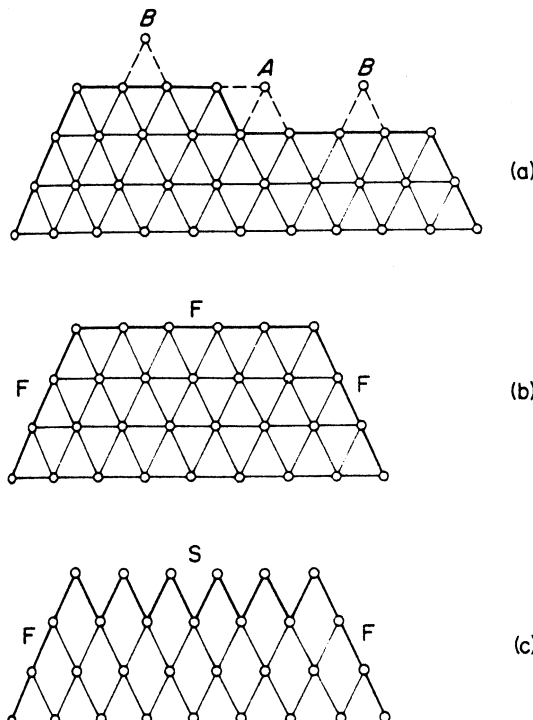


Figure 6.34. (a) Two-dimensional crystal. Each circle represents a growth unit of Kossel's repeatable step. (b) and (c) Projection of a three-dimensional crystal along a PBC. Each circle represents a PBC. An F-face results when neighbouring PBCs are linked together by strong bonds, otherwise an S-face develops

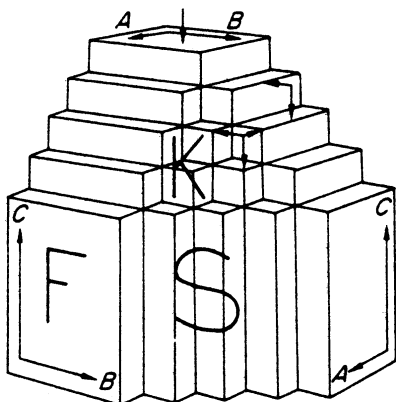


Figure 6.35. Crystal with three PBCs parallel to [100] (A), [010] (B), and [001] (C). The F-faces are (100), (010) and (001). The S-faces are (110), (101) and (011). The K-face is (111). (After Hartman, 1963)

of Kossel's repeatable step (*Figure 6.35*). In terms of crystal structure dependent growth, therefore, the growth form should be bounded by F-faces only, although not all F-faces need be present.

The Hartman–Perdok approach is applied by making projections of the crystal structure parallel to a PBC and tabulating all the bonds. The packing of the chains determines the F-faces, provided that the chains are bonded by strong bonds. Sometimes it is easier to recognize the slices, and in that case the PBC may be found as the intersection of two slices.

Some reported examples of the use of PBC analysis to predict crystal morphology include: hexamethylenetetramine (Hartman and Perdok, 1955), calcium sulphate (gypsum) (van Rosmalen, Marchée and Bennema, 1976), anthracene (Hartman, 1980), magnesium hydrogenphosphate (newberyite) (Boistelle and Abbona, 1981), sodium sulphite and potassium sulphate (Follner and Schwarz, 1982), succinic acid (Davey, Mullin and Whiting, 1982), sucrose (Aquilano *et al.*, 1983).

Docherty and Roberts (1988) developed an alternative technique which included the computation of surface attachment energies: faces with the lowest attachment energies will be the slowest growing and hence the most dominant morphologically (Bennema and Hartman, 1980). This approach led to the successful modelling of the theoretical morphologies of molecular crystals, e.g. anthracene, biphenyl and β -succinic acid. In a similar manner, Clydesdale and Roberts (1991) predicted the structural stability and morphologies of crystalline C_{18} – C_{28} *n*-alkanes. Anwar and Boateng (1998) have shown how crystallization from solution can be simulated using the method of molecular dynamics for a model solute/solvent system consisting of atomic species characterized by the Leonard-Jones potential function. Accounts of molecular modelling techniques, based on computer simulation and computational chemistry, are given by Docherty and Meenan (1999) and Myerson (1999).

6.4.2 Interface structure

Consideration of the structure of a growing crystal face can provide additional information to assist in the task of crystal morphology prediction. The surface roughness (on the molecular level) quantified by the α -factor (section 6.1.7) is governed by energetic factors arising from fluid–solid interactions at the interface between the crystal and its growth environment. The degree of roughness of a given crystal face can have an important bearing on the growth mechanism controlling its development. A significant change in the α -factor could considerably alter the face growth potential and hence affect the overall crystal habit.

A change of solvent often changes the crystal habit and this may sometimes be explained in terms of interface structure changes. In general, the higher the solubility of the solute in the solvent, the lower the α -value and hence the rougher the surface. A smooth face (high α -value) would favour growth by the BCF screw-dislocation mechanism, a rough face (low α -value) would favour diffusion-controlled growth, while a face of intermediate roughness would tend to grow by the B + S mechanism. Since these three mechanisms imply different $v-\sigma$ relationships (section 6.1.7), the face growth rates could be quite different in different solvents, and any differences in the relative rates of growth would manifest themselves in a habit change.

A detailed study on solvent effects relating to the growth of succinic acid crystals from water and isopropanol solutions was reported by Davey, Mullin and Whiting (1982). The faster growth of the (010) and (001) faces in water than in isopropanol resulted in a succinic acid habit modification from platelets to needles, as shown in *Figure 6.36*. Calculated α -factors for the two faces were found to be similar for both solvents, so the change of habit was considered to result from chemical interaction with the solvent. Succinic acid interacts, pre-

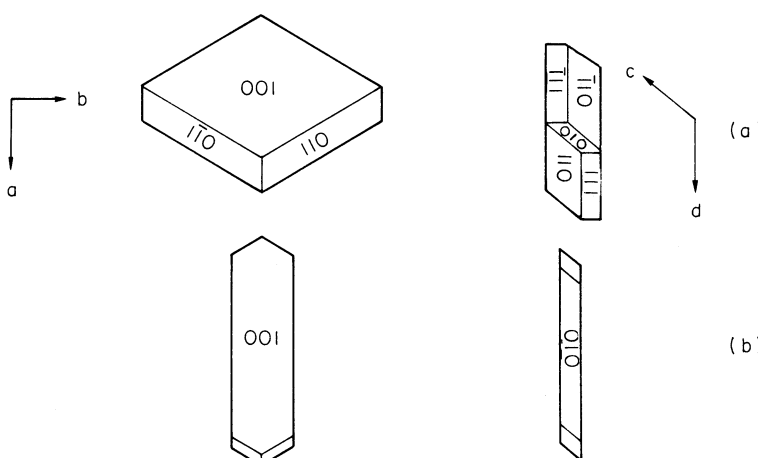


Figure 6.36. Habits of succinic acid crystals grown from (a) water (b) isopropanol. (After Davey, Whiting and Mullin, 1982)

sumably through hydrogen bonding, more strongly with isopropanol than with water, and the stronger adsorption would reduce the face growth rates below those in aqueous solution. On the (001) faces, the carboxylic acid groups are normal to the surface and adsorption would reduce surface diffusional flux to the growth steps. On the (010) faces, the carboxylic acid groups are parallel to the surface and adsorption would be active in blocking kink sites. This appears, therefore, to be a case in which adsorption effects dominate the growth kinetics. In another attempt to explain the habit changes of succinic acid in water/isopropanol solvents, van der Voort (1991) assumed that solvent interactions determine diffusion rates.

The adsorption of an impurity on a crystal face can have a similar effect to a change of solvent. Since adsorption reduces the interfacial tension, it will also reduce the α -factor and consequently roughen the surface. If adsorption is selective, i.e. only on to specific faces of the crystal, or to different extents on different faces, any significant change from the smooth to rough condition could lead to faster growth on those faces and hence to a habit change.

Crystal growth enhancement by the adsorption of a foreign species appears to be contrary to the commonly held view of the action of an additive in which foreign species adsorb at various sites on a crystal face, impede the flow of growth layers and reduce the growth rate (section 6.2.8). However, the two effects can sometimes be seen in the same system, with growth enhancement occurring at low impurity levels followed by a reversal at higher levels when the blocking effect becomes dominant. An example is shown in *Figure 6.37* where the cube (100) and octahedral (111) faces of lead nitrate growing in the presence of increasing amounts of methylene blue (Bliznakov, 1965) both exhibit a reversal effect at the low impurity level of approximately 5 mg L^{-1} . Similar examples have been reported with other systems by Budz, Jones and Mullin (1986) and Eidelman, Azoury and Sarig (1986).

The chemisorption of an impurity can cause chemical changes in the crystal surface that give it a new structural appearance. The growth of octahedral

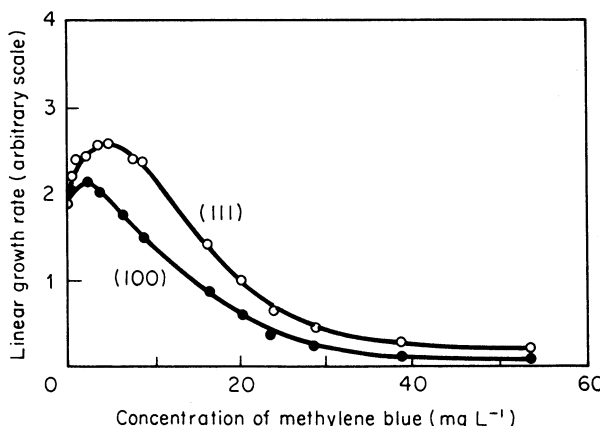


Figure 6.37. The influence of methylene blue on the (100) and (111) face growth rates of lead nitrate at 25°C and $S = 1.08$, showing a reversal of effect. (After Bliznakov, 1965)

sodium chloride crystals from solutions containing cadmium chloride results not from the simple adsorption of Cd^{2+} , but from the formation of a new phase, $\text{CdCl}_2 \cdot 2\text{NaCl} \cdot 3\text{H}_2\text{O}$, which has an epitaxial fit with the {111} planes of NaCl causing the (111) growth rate to decrease and hence dominate the habit (Boistelle and Simon, 1974).

6.4.3 Structural compatibility

It is usually assumed that there is some form of affinity between an active impurity and the crystallizing species, and this can take a large variety of forms. For example, there may be some degree of structural compatibility between ionic groups in the modifying agent and the crystal, e.g. as in the case of calcium carbonate being modified by metaphosphates, or nitrilotriacetamide and nitrilotripropionamide for modifying NaCl and KCl, respectively (Sarig, Glasner and Epstein, 1975). There may be some structural similarity with the crystal to be modified, particularly in organic systems, and this has led to the use of the term ‘tailored’ crystal growth. A tailored additive usually has two parts, one which is structurally compatible with a grouping on one of the crystal faces and the other which acts as a repellent, i.e., after integration it will then disrupt the subsequent bonding sequence and hence retard the growth process on that face.

A simple example of a tailor-made habit modifier for benzamide was reported by Berkovitch-Yellin *et al.* (1982). This substance normally crystallizes from ethanol solution in the form of platelets, with the slowest growth in the *c* direction. During growth the benzamide molecules develop a ribbon pattern in which hydrogen bonded cyclic dimers are interlinked by N—H \cdots O bonds along the *b* axis. The ribbons are stacked along the *a* axis to yield (001) layers. Three different impurities, benzoic acid, *o*-toluamide and *p*-toluamide, which all bear a structural resemblance to benzamide but contain substituent groups that interfere with the bonding, were found to be capable of retarding the growth rates along the *b*, *a* and *c* axes, respectively.

Figure 6.38 demonstrates the action of benzoic acid which, after substituting for a benzamide molecule in the lattice by H bonding, repels the next incoming benzamide molecule as it encounters an O \cdots O repulsion due to the lone pair electrons of the benzoic acid carbonyl oxygen. The rate of growth along the *c* axis is thus impeded.

A tailored modifier does not always have to be deliberately added to a crystallizing system; it may already exist, e.g., as a synthesis by-product of a chemical reaction. If its presence causes a crystal habit problems, it must be removed or deactivated. On the other hand, it may have a beneficial effect. These are both commonly encountered cases in the manufacture of organic chemicals. A simple, but industrially important, example is the effect of biuret on the crystallization of urea (Davey, Fila and Garside, 1986). In the synthesis of urea (NH_2CONH_2) from ammonia and carbon dioxide a small amount of biuret ($\text{NH}_2\text{CONHCONH}_2$), a condensation dimer, is formed. The presence of biuret is actually beneficial because from pure aqueous solution urea crystals form as elongated [001] needles that are difficult to process. Biuret retards growth in the

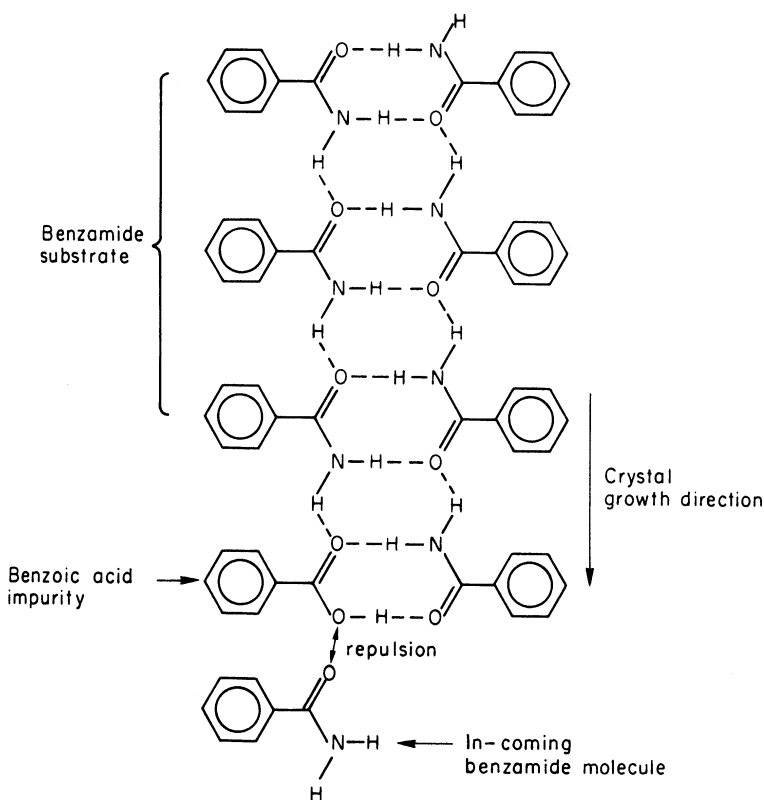


Figure 6.38. Benzoic acid, as an impurity, retarding the growth of benzamide. (After Berkovitch-Yellin *et al.*, 1982)

[001] direction resulting in short stubby urea crystals which are more easily handled in the subsequent downstream processes of filtration, washing and drying (section 9.7).

The needle-like morphology of urea results from the strong intermolecular hydrogen bonding along the urea crystal *c*-axis, as shown by the dotted lines in Figure 6.39. The urea structure is such that the {001} surfaces cannot easily discriminate between two urea molecules and one biuret molecule, so biuret molecules can easily become attached to the lattice at growth sites in the [001] direction. However, subsequent urea molecules attempting to attach to a biuret-contaminated surface meet a resistance since the NH₂ groups in the crystal surface that are needed to form hydrogen bonds are now missing. The growth rate in the [001] direction is thus effectively reduced, and stubby crystals are the result. This example illustrates the general rule that the most effective habit modifiers are those that are able to enter the growing surface and yet once there they disrupt further growth. To perform this function effectively the additive molecule must resemble the crystallizing molecule while containing some small difference in stereochemistry or functionality, rendering it capable of inhibiting growth in a selected direction (Davey and Garside, 2000).

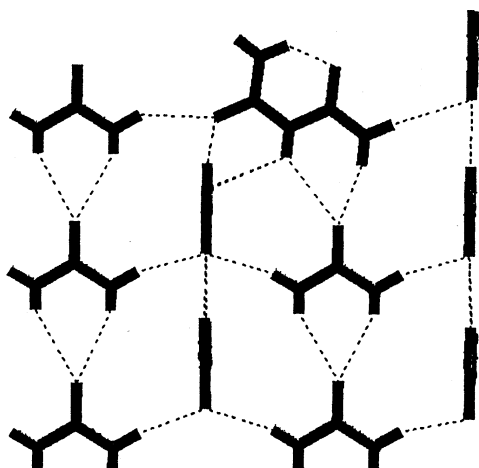


Figure 6.39. Showing a biuret molecule occupying two urea sites on the fast growing (001) face and impeding further growth. (After Davey and Garside, 2000).

Authoritative account of the control of crystal morphology by the use of tailor-made additives have been given by Davey, Polywka and Maginn (1991), Popovitz-Biro *et al.* (1991), Myerson (1999) and Davey and Garside (2000).

6.4.4 Industrial importance

Most habit modification cases reported in the literature have been concerned with laboratory investigations, but the phenomenon is of the utmost importance in industrial crystallization and by no means a mere laboratory curiosity. Certain crystal habits are disliked in commercial crystals because they give the crystalline mass a poor appearance; others make the product prone to caking (section 7.6), induce poor flow characteristics or give rise to difficulties in the handling or packaging of the material. For most commercial purposes a granular or prismatic habit is usually desired, but there are specific occasions when other morphologies, such as plates or needles, may be wanted.

In nearly every industrial crystallization some form of habit modification procedure is necessary to control the type of crystal produced. This may be done by controlling the rate of crystallization, e.g. the rate of cooling or evaporation, the degree of supersaturation or the temperature, by choosing a particular solvent, adjusting the solution pH, deliberately adding an impurity that acts as a habit modifier, or even removing or deactivating some impurity that already exists in the solution. A combination of several of the above methods may have to be used in specific cases, as seen in the examples quoted in section 6.2.8.

Many dyestuffs act as powerful habit modifiers for inorganic salts. Buckley (1952) has summarized a large number of case histories giving an indication of the concentrations necessary to induce the required change, but these additives do not nowadays find any significant industrial application.

Surface-active agents (surfactants) are frequently used to change crystal habits. Common anionic surfactants include the alkyl sulphates, alkane sulphon-

ates and aryl alkyl sulphonates. Quaternary ammonium salts are frequently used as cationic agents. Non-ionic surfactants only occasionally find application as habit modifiers.

Polymeric substances such as polyvinylalcohol, polyacrylates, polyglutamates, polystyrene sulphonates, alginates, polyacrylamides, etc., have also found application, as have long-chain and proteinaceous materials like sodium carboxymethylcellulose, gelatin and phosphoproteins. Sodium triphosphate, sodium pyrophosphate, organic derivatives of phosphonic acid (H_3PO_3), low molecular weight organic acids, such as citric, succinic and tartaric and their derivatives, are also useful habit modifiers.

The trace presence of foreign cations can exert an influence on the crystal habit of inorganic salts. Some act by simple substitution in the lattice, e.g. Cd^{2+} for Ca^{2+} in calcium salts or Ca^{2+} for Mg^{2+} in magnesium salts, as a result of similar ionic radii and charge. Trivalent cations, particularly Cr^{3+} and Fe^{3+} , have a powerful effect on the morphology of salts such as ammonium and potassium dihydrogenphosphates (Mullin, Amatavivadhana and Chakraborty, 1970; Davey and Mullin, 1974, 1976) and ammonium sulphate (Larson and Mullin, 1973). These trivalent cation habit modifiers are not only powerful in effect, i.e., active at very low concentrations in the system, but also that above some critical concentration they begin to have a severe disruptive effect on the overall crystal growth process, resulting in the production of unacceptable crystalline products. For example, at a Cr^{3+} concentration of 5 ppm the normal orthorhombic crystal habit of ammonium sulphate changes with the appearance of higher index faces, while at around 20 ppm large grotesque non-faceted crystals are produced (*Figure 6.40*).

Complex cations, like $Fe(CN)_6^{4-}$, have a remarkable influence on sodium chloride (*Figure 6.41*). At concentrations of around 0.1%, excrescences develop at the corners of the normal cubic crystals producing large hard crystals with a skeletal appearance, often referred to as dendrites (see *Figure 8.3*). At around 1% $Fe(CN)_6^{4-}$, however, the product changes to soft friable particles with little or no outward appearance of crystallinity (Cooke, 1966).

Phoenix (1966) has reported on the effects of a wide variety of inorganic and organic additives on $NaCl$, $NaBr$, KCl , KCN , K_2SO_4 , NH_4Cl , NH_4NO_3 and $(NH_4)_2SO_4$. A considerable amount of valuable quantitative information is given concerning the effects of the different additives on crystal habit, growth and dissolution rates, and anti-caking effectiveness. The influence of ferrocyanide ions in producing dendritic crystals of $NaCl$ is discussed in some detail.

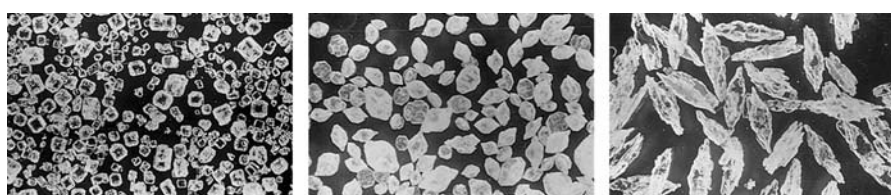


Figure 6.40. Habit changes in ammonium sulphate crystals caused by traces of impurity: (a) pure solution, (b) 5 ppm Cr^{3+} , (c) 20 ppm Cr^{3+} . (Larson and Mullin, 1973)



Figure 6.41. Habit changes in sodium chloride crystals caused by traces of impurity: (a) pure solution, (b) 0.1% $\text{Fe}(\text{CN})_6^{4-}$, (c) 1% $\text{Fe}(\text{CN})_6^{4-}$. (Cooke, 1966)

There are literally thousands of reports in the scientific literature concerning the effects of impurities on the growth of specific crystals, and it would be superfluous to attempt a summary here. General reviews on the influence of additives in the control of crystal morphology have been made by Kern (1965), Boistelle (1976), Davey (1979), Botsaris (1982), Nancollas and Zawacki (1984), van Rosmalen, Witkamp and de Vreugd (1989), Davey *et al.* (1991) and Pfefer and Boistelle (1996).

The selection of a suitable habit modifier for the industrial production of crystals of a particular form normally begins with a series of laboratory-scale screening tests covering a wide range of potential additives at different concentrations. It is usually necessary to conduct further trials with the more promising modifiers to attempt to identify the ones that should prove efficacious on the industrial scale. Quite clearly, all these procedures can be extremely time-consuming and costly, but ultimate success depends on the key step of deciding which additive is likely to be potentially useful. There is a rapidly growing interest, therefore, in an alternative procedure to eliminate guesswork and serendipity from the initial selection process, involving the use of computer modelling techniques to match additive molecular species with the molecular configurations on the specific faces of the crystal that need to be influenced. This is a rapidly developing field of activity, but it should be understood that whilst the molecular modelling approach to habit modification undoubtedly holds great promise for the future, it is first necessary to be in possession of detailed crystallographic data and quantifications of intermolecular bond strengths at relevant crystal faces. Unfortunately, this information is not always readily available. Nevertheless, there are already several reported examples of the successful application of the molecular modelling approach to habit modification (Davey, Polywka and Maginn, 1991; Lewtas *et al.*, 1991; Lee *et al.*, 1996; Myerson, 1999; Davey and Garside, 2000; Winn and Doherty, 2000).

Maximum crystal size

Theoretically there is no limit to a product crystal size, but there is generally a practical limit. It is common experience that some crystals do not normally grow beyond a certain size in agitated industrial crystallizers (*Figure 6.42*), although there is no single clear-cut answer to this problem.

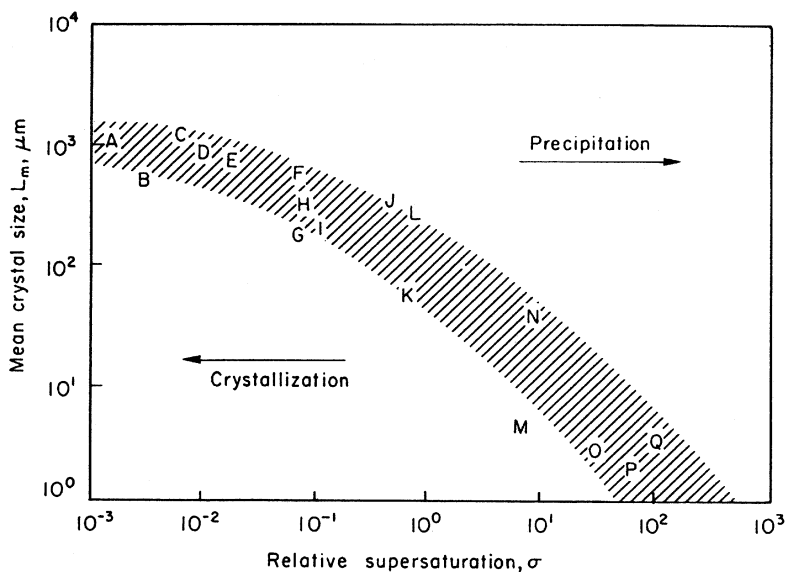


Figure 6.42. Maximum mean crystal sizes obtained in an MSMPR crystallizer: A, KCl; B, NaCl; C, $(\text{NH}_2)_2\text{CS}$; D, $(\text{NH}_4)_2\text{SO}_4$; E, KNO_3 ; F, Na_2SO_4 ; G, K_2SO_4 ; H, $\text{NH}_4\text{Al}(\text{SO}_4)_2$; I, $\text{K}_2\text{Cr}_2\text{O}_7$; J, $\text{KAl}(\text{SO}_4)_2$; K, KClO_3 ; L, $\text{NiSO}_4(\text{NH}_4)_2\text{SO}_4$; M, BaF_2 ; N, CaCO_3 ; O, TiO_2 ; P, CaF_2 ; Q, BaSO_4 . (After Mersmann and Kind, 1988)

Some crystals have such low growth rates that excessive residence times would be necessary to produce large crystals. For example, at a linear growth rate of 10^{-7} m s^{-1} a nucleus would grow to 1 mm in just over 1 h, but at 10^{-9} m s^{-1} it would require around 6 days. Growth rates exhibited by inorganic salts in aqueous solution generally lie well within this range (Table 6.1). Of course, increased residence time alone in an agitated crystallizer may not greatly influence the product size because of the inevitable occurrence of secondary nucleation (section 9.1.1) which greatly increases the number of product crystals and consequently inhibits the development of large crystals. Growth rates can be increased by raising the operating level of supersaturation, but nucleation rates are even more sensitive to supersaturation and play the dominant role.

The presence of impurities in the system can also have a significant effect. For example, crystallization of copper and cadmium sulphates from plating-bath liquors, to which gelatin has been added, produces crystals no larger than 1 μm , yet both of these salts can readily be crystallized from normal aqueous solution as large crystals ($> 1 \text{ mm}$).

Some crystals appear to become prone to attrition once they have been grown beyond a certain critical size in an agitated crystallizer. To some extent this can be attributed to increased damage from the agitator as higher rotational speeds are needed to keep them in suspension. Sometimes the critical size coincides with the onset of polycrystalline growth which tends to make the crystals friable. Polycrystalline growth, however, may not only render the crystals mechanically weak, but may even make the crystals thermodynamically

unstable (the Gibbs–Thomson effect – section 3.7) and dissolution would tend to occur at sharp edges and grain boundaries, i.e. at regions of very small radius, and cause the crystal to achieve a rounded shape. It is possible, therefore, that opaque egg-shaped crystals produced in many industrial crystallizers, are as much the result of sequences of crystallization–dissolution as of attrition.

6.5 Polymorphs and phase transformations

It is not uncommon in crystallization processes for the first crystalline phase to make its appearance to be metastable, e.g. a polymorph or hydrate (Ostwald's rule of stages – section 5.7). Some metastable phases rapidly transform to a more stable phase while others can exhibit apparent stability for an exceptionally long time. Some transformations are reversible (enantiotropic) while others are irreversible (monotropic), as explained in sections 1.8 and 4.2.1. In some cases, the metastable phase may have more desirable properties than the stable phase, e.g., a metastable pharmaceutical product may be more pharmacologically active than the stable form. If the required metastable form is first to crystallize, it is important to isolate and dry it quickly to prevent it transforming to the stable form. Once in the dry condition a metastable form can often remain unchanged indefinitely. If the stable polymorph is required, it is essential to create conditions and allow sufficient time in the crystallizer for total transformation to the more stable phase to be ensured.

Polymorphism is commonly encountered in crystalline substances. Calcium carbonate, for example, has three polymorphs, ammonium nitrate has five (section 1.8), and some organic compounds have many more. Aspirin, for example, was once thought to have 6 or 8 and phenobarbitone as many as 13, but it is always worth keeping in mind the somewhat provocative comment, generally attributed to McCrone (Dunitz and Bernstein, 1995), that the number of polymorphs discovered often seems to be proportional to the time and money spent looking for them.

Because polymorphs differ in the type of lattice, or in the spacing of the lattice points, they can exhibit different crystalline shapes and may often be readily identified by visual or microscopic observation. These characteristics, however, should not be confused with changes in crystal habit (section 6.4) which are caused solely by changes in the relative rates of growth of specific faces and do not affect the basic physical properties of the substance.

All crystals of one given substance, which may exhibit different habits, have identical physical properties. On the other hand, the different polymorphs of a given substance, which may also differ in habit, will exhibit different physical properties: density, hardness, melting point, solubility, reactivity, thermal properties, optical and electrical behaviour, etc. Each polymorph constitutes a separate phase of the given substance, in the Gibbs' phase rule sense, whereas crystals of different habit constitute the same phase. Polymorphs may transform in the solid state, but crystals of different habit cannot.

Strictly speaking, hydrates and other solvates are not polymorphs because they are different chemically from their parent compounds, although they do

have some similar characteristics to polymorphs such as being capable of transformation to more stable forms. Similarly, enantiomorphs (section 1.9) are not true polymorphs, although they share many of their characteristics, e.g., they do have different lattice structures, yet they are chemically identical. Furthermore, unlike polymorphs they have identical solubilities and/or melting points and cannot transform into one another. The separation of mixtures of enantiomers is discussed in section 7.1.3. Bernstein, Davey and Henk (1999) have drawn attention to a little appreciated phenomenon of the simultaneous crystallization of different polymorphs. They use the term ‘concomitant polymorphs’ to describe these mixtures that can occur and cause problems in industrial processes since the product crystals may show erratic variations in habit, colour, melting point, dissolution rates, etc., despite any evidence of process changes or impurity contamination.

Polymorphs and solvates can be identified and characterized by several analytical techniques including powder X-ray diffraction, IR and NMR spectroscopy. Differential scanning calorimetry (DSC) is useful for monitoring phase transformations and the hot-stage microscope is best for the identification of concomitant polymorphs.

Under specified conditions of temperature and pressure, except at a transition point, only one polymorph is thermodynamically stable. All others are unstable and potentially capable of transforming to the stable polymorph. Whether they will do so, however, is another matter entirely. The more stable polymorph has the lower free energy at a given temperature. If polymorph II is more stable than polymorph I then the chemical potential of the species in the solid phase II is lower than that in solid phase I, i.e.

$$\mu_{\text{II}} < \mu_{\text{I}} \quad (6.129)$$

Under equilibrium conditions, i.e. for the solid phase in contact with its saturated solution, the chemical potentials are identical for each species in the solid and solution phases, so it is possible to write

$$\mu_0 + \mathbf{R}T \ln a_{\text{II}} < \mu_0 + \mathbf{R}T \ln a_{\text{I}} \quad (6.130)$$

where μ_0 is the standard chemical potential and a is the solution activity, both being expressed on a common basis (section 3.6.1). Therefore,

$$a_{\text{II}} < a_{\text{I}} \quad (6.131)$$

and, since activity a and concentration c are related,

$$c_{\text{II}} < c_{\text{I}} \quad (6.132)$$

which leads to the important statement that, at a given temperature, the more stable phase will always have the lower solubility *in any given solvent*. Similarly, at a given pressure, the more stable phase will always have the higher melting point, but this information cannot be regarded as an infallible guide to the relative stability at some other temperature well below the melting point.

Typical solubility diagrams for substances exhibiting monotropic and enantiotropic behaviour are shown in *Figure 6.43*. In *Figure 6.43a*, form II, having

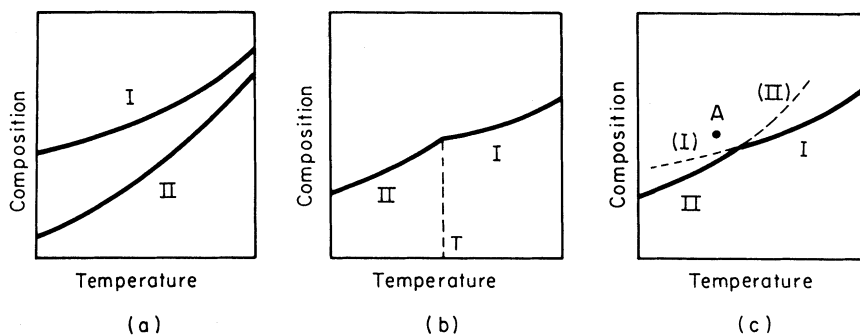


Figure 6.43. Solubility curves exhibiting (a) monotropy, (b) enantiotropy, (c) enantiotropy with metastable phases

the lower solubility, is more stable than form I. These two non-interchangeable polymorphs are monotropic over the whole temperature range depicted.

In *Figure 6.43b*, form II is stable at temperatures below the transition temperature T and form I is stable above T . At the transition temperature both forms have the same solubility and reversible transformation between these two enantiotropic forms I and II can be effected by temperature manipulation. *Figure 6.43c*, however, depicts the intervention of metastable phases (the broken line extensions to the two solubility curves) which bear evidence of the importance of kinetic factors which for a time may override thermodynamic considerations. For example, if a solution of composition and temperature represented by point A (supersaturated with respect to both I and II) is allowed to crystallize it would not be unusual if the metastable form I crystallized out first even though the temperature would suggest that form II is the stable form. This would simply be an example of Ostwald's rule (section 5.7) being followed. This behaviour would occur, for example, if form II had the faster nucleation and/or crystal growth rates. However, if the crystals of form I were kept in contact with the mother liquor, transformation could occur as the more soluble form I crystals dissolve and the less soluble form II crystals nucleate and grow.

An example of solvent-mediated transformation may be seen in *Figure 6.44* which comprises six frames from a time-lapse cine-micrograph showing metastable anhydrous sodium sulphate dissolving while the stable phase $\text{Na}_2\text{SO}_4 \cdot 10\text{H}_2\text{O}$ nucleates and grows. *Figure 6.45* shows two stages in the transformation of metastable vaterite into stable phase calcite crystals during the precipitation of calcium carbonate from aqueous solution.

Transformation is not certain even though a system enters a condition that will theoretically allow it. Transformation can only be ensured if a more stable solid phase is already present, is introduced, e.g. by deliberate seeding, or makes its appearance by nucleation. The rate of transformation may be influenced by retarding the rate of dissolution of the less stable species, e.g. by introducing specific impurities that act as inhibitors (Zhang and Nancollas, 1991).

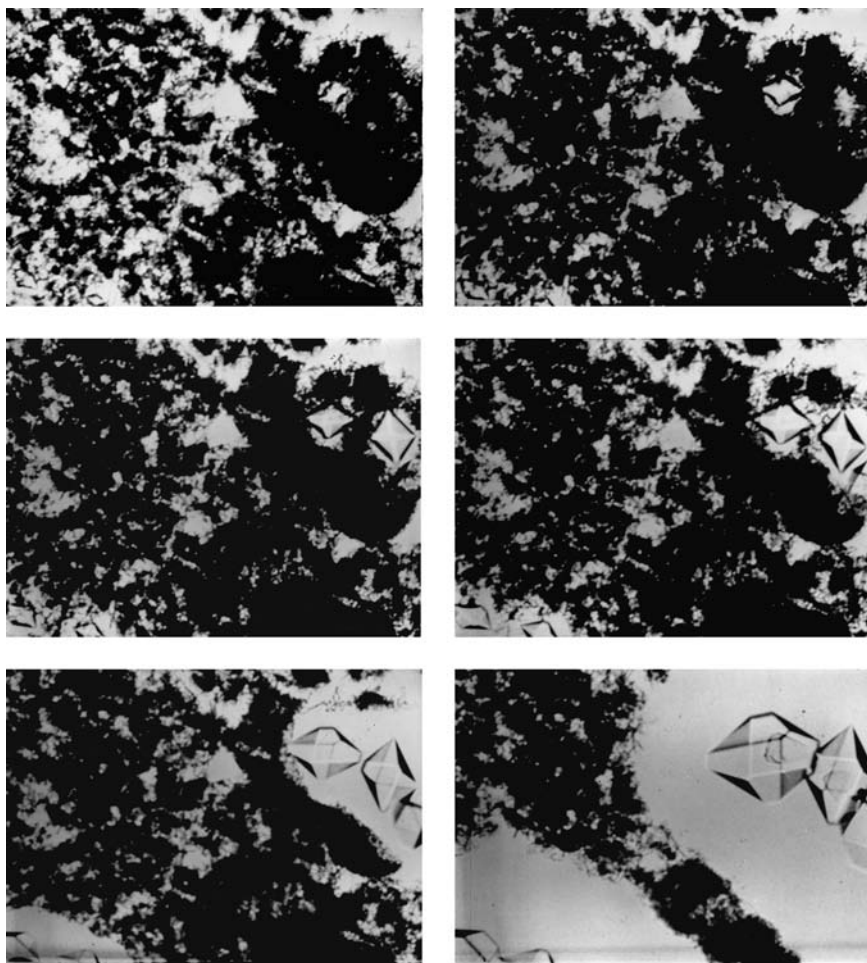


Figure 6.44. Six frames from a sequence of time-lapse cinemicrographs showing the solvent-mediated transformation of anhydrous Na_2SO_4 to $\text{Na}_2\text{SO}_4 \cdot \text{H}_2\text{O}$ at ambient temperature

Cardew and Davey (1985) proposed a model for solvent-mediated phase transformations with which they were able to simulate kinetic data for the α - β polymorphic transformation of copper phthalocyanine (Honigman and Horn, 1973). Solution-mediated transformations have been reported for stearic acid (Sato and Boistelle, 1984; Sato, Suzuki and Okada, 1985), magnesium phosphate hydrates (Boistelle, Abbona and Madsen, 1983) and L-glutamic acid (Kitamura, 1989) and L-histidine (Kitamura, Furukawa and Asaeda, 1994). In the cooling crystallization of L-glutamic acid, the metastable α form is the first to nucleate and grow, resulting in a crop of 100% α which if separated and dried quickly can be maintained indefinitely (Kitamura, 1989). On the other hand, if the α form is kept in contact with the crystallization mother liquor the solvent-mediated transformation to the β form, the stable polymorph, quickly

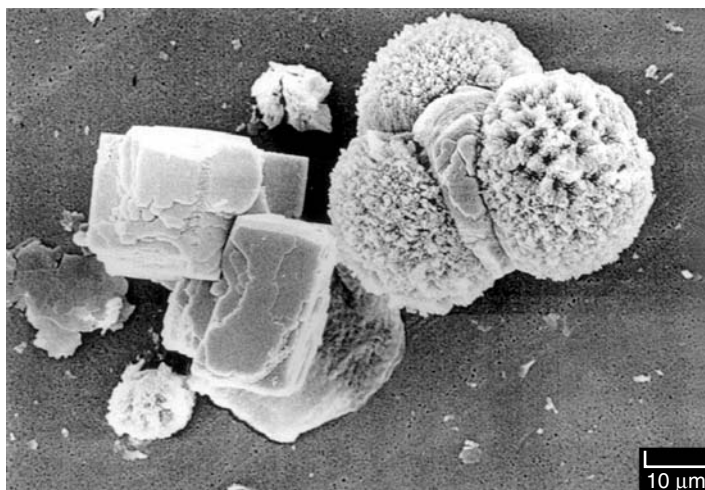


Figure 6.45. Solvent-mediated transformation of vaterite to calcite

ensues. Davey *et al.* (1997) have further examined this interesting system and described a molecular modelling technique that has led to the identification of additives that can selectively inhibit the $\alpha \rightarrow \beta$ transformation and allow kinetics to dominate the crystallization process so that the stable β polymorph is suppressed and the metastable α form stabilized.

Phase transformations can also occur in the solid state, and this mode is particularly common in organic solids held close to their melting point. The roles of both solid-state and solvent-mediated polymorphic transformations have been studied with ammonium nitrate by Davey, Guy and Ruddick (1985) and with oleic acid by Suzuki, Ogaki and Sato (1985).

The industrial process implications of polymorphic crystallizations are discussed in section 7.3.

6.6 Inclusions

Crystals generally contain foreign impurities, solid, liquid or gas, and the pockets of impurity are called ‘inclusions’. The term ‘occlusion’ has also been used in this connection, but it has also been applied to the surface fluid that becomes trapped between agglomerated crystals and left behind after filtration. For this reason, the term ‘inclusion’ is preferred because it tends to emphasize the entrapment of impurity *inside* a crystal.

Inclusions are a frequent source of trouble in industrial crystallization. Crystals grown from aqueous solution can contain up to 0.5% by mass of liquid inclusions, and their presence can significantly affect the purity of analytical reagents, pharmaceutical chemicals and foodstuffs such as sugar. Inclusions can cause caking (section 7.6) of stored crystals by the seepage of liquid if the crystals become broken.

Fluid inclusions may often be observed with the aid of a simple magnifying glass, although a more detailed picture is revealed under a low-power microscope with the crystal immersed in an inert liquid of similar refractive index. Alternatively the crystal may be immersed in its saturated solution and the type of inclusion may be identified by raising the temperature slightly to dissolve the crystal: if the inclusion is a liquid, concentration streamlines will be seen as the two fluids meet; if it is a vapour, the bubble will rise to the surface.

A number of terms have been used to describe inclusions, some of which are self-explanatory, such as bubbles, fjords (parallel channels), veils (thin sheets of small bubbles), clouds (random clusters of small bubbles), negative crystals (faceted inclusions) and so on. Most frequently inclusions are distributed randomly throughout the crystal, but sometimes they show a remarkable regularity, e.g. as in hexamine (Denbigh and White, 1966; Bourne and Davey, 1977) and ammonium perchlorate (Williams, 1981). Sometimes hour-glass or Maltese cross patterns may appear, e.g. as in sucrose (Powers, 1969/70; Mantovani *et al.*, 1985). Several examples of different types of inclusion in crystals are illustrated in *Figure 6.46*.

Inclusions may be classified as primary (formed during growth) or secondary (formed later). Primary fluid inclusions constitute samples of fluid in which the crystals grew. Secondary inclusions give evidence of later environments and are

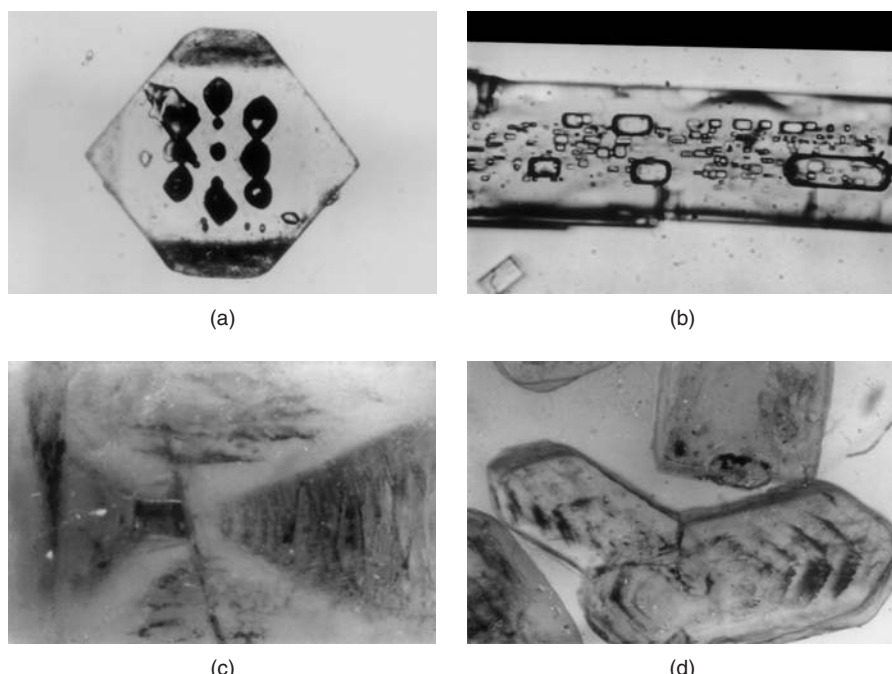


Figure 6.46. Some examples of liquid inclusions in crystals: (a) a regular pattern in ammonium perchlorate, (b) random aligned inclusions in potassium iodide, (c) an 'hour-glass' pattern in sucrose and (d) 'herring-bone' inclusions in sucrose

often formed as a result of crystals cracking due to internal stresses created during growth, incorporating mother liquor by capillary attraction and resealing later.

Inclusions readily form in a crystal that has been subjected to dissolution: rapid growth occurs on the partially rounded surfaces and entraps mother liquor. The rapid healing of dissolution etch pits will do the same. These 'regeneration' inclusions which usually lie in lines, i.e. along the former crystal edges, are characteristic of crystals grown from seeds.

Interrupted growth generally leads to inclusions. Brooks, Horton and Torgesen (1968) attributed the formation of inclusions in ADP and NaClO₄ crystals to the introduction of a sudden upward step-change in supersaturation. Belyustin and Fridman (1968) suggested that layer growth by the advancement of steps across the surface could be used to explain inclusions in KDP and NaClO₄. They concluded that the development of an inclusion at any point is governed by local conditions, more specifically by the concentration gradient along the height of a growth step. A critical step height was postulated beyond which a layer of solution can be trapped.

Large crystals and/or fast growth increase the likelihood of inclusions. Denbigh and White (1966) found that crystals of hexamine grew regularly when they were quite small, but after they had grown larger than about 70 µm, cavities began to form at the centre of the faces and these were later sealed over to produce a regular pattern of inclusions in the crystals. Cavities appeared to form, however, only if the growth rate exceeded a certain value when the crystal had reached its critical size. Similar conclusions concerning critical size and growth rate criteria have also been recorded for ammonium perchlorate (Williams, 1981) and terephthalic acid (Myerson and Saska, 1984). The much earlier work of Yamamoto (1939), however, had already identified the need to combine both size and growth rate when assessing inclusion potential. Some of Yamamoto's recalculated data for NaCl are presented in *Table 6.2* where it can be seen that the key factor is not the linear, but the

Table 6.2. Growth rate and appearance of sodium chloride crystals*

Crystal size L (10^{-4} m)	Growth velocity dL/dt (10^{-7} m s ⁻¹)	Volumetric growth rate [†] dV/dt (10^{-15} m ³ s ⁻¹)	Crystal appearance
1.0	2.9	9	transparent
1.2	2.9	13	transparent
1.2	3.8	16	transparent
2.0	1.4	17	transparent
1.7	2.6	23	opaque
1.5	3.7	25	opaque
1.8	4.1	40	opaque
2.0	3.7	44	opaque
3.0	1.8	49	opaque

* Calculated from data of Yamamoto (1939)

† Volumetric rate increase $dV/dt = 3L^2 \cdot dL/dt$

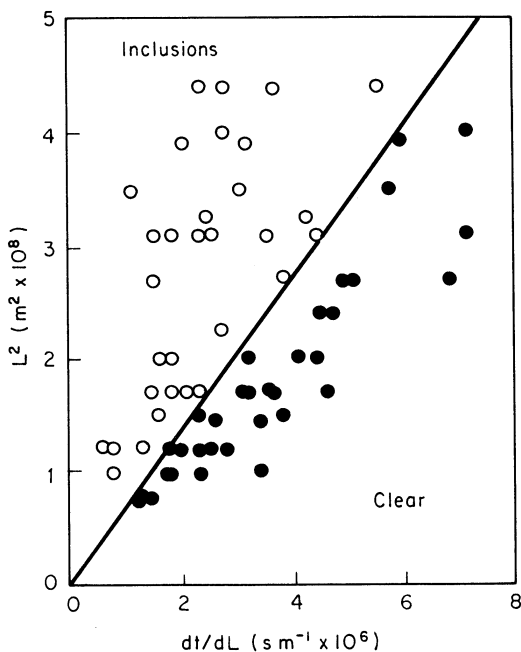


Figure 6.47. Criteria for the avoidance of mother liquor inclusions in sodium chloride crystals. (After Yamamoto, 1939)

volumetric, growth rate that is important. Figure 6.47 suggests another way of setting a dividing line between the inclusion and inclusion-free zones.

The questions of why a cavity often forms at a face centre and why it subsequently seals over have been the subjects of much speculation. The work of Bunn (1949) and Humphreys-Owen (1949) showed that the supersaturation is generally lower at the centre of the crystal face than at the edges, but small crystals tend to grow layerwise away from the centres. Bunn's explanation for this unexpected finding was that the diffusion field around a small crystal would tend to develop spherical symmetry and this results in the component of the concentration gradient normal to the face being greater near the centre than near the edges, thus causing more solute to be transported to the centre. However, when the crystal is large enough, the above situation is reversed (Denbigh and White, 1966) and the corners and edges grow more rapidly than the face centres, and cavities form. Later, when the face grows beyond a certain size, growth layers are generated on the macroface, grow inwards and meet to seal the inclusion, as indicated diagrammatically in Figure 6.48 (Murata and Honda, 1977; Dzyuba, 1983; Sato, 1988).

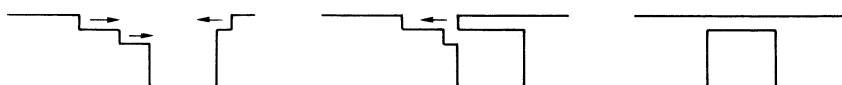


Figure 6.48. Development of a mother liquor inclusion by the interaction of growth layers of different height and velocity

The adsorption of impurities, including the solvent, on the crystal surface can also lead to impeded growth and hence to inclusions. There is evidence that crystals reject impurity during growth, and for this reason liquid inclusions may be richer in impurities than the mother liquor from which the crystals grew. Growth instabilities on crystal faces resulting in dendritic growth can also lead to the trapping of mother liquor by the side-branching and impingement of dendrites (Myerson and Kirwan, 1977). Solid particles may also be included into the crystal particularly at the nucleation stage when foreign bodies act as heteronuclei. Saito *et al.* (1998, 1999) have shown that physical contacts between crystals and/or the temporary attachment of small crystal fragments, such as attrition nuclei, significantly enhance the growth rate of the particular face for a short period during which generated macrosteps interact and entrap mother liquor. This work was carried out with sodium chloride crystals, but the mechanisms postulated could be of more general application.

Inclusions may sometimes be prevented if the crystals are grown in the presence of certain ionic impurities, e.g. traces of Pb^{2+} and Ni^{2+} allow near-perfect crystals of ADP to be grown for piezoelectric use; traces of Pb^{2+} help good crystals of NaCl to be grown. Anionic surfactants are particularly effective for eliminating inclusions in ammonium perchlorate growth from aqueous solution (Hiquily and Laguerie, 1984). A change of solvent may have a significant effect. Hexamine, which readily develops inclusions when grown from aqueous solution, contains none when grown from methanol or ethanol. An increase in the viscosity of the mother liquor may also help; small amounts of carboxymethyl cellulose added to the solution have been known to have a beneficial effect. Ultrasonic vibrations have also been tried with moderate success.

Under isothermal conditions inclusions may change shape or coalesce as the internal system adjusts itself towards the condition of minimum surface energy. If the temperature is raised, negative crystals (faceted inclusion cavities) may be formed by a process of recrystallization. Fluid inclusions cannot be removed by heating alone. In fact even heating to decrepitation frequently fails to destroy all the inclusions. However, liquid inclusions can actually move under the influence of a temperature gradient. Since solubility is temperature dependent, crystalline material dissolves on the high solubility side of the inclusion, diffuses across the liquid and crystallizes out on the low solubility side (Wilcox, 1968). Henning and Ulrich (1997) measured migration rates of water inclusions in crystal layers of captolactam induced by temperature gradients. Migration progressed towards the warm surface at rates proportional to the temperature gradient while inclusions increased in size and changed their shape. Large inclusions moved faster than small ones. The relevance of these observations to industrial solid-layer melt crystallization processes (section 8.4) was discussed.

A general review of inclusions has been written by Deicha (1955). Powers (1969/70) and Mantovani *et al.* (1985) give comprehensive accounts of inclusions in sugar crystals, and a world-wide coverage of research on inclusions, although mainly of geological interest, is provided by the annual COFFI (1968 ff) reviews. A practical guide to fluid inclusion studies, with a geological bias, has been written by Shepherd, Rankin and Alderton (1985).

7 Recrystallization

7.1 Recrystallization schemes

It is often possible to remove the impurities from a crystalline mass by dissolving the crystals in a small amount of fresh hot solvent and cooling the solution to produce a fresh crop of purer crystals, provided that the impurities are more soluble in the solvent than is the main product. This step may have to be repeated many times before a yield of crystals of the desired purity is obtained, depending on the nature of the phase equilibria exhibited by the particular multicomponent system (Chapter 4). A eutectic system, for example, can yield a near-pure crystal product in one step (see *Figure 4.4*) whereas a solid solution system would need many (see *Figure 4.7*).

A simple crystallization scheme is shown in *Figure 7.1*. An impure crystalline mass AB (A is the less soluble pure component, B the more soluble impurity) is dissolved in the minimum amount of hot solvent S and then cooled. The crop of crystals X_1 will contain less impurity B than the original mixture: but if the desired degree of purity has not been achieved, the procedure can be repeated: crystals X_1 are dissolved in more fresh solvent S and recrystallized to give a crop X_2 , and so on.

In a sequence of operations of the above kind the losses of the desired component A can be considerable, and the final amount of ‘pure’ crystals may easily be a minute fraction of the starting mixture AB . This question of yield from recrystallization processes is of paramount importance, and many schemes have been designed with the object of increasing both yield and separation efficiency. The choice of solvent depends on the nature of the required substance A and the impurity B . Ideally, B should be very soluble in the solvent at the lowest temperature employed, and A should have a high temperature coefficient of solubility so that high yields of A can be obtained from operation within a small temperature range. Some of the factors affecting the choice of a solvent are discussed in section 3.2.

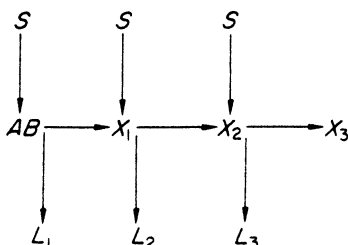


Figure 7.1. Simple recrystallization

A modification of the simple recrystallization scheme in *Figure 7.2*: additions of the original impure mixture AB are made to the system at certain intervals. The first two stages are identical with those illustrated in *Figure 7.1*, but the crystals X_2 are set aside and fresh feedstock AB is dissolved by heating in mother liquor L_2 . On cooling, a crop of crystals X_3 is obtained and a mother liquor L_3 , which is discarded. Crystals X_3 are recrystallized from fresh solvent to give a crop X_4 , which is set aside; the mother liquor L_4 can, if required, be used as a solvent from which more feedstock can be crystallized. If the crops X_2 , X_4 , X_6 , etc. are still not pure enough, they can be bulked together and recrystallized from fresh solvent.

The triangular fractional recrystallization scheme shown in *Figure 7.3* makes better use of the successive mother liquor fractions than does that of *Figure 7.2*. Again, A and B are taken to be the less and more soluble constituents, respectively. The mixture AB is dissolved in the minimum amount of hot solvent S , and then cooled. The crop of crystals X_1 which is deposited is separated from the mother liquor L_1 and then dissolved in fresh solvent. The cooling and separating operations are repeated, giving a further crop of crystals X_2 and a mother liquor L_2 . The first mother liquor L_1 is concentrated to yield a crop of crystals X_3 and a mother liquor L_3 . Crystals X_3 are dissolved by warming in mother liquor L_2 and then cooled to yield crystals X_5 and liquor L_5 . Crystals X_2 are dissolved in fresh hot solvent and cooled to yield crystals X_4 and liquor L_4 . Liquor L_3 is concentrated to give crystals X_6 and liquor L_6 . The scheme can be continued until the required degree of separation is effected. The less soluble substance A is concentrated in the fractions on the left-hand

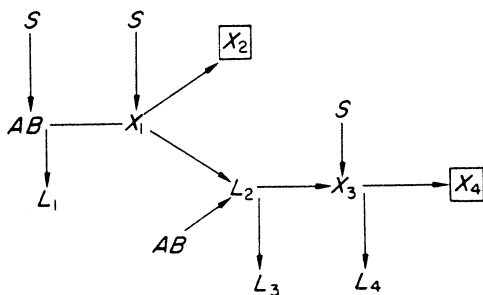


Figure 7.2. Simple recrystallization with further additions of feedstock

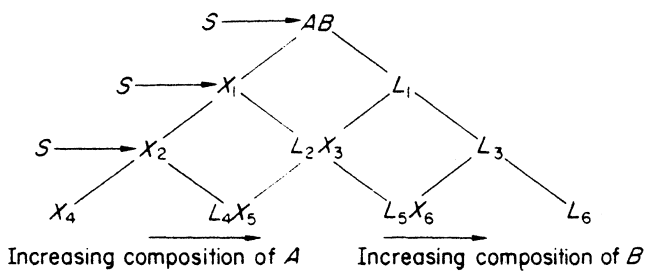


Figure 7.3. Fractional recrystallization of a solution (triangular scheme)

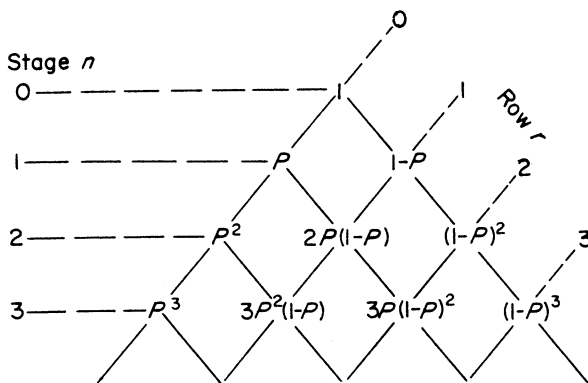


Figure 7.4. Analysis of the triangular fractional crystallization

side of the diagram, the more soluble constituent *B* on the right-hand side. If any other substances with intermediate solubilities were present, they would be concentrated in the fractions in the centre of the diagram.

If the starting material contained a unit quantity of component *A*, and each crystallization step resulted in the deposition of a proportion *P* of this component, the proportions of *A* which would appear at any given point in the triangular scheme (see *Figure 7.4*) would be given by a term in the binomial expansion

$$[P + (1 - P)]^n = 1 \quad (7.1)$$

$$p_{n,r} = \frac{n!}{r!(n-r)!} \cdot P^{n-r}(1 - P)^r \quad (7.2)$$

where $p_{n,r}$ = proportion of *A* at a point represented by row *r* and stage *n*. Thus, for example,

$$\begin{aligned} p_{3,2} &= \frac{3!}{2!} \cdot P^{(3-2)}(1 - P)^2 \\ &= 3P(1 - P)^2 \end{aligned}$$

A modification of the triangular scheme is shown in *Figure 7.5*. In this case further quantities of the feedstock *AB* are added to the system by dissolving it in successive mother liquors on the right-hand side of the diagram. This scheme is particularly useful if component *A* has a high temperature coefficient of solubility.

Several other much more complex schemes for fractional recrystallization can be used, their aim being to increase the yield of the desired constituent by further re-use of the mother liquors. A detailed account of these methods has been given by Tipson (1956). *Figure 7.6* illustrates two of them. In the 'diamond' scheme (*Figure 7.6a*) the outermost fractions are set aside when they have reached a predetermined degree of purity, and fractionation is continued until all the material is obtained either in a crystalline form or in solution in a final mother liquor. If necessary, various crystal fractions can be bulked

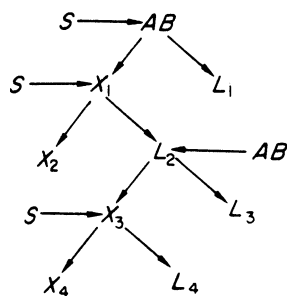


Figure 7.5. Simple recrystallization with further additions of feedstock

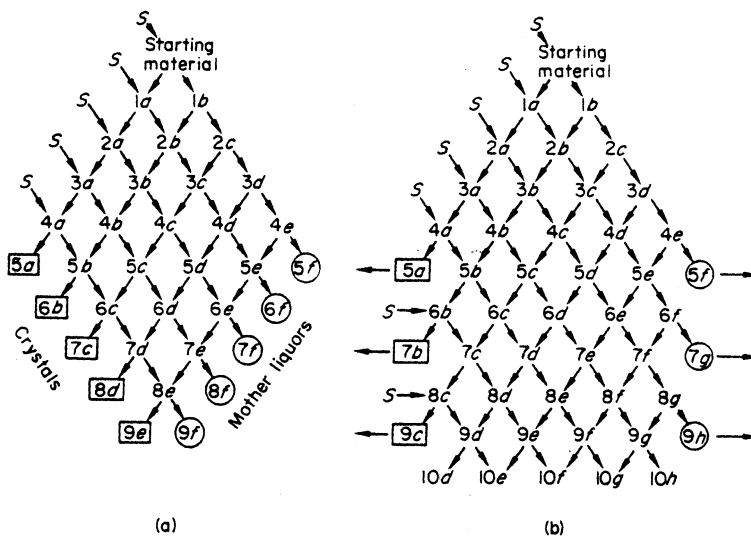


Figure 7.6. Fractional recrystallization schemes: (a) diamond; (b) double withdrawal. (After Tipson, 1956)

together and recrystallized, and in a similar manner the mother liquors can receive further treatment.

Unfortunately, the various fractions obtained by the diamond scheme will differ in composition, and relatively pure crystals will be mixed with relatively impure ones. This difficulty can be overcome by the use of the 'double-withdrawal' scheme shown in *Figure 7.6b*. The procedure is the same as that used in the diamond scheme up to the point where no further fresh solvent is used (line 5 in *Figure 7.6a*). At this point it is assumed that crystals 5a and mother liquor 5f have reached the desired degree of purity, and they are both set aside from the system. Fresh solvent is then added to the crystal crop 6b to yield a purer crop 7b, which is arranged to have a purity similar to that of crop 5a. Crop 7b is set aside, crop 8c crystallized from pure solvent, and so on.

Theoretical analyses and surveys of the factors affecting the choice of different fractional crystallization schemes have been made by Doerner and Hoskins

(1925), Sunier (1929), Garber and Goodman (1941) and Tipson (1956). Joy and Payne (1955) have discussed problems associated with the fractional crystallization of similar substances where one substance is present in very small amount. The use of the Chlopin (1925) and Doerner and Hoskins (1925) relationships, which describe the distribution of isomorphous impurities between solid and solution phases, is further discussed in section 7.2.3.

Procedures for the design of industrial fractional crystallization processes for multicomponent systems, utilizing appropriate eutectic and solid solution phase diagrams, have been described by Fitch (1970, 1976), Chang and Ng (1998), Cisternas (1999), Cesar and Ng (1999) and Wibowo and Ng (2000).

Theoretical stages

The number of theoretical stages required in a process of fractional crystallization from solution can be analysed by the well-known McCabe–Thiele and Ponchon–Savarit graphical methods commonly used for fractional distillation (Matz, 1969). In the Ponchon–Savarit diagram (upper section of *Figure 7.7*) the abscissa records crystal compositions, x , or mother liquor concentrations, y . The ordinate represents the solvent–solute mass ratio, N . The system used here as an example is lead and barium nitrates in water, which form a continuous series of solid solutions with no hydrate formation. The N – x curve, therefore, is the abscissa of the diagram ($N = 0$) and the N – y curve has no discontinuities. The region between the N – x and N – y curves represents solid–liquid mixtures. As in similar diagrams for liquid–liquid and vapour–liquid systems, this area is interlaced with tie-lines whose end-points correspond to the solid (x) and liquid (y) phase compositions in equilibrium.

Equilibrium values from the upper Ponchon–Savarit diagram are used to construct the equilibrium curve in the lower McCabe–Thiele diagram as follows. For a given tie-line, a vertical line is drawn down from the end-point on the N – y curve on to the diagonal ($x = y$) in the lower diagram. A horizontal line is then drawn to the left to meet the vertical from the other end-point of the tie-line on the N – x curve. The intersection gives a point on the equilibrium curve. This procedure is repeated.

The inlet and exit streams (F = feed, C = crystals, S = solution) can be located on the operating diagram. Points S_1 and C_0 represent the solution leaving and the crystal ‘reflux’ entering the top (stage 1) of the crystallization section. Points S_{n+1} and C_n represent the solution ‘reflux’ entering and the crystals leaving the bottom (stage n) of the concentration section. The minimum crystal reflux ratio, R_{\min} , is obtained by extending the tie-line through F to meet the vertical from C_0 at P . Then

$$R_{\min} = \frac{\text{distance } PS_1}{\text{distance } S_1 C_0} \quad (7.3)$$

For reflux ratio $R > R_{\min}$ (where $R = QS_1/S_1C_0$) the operating line passes through F more steeply than the tie-line and determines the solution and crystal ‘poles’ Q and W . Arbitrarily drawn lines radiating from these poles are used in

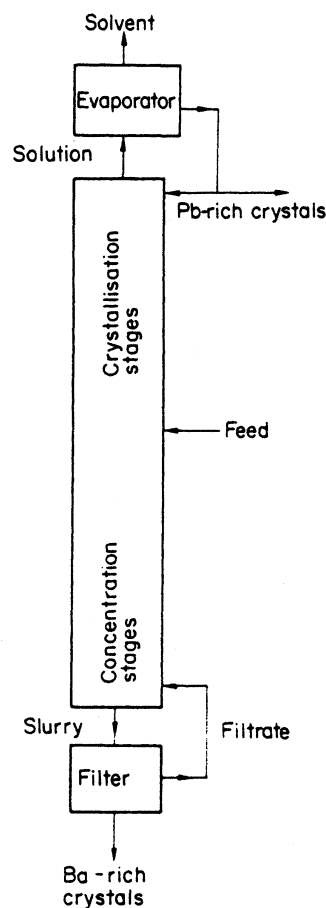
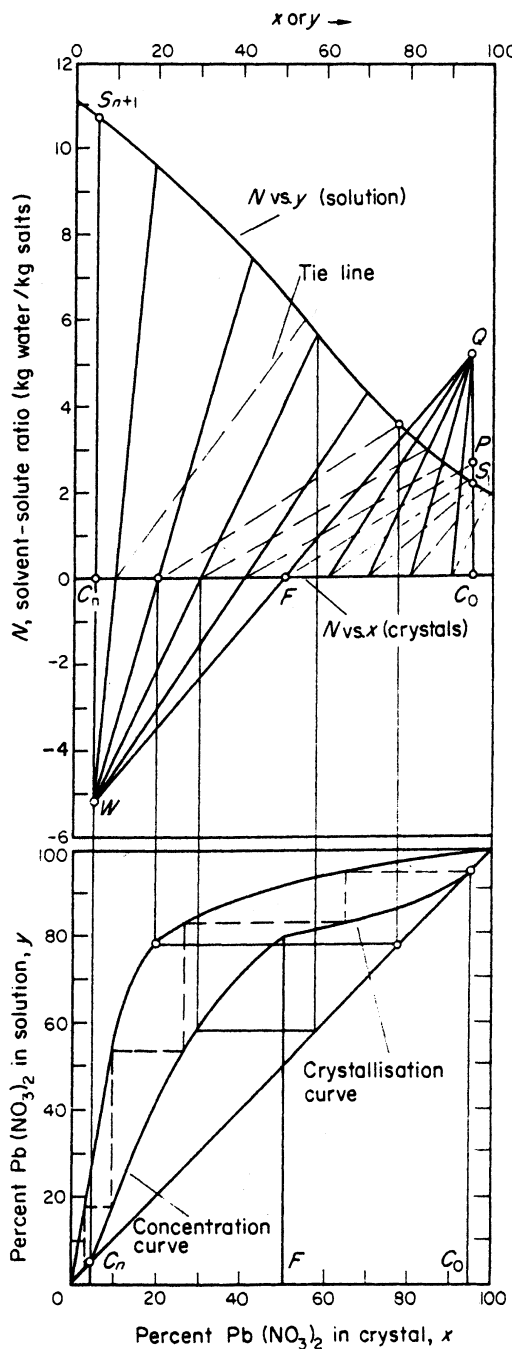


Figure 7.7. Ponchon-Savarit and McCabe-Thiele diagrams for the fractional crystallization of lead and barium nitrates from aqueous solution. (After Matz, 1969)

the construction of the ‘crystallization’ and ‘concentration’ curves in the lower McCabe–Thiele diagram, in the same way as the tie-lines are used to construct the equilibrium curve.

The continuous fractional crystallization of a mixture of $\text{Pb}(\text{NO}_3)_2$ (the more soluble component) and $\text{Ba}(\text{NO}_3)_2$ (the less soluble) is shown diagrammatically at the right of *Figure 7.7*. This scheme is similar to that for fractional distillation or countercurrent extraction, but it is not essential to operate the process in a column; any arrangement of contact vessels which provides the necessary stage-wise countercurrent contact of solid and liquid phases would suffice. In the scheme depicted $\text{Ba}(\text{NO}_3)_2$ crystallizes out in the upper ‘crystallization’ section, above the feed entry point, and $\text{Pb}(\text{NO}_3)_2$ dissolves in the lower ‘concentration’ section. The crystals, which progress downwards, are therefore enriched in Ba, and the solution, which progresses upwards, is enriched in Pb. The Ba-rich crystals are removed through a filter and the filtrate is returned to the column as ‘reflux’. The Pb-rich solution leaving the top of the column is evaporated to yield Pb-rich crystals, some of which are returned as ‘reflux’ at the top of the column.

To produce crystals containing 95 per cent $\text{Ba}(\text{NO}_3)_2$ at the top and 95 per cent $\text{Pb}(\text{NO}_3)_2$ at the bottom from a 50 per cent feedstock, using a reflux ratio of 1.36, four theoretical stages would be adequate as shown. The upper Ponchon–Savarit diagram could also be used to determine the number of theoretical stages.

7.2 Resolution of racemates

The resolution of racemic mixtures, i.e., the separation of at least one of the enantiomers in pure form, is an important step in the manufacture of chiral products in the pharmaceutical, agrochemical, flavour and perfumery industries and for other specialty chemicals. The necessity to resolve racemic mixtures is particularly strong in the pharmaceutical industry since the two component enantiomers (see section 1.9 for definition of terms) in the equimolar mixture can have very different pharmacological activities. Thalidomide is a frequently quoted example: one stereoisomer was the beneficial agent for preventing morning sickness in pregnant women while the other caused serious birth defects.

A crystalline racemate, may be either a *conglomerate* (an equimolar physical mixture of two enantiomorphs) or a *racemic compound* (two enantiomers homogeneously distributed in the crystal lattice). Conglomerates, the much rarer (< 10%) of the two types of racemate are easier to resolve. The mixture of **D** and **L** crystals can sometimes be distinguished under a microscope and in very rare cases can even be separated by hand, as in the case of sodium ammonium tartrate (section 1.9.1). In practice, however, manual sorting is impossible and resolution by crystallization is the usual means of producing at least one of the **D** or **L** enantiomers in pure form. The **D**, **L** system of molecular classification, which is still commonly encountered, is being used here as an alternative to the more rigorous **R**, **S** system (section 1.9) since the

symbols R and S are used in the following phase diagrams to denote racemate and solvent respectively.

The phase equilibria for a racemic mixture can be represented on a binary phase diagram with composition as the abscissa and temperature as the ordinate. *Figure 7.8a* represents a conglomerate system and *Figure 7.8b* indicates the formation of a racemic compound. Both of these diagrams are symmetrical, unlike those for non-chiral systems (as in *Figures 4.4* and *4.5*). For example, a conglomerate system has one eutectic point, at the 50 : 50 D : L composition. Any solution to the left of it can produce pure D crystals and solutions to the right yield pure L crystals. On the other hand, the racemic compound system has two eutectic points equidistant from the 50% mark representing the composition of the racemic compound which cannot be resolved into either of the pure enantiomers in a single crystallization operation.

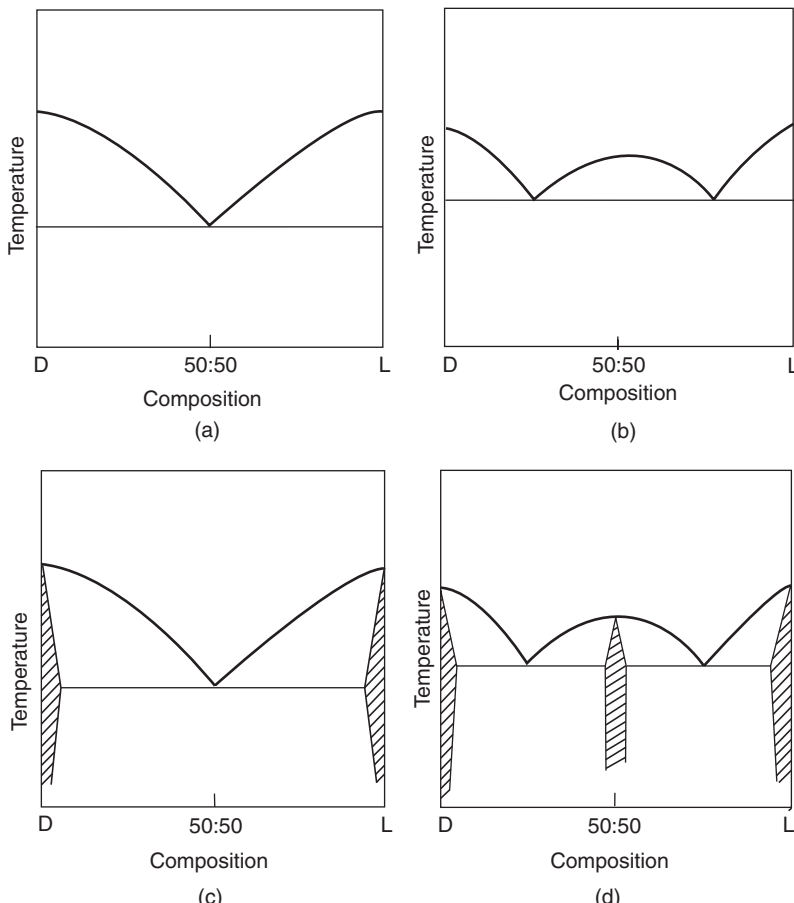


Figure 7.8. Phase diagrams: (a) and (c) for conglomerates; (b) and (d) for racemic compounds. (c) and (d) illustrate the potential existence of very narrow zones of terminal solid solutions (After Jacques, Collet and Wilen, 1981)

At this point an explanation of the term ‘pure’ might be helpful. For many industrially bulk-produced organic chemicals a purity of >95% is often accepted as justifying the designation ‘pure’. For some specialty chemicals a purity of >99% may be demanded. For purities >99.9% the term ‘ultra pure’ is frequently applied. For many chiral products, an enantiomeric purity of around 98% can be acceptable since up to about 2% of the other enantiomer usually has little or no adverse effect on the activity of the product. In any case, a crystallization operation cannot produce 100% pure crystals for a variety of reasons, e.g., they can be contaminated with residual solution- or reaction-based impurities that have not been removed by washing, or have been incorporated into the crystal interstitially or as liquid inclusions, and so on. Furthermore, account should be taken of what has been called *terminal solid solutions*, which inevitably accompany both eutectic and chemical compound systems, as shown in Figures 7.8b and 7.8c where the zones of miscibility (solid solutions), are identified by the shaded areas which are greatly enlarged for ease of visualization (Jacques, Collet and Wilen, 1981). These very narrow zones are generally impossible to detect with any certainty since the melting point or solubility data needed to draw the phase diagram are insensitive to such small quantities of impurity.

A mixture of D and L enantiomers in the presence of a solvent S constitutes a ternary system in which the equilibria are best represented on a triangular diagram (see section 4.6.3). The effects of temperature on solubility and phase change can also be included. Figure 7.9a shows the transition of a racemic compound R, stable at the lower temperatures t_1 and t_2 , to a conglomerate at the higher temperature t_3 .

Phase diagrams such as those depicted in Figures 7.8 and 7.9 can readily be constructed by measuring the solubilities of a range of mixtures of the two enantiomers and determining their equilibria by methods described in section 4.5. At all times during equilibrium determination undissolved solid must

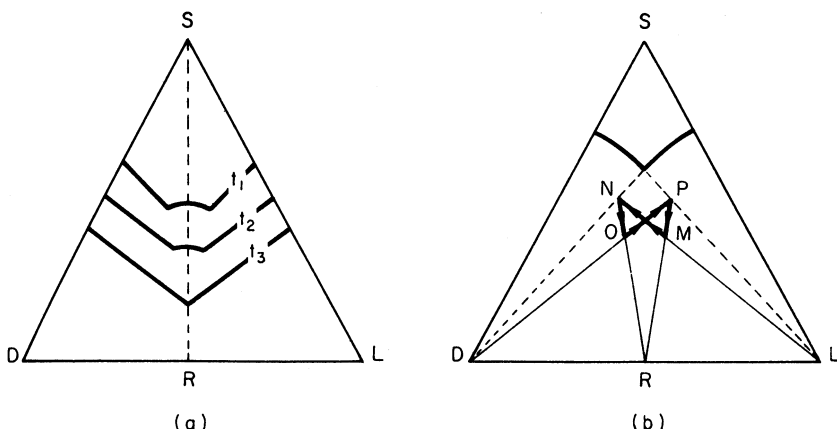


Figure 7.9. Resolution of racemates: (a) isotherms on a ternary diagram (temperature $t_1 < t_2 < t_3$); (b) simple recrystallization procedure for a conglomerate. (S = solvent, R = racemic composition, 50% D:L)

remain in agitated contact with solution. Equilibration in such systems can take some considerable time and it is recommended that samples are analysed at 1-day intervals until equilibrium is achieved, preferably from both the over- and under-saturated conditions (section 3.9). Subsequent analyses of the equilibrium saturated solutions and their corresponding solid phases can be made by the appropriate techniques described in section 3.9.1.

A simple recrystallization procedure for the resolution of conglomerate systems is shown in *Figure 7.9b*. A convenient starting point is point M, representing a metastable aqueous solution containing the racemate R and a slight excess of enantiomer L. This solution may first be prepared at an elevated temperature and then cooled to the phase diagram temperature. At point M the solution is supersaturated with respect to both enantiomers, but more supersaturated with respect to L. Enantiomer L is induced to crystallize alone by adding a few L seeds and the mother liquor composition moves from M to N following the line LMN to the extent that at N its optical rotation is roughly of equal magnitude, but opposite sign, to that at M. The now dextrorotatory mother liquor is then separated from the L crystals and used to dissolve an equivalent mass of racemate R to yield, by heating and subsequent cooling, a metastable supersaturated solution O. D seeds are then added to induce crystallization of enantiomer D and the mother liquor composition changes from O towards P. At P enantiomer D is recovered, more racemate R is dissolved in the mother liquor, and the cycle is repeated. A possible flow scheme, with a recycle loop, for the continuous seeded crystallization of a conglomerate system is shown in *Figure 7.10*.

Examples of different crystallization procedures have been given by Secor (1963); Collet, Brienne and Jacques (1980); Jacques, Collet and Wilen (1981); Asai (1983); Samant and Chandalla (1985); Sheldon (1993); Collins, Sheldrake and Crosby (1995).

Racemic compound systems, which account for more than 90% of all racemic mixtures, cannot be resolved by direct crystallization, but a common

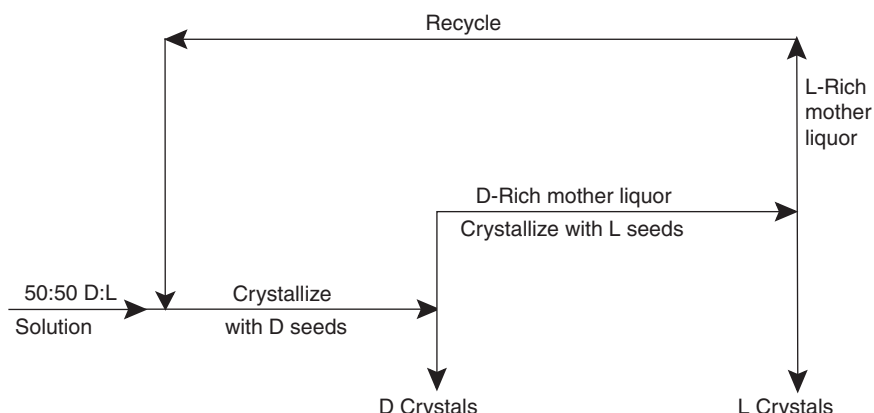


Figure 7.10. Flow diagram for the continuous crystallization of a conglomerate system. (After Stahly and Byrn, 1999)

route to resolution is to react the 50 : 50 mixture of the (+) and (−) enantiomers with an optically pure resolving agent, e.g., an acid or base (most usually an amine), to give a mixture of diastereomers which are non-enantiomeric (++) and (−+) and hence have different physical properties. For example, a racemate of an acidic substance A with, say, the dextro form of an optically active base B will give



and the two salts (+)-A · (+)-B and (−)-A · (+)-B can be separated by fractional crystallization. The phase diagram of such a mixture is generally asymmetric and crystallization will yield crystals enriched in one of the isomers. Practical examples have been given by Jacques, Collet and Wilen (1981); Yokota *et al.* (1998) and Stahly and Byrn (1999).

Crystallization from the melt (usually at low temperature) is also a possibility for recovering enantiomers. A temperature–composition phase diagram for a conglomerate is the same as that for a eutectic system containing two components D and L (section 4.3.1). The special feature of the conglomerate diagram is its symmetry, which arises from the thermodynamic identity of the D and L enantiomers (melting point, enthalpy of fusion, etc.) giving the eutectic an equimolar racemic composition R (*Figure 7.11*). The following procedures are possible.

The liquid conglomerate is supercooled, following a path from say X through E to point Y below the solidus. The two liquidus curves for D and L may be extended (dotted lines) beyond E into the metastable region. At point Y, seeds of one of the enantiomorphs are added. L seeds, for example, cause L crystals to be deposited and the residual liquid becomes richer in D. By the mixture rule (section 4.3), one mole of racemate gives MY/MO mole of pure L and YO/MO

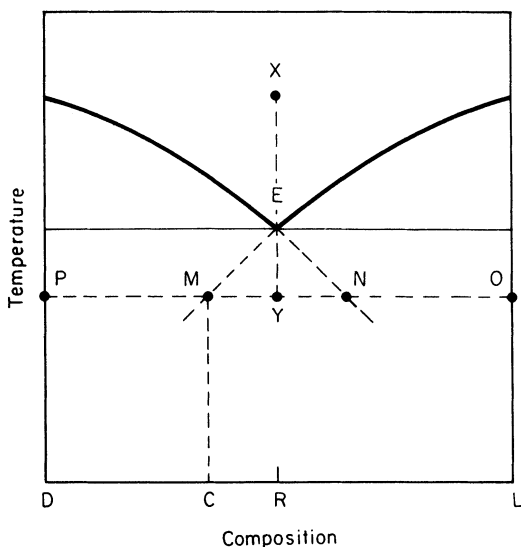


Figure 7.11. Recrystallization of a conglomerate from the melt

mole of residual liquid of composition c . The L crystals are then separated and the D-rich liquid is seeded with D to give a crop of D crystals. This process of alternate L and D seeding can be repeated.

The yield from each crystallization depends on the ratio MN/PN, which increases with the supercooling EY. It is, of course, necessary to find the optimal conditions of temperature and agitation which allow maximum yields of D and L without disturbing the metastable conditions on which the process depends (Collet, Brienne and Jacques, 1980).

Sublimation (section 8.3) could have a role to play in the separation of enantiomers since the vapour phase arising from a solid mixture of enantiomers is always racemic, irrespective of the ratio of enantiomers present in the solid. Therefore, if the starting solid contains unequal amounts of enantiomer, sublimation will increase the purity of the major component in the residual solid phase. There does seem to be a possibility for improving the purity of near-pure enantiomers, e.g. those that had been partially resolved by other methods. However, as only a few experimental studies of enantiomer separation by sublimation have so far been recorded, the technique must still be regarded as speculative (Jacques, Collet and Wilen, 1981).

7.3 Isolation of polymorphs

The ability of a single compound to crystallize in more than one crystallographic form (polymorphism) is encountered in a wide range of industries including pharmaceuticals, dyestuffs, agrochemicals, photochemicals, and other specialty compounds, both organic and inorganic. Similarly, it may also be possible to crystallize several different solvates, e.g., hydrates, which although not strictly speaking polymorphs can also be included in the general considerations outlined below.

As described in section 6.5, the different polymorphs of a given substance, although chemically identical, exhibit different physical properties that can considerably affect the end-use of the material. For example, one polymorph of a pharmaceutical compound may have quite significant differences in bioavailability and pharmacological action from another. It is essential, therefore, when investigating a new chemical substance with a view to eventual industrial production, to investigate at an early stage the possibility of the existence of different polymorphs or solvates and how they may be isolated. Without such an investigation, new phases may make a sudden appearance years after the development of the first form and this can often be very inconvenient. However, as Bavin (1989) has pointed out, the existence of different polymorphs or solvates need not always be considered as a problem. Indeed, if discovered early enough, they may have potential commercial advantages in allowing increased patent coverage and greater flexibility in, for example, the formulation of pharmaceuticals.

For monotropic polymorphs (*Figure 6.42a*) only one form is thermodynamically stable at all temperatures in the range considered. All other forms are metastable and potentially capable of transforming into the stable form. For

enantiotropic polymorphs (*Figure 6.42b*) two or more forms are thermodynamically stable over different temperature ranges. In these cases it is essential to identify the transition temperatures as accurately as possible since they mark boundaries that should be avoided when planning processing operations. Furthermore, compounds with transition temperatures in the ambient range are likely to cause problems in subsequent storage and use.

A number of guidelines for the laboratory procedures that can be adopted in the preliminary search for possible polymorphs or solvates have been proposed Bavin (1989) and Nass (1991). These include: crystallizing from a wide range of solvents (polar, non-polar, hydrophilic and hydrophobic) at different temperatures; chilling saturated solutions rapidly; precipitation by rapid quenching with a liquid non-solvent; heating excess solid with a high boiling solvent; crystallization from the melt or by sublimation, and so on. The identity and purity of all product crystals should then be checked by appropriate analytical techniques (McCauley, 1991). See also section 3.9.1.

Once the polymorphs or solvates have been isolated and identified, samples can be used as seed crystals in subsequent crystallization operations to promote the production of a specific form. Seeding is particularly necessary in cases involving the so-called concomitant polymorphs (Bernstein, Davey and Henk, 1999), the phenomenon of different polymorphs crystallizing simultaneously (section 6.5). It is important to identify any process conditions that could result in polymorphic transformation, e.g., the initiation of a solvent-mediated transformation in monotropic systems during a drying operation. Solid phase transformations can be temperature dependent, but they can also occur during energetic processes such as grinding or tabletting (Pirttimaki *et al.*, 1993).

The process implications of polymorphism in organic compounds has been considered by Nass (1991) who outlined some general recommendations for the batch cooling crystallization of a desired polymorph, either stable or metastable. First, it is necessary to isolate and identify each polymorph and to generate solubility data in more than one solvent in order to determine if the system is monotropic or enantiotropic. This information will help in the selection of a solvent for the industrial process, although the ultimate choice will also have to include considerations of process yield, solvent recovery costs, hazards, etc.

For enantiotropic systems the temperature range of the crystallization process will be determined by the particular polymorph required. If it is metastable below the transition temperature, crystallization should begin just above transition temperature, where the kinetics are relatively slow. Seeding with the desired polymorph at this point is recommended. If the required polymorph is stable below the transition temperature, seeding should be commenced just below the transition temperature.

Seeding is also recommended for monotropic systems. For the stable polymorph, the temperature after seeding should be held constant for a predetermined time to allow the solution to desupersaturate, after which an appropriate cooling profile (section 7.5.5) should be adopted to maintain a constant controlled supersaturation. If the metastable polymorph is required, and the

solution is supersaturated with respect to the stable form, the solution should be seeded with the metastable form and cooled rapidly to avoid any solvent-mediated transition. As noted above, the drying conditions for metastable polymorphs must be chosen carefully to avoid any solvent-mediated transformation occurring.

7.4 Recrystallization from supercritical fluids

At temperatures and pressures above the critical point, where liquid and vapour phases are no longer distinguishable (section 4.2) supercritical fluids (SCFs) exhibit very different properties from those of their corresponding liquid and gaseous phases. For example, the dielectric constant of liquid water (~ 81) falls to around 2 for supercritical water at which value, since it no longer acts as a polar solvent, it can dissolve many organic compounds and provide a medium for recrystallization. On the other hand inorganic salts are virtually insoluble in supercritical water. Solute solubilities in supercritical fluids can undergo considerable changes with relatively small changes in pressure, and at constant pressure they generally pass through a minimum with temperature. These characteristics give the possibility of separating different solutes, by manipulating pressure or temperature in the so-called ‘cross-over’ region (*Figure 7.12*). Rapid depressurization, for example, creates high supersaturation, fast nucleation rates and consequently large numbers of small crystals. Chang and Randolph (1989) showed how small ($< 1 \mu\text{m}$) uniform particles of β -carotene, a vitamin A precursor, could be precipitated by rapidly expanding a solution in supercritical ethylene (critical point, 10°C and 50 bar) through a nozzle.

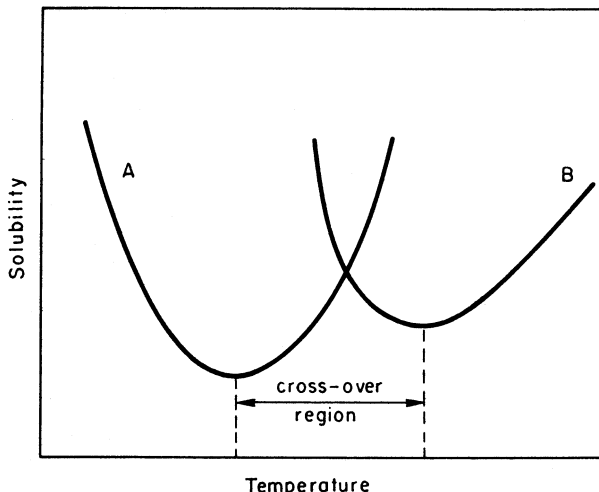


Figure 7.12. Solubility curve minima exhibited by two different solutes A and B in a supercritical fluid

Of all the solvents considered in recent years as possible SCFs for crystallization processes, the only two that now command any notable attention are water and CO₂ primarily because they are non-flammable, non-toxic, low-cost and readily available. Of these, CO₂ is attracting greater support on account of its more accessible critical point (31 °C and 74 bar) compared with that of water (374 °C and 220 bar).

One problem with SCFs as crystallization solvents is that the solubilities of most organic compounds are generally low. Whilst the supersaturations developed can appear to be high when expressed as the ratio c/c^* (section 3.12.1), they are usually low when expressed as a mass concentration driving force ($c - c^*$) and the consequent low yields and productivity can make the process appear commercially unattractive. Nevertheless, SCF crystallization could still be profitable in, for example, the separation of isomers and polymorphs and the purification of high-value products such as pharmaceuticals. Attempts have been made to increase solubility in SCFs by adding small amounts of a low molecular weight organic liquid, e.g. an alcohol or ketone, as a co-solvent (Dobbs, Wong and Johnston, 1986) although this can present subsequent downstream separation problems in an industrial process.

Some recent examples of exploratory crystallizations using supercritical CO₂ have been described by Mohamed, Debendetti and Prud'homme (1989); Kelley and Chimowitz (1989); Sako, Satu and Yamane (1990); Berends, Bruinsma and van Rosmalen (1993); Liu and Nagahama (1996); Tai and Cheng (1997); Shekunov, Hanna and York (1999).

Attention has recently been drawn to the possible advantages of 'nearcritical' rather than supercritical water as a benign solvent for both organic and ionic compounds (Eckert, Liotta and Brown, 2000). Nearcritical water is defined as liquid water at temperatures between about 250 and 300 °C and at its corresponding vapour pressure. Like ambient water, nearcritical water can hydrate ions, but it can also dissolve non-polar organic compounds. Polar organics are virtually insoluble in nearcritical water making it a good solvent in which to conduct chemical syntheses. Whilst no crystallization applications have yet been reported, the potential does appear to exist.

7.5 Zone refining

For the removal of the last traces of impurity from a substance, fractional crystallization from the melt cannot be applied with any degree of success. Apart from the fact that an almost infinite number of recrystallization steps would be necessary, there would only be a minute quantity of the pure substance left at the end of the process. High degrees of purification combined with a high yield of purified material can, however, be obtained by the technique known as zone melting or zone refining, originally developed by Pfann (1966) for the purification of germanium for use in transistors. Purification by zone refining can be effected when a concentration difference exists between the liquid and solid phases that are in contact during the melting or solidification of a solid solution. The method is best explained by means of a phase diagram.

Figure 7.13a shows a phase diagram for two substances A and B that form a simple solid solution: in this case the melting point of A is higher than that of B. When a homogeneous melt M of composition x is cooled solid material will first be deposited at some temperature T . The composition of this solid, which is in equilibrium with the melt of composition x (point L on the liquidus), is given by point S^* on the solidus. As cooling proceeds, more solid is deposited, and the concentration of B in the solid increases towards S. A similar reasoning may be applied to the reversed melting procedure starting from temperature T' , where a liquid of composition L^* is in equilibrium with a solid S of composition x . The solidification of a homogeneous molten mixture M yields a solid with an overall composition x , but owing to segregation the solid mixture is not homogeneous. Adjustments in the composition of the successive depositions of solid matter will not take place because of the very slow rate of diffusion in the solid state. The further apart the liquidus and solidus lines are, the greater will be the difference in concentration between the deposited solid and residual melt.

A measure of the expected efficiency of separation is given by a factor known as the segregation coefficient k . The significance of this coefficient can be seen in *Figure 7.13b*, where the liquidus and solidus for a binary solid solution in the regions of low B and low A concentrations are represented by straight lines. As zone melting is only useful for the refining of substances with low impurity contents, these are the regions that are of interest. For dilute solutions the segregation coefficient k is defined by

$$k = \frac{\text{concentration of impurity in solid}}{\text{concentration of impurity in liquid}} \quad (\text{at equilibrium}) \quad (7.4)$$

$$= \frac{\text{slope of liquidus}}{\text{slope of solidus}} = \frac{l}{s}$$

In *Figure 7.13b* it can be seen that $k_1 = l_1/s_1$ and $k_2 = l_2/s_2$, and also that $s_1 > l_1$ and $s_2 < l_2$. In general, therefore, it may be said that

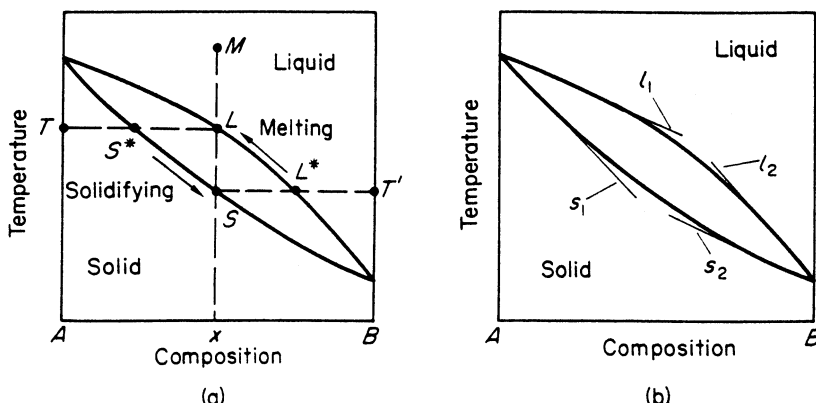


Figure 7.13. Phase diagram for simple solid solution: (a) solidification of a mixture; (b) liquidus and solidus drawn as straight lines in regions of near-pure A and B

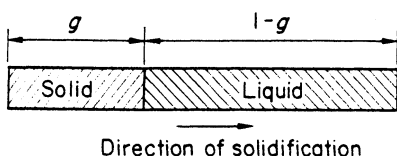


Figure 7.14. Molten bar of unit length undergoing progressive directional solidification

$k < l$ when the impurity lowers the melting point
and

$k > l$ when the impurity raises the melting point

When $k < l$, the impurity will concentrate in the melt, when $k > l$ in the solidifying mass. The nearer the value of k approaches unity, i.e. the closer the liquidus and solidus approach, the more difficult the segregation becomes. When $k = 1$, no zone refining is possible.

The impurity concentration at any point along a solid bar or ingot that was originally molten and then progressively cooled and solidified along its length (*Figure 7.14*) can be expressed in terms of the segregation coefficient. The concentration C of impurity (solute) in the solid at the solid–liquid interface is given by

$$C = kC_l \quad (7.5)$$

where C_l is the concentration of impurity in the liquid phase at the interface. At any distance g along the bar of unit length, the concentration C at the solid–liquid interface is given by the equation

$$C = kC_0(1 - g)^{k-1} \quad (7.6)$$

where C_0 is the initial concentration of the impurity in the homogeneous molten bar.

The distribution of impurity along a bar subjected to this process of *directional solidification* can be calculated from equation 7.6. The greater the deviation of k from unity, the greater the concentration gradient along the bar.

7.5.1 Constitutional supercooling

When a crystal grows in a melt or solution, impurity is rejected at the solid–liquid interface. In a stagnant fluid, e.g. with the crystalline phase gradually advancing into an unstirred melt, the impurity may not be able to diffuse away fast enough, in which case it will accumulate near the crystal face and lower the melting point in that region. Thus the effective temperature driving force, $\Delta T = T^* - T$, is decreased and the crystal growth rate is retarded. However, the melting point in the main bulk of the melt remains unaffected, so ΔT increases away from the interface.

This condition, known as *constitutional supercooling*, represents an instability and the advancing face usually breaks up into finger-like cells, which progress in a more or less regular bunched array. In this manner heat of crystallization is more readily dissipated and the tips of the projections advance

clear of the concentrated impurity and grow under conditions of near-maximum driving force. Impure liquid may be entrapped in the regions between the fingers, and a succession of regular inclusions may be left behind. At low constitutional supercooling, i.e. in a relatively pure system, the advancing interface is generally cellular. At high constitutional supercooling (high impurity) dendritic branching may occur. This sort of behaviour is common in, for example, the casting of metals.

7.5.2 Zone purification

Directional solidification is not readily adaptable for purification purposes, because the impurity content varies considerably along the bar at the end of the operation. The end portion of the bar, where the impurity concentration is highest, could be rejected and the process repeated after a remelting operation, but this would be extremely wasteful.

The technique known as *zone melting* does lend itself to repetitive purification without undue wastage. In this process a short molten zone is passed along the solid bar of material to be purified. If $k < 1$, the impurities pass into the melt and concentrate at the end of the bar. If $k > 1$, the impurities concentrate in the solid; thus in this case a cooled solid zone could be passed through the melt. The sequence of operations for molten zone refining is shown in *Figure 7.15a,b*. Although the impurity concentration in the bar, after the rejection of the high-impurity end portion, is much lower than initially, there is a considerable concentration gradient along the bar. In order to make the impurity concentration uniform along the bar, the process known as *zone levelling* must be employed; further zoning is carried out in alternate directions until a homogeneous mid-section of the bar is obtained (*Figure 7.15c*). Both the high- and low-impurity ends of the bar are discarded.

7.5.3 Zone refining methods

A few of the basic arrangements used in zone refining (Parr, 1960) are shown in *Figure 7.16*. *Figure 7.16a* shows the material contained in a horizontal crucible along which a heater is passed; or the crucible may be pulled through a stationary heater, and the molten zone travels through the solid. Several zones may be passed simultaneously at fixed intervals along the bar (*Figure 7.16b*) in order to reduce purification time. It is essential that the heaters be spaced at a sufficient distance to prevent any spread of the molten zones; for materials of high thermal conductivity and substances that exhibit high degrees of supercooling, alternate cooling arrangements may have to be fitted between the heaters. The ring method (*Figure 7.16c*) permits a simple multi-pass arrangement. The vertical tube method (*Figure 7.16d*) is useful when impurities that can sink or float in the melt are present. A downward zone pass can be used in the former case, an upward pass in the latter.

Different methods of heating may be used to produce molten zones; the choice of a particular method is usually governed by the physical characteristics

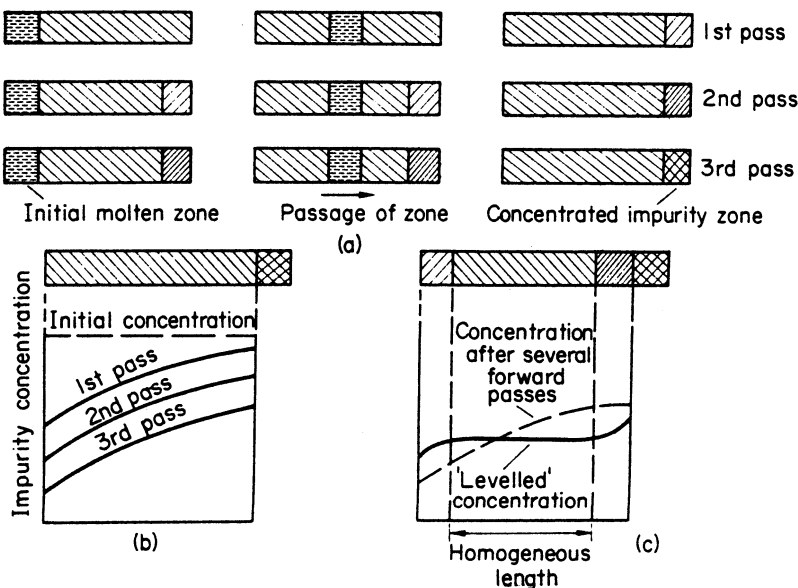


Figure 7.15. (a) and (b): A 3-pass zone refining operation; (c) zone levelling

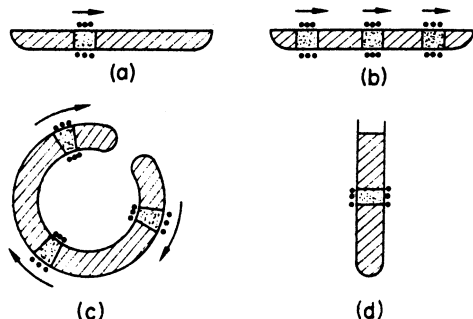


Figure 7.16. Simple methods of zone refining: (a) horizontal, single-pass; (b) horizontal concurrent passes; (c) continuous concurrent passes in 'broken ring' crucible; (d) vertical tube, upward or downward passes. (After Parr, 1960)

of the material undergoing purification. Resistance heating is widely employed, and direct-flame and focused-radiation heating are quite common. Heat can be generated inside an ingot by induction heating, and this method is often used for metals and semiconductors. Heating by electron bombardment or by electrical discharge also have their specific uses. Solar radiation, focused by lenses or reflectors, affords an automatic method for zone movement, on account of the sun's motion.

The speed of zoning is a factor that can have a considerable effect on the efficiency of zone refining. The correct speed is that which gives a uniform zone passage and at the same time permits impurities to diffuse away from the

solidifying face into the melt. If the zone speed is too fast, irregular crystallization will occur at the solidifying face, and impure melt will be trapped before it can diffuse into the bulk of the moving zone (*Figure 7.17a*). For the purification stages, the speed of zoning can vary from about 50 to 200 mm h⁻¹ and speeds of about 5 to 15 mm h⁻¹ are common for zone levelling.

The tube or crucible that contains the material undergoing purification should not provide a source of contamination and must be capable of withstanding thermal and mechanical stresses. The purified solid must be easily removable from its container, so the melt should not wet the container walls. The choice of the container material depends on the substance to be purified. Glass and silica are commonly used for organic substances, and silica for many sulphides, selenides, arsenides and antimonides; graphite-lined silica is often used for metals.

External contamination can be prevented by dispensing with the use of a conventional container. For example, a vertical zone refining technique that uses a ‘floating zone’ is shown in *Figure 7.17b*. The bar of material is fixed inside a container tube without touching the walls and the annulus between the bar and tube may contain a controlled atmosphere. Surface tension plays a large part in preventing the collapse of the molten zone, but the control of such a zone demands a high degree of experimental skill.

Although the largest applications of zone refining are in the fields of semiconductors and metallurgy, the technique has been used very successfully for the purification of a large number of chemical compounds. Herington (1963), for example, reports the particular application of zone refining to the preparation of very pure organic compounds. Nicolau (1971) has described the purification of inorganic salts by zone refining in the presence of a solvent, which allows operation at temperatures much lower than the melting point. He calls the technique zone-dissolution-crystallization, and describes the production of reagent-grade di-sodium phosphate, ammonium alum and copper sulphate from impure commercial-grade chemicals.

Comprehensive accounts of zone refining and its applications have been given by Pfann (1966), Schildknecht (1966), Zief and Wilcox (1967), Shah (1980) and Sloan and McGhie (1998).

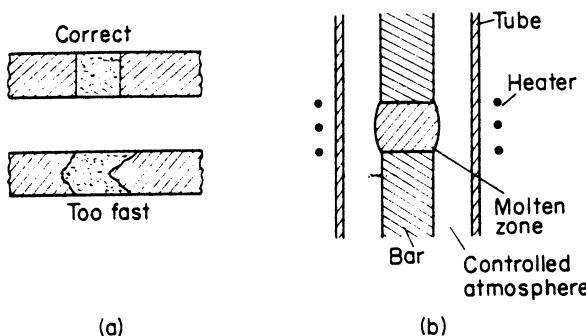


Figure 7.17. (a) Influence of zone speed; (b) floating-zone technique

7.6 Single crystals

There is a large demand nowadays for single, pure and defect-free crystals of innumerable substances, e.g. for the scientific appraisal of the chemical and physical properties of pure solids, for use in solid-state electronics, where crystals of certain substances are required for their dielectric, piezoelectric, paramagnetic and semiconductor properties, and for optical and laser materials and synthetic gem-stones (see *Table 7.1*).

The production of large single crystals demands exacting techniques, but broadly speaking there are three general methods available, viz. growth from solutions, from melts, and from vapours. There are many variations, however, in the processing techniques available within these three groups.

This subject is somewhat outside the main theme of the present book, so only a brief summary will be attempted here. However, several comprehensive accounts have been made of this specialized aspect of crystallization practice (Laudise, 1970; Faktor and Garrett, 1974; Pamplin, 1980; Hurle, 1993).

7.6.1 Low temperature solution growth

Slow crystallization from solution in water or organic solvents has long been a standard method for growing large pure crystals of inorganic and organic substances. Basically, a small crystal seed is immersed in a supersaturated solution of the given substance and its growth is regulated by a careful control of the temperature, concentration and degree of agitation of the system. For instance, a tiny selected crystal may be mounted on a suitable support and suspended in a vessel containing a solution of the substance, maintained at a fixed temperature. Slow rotation of the vessel will give an adequate movement of the solution around the crystal, and slow, controlled evaporation of the solvent will produce the degree of supersaturation necessary for crystal growth. Alternatively, the vessel may remain stationary and the growing crystal, or several suitably mounted crystals, may be gently rotated in the solution.

The actual operating conditions vary according to the nature of the crystallizing substance and solvent; the optimum supersaturation and solution movement

Table 7.1. Some uses of single crystals

Uses	Substances
Piezoelectric	quartz, Rochelle salt, ammonium and potassium dihydrogen phosphates, ethylenediamine tartrate, triglycine phosphate
Optical materials	CaF_2 , $\alpha\text{-SiO}_2$
Lasers	ruby, sapphire
Paramagnetic materials	$\alpha\text{-Al}_2\text{O}_3$, TiO_2 , CaF_2
Semiconductors	Ge, Si, GaAs
Luminescence and fluorescence	ZnS and CsS activated with Ag, Tl, Cr, Mn and Cu salts; various organic crystals
Gem-stones	alumina (sapphire and ruby), diamond

past the crystal must be found by trial and error. Generally speaking, the degree of supersaturation must not be high, and in any case the solution must never be allowed to approach the labile condition. The degree of supersaturation should be kept as constant as possible to ensure a constant rate of deposition of solute on the crystal seed. Holden (1949) states that, for salts with solubilities in the approximate range 20–50 per cent by mass, the maximum linear growth rate that can be tolerated by the fastest-growing faces of a crystal is about 1–3 mm per day; faster rates tend to give imperfections. Single crystals are better grown by a cooling than by an evaporation process, as supersaturation can then be much more closely controlled.

A typical example of a cooling-type growth unit is shown in *Figure 7.18a*. The carefully selected seed crystals are supported on a rotating arm, which is submerged in the gently agitated system, and grow under carefully controlled conditions. A very slow cooling rate is used, often less than $0.1\text{ }^{\circ}\text{C h}^{-1}$. Torgesen, Horton and Saylor (1963) have given a detailed description of an apparatus and procedure for growing large single crystals by this method. Single crystals can also be grown by holding them in a fixed position in a growth cell of the type described in section 6.2.2 (*Figure 6.12*) through which solution of the required level of supersaturation flows at a controlled steady rate.

7.6.2 High temperature solution growth

Many substances normally considered insoluble in water have an appreciable solubility at elevated temperatures and pressures. This property is utilized in the technique called ‘hydrothermal crystallization’, which is basically crystallization from aqueous solution at high temperature (350–550 °C) and pressure (1–3 k bar). The operation is carried out in a steel autoclave (*Figure 7.18b*), which can be provided with a silver or platinum liner for protection. The technique has proved satisfactory for the growth of silica and aluminosilicates from aqueous alkaline solutions. Quartz crystal, the ideal piezoelectric material, is now grown in this manner on a commercial scale.

Molten salt solvents may also be used for high-temperature solution growth in the technique normally called ‘flux growth’. Oxide crystals, like yttrium aluminium garnet, $\text{Y}_3\text{Al}_5\text{O}_{12}$, for example, may be grown from ionic solvents such as $\text{PbO}-\text{PbF}_2-\text{B}_2\text{O}_3$, while metallic solvents are suitable for covalently bonded semiconductors such as Si, GaAs and InP, while diamond can be crystallized from molten Ni–Fe alloys.

Hydrothermal and flux growth and their industrial applications have been the subjects of several comprehensive reviews (Lobachev, 1971; Elwell and Scheel, 1975; Elwell, 1980; Wanklyn, 1983).

7.6.3 Growth in gels

A room-temperature method, particularly useful for the production of single crystals of substances that are thermally unstable or have a very low solubility in water, is the technique of growth in a gel. The gel provides a kind of

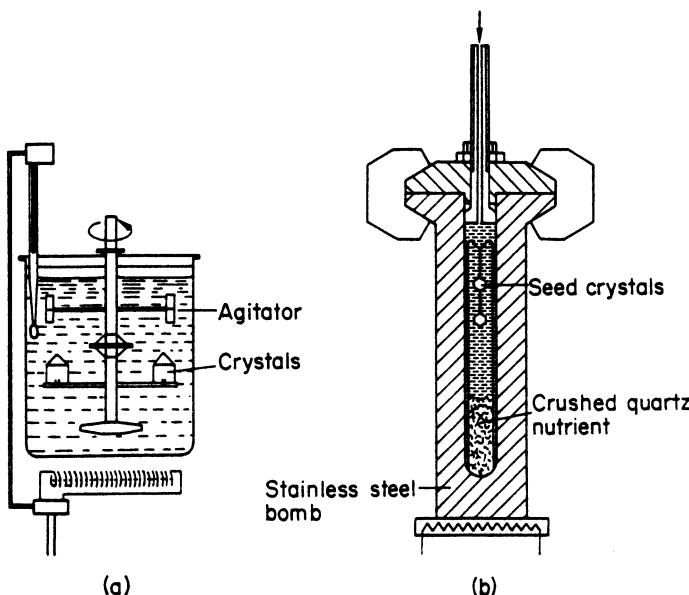


Figure 7.18. Crystallization from solution: (a) temperature-lowering methods, (b) hydro-thermal growth

protective barrier for the growing crystals; it eliminates turbulence, yet it imposes no strain on the crystals, and permits a steady diffusion of the growth components. The diffusion and reaction processes are retarded and very much larger crystals are grown than could be produced by normal reaction and precipitation techniques.

One technique for growth by controlled diffusion in a gel may be illustrated by the growth of calcium tartrate tetrahydrate crystals by reacting calcium chloride with D-tartaric acid in a silica gel (Rubin, 1969). A freshly made solution of sodium metasilicate (21.6 g in 250 cm³ of water, density 1.034, acidified to pH 3.5 with normal tartaric acid solution) is poured into test-tubes (6 × 1 in, two-thirds full) sealed to prevent loss of water and allowed to set over a period of 3 days at 40 °C. A normal solution of calcium chloride is then carefully pipetted on to the gel and nucleation immediately takes place at the gel-nutrient interface. After several hours single crystals appear below the interface and grow until they can no longer be supported by the gel. Crystals from 2 to 10 mm have been grown by this method over a period of a few weeks. Doped crystals can also be grown by doping the nutrient solution.

Surveys of growth in gels have been made by Henisch (1988) and Arora (1981).

7.6.4 Growth from the melt

A single crystal can be grown in a pure melt in a manner similar to that described earlier for growth in a solution. For example, a small crystal seed could be rotated in a supercooled melt, or the melt could flow past a fixed seed

in a growth cell. However, these methods do not find any significant application. The most widely used techniques for the production of single crystals from the melt can be grouped into four categories: the withdrawal or pulling techniques, the crucible methods, flame fusion and zone refining. The latter method has been described in some detail above.

The pulling techniques are typified by the Kyropoulos and Czochralski methods. In both cases a small, carefully selected seed crystal is partially immersed in a melt, kept just above its melting point, and the growing crystal is maintained just below its melting point by holding it on a water-cooled rod or tube (see Figure 7.19). The apparatus is usually kept under reduced pressure or supplied with an inert atmosphere. Silicon, germanium, bismuth, tin, aluminum, cadmium, zinc, intermetallic compounds, and many organic substances have been grown as large strainfree single crystals in this manner.

The main difference between the methods of Kyropoulos (see Figure 7.19a) and Czochralski (see Figure 7.19b) is that in the former the seed is permitted to grow into the melt, while in the latter the seed is withdrawn at a rate that keeps the solid–liquid interface more or less in a constant position. Pull rates depend on the temperature gradient at the crystal–melt interface and can vary from 1 to 40 mm h^{-1} . The steeper the gradient the faster the growth rate and, hence, the faster the permissible rate of withdrawal.

Compounds that dissociate on melting cannot be grown by the vertical pulling technique unless means are provided for suppressing dissociation. A simple elegant means is provided by the *liquid encapsulation* technique (Mullin,

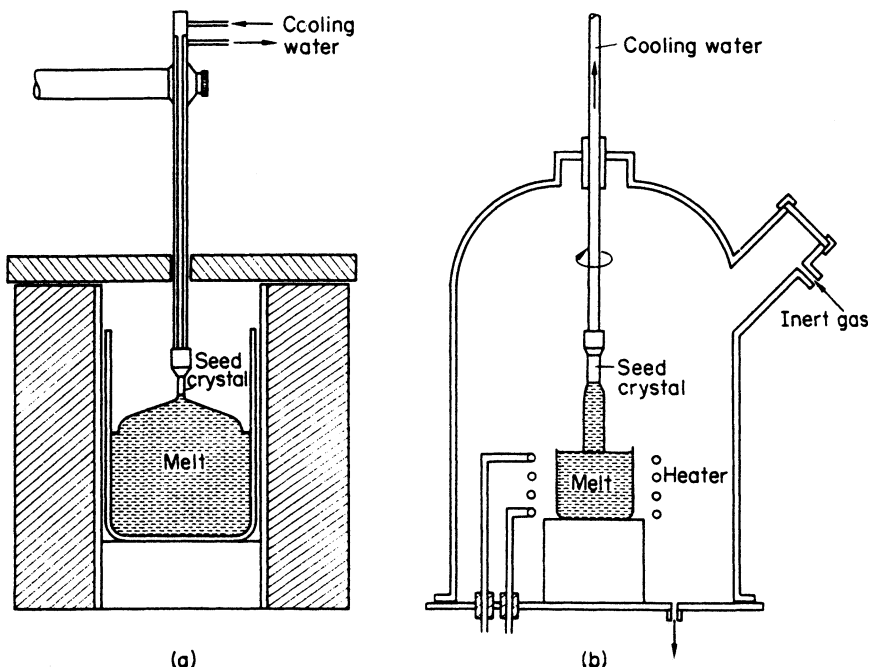


Figure 7.19. Crystal pulling and withdrawal techniques: (a) Kyropoulos, (b) Czochralski

Straughan and Bricknell, 1965) in which the melt surface is covered by a floating layer of transparent liquid. The encapsulant, e.g. boric oxide, B_2O_3 , a low-melting-point glass, acts as a liquid seal provided that the inert gas pressure on its surface is greater than the dissociation pressure of the compound. As the crystal is pulled from the melt, a thin film of encapsulant adheres to its surface and suppresses dissociation. The technique is particularly useful for the growth of semiconductor and metal crystals; even highly dissociable compounds such as GaP (vapour pressure 35 bar at 1470 °C) can be grown successfully on a commercial scale by this technique.

An example of the crucible method is that due to Bridgman and Stockbarger (see *Figure 7.20a*). The melt is contained in a crucible with a conical bottom which is lowered slowly from a hot to a cold zone. The two sections of the furnace, which are kept at about 50 °C above and below the melting point of the substance, respectively, are isolated by a thermal shield. The bulk of the solidified material, apart from the tip of the cone where the nuclei gather, is a single crystal. This method has proved successful for many semiconductor materials and alkali halides.

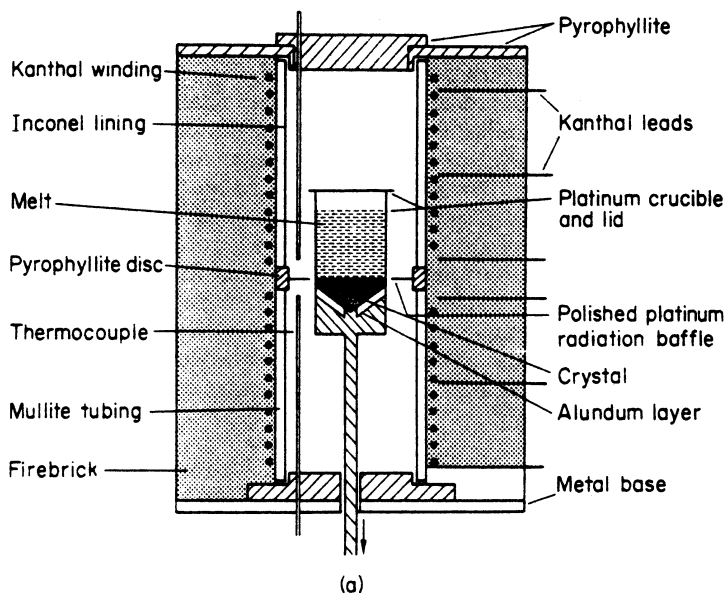
The flame fusion technique (see *Figure 7.20b*) was originally devised in 1904 by Verneuil for the manufacture of artificial gemstones, such as corundum (white sapphire) and ruby. This method is now used for the mass production of jewels for watches and scientific instruments. A trickle of fine alumina powder plus traces of colouring oxides is fed at a controlled rate into an oxyhydrogen flame. Fusion occurs and the molten droplets fall on to a ceramic collecting rod. A seed crystal cemented to the rod is fused in the flame and the rod is lowered at a rate that allows the top of the growing crystal (known as a *boule*) to remain just molten. Renewed interest has recently been shown in this method for the production of rubies for lasers.

Melt growth techniques have been reviewed by Pamplin (1980), Sloan and McGhie (1998) and Hurle (1993).

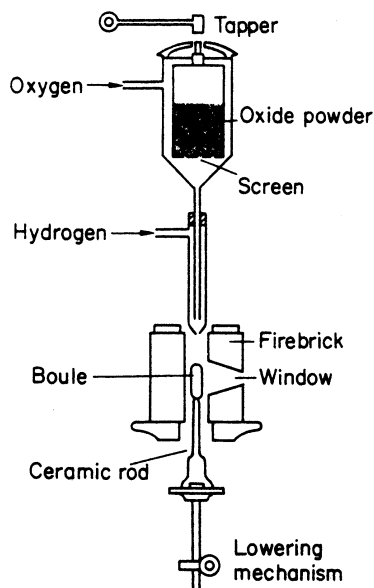
7.6.5 Growth from vapour

Crystal growth from a vapour by direct condensation, without the intervention of the liquid phase, can be used to produce small strain-free single crystals of substances that sublime readily. Large single crystals cannot be grown by this method. A number of techniques are available. For example, a gas stream, such as N_2 or H_2S , may be passed over a sublimable substance, such as cadmium sulphide, in a heated container. The vapours then pass to another part of the apparatus, where they condense, in crystalline form, on a cold surface.

Sublimation in sealed tubes is also used for the preparation of single crystals of metals, such as zinc and cadmium, and non-metallic sulphides. A quantity of the material is placed at one end of the tube, along which a temperature gradient is maintained, so that sublimation occurs at the hot end and crystallization at the other. An electric furnace with a number of independently controlled windings is used to maintain the temperature gradient to give a rate of sublimation sufficiently slow for the grown crystals to be single and not polycrystalline.



(a)



(b)

Figure 7.20. (a) The Bridgman–Stockbarger technique; (b) the Verneuil boule furnace

Vapour phase growth techniques have been reviewed by Faktor and Garrett (1974), Pamplin (1980), Hurle (1993) and Krabbes (1995).

8 Industrial techniques and equipment

8.1 Precipitation

Precipitation is a widely used industrial process. It is also a very popular laboratory technique, especially in analytical chemistry, and the literature on this aspect of the subject is voluminous (see Kolthoff *et al.*, 1969). Precipitation plays an important role not only in chemistry but also in metallurgy, geology, physiology, and other sciences. In the industrial field, the manufacture of photographic chemicals, pharmaceuticals, paints and pigments, polymers and plastics utilizes the principles of precipitation. For the production of ultrafine powders precipitation may be considered a useful alternative to conventional crystallization followed by milling.

The term *precipitation* very often refers to nothing more than fast crystallization, although sometimes it also implies an irreversible process, e.g. many precipitates are virtually insoluble substances produced by a chemical reaction, whereas the products of most conventional crystallization processes can usually be redissolved if the original conditions of temperature and solution concentration are restored. Another distinguishing feature of precipitation processes is that they are generally initiated at high supersaturation, resulting in fast nucleation and the consequent creation of large numbers of very small primary crystals. Although precipitation, like all crystallization processes, consists of three basic steps (supersaturation, nucleation and growth) two subsequent secondary steps usually have a profound effect on the final crystalline product. The first is *agglomeration*, which generally occurs soon after nucleation, and the second is *ageing*, a term used to cover all irreversible changes that take place in a precipitate after its formation.

A common method for producing a precipitate is to mix two reacting solutions together as quickly as possible, but the analysis of this apparently simple operation is exceedingly complex. Primary nucleation does not necessarily commence as soon as the reactants are mixed, unless the level of supersaturation is very high, and the mixing stage may be followed by an appreciable time lag before the first crystals can be detected. This event, which is often referred to as the end of the *induction period*, depends on the supersaturation, temperature, efficiency of mixing, intensity of agitation, presence of impurities, and so on. As explained in section 5.5, however, an experimentally measured induction period is not identical with the critical nucleation time since critical nuclei have to grow before they can be detected. Primary nucleation, both homogeneous and heterogeneous, together with growth of the nuclei, may continue for some time until sufficient crystal surface area has been created to cause a rapid desupersaturation. This event, which will be referred to as the end of the *latent period*, can be virtually identical with the experimental induction period at high supersaturations

(see *Figure 5.12*). Secondary nucleation is probably a rare event in precipitating systems.

Some indication of the particular nucleation and/or growth mechanisms predominating during the early stages of precipitation may be gained by plotting measured induction periods as a function of (1) $(\log S)^{-2}$, (2) $(\log S)^{-1}$ and (3) $\log(S^{-1})$. A straight line obtained from any of these plots can give an indication of the predominant mechanism. For example, (1) suggests either homogeneous nucleation or primary nucleation followed by diffusion-controlled growth, (2) indicates polynuclear growth, and (3) screw-dislocation growth. Further support for such mechanisms, however, must be sought by evaluating a relevant physical property from the slope of such functions (e.g. interfacial tension, see section 5.5) and assessing its validity (Söhnle and Mullin, 1978b, 1988a; Söhnle and Garside, 1992).

8.1.1 Agglomeration

Small particles in liquid suspension have a tendency to cluster together. Such terms as ‘agglomeration’, ‘aggregation’, ‘coagulation’ and ‘flocculation’ have all been applied in this area, although without any generally accepted rules of definition. For simplicity, therefore, the term ‘agglomeration’ will be used exclusively in this section.

Interparticle collision may result in permanent attachment if the particles are small enough for the van der Waals forces to exceed the gravitational forces, a condition that generally obtains for sizes $<1\text{ }\mu\text{m}$. Smoluchowski (1918) showed that the half-time, t^* , the time needed to have the number of particles in a monodisperse system, may be expressed as

$$t^* = [n_t/(n_0 - n_t)]t \quad (8.1)$$

where n_t and n_0 are the number of particles present at time t and in the original monodispersion ($t = 0$), respectively. For a binary collision process in a water-dispersed phase, in which all collisions are effective, Walton (1967) suggested that $n_0 t^* \sim 2 \times 10^{11}$. If an agglomerated system were arbitrarily defined as one in which more than 10% of the particles have aggregated in less than 1000 s, then aqueous systems containing less than 10^7 particles/cm 3 can be said to be non-agglomerating. The rather interesting conclusion to be drawn from this is that agglomeration may not be expected in systems where heteronucleation occurs since the number of heteronuclei is generally much less than 10^7 cm^{-3} , in fact it can be less than 10^4 cm^{-3} . On the other hand, agglomeration is quite common in systems that have nucleated homogeneously when n often exceeds 10^7 cm^{-3} . Of course, not all interparticle collisions result in permanent contact and in lyophobic systems charge stabilization greatly decreases the rate of agglomeration.

An over-simplified but graphic example of the interactive effects of supersaturation, nucleation and growth in the development of precipitated particles is given by Füredi-Milhofer and Walton (1969), who considered the homogeneous nucleation of three different systems at an arbitrary value of

supersaturation $S (=c/c^*, \text{ see section 3.12.1}) = 100$. The three solubilities, c^* are $10^{-7}, 10^{-4}$ and $10^{-1} \text{ mol L}^{-1}$, respectively, so the respective solution concentrations, c , at the onset of nucleation are $10^{-5}, 10^{-2}$ and 10 mol L^{-1} . If the number of particles nucleated is say 10^6 cm^{-3} , it may be concluded that the maximum particle sizes expected from such precipitations are 1, 10 and $100 \mu\text{m}$, respectively. Of course, this is a very crude calculation, but the results do show an order of magnitude agreement with practical experience.

Another way to look at the problem is to estimate the approximate nucleated particle size if the solutions of the above three substances were all of the same concentration, e.g. 1 mol L^{-1} . The supersaturation of the first solution is $S = 10^7$ and this would nucleate homogeneously, forming particles around 1 nm and producing a colloidal system (gel). These small primary particles would ultimately agglomerate, but the gel could remain stable for long periods if left undisturbed. The second solution ($S = 10^4$) would also nucleate homogeneously forming primary particles around $0.1 \mu\text{m}$ which again would agglomerate easily, but a conventional precipitate would rapidly develop. The third solution ($S = 10$) would probably nucleate heterogeneously, yielding crystals around $10 \mu\text{m}$ which could, under favourable conditions, remain discretely dispersed.

Smoluchowski (1918) distinguished between two types of agglomeration for colloidal particles in suspension:

1. Perikinetic (static fluid, particles in Brownian motion)
2. Orthokinetic (agitated dispersions).

Both modes can occur in precipitation processes, but in a stirred precipitator orthokinetic agglomeration clearly predominates. From the Smoluchowski kinetic expressions for perikinetic and orthokinetic agglomeration it can be deduced (Söhnel and Mullin, 1991) that the relationship between agglomerate size D and time t may be expressed by

$$D^3(t) = A_1 + B_1 t \quad (\text{perikinetic}) \quad (8.2)$$

and

$$\log D(t) = A_2 + B_2 t \quad (\text{orthokinetic}) \quad (8.3)$$

where A and B are particle–fluid system constants. *Figure 8.1* shows plots of these two equations for the early stages (first few minutes) of barium tungstate precipitation in an agitated vessel. The linear plot for equation 8.3, and not for equation 8.2, demonstrates that the agglomeration was orthokinetic rather than perikinetic.

Equations 8.2 and 8.3 are strictly applicable only to the early stages of agglomeration since they imply an unlimited increase of agglomerate size with time, which is unrealistic. Indeed, an upper limiting agglomerate size D_{\max} is often reached, after a certain time and in many cases this can be comparable with the Kolmogoroff microscale of turbulence (typically around $25 \mu\text{m}$ in stirred vessels). D_{\max} is also a function of the mixing intensity and often satisfies a relationship (Tomi and Bagster, 1978) of the form

$$D_{\max} \propto R^{-n} \quad (8.4)$$

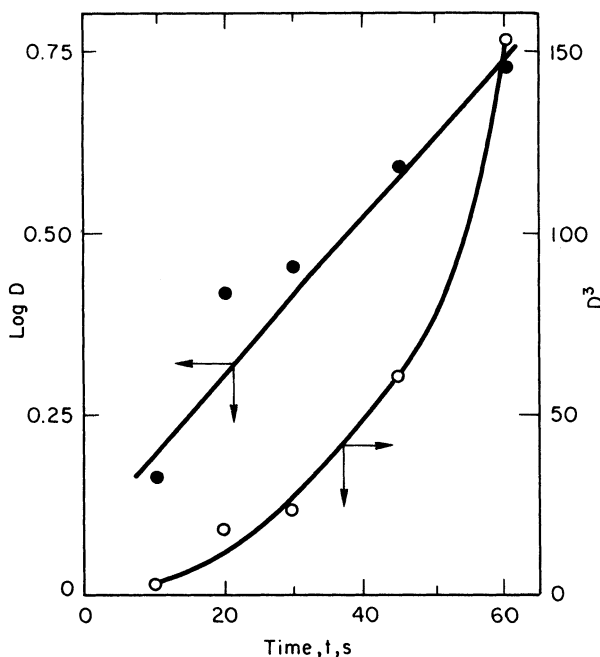


Figure 8.1. Plots of equations 8.2 [○] and 8.3 [●] for data from the precipitation of barium tungstate at an initial concentration of 3 mol m^{-3} . D is the median particle size (μm). (After Söhnel and Mullin, 1991)

where R is the stirrer speed and exponent n acquires a value of 0 or 3 when viscous or inertial forces, respectively, acting on the agglomerated particles are dominant. In the transition region n adopts some intermediate value.

An example of the time-development of a precipitate is shown in *Figure 8.2* which traces the particle size distribution of strontium molybdate precipitated batchwise by mixing aqueous solutions of SrCl_2 and Na_2MoO_4 . In this particular case the final steady-state distribution produced under agitated conditions is approached in around five minutes after mixing the reactants and remains constant up to 1 hour. The final size distribution and the behaviour of the primary particles are also influenced by the agitator speed in the reaction vessel and the reactant solution concentrations, but an indication of the development can be seen in the selected photomicrographs (taken from different runs) in *Figure 8.3*. Towards the end of the induction period ($\sim 15\text{ s}$) the crystals appear mainly as discrete spheres (*Figure 8.3a*). Within about 1 min., however, the crystals become elongated (*Figure 8.3b*). After about 30 min., virtually all the crystals are agglomerated (*Figure 8.3c*).

Useful surveys of agglomeration kinetics have been made by Nývlt *et al.* (1985), Söhnel and Garside (1992) and Wachi and Jones (1995). Recent papers on the subject by Collier and Hounslow (1999) and Zauner and Jones (2000a) are also noteworthy.

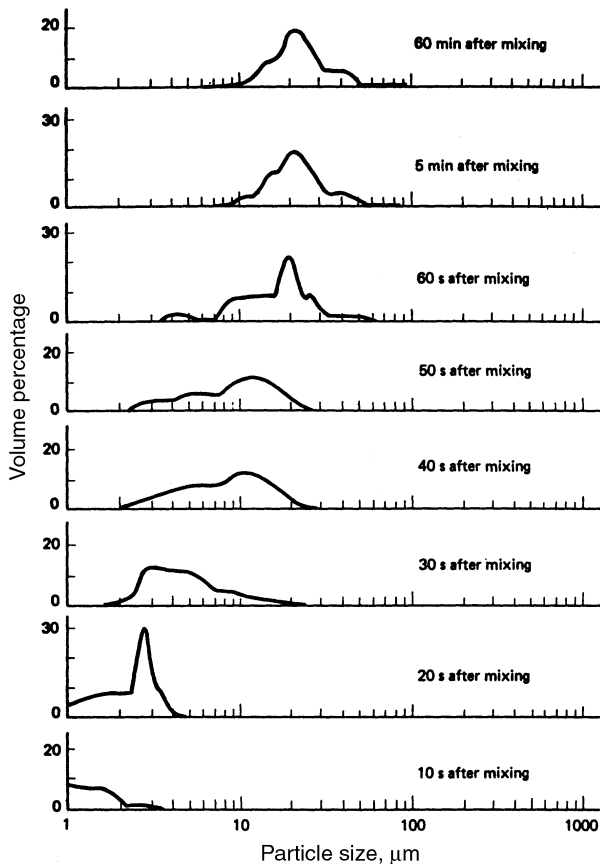


Figure 8.2. Volume percentage particle size distribution of SrMoO_4 particles precipitated batchwise as a function of the time after mixing the reacting solutions. (After Söhnel, Mullin and Jones, 1988)

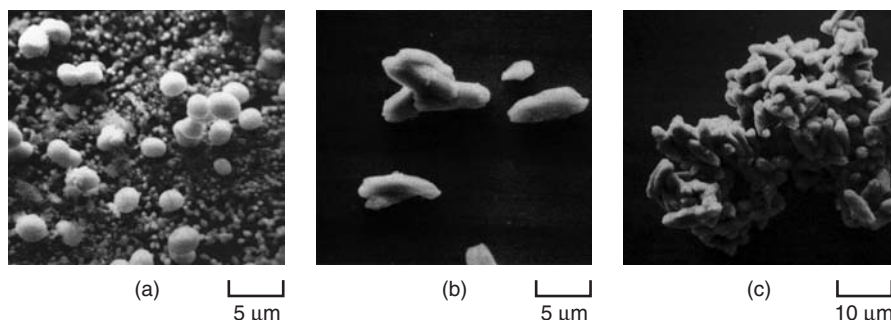


Figure 8.3. Particles of precipitated SrMoO_4 observed by SEM (a) towards the end of the induction period, (b) after 1 min. and (c) after 30 min. (After Söhnel, Mullin and Jones, 1988)

8.1.2 Ageing

Ripening

When solid particles are dispersed in their own saturated solution there is a tendency for the smaller particles to dissolve and the solute to be deposited subsequently on the larger particles. Thus the small particles disappear, the large grow larger and, theoretically, the particle size distribution should ultimately change towards that of a monosized dispersion. The reason for this behaviour lies in the tendency of the solid phase in the systems to adjust itself to achieve a minimum total surface free energy. This process of particle coarsening was first called ‘Ostwald ripening’ by Liesegang (1911), after the proposer of the mechanism (Ostwald, 1896).

The driving force for ripening is the difference in solubility between small and large particles, as given by the size–solubility (Gibbs–Thomson) relationship (equation 3.58) which for the present purpose may be written as

$$\ln \left[\frac{c(r)}{c^*} \right] = \frac{2\gamma v}{\nu R T r} \quad (8.5)$$

where v = molar volume of the solute, $c(r)$ = solubility of small particles of size r , c^* = equilibrium saturation for large particles ($r \rightarrow \infty$), γ = interfacial tension and ν = number of ions in a formula unit. As discussed in section 3.7 a significant increase in solubility occurs when $r < 1 \mu\text{m}$. From equation 8.5, expanding the logarithm for $c(r)/c^* \sim 1$ (ripening takes place at very low supersaturations), we get

$$c(r) - c^* \approx \frac{2\gamma v c^*}{\nu R T r} \quad (8.6)$$

If mass transport is possible between the particles in a polydisperse precipitate, the large will grow at the expense of the small. If the growth kinetics are first-order, diffusion-controlled, then for a change in particle radius with time (see equation 6.37)

$$\frac{dr}{dt} = \frac{Dv[c - c(r)]}{r} \quad (8.7)$$

where c is the average bulk solution concentration, and from equation 8.6

$$\frac{dr}{dt} = \frac{Dv}{r} \left[(c - c^*) - \frac{2\gamma v c^*}{\nu R T r} \right] \quad (8.8)$$

where $c - c^*$ is always positive during precipitation. Setting equation 8.8 equal to zero, it follows that all particles of size

$$r = \frac{2\gamma v c^*}{\nu R T (c - c^*)} \quad (8.9)$$

are in equilibrium with the bulk solution ($dr/dt = 0$). All particles smaller than this will dissolve ($dr/dt < 0$), and all particles larger will grow ($dr/dt > 0$).

The speed with which ripening occurs depends to a large extent on the particle size and solubility. For example, small crystals of a moderately soluble salt such as K_2SO_4 with a solubility $c_1^* \sim 10^3 \text{ mol m}^{-3}$ will age much faster than those of the almost insoluble BaSO_4 ($c_2^* \sim 10^{-2} \text{ mol m}^{-3}$) if kept in solutions of the same supersaturation, say $S = c/c^* = 1.1$. The driving force, for mass transfer $\Delta c_1 = (S - 1)c_1^* = 10^2$ and $\Delta c_2 = 10^{-3} \text{ mol m}^{-3}$, and if a growth law $R_G = K_G \Delta c^n$ is assumed (equation 6.14), with the growth coefficients not differing by more than an order of magnitude, the relative growth rates of the two salts are $\sim 10^5 : 1$ for first-order growth kinetics rising to $\sim 10^{12} : 1$ for second-order.

For diffusion-controlled growth kinetics it can be shown (Nielsen, 1964; Hanitzsch and Kahlweit, 1969) that the linear growth velocity approximates to

$$\frac{dr}{dt} \approx \frac{\gamma v^2 D c^*}{3\nu \mathbf{R} T r^2} \quad (8.10)$$

which on integration gives

$$t \approx \frac{\nu \mathbf{R} T r^3}{\gamma v^2 D c^*} \quad (8.11)$$

thus the smaller the particle size, r , or the higher the solubility, c^* , the faster ripening process.

Of course, the ripening process, which occurs at very low supersaturation, is probably more likely to be controlled by a surface reaction than by a diffusion process, and under these circumstances ripening could be considerably retarded. For surface reaction growth kinetics the linear growth velocity obeys a relationship such as

$$\frac{dr}{dt} = k(c - c^*)^n \quad (8.12)$$

where k is a growth rate constant, and if an arbitrary value of $n = 2$ is assumed, then

$$t = \left(\frac{\nu \mathbf{R} T}{\gamma v c^*} \right)^2 \frac{r^3}{k} \quad (8.13)$$

Therefore, from equations 8.11 ($t = t_D$) and 8.13 ($t = t_R$)

$$t_R \approx \left(\frac{\nu \mathbf{R} T D}{\gamma k c^*} \right) t_D \quad (8.14)$$

Substituting typical values in equation 8.14 for a relatively insoluble salt such as PbSO_4 ($T = 300 \text{ K}$, $D = 10^{-9} \text{ m}^2 \text{ s}^{-1}$, $\gamma = 10^{-1} \text{ J m}^{-2}$, $R = 8.3 \text{ J mol}^{-1} \text{ K}^{-1}$, $c^* = 10^{-1} \text{ mol m}^{-3}$, $k = 10^{-6} \text{ m}^7 \text{ mol}^{-2} \text{ s}^{-1}$, $\nu = 2$), we get $t_R \simeq t_D$, which indicates that the interfacial reaction can exert a dominant effect on the ripening process. Any additive to the system which slows down the surface reaction step will automatically retard the ripening process and thus stabilize the

suspension. Substances such as gelatin and carboxymethyl cellulose are commonly used for this purpose.

Ripening can change the particle size distribution of a precipitate over a period of time, even in an isothermal system, but the change can be accelerated by the use of controlled temperature fluctuations. This process, known as ‘temperature cycling’, has been utilized to alter the physical characteristics of organic and inorganic precipitates (Carless and Foster, 1966; Nývlt, 1973; Brown, Marquering and Myerson, 1990).

Kahlweit (1975) has made a comprehensive analysis of ripening mechanisms. Sugimoto (1978) has critically assessed relationships between diffusion-controlled and reaction-controlled ripening and reviewed the experimental determination of the respective kinetic constants.

Phase transformation

Although Ostwald ripening is rightly regarded as an important ageing process for a precipitate that remains in contact with its mother liquor, particularly if the primary crystals are smaller than 1 µm, it is not the only ageing process that can be encountered. Nor is it always the most important one.

Another frequent occurrence is the first-precipitation of a metastable phase (Ostwald’s rule of stages – section 5.7) followed by a phase transformation to the final product. The metastable phase may be an amorphous precipitate, a polymorph of the final material, a hydrated species or some system-contaminated substance.

Magnesium hydroxide, precipitated by mixing aqueous solutions of MgCl₂ and NaOH, affords a particularly good example of a complex ageing process (Mullin *et al.*, 1989a). After the first few seconds the mean agglomerate size (~20 µm) decreased steadily with time. Mechanical breakdown of the agglomerates, under agitated conditions, at first suspected, was not responsible because the precipitate specific surface area also decreased with time. The paradox was shown to be the result of the first-precipitation of a complex species (probably MgOH · OCl · 2H₂O) which subsequently dehydrated and decomposed to yield Mg(OH)₂. The consequent agglomerate shrinkage caused the primary platelet crystals (~40 nm) to cement together resulting in a specific area reduction.

Calcium sulphate in water exhibits a phase transition near 100 °C between the dihydrate (gypsum) and the hemihydrate initiated by the dissolution of gypsum and the subsequent nucleation and growth of hemihydrate (Nancollas and Reddy, 1974). Dissolution–recrystallization mechanisms have been advanced for many similar transformations involving hydrates, e.g. calcium phosphates (Nancollas and Tomazic, 1974; Brečević and Füredi-Milhofer, 1976) and for polymorphic transformations, e.g. copper phthalocyanine (Honigmann and Horn, 1973). Solid-state transformations, frequently encountered in polymorphic changes, are occasionally encountered in hydrate transitions, e.g. calcium oxalate (Gardner, 1976).

Polymorphs and their transformations are discussed in section 6.5.

Precipitate morphology

The morphological development of a precipitate is a complex combination of a variety of processes, including nucleation, growth, habit modification, phase transformation, ripening, agglomeration, and so on. The dominant system parameters are supersaturation and the level of active impurities, although in some aqueous systems pH can also exert a profound effect.

The dominant influence of supersaturation on the particle size characteristics of a precipitate has been summed up in the so-called Weimarn laws of precipitation (Weimarn, 1926) which, whilst open to criticism from a theoretical point of view, still give useful guidelines for batch precipitation behaviour. The 'laws' cannot be expressed concisely, but *Figure 8.4* assists in their interpretation:

1. As the concentration of reacting substances in solution is increased, i.e. as the initial supersaturation is increased, the mean size of the precipitate particles (measured at a given time after mixing the reactants) increases to a maximum and then decreases. As the time at which measurement is made is increased, the maximum is displaced towards lower initial supersaturations and higher mean sizes.
2. For a completed precipitation, the precipitate mean size decreases as the initial supersaturation is increased.

In addition to confirming the well-known beneficial effect of using reasonably dilute reactants to produce coarse precipitates, the laws demonstrate that excessive dilution can be detrimental, a fact that is not always fully appreciated. Experimental evidence for the Weimarn laws has been provided by Mullin and Ang (1977) for the precipitation of nickel ammonium sulphate.

Some measure of control over nucleation and growth, and hence of precipitation, may also be exercised by the addition of substances, such as surfactants

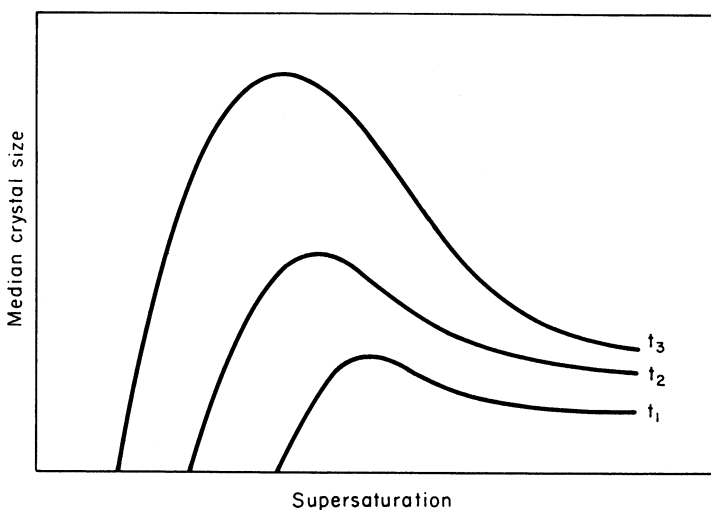


Figure 8.4. Weimarn's 'laws' of precipitation. Time $t_1 < t_2 < t_3$

and polyelectrolytes. Impurities in the system, whether deliberately added or already present, can have a powerful influence on the morphology of the final precipitated particles.

Walton (1967) and Füredi-Milhofer (1969) has described how, due to the build-up of impurities in the crystal face boundary layer, the predominant growth of crystal corners operating in a periodic mode can lead to the development of dendritic-like structures (*Figure 8.5*). Particles of this type, commonly seen for example in precipitates such as Bayer hydrate (alumina hydrate), give the impression of being developed by the partial agglomeration of small platelets (an explanation frequently found in the literature), but the true mechanism is probably one of periodic growth (Gnyra, Jooste and Brown, 1974). Another type of precipitated particle that is often confused with a true agglomerate is the one that results from crystalline out-growths emanating from different surfaces of an original heteronucleus. Subsequent growth leads to the development of a particle that looks deceptively like an agglomerate.

Another interesting growth form exhibited by several substances is the development of regular isometrical shapes towards the end of the precipitation process. The phenomenon was described for the case of barium sulphate by Melikhov and Kelebeev (1979) who proposed the mechanism that, in a strongly supersaturated solution, homogeneous nucleation followed by growth yields isotropic crystals of about 2 nm in size. Their surfaces then develop zones with enhanced growth rates which lead to the formation of anisotropic needles,

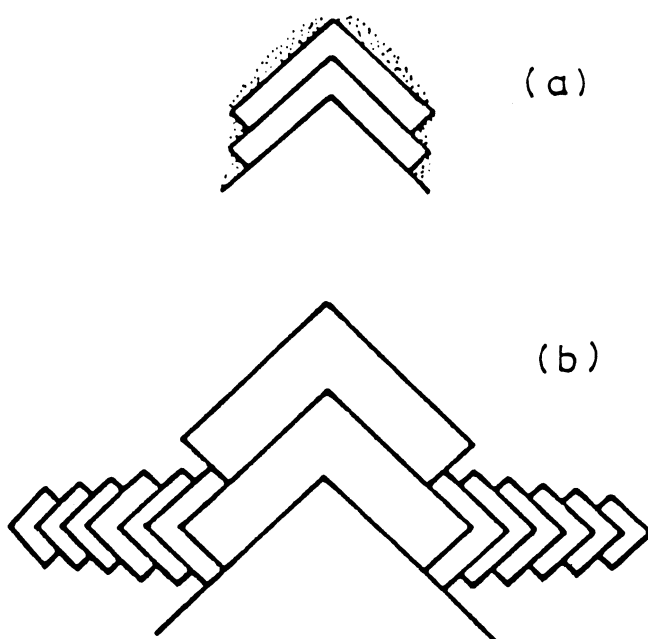


Figure 8.5. *Representation of the development of a crystal dendrite: (a) the corners, which are not blocked by impurity, grow preferentially; (b) periodic growth leads to the development of a dendrite-type crystal. (After Walton, 1967)*

the rapidly growing faces of which have different crystallographic orientations. The needle crystals then adhere, first by end to end contacts, forming ring structures which subsequently, i.e. at a lower supersaturation, agglomerate in a side to side fashion to form isometrical cellular particles.

It often appears that, for a given system, there is a certain level of supersaturation for maximum agglomeration. It is as if under these conditions the crystal surfaces become 'sticky'. It is interesting to speculate on the link between this behaviour and the character of the adsorption layer (loosely bonded, partially integrated groups of the crystallizing species) surrounding a growing crystal. At very low supersaturations, the adsorption layer will be thin and strongly attracted to the crystal face and the growth units will be readily incorporated at the growth sites. At very high supersaturations the adsorption layer will be thick and the outer layers of growth units will only be loosely attracted to the parent crystal. Under these conditions fluid shearing, as the crystal moves through the solution, can sweep portions of the loosely bound growth units into the solution where, because they are already partially integrated, they become nuclei. However, at some intermediate level of supersaturation the adsorption layer may be neither 'thick' nor 'thin' and contact between two crystals in the same condition could rapidly result in a permanent bond through their integrated adsorption layers.

Amorphous precipitates

A substance capable of exhibiting crystallinity is sometimes precipitated in an amorphous form. Kolthoff *et al.* (1969) have suggested that there is a competition between the 'aggregation' and 'orientation' velocities of the molecular species concerned and the former sometimes dominates, although this is undoubtedly an oversimplification.

Aggregation (non-crystalline) and orientation (crystalline) are both influenced by supersaturation and temperature, but the type of species is also very important. For example, strongly polar salts, such as lead iodide, silver chloride and barium sulphate, invariably precipitate in crystalline form. Carbonates of calcium and barium and hydroxides of magnesium and zinc do likewise, but there is evidence in some of these cases of the prior precipitation of hydrated short-lived precursor phases (Mullin *et al.*, 1989; Brečević and Nielsen, 1990). Hydrous oxides like hydrous ferric oxide (*o*-ferric hydroxide) are generally amorphous, especially when precipitated from cold solution.

Amorphous precipitates can transform, often quite rapidly, into a crystalline product on ageing, but the ageing process can sometimes be accompanied by chemical change. Hydrous ferric oxide affords such an example: a polymer containing eight atoms of Fe agglomerates into a chain structure containing more than 50 atoms of Fe which dehydrates on ageing to a yellow amorphous ferric acid with a ring structure and finally yields crystalline goethite.

In recent years there has been an increasing realization that manufactured crystalline products can contain small amounts of molecular disorder which can be highly detrimental to product quality, particularly in the pharmaceutical industry. Amorphous regions in a crystal are thermodynamically

unstable and, if located near the surfaces of water-soluble substances, the particles can readily absorb atmospheric water vapour and initiate undesirable physical and chemical changes. Buckton and Darcy (1999) have critically reviewed some of the analytical techniques, including vapour sorption, DSC, powder X-ray diffraction and IR spectrometry, that can be used to characterize partially amorphous materials. An interesting method has been proposed by Kishishita, Kishimoto and Nagashima (1996) for interpreting X-ray diffraction patterns to provide information on a property described as 'crystal texture'. The two quantities evaluated are the degree of crystallinity and the preferred orientation of molecular units, both of which are shown to be influenced by the rate of crystallization or grinding the dry crystalline product.

8.1.3 Co-precipitation

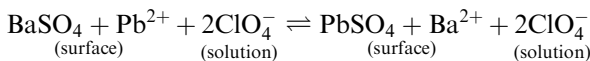
To some extent, all precipitates are contaminated with materials originating from solution in the mother liquor. The general term 'co-precipitation' may be used to cover the many different types of impurity incorporation that can occur, including the surface adsorption and lattice entrapment of foreign ions and solvent molecules, the physical inclusion of pockets of mother liquor, and so on.

Adsorption phenomena

The adsorption of salts having an ion in common with the precipitate roughly follows the Paneth–Fajans–Hahn adsorption rule which postulates that the less soluble the salt, the more easily is it incorporated into a precipitate. For example barium chloride is more readily adsorbed by barium sulphate than is barium iodide, which is much more soluble than the chloride.

The dissociability of the adsorbed salt is also important. Adsorption decreases as the degree of dissociation of the adsorbed salt increases. The deformability of the foreign ion also has an influence. With anions, which are generally more easily deformed than cations, the deformability increases with size. Dyestuff anions, for example, are highly deformable and this property is utilized in the application of adsorption indicators used in volumetric analysis.

Salts having no ion in common with the precipitate can also be incorporated. The ions in a lattice surface exhibit residual valence forces and will readily attract foreign ions of opposite charge. Some complex 'surface exchange' reactions may occur (Kolthoff *et al.*, 1969). For example, when a barium sulphate precipitate is shaken with a dilute solution of lead perchlorate, the lead ions are strongly attracted by the barium sulphate since lead sulphate is slightly soluble and it fits into the barium sulphate lattice. On the other hand, the perchlorate ions show no pronounced tendency to adsorb since barium perchlorate is quite soluble. Thus, both Ba^{2+} , Pb^{2+} and SO_4^{2-} are strongly attracted by the BaSO_4 lattice surface whereas ClO_4^- is not, and the following surface exchange reaction takes place:



As a result, Ba^{2+} in the surface is partly replaced by Pb^{2+} and an equivalent amount of Ba^{2+} enters the solution. This exchange adsorption occurs even though the solubility product of lead sulphate is not exceeded.

Precipitates originating from colloidal solutions (sols or gels) are also liable to be contaminated with the *counterions*. For example, a colloidal solution of silver iodide may be prepared by mixing dilute solutions of silver nitrate and potassium iodide. The colloidal particles are stabilized by adsorbed I^- and an equivalent amount of K^+ (the counterion) is present. The AgI sol may be flocculated by the addition of an electrolyte, e.g. KNO_3 , but the precipitate will be contaminated with adsorbed KI which is difficult to remove by washing. However, counterions can often be readily replaced by other ions. For example, if the above contaminated AgI precipitate is washed with dilute H_2SO_4 , K^+ may be replaced by H^+ . Many such examples are available in textbooks of analytical chemistry (e.g. see Kolthoff *et al.*, 1969).

Solid solution formation

Mixtures of components that exhibit solid solution behaviour cannot be separated in a single step as can, for example, simple eutectic systems. Multistage or fractional precipitation schemes must therefore be employed (section 7.1). The distribution of an impurity between the solid (i.e. solid solution) and liquid phases may be represented by the Chlopin (1925) equation:

$$\frac{x}{y} = D \left(\frac{a-x}{b-y} \right) \quad (8.15)$$

where a and b are the amounts of components A and B in the original solid, x and y are the amounts of A and B in the crystallized solid and $a-x$ and $b-y$ are the amounts of A and B retained in the solution. D is a distribution coefficient. Alternatively, the logarithmic Doerner–Hoskins (1925) equation may be used:

$$\ln(a/x) = \lambda \ln(b/y) \quad (8.16)$$

The constant λ has been called a heterogeneous distribution coefficient to distinguish it from the homogeneous distribution coefficient D in equation 8.15. Under ideal conditions $D = \lambda$.

If component A is the impurity, $\lambda > 1$ indicates that the impurity will be enriched in the precipitate. Conversely, if $\lambda < 1$ it will be depleted. A schematic diagram of the effect of precipitation rate on λ is shown in *Figure 8.6* (Walton, 1967). In enrichment systems, $\lambda \rightarrow \lambda_e = D_e$ as the precipitation rate tends to zero. For fast rates of precipitation $\lambda \rightarrow 1$. For depletion systems, an analogous situation exists with $\lambda \rightarrow \lambda_d = D_d$ for very slow precipitation and $\lambda \rightarrow 1$ for rapid precipitation.

Both the Chlopin and Doerner–Hoskins relationships have been widely used to correlate the results of fractional precipitation and recrystallization schemes

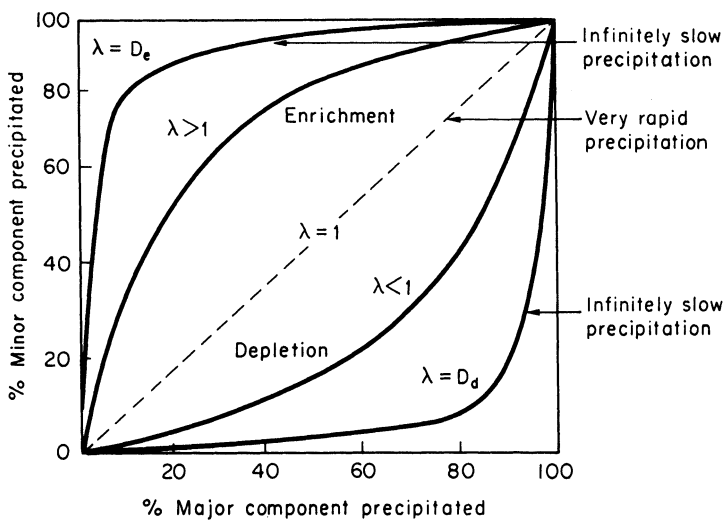


Figure 8.6. The effect of precipitation rate on the distribution coefficient λ (equation 8.16). (After Walton, 1967)

(see section 7.1), although neither is entirely satisfactory from a theoretical point of view.

General problems associated with the fractional precipitation of mixtures of similar substances when one is present in a very small amount have been discussed by Joy and Payne (1955) and Gordon, Salutsky and Willard (1959).

Incorporation of solvent

Solvent molecules are frequently found in association with precipitated materials. For example, crystalline substances often form with water molecules located at specific sites, e.g. water of crystallization, held in co-ordination complexes around lattice cations. Extraneous inclusion of water molecules can occur if a co-precipitated cation carries solvation molecules with it. Massive incorporation of solvent, together with other soluble impurities can occur in random pockets (inclusions) as a result of the physical entrapment of mother liquor. Fast crystal growth, leading to growth instabilities, dendrite formation, crystal agglomeration, etc., can all contribute to this undesirable feature. An account of liquid inclusions in crystals is given in section 6.6.

8.1.4 Precipitation diagrams

The inherent complexities of precipitation in multicomponent systems influence the system equilibria, nucleation and growth mechanisms and precipitate characteristics. The graphical procedures developed by Tezak (1966) and Füredi (1967) afford an interesting approach towards an understanding of the underlying principles. If two precipitating components, e.g. with interacting anions or cations, are mixed in increasingly dilute solution, a limit will eventually be

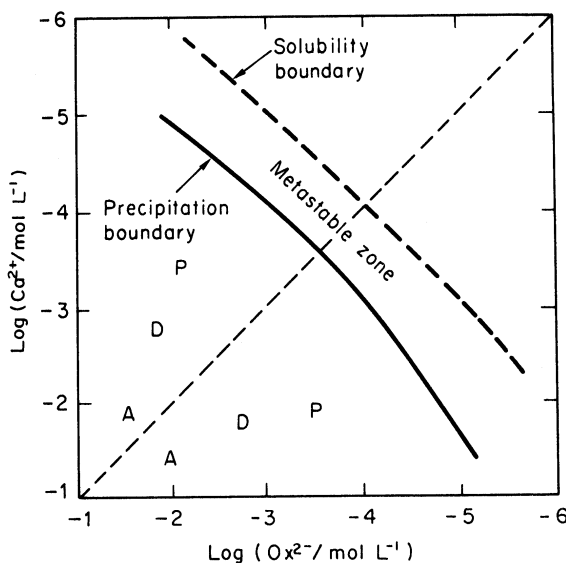


Figure 8.7. Precipitation boundary (24 h) for calcium oxalate at 25°C. P = plates, D = dendrites, A = agglomerates

reached where no precipitate will appear, even after a very long time. Tezak called this limit the 'precipitation boundary'. A range of reactant concentrations is normally covered. For example, the concentration of one component can be varied while the concentrations of all the others are kept constant. In this way, the maximum concentration attainable before the onset of precipitation, i.e. the precipitation boundary, may be determined.

The precipitation boundary for some arbitrary 'long period of time', e.g. 24 hours, may be drawn on the diagram as shown in *Figure 8.7*. The solubility curve is also depicted and its contours reflect any complexing that occurs in solution and the resulting equilibria. The zone between the two curves represents the condition of metastability. The dotted diagonal representing equivalent concentrations of the initially added precipitating components, divides the precipitation diagram into two symmetrical parts, in each of which one of the precipitating components is in excess. Any line parallel to the equivalence line represents a different constant ratio of the precipitating components. The diagram may also be used to indicate observed particulate characteristics such as size, morphology, agglomeration, etc.

The analysis of solubility curves and precipitation boundaries is illustrated for the precipitation of silver bromide (mixing aqueous solutions of KBr and AgNO₃) in *Figure 8.8* (Füredi, 1967). The curves are approximated by tangents and the values of the slopes, *b*, of the various parts of the curve determine the compositions of the complexes. For example, slope *b* = -1 for this 1-1 electrolyte represents the solubility product and slope *b* = 0 represents the complex AgBr (aq). The other portions of the curve represent the compositions of the other complexes AgBr⁽ⁿ⁻¹⁾⁻ and Ag_{*m*}Br^{(m-1)+} where the slope

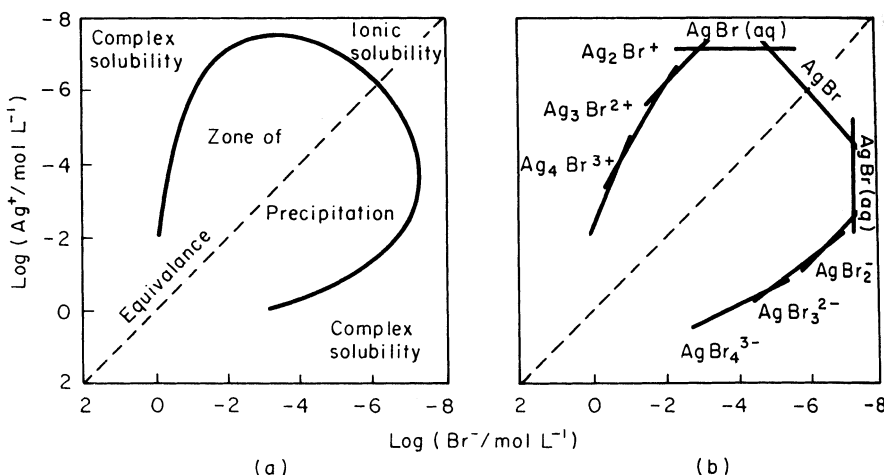


Figure 8.8. Precipitation-solubility curves for silver bromide in aqueous solution (a) smoothed experimental points, (b) curve approximated by tangents. (After Füredi, 1967)

$b = ny - (mx/y)$. In this case only mononuclear complexes were considered, i.e. $x = y = m = 1$.

The precipitation boundary may or may not coincide with the solubility curve since its position in the diagram depends on the time and method of detection of the onset of precipitation. In effect, it establishes the metastable zone for the given system. If a stable precipitate is formed at low levels of supersaturation the precipitation boundary and solubility curve may be assumed to be virtually coincident. In cases where they do not coincide, the composition of the critical nuclei may be determined from the slopes of the precipitation boundary while the compositions of the corresponding bulk equilibrium solid phases may be obtained from the solubility curve. Hence, comparison of the two curves can yield information as to whether the composition of both nuclei and precipitate is the same or if the bulk solid phase is formed by a solid-state transformation from a metastable precursor. A useful account of the significance of the zones on a precipitation diagram has also been given by Nielsen (1979).

Another type of ‘precipitation diagram’ has been proposed for assessing hydrometallurgical processes involving the selective precipitation of metal hydroxides and salts (Monhemius, 1977). Each diagram illustrates the relative solubilities of a particular hydroxide or salt of a range of metals and enables estimation of theoretical solubilities at any acidic pH.

The sulphide precipitation diagram in Figure 8.9 is essentially a plot of cation activity against sulphide ion activity. pH is also recorded for systems containing H_2S at atmospheric pressure.

The use of the diagram is illustrated as follows. Assess the feasibility of removing copper from a solution containing $30 \text{ g L}^{-1} \text{ Zn}$ and $2 \text{ g L}^{-1} \text{ Cu}$ at pH 0 by precipitation with gaseous H_2S . If the solution is saturated with H_2S at atmospheric pressure, the sulphide ion activity $\log\{\text{S}^{2-}\}$ at pH 0 will be -21 ,

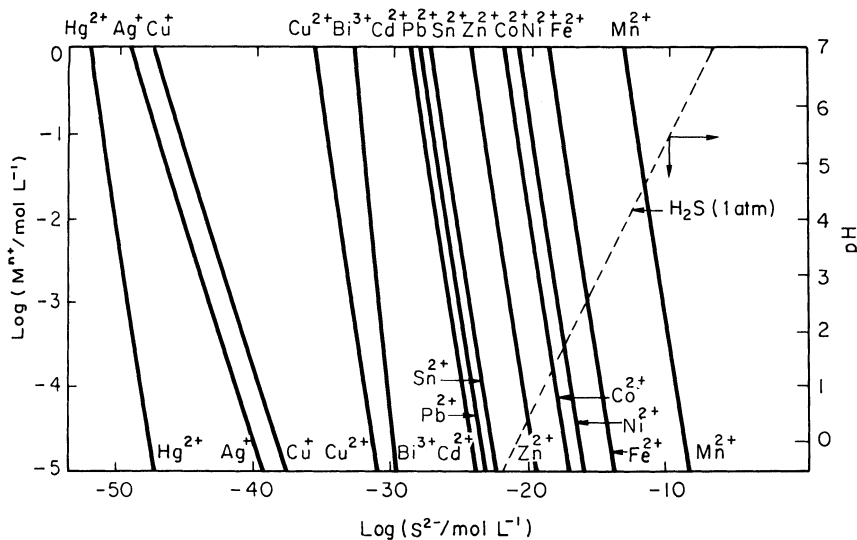


Figure 8.9. Sulphide precipitation diagram at 25 °C. (H₂S at atmospheric pressure). (After Monhemius, 1977)

at which the equilibrium activity of copper in solution, as either Cu^+ or Cu^{2+} , is much less than 10^{-5} molar (below the graph), i.e. the copper is virtually insoluble. However, at $\log\{\text{S}^{2-}\} = -21$ the solubility of zinc is also low ($\log\{\text{Zn}^{2+}\} = -3.5$) so much of the zinc would be co-precipitated with the copper. To prevent this occurring, the input of H₂S could be controlled so that the solution always remains undersaturated with respect to it. For example, by keeping $\log\{\text{S}^{2-}\}$ lower than say -25 the copper should precipitate, as the sulphide, and zinc should remain in solution.

8.1.5 Techniques of precipitation

Precipitation by direct mixing

The precipitation of a solid product as the result of the chemical reaction between gases and/or liquids is a standard method for the preparation of many industrial chemicals. Precipitation occurs because the gaseous or liquid phase becomes supersaturated with respect to the solid component. A crude precipitation operation, therefore, can be transformed into a crystallization process by careful control of the degree of supersaturation.

A common method for producing a precipitate is to mix two reactant solutions together as quickly as possible, but the analysis of this apparently simple operation can be exceedingly complex. Precipitation processes, almost by definition, involve the creation of highly supersaturated systems and the main practical difficulty is to maintain reasonably uniform conditions throughout the reaction vessel. The choice of the method of mixing the reactants is therefore very important and the aim should be to avoid any accidental development of zones of excessive supersaturation. The sequence of reactant mixing can

also be of critical importance: A added to B to produce a precipitate C can often yield a very different product from that which results from the addition of B to A. The development of local pockets of reactants in non-stoichiometric ratios, undesirable pH levels, and so on, can have highly detrimental effects.

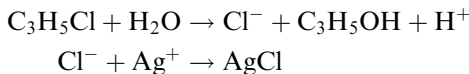
Further comments on the complexity of mixing processes during precipitation operations are made in section 8.1.7.

Primary nucleation does not necessarily commence as soon as the reactants are mixed, unless the level of supersaturation is very high. The mixing stage may be followed by an appreciable time lag (induction period) which depends on the temperature, supersaturation, efficiency of mixing, state of agitation, presence of impurities, and so on, before nuclei appear. Some time after the induction period a rapid desupersaturation ensues (see *Figure 5.12*) during which both primary (homogeneous and heterogeneous) and possibly secondary nucleation may occur together, but the predominant process at this stage is growth of nuclei. Particle agglomeration followed by ripening or other ageing processes can lead to subsequent particle coarsening.

Precipitation from homogeneous solution

For the purpose of gravimetric analysis, where it is necessary to effect an efficient separation of solid from liquid, it is generally accepted that precipitation should be carried out slowly from dilute solution. However, some substances, such as the hydroxides and basic salts of aluminium, iron and tin, demand extremely high dilutions and excessively long times for dense particles to be produced. The method known as precipitation from homogeneous solution (PFHS) allows coarse precipitates to be produced in relatively short times (Gordon, Salutsky and Willard, 1959).

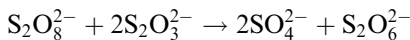
Briefly, the technique of PFHS consists of slowly generating the precipitating agent homogeneously within the solution by means of a chemical reaction. Undesirable concentration effects are eliminated, a dense granular precipitate is formed and co-precipitation is minimized. For example, silver chloride crystals can be produced in aqueous solution by the reactions:



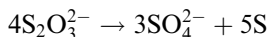
The growth kinetics of this process are reported to be second order and surface reaction controlled. The precipitation of silver iodide in ethanol by the reaction



is reported to be first order and diffusion controlled. Also first order and diffusion controlled are the precipitation of barium sulphate by a persulphate–thiosulphate reaction in the presence of Ba^{2+} :



and the production of sulphur (as a spherical monodisperse sol) by the decomposition of thiosulphate in acid solution:



Other PFHS methods that have been used for the production of crystalline precipitates by the controlled generation of the required anions in an appropriate aqueous solution include the hydrolysis of allyl chloride (Cl^-), dimethyl oxalate ($\text{C}_2\text{O}_4^{2-}$), triethylphosphate (PO_4^{3-}), dimethylsulphate (SO_4^{2-}) and thioacetamide (S^{2-}).

PFHS plays a very important role in analytical chemistry. It is also being used in studies of co-precipitation and nucleation phenomena because the slow controlled precipitation allows a close approach to equilibrium between the solid and solution. The applications of PFHS on the industrial scale have so far been limited, but it does appear to be a promising technique. Fractional precipitation methods are generally improved by PFHS and it has been applied to the difficult separation of radium and barium, for the production of carriers for radioactive materials and for the preparation of monodisperse suspensions of pigments and polishing agents.

Reviews of precipitation from homogeneous solution have been made by Gordon, Salutsky and Willard (1959); Cartwright, Newman and Wilson (1967); Matijević (1994).

Salting-out

A solution can be made supersaturated, with respect to a given solute, by the addition of a substance that reduces the solubility of the solute in the solvent. The added substance, which may be a liquid, solid or gas, is generally referred to as the 'precipitant' and the operation is known by a variety of terms. In the pharmaceutical industry, for example, for the precipitation/crystallization of organic substances from water-miscible organic solvents by the controlled addition of water to the solution, the term 'watering-out' is commonly used. The descriptions 'drowning-out', 'quenching' and 'solventing-out' have also been applied to the precipitation of electrolytes from aqueous solution by the addition of a water-miscible organic solvent. However, despite the fact that no single designation can be appropriate for all cases, the term 'salting-out' will be used for convenience throughout this section.

The properties required of a liquid precipitant are that it be miscible with the solvent of the original solution, at least over the ranges of concentration encountered, that the solute be relatively insoluble in it, and that the final solvent-precipitant mixture, if comprising valuable components, be readily separable, e.g. by distillation.

Salting-out has many advantages. For example, highly concentrated initial solutions can be made by dissolving an impure crystalline material in a suitable solvent. If the solute is very soluble in the chosen solvent, dissolution may be effected at low temperature and this is advantageous for the processing of heat-sensitive substances. By choosing a suitable precipitant, a high solute recovery

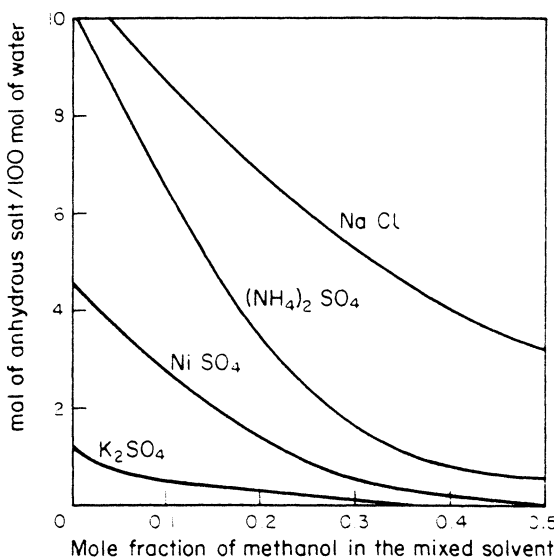


Figure 8.10. Solubility of some common salts in methanol–water mixtures at 20 °C

yield may be obtained (see *Figure 8.10*). Furthermore, better purification is often obtained than that from a straightforward crystallization operation since the mixed mother liquor often retains more of the undesirable impurities than does the original solvent. However, salting-out can have the disadvantage of needing a separation unit to handle fairly large quantities of mother liquor if the solvent and precipitant have to be recovered.

A slight dilution of the salting-out agent with the system solvent can be extremely beneficial in avoiding excessive nucleation in the regions of primary contact. This procedure, demonstrated with aqueous acetone used as a precipitant for potassium sulphate from aqueous solution, appears to offer considerable advantages for industrial processing in cases where very small primary crystals need to be avoided (Mullin, Teodossiev and Söhnel, 1989). A general model for controlled precipitant dosage rate addition in batch precipitation has been proposed by Jones and Teodossiev (1988).

Another possibility for reducing supersaturation levels, and hence nucleation rates, is to use an air-diluted precipitant. This is quite easy to arrange if the precipitant is a volatile organic liquid. A practical example of this technique is the foam column described by Halasz and Mullin (1987) which was used for the controlled precipitation of potash alum crystals from aqueous solution using air saturated with 2-propanol (*Figure 8.11*).

The use of hydrotropes, substances which possess the property of selectively enhancing the aqueous solubility of sparingly-soluble compounds, can afford an opportunity for mixture separation. Colônia, Dixit and Tavare (1998) describe an example of the use of a hydrotrope for the separation of the *o*- and *p*-isomers of chlorobenzoic acid from a 42/58% mixture, a typical ratio for the product from an industrial reactor. Sodium butyl monoglycol sulphate, used as a 50% aqueous solution, is a suitable hydrotrope in which the *ortho*-

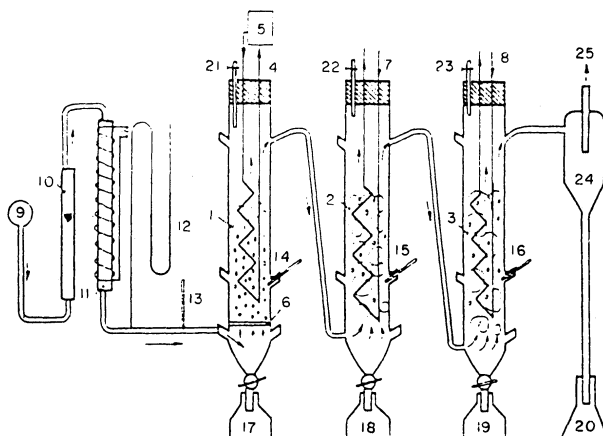


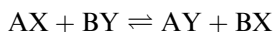
Figure 8.11. Controlled precipitation in a series of foam columns using an air-diluted vapour-phase alcohol as the precipitant for potash alum from aqueous solution. 1, alcohol evaporator; 2, 3, precipitation columns; 4, heater coil; 5, thermostat; 6, sintered glass distributor; 7, 8, cooling coils; 9, compressed air supply; 10, Rotameter; 11, preheater; 12, manometer; 13–16, thermometers; 17–20, sampling vessels; 21–23, inlet tubes; 24, cyclone; 25, vent to atmosphere. (After Halasz and Mullin, 1987)

isomer has a much higher solubility than the *para*- and from which crystals of > 99% pure *para*- can be precipitated when water is added in a controlled manner.

Gases or solids may be used as precipitants so long as they meet the requirement of being soluble in the original solvent and do not react with the solute to be precipitated. Ammonia can assist in the production of potassium sulphate by the reaction of calcium sulphate and potassium chloride. In water alone the yield is low, but in aqueous ammonia it is greatly improved. Hydrazine can act in a similar manner (Fernandez-Lozano and Wint, 1979). High pressure CO₂ has been used to precipitate sulphathiazole from solution in ethanol; the precipitation rate, crystal size and habit can be controlled by varying the CO₂ pressure (Kitamura *et al.*, 1997).

An example of the use of a solid precipitant is the addition of sodium chloride crystals for the salting-out of organic dyestuffs. The sodium chloride acts through the solution phase, i.e. it must dissolve in the water present before it can act as a precipitant, although its precise mode of action is probably quite complex.

Crystalline salts can be added to solutions to precipitate other salts as a result, for example, of the formation of a stable salt pair. This behaviour is encountered when two solutes, AX and BY, usually without a common ion, react in solution and undergo a double decomposition (metathesis):



The four salts AX, BY, AY and BX constitute a reciprocal salt pair. One of these pairs, AX, BY or AY, BX is a stable pair (compatible salts), which can coexist in solution, and the other an unstable salt pair (incompatible salts) which cannot (section 4.7.2).

Garrett (1958) has described the large-scale production of potassium sulphate from solid glaserite ore ($3\text{K}_2\text{SO}_4 \cdot \text{Na}_2\text{SO}_4$) which is added to an aqueous solution of potassium chloride. Conversion to a stable salt pair occurs, the Na_2SO_4 and KCl remain in solution and K_2SO_4 is precipitated. Mazzarotta (1989) studied the cooling crystallization of potassium sulphate from aqueous solutions of glaserite and reported the effects of traces of calcium on the nucleation and growth kinetics.

Further reference is made to the use of salting-out in crystallization processes in section 8.4.6.

8.1.6 Industrial applications

It is not possible to attempt a comprehensive survey of the enormous range of industrial precipitation practice, but the examples below will serve to indicate something of its diversity. A few references are listed for each topic to serve as an introduction to relevant literature.

Precipitated calcium carbonate is widely used industrially, with different applications usually demanding different physical and granulometric properties. Three different crystallographic forms of CaCO_3 can be precipitated (calcite, aragonite and vaterite) depending on the supersaturation, temperature, presence of trace impurities, etc. Kinetic studies have been reported by Maruscak, Baker and Bergougnou (1971). Roques and Girou (1974), Schierholz and Stevens (1975), Hostomský and Jones (1991), Wachi and Jones (1991, 1995) and Kabascı *et al.* (1996). Reddy (1978) has made a general survey of CaCO_3 precipitation from waste-waters, and a good introduction to the geochemical literature on CaCO_3 precipitation is given by Kitano, Okumara and Idogaki (1980). There are many reports of the effects of ionic and other trace impurities, e.g. Reddy and Nancollas (1976) and Söhnel and Mullin (1982).

Calcium sulphate can crystallize from aqueous solution as the dihydrate (gypsum), hemihydrate (α and β forms) or the anhydrous salt (anhydrite: α , β and ‘insoluble’ forms), many of which can coexist in contact with solution in metastable equilibrium. The solubilities of all forms of calcium sulphate decrease with increasing temperature (gypsum only above 32 °C) so CaSO_4 scale commonly forms on heat-transfer surfaces. Precipitation of calcium sulphate at elevated temperatures, a topic of interest in water-cooling towers, petroleum drilling operations, evaporative seawater desalination plants, etc., has been studied by Nancollas and Gill (1979). Simulations of calcium sulphate precipitation as encountered in the phosphoric acid wet process, have included studies of nucleation and growth kinetics (e.g. Amin and Larson, 1968; Sikdar, Ore and Moore, 1980) and the effects of trace impurities (e.g. Sarig and Mullin, 1982; Budz, Jones and Mullin, 1986).

The precipitation of alumina trihydrate (Bayer hydrate) from caustic (sodium aluminate) solution is an important step in the production of alumina from bauxite by the Bayer process. The reaction



is normally carried out in the presence of alumina trihydrate seeds to induce the formation of the appropriate species. Agglomeration plays an important part in the development of the final product. Kinetic studies of Bayer hydrate precipitation include those of Misra and White (1971) and Halfon and Kaliaguine (1976).

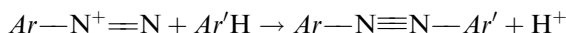
Magnesium is recovered from seawater and brines on a large scale worldwide by the precipitation of its hydroxide. Some processes use lime as the precipitant while others use calcined dolomite (dolime) which reacts with MgCl₂ according to



thus enhancing the magnesium yield for a given quantity of seawater. Laboratory studies of Mg(OH)₂ precipitation pertinent to the industrial process have been described by Phillips, Kolbe and Opperhauser (1977), Söhnle and Maracek (1978), Petric and Petric (1980) and Mullin, Murphy, Söhnle and Spoors (1989).

Photographic emulsions consist of dispersions of silver halide crystals, around 1 µm in size, in a protective colloid such as gelatin. The light sensitivity of the finished photographic emulsion is to a large extent dependent on the crystal size distribution. Emulsions of high light sensitivity are based on silver bromide containing small percentages of silver iodide. Most commercial photographic emulsions are made by adding silver nitrate solution slowly to an agitated vessel containing an aqueous solution of gelatin containing excess halide. After precipitation of the silver halide, the dispersion may be held at a given temperature to permit ripening (Margolis and Gutoff, 1974; Leubner, Jagganathan and Wey, 1980).

Many pigments, such as Prussian blue, iron oxide reds and yellows, and the chromate pigments, are manufactured by precipitation processes. The most important group of synthetic organic pigments (Abrahart, 1977) are the azo group produced by the diazotization of an aromatic amine followed by coupling the soluble diazo compound with a suitable agent to form an azo linkage. This latter step is the precipitation stage:



where Ar and Ar' represent different aryl groups. The colour of a pigment depends on the physical form in which it is precipitated and this, in turn, depends on the kinetics of the coupling reaction and the subsequent nucleation and growth steps. The important variables include concentration, temperature, pH, time and presence of impurities and/or additives. Stringent particle size and size distribution limits around 0.2 µm are usually specified. The respective merits of batch and continuous coupling methods have been discussed by Nobbs and Patterson (1977). Gutoff and Swank (1980) report a pilot-scale (300 g/h) study in which amorphous spherical dye particles can be obtained continuously by precipitation from solution in a water-miscible solvent by the addition of water.

Crystalline sucrose develops interesting physicochemical properties when its specific surface exceeds about 2000 cm² g⁻¹, which corresponds roughly to

a crystal size of around 20 µm. Sucrose crystals of this size and smaller are of importance for icing sugar and for use as seed material in large-scale sugar-boiling practice. Such small crystals are normally produced by comminution, e.g. in hammer mills, or in the latter case by ball-milling in the presence of a liquid such as isopropanol. Precipitation, however, would appear to offer an alternative procedure with potential advantages. Sucrose may be precipitated from aqueous solution by the addition of a water-miscible organic liquid. Of a wide range of precipitants studied by Kelly and Mak (1975), 2-methoxy ethanol gave the smallest discrete crystals (about 5 µm) with the best physical properties.

There is an increasing use of precipitation for the production of colloidal nanoparticles in such fields as pharmacy and cosmetics. Plasari, Grisoni and Villermieux (1997) reported an extensive study on the production of ethylcellulose nanoparticles from solution in ethanol by drowning-out with water. The most important process parameter controlling the product particle size distribution was found to be the ethylcellulose concentration in the ethanolic solution. Contrary to all expectations, other parameters such as type of agitator and speed, solvent:nonsolvent ratio and temperature had practically no influence. In addition, the particle size distribution was insensitive to scale-up and a distinct double population of single nanoparticles (<100 nm) and aggregates (>200 nm) was obtained in all runs. A comparison was made between the experimental results and predictions made from classical nucleation theories and aggregative growth models.

Salting-out is commonly used for the recovery of proteins from solution since their solubility is considerably reduced by increasing the ionic strength. Ammonium and sodium sulphates are most commonly used for this purpose. The control of pH is of critical importance: a protein molecule may be represented as a dipolar ion and pH determines the overall net charge on the molecule. A protein exhibits its minimum solubility at the isoelectric point (zero net charge) and for a pure protein this can be very sharp, the solubility increasing greatly even at 0.5 pH on either side of the minimum. Detailed studies have been reported by Hoare (1982) and Nelson and Glatz (1985). Richardson, Hoare and Dunnill (1990) have developed a framework for optimizing the design and operation of the fractional precipitation of proteins. They illustrate their method experimentally by the precipitation of the enzyme alcohol dehydrogenase from clarified baker's yeast homogenate using saturated ammonium sulphate solution, a system that represents a typical industrial microbial protein source and precipitating agent.

Until comparatively recently, the only reported stable inorganic hydrosols were primarily sols of elements such as gold, sulphur, selenium, etc. and compounds such as silica, lead iodate, silver halides, etc. A considerable amount of attention is now being paid, however, to the preparation of mono-dispersed hydrous metal oxides, which are chemically considerably more complex than other crystalline or stoichiometrically well-defined materials and are of interest as potential catalysts. Examples include the hydrous oxides of chromium and aluminium (spheres) and copper and iron (polyhedra) with particle sizes < 1 µm. One manufacturing procedure consists of ageing aqueous

solutions of metal salts at elevated temperatures under controlled conditions of concentration, pH and temperature for several hours in the presence of complexing anions, notably sulphate or phosphate (Catone and Matijevich, 1974). Her, Matijevich and Wilcox (1990) describe a continuous precipitation method for yttrium basic carbonate, in a tubular reactor containing static in-line mixing elements, in which aqueous solutions of an yttrium salt and urea are brought into contact and subsequently aged.

Methods and equipment

Although precipitation is a widely used industrial process, it is disappointing, to say the least, to find so few informative published reports on its large-scale applications. The vast majority of papers in the scientific and technical literature refer to laboratory, and very occasionally to small pilot-scale, operation. Nevertheless, there is a wealth of published information available although it is scattered widely across the boundaries of many disciplines.

Most industrial precipitation units are simple in construction. The prime aim is usually to mix reacting fluids rapidly and to allow them to develop a precipitate of the desired physical and chemical characteristics. Batch operation is more often favoured for industrial precipitation than is the truly continuous mode, although the merits of semi-continuous operation deserve serious consideration, i.e. a continuous reactant mixing step from which the product stream passes to batch-operated agitated hold-up tanks to permit equilibration, phase transformation, ripening, etc. The hold-up tanks may be arranged in a sequenced battery or in a continuous cascade system (see section 9.1.2).

A distinct advantage of batch precipitation, widely acknowledged in the pharmaceutical industry, is that the vessel can be thoroughly washed-out at the end of each batch to prevent the seeding of the next charge with an undesirable phase that might have arisen from transformation, rehydration, dehydration, air oxidation, etc., during the batch cycle. Continuous precipitation systems often undesirably self-seed after some operating time, resulting in the need for frequent shut-down and wash-out.

Seeded precipitations are occasionally encountered, but very large amounts of seed material are generally required compared with those normally utilized in conventional crystallization processes (section 8.4.5). It is not uncommon, for example, to recycle up to 50 per cent of the magma through a loop system in a seeded precipitator to provide the seed surface area needed.

Several assessments of experimental data from continuously operated precipitators, utilizing the population balance (section 8.1.1), are of particular interest, e.g. the MSMPR studies on calcium carbonate by Baker and Bergognou (1974), calcium sulphate hemihydrate in phosphoric acid (Sikdar, Ore and Moore, 1980) and silver bromide in aqueous gelatin suspension (Wey, Terwilliger and Gingello, 1980).

Batch precipitation is more complex than continuous precipitation since the basic mechanisms of nucleation and growth can change during the batch period. The development process is generally further complicated by the intervention of agglomeration and ripening. The accounts by Margolis and Gutoff

(1974) and Tavare, Garside and Chivate (1980), Mersmann and Kind (1988) and Söhnle, Chianese and Jones (1991) highlight some of the problems involved. The report by Bryson, Glasser and Lutz (1976) is one of the few attempts to compare batch and continuous operation: laboratory-scale data are presented for the precipitation of ammonium paratungstate from boiling aqueous solutions of ammonium tungstate.

Reports on truly continuous precipitation on an industrial scale are a rarity. The study by Stevenson (1964), therefore, is quite interesting not only because it reports a pilot-plant study of a continuous precipitation (of ammonium diuranate by reacting uranyl nitrate solution with ammonia) but also because a design route for a multistage continuous unit operated with feedback is proposed. Regrettably, there does not appear to have been any follow-up to this work.

The two-stage precipitator (*Figure 8.12*) described by Aoyama, Kawakami and Miki (1979) appears to contain features that could serve other applications. In the particular process considered, the feed liquor containing 100 kg m^{-3} of NaOH and 40 kg m^{-3} of Al^{3+} passes into a suspension of aluminium hydroxide seeds kept at 60°C . Comparatively small crystals of aluminium hydroxide are suspended in the upper zone A by solution liquor flowing upwards from zone B. As the crystals develop, either by growth or by agglomeration, they fall into the lower zone B where they continue to grow. An average slurry density of about 25 per cent by mass in zone B allowed particles of around $100 \mu\text{m}$ mean size to be produced at approximately 0.75 ton h^{-1} .

8.1.7 Mixing techniques

The mixing of a reactant feedstock stream with the contents of a precipitation vessel is of critical importance in the control of precipitate development. It is

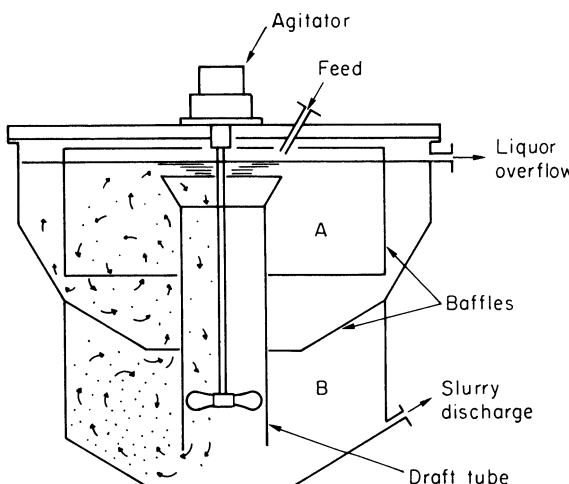


Figure 8.12. A seeded two-stage precipitator for the recovery of aluminium hydroxide. (After Aoyama, Kawakami and Miki, 1979)

essential to achieve good overall mixing to smooth-out supersaturation peaks in local regions. Both micromixing and macromixing are involved. The former is concerned with mixing at or near the molecular level, and is influenced by fluid physical properties and local conditions. The latter, which is concerned with bulk fluid movement and blending, is influenced by agitator speed, vessel geometry, etc. A third scale of mixing, named *meso-mixing* by Baldyga and Bourne (1997, 1999), is the turbulent dispersion of an incoming fresh feedstock plume within a precipitator. These three types of mixing are often considered independently, but their contributions to the overall effects of mixing on the precipitation process are extremely complex (Garside and Tavare, 1985; Söhnle and Mullin, 1987; Villermaux, 1988; Rice and Baud, 1990; Marcant and David, 1991; Söhnle and Garside, 1992; Mersmann, 1995; Baldyga and Bourne, 1999).

The position of the feedstock entry point(s) can have a great influence on the precipitate quality. A few examples of the many choices available are shown in Figure 8.13. If two reactant feedstocks A and B are involved, A could be fed on or near the surface of reactant B already in the vessel in the so-called 'single-jet' mode (Figure 8.13a) or A could be introduced into the intensely agitated zone near the impeller blade (Figure 8.13b). The latter procedure often results in the production of larger primary crystals since the good mixing keeps local levels of supersaturation low at the first point of contact and minimizes the nucleation rate. Reactant B could be introduced as a single jet into reactant A charged first into the vessel, if required. The sequence of reactant additions often has a significant effect on the characteristics of the precipitate produced.

Alternatively, both reactant streams A and B may be introduced to the vessel simultaneously, in the so-called 'double-jet' mode, and again several choices emerge. For example, streams A and B could be introduced together near the surface (Figure 8.13c), or near the impeller tip (not illustrated). On the other hand, the two streams could be premixed before entering the vessel as a single jet (Figure 8.13d) at some appropriate point.

Premixing of feedstocks is often used because it can provide a means of exerting some control over the initial supersaturation levels. Impinging jets or

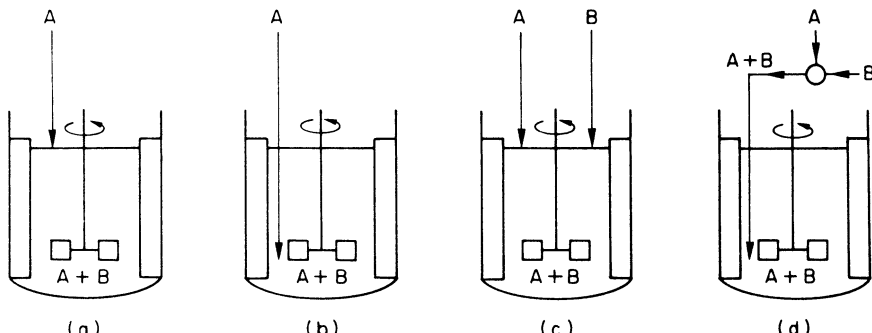


Figure 8.13. Some possibilities for introducing reactant feedstock streams to a precipitation vessel

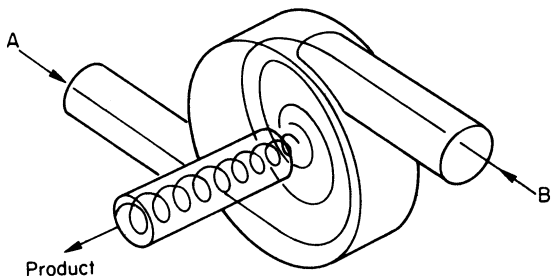


Figure 8.14. A vortex mixer for premixing feedstocks. (Courtesy of AEA Technology, Harwell)

in-line mixers of a variety of designs (e.g. see *Figure 8.14*) may be used for premixing purposes, some of which will allow complete mixing to be achieved in a matter of milliseconds (Demyanovich and Bourne, 1989).

Controlled double-jet precipitation, which attempts to control primary nucleation and the subsequent processes of crystal growth, ripening and agglomeration, is a technique that has been used for many years in the photographic industry for the production of silver halide microcrystals ($< 5 \mu\text{m}$). It can also be used, with suitable adaptation, for the production of other sparingly soluble salts. A comprehensive survey of the wide range of related procedures that have been used in the past 40 years to produce monodisperse micro-particles, together with detailed accounts of experimental studies using variations of controlled double-jet precipitation has been made by Stávek *et al.* (1992).

A precipitation process can be operated under batch, semi-batch or continuous conditions, each of which will have its own distinct influence on the product crystal size distribution in addition to the combined influences of feedstock entry positions, variations in the reactant addition rate profile and mixing intensity (Tavare and Garside, 1990; Söhnel and Garside, 1992).

Guidelines for the choice of optimum reactant solution concentrations in a precipitation process have been proposed by Lindberg and Rasmussen (2000) who showed that larger crystals are produced when the feed concentration is kept low in the early stages of the process and then allowed to increase with time in a controlled manner. The term *programmed feed concentration* is introduced for this mode of operation in allusion to the method of *programmed cooling* for batch crystallizers described in section 8.4.5.

CFD modelling

Considerable advances have been made in recent years, using computational fluid dynamics (CFD), towards a better understanding of mixing effects and their influence on precipitation processes (Leeuwen, Bruinsma and van Rosmalen, 1996; Wei and Garside, 1997; Leeuwen, 1998; Al-Rashed and Jones, 1999; Zauner and Jones, 2000b). Several commercial and private CFD packages are now available to facilitate solution of the relevant mass, momen-

tum and energy conservation equations, and many will also incorporate precipitation kinetics and population balance modelling.

Most of the experimental work aimed at verifying CFD modelling procedures has so far been performed on small-scale laboratory equipment, but encouraging progress is being made. For example, Leeuwen (1998) developed a three-compartment model which describes in considerable detail the initial turbulent mixing of the feed streams with the surrounding bulk fluid in a continuous stirred tank reactor. He compared the findings with experimental results for BaSO₄ precipitation with jet mixing in a 2½ L reactor. Zauner and Jones (2000b) developed another approach to the scale-up of both continuous and semibatch precipitation of calcium oxalate in reactors ranging in size from 0.3 to 25 L equipped with a variety of agitators. Residence time/feed time, feed concentration, feed point position, feed tube diameter, impeller type and stirring rate were varied. A segregated-feed model was developed, coupling CFD and population balance data, which could lead to the reliable scale-up of precipitation processes. It is interesting to note that conventional scale-up criteria (equal power input per unit mass, equal tip speed, equal stirring rate, etc.) were found incapable of predicting the observed effects of mixing conditions on the particle size distribution.

At the time of writing, CFD techniques and the interpretation of their results are still in their infancy, but with ever increasing computational power becoming available, substantial advances towards unravelling the complexities of mixing processes may confidently be expected in the very near future.

8.2 Crystallization from melts

As explained in section 3.1, the term 'melt' strictly refers to a liquid close to its freezing point, but in its general industrial application it tends to encompass multicomponent liquid mixtures that solidify on cooling. Melt crystallization is the common term applied to the controlled cooling crystallization and separation of such systems with the objective of producing one or more of the components in relatively pure form.

Melt crystallization is often considered to be commercially attractive since it offers the potential for low-energy separation compared with distillation, because latent heats of fusion are generally much lower than latent heats of vaporization. The best example in *Table 8.1* is that of water where there is almost a 7 : 1 difference in the two heat quantities. A further advantage of melt crystallization over distillation is that it operates at much lower temperatures, and this can be very helpful when processing thermally unstable substances. In practice, however, the benefits of low-energy separation for industrial melt crystallization can be outweighed by operational problems associated with the need to separate purified materials from impure residues. Operating costs can also escalate if refrigeration, rather than normal cooling water, is required. Technical limitations to the theoretical possibilities for melt crystallization have been discussed in some detail by Wintermantel and Wellinghoff (1994).

Table 8.1. Enthalpies of crystallization and distillation

Substance	Crystallization		Distillation	
	Melting point, °C	Enthalpy of crystallization, kJ kg ⁻¹	Boiling point, °C	Enthalpy of vaporization, kJ kg ⁻¹
<i>o</i> -Cresol	31	115	191	410
<i>m</i> -Cresol	12	117	203	423
<i>p</i> -Cresol	35	110	202	435
<i>o</i> -Xylene	-25	128	141	347
<i>m</i> -Xylene	-48	109	139	343
<i>p</i> -Xylene	13	161	138	340
<i>o</i> -Nitrotoluene	-4.1	120	222	344
<i>m</i> -Nitrotoluene	15.5	109	233	364
<i>p</i> -Nitrotoluene	51.9	113	238	366
Benzene	5.4	126	80	394
Water	0	334	100	2260

8.2.1 Basic principles

Not all melts are amenable to separation by crystallization. The phase equilibria (Chapter 4) will generally decide the feasibility of the process and often give guidance to the choice of the basic procedure to be followed. Only a eutectic system (*Figure 8.15a*) will allow the crystallization of a pure component from a melt in one step, but a solid solution system (*Figure 8.15b*) requires a sequence of fractionation steps to yield high-purity products.

The crystallization of a single component (different for feedstocks to the left or right of the eutectic point) in one step from a eutectic system has already

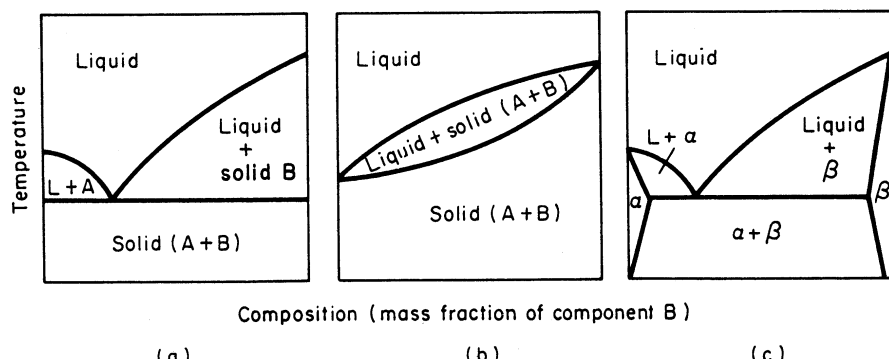


Figure 8.15. Some binary solid–liquid phase diagrams encountered in melt crystallization: (a) simple eutectic; (b) simple solid solutions; (c) eutectic with limited solid solubility (α and β are solid solutions)

been discussed in section 4.3.1 (*Figure 4.4*). The repeated melting and freezing steps necessary to produce crystalline products of increasing purity from a solid solution system are described in section 4.3.3 (*Figure 4.7a*). *Figure 8.15c* shows a binary eutectic system with limited solid solubility, which would prevent a one-step crystallization from producing a pure component. The existence of this type of system should be suspected if product contamination persists in a sequence of melt crystallization steps.

Other more complex systems may be encountered, however, including minimum melting solid solutions, eutectics with compound formation, etc., but in a comprehensive survey of binary organic mixtures, Matsuoka (1991) estimated that over 50% exhibited simple eutectic behaviour, about 25% formed intermolecular compounds and about 10% formed solid solutions of one kind or another. Interestingly, fewer than 2% formed simple solid solutions (*Figure 8.15b*).

Ternary eutectics

The Jänecke projection (section 4.4) in *Figure 8.16* shows the phase equilibria for the ternary system, *ortho*-, *meta*- and *para*-nitrotoluene; the three pure components are represented by the letters *O*, *M* and *P*, respectively, at the apexes of the triangle. Four different eutectics can exist in this system, three binaries and one ternary:

Symbol	Eutectic points Components	Per cent by mass			Temperature °C
		<i>O</i>	<i>M</i>	<i>P</i>	
<i>A</i>	<i>O</i> - <i>M</i>	52	48	—	-31.7
<i>B</i>	<i>O</i> - <i>P</i>	76	—	24	-16.3
<i>C</i>	<i>M</i> - <i>P</i>	—	67	33	-2.8
<i>D</i>	<i>O</i> - <i>M</i> - <i>P</i>	42	44	14	-40.0

Figure 8.16 may be used to assess a cooling process for mononitrotoluene (Coulson and Warner, 1949). For example, if the crystallizer is supplied with a liquid feedstock containing 3.0% *ortho*, 8.5% *meta* and 88.5% *para*, it is a simple matter to estimate the potential yield of *p*-nitrotoluene, choosing an operating temperature of say 20 °C, as follows.

Point X in *Figure 8.16* represents the composition of feedstock located between the 40 and 50 °C isotherms. By interpolation, the temperature at which this system starts to freeze can be estimated as about 46 °C. As point X lies in the region PBDC, pure *para*- will crystallize out once the temperature falls below 46 °C, and the composition of the mother liquor will follow line XYZ (i.e. away from point P) as cooling proceeds. At point Z (about -15 °C) on curve DC, *meta*- also starts crystallizing out. It is not necessary, however, to cool to near -15 °C in order to get a high yield of *para*-, as the following data, based on 100 kg of feedstock, show:

Temperature, °C	Para- deposited, kg	Mother liquor, kg	Composition of mother liquor (mass per cent)		
			O	M	P
46	0	100	3.0	8.5	88.5
40	39.6	60.4	5.0	14.0	81.0
30	66.7	33.3	8.7	24.8	66.5
20	75.0	25.0	12.0	34.0	54.0
10	79.6	20.4	14.7	41.6	43.7
0	82.3	17.7	16.7	48.0	35.3
-10	84.8	15.2	19.0	53.9	27.1

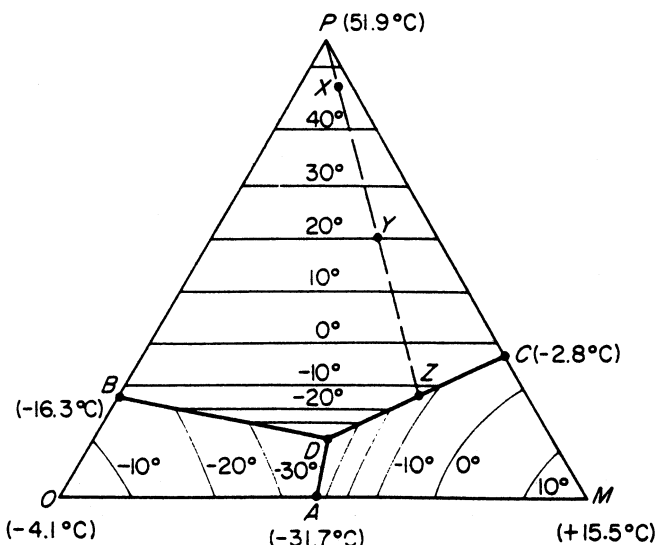


Figure 8.16. Phase diagram for the ternary system o-, m- and p-nitrotoluene (point D = -40.0 °C)

The above mother liquor compositions are read off Figure 8.16 at the point at which the line P → Z cuts the particular isotherm. The total mass of para-crystallized out is calculated by the mixture rule. For example, for 100 kg of original mixture X at 20 °C (point Y)

$$\text{para-deposited} = 100 \left(\frac{\text{distance XY}}{\text{distance PY}} \right) = 75 \text{ kg}$$

which is equivalent to a recovery of about 85 %.

8.2.2 Processes and equipment

Simple agitated vessels, such as those commonly used in solution crystallization (section 8.4), rarely find application in melt crystallization processes. One of the

main reasons is the difficulty in maintaining efficient mixing in the high-density magmas normally encountered; it is not uncommon for more than 90% of a melt to crystallize compared with less than 30% of a solution. Massive encrustation on the heat-transfer surfaces is another common problem in melt crystallization, on account of the large temperature driving forces generally used.

The possibility of overcoming encrustation problems by applying direct contact cooling techniques (section 8.4.1) has been explored for the separation of organic eutectic systems by suspension melt crystallization (Kim and Mersmann, 1997; Bartosch and Mersmann, 1999). These laboratory studies, which utilized both gas (air) and liquid (water) as coolants were aimed at measuring heat transfer and kinetic data and observing the crystal product characteristics. Eventual industrial application (section 8.2.3) appears possible.

Sweat-tank crystallizers

Batch-operated, non-agitated sweat-tank crystallizers were first developed towards the end of the 19th century for the processing of phenolic feedstocks in the coal-tar industry. A batch of melt is charged into a tank virtually filled with coils or fin-tubes that can carry either cooling water or steam. The batch is cooled until it almost completely solidifies: crystals first adhere to the cooling surfaces. In the second part of the cycle, steam is introduced to the heat transfer elements and the adhering crystalline mass begins to melt, impurity inclusions are sweated-out and the resulting melt washes away adhering impurities on the crystals. The run-off melt is continuously analysed, and when it reaches the required product purity, it is directed to a product receiver as the rest of the charge is melted.

These principles were embodied in the Proabd refiner (Société Proabd, 1959; Molinari, 1967a) which also incorporated a feature to prevent the melt run-off outlet in the bottom of the tank becoming blocked with crystal during the cooling cycle. One proposed method was to fill the bottom of the tank, up to the first set of cooling coils, with an immiscible, high-density, low-melting fluid which is first run off when the melting process is commenced. For naphthalene, for example, a suitable fluid would be a concentrated solution of sodium hydroxide.

The Sulzer static melt crystallizer with close-packed cooling plates (*Figure 8.17*) is a more recent refinement of the sweat-tank concept in which the freezing and subsequent melting sequences are time-controlled, the heat transfer fluid temperature being lowered and raised according to a pre-set programme. Production rates up to 20 000 ton/year and product purities up to 98% are claimed.

Scraped-surface chillers

A robust mechanical unit that can cope with most encrustation problems is the scraped-surface heat exchanger, often referred to as a ‘scraped-surface chiller’ when used in crystallization operations. The unit is essentially a double-pipe heat exchanger fitted with an internal scraping device to keep the heat transfer

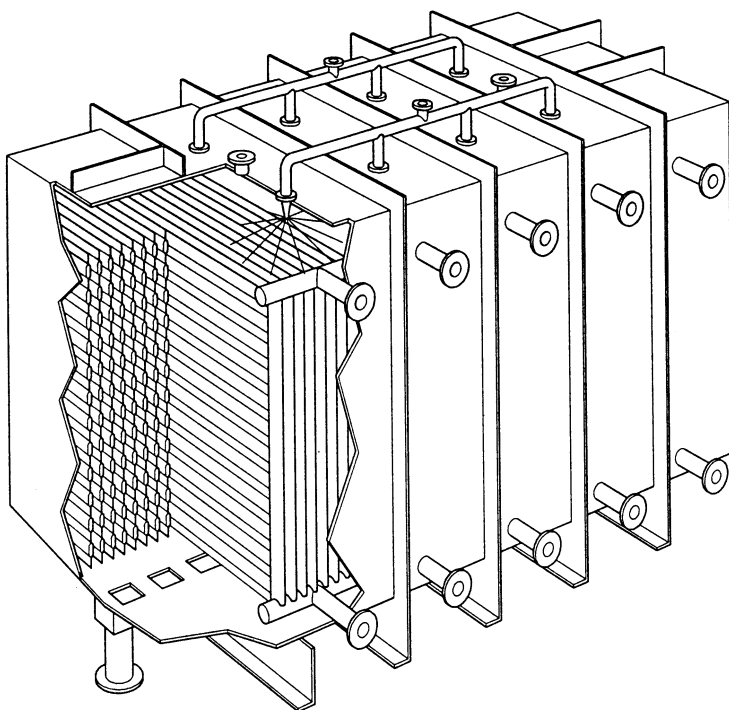


Figure 8.17. The Sulzer static melt crystallizer

surface clean. The annulus between the two concentric tubes contains the cooling fluid, which moves countercurrently to the crystallizing solution flowing in the central pipe. Located in the central pipe is a shaft upon which scraper blades, generally spring-loaded, are fixed. The units range in internal diameter from about 150–500 mm and in length up to about 3 m. The close-clearance scraper blades rotate at a relatively slow speed (10–60 rev/min) and, operating with a $\Delta T > 15^\circ\text{C}$, an overall heat transfer coefficient in the range 0.2–1 $\text{kW m}^{-2} \text{K}^{-1}$ may be expected (Armstrong, 1969).

It should be noted, incidentally, that scraped-surface heat exchangers used with homogeneous liquid feedstocks and products normally operate at much higher rotor speeds (up to 2000 rev/min) than those of crystallization units and give overall heat transfer coefficients up to 4 $\text{kW m}^{-2} \text{K}^{-1}$ (Skelland, 1958).

Scraped-surface chillers are employed for the crystallization of fats and waxes and the processing of viscous materials such as lard, margarine and ice cream (Bailey, 1950; Swern, 1979; Timms, 1991). They are also used for the freeze-concentration of foodstuffs such as fruit juices, vinegar, tea and coffee (section 8.4.7). The crystals produced by scraped-surface crystallizers are generally very small since nucleation and crystal breakage can be excessive. Indeed, in some processes, scraped-surface units are often installed for the sole purpose of providing nuclei for the growth zone of another crystallizer (see Figures 8.19 and 8.20). A particular advantage of the scraped-surface crystallizer is that the amount of process liquor hold-up is very low.

Column crystallizers

A process for the fractional crystallization of a melt in a countercurrent column was first patented by P. M. Arnold in 1951. In 1961, H. Schildknecht utilized a spiral conveyor to transport the solids up or down the column. These techniques, together with other later refinements, may now be seen in several commercial-scale melt crystallizers.

The principles of column crystallization are shown in *Figure 8.18*. In the end-fed unit (*a*), a slurry feedstock enters at the top of the column, the crystals fall countercurrently to upflowing melt, and there is a heat and mass interchange between the solid and liquid phases. When the purified crystals migrate to the lower zone, they are remelted to provide high-purity melt for the upflow stream. The centre-fed column (*b*) takes a liquid feedstock. Crystals conveyed downwards by means of a screw conveyor are subjected to a surface washing action as they come into contact with the counterflowing melt. The high-purity crystals reaching the bottom of the column are melted by the heater and a liquid product is removed. Some Schildknecht-type columns are operated in the reverse mode, i.e. with a heater at the top and a freezer at the bottom, in which case the crystals are transported up the column. Although successful as a laboratory apparatus (<200 mm diameter), no large-scale industrial applications of the Schildknecht column have yet been reported.

Models for and analyses of column crystallizer operation have been discussed by Bolsaitis (1969); Player (1969); Albertins, Gates and Powers (1967); Gates and Powers (1970); Henry and Powers (1970); and Betts and Girling (1971).

An early example of the commercial application of countercurrent column crystallization was the Phillips *p*-xylene process (McKay and Goard, 1965; McKay, 1967). A concentrated *p*-xylene feedstock is cooled from about 10 °C to -18 °C in a scraped-surface chiller cooled with ethylene (*Figure 8.19*) to produce a slurry containing about 40 % of crystals by mass. This slurry feedstock

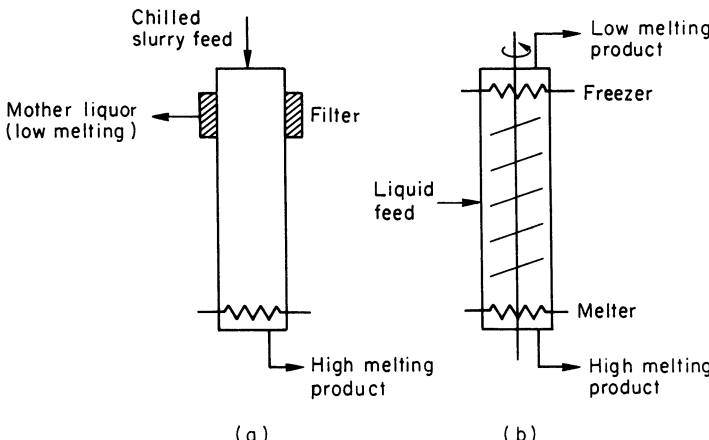


Figure 8.18. Column crystallizers: (a) end-fed column (Arnold type), (b) centre-fed column with spiral conveyor (Schildknecht type)

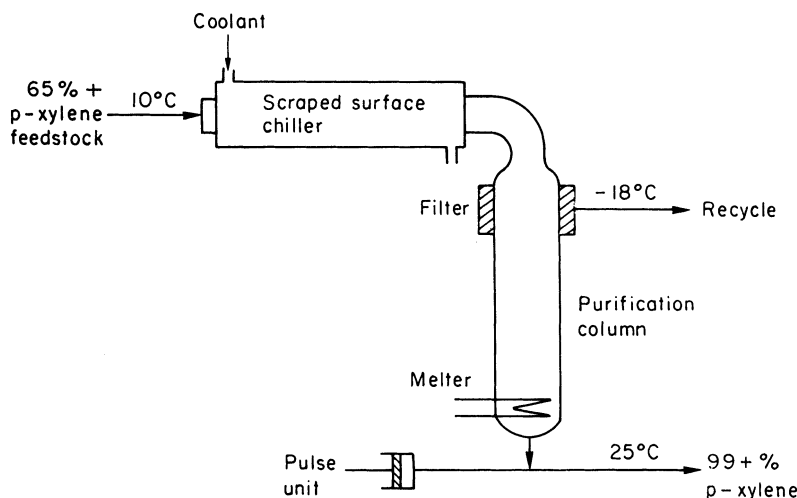


Figure 8.19. Phillips countercurrent pulsed column for the production of p-xylene

passes into a pulsed purification column which acts predominantly as a countercurrent wash unit, removing adhering impurities from the crystal surfaces, although a small amount of melting and recrystallization does take place. A high purity p-xylene melt emerges from the heater section at the base of the column. A filter at the top of the column prevents crystals from being carried out with the spent mother liquor, which is recycled. An important function of the pulse action is to keep the filters clear by inducing a reverse flow through the filter medium during part of the pressure pulse cycle. Columns of up to 70 cm diameter have been operated.

Brodie purifier

The Brodie purifier (Brodie, 1971) is a countercurrent melt purification system with the added feature of an imposed temperature gradient between the residue and product outlets. The unit thereby acts as a countercurrent multistage fractionator with partial melting and recrystallization occurring along its length.

The essential features are shown in *Figure 8.20*. The heat exchangers, provided with slow-moving scraper-conveyors, are arranged into refining and recovery sections separated by the feed inlet point. Feedstock enters continuously and flows through the recovery section towards the cold end (low-melting residue outlet) while crystals formed by cooling are conveyed countercurrently through the refining section towards the warm end (inlet to the purification column). During their passage they are continually subjected to partial melting, releasing low-melting impurities which flow back with the liquid stream. The interconnected scraped-surface heat exchangers are of progressively smaller diameter to maintain reasonably constant axial flow velocities and minimize back-mixing. A final purification stage is provided by the vertical column purification zone in which the crystals fall countercurrently to an upflow of high-purity melt produced from the melter at the base of the column.

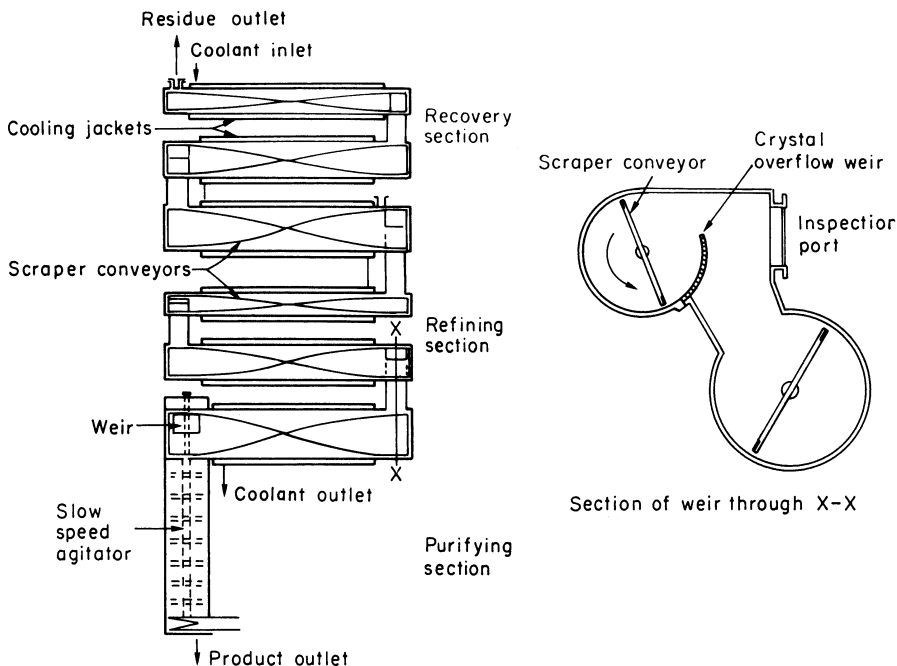


Figure 8.20. The Brodie purifier

Brodie units have been successfully employed for the production of high-purity *p*-dichlorobenzene and naphthalene at rates up to 7500 ton/year (Molinari and Dodgson, 1974).

TSK process

The Tsukishima Kikai countercurrent cooling crystallization process (frequently referred to as the TSK 4C process) is a development of Brodie technology with the scraped-surface chillers replaced by several cooling crystallizers connected in series. The flow sheet in *Figure 8.21* shows three conventional agitated cooling crystallizers connected in series. Feed enters the first stage vessel and partially crystallizes. The first stage slurry is continuously pumped to a hydrocyclone to be concentrated before passing to a Brodie-type column. After passing through a settling zone in the crystallizer, clear melt overflows to the next stage. Slurry pumping towards the purifying column and clear melt overflow from each stage result in a countercurrent flow of liquid and solid phases. The process has been applied to the large-scale production of *p*-xylene (Takegami, Nakamaru and Morita, 1984).

TNO column

The essential features of the TNO (Toegepast-Natuurwetenschappelijk Onderzoek) column are shown in *Figure 8.22* (Arkenbout, 1976, 1978). A crystal

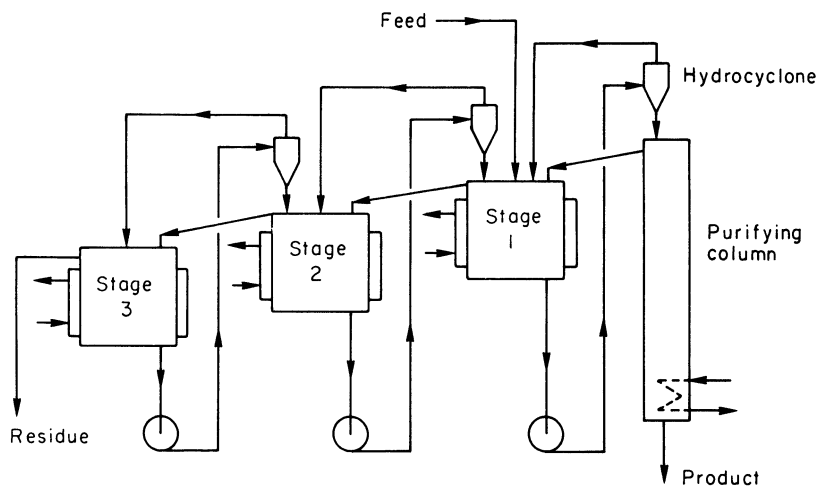


Figure 8.21. TSK countercurrent cooling melt crystallization process

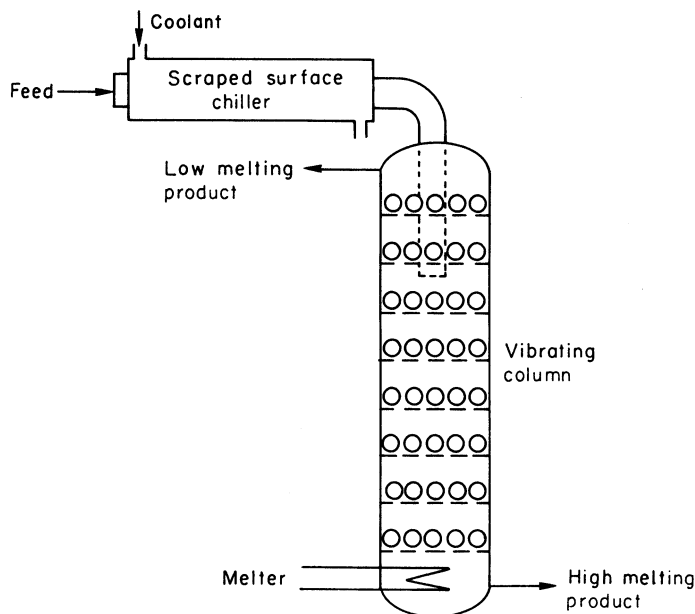


Figure 8.22. The TNO vibrating ball and plate column

slurry is produced in a scraped-surface chiller at the top of the column and passes downwards through a series of vibrating sieve trays, each loaded with a single layer of metal balls. The action of the balls is to crush the crystals, assist their passage through the perforated trays and expose fresh surfaces to the countercurrent melt flow. Successful results have been reported with benzene-thiophene in 80 mm diameter laboratory columns, and trials have been

reported on a pilot-scale 500 mm diameter column (Arkenbout, 1978). Scale-up to commercial size, however, has not yet been achieved.

Sulzer MWB process

The Sulzer MWB process (Fischer, Jančić and Säxer, 1984) is a melt crystallizer that operates basically by crystallization on a cold surface, but with features which allow it to operate effectively as a multistage separation device. Consequently, it can be used to purify solid solution as well as eutectic systems.

The effective multistage countercurrent scheme is illustrated for four-stage operation in *Figure 8.23a*. Stage 1, is fed with melt L_2 and recycle liquor $L_1 - L$, where L is the reject impure liquor stream. A quantity of crystals C_1 is deposited in stage 1. In stage 2 the melted crystals C_1 are contacted with melt L_3 and fresh feedstock F . Subsequent crystallization yields crystals C_2 and melt L_3 . Stages 3 and 4 follow similar patterns and, in this example, the final high-purity stream C_4 , after being remelted, is split into product C and recycle melt $C_4 - C$.

Only one crystallization vessel, a vertical multitube heat exchanger, is needed. The crystals are not transported; they remain inside the vessel, deposited on the internal surfaces of the heat exchanger tubes until they are melted by

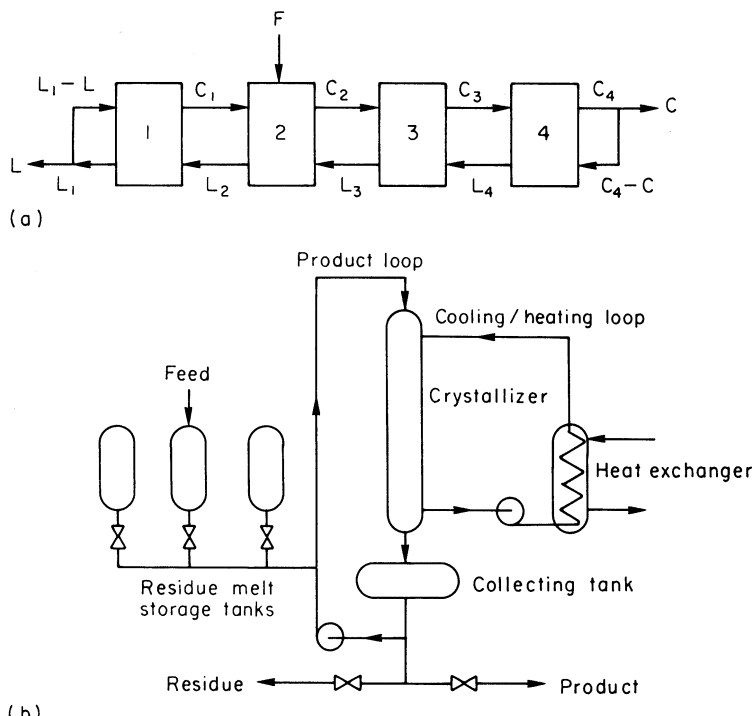


Figure 8.23. The Sulzer MWB process: (a) multistage flow diagram (C = crystal, L = liquor); (b) plant layout (A = crystallizer, B = melt collection tank, C = residue melt storage tank, D = heat exchanger, E = pump)

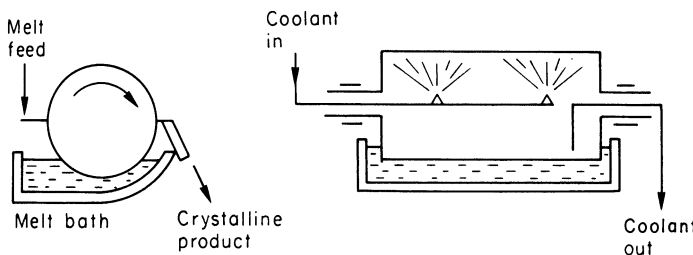


Figure 8.24. Rotary drum crystallizer

the appropriate incoming warm liquor stream. The control system linking the storage tanks and crystallizer consists of a programme timer, actuating valves, pumps and the cooling loop (*Figure 8.23b*).

The MWB process has achieved remarkable success in the recent years, finding large-scale industrial applications in the purification of a wide range of organic substances and the separation of fatty acids (Jančić, 1989). Production rates >100 000 ton/year from groups of linked units are possible.

Rotary drum crystallizers

The rotary drum crystallizer (*Figure 8.24*) is another example of crystallization on a chilled surface. A horizontally-mounted cylinder, partially immersed in the melt, or supplied with feedstock in some other way, is supplied with coolant fluid entering and leaving the inside of the hollow drum through trunnions. As the drum rotates, a thin crystalline layer forms on the cold surface and this is removed with a scraper knife.

Agitation of the melt, as near to the drum as possible, appears to have a marked effect on the efficiency, as does the drum rotational speed. The optimum drum speed must be found by trial and error. Decreasing the speed offers two advantages: increased contact time which gives a closer approach to equilibrium and hence improved separation, and better drainage of impure mother liquor off the drum as it emerges from the melt. Decreases in the speed, however, reduce the production rate, so a compromise must be reached.

Rotary drum behaviour and design for melt crystallization have been discussed in some detail by Chaty and O'Hern (1964); Chaty (1967); Svalov (1970); Toyokura *et al.* (1976a); Gel'perin and Nosov (1977); and Gel'perin, Nosov and Parokonyi (1978), although much of the information relates to laboratory, pilot-plant and theoretical studies. Bamforth (1965) describes an early use of rotary drum crystallizers for the recovery of sodium sulphate decahydrate from rayon spin-bath liquors.

Continuous belt crystallizer

The Sandvik continuous cooled belt crystallizer (*Figure 8.25*) may be considered as an alternative to the rotary cooled drum. The underside of the steel belt is sprayed with cooling water to provide a controlled temperature gradient along

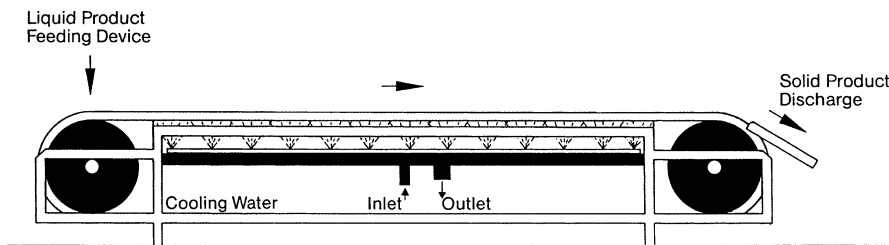


Figure 8.25. The Sandvik continuous belt crystallizer

the belt. Melt is fed at one end and crystals are removed at the other, generally in the form of thin flakes. The unit can also produce small pastilles if the melt is introduced on the belt through a drop-forming feeder. It has also been used for wax processing. Belt crystallizers have also been used to produce aluminium sulphate flakes and/or pastilles when fed with a highly concentrated seeded aqueous solution which rapidly solidifies on contact with the cold surface.

8.2.3 Alternative procedures

Most melt crystallizations normally involve, as a basic step, feeding melt onto a cold surface where it solidifies. Many variations of this procedure have been described above. There are, however, several alternative procedures that merit attention.

Direct contact cooling

In this process a melt is cooled and crystallized by direct contact with an inert coolant (gas or liquid) which maintains the crystals in suspension in the crystallizer. This technique has already been exploited in the desalination of sea-water by freezing (section 8.4.1 and 8.4.7) and is also a well-established technique in the crystallization of inorganic salts from solution (section 8.4.1). It is only in recent years, however, that the application to organic melts has been explored, but so far only laboratory scale results have been reported. One example of such a study is described by Kim and Mersmann (1997) who examined the separation of n-decanol/n-dodecanol, a simple eutectic mixture, using air as the gaseous coolant (*Figure 8.26*) and water and liquefied butane as the liquid coolants. Bartosch and Mersmann (1999) extended this study on the same eutectic mixture with a view to providing design information. Good separations were achieved with air at atmospheric pressure, but they identified a potential problem with the liquid–solid separation step which could adversely influence the product purity.

Adiabatic evaporative cooling

An early report of adiabatic evaporative cooling (Takegami, 1993) considered the purification of caprolactam (melting point 69 °C) in the presence of water

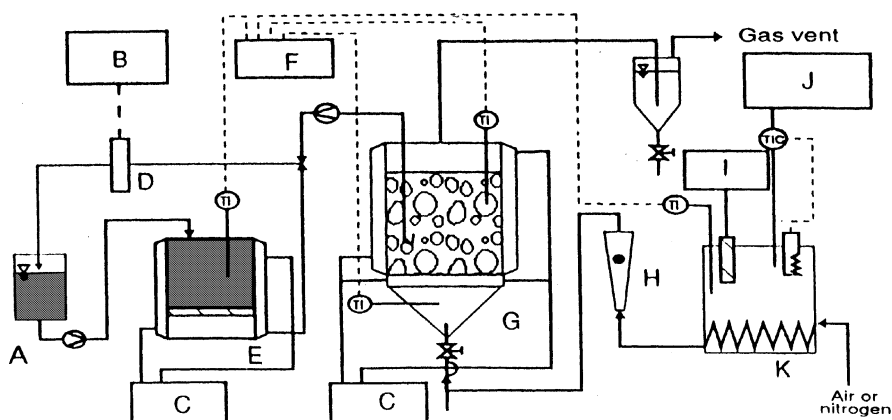


Figure 8.26. Apparatus for melt DCC crystallization, using air as a coolant. A = Reservoir; B = Data acquisition system; C = Thermostatic baths and circulators; D = Particle analysis sensor; E = Dilution tank; F = Temperature recorder; G = Crystallizer; H = Flowmeter; I = Refrigerator; J = Temperature programming controller; K = Heat exchanger. (After Kim and Mersmann, 1997)

which was evaporated under reduced pressure. The process was also considered for application to acrylic acid (m.p. 14 °C) and biphenol (m.p. 157 °C). A more recent account of the theoretical considerations leading to the selection of optimum conditions for this procedure has been given by Diepen, Bruinsma and van Rosmalen (2000). Caprolactam was crystallized from water mixtures by evaporating of water under reduced pressure; the actual cooling takes place in a condenser without any solid phase being present. The optimum process conditions were found to be 5% water, a pressure of 42 mbar and the temperature of 53 °C.

Prilling

The name ‘prilling’ is given to a melt-spray crystallization process that results in the formation of solid spherical granules. It is employed widely in the manufacture of fertilizer chemicals such as ammonium nitrate, potassium nitrate, sodium nitrate and urea.

In the ammonium nitrate prilling process (Shearon and Dunwoody, 1953) a very concentrated solution, containing about 5% water, is sprayed at 140 °C into the top of a 30 m high, 6 m diameter tower in which the droplets fall countercurrently to an up-flowing air stream that enters the base of the tower at 25 °C. The droplets, suddenly chilled when they meet the air stream, solidify into 0.5–2 mm diameter prills which are removed from the bottom of the tower at 80 °C. As they still contain about 4% water, they are dried at a temperature not exceeding 80 °C to ensure that no phase transition occurs (see section 1.8). They may then be dusted with diatomaceous earth or some other coating agent to prevent caking (section 9.6). The prills made by this process are reported to

have twice the crushing strength of those formed by the spray drying of fused water-free ammonium nitrate.

An interesting method of prilling has been developed for the processing of calcium nitrate in a form suitable for use as a fertilizer (van den Berg and Hallie, 1960). Calcium nitrate, which is hygroscopic, is produced as a by-product in the manufacture of nitrophosphate fertilizer. The process consists of crystallizing droplets of calcium nitrate in the form of prills in a mineral oil to which seed crystals have been added. A spray of droplets of the concentrated solution, formed by allowing jets of the liquid at 140 °C to fall on to a rotating cup, fall into an oil-bath kept at 50–80 °C. The prills are removed, centrifuged to remove surplus oil, and packed into bags. Because of the thin film of oil which remains on the particles, the material is less hygroscopic than it would normally be, there is no dust problem on handling, and the tendency to cake on storage is minimized.

In another technique, molten urea is sprayed at 148 °C onto cascading seed granules (<0.5 mm) in a rotating drum until they grow into product sized particles (2–3 mm). Heat released by the solidifying melt is removed primarily by evaporation of a fine mist of water sprayed into air that is passed through the granulation drum (Shirley, Nunelly and Cartney, 1982).

Problems associated with the design of prilling towers have been discussed by Roberts and Shah (1975); Schweizer, Corelli and Widmer (1975); and Scheffler and Henning (1979). The merits of prilling have been compared with granulation by Ruskam (1978).

High pressure crystallization

Pressure, as well as temperature, can alter the equilibrium relationships in a melt-crystal system. Figure 8.27a shows the relationship between pressure and volume in a liquid crystallizing under the influence of pressure. Curve AB (the liquidus) shows the volume decrease as the liquid is compressed isothermally. With a pure liquid, crystallization commences at some point B and proceeds at

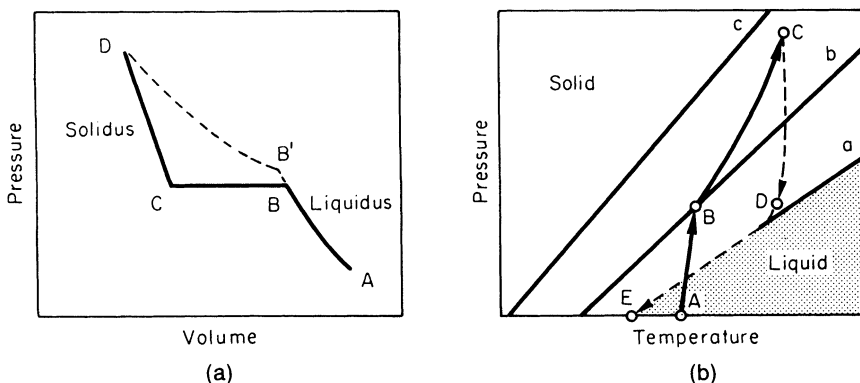


Figure 8.27. High pressure crystallization: (a) compression curve showing a solid-liquid transition, (b) pressure-temperature relationship in an adiabatic compression

constant pressure until all the liquid is solidified (point C). Beyond this point, any solid phase compression requires a sharp pressure increase along curve CD (the solidus). If the liquid is impure, crystallization will not normally occur until some higher pressure than B is applied, e.g. at some point B'. As the major component crystallizes, the concentration of the impurity species in the remaining liquid increases and, consequently, higher and higher pressures are required to continue crystallization, following an exponential path from B' to D where the curve approaches the solidus and crystallization is virtually complete.

The pressure difference between the liquid–solid equilibrium curves for pure and impure materials corresponds to the freezing temperature depression caused by the presence of an impurity. The pressure increase accompanying the increase in pure crystalline material deposited is related to the concentration of impurities in the liquid. With this information, therefore, the mother liquor composition at any stage can be estimated from the system pressure. Consequently, a highly pure solid phase can be obtained by separating the liquid phase from the solid phase while maintaining an appropriate pressure corresponding to the desired solid fraction or mother liquor composition.

Figure 8.27b shows liquid–solid equilibrium lines in terms of pressure and temperature. Line *a* represents the pure component, line *b* represents the impure feedstock and line *c* represents the eutectic. The sequences of a pressure crystallization operation are as follows. A liquid feedstock is adiabatically compressed from point A to point B and this is accompanied by compression heat generation. On further increasing the pressure up to point C, slightly below the eutectic line, nucleation occurs and crystal growth proceeds. The temperature rise on this occasion is caused by both compression and latent heat release. In this step, the impurities are concentrated in the mother liquor which is then separated from the solid phase by releasing it from the pressure vessel. When most of the mother liquor is discharged, its pressure decreases to atmospheric, while the crystals, maintained at the initial separation pressure, are purified by ‘sweating’. After separation, at point D, the purified crystals gradually approach the equilibrium state along line *a* at point E (atmospheric pressure).

Amongst the successful separations so far reported (Moritoki, 1984), using pressures up to 3000 bar, are those of *p*-xylene from *m*–*p* mixtures, *p*-cresol from *m*–*p* mixtures, and mesitylene from its isomers.

8.3 Sublimation

So far, in the discussion of industrial crystallization processes, only the crystallization of a solid phase from a supersaturated or supercooled liquid phase has been considered. However, the crystallization of a solid substance can be induced from a supersaturated vapour by the process generally known as ‘sublimation’. Strictly speaking, of course, the term sublimation refers only to the phase change solid → vapour without the intervention of the liquid phase. In its industrial application, however, the term is commonly used to include the condensation (crystallization) process as well, i.e. solid → vapour

→ solid, even though the second step should more properly be referred to as *desublimation*.

In practice, for heat transfer reasons, it is often desirable to vaporize the substance from the liquid state, so the complete series of phase changes in an industrial sublimation process can be solid → liquid → vapour → solid. It is on the condensation side of the process that the appearance of the liquid phase is prohibited. The supersaturated vapour must condense directly to the crystalline solid state.

Organic compounds that can be purified by sublimation include:

2-aminophenol	naphthalene
anthracene	2-naphthol
anthranilic acid	phthalic anhydride
anthraquinone	phthalimide
benzanthrone	pyrogallol
benzoic acid	salicylic acid
1,4-benzoquinone	terephthalic acid
camphor	thymol

Inorganic compounds and elemental substances include:

aluminum chloride	magnesium
arsenic	molybdenum trioxide
arsenic (III) oxide	sulphur
calcium	titanium tetrachloride
chromium (III) chloride	uranium hexafluoride
iodine	water (ice)
iron (III) chloride	zirconium tetrachloride

The sublimation of ice is an important operation in the freeze-drying of foods and biological products.

Reviews of the industrial applications of sublimation techniques have been made by Kemp (1958); Holden and Bryant (1969); Mellor (1978); Kudela and Sampson (1986). The basic principles of vaporization and condensation have been discussed by Rutner, Goldfinger and Hirth (1964); Strickland-Constable (1968); and Mellor (1978).

8.3.1 Basic principles

The mechanism of a sublimation process can be described with reference to the pressure–temperature phase diagram in *Figure 8.28*. The significance of the P–T diagram applied to one-component systems has already been discussed in section 4.2. The phase diagram is divided into three regions, solid, liquid and vapour, by the sublimation, vaporization and fusion curves. These three curves intersect at the triple point T. The position of the triple point in the diagram is of the utmost importance: if it occurs at a pressure above atmospheric, the solid cannot melt under normal atmospheric conditions, and true sublimation, i.e. solid → vapour, is easy to achieve. The triple point for carbon dioxide, for

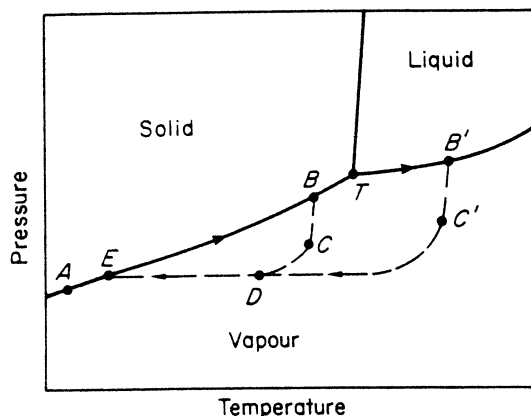


Figure 8.28. True and pseudo-sublimation cycles

example, is -57°C and 5 bar, so liquid CO_2 does not form when solid CO_2 is heated at atmospheric pressure (1 bar); the solid simply vaporizes. If the triple point occurs at a pressure less than atmospheric, however, certain precautions are necessary if the phase changes solid \rightarrow vapour (sublimation) or vapour \rightarrow solid (desublimation) are to be controlled. For example, because the triple point for water is 0.01°C and 6 mbar, ice melts when it is heated above 0°C at atmospheric pressure. For ice to sublime, it is necessary to keep both the temperature and pressure below the triple point values.

For industrial processing, it is not uncommon for liquefaction to be allowed in the vaporization stage, to facilitate better heat transfer, but this must never be allowed in the desublimation (crystallization) step. The condensation equipment, therefore, must operate well below the triple point. If liquefaction is employed before vaporization, the operation is often called *pseudo-sublimation*.

Both true and pseudo-sublimation cycles are depicted in Figure 8.28. For the case of a substance with a triple point at a pressure greater than atmospheric, true sublimation occurs. The complete cycle is given by path ABCDE. The original solid A is heated to some temperature represented by point B. The increase in the vapour pressure of the substance is traced along the sublimation curve from A to B. The condensation side of the process is represented by the broken line BCDE. As the vapour passes out of the vaporizer into the condenser, it may cool slightly, and it may become diluted as it mixes with some inert gas such as air. Point C, therefore, representing a temperature and partial pressure slightly lower than point B, can be taken as the condition at the inlet to the condenser. After entering the condenser the vapour mixes with more inert gas, and the partial pressure of the substance and its temperature will drop to some point D. Thereafter the vapour cools essentially at constant pressure to the conditions represented by point E, the temperature of the condenser.

When the triple point of the substance occurs at a pressure less than atmospheric, the heating of the solid may easily result in its temperature and vapour pressure exceeding the triple point conditions. The solid will then melt in the vaporizer: path A to B' in Figure 8.28 represents such a process. However, great

care must be taken in the condensation stage; the partial pressure of the substance in the vapour stream entering the condenser must be reduced below the triple point pressure to prevent initial condensation to a liquid. The required partial pressure reduction can be brought about by diluting the vapours with an inert gas, but the frictional pressure drop in the vapour lines is generally sufficient in itself. Point C represents the conditions at the point of entry into the condenser, and the condensation path is represented by C'DE.

Fractionation

The separation of two or more sublimable substances by fractional sublimation is theoretically possible if they form true solid solutions. The phase diagram for a binary solid solution system, at a pressure below the triple point pressures of the two components, is shown in *Figure 8.29a*. Points A and B represent the equilibrium sublimation temperatures of pure components A (the more volatile) and B, respectively, at the given pressure. The lower curve represents the sublimation temperatures of mixtures of A and B while the upper curve represents the solid-phase condensation temperatures, often called ‘snow points’. From *Figure 8.29b* it can be seen that if a solid solution (e.g. point S) were to be partially sublimed (e.g. heated to some temperature X), the resulting vapour phase (point Y) would be enriched in component A and residual solid (point Z) would be depleted. The mass proportion of vapour to remaining solid is given by the ratio of the distance XZ/YX (the mixture rule – see section 4.3.1). A repeated procedure of vapour condensation and solid vaporization gives the possibility of fractionation, although the practical difficulties in operating such a separation process may be considerable.

Experimental studies on fractional sublimation have been described by Gillot and Goldberger (1969); Vitovec, Smolik and Kugler (1978); Matsuoka (1984); and Eggers *et al.* (1986).

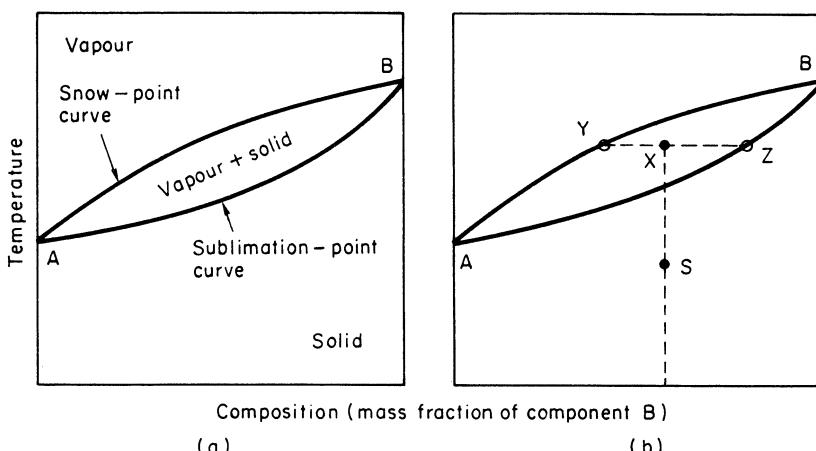


Figure 8.29. (a) Phase diagram for a two-component solid-solution system at a pressure below the triple points of the two components A and B; (b) fractional sublimation

Vaporization and condensation

The maximum theoretical rate of vaporization V ($\text{kg m}^{-2} \text{s}^{-1}$) from the surface of a pure liquid or solid under its own vapour pressure is given by the Hertz–Knudsen equation, which can be derived from the kinetic theory of gases:

$$V = P_s(M/2\pi\mathbf{R}T_s)^{1/2} \quad (8.17)$$

P_s is the vapour pressure (Pa) at the surface temperature T_s (K), M is the molar mass (kg kmol^{-1}) and \mathbf{R} the gas constant ($8.314 \times 10^3 \text{ J kmol}^{-1} \text{ K}^{-1}$).

In practice, however, the actual vaporization rate may be less than that predicted by equation 8.17 and it is conventional to include a correction factor α (≤ 1), generally referred to as an ‘evaporation coefficient’:

$$V = \alpha P_s(M/2\pi\mathbf{R}T_s)^{1/2} \quad (8.18)$$

A laboratory technique suitable for measuring values of α for sublimable solid materials is described by Sherwood and Johannes (1962).

Rates of sublimation of pure solids into turbulent air streams have been successfully correlated (Plewes and Klassen, 1991) by the Gilliland–Sherwood equation:

$$d/x = 0.023 Re^{0.38} Sc^{0.44} \quad (8.19)$$

where d is a characteristic dimension of the vaporization chamber, x the effective film thickness at the vapour–solid interface, and Re and Sc the dimensionless Reynolds and Schmidt numbers, respectively.

Desublimation is generally a transient operation, with the processes of simultaneous heat and mass transfer additionally complicated by the effects of spontaneous condensation in the bulk gaseous phase (Ueda and Takashima, 1977). Several steps, which may or may not be independent of one another, can be involved in the condensation of a solid phase from a vapour. The first step, after the creation of supersaturation in the vapour phase, is nucleation, which may be homogeneous but under most circumstances is probably predominantly heterogeneous. This event is then followed by both crystal growth and agglomeration in the formation of the final crystal product. A simple laboratory technique for making kinetic measurements in subliming systems was described by Strickland-Constable (1968) who compared the solid evaporation and growth rates of benzophenone under comparable conditions.

In practice, the two most common ways of creating the necessary supersaturation for crystal nucleation and subsequent growth are by cooling through a metal surface (which can lead to either a glassy or a multicrystalline deposit, both of which necessitate mechanical removal) or by dilution (e.g. with an inert gas) which, under suitable conditions, can produce an easily handled loose crystalline mass.

A study of the condensation of several sublimable materials in a fluidized bed was reported by Ciborowski and Wronski (1962) and a summary of a study on heat and mass transfer processes in a fluidized bed desublimation unit was reported by Knuth and Weinspach (1976). The measurement and correlation of

condensation heat transfer rates in a pilot plant connected to an industrial phthalic anhydride desublimation unit has been described by Bilik and Krupiczka (1983). Krupiczka and Pyschny (1990) have proposed a mathematical model for desublimation to assist the selection of the optimum cooling conditions for smooth and fin-tube heat exchangers. Comparisons are made with industrial-scale data for phthalic anhydride.

8.3.2 Processes and equipment

Sublimation techniques can be classified conveniently into three basic types: simple, vacuum and entrainer.

In *simple sublimation* the solid material is heated and vaporized, and the vapours diffuse towards the condenser. The driving force for diffusion is the partial pressure difference between the vaporizing and the condensing surfaces. The vapour path between vaporizer and condenser should be as short as possible to reduce the resistance to flow. Simple sublimation has been practised for centuries; ammonium chloride, iodine and 'flowers' of sulphur have all been sublimed in this manner, often in the crudest of equipment.

Vacuum sublimation is a natural follow-on from simple sublimation. The transfer of vapour from the vaporizer to the condenser is enhanced by reducing the pressure in the condenser, which thus increases the partial pressure driving force. Iodine, pyrogallol and many metals have been purified by this type of process. The exit gases from the condenser usually pass through a cyclone or scrubber to protect the vacuum-raising equipment and to minimize the loss of product.

In *entrainer sublimation* an inert gas is blown into the vaporization chamber of a sublimer to increase the rate of flow of vapours to the condensing equipment and thus increase the yield. Such a process is known as 'entrainer' or 'carrier' sublimation. Air is the most commonly used entrainer, but superheated steam can be employed for substances that are relatively, insoluble in water, e.g. anthracene. When steam is used as the entrainer, the vapours may be cooled and condensed by direct contact with a spray of cold water. In this manner an efficient recovery of the sublimate is made, but the product is obtained in the wet state.

The use of an entrainer in a sublimation process has many desirable features. It enhances the flow of vapours from the sublimer to the condenser, as already mentioned: it also provides the heat needed for sublimation, and thus an efficient means of temperature control is provided. The technique of entrainer sublimation, whether by gas flow over static solid particles or through a fluidized bed, is ideally suited to continuous operation.

The purification of salicylic acid provides a good example of the use industrially of entrainer sublimation. Air may be used as the carrier gas; but as salicylic acid can be decarboxylated in hot air, a mixture of air and CO₂ is often preferred. The process shown in *Figure 8.30* is carried out batchwise. A 5–10 per cent mixture of CO₂ in air is recycled through the plant, passing over heater coils before over the containers, e.g. bins or trays, holding the impure salicylic acid in the vaporizer. The vapours then pass to a series of air-cooled

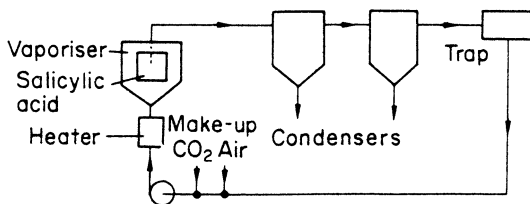


Figure 8.30. An entrainer sublimation process used for salicylic acid purification

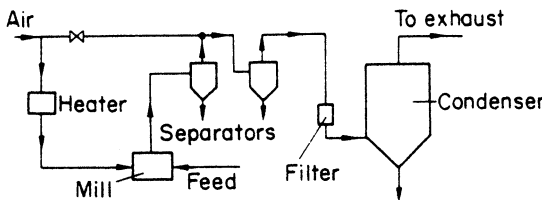


Figure 8.31. A typical continuous sublimation unit

chambers, where the sublimed salicylic acid is deposited. A trap removes any entrained sublimate before the gas stream is returned to the heater. Make-up CO₂ and air are introduced to the system as required, and the process continues until the containers are emptied of all volatile matter.

A typical example of a continuous sublimation plant is shown in Figure 8.31. The impure material is pulverized in a mill, and hot air or any other suitable gas mixture blows the fine particles, which readily volatilize, into a series of separators, e.g. cyclones, where non-volatile solid impurities are removed; a filter may also be fitted in the vapour lines to remove final traces of impurity. The vapours then pass to a series of condensers. The exhaust gases can be recycled or passed to atmosphere through a cyclone or wet scrubber.

Product yield

The yield from an entrainer sublimation process can be estimated as follows. The inert gas mass flow rate G and mass rate of sublimation S are related by

$$\frac{G}{S} = \frac{\rho_G p_G}{\rho_S p_S} \quad (8.20)$$

where p_G and p_S are the partial pressures of the inert gas and vaporized substance, respectively. In the vapour stream, and ρ_G and ρ_S are their respective vapour densities. The total pressure, P , of the system will be the sum of the partial pressures of the components

$$P = p_G + p_S$$

so equation 8.20 can be written

$$S = G \left(\frac{\rho_S}{\rho_G} \right) \left(\frac{p_S}{P - p_S} \right) \quad (8.21)$$

or, in terms of the molecular weights of inert gas, M_G , and the material being sublimed, M_S ,

$$S = G \left(\frac{M_S}{M_G} \right) \left(\frac{p_S}{P - p_S} \right) \quad (8.22)$$

The theoretical maximum yield from an entrainer sublimation process is the difference in the sublimation rates corresponding to the conditions in the vaporization and condensation stages, respectively.

For example, salicylic acid ($M_S = 138$) is to be purified by entrainer sublimation with air ($M_G = 29$) at 150°C . The vapours pass to a series of condensers, the internal temperature and pressure of the last being 40°C and 1 bar (10^5 Pa). The air flow rate is 2000 kg h^{-1} and the pressure drop between the vaporizer and the last condenser is 15 mbar. The vapour pressures of salicylic acid at 150°C and 40°C are 14.4 and 0.023 mbar, respectively. Therefore, assuming saturated conditions:

Vaporization stage ($P = 1.015 \text{ bar}$, $p_S = 0.0144 \text{ bar}$):

$$S_v = 2000 \left(\frac{138}{29} \right) \left(\frac{0.0144}{1.015 - 0.0144} \right) = 137 \text{ kg h}^{-1}$$

Condensation stage ($P = 1 \text{ bar}$, $p_S = 2.3 \times 10^{-5} \text{ bar}$):

$$S_c = 2000 \left(\frac{138}{29} \right) \left(\frac{2.3 \times 10^{-5}}{1 - 2.3 \times 10^{-5}} \right) = 0.22 \text{ kg h}^{-1}$$

In this particular example, therefore, the loss from the condenser exit gases is only 0.22 kg h^{-1} and the theoretical maximum yield is virtually 137 kg h^{-1} . This maximum yield will only be obtained, however, if the air is saturated with salicylic acid vapour at 150°C , and saturation will only be approached if the air and salicylic acid are contacted for a sufficient period of time at the required temperature. A fluidized-bed vaporizer may allow these optimum conditions to be approached; but if air is simply blown over bins or trays containing the solid, saturation will not be reached and the actual rate of sublimation will be less than that calculated. In some cases the degree of saturation achieved may be as low as 10 per cent of the possible value.

The calculated loss of product in the condenser exit gases is only a minimum value. Any other losses due to solids entrainment will depend on the design of the condenser and cannot be calculated theoretically. An efficient exit-gas scrubber can, of course, minimize these losses.

Fractional sublimation

As mentioned above in section 8.3.1, the separation of two or more sublimable substances by fractional sublimation is theoretically possible if the sublimable substances form true solid solutions, but there have been no reports yet of the large-scale commercial exploitation of fractional sublimation. On the other hand, a laboratory-scale process known as thin-film fractional sublimation (Gillot and Goldberger, 1969) has been successfully applied to the separation

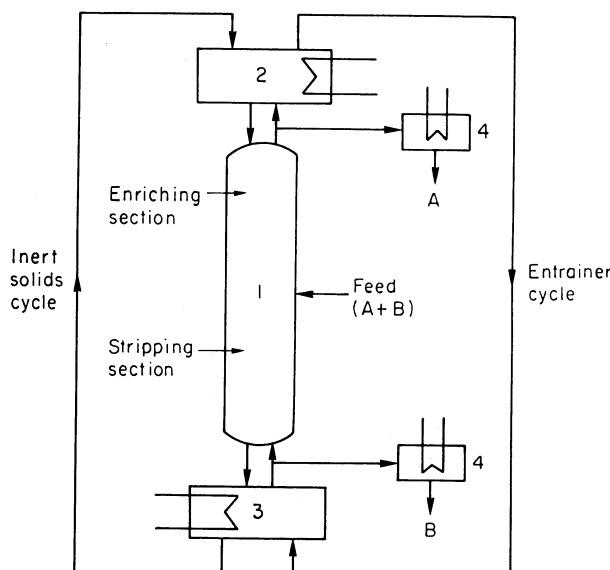


Figure 8.32. Thin-film fractional sublimation column: 1, fractionation column; 2, reflux condenser; 3, vaporizer; 4, condenser. (After Gillot and Goldberger, 1969)

of volatile solid mixtures such as hafnium and zirconium tetrachlorides, *p*-dibromobenzene and *p*-bromochlorobenzene, and anthracene and carbazole (Figure 8.32). A stream of inert non-volatile solids (e.g. glass beads or sand) is fed to the top of a vertical fractionation column to fall countercurrently to the uprising supersaturated vapour. Vapour movement is facilitated by an up-flowing entrainer gas stream. The temperature of the in-flowing solids is maintained well below the snow-point temperature of the vapour and consequently the solids become coated with a thin film (< 10 µm) of sublimate which acts as a reflux for the enriching section of the column, above the feed entry point.

Sublimation equipment

There are virtually no standard forms of sublimation or desublimation equipment in common use. Most industrial units, particularly on the condensation side of the process, have been developed on an *ad hoc* basis for a specific substance and duty. The most useful source of information on equipment types is the patent literature, but this has the severe drawback that it offers no evidence that a process has been, or is even capable of being, put into practice.

A wide variety of vaporization units have been used, or proposed, for large-scale operation depending on the manner in which the solid feedstock is to be vaporized. For example (Holden and Bryant, 1969):

1. A bed of dry solids, without entrainer gas. This is the simplest arrangement.
2. Dry solids suspended in a non-volatile heavy liquid.
3. Solids suspended in a boiling (entrainer) liquid where the entrainer gas is formed *in situ*.

4. Entrainer gas flowing through a fixed bed of solid particles.
5. Entrainer gas bubbling through a melted feedstock, i.e. vaporization takes place above the triple point pressure.
6. Entrainer gas flowing through a dense phase fluidized bed of the solid particles.
7. Entrainer gas flowing through a dilute phase of the solid particles, e.g. in a transfer-line vaporizer where the solid and gas phases are in concurrent flow, or a raining solids unit where the solids and entrainer may be in counter-current flow.
8. Vacuum sublimation for cases where the vapour phase consists essentially of the sublimate, i.e., when vaporization takes place below the triple-point pressure without the aid of an entrainer gas.

Sublimer condensers usually take the form of large air-cooled chambers which tend to give very low heat transfer coefficients, probably not greater than about $5\text{--}10 \text{ W m}^{-2} \text{ K}^{-1}$. This is only to be expected because deposits of sublimate on the condenser walls act as an insulator. In addition, vapour velocities within the chambers are generally very low. Quenching of the vapours with cold air in the chamber may increase the rate of heat removal, but excessive nucleation is likely and the product crystals will be very small. The condenser walls may be kept clear of solid by the use of internal scrapers, brushes and other devices. All vapour lines in sublimation units should be of a large diameter, adequately insulated and, if necessary, provided with trace heating to minimize blockage due to the build-up of sublimate.

One of the main hazards of air-entrainment sublimation is the risk of fire; many substances that are considered to be quite safe in their normal state can produce explosive mixtures with air. All electrical equipment should be flame-proof, and all parts of the plant should be earthed (grounded) efficiently to avoid the build-up of static electricity. Vacuum operation after nitrogen purging can provide a much safer processing environment.

The totally enclosed List sublimation unit (*Figure 8.33*) is provided with self-cleaning heat exchange surfaces and operates semi-continuously under reduced pressure without the aid of a carrier gas. Accumulated impurities are discharged from the sublimator periodically. Batch and continuous modifications of this unit are available (Schwenk and Raouzeos, 1995) and have been successfully applied industrially for the purification of anthraquinone, dyestuffs intermediates, metal-organic compounds and pharmaceuticals with production rates ranging from 300 to 10 000 ton/year.

Calculation of the density of deposited layers of sublimate, and of associated variables, as an aid towards the optimization of sublimate condenser design, is discussed by Wintermantel, Holzknecht and Thoma (1987). The starting point of the analysis is the assumption that the growth of sublimate layers is governed mainly by heat and mass transfer; the model is based on conditions in the diffusion boundary layer. The main process-determining factors (growth rate, mass transfer, and gas concentration) are accounted for. The derived theoretical relationship is shown to fit experimental data.

A variant on the large-chamber desublimation condenser is a crystallization chamber fitted with gas-permeable walls. Vapour and carrier gas is cooled by

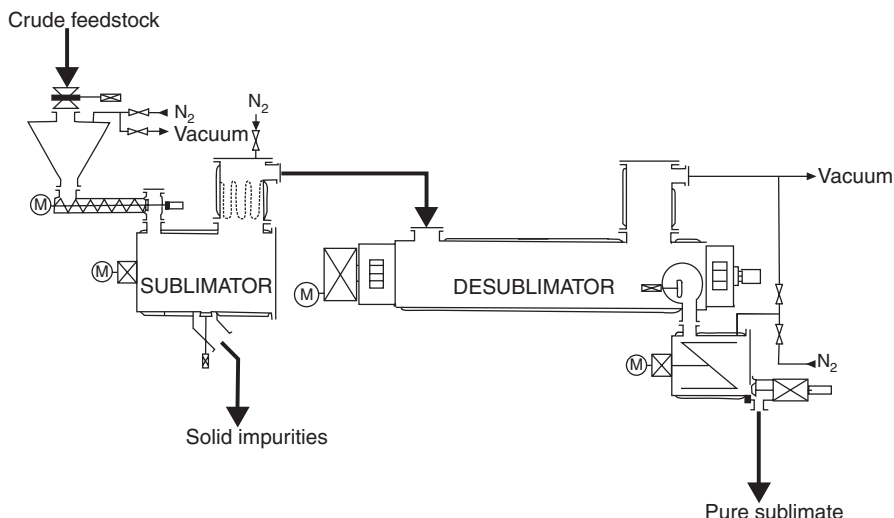


Figure 8.33. The List AG semi-continuous vacuum sublimation unit. (After Schwenk and Raouzeos, 1995)

evaporation of water dispersed in the cooling space formed by porous walls through which the inert gas, which protects the internal walls from solid deposits, passes into the cooling space. Crystallization takes place in the bulk vapour–gas mixture by direct contact with the dispersed water. Vitovec, Smolik and Kugler (1978) used such a system for the partial separation of a mixture of phthalic anhydride and naphthalene using nitrogen as entrainer.

Fluidized-bed condensers (desublimation units) have been considered for large-scale application although most of the published reports are concerned with laboratory-scale investigations (Knuth and Weinsbach, 1976).

8.4 Crystallization from solution

The large numbers of different industrial solution crystallizers in existence may be classified into a few general categories. Terms such as batch or continuous, agitated or non-agitated, controlled or uncontrolled, classifying or non-classifying, circulating liquor or circulating magma, etc., are useful for this purpose, but classification of crystallizers according to the method by which supersaturation is achieved is still probably the most widely used method; thus we have cooling, evaporating, vacuum, reaction, etc., crystallizers.

Many of these classes are self-explanatory, but some require definition. For example, the term *controlled* refers to supersaturation control. The term *classifying* refers to the production of a selected product size by classification in a fluidized bed of crystals. In a *circulating-liquor* crystallizer the crystals remain in the crystallization zone; only the clear mother liquor is circulated, e.g., through a heat exchanger. In the *circulating-magma* crystallizer the crystals

and the mother liquor are circulated together. Any given crystallizer may well belong to several of the above types, as the following examples will show.

8.4.1 Cooling crystallizers

Non-agitated vessels

The simplest type of cooling crystallizer is the unstirred tank: a hot feedstock solution is charged to the open vessel where it is allowed to cool, often for several days, predominantly by natural convection. Metallic rods may be suspended in the solution so that large crystals can grow on them and reduce the amount of product that sinks to the bottom of the crystallizer. The product is removed by hand.

Because cooling is slow, large interlocked crystals are usually obtained and retention of mother liquor is unavoidable. As a result, the dried crystals are generally impure. Because of the uncontrolled nature of the process, product crystals range from a fine dust to large agglomerates.

Labour costs are generally high, but the method may be economical for small batches because capital, operating, and maintenance costs are low. However, the productivity of this type of equipment is low and space requirements are high.

Agitated vessels

The installation of an agitator in an open-tank crystallizer generally results in smaller, more uniform crystals and reduced batch time. The final product tends to have a higher purity because less mother liquor is retained by the crystals after filtration and more efficient washing is possible. Vertical baffles may be fitted inside the vessel to induce better mixing, but they should terminate below the liquor level to avoid excessive encrustation. For the same reason, water jackets are usually preferred to coils for cooling purposes and, where possible, the internal surfaces of the crystallizer should be smooth and crevice-free (section 9.5).

An agitated cooler is more expensive to operate than a simple tank crystallizer, but it has a much higher productivity. Labour costs for product handling may still be rather high. The design of tank crystallizers varies from shallow pans to large cylindrical tanks.

The use of external circulation allows good mixing inside the crystallizer and high rates of heat transfer between the liquor and coolant (*Figure 8.34a*). An internal agitator may be installed in the crystallization tank if needed. The liquor velocity in the tubes is high; therefore, small temperature differences are usually adequate for cooling purposes and encrustation on heat-transfer surfaces can be reduced considerably. The unit shown may be used for batch or continuous operation.

The large agitated cooling crystallizer shown in *Figure 8.34b* has an upper conical section which slows down the upward velocity of liquor and prevents the crystalline product from being swept out with the spent liquor. An agitator located in the lower region of a draft tube circulates the crystal slurry (magma)

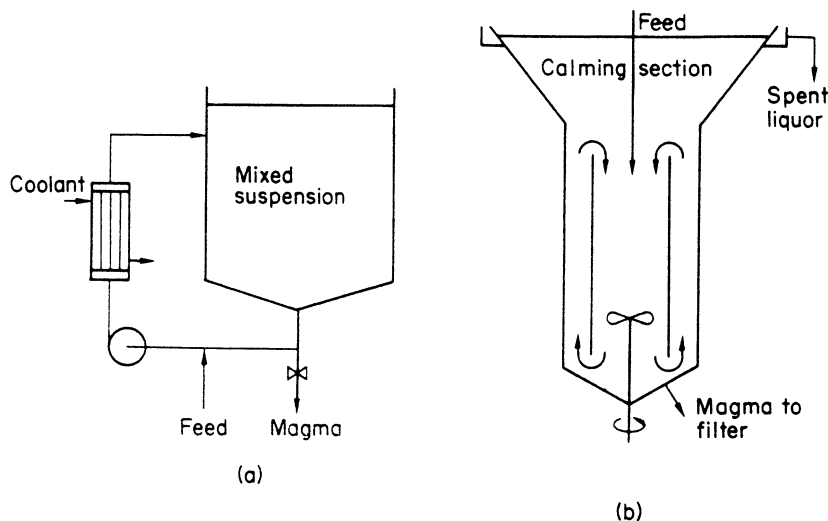


Figure 8.34. Agitated tank crystallizers: (a) external circulation through a heat exchanger, (b) internal circulation with a draft tube

through the growth zone of the crystallizer. If required, cooling surfaces may be provided inside the crystallizer. Units of this type, called Pachuca growth-type crystallizers, have been used for the large-scale production of borax from natural brines at Trona, California (Garrett, 1958).

The batch time of a cooling crystallizer is often prolonged because of the build-up of crystal encrustation on the cooling coils, or other heat exchange surfaces, resulting in progressively lower heat transfer coefficients. One way of overcoming this problem is to carry out the cooling process in two steps (Nývlt, 1978). In the first stage, operated with a high temperature difference across the heat exchanger, rapid cooling is allowed to proceed until a significant amount of encrustation is deposited on the cooling surfaces. At this point, the contents of the first vessel are discharged into a second vessel where cooling continues, this time under the influence of a lower temperature difference selected so that encrustation is avoided. The total batch time of these two stages can be very much shorter than that of a conventional previously single-stage operation, and the cooling water consumption significantly reduced. A worked example is given in section 9.3.3 (example 9.4).

In practice, if the two vessels are arranged one above the other, the following sequence of operations can be adopted. Hot feedstock solution is charged to the upper stage 1 crystallizer where it is quickly cooled to the predetermined temperature and then discharged into the lower stage 2 vessel to be cooled to the final batch temperature before discharging the magma, e.g. to a centrifuge. Meanwhile, the upper vessel is charged with fresh hot feedstock, during which operation the encrustations that had formed are dissolved. Fast cooling can then begin again and the cycle repeated.

A unit called the ‘twin’ or ‘double’ crystallizer is claimed to give a product with a very narrow size distribution (Nývlt, 1971). It consists of two intercon-

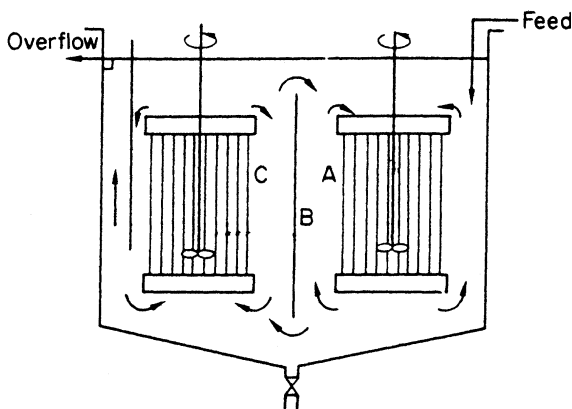


Figure 8.35. The 'twin' or 'double' crystallizer

nected simple crystallizers, each section operating at a different temperature (*Figure 8.35*). Hot feed liquor enters and mixes with the circulating contents of the crystallizer, which pass downwards through the water-cooled draft tube, A, under the influence of an agitator. Part of the cooled magma passes under the adjustable gate, B, into the second compartment of the crystallizer, where it mixes with the circulating magma in the second draft tube, C, operated at a lower temperature. A back-flow of magma occurs above the gate. Large crystals migrate to the bottom of the crystallizer and are discharged. The mother liquor exit is located behind the baffle. If both sections of the crystallizer operate with supersaturated solution, the system functions essentially as crystallizers in series. If one section operates slightly above the saturation temperature, the excess fines are dissolved and coarse crystals with rounded edges are produced. A detailed analysis of the performance of a double crystallizer is given by Skřivánek *et al.* (1976).

Trough crystallizers

The first truly continuous crystallizer to be introduced to the chemical industry, between 1905 and 1910, was the Wulff–Bock unit (*Figure 8.36*), frequently referred to as the crystallizing cradle or rocking crystallizer. It consists of a long shallow trough, about 1.2 m wide, rocked on supporting rollers. The solution to be crystallized is fed in at one end and the crystals are discharged at the other end, continuously. Transverse baffles may be fitted inside the trough to prevent longitudinal surging of the liquor, so the charge flows in zigzag fashion along the unit. The slope of the trough, towards the discharge end, is varied according to the required residence time of the liquor in the crystallizer.

One of the advantages of the Wulff–Bock crystallizer is the complete absence of moving parts in the crystallization zone. Several units may be joined together and assemblies up to 30 m in total length have been installed. No external cooling is employed; heat is lost by natural convection to the atmosphere. High degrees of supersaturation, therefore, are not encountered at any point within

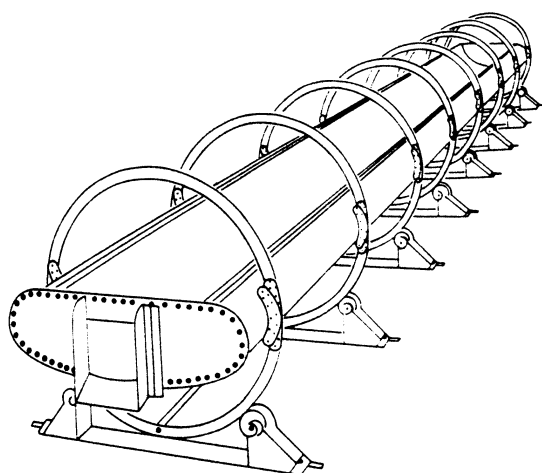


Figure 8.36. *Wulff–Bock crystallizer. (After Griffiths, 1925)*

the unit and crystallization occurs slowly. The gentle agitation prevents crystal attrition and very large (~ 1 cm) uniform crystals, e.g. of sodium thiosulphate, have been grown at production rates of 2–3 ton/day (Griffiths, 1925). Potassium chloride, potassium permanganate, sodium acetate, sodium sulphate and sodium sulphite have also been produced commercially in this manner. Only a few Wulff–Bock crystallizers still remain in service.

The Swenson–Walker crystallizer (Figure 8.37) developed in the early 1930s is a well-known example of a trough crystallizer with internal agitation and

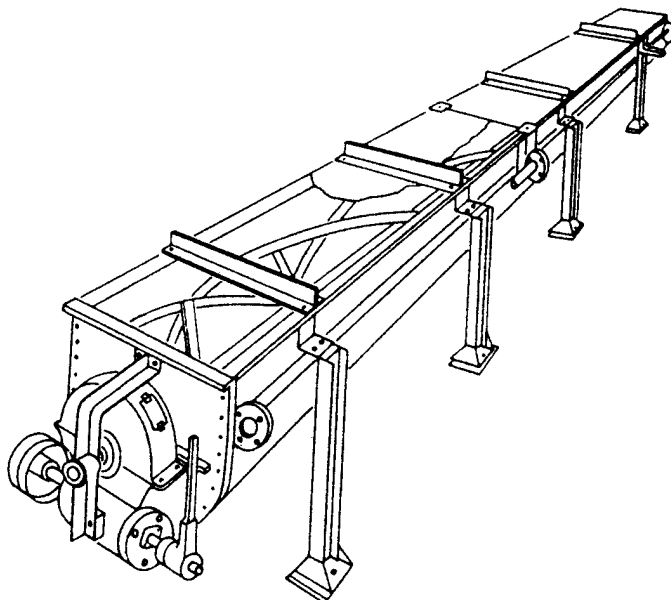


Figure 8.37. *Swenson–Walker crystallizer. (After Seavoy and Caldwell, 1940)*

a cooling system. Each unit consists of a semi-cylindrical trough up to about 1 m wide and 3–5 m long, generally fitted with a water-cooled jacket. Several units may be linked together. A helical agitator-conveyor rotates at a slow speed (5–10 rev/min) inside the trough to aid the growth of the crystals by lifting them and then allowing them to fall back through the solution. The system is kept in gentle agitation and the crystals are conveyed along the trough. Overall heat transfer coefficients of $\sim 50\text{--}105 \text{ W m}^{-2} \text{ K}^{-1}$ based on a logarithmic mean temperature difference between solution and cooling water, may be expected. Moderately sized and fairly uniform crystals can be obtained from this type of crystallizer and production rates of up to 20 ton/day of salt such as sodium phosphate and sodium sulphate have been reported from a single unit (Seavoy and Caldwell, 1940).

Crystallizers similar to the Swenson-Walker type with semi-cylindrical (U-type) or nearly cylindrical (O-type) cross-section have been used for many years in the sugar industry for the crystallization of concentrated molasses. Units fitted with water-cooled jacket are still employed, but these show poor heat transfer characteristics; scraper-stirrers are not permitted on account of the damage they do to the crystals. Accordingly, many other types of cooling arrangement have been tried (Seavoy and Caldwell, 1940).

Cooling disc crystallizer

The first cooling disc crystallizer to be developed, in the early 1930s, was the Werkspoor ‘rapid’ crystallizer which has widely used in the sugar industry for the processing of after-product massecuite. It was an open trough machine containing a horizontally mounted slow-speed agitator-cooler in the form of hollow discs through which cooling water was circulated. The discs had segmental openings to enable the crystal slurry to flow through the machine countercurrently to the cooling medium. This crystallizer subsequently found another large-scale application in the recovery of Glauber’s salt from rayon spin-bath liquors (Bamforth, 1965).

In the modern Gouda cooling disc crystallizer (*Figure 8.38*) the discs themselves are not heat exchangers. This multistage crystallizer consists of an open or closed trough, the latter being designed for the processing of toxic and flammable materials. The trough is effectively divided into a number of compartments by fixed vertical plate heat exchangers between which discs with segmental openings slowly rotate. Wipers on the discs can help to keep the cooling surfaces free from crystalline deposits. The crystal slurry flows from

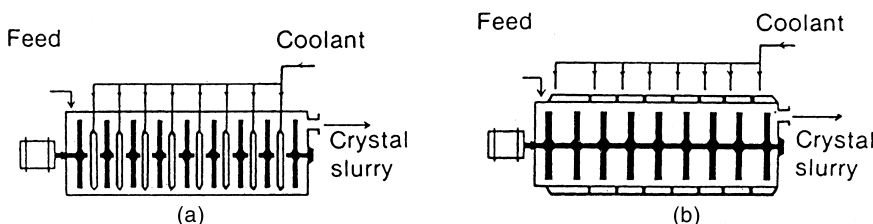


Figure 8.38. The Gouda MF cooling disc crystallizer (a) open type, (b) closed type

one compartment to the next, through bottom openings in the heat exchangers, and the temperature decreases stepwise. Applications in a wide range of solution crystallizations are claimed.

Rotary crystallizers

Rotating cylinders, similar in some respects to those used as rotary driers or kilns, have been used for the crystallization of solutions. The cylinder slopes slightly from the feed liquor inlet down to the crystal magma outlet. Cooling may be provided either by cold air blown through the cylinder or by water sprayed over the outside. In the former case internal baffles disturb the liquor on the inside wall and cause it to rain through the air stream. In the latter case internal scraper devices prevent excessive build-up of crystal on the walls.

Bamforth (1965) describes several different units used for the recovery of ferrous sulphate from pickle liquors and sodium sulphate from spin-bath liquors.

Internally chilled rotating drum crystallizers (see *Figure 8.24*) are normally associated with melt crystallization (section 8.2), but have also found occasional application for crystallization from solution. Sodium sulphate and barium hydroxide hydrates, for example, have been produced commercially in this manner.

Scraped-surface crystallizers

High heat transfer coefficients, up to $1 \text{ kW m}^{-2} \text{ K}^{-1}$, and hence high production rates, are obtainable with double-pipe, scraped-surface heat exchangers. Although mainly employed in the crystallization of fats, waxes and other organic melts (section 8.2.2) and in freeze concentration processes (section 8.4.7), scraped-surface chillers have occasionally been employed for crystallization from solution. Because of the high turbulence and surface scraping action, however, the size of crystal produced is extremely small.

Oslo-Krystal cooling crystallizer

Towards the end of the First World War, investigations were carried out in Norway by Isaachsen and Jeremiassen into the problems associated with the continuous production of large uniform crystals, in particular of sodium chloride. These investigations subsequently led to the development, by Jeremiassen, of a method for maintaining a stable suspension of crystals within the growth zone of a crystallizer. The practical application of this method has been incorporated in a continuous classifying crystallizer known by the names Oslo or Krystal (Jeremiassen and Svane, 1932). Bamforth (1965) has given a concise account of the design and uses of these versatile and compact units.

There are several basic forms of the Oslo apparatus, but all units based on the original Jeremiassen process have one feature in common – a concentrated solution, which is continuously cycled through the crystallizer, is supersaturated in one part of the apparatus, and the supersaturated solution is conveyed to another part, where it is gently released into a mass of growing

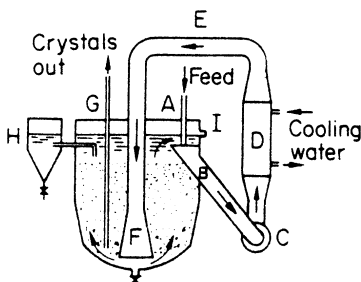


Figure 8.39. Oslo-Krystal cooling crystallizer

crystals. These units, therefore, belong to the ‘circulating liquor’ type of crystallizer.

The operation of the Oslo cooling crystallizer (*Figure 8.39*) may be described as follows. A small quantity of warm concentrated feed solution (0.5 to 2 per cent of the liquor circulation rate) enters the crystallizer vessel at point A, located directly above the inlet to the circulation pipe B. Saturated solution from the upper regions of the vessel, together with the small amount of feed liquor, is circulated by pump C through the tubes of heat exchanger D, which is cooled rapidly by a forced circulation of water or brine. On cooling, the solution becomes supersaturated, but not sufficiently for spontaneous nucleation to occur, i.e. metastable, and great care is taken to prevent it entering the labile condition. The temperature difference between the process liquor and coolant should not normally exceed 2 °C. The supersaturated solution flows down pipe E and emerges from the outlet F, located near the bottom of the crystallizer vessel, directly into a mass of crystals growing in the vessel. The rate of liquor circulation is such that the crystals are maintained in a fluidized state in the vessel, and classification occurs by a hindered settling process. Crystals that have grown to the required size fall to the bottom of the vessel and are discharged from outlet G, continuously or at regular intervals. Any excess fine crystals floating near the surface of the solution in the crystallizer vessel are removed in a small cyclone separator H, and the clear liquor is introduced back into the system through the circulation pipe. A mother liquor overflow pipe is located at point I.

Like all other cooling crystallizers, this unit can only be used to advantage when the solute shows an appreciable reduction in solubility with decrease in temperature. Examples of some of the salts that can be crystallized in this manner are sodium acetate, sodium thiosulphate, saltpetre, silver nitrate, copper sulphate, magnesium sulphate and nickel sulphate. Bamforth (1965) reports the production of 7 ton/day of 10 × 5 mm sodium thiosulphate crystals in a 2 m diameter 6 m high vessel with 200 m² heat exchange surface.

Direct contact cooling

The simplest form of direct contact cooling (DCC) is effected by blowing air into a hot crystallizing solution. Cooling takes place predominantly through

the evaporation of water and the air flow also serves as a means of agitation. In recent years a considerable amount of attention has been given to the possibility of using other direct contact coolants for crystallization processes.

By avoiding the use of a conventional heat exchanger, a DCC crystallizer avoids the troublesome problems associated with encrustation on heat transfer surfaces (section 9.5). The coolant in a DCC process can be a solid, liquid or gas, and heat is extracted by the transfer of sensible and/or latent heat (vaporization or sublimation).

Four main modes of action can be specified depending on the degree of solubility of the coolant in the solution and the manner in which heat is transferred. Within each mode of operation further sub-divisions of procedure may be possible:

1. *Immiscible/boiling DCC.* The coolant, solid or liquid, is substantially insoluble in the solution and its latent heat of phase change (of sublimation or vaporization) is the main cause of heat removal.
2. *Immiscible/non-boiling DCC.* The coolant, solid, liquid, or gas, is substantially insoluble in the solution and its sensible heat is utilized for cooling purposes.
3. *Miscible/boiling DCC.* The coolant, usually a liquid, is substantially soluble in the solution and its latent heat of vaporization is utilized.
4. *Miscible/non-boiling DCC.* The coolant, usually a liquid, is substantially soluble in the solution and its sensible heat is utilized.

Examples of proposed DCC coolants include liquid butane for the seawater desalination process (section 8.4.7) and methyl ethyl ketone for the Dilchill lubricating oil dewaxing process (Bushnell and Eagen, 1975). Chlorinated hydrocarbons, fluorocarbons and CO₂ have also found application in specific cases.

The continuous DCC crystallizer shown in *Figure 8.40* has been used for the large-scale production of calcium nitrate tetrahydrate (Černý, 1963). Aqueous feedstock enters at the top of the crystallizer at 25 °C and flows countercurrently to the immiscible coolant droplets, e.g. petroleum, introduced into the draft tube at -15 °C. The magma, containing crystals of mean size ~500 µm, is discharged at -5 °C. The low-density coolant collects in the upper layers and passes to a cyclone to separate aqueous solution droplets before being recycled.

The thermal efficiencies of the Černý and similar column crystallizers have been discussed by Letan (1973) in the light of data obtained for the crystallization of MgCl₂ · 6H₂O from aqueous solution using kerosene as a coolant. Shaviv and Letan (1979) studied the effect of operating conditions (temperature, droplet size and hold-up) on the same process.

Examples of the use of DCC crystallization for the recovery of valuable components from waste liquids are given by Toyokura *et al.* (1976a) and Nagashima and Yamasaki (1979) who report data on pilot plant units using CCl₂F₂ as coolant to recover 5 ton/day of sodium hydroxide. Duncan and Phillips (1976) have discussed the potential application of DCC crystallization to the production of *p*-xylene, using CClF₃, liquid nitrogen and liquid natural gas as coolants. Mullin and Williams (1984) have compared indirect

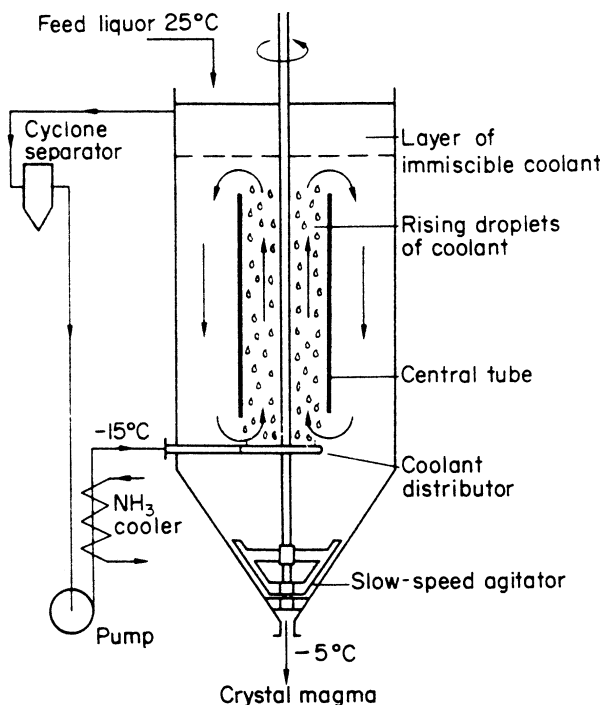


Figure 8.40. The Černý direct-coolant crystallizer. (After Bamforth, 1965)

cooling with DCC, using iso-octane, for the crystallization of potassium sulphate. Kim and Mersmann (1997) and Bartosch and Mersmann (1999) have explored the possibility of using DCC crystallization to separate individual components from eutectic organic melts (section 8.2.3).

A general review of DCC crystallization by Casper (1981) outlines a number of processes and equipment details.

8.4.2 Evaporating crystallizers

When the solubility of a solute in a solvent is not appreciably decreased by a reduction in temperature, supersaturation of the solution can be achieved by removal of some of the solvent. A number of evaporation techniques are available.

Solar evaporation

The evaporation of brines in shallow ponds, using energy from solar radiation, has been practised for thousands of years and still provides an important means of recovering salts from saline waters in many parts of the world (Sonnenfeld, 1984). An excellent example is the recovery of salts from Dead Sea waters (Novomeysky, 1936).

In principle, the technique is simple, but control of the complex solar evaporation process still presents a considerable number of technical problems (Finkelstein, 1983). Bonython (1966) has given a comprehensive analysis of the many factors that can determine the rate of evaporation from solar ponds. The use of organic dyes or the encouragement of the growth of certain naturally coloured microorganisms in the brine to assist the trapping of incoming solar radiation has received a lot of attention in recent years. A study to compare the relative efficiencies of dyestuffs and suspensions of halophilic bacteria was made by Jones, Ewing and Melvin (1981).

Attempts to model solar pond operations have been made for existing commercial productions of $\text{Na}_2\text{CO}_3 \cdot 10\text{H}_2\text{O}$ (Manguo and Schwartz, 1985) and KCl (Klein *et al.*, 1987). The use of weather-station data in the design and operation of solar ponds is discussed by Butts (1993) and correlations for solar evaporation rates using weather variables have been proposed by Lukes and Lukes (1993).

Steam-heated evaporators

Most evaporation units are steam heated and a typical evaporator body used in evaporative crystallization is the short-tube vertical type in which steam condenses on the outside of the tubes (*Figure 8.41*). A steam chest, or calandria, with a large central downcomer allows the magma to circulate through the tubes; during operation the tops of the tubes are just covered with liquor. To increase the rate of heat transfer, especially in dealing with viscous liquors, a forced circulation of liquor may be effected by installing an impeller in the downcomer.

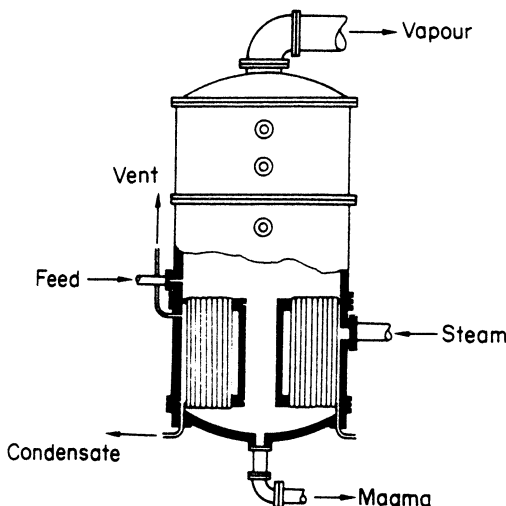


Figure 8.41. A typical crystallizing evaporator containing a calandria with a large central downcomer

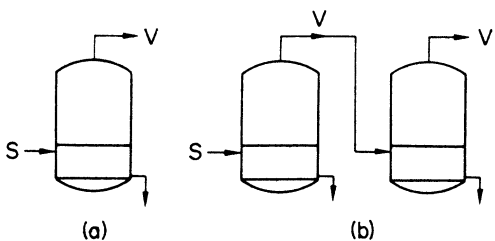


Figure 8.42. Principle of multiple-effect evaporation: (a) single-effect; (b) double-effect

Multiple-effect evaporation

Low pressure steam, i.e. <4 bar, is normally used in evaporators, and frequently by-product steam ($\sim 1.5\text{--}2$ bar) from some other process is employed. Nevertheless, 1 kg of steam cannot evaporate more than 1 kg of water from a liquor, and for very high evaporation duties the use of process steam as the sole heat source can be very costly. However, if the vapour from one evaporator is passed into the steam chest of a second evaporator, a great saving can be achieved. This is the principle of the method of operation known as multiple-effect evaporation (Figure 8.42). As many as six effects have been used in practice.

It is beyond the scope of this book to deal in any detail with the subject of multiple-effect evaporation; all standard chemical engineering textbooks contain adequate accounts of this method of operation, but two important points may be made here. First, multiple-effect evaporation increases the *efficiency* of steam utilization (kg of water evaporated per kg of steam used) but reduces the *capacity* of the system (kg of water evaporated). The well-known equation for heat transfer may be written

$$Q = UA\Delta T$$

where Q is the rate of heat transfer, U the overall heat transfer coefficient, A the area of the heat exchanger, and ΔT the driving force, the temperature difference across the heat transfer septum. The area A is usually fixed, so the variables to consider are Q , U and ΔT . Q will be reduced by heat losses from the equipment, U by sluggish liquor movement and scaling in the tubes of the calandria, by the increase in the boiling point of the liquor as it gets more and more concentrated. These and many other factors prevent the achievement of the ideal condition:

1 effect : 1 kg steam \rightarrow 1 kg vapour

2 effects : 1 kg steam \rightarrow 2 kg vapour

3 effects : 1 kg steam \rightarrow 3 kg vapour, etc.

Nevertheless a close approach to this ideality can often be produced. Some of the evaporators in a multiple-effect system are frequently operated under reduced pressure to reduce the boiling point of the liquor and thereby increase the available ΔT .

Before leaving this brief account of multiple-effect evaporation, mention may be made of the various methods of feeding that can be employed. *Figure 8.43* shows, in diagrammatic form, the possible feed arrangements. In all cases fresh process steam enters effect number one. S denotes live steam, F the feed solution, V vapour passing to the condenser system, and L the thick liquor, or crystalline magma, passing to a cooling system or direct to a centrifuge. Pumps are indicated on these diagrams to indicate the number required for each of the systems. In all cases the vapours flow in the direction of effects $1 \rightarrow 2 \rightarrow 3 \rightarrow$, etc.

In the forward-feed arrangement (*Figure 8.43a*) liquor as well as vapour pass from effect $1 \rightarrow 2 \rightarrow 3 \rightarrow$, etc. As the last effect is usually operated under reduced pressure, a pump is required to remove the thick liquor; a feed pump is also required. The transfer of liquor between the intermediate effects is automatic as the pressure decreases in each successive effect. Suitable control valves are installed in the liquor lines. The disadvantages of a forward-feed arrangement are (a) the feed may enter cold and consequently require a considerable amount of live steam to heat it to its boiling point; (b) the thick liquor, which flows sluggishly, is produced in the last effect, where the available ΔT is lowest; (c) the liquor pipelines can easily become steam-blocked as the liquor flashes into the evaporator body.

In the backward-feed arrangement (*Figure 8.43b*) the thick liquor is produced in effect 1, where the ΔT is highest; the liquor is more mobile on account of the higher operating temperature. Any feed preheating is done in the last effect, where low-quality steam (vapour) is being utilized. More pumps will be required in backward feeding than in forward feeding; the liquor passes into each effect in the direction of increasing pressure. No feed pump is necessary, as the last effect is under reduced pressure. Liquor does not flash as it enters an evaporator body, so small-bore liquor lines can be used. Backward feeding is best for cold feed liquor.

In the parallel-feed arrangement (*Figure 8.43c*) one feed pump is required, and predetermined flows F_1 , F_2 and F_3 are passed into the corresponding effects. A thick liquor product is taken from each effect: for this purpose pumps are generally necessary. Parallel feeding is often encountered in crystallization practice, e.g. in the salt industry, and it is useful if a concentrated feedstock is being processed.

In *Figure 8.43d* a 5-effect system is chosen to illustrate the mixed-feed arrangement. Many different sequences are possible; the one demonstrated is as follows. Feed enters an intermediate effect (number 3 in this case) wherefrom the liquor flows in forward-feed arrangement to the last effect, is then pumped to effect number 2 and from there flows in backward-feed arrangement to the first effect. Some of the advantages of this method of feeding are (a) fewer pumps are required compared with backward feeding; (b) the final evaporation is effected at the highest operating temperature; and (c) frothing and scaling problems are claimed to be minimized. Caustic soda evaporation is often carried out on a mixed-feed basis.

An alternative to multiple-effect evaporation is vapour recompression. The principle of the method is to raise the temperature of the vapour leaving the

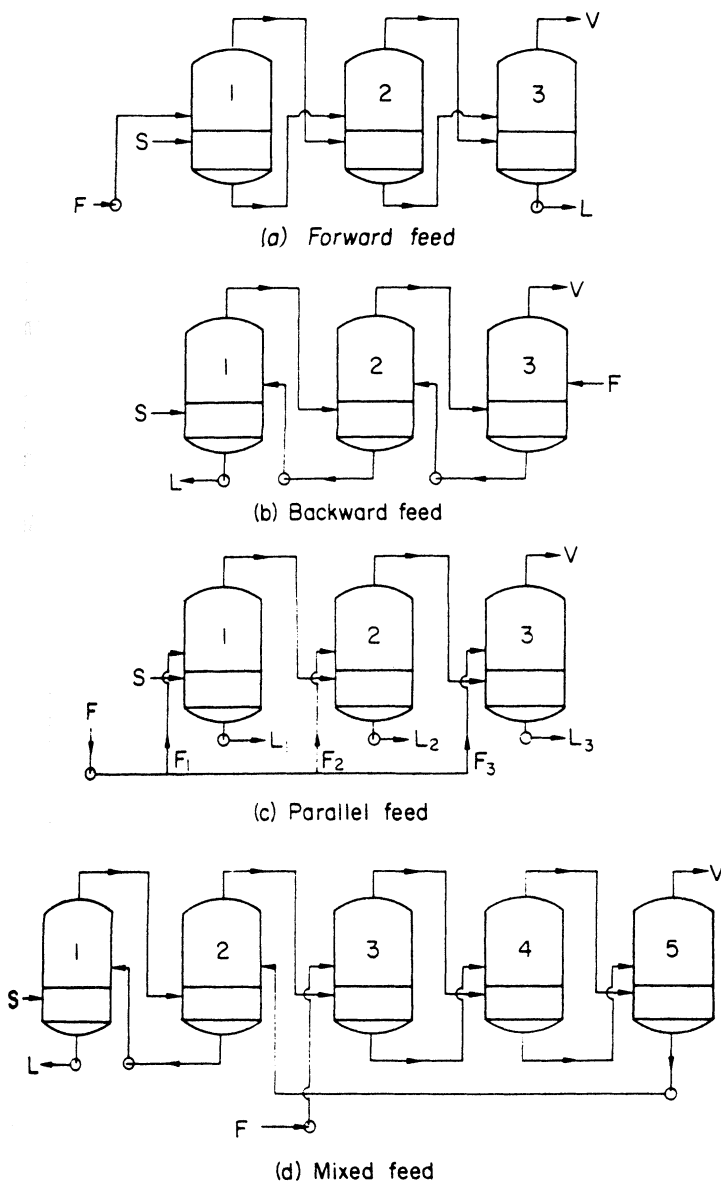


Figure 8.43. Various feeding arrangements in multiple-effect evaporators

evaporator, by raising its pressure, and passing it back into the evaporator heat exchanger. The recompression may be effected either mechanically (with a compressor) or thermally (with an injection of high pressure steam). An advantage of vapour recompression is that only one evaporator body is needed. A disadvantage is that it is not applicable to systems with high boiling point elevations. An economic comparison of multi-effect and vapour recompression evaporation has been made by Wöhlk (1982). King (1984) discusses some of the

merits of mechanical vapour recompression and outlines the optimization of operation for the production of $\text{Na}_2\text{SO}_4 \cdot 10\text{H}_2\text{O}$.

Forced circulation evaporators

The typical forced circulation evaporator-crystallizer shown in *Figure 8.44a* is a circulating magma unit operated under reduced pressure. Magma is circulated from the conical base of the evaporator body through the vertical tubular heat exchanger and reintroduced tangentially into the evaporator below the liquor level to create a swirling action and prevent flashing. Feedstock enters on the pump inlet side of the circulation system. The liquor level in the separator (the evaporator body) is kept above the top of the heat exchanger to prevent boiling in the tubes. The fine crystals are recirculated through the heat exchanger. *Figure 8.44b* shows, for comparison with *Figure 8.44a*, a forced circulation vacuum (flash cooling) crystallizer which operates without a heat exchanger, thus avoiding any problems with tube scaling. Crystallizers of this type are described in section 8.4.3.

To minimize liquid droplet entrainment into the vapour space above the boiling liquid surface in a forced circulation crystallizer, a common cause of crystal encrustation on the walls, the evaporation rate must be controlled to limit the upward vapour velocity to below a critical value depending on the liquor and vapour densities, the latter quantity depending on the operating pressure in the vapour chamber (see section 9.3.1). Forced circulation crystallizers are widely used for a variety of substances such as NaCl , $(\text{NH}_4)_2\text{SO}_4$, Na_2SO_4 , FeSO_4 , NiSO_4 , citric acid, etc. In general, relatively small crystals (median size < 0.5 mm) are produced.

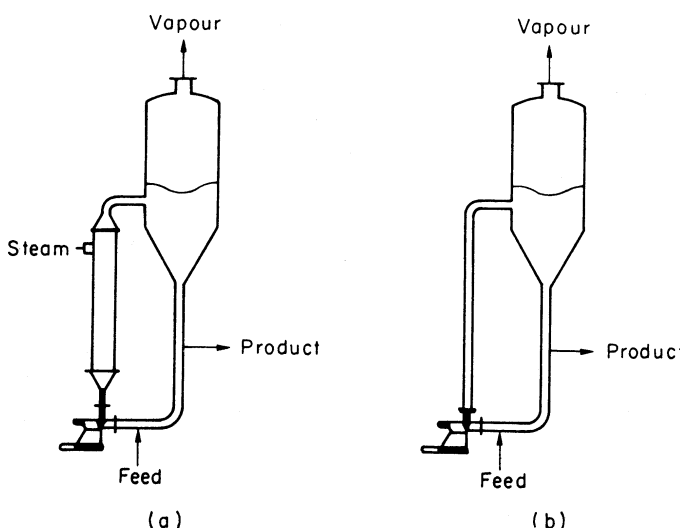


Figure 8.44. Forced circulation (a) evaporating crystallizer, (b) vacuum (flash cooling) crystallizer

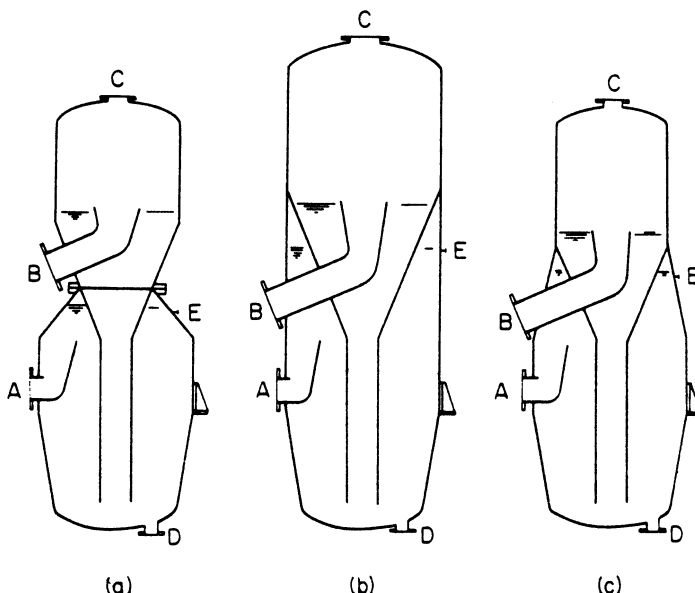


Figure 8.45. Oslo-Krystal evaporator types: (a) waisted, (b) and (c) monolithic. A and B, circulating liquor outlet and inlet; C, vapour outlet; D, crystal magma outlet; E, liquor overflow. (After Bamforth, 1965)

Oslo-Krystal evaporating crystallizer

The principles of the Oslo-Krystal process, already referred to above in connection with cooling crystallizers, can also be applied to evaporative crystallization. Three forms of the Oslo-Krystal evaporating crystallizer are shown in *Figure 8.45*. The construction of these crystallizers, commonly used in multiple-effect systems, is of the ‘closed’ form, i.e. the vaporizer is directly connected with the crystallizer body to form a sealed unit.

There are two basic types, the waisted (a) and the monolithic (b and c). One advantage of the latter is that the conical downcomer, which joints the vaporizer and crystallizer sections and contains highly supersaturated (metastable) solution, is insulated from external conditions by mother liquor within the crystallizer. The circulating liquor inlet and outlet, A and B, are connected through a heat exchanger and pump. Liquor velocities of $1.5\text{--}2\text{ m s}^{-1}$ are commonly used through the tubes to minimize crystal depositions.

Bamforth (1965) has given operating details of several Oslo-Krystal plants producing ammonium sulphate. Oslo-Krystal evaporating crystallizers have also been used for the manufacture of ammonium nitrate, borax, boric acid, sodium chloride, sodium dichromate and oxalic acid. In the case of sodium chloride, this type of crystallizer can, when operated under appropriate conditions, also produce spherical crystals of a median size 2–3 mm as opposed to the $<0.5\text{ mm}$ cubic crystals normally produced in a conventional forced circulation evaporating crystallizer. An example of this interesting and commercially useful crystalline form is shown in *Figure 8.46* where a microscopic inspection of

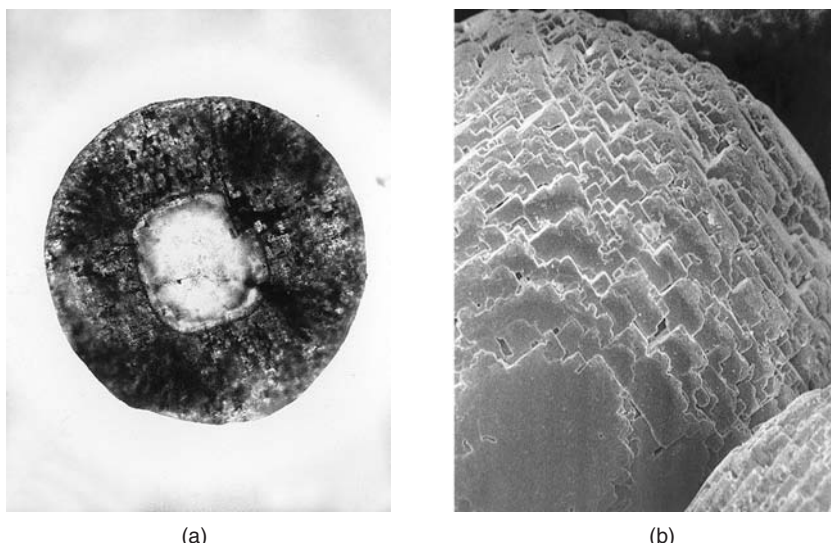


Figure 8.46. (a) A section through a 1 mm spherical crystal of sodium chloride showing an inner core of a 0.3 mm cubic crystal surrounded by a polycrystalline shell, (b) an SEM view of the surface of the outer shell. (Courtesy of ICI Ltd. Mond Division)

a section through a 1 mm sphere reveals at its centre a conventional 0.3 mm cubic crystal of salt, surrounded by a tightly bonded polycrystalline spherical shell.

Wetted-wall evaporative crystallizer

A somewhat unusual application of the wetted-wall column, frequently used in gas–liquid mass transfer operations, has been reported by Chandler (1959). A hot concentrated solution is fed into a horizontal pipe, and cold air is blown in concurrently at a velocity of about 30 m s^{-1} . The liquid stream spreads over the internal surface of the pipe and cools, mainly by evaporation (see *Figure 8.47*). The crystal slurry and air leave from the same end of the pipe. Only small

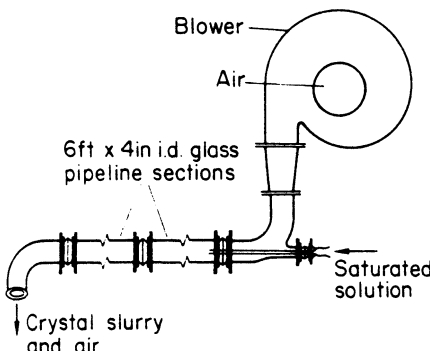


Figure 8.47. Arrangement of a wetted-wall evaporative crystallizer. (After Chandler, 1959)

Table 8.2. Approximate theoretical capacity of a 4 in diameter wetted-wall evaporative crystallizer, based on a 3000 lb h⁻¹ solution flow rate and a solution temperature drop from 100 to 67 °C (after J. L. Chandler, 1959)

Solute	Crystal yield, lb h ⁻¹ of anhydrous salt			Deposited crystalline phase
	Due to cooling	Due to evaporation	Total	
NaCl	66	60	126	anhyd.
CuSO ₄	912	115	1027	5H ₂ O
CaCl ₂	570	240	810	2H ₂ O
CuCl ₂	480	161	641	2H ₂ O
Al ₂ (SO ₄) ₃	750	137	887	18H ₂ O
BaCl ₂	313	90	403	2H ₂ O
Ba(NO ₃) ₂	352	52	404	anhyd.
K ₂ SO ₄	150	37	187	anhyd.
KNO ₃	3480	375	3855	anhyd.
CH ₃ · COOK	1560	625	2185	$\frac{1}{2}$ H ₂ O
K ₂ SO ₄ · Al ₂ (SO ₄) ₃	3600	227	3827	24H ₂ O
MgSO ₄	165	65	230	6H ₂ O
MgCl ₂	300	111	411	6H ₂ O
MnCl ₂	159	175	334	2H ₂ O
(NH ₄) ₂ SO ₄	398	157	555	anhyd.
NH ₄ Cl	580	117	697	anhyd.
Na ₃ PO ₄	1350	180	1530	12H ₂ O
Na ₂ HPO ₄	486	155	641	2H ₂ O
NaH ₂ PO ₄	1830	372	2202	anhyd.
CH ₃ · COONa	811	258	1069	anhyd.

crystals can be produced by this method, and because of the evaporative loss of solvent only aqueous solutions can be handled. Nevertheless the equipment required is quite simple and relatively inexpensive.

Although the pilot plant work described by Chandler was carried out on a small (100 cm diam.) unit and confined to the crystallization of sodium chloride, the wetted-wall crystallizer could be scaled up to larger sizes and used for other systems. The potential throughput of this small unit, however, could be quite high, depending on the temperature-solubility characteristics of the solute-solvent system, as indicated in *Table 8.2*.

8.4.3 Vacuum crystallizers

The term ‘vacuum’ crystallization is capable of being interpreted in many ways; any crystallizer that is operated under reduced pressure could be called a vacuum crystallizer. Some of the evaporators described above could be classified in this manner, but these units are better, and more correctly, described as reduced-pressure evaporating crystallizers. The true vacuum crystallizer operates through *flash cooling*; supersaturation is achieved by simultaneous evaporation and cooling of the feed solution as it enters the vessel.

To demonstrate the operating principles of these units, consider a hot saturated solution introduced into a lagged vessel maintained under vacuum. If the feed temperature is higher than that at which the solution would boil under the low pressure existing in the vessel, the feed solution will cool adiabatically to this temperature. The sensible heat liberated by the solution, together with any heat of crystallization liberated owing to the deposition of crystals at the lower temperature, causes the evaporation of a small amount of the solvent, which in turn results in the deposition of more crystals owing to the increased concentration. One of the attractions of 'vacuum' operation is the absence of a heat exchanger and the consequent elimination of tube-scaling problems.

Vacuum crystallizers may be operated batchwise or continuously. In batch operation, the vessel is charged to a predetermined level with hot concentrated solution. As the pressure inside the vessel is reduced, the solution begins to boil and cool until the limit of the condensing equipment is reached. In order to increase the capacity of the condenser, and thereby increase the crystal yield, the vapour leaving the vessel can be compressed before condensation by the use of a steam-jet booster. The vacuum equipment usually consists of a two-stage steam ejector.

Some form of agitation normally has to be provided to maintain reasonably uniform temperatures throughout the batch and to keep the crystals suspended in the liquor. Crystalline deposits around the upper portions of the inner walls of the vessel cause little inconvenience because, as the unit is operated batchwise, the next charge will redissolve the deposit. When the batch reaches the required temperature, i.e. the desired degree of crystallization, it is discharged to a filtration unit. Small crystals, rarely much larger than about $250\text{ }\mu\text{m}$, are obtained from this type of crystallizer.

In a continuously operated vacuum crystallizer the feed solution should reach the surface of the liquor in the vessel quickly, otherwise evaporation and cooling will not take place, because, owing to the hydrostatic head of solution, the boiling point elevation becomes appreciable at the low pressures ($<20\text{ mbar}$) used in these vessels, and the feed solution will tend to migrate down towards the bottom outlet. Care must be taken, therefore, either to introduce the feed near the surface of the liquor in the vessel or to provide some form of agitation.

As in the batch-operated units, crystalline deposits build up on the upper walls of the vessel. One way of overcoming this troublesome feature is to allow a small quantity of water to flow as a film down the walls at a rate less than the normal vaporization rate, so that no serious dilution of the charge occurs. A forced-circulation continuous vacuum crystallizer is shown in *Figure 8.44b*.

Draft-tube agitation

Vacuum crystallizers of the type shown in *Fig. 8.44b* generally produce small crystals ($<300\text{ }\mu\text{m}$) with a wide size distribution as a result of uncontrolled nucleation caused by a combination of feedstock 'flashing' on entry to the vessel and vigorous agitation.

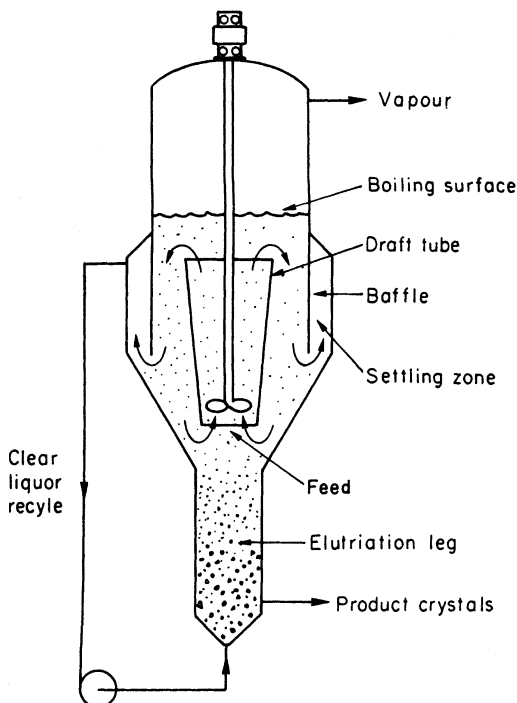


Figure 8.48. Swenson draft-tube-baffled (DTB) crystallizer

A vacuum unit capable of producing larger crystals of narrow size distribution is the Swenson draft-tube baffled (DTB) crystallizer (*Figure 8.48*) which has been described and compared with other types by Newman and Bennett (1959). A relatively slow-speed propeller agitator is located in a draft tube which extends to a few inches below the liquor level in the crystallizer. Hot, concentrated feedstock enters at the base of the draft tube. The steady movement of magma and feedstock up to the surface of the liquor produces a gentle, uniform boiling action over the whole cross-sectional area of the crystallizer. The degree of supercooling thus produced is very low ($< 1^{\circ}\text{C}$), and in the absence of violent flashing, both excessive nucleation and salt build-up on the inner walls are minimized. The internal baffle in the crystallizer forms an annular space in which agitation effects are absent. This provides a settling zone that permits regulation of the magma density and control of the removal of excess nuclei. An integral elutriating leg may be installed underneath the crystallization zone (as depicted in *Figure 8.48*) to effect some degree of product classification.

The DTB crystallizer can also be operated as a conventional evaporator-crystallizer by incorporating a steam-heated heat exchanger in the clear liquor recycle line. In this case, however, an elutriating leg is not normally installed and the recycled hot liquor stream enters directly into the draft-tube. Detailed design calculations for a forced circulation evaporative crystallizer of the DTB type to produce 75 ton/day of $>200\text{ }\mu\text{m}$ urea crystals have been described by Bennett (1992).

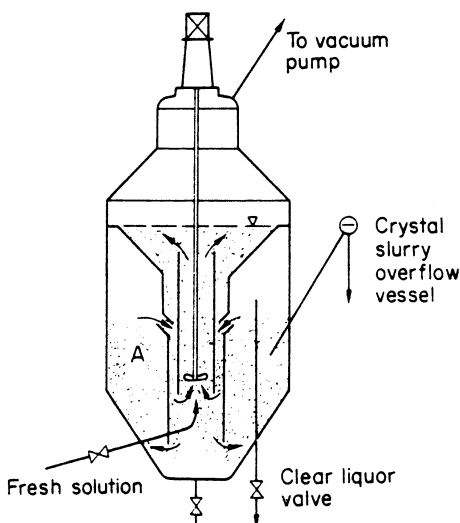


Figure 8.49. Standard Messo turbulence crystallizer

The Standard Messo turbulence crystallizer (*Figure 8.49*) is another draft-tube agitated unit. Two liquor flow circuits are created by concentric pipes: an outer ejector tube with a circumferential slot and an inner guide tube. Circulation is effected by a variable-speed agitator in the guide tube. The principle of the Oslo crystallizer is utilized in the growth zone; partial classification occurs in the lower regions, and fine crystals segregate in the upper region. The primary circuit is created by a fast upward flow of liquor in the guide tube and a downward flow in the annulus; liquor is thus drawn through the slot between the ejector tube and the baffle, and a secondary flow circuit is formed in the lower region of the vessel. Feedstock is introduced into the guide tube and passes into the vaporizer section where flash evaporation takes place. Nucleation, therefore, occurs in this region, and the nuclei are swept into the primary circuit. Mother liquor can be drawn off via a control valve, thus providing a means of controlling crystal slurry density.

The Escher-Wyss Tsukishima double propeller (DP) crystallizer (*Figure 8.50*) is essentially a draft-tube agitated crystallizer with some novel features. The DP unit contains an annular baffled zone and a double-propeller agitator which maintains a steady upward flow inside the draft tube and a downward flow in the annular region. Very stable suspension characteristics are claimed.

Fluidized-bed agitation

As described above, the Oslo-Krystal unit is a fluidized-bed agitated crystallizer in which the gentle action minimizes secondary nucleation and allows large crystals to grow. Oslo-Krystal vacuum crystallizers can be of the ‘open’ (*Figure 8.51*) or ‘closed’ (*Figure 8.45*) types. In the former the crystallization zone is at atmospheric pressure. In the latter all parts of the equipment are under reduced pressure.

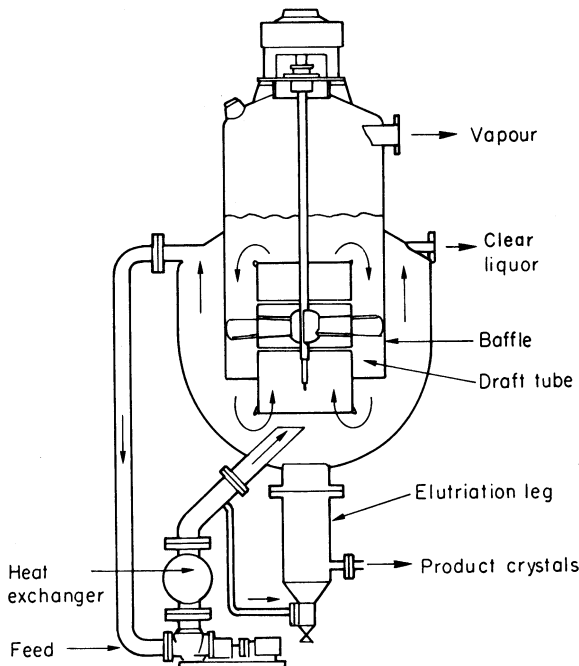


Figure 8.50. Escher-Wyss Tsukishima double propeller (DP) crystallizer

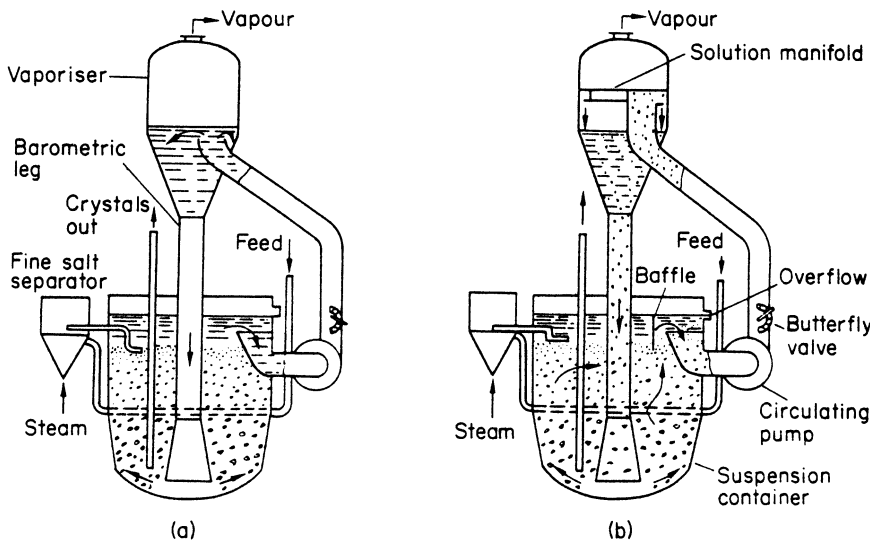


Figure 8.51. An Oslo-Krystal vacuum crystallizer showing two different methods of operation: (a) classified suspension, (b) mixed suspension. (After Saeman, 1956)

Two different methods of operation are shown in Figure 8.51 with (a) a classified suspension (circulating liquor) and (b) a mixed suspension (circulating magma). Classified operation, while capable of producing large regular

crystals, limits productivity because both the liquor velocity and the mass of crystals in suspension have to be restricted to keep the fines level below the pump inlet. Modification to magma circulation can improve the productivity considerably, because higher circulation rates and magma densities can be employed. Furthermore, the suspension volume is increased because magma circulates through the vaporizer and downcomer. In this type of operation, however, the bulk classifying action is lost, and it is necessary to provide a secondary elutriation zone in the suspension to permit segregation and removal of excess nuclei. Fines can be redissolved with live steam and the resulting solution fed to the vaporizer.

One of the major factors in the successful operation of any controlled suspension crystallizer is the incorporation of a suitable fines trap. The earlier the excess nuclei are collected and destroyed the more efficient will be the process. In practice, fines are most economically removed when they reach 5 to 10% of the average product size (Saeman, 1956).

Multistage vacuum crystallizer

The Standard Messo multistage vacuum crystallizer (*Figure 8.52*) provides a number of cooling stages in one vessel. The horizontal cylinder is divided into several compartments by vertical baffles that permit underflow of magma from one section to another but isolate the vapour spaces. Each vapour space is kept at its operating pressure by a thermocompressor, which discharges to a barometric condenser.

Hot feedstock is sucked into the first compartment, which is operated at the highest pressure and temperature (say 100 mbar and 45 °C). Flash evaporation and cooling occur, and the resulting crystal slurry passes into the successive compartments, where the pressure is successively reduced and evaporation and cooling continue. In the last compartment the temperature and pressure may be 10 °C and 10 mbar, for example. Agitation is provided by the boiling action in

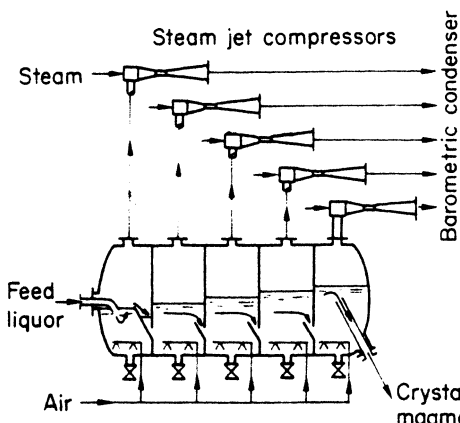


Figure 8.52. Standard Messo multistage vacuum crystallizer

the compartments supplemented by air spargers. Mother liquor or magma is withdrawn from the last stage through a barometric leg or by means of a pump. Industrial units in a variety of sizes have been installed for the recovery of sodium sulphate from spin-bath liquors, the regeneration of pickling liquors, etc.

8.4.4 Crystal yield

The theoretical crystal yield for simple cooling or evaporating crystallization can be estimated from the solubility characteristics of the solution. For aqueous solutions, the following general equation applies (section 3.5):

$$Y = \frac{WR[c_1 - c_2(1 - V)]}{1 - c_2(R - 1)} \quad (8.23)$$

where c_1 is the initial solution concentration, kg anhydrous salt per kg water; c_2 is the final solution concentration, kg anhydrous salt per kg water; W is the initial mass of water, kg; V is the water lost by evaporation, kg per kg of original water present; R is the ratio of molecular masses of hydrated to anhydrous salts; and Y is the crystal yield, kg.

The actual yield may differ slightly from that calculated from equation 8.23. For example, if the crystals are washed with fresh solvent after filtration, losses may occur through dissolution. On the other hand, if mother liquor is retained by the crystals, an extra quantity of crystalline material will be deposited on drying. Furthermore, published solubility data usually refer to pure solvents and solutes. Because pure systems are rarely encountered industrially, solubilities should always be checked on the actual working liquors.

Before equation 8.23 can be applied to vacuum (flash cooling) crystallization, the quantity V must be estimated:

$$V = \frac{qR(c_1 - c_2) + C(t_1 - t_2)(1 + c_1)[1 - c_2(R - 1)]}{\lambda[1 - c_2(R - 1)] - qRc_2} \quad (8.24)$$

where λ is the latent heat of evaporation of the solvent, J kg^{-1} ; q is the heat of crystallization of the product, J kg^{-1} ; t_1 is the initial temperature of the solution, $^{\circ}\text{C}$; t_2 is the final temperature of the solution, $^{\circ}\text{C}$; C is the specific heat capacity of the solution, $\text{J kg}^{-1} \text{K}^{-1}$; and c_1 and c_2 have the same meaning as in equation 8.23.

As an example, the theoretical yield of sodium acetate crystals ($\text{CH}_3\text{COONa} \cdot 3\text{H}_2\text{O}$) obtainable from a vacuum crystallizer operating with an internal pressure of 20 mbar, supplied with 2000 kg h^{-1} of a sodium acetate solution (0.4 kg/kg of water) at 80°C , may be calculated as follows.

Boiling point elevation	$= 11.5^{\circ}\text{C}$
Heat of crystallization, q	$= 144 \text{ kJ/kg}$ of trihydrate
Heat capacity of the solution	$= 3.5 \text{ kJ kg}^{-1} \text{ K}^{-1}$
Latent heat of water at 20 mbar, $\lambda = 2.46 \text{ MJ kg}^{-1}$	
Boiling point of water at 20 mbar	$= 17.5^{\circ}\text{C}$

Solubilities of sodium acetate in water are given in the Appendix, *Table A.4*.

$$\text{Equilibrium temperature of liquor} = 17.5 + 11.5 = 29^\circ\text{C}$$

$$\text{Initial concentration, } c_1 = 0.4/0.6 = 0.667 \text{ kg/kg of solvent}$$

$$\text{Final concentration at } 29^\circ\text{C, } c_2 = 0.539 \text{ kg/kg of solvent}$$

$$\text{Initial mass of water} = 0.6 \times 2000 = 1200 \text{ kg}$$

$$\text{Ratio of molecular masses, } R = 136/82 = 1.66$$

The vaporization, V , is calculated from equation 8.24

$$V = 0.153 \text{ kg/kg of water present originally}$$

This value of V substituted in equation 8.23 gives the crystal yield

$$Y = 660 \text{ kg of sodium acetate trihydrate}$$

8.4.5 Controlled crystallization

Selected seed crystals are sometimes added to a crystallizer to control the final product size. The effects of cooling rate and seeding are shown in *Figure 8.53* (Griffiths, 1925). When an unseeded solution is cooled rapidly (*Figure 8.53a*), cooling proceeds at constant concentration until the limit of the metastable zone is reached, where nucleation occurs. The temperature increases slightly due to the release of latent heat of crystallization, but cooling reduces it and more nucleation occurs. This results in a short period of instability after which the temperature and concentration subsequently fall as indicated. In such a process, both nucleation and growth are uncontrolled.

Figure 8.53b demonstrates the slow cooling of a seeded solution in which temperature and solution composition are controlled within the metastable zone throughout the cooling cycle. Seeds are added as soon as the solution becomes supersaturated. Crystal growth occurs at a controlled rate only on the added seeds; spontaneous nucleation is avoided because the system is never

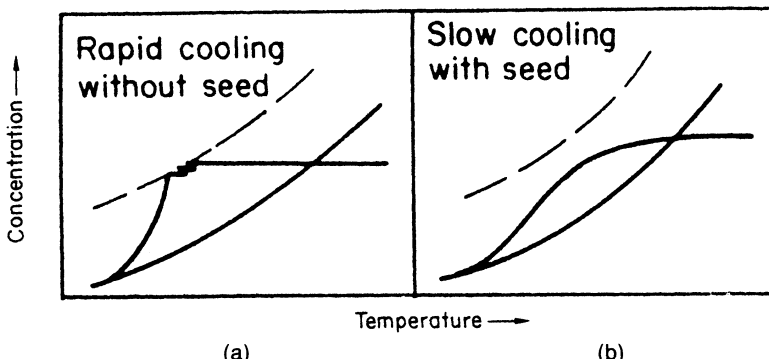


Figure 8.53. The effect of cooling rate and seeding on a crystallization operation: (a) uncontrolled and (b) controlled cooling

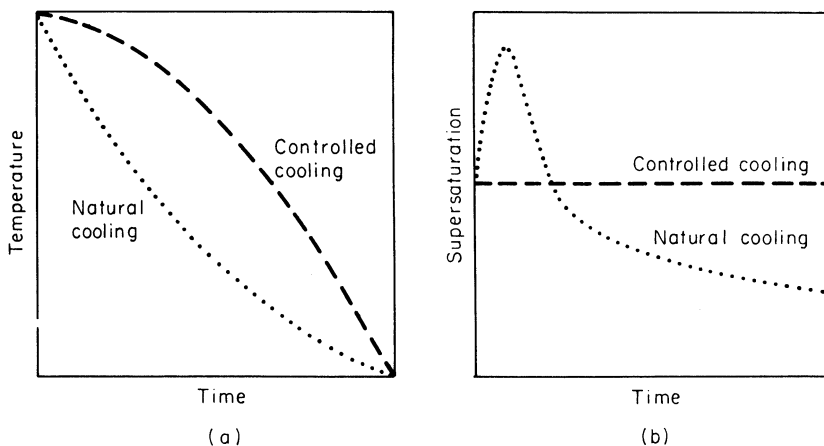


Figure 8.54. Cooling modes for a batch crystallizer: (a) natural cooling, (b) controlled (constant supersaturation) cooling

allowed to become labile. This batch operating method is known as *controlled crystallization*; many modern large-scale crystallizers operate on this principle.

If crystallization occurs only on the added seeds, the mass M_s of seeds of size L_s that can be added to a crystallizer depends on the required crystal yield Y (equation 8.23) and the product crystal size L_p :

$$M_s = YL_s^3 / (L_p^3 - L_s^3) \quad (8.25)$$

The product crystal size from a batch crystallizer can also be controlled by adjusting cooling or evaporation rates. Natural cooling (Figure 8.54a), for example, produces a supersaturation peak in the early stages of the process when rapid, uncontrolled heavy nucleation inevitably occurs. However, nucleation can be controlled within acceptable limits by following a cooling path that maintains a constant low level of supersaturation (Figure 8.54b).

The calculation of optimum cooling curves for different operating conditions is complex (Mullin and Nývlt, 1971; Jones and Mullin, 1974), but the following simplified relationship is often adequate for general application:

$$\theta_t = \theta_0 - (\theta_0 - \theta_f)(t/\tau)^3 \quad (8.26)$$

where θ_0 , θ_f , and θ_t are the temperatures at the beginning, end, and any time t during the process, respectively, and τ is the overall batch time.

The subject of controlled (programmed) crystallization is considered in more detail in sections 9.1.4 and 9.9 (example 9.3).

8.4.6 Miscellaneous crystallization techniques

Salting-out crystallization

A solute can be deposited from solution by the addition of another substance (a soluble solid, liquid or gas) which effectively reduces the original solute

solubility. The process is often referred to as ‘salting out’, although it applies to electrolytes and non-electrolytes alike. A slow addition of the salting-out agent can change a fast precipitation of the solute into a more controlled crystallization process. For convenience, this topic is dealt with in more detail as one of the techniques of precipitation in section 8.1.5.

Several potential applications of salting-out crystallization have been reported for the production of pure inorganic salts from aqueous solution (Gee, Cunningham and Heindl, 1947), the recovery of fertilizer-grade salts from seawater (Fernandez-Lozano, 1976) and the separation of inorganic salt mixtures (Alfassi and Mosseri, 1984). The recovery of inorganic salts from concentrated aqueous solution is considered by Weingaertner, Lynn and Hanson (1991) who propose a process in which the filtered mother liquor is regenerated into two phases, aqueous and organic, by change of temperature and addition of more feedstock. Both phases are then recycled. Detailed examples are given for the recovery of sodium chloride using 2-propanol or diisopropylamine and sodium carbonate using 1-propanol or 1-butanol. The kinetics of the salting-out crystallization of anhydrous sodium sulphate, from dilute aqueous solutions of sulphuric acid using methanol, have been studied by Mina-Mankarios and Pinder (1991). The effects of trace quantities of Cr^{3+} were also reported.

Reaction crystallization

The production of a solid crystalline product as the result of chemical reaction between gases and or liquids is a standard method for the preparation of many industrial chemicals. Crystallization occurs because the gaseous or liquid phase becomes supersaturated with respect to the reaction product. A precipitation operation (section 8.1.5) can be transformed into a crystallization process by moderation and control of the degree of supersaturation.

Reaction crystallization is practised widely, especially in industries where valuable waste gases are produced. For instance, ammonia can be recovered from coke oven gases by converting it into ammonium sulphate by reaction with sulphuric acid. Agitation of the crystals within the reaction vessel is effected by a combination of the vigorous nature of the exothermic reaction and air sparging. The heat of reaction is removed by the evaporation of water added to the reaction zone. Bamforth (1965) gives a detailed heat and materials balance for a commercial installation producing 32 ton h^{-1} of $(\text{NH}_4)_2\text{SO}_4$.

Another example of a reaction crystallizer is the carbonation tower method used for the production of sodium bicarbonate by the interaction between brine and flue gases containing about 10–20 per cent of carbon dioxide. A 15 m high tower is kept full of brine, and the flue gas, which enters at the bottom of the tower, flows upwards countercurrently to the brine flow. Carbonated brine is pumped continuously out of the bottom of the tower. To effect efficient absorption of CO_2 , internal rotating screens continually redisperse the gas stream in the form of tiny bubbles in the liquor. The operating temperature is controlled at about 38 °C, which has been found from experience to give both good absorption and crystal growth (Hou, 1942; Garrett, 1958).

A more recent example is flue-gas desulphurization, an environmental protection process employed for the removal of SO₂ from coal-fired power station flue gases. One widely used method is to absorb the SO₂ in an aqueous suspension of finely crushed limestone in an agitated vessel or spray tower. The resulting CaSO₃ solution is passed to an air-sparged tank where it is oxidized to precipitate CaSO₄ · 2H₂O which can find use in cement or wall-board manufacture. Another desulphurization technique can produce a fertilizer-grade (NH₄)₂SO₄ by countercurrent scrubbing flue gases with aqueous ammonia (Wallach, 1997; AIChE, 2000).

A number of laboratory studies have been recorded recently aimed at characterizing the kinetics of both the chemical reaction and crystallization steps in a reaction crystallization process. Examples of liquid phase reactions studied for this purpose are the crystallization of salicylic acid from aqueous solutions of sodium salicylate using dilute sulphuric acid (Franck *et al.*, 1988) and the crystallization of various calcium phosphates by reacting equimolar aqueous solutions of calcium nitrate and potassium phosphate (Tsuge, Yoshizawa and Tsuzuki, 1996). Several aspects of crystal size distribution control in semi-batch reaction crystallization have been considered by Aslund and Rasmuson (1990) who studied the crystallization of benzoic acid by reacting aqueous solutions of sodium benzoate with HCl. An example of crystallization arising from a gas-liquid reaction in an aqueous medium is the precipitation of calcium carbonate from the reaction between calcium hydroxide and CO₂ (Wachi and Jones, 1995).

Adductive crystallization

The simple crystallization of a binary eutectic system only produces one of the components in pure form, while the residual mother liquor composition progresses towards that of the eutectic (section 4.3.1). There is often a need, however, to produce both components in pure form, and one way in which this may be achieved is to add a third component to the system which forms a compound with one of the binary components. Phase diagrams for systems with compound formation are discussed in section 4.3.2.

A typical sequence of operation would be as follows. A certain substance X is added to a given binary mixture of components A and B so that a solid complex, say A · X, is precipitated. Component B is left in solution. The solid and liquid phases are separated, and the solid complex is split into pure A and X by the application of heat or by dissolution in some suitable solvent.

The best-known example of compound formation in solvent-solute systems is the formation of hydrates, but other solvates, e.g. with methanol, ethanol and acetic acid, are known. In these cases the ratio of the molecules of the two components in the solid solvate can usually be expressed in terms of small integers, e.g. CuSO₄ · 5H₂O or (C₆H₅)₂NH · (C₆H₅)₂CO (diphenylamine · benzophenone). There are, however, several other types of molecular complex that can be formed which are not necessarily expressed in terms of simple ratios. These complexes are best considered not as chemical compounds but as strongly bound physical mixtures.

Clathrate compounds are of this type: molecules of one substance are trapped in the open structure of molecules of another. Hydroquinone forms clathrate compounds with SO_2 and methanol, for example. Urea and thiourea also have the property of forming complexes, known as adducts, with certain types of hydrocarbons. In these cases molecules of the hydrocarbons fit into 'holes' or 'channels' in the crystals of urea or thiourea; the shape and size of the molecules determine whether they will be adducted or not.

It is open to question whether adduct formation can really be considered as a true crystallization process, but the methods of operation employed are often indistinguishable from conventional crystallization methods. Several different names have been given to separation techniques based on the formation of adducts, but the name additive crystallization is probably the best and will be used here.

Several possible commercial applications of additive crystallization have been reported. For example, the system *m*-cresol-*p*-cresol forms two eutectics over the complete range of composition, and the separation of the pure components cannot be made by conventional crystallization. Savitt and Othmer (1952) described the separation of mixtures of these two components by the use of benzidine to form a solid addition compound with *p*-cresol. Actually both *m*-cresol and *p*-cresol form addition compounds with benzidine, but the *meta*-compound melts at a lower temperature than the *para*-. If the process is carried out at an elevated temperature the formation of the *meta*- complex can be avoided. The method consists of adding benzidine to the *meta*-*para*- mixture at 110 °C. The *p*-cresol · benzidine crystallizes out, leaving the *m*-cresol in solution. The crystals are filtered off, washed with benzene to remove *m*-cresol, and the washed cake is distilled under reduced pressure to yield a 98 per cent pure *p*-cresol.

In a somewhat similar manner *p*-xylene can be separated from a mixture of *m*- and *p*-xylene; this binary system forms a eutectic. Carbon tetrachloride produces an equimolecular solid compound with *p*-xylene, but not with *o*- or *m*-xylene. Egan and Luthy (1955) reported on a plant for the production of pure *p*-xylene by crystallization *meta*-*para*- xylene mixtures in the presence of carbon tetra-chloride. Up to 90 per cent of the *para*- isomer was recovered by distillation after splitting the separated solid complex. The *meta*- isomer was recovered by fractionally crystallizing the CCl_4 -free mother liquor. Perfect separation of *p*-xylene is not possible, because the ternary system CCl_4 /*m*-xylene/ CCl_4 :*p*-xylene forms a eutectic, but fortunately the concentration of the complex $\text{CCl}_4 \cdot p\text{-xylene}$ in this eutectic is very low. Several commercial clathration processes for the separation of *m*-xylene from C₈ petroleum reformate fractions using a variety of complexing agents have been operated (Sherwood, 1965).

Separation processes based on the formation of adducts with urea, thiourea and other substances have been described by several authors (Findlay and Weedman, 1958; Hoppe, 1964; Santhanam, 1966; McCandless, 1988; Jadhav, Chivate and Tavare, 1991, 1992; Kitamura and Tanaka, 1994).

Urea forms addition complexes with straight-chain, or nearly straight-chain, organic compounds such as paraffin and unsaturated hydrocarbons (> 6 carbon atoms), acids, esters and ketones. Thiourea forms rather less stable

complexes with branched-chain hydrocarbons and naphthenes, e.g. cyclohexane. For example, if a saturated aqueous solution of urea in methanol is added to an agitated mixture of cetane and iso-octane, a solid complex of cetane-urea is formed almost immediately, deposited from the solution in the form of fine needle crystals. The iso-octane is left in solution. After filtration and washing the complex is heated or dissolved in water, and pure cetane is recovered by distillation. If thiourea is used instead of urea, iso-octane can be recovered leaving the cetane in solution.

Extractive crystallization

As described above, adductive crystallization is one method for separating a binary eutectic mixture into its component parts. Another possibility is to alter the solid–liquid phase relationships by introducing a third component, usually a liquid called the solvent. This process is known by the name ‘extractive crystallization’.

Chivate and Shah (1956) discussed the use of extractive crystallization for the separation of mixtures of *m*- and *p*-cresol, a system in which two eutectics are formed. Acetic acid was used as the extraction solvent. Details of the relevant phase equilibria encountered in the various combinations of systems were given together with an account of the laboratory investigations. While it was shown that acetic acid is not a particularly good solvent for the separation process in question, it was clearly indicated that extractive crystallization, provided a suitable solvent is chosen, has a large number of potential applications. Dikshit and Chivate (1970) have reported ternary phase equilibria for the separation of *o*- and *p*-nitrochlorobenzenes by extractive crystallization with *p*-dichlorobenzene, and have proposed general methods for predicting the selectivity of a solvent.

A procedure for screening solvents for both adductive and extractive crystallization has been proposed by Tare and Chivate (1976a) who also described (1976b) adductive and extractive routes towards the separation of *o*- and *p*-nitrochlorobenzene using *p*-dibromobenzene. Gaikar, Mahapatra and Sharma (1989) have described procedures for the separation of other close-boiling organic mixtures. Rajagopal, Ng and Douglas (1991) have formulated a systematic procedure for extractive crystallization separations. Design equations are proposed for flow-sheet analysis and design variables and constraints are identified. A worked example is outlined for the recovery of *p*-xylene from a *m*-xylene mixture using pentane as the solvent. In a further contribution, Dye and Ng (1995) demonstrate that extractive crystallization can offer a way to by-pass eutectics in multicomponent systems and to recover individual components.

Weingaertner, Lynn and Hanson (1991) have assessed the recovery of inorganic salts from concentrated aqueous solution in a process that they called ‘extractive crystallization’, but in part follows conventional salting-out procedures (sections 8.1.5 and 8.4.6). Enhanced recovery of salt and economical use of solvent are achieved, however, by generating a two-phase change in the filtered mother liquor, by temperature and composition manipulation, and the

use of recycling. Amongst the examples examined are the recovery of sodium chloride using 2-propanol and sodium carbonate using 1-propanol.

Freeze crystallization

Large-scale crystallization by freezing has been practised commercially since the 1950s when the first successful continuous column crystallizers were developed for use in the petrochemicals industry, particularly for *p*-xylene. Some of these processes have already been discussed in section 8.2.2. The present section will be devoted to the freezing of aqueous systems and the removal of water, as ice, either as the required product or as the unwanted component of the mixture.

One of the great engineering challenges of the present day is the search for the ideal process to produce fresh water from seawater. Desalination by crystallization offers several possible routes. The main freezing processes being pursued at the present time (Barduhn, 1975) are

1. Vacuum flash freezing
2. Hydrate freezing
3. Immiscible refrigerant freezing

The first of these processes utilizes the cooling effect of vaporization. Seawater is sprayed into a low-pressure chamber, where some of the water vapour flashes off and the brine partially freezes. The ice–brine slurry is separated, and the ice crystals are washed and remelted. Commercial units based on this principle have been operated.

The hydrate processes utilize the fact that certain substances can form inclusion compounds with water, loosely called ‘hydrates’, as described above in the section dealing with adductive crystallization. These crystalline substances are separated from the residual brine and decomposed to recover the hydrating agent. Propane is one of the most promising hydrating agents. One of the important advantages of the hydrate processes is that they operate close to ambient temperature (10–15 °C) and energy costs are minimized. One of the main disadvantages is the difficulty in growing crystals with good filtration and washing characteristics. Light, feathery crystals are quite common, and the compacted beds have a low permeability. The success of the hydrate processes, therefore, appears to hinge on developing a reliable method of controlling the crystal habit.

The indirect freezing processes, i.e. those in which brine is crystallized in some form of heat exchanger, have largely been abandoned, but the direct contact between brine and refrigerant is a very promising technique. The direct contact between liquid *n*-butane (which does not form a ‘hydrate’) and seawater has been widely investigated (Denton *et al.*, 1970). One approach is shown in *Figure 8.55*. Precooled brine (3.5 per cent dissolved salts) is fed to the crystallizer and liquid butane, which is sparged into the slurry, boils under reduced pressure (0.86 bar). Agitation is not usually necessary in the crystallizer in view of the vigorous boiling action of the butane. The slurry of ice crystals is pumped to the wash column. Butane vapour leaving the crystallizer is compressed (1.1 bar) before entering the ice melter where it is liquefied and, after separation from the water, is pumped back into the crystallizer. The compressor, therefore,

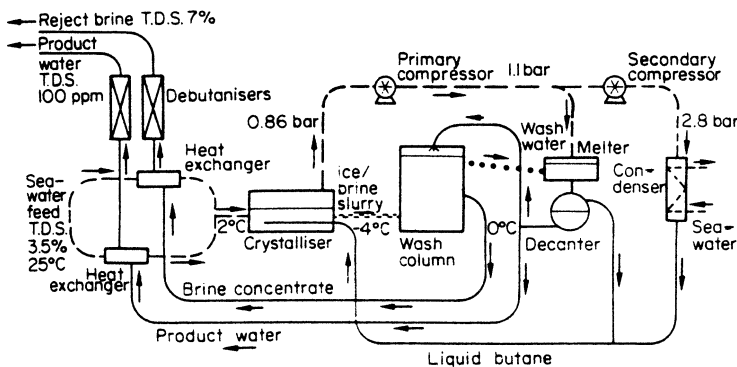


Figure 8.55. Immiscible refrigerant (*n*-butane) freeze desalination process (U.K. A.E.R.E., Harwell)

provides the energy input to the system. A hydraulic piston wash column provides a simple method for both separating the bulk of the mother liquor from the ice and providing countercurrent flow for washing the ice crystals free from residual brine.

An attraction of freezing over evaporation for the removal of water from solutions is the potential for saving heat energy: the enthalpy of crystallization of ice (334 kJ kg^{-1}) is only one seventh of the enthalpy of vaporization of water (2260 kJ kg^{-1}). In practice, however, the overall process energy consumptions, taking into account the other ancillary separation operations needed, are often comparable.

A definite advantage of freeze crystallization, important in many food industry applications, is that volatile flavour components that are normally lost during conventional evaporation can be retained in a freeze-concentrated product. In fact, at present, freeze crystallization finds its main application in the food industry, for the concentration of fruit juices, etc. Indirect-contact freezing processes are normally used, e.g. the liquid feedstock is crystallized in a scraped-surface heat exchanger (section 8.2.2) and the resulting ice slurry passes to a wash column where the crystals are separated and washed to recover valuable product. The wash column is the key item in the process. *Figure 8.56* shows an example of the Genco system of freeze crystallization.

Reviews of the potential of industrial freeze crystallization have been made by Heist (1981) and Casper (1981).

The subject of gas hydrates has become highly topical in recent years (Sloan, 1997), particularly since the discovery of vast amounts of natural gas hydrates under ocean floor sediments at depths $>500 \text{ m}$ and in polar permafrost regions. Gas hydrates are clathrate compounds in which variable (non-stoichiometric) amounts of gas, e.g., methane, ethane and propane, are trapped within ice crystal lattice ‘cages’. The amount of entrapped gas increases with lowering temperature and increasing pressure. It has been estimated that world-wide the amount of methane trapped in gas hydrates is around $2 \times 10^{16} \text{ m}^3$ at STP, which is roughly equivalent to twice the mass of carbon in all conventional

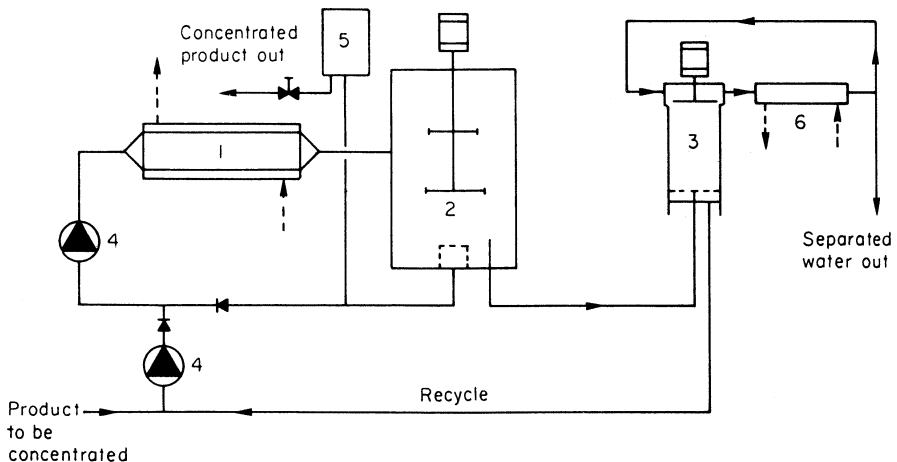


Figure 8.56. Grenco freeze concentration process (single stage). 1, scraped surface heat exchanger; 2, agitated recrystallizer; 3, wash column with bottom perforated piston and top ice scraper; 4, circulating pumps; 5, concentrated product expansion vessel; 6, ice melter

gas, oil and coal deposits combined. Although the commercial recovery of methane from natural hydrate sources has not yet been achieved, very active international research programmes are at present being pursued (Max and Dillon, 2000).

Emulsion crystallization

Organic substances may be purified by fractional crystallization from the melt or from organic solvents, but these operations frequently present difficulties in large-scale production. In the latter case, apart from expensive solvent losses and the potential fire and explosion hazards, yields are often low on account of the high solubility of the crystals. A method known as emulsion crystallization described by Holeci (1965) appears to be free from these shortcomings.

Briefly, crystallization is carried out by cooling from an aqueous emulsion. Impurities, in the form of eutectic mixtures, remain in the emulsion, from which they may be recovered by further cooling. The organic substance should be (a) practically insoluble in water and (b) able to melt and solidify in a heterogeneous aqueous medium, and remain stable.

The organic melt is emulsified in water with the aid of a suitable nonionic agent and stabilized by a protective colloid, e.g. potato starch gelatinized with water. The system is crystallized by cooling, and the crystals are separated from the emulsion and washed with water. The operation may be repeated if required. A typical example is shown in *Figure 8.57* where five or six emulsion-crystallization cycles yield an almost pure naphthalene at an overall yield of 70 per cent compared with a less pure product at a 2 per cent yield by seven conventional fractional crystallization steps. The high efficiency of the emulsion crystallization is apparently due to the fact that crystal agglomeration does

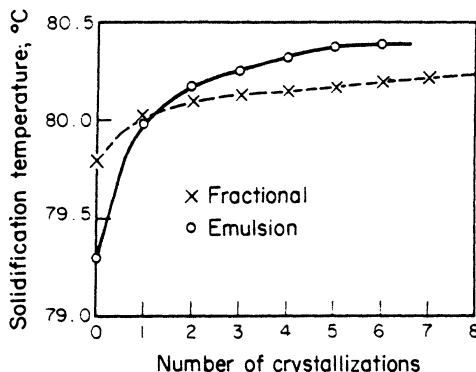


Figure 8.57. Comparison of fractional and emulsion crystallization cycles for the purification of naphthalene. (After Holeci, 1965)

not occur to any great extent and the impure emulsion is readily washed away with water.

Although there has not been any published report of commercial exploitation of this technique so far, other reports along similar lines tend to suggest that there could still be potential applications for emulsion-phase crystallization procedures (Sun, 1971; Dow Chemical Co., 1978; Davies, Ming and Garside, 1990; Davey, Hilton and Garside, 1997; Espitalier *et al.*, 1997).

Spray crystallization

The term ‘spray’ crystallization is really a misnomer; strictly speaking, individual crystals are not grown by this method – solid is simply deposited from a very concentrated solution by a technique similar to that used in spray drying. Size and shape of the solid particles depend to a large extent on those of the spray droplets. The spray method is often employed when difficulties are encountered in the conventional crystallization techniques, or if a product with better storage and handling properties can be produced.

Anhydrous sodium sulphate can be manufactured by spray crystallization. Below 32.4 °C sodium sulphate crystallizes from solution in the form of the decahydrate: above this temperature the anhydrous salt is formed. However, anhydrous sodium sulphate has an inverted temperature-solubility characteristic (see *Figure 3.1b*), and trouble is encountered with scale formation on the heat transfer surfaces of conventional evaporating crystallizers when operating temperatures in excess of 32.4 °C are used. In a plant described by Holland (1951) a concentrated solution of sodium sulphate was sprayed, or splashed, in the form of tiny droplets into a chamber through which hot gases flowed. The gases entered at about 900 °C. The continuously operated unit produced a powdered anhydrous product.

In recent years an increasing interest has been paid to the utility of the spray technique for commercial production purposes, and a number of studies have been made to ascertain the important variables affecting the growth of solid particles in gas-solid fluidized beds. Metheny and Vance (1962), for example,

have reported pilot-scale trials for the production of crystalline granules of $(\text{NH}_4)_2\text{SO}_4$, NaCN, CaCl_2 and NaOH by the spraying of solution onto seed crystals introduced into a fluidized bed. Similar studies have been made with $\text{Na}_2\text{SO}_4 \cdot 10\text{H}_2\text{O}$, $\text{Al}(\text{NO}_3)_3$, CaCl_2 and $\text{Ca}(\text{NO}_3)_2 \cdot 4\text{H}_2\text{O}$ (Markvart, Vaneček and Drbohlav, 1962).

Analyses of the kinetics of particle growth in fluidized beds have been made by several authors (Grimmett, 1964; Shakova *et al.*, 1973; Uemaki and Mathur, 1976; Smith and Nienow, 1983).

The spray crystallization of a solution has some features in common with prilling, the melt crystallization technique described in section 8.2.2.

Spherical crystallization

Fine crystals of pharmaceutical substances are frequently granulated to impart good flow properties and to assist tabletting procedures. An interesting technique for transforming fine crystals into dense spherical agglomerates during the crystallization process, hence the name *spherical crystallization*, appears to have potential application in the pharmaceutical industry.

The method is based on the addition to a crystallizing system of a small amount of an immiscible liquid that preferentially wets the developing fine crystals and encourages them to compact into spherical agglomerates $\sim 250\text{--}1000\,\mu\text{m}$. The technique stems from work that established successful granulation procedures, starting with dry crystals, using carbon tetrachloride as a 'bridging agent' (Capes and Sutherland, 1967), but chloroform appears to be the preferred organic liquid for use in association with crystallization from aqueous solution. An example of spherical crystallization is that of salicylic acid which may be agglomerated by adding an ethanolic solution of it to a well-dispersed 30:1 mixture of water and chloroform. Alternatively an aqueous solution of salicylic acid may be added to a solution of chloroform in ethanol. Several pharmaceutical substances have been successfully processed by this technique (Kawashima, 1984; Kawashima, Okumura and Tekenaka, 1984).

Kerosene has been used as a binding agent for the production of spherical agglomerates of precipitated inorganic substances, e.g. calcium carbonate (Bos and Zuiderweg, 1985; Kawashima *et al.*, 1986).

9 Crystallizer design and operation

Many of the difficulties facing designers of industrial crystallizers arise from the shortage of basic data in the technical literature. However, not only are published data scarce, they are so frequently unreliable. It is not uncommon to find different investigators reporting crystal growth rates for the same substance differing by an order of magnitude or more. In such cases it is often impossible to select the appropriate value for a given situation, usually because some important parameter has not been specified, or perhaps not even measured. Reliable nucleation data applicable to industrial systems are seldom, if ever, available in the literature.

The unit operation of crystallization is governed by some very complex interacting variables. It is a simultaneous heat and mass transfer process with a strong dependence on fluid and particle mechanics. It takes place in a multiphase, multicomponent system. It is concerned with particulate solids whose size and size distribution, both incapable of unique definition, vary with time. The solids are suspended in a solution which can fluctuate between a so-called metastable equilibrium and a labile state, and the solution composition can also vary with time. The nucleation and growth kinetics, the governing processes in this operation, can often be profoundly influenced by mere traces of impurity in the system; a few parts per million may alter the crystalline product beyond all recognition.

It is perhaps no wonder that crystallization was once called an art rather than a science, but to do so today would be to ignore the tremendous advances that have been made over the past three or more decades in both the theory and practice of the subject. The object of this chapter is to describe some of the recent developments in the area of crystallizer design and operation and to demonstrate how simple laboratory scale tests, some of which have been described in earlier chapters, can provide basic design information.

9.1 Crystal size distribution (CSD)

One of the earliest investigations aimed at studying the size distribution of crystals in a continuous crystallizer was made by Montillon and Badger (1927) with $\text{Na}_2\text{SO}_4 \cdot 10\text{H}_2\text{O}$ and $\text{MgSO}_4 \cdot 7\text{H}_2\text{O}$. Shortly afterwards McCabe (1929) analysed the problem of crystal size distribution (CSD) and developed the ΔL law, making the following assumptions: (a) all crystals have the same shape; (b) they grow invariantly, i.e. the growth rate is independent of crystal size; (c) supersaturation is constant throughout the crystallizer; (d) no nucleation occurs; (e) no size classification occurs in the crystallizer; (f) the relative velocity between crystals and liquor remains constant. For a full account of the

derivation of the ΔL law reference should be made to the original paper, but the main steps are briefly as follows.

The mass of one crystal of a chosen characteristic size L (section 2.14.2) is given by $\alpha\rho_c L^3$, where α is a volume shape factor (section 2.14.3) and ρ_c is the crystal density. The number of crystals, dN , of size L in a mass dM is thus $dN = dM/\alpha\rho_c L^3$. Assuming no nucleation, the number of seeds dN_s of size L_s is equal to the number of product crystals dN_p of size L_p , i.e.

$$\frac{dM_s}{\alpha\rho_c L_s^3} = \frac{dM_p}{\alpha\rho_c L_p^3} = \frac{dM_p}{\alpha\rho_c (L_s + \Delta L)^3}$$

where ΔL is the growth increment. Therefore

$$\begin{aligned} dM_p &= \left(\frac{L_s + \Delta L}{L_s} \right)^3 dM_s \\ M_p &= \int_0^{M_s} \left(1 + \frac{\Delta L}{L_s} \right)^3 dM_s \end{aligned} \quad (9.1)$$

where M_p is the product crystal yield obtained from an initial mass of seed crystals, M_s .

McCabe recognized that the ideal conditions assumed in this derivation are unlikely to be attained in a real crystallizer. Temperature and supersaturation gradients are unavoidable; invariant growth is comparatively rare; different crystal faces usually grow at different rates; crystal growth rates may be dependent on solution velocity, in which case large crystals may grow faster than small; and so on. However, an interesting feature of the derivation is that the dependence of growth on supersaturation need not be known. Despite its limitations, the ΔL law still provides an interesting, if oversimplified, approach to the development of a CSD.

One use of the law is demonstrated by the following example. If a quantity of seed crystals of known CSD is added to a crystallizer, it is possible to estimate the CSD of the final product by the following procedure.

- Find the value of ΔL compatible with the product yield M_p calculated from solubility data and the mass of added seeds M_s . This involves a trial and error evaluation of equation 9.1, which may be integrated graphically (plot M_s versus $(1 + \Delta L/L_s)^3$; the area enclosed under $M_s = 0$ and $M_s = \text{mass of seeds added}$ is equal to M_p).
- Plot the integral curve of equation 9.1 (M_p versus M_s) using the correct value of ΔL .
- Plot the CSD curve, e.g. from sieve test data, of the product crystals (M_p versus L_p) remembering that $L_p = L_s + \Delta L$. For comparison purposes, this plot may be made on the same diagram as the CSD curve of the seed crystals (M_s versus L_s).

The tedious trial and error solution of equation 9.1 to find the appropriate value of ΔL , as outlined in step 1, may be simplified by the use of a nomograph (Figure 9.1) (Hooks and Kerze, 1946). For example, Table 9.1 shows a seed sieve analysis based on 100 g and gives the values of $(1 + \Delta L/L_s)^3$ for a first

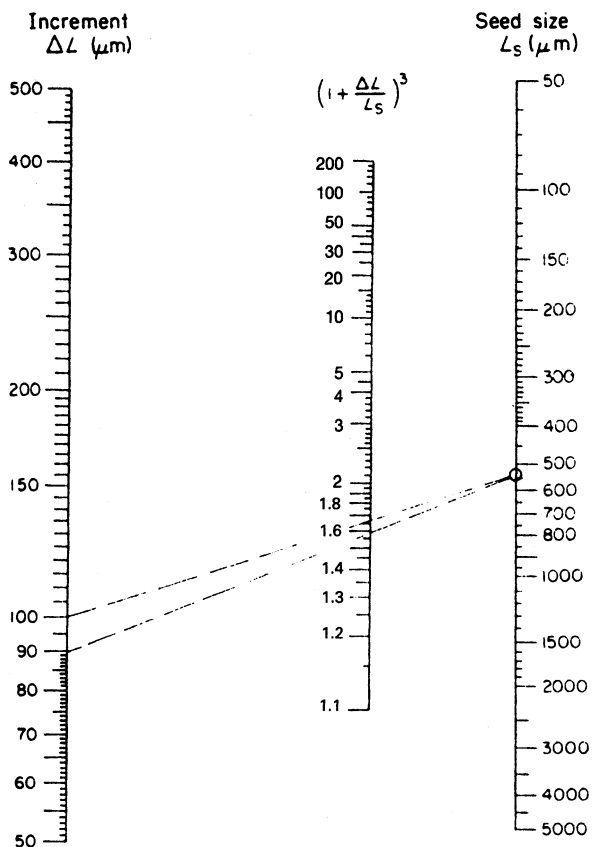


Figure 9.1. Nomograph to aid solution of the McCabe ΔL law

Table 9.1. Solution of the ΔL law (equation 9.1)

L_s μm	M_s g	$(1 + \Delta L/L_s)^3$	$\Delta L = 100 \mu\text{m}$	$\Delta L = 90 \mu\text{m}$
1400	0	1.23	1.21	
1180	0.1	1.28	1.25	
1000	3.0	1.33	1.30	
850	15.7	1.41	1.35	
710	28.7	1.49	1.43	
600	54.5	1.60	1.52	
500	74.1	1.74	1.64	
425	87.4	1.91	1.78	
355	93.7	2.12	1.97	
300	97.3	2.40	2.20	
250	98.3	2.78	2.52	
212	99.5	3.25	2.89	
180	100	3.88	3.38	

trial using $\Delta L = 100 \mu\text{m}$. A plot of these values against M_s , as explained in step 1, gives an area $M_p = 165$. If, for example, $M_p = 1.57 M_s$, then the correct value of ΔL is found from the nomograph as follows. Draw a line from $\Delta L = 100 \mu\text{m}$ through $(1 + \Delta L/L_s)^3 = 1.65$ and extend it to the L_s scale (at 520 μm). Now draw a line from this point on the L_s scale through $(1 + \Delta L/L_s)^3 = 1.57$ and extend it to the ΔL scale. The desired value of ΔL is found to be 90 μm . Column 4 in *Table 9.1* can now be completed and a plot of M_s versus $(1 + \Delta L/L_s)^3$ yields the correct value of $M_p = 157$. It is interesting to note that the focal point on the L_s scale is near the maximum of the size distribution curve of the seeds plotted on a differential basis (between 500 and 600 μm).

The postulation of the ΔL law, despite its many limitations, was a most significant step forward: it paved the way for a better understanding of the complex behaviour of crystallizers.

The next important contribution was made by Bransom, Dunning and Millard (1949) who, like McCabe, considered a perfectly mixed crystallizer, now commonly referred to as a mixed-suspension mixed-product removal (MSMPR) crystallizer (section 9.1.1). In addition, however, they considered the more realistic case where spontaneous nucleation and subsequent growth occurs. They also assumed a ‘first-order’ growth law

$$\frac{dL}{dt} = k\Delta c^g \quad (9.2)$$

where $\Delta c = c - c^*$ is the supersaturation, i.e. concentration driving force, k is a growth rate constant and $g = 1$. Their derived mass–size CSD relation may be written in the form

$$M(L) = AL^3 \exp(-BL) \quad (9.3)$$

$M(L)$ is the mass of crystals of size between L and $L + \Delta L$. A and B are constants for a given system. Equation 9.3 was verified experimentally for the laboratory-scale crystallization of cyclonite (cyclomethylene trinitramine).

Another notable contribution was made by Saeman (1956) who derived equations, based on a first-order growth law, for the form of the steady-state size distribution in mixed suspensions. The assumption of size-independent growth was also made and the cumulative mass–size distribution was expressed in the form

$$\int_0^L M(L) dL = K \left\{ 6 - \left[6 + 6 \left(\frac{L}{L_\tau} \right) + 3 \left(\frac{L}{L_\tau} \right)^2 + \left(\frac{L}{L_\tau} \right)^3 \right] \exp \left(-\frac{L}{L_\tau} \right) \right\} \quad (9.4)$$

K is a constant and L_τ is the size of a crystal grown from a nucleus (zero size) in the ‘draw-down’ time, τ , i.e. the overall residence time, defined as the ratio of the mass of crystals in suspension to the crystal production rate, or the volume of suspension to the volumetric feed rate. Saeman also compared the cases of mixed-suspension, classified-product removal (MSCPR) with MSMPR operation and showed, for example, that the age of a product mean size crystal was

four times the overall residence time for the former and three times for the latter (equation 9.36).

The basic equations of Bransom, Dunning and Millard and Saeman, had apparently already been anticipated by Peet (1931), but his pioneering work had remained unpublished in the archives of the American Potash and Chemical Corporation at Trona (Randolph, 1965).

Bransom (1960) later considered the more general case where crystal growth may be size dependent and ‘non-first-order’ with respect to supersaturation:

$$\frac{dL}{dt} = k L^b \Delta c^g \quad (9.5)$$

where k is a constant, $b > 0$ and $g > 1$. The resulting CSD equation for a continuous MSMPR crystallizer becomes

$$M(L) = A L^{3-b} \exp(-B L^{1-b}) \quad (9.6)$$

where A and B are constants (Randolph, 1965). For the case of size-independent growth ($b = 0$), equation 9.6 reduces to equation 9.3.

Another early paper was that of Robinson and Roberts (1957) who derived mathematical relationships for residence times, and hence the CSDs, in a cascade series of perfectly mixed crystallizers (section 9.1.2).

9.1.1 The population balance

For a complete description of the crystal size distribution (CSD) in a continuously operated crystallizer it is necessary to quantify the nucleation and growth processes and to apply the three conservation laws of mass, energy and crystal population. The importance of the population balance, in which all particles must be accounted for, has been a central feature in the pioneering work of Randolph and Larson (1962, 1988).

The crystal population density, n (number of crystals per unit size per unit volume of system) is defined by

$$\lim_{\Delta L \rightarrow 0} \frac{\Delta N}{\Delta L} = \frac{dN}{dL} = n \quad (9.7)$$

where ΔN is the number of crystals in the size range ΔL per unit volume. The value of n depends on the value of L at which the interval dL is taken, i.e. n is a function of L (*Figure 9.2a*). The number of crystals in the size range L_1 to L_2 is thus given by

$$\Delta N = \int_{L_1}^{L_2} n dL \quad (9.8)$$

Application of the population balance is most easily demonstrated with reference to the case of a continuously operated MSMPR crystallizer (*Figure 9.3*) assuming (a) steady-state operation, (b) no crystals in the feed stream, (c) all

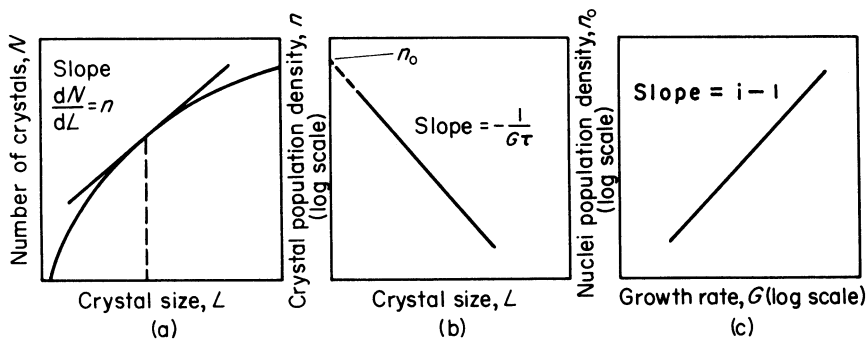


Figure 9.2. Population plots characterizing the crystal size distribution, and the nucleation and growth kinetics for a continuous MSMPR crystallizer

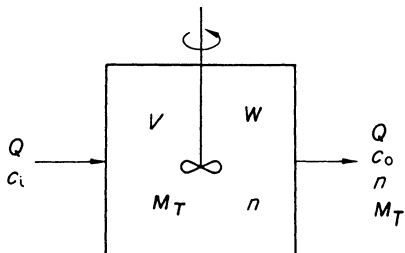


Figure 9.3. A continuous mixed-suspension, mixed-product removal (MSMPR) crystallizer

crystals of the same shape, characterized by a chosen linear dimension L , (d) no break-down of crystals by attrition, and (e) crystal growth rate independent of crystal size.

A population balance (input = output) in a system of volume V for a time interval Δt and size range $\Delta L = L_2 - L_1$ is

$$n_1 G_1 V \Delta t = n_2 G_2 V \Delta t + Q \bar{n} \Delta L \Delta t \quad (9.9)$$

where Q is the volumetric feed and discharge rate, G the crystal growth rate (dL/dt), and \bar{n} the average population density. As $\Delta L \rightarrow 0$,

$$\frac{d(nG)}{dL} = -\frac{Qn}{V} \quad (9.10)$$

Defining the liquor and crystal mean residence time $\tau = V/Q$ and assuming that growth is independent of size (ΔL law), i.e. $dG/dL = 0$, then

$$\frac{dn}{dL} = -\frac{n}{G\tau} \quad (9.11)$$

which on integration gives

$$n = n_0 \exp(-L/G\tau) \quad (9.12)$$

Equation 9.12 is the fundamental relationship between crystal size L and population density n characterizing the CSD. The quantity n_0 is the population density of nuclei (zero-sized crystals). A plot of $\log n$ versus L should give a straight line with an intercept at $L = 0$ equal to n_0 and a slope of $-1/G\tau$ (Figure 9.2b). Therefore, if the residence time τ is known, the crystal growth rate, G , can be calculated.

Furthermore, CSD data can be used to give information on the nucleation and growth kinetics. For example, the number nucleation rate, B , can be expressed as a function of the supersaturation, Δc :

$$B = \frac{dN}{dt} \Big|_{L=0} = k_1 \Delta c^b \quad (9.13)$$

The crystal growth rate G can be expressed in a similar manner:

$$G = \frac{dL}{dt} = k_2 \Delta c^g \quad (9.14)$$

as

$$\frac{dN}{dt} \Big|_{L=0} = \frac{dN}{dL} \Big|_{L=0} \cdot \frac{dL}{dt}$$

the nucleation rate may be expressed in terms of the growth rate by

$$B = n_0 G \quad (9.15)$$

or

$$B = k_3 G^i \quad (9.16)$$

where

$$i = b/g \quad (9.17)$$

Consequently

$$n_0 = k_4 G^{i-1} \quad (9.18)$$

so a plot of $\log n_0$ versus $\log G$ should give a straight line of slope $i - 1$ (Figure 9.2c) or a plot of $\log B$ versus $\log G$ should give a line of slope i . Thus the kinetic order of nucleation, b , may be evaluated if the kinetic order of growth, g , is known.

The uses of these relationships for the evaluation of nucleation and growth kinetics from experimental data have been discussed in section 6.2.5 and a worked example is given in section 9.2.

Moments of the distribution

Equation 9.12 is a number-size distribution relationship. Other distributions can be obtained in the following manner. From equations 9.8 and 9.12, the number of crystals, N , up to size L is given by

$$\begin{aligned}
N &= \int_0^L n \, dL \\
&= \int_0^L n_0 \exp(-L/G\tau) \, dL \\
&= n_0 G\tau [1 - \exp(-L/G\tau)]
\end{aligned} \tag{9.19}$$

Equation 9.19 is the *zeroth moment* of the distribution, and for large values of L ($L \rightarrow \infty$) it reduces to the total number of crystals in the system:

$$N_T = n_0 G\tau \tag{9.20}$$

The *first moment* of the distribution, which is not of any great utility, is the cumulative length (all the crystals laid side by side, if L is the sieve size):

$$\begin{aligned}
\mathcal{L} &= \int_0^L nL \, dL \\
&= \int_0^L n_0 L \exp(-L/G\tau) \, dL \\
&= n_0 (G\tau)^2 [1 - \exp(-L/G\tau) - (L/G\tau) \exp(-L/G\tau)]
\end{aligned} \tag{9.21}$$

and for $L \rightarrow \infty$

$$\mathcal{L}_T = n_0 (G\tau)^2 \tag{9.22}$$

The *second moment* gives the surface area:

$$A = \beta \int_0^L nL^2 \, dL \tag{9.23}$$

where β is a surface shape factor (section 2.14.3). For $L \rightarrow \infty$

$$A_T = 2\beta n_0 (G\tau)^3 \tag{9.24}$$

The *third moment* gives the mass:

$$M = \alpha \rho_c \int_0^L nL^3 \, dL \tag{9.25}$$

where α is a volume shape factor and ρ_c is the crystal density. For $L \rightarrow \infty$

$$M_T = 6\alpha \rho_c n_0 (G\tau)^4 \tag{9.26}$$

These equations can be simplified in dimensionless form using a relative size by putting $X = L/G\tau$, i.e. the ratio of crystal size to the size of a crystal that has grown for a period equal to the residence time τ . Thus,

$$\frac{N}{N_T} = N(X) = 1 - \exp(-X) \tag{9.27}$$

$$\frac{\mathcal{L}}{\mathcal{L}_T} = \mathcal{L}(X) = 1 - (1 + X) \exp(-X) \tag{9.28}$$

$$\frac{A}{A_T} = A(X) = 1 - \left(1 + X + \frac{X^2}{2}\right) \exp(-X) \quad (9.29)$$

$$\frac{M}{M_T} = M(X) = 1 - \left(1 + X + \frac{X^2}{2} + \frac{X^3}{6}\right) \exp(-X) \quad (9.30)$$

By use of the relative size, X , the CSD can be analysed without knowing the dependence of growth rate on supersaturation. Equation 9.30, which is identical in form with equation 9.4, represents the cumulative mass distribution. The differential mass distribution is represented by

$$\frac{dM(X)}{dX} = \frac{1}{6} X^3 \exp(-X) \quad (9.31)$$

These relationships are shown in *Figure 9.4* where it is seen that the mixed product shows a dominant size fraction for $X = 3$, at the peak of the mass distribution curve. This is sometimes referred to as the *modal* or *dominant* size. The *median* size of the distribution, at 0.5 mass fraction on the cumulative curve, occurs at $X = 3.67$.

Mass balance constraint

The total solids content, M_T , and hence the production rate of an MSMPR crystallizer are both controlled by the feedstock and operating conditions. Equation 9.26 is, in effect, a growth rate constraint because for a given population density of nuclei only one value of G will satisfy the mass balance. The mass of crystals dM in a given size range dL is

$$dM = n\alpha\rho_c L^3 dL \quad (9.32)$$

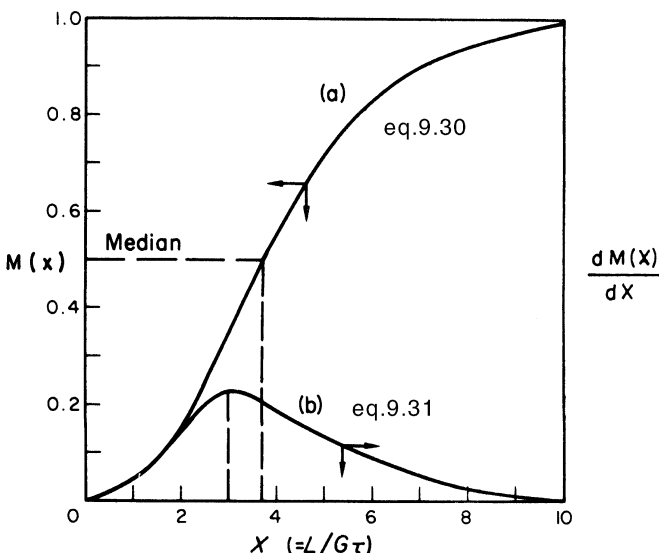


Figure 9.4. Mass distributions for MSMPR operation: (a) cumulative, and (b) differential

so the mass fraction in that size range is dM/M_T . Therefore, the mass distribution is given by

$$\frac{M(L)}{dL} = \frac{nL^3}{6n_0(G\tau)^4} \quad (9.33)$$

which, from the population density relationship (equation 9.12), becomes

$$\frac{M(L)}{dL} = \frac{\exp(-L/G\tau)L^3}{6(G\tau)^4} \quad (9.34)$$

The maximum of this mass distribution (the modal or dominant size, L_D , of the CSD) is found by maximizing equation 9.34:

$$6(G\tau)^4 \frac{d}{dL} \cdot \frac{M(L)}{dL} = 3L^2 \exp(-L/G\tau) - \frac{L^3}{G\tau} \exp(-L/G\tau) = 0 \quad (9.35)$$

which gives the modal size

$$L_D = 3G\tau \quad (9.36)$$

The median size of the mass distribution may be expressed as

$$L_M = 3.67G\tau \quad (9.37)$$

i.e. 50% by mass of the product from an MSMPR crystallizer is larger, or smaller, than $3.67G\tau$.

CSDs may be conveniently classified by the median size and the coefficient of variation. The CV , which quantifies the size spread, is a statistical property related to the standard deviation of a Gaussian distribution and is normally expressed as a percentage by

$$CV = 100 \left[\frac{L_{84\%} - L_{16\%}}{2L_{50\%}} \right] \quad (9.38)$$

The values of $L_{84\%}$, $L_{50\%}$ ($= L_M$) and $L_{16\%}$ may be obtained from a cumulative mass distribution curve, as described in section 2.14.4. The higher the CV the broader the spread, $CV = 0$ denoting a monosized distribution. The CV for a Gaussian distribution is 52%, but the product from an MSMPR crystallizer, which generally conforms more to a gamma function distribution (equation 2.78), has a CV of $\sim 50\%$.

The simplified information flow diagram for an MSMPR crystallizer in *Figure 9.5* demonstrates several interacting processes that contribute to the development of the product CSD. Supersaturation, created by cooling, evaporation, reaction, etc., influences the rates of both nucleation and crystal growth, the product CSD and consequently the total crystal surface area available in the crystallizer. In turn, the crystal surface area influences the supersaturation, thus creating a feedback loop. More complex schemes can be drawn showing other influences, such as the effect of hydrodynamics on both nucleation and growth, and other feedback loops, caused by agglomeration or secondary nucleation effects (Randolph and Larson, 1988).

The products from a number of large-scale industrial crystallizers of the forced-circulation and DTB types have been reported (Bennett, 1962) to have

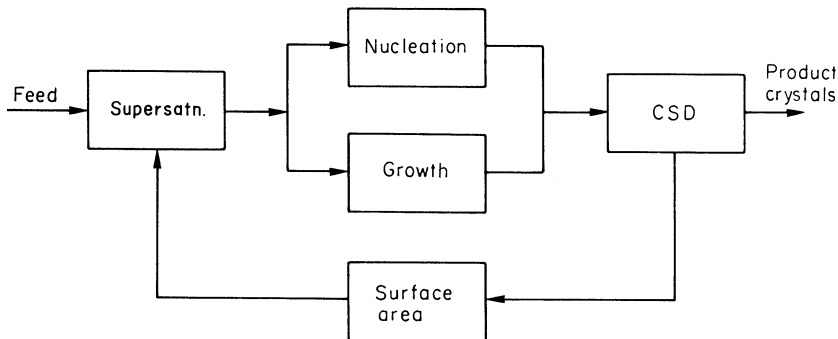


Figure 9.5. A simple information flow diagram for a continuous MSMPR crystallizer

CVs in the range 30–50%, although sodium chloride appeared consistently to be lower (20–30%). Industrial CV data have also been reported by Palmer (1970) for a large number of substances crystallized in Oslo-Krystal units.

The magma density M_T in a crystallizer can significantly influence the production of secondary nuclei and this effect may be represented by extending equation 9.16 to

$$B = K_R M_T^j G^i \quad (9.39)$$

where K_R is a rate constant related to the kinetic constants of equations 9.13 and 9.14. Incorporating equation 9.15, equation 9.26 may be written

$$M_T = 6\alpha\rho_c(B/G)(G\tau)^4 \quad (9.40)$$

which, characterizing the crystals by the modal size L_D (equation 9.36), gives:

$$M_T = \frac{2\alpha\rho_c B L_D^4}{27G} \quad (9.41)$$

Alternatively, if the CSD were to be characterized by the median size L_M (equation 9.37), the relationship may be written

$$M_T = \frac{\alpha\rho_c B L_M^4}{30G} \quad (9.42)$$

Substituting for M_T in equation 9.39, assuming the simplest case of $j = 1$, which appears to have some practical justification, equation 9.41 and equation 9.42, respectively, give

$$G = \left[\frac{27}{2\alpha\rho_c K_R L_D^4} \right]^{1/(i-1)} \quad (9.43)$$

and

$$G = \left[\frac{30}{\alpha\rho_c K_R L_M^4} \right]^{1/(i-1)} \quad (9.44)$$

Equations 9.41–9.44 are useful for basic design calculations (see section 9.3.2).

Effect of residence time

For a constant magma density, equation 9.26 indicates that for different residence times τ_1 and τ_2 :

$$6\alpha\rho_c n_{01}(G_1\tau_1)^4 = 6\alpha\rho_c n_{02}(G_2\tau_2)^4 \quad (9.45)$$

i.e.

$$\frac{n_{02}}{n_{01}} = \left(\frac{G_1\tau_1}{G_2\tau_2}\right)^4 \quad (9.46)$$

which, from equation 9.18, may be written

$$\frac{n_{02}}{n_{01}} = \left(\frac{\tau_1}{\tau_2}\right)^{4(i-1)/(i+3)} \quad (9.47)$$

or

$$\frac{G_2}{G_1} = \left(\frac{\tau_1}{\tau_2}\right)^{4/(i+3)} \quad (9.48)$$

The effect of residence time on the median crystal size L_M (from equation 9.37) is

$$\frac{L_{M2}}{L_{M1}} = \left(\frac{\tau_1}{\tau_2}\right)^{(1-i)/(i+3)} \quad (9.49)$$

Keeping the magma density constant and doubling the residence time ($\tau_2 = 2\tau_1$), the following effects might be noted:

1. For a relative kinetic order $i < 1$, a comparatively rare occurrence, the median crystal size would decrease slightly.
2. For $i = 1$, the median crystal size would be unaffected (equation 9.49) even though the crystal growth rate had been halved (equation 9.48).
3. For $i > 1$, the median crystal size would increase, but for a fairly typical value of $i = 2$ the increase would only amount to about 15% (equation 9.49).

The conclusion, therefore, is that residence time manipulation is not usually a very effective means of adjusting product crystal size.

Effect of magma density

For a constant residence time, changes in magma density, e.g. by changing the feedstock concentration, can be analysed in a similar manner to that above to yield the following relationships:

$$\frac{n_{02}}{n_{01}} = \left(\frac{M_{T2}}{M_{T1}}\right)^{(i-1)/(i+3)} \quad (9.50)$$

$$\frac{G_2}{G_1} = \left(\frac{M_{T2}}{M_{T1}} \right)^{1/i+3} \quad (9.51)$$

$$\frac{L_{D2}}{L_{D1}} = \left(\frac{M_{T2}}{M_{T1}} \right)^{1/i+3} \quad (9.52)$$

The magma density can significantly influence secondary nucleation (equation 9.39) and this interaction should not be ignored. Accordingly, equation 9.18 can be modified to

$$n_0 \propto M_T^j G^{i-1} \quad (9.53)$$

giving

$$\frac{n_{02}}{n_{01}} = \left(\frac{M_{T2}}{M_{T1}} \right)^{(i+4j-1)/(i+3)} \quad (9.54)$$

and

$$\frac{G_2}{G_1} = \left(\frac{M_{T2}}{M_{T1}} \right)^{(1-j)/(i+3)} \quad (9.55)$$

The secondary nucleation rate is often assumed to be directly proportional to the magma density ($j = 1$) which gives

$$\frac{G_2}{G_1} = \left(\frac{M_{T2}}{M_{T1}} \right)^0 = 1 \quad (9.56)$$

and

$$\frac{n_{02}}{n_{01}} = \frac{M_{T2}}{M_{T1}} \quad (9.57)$$

Equations 9.56 and 9.57 suggest, therefore, that the crystal growth rate is independent of M_T and that the population density of nuclei is proportional to M_T , regardless of the relative kinetic order i , so that it might be expected that there would be little or no change in CSD from a change of magma density.

Effect of agitation

Although the effects of residence time and magma density changes *alone* would appear to have little or no influence on the CSD, their combined effects together with those of agitation cannot be ignored. For example, a combination of equations 9.15 and 9.26 gives

$$\log(B/M_T) = \log(1/6\alpha\rho_c\tau^4) - 3 \log G \quad (9.58)$$

which when plotted gives a series of lines, each of slope -3 , for different residence times (Figure 9.6).

The effect of agitation may be incorporated in an extension of equation 9.39:

$$B \propto M_T^j G^i N^s \quad (9.59)$$

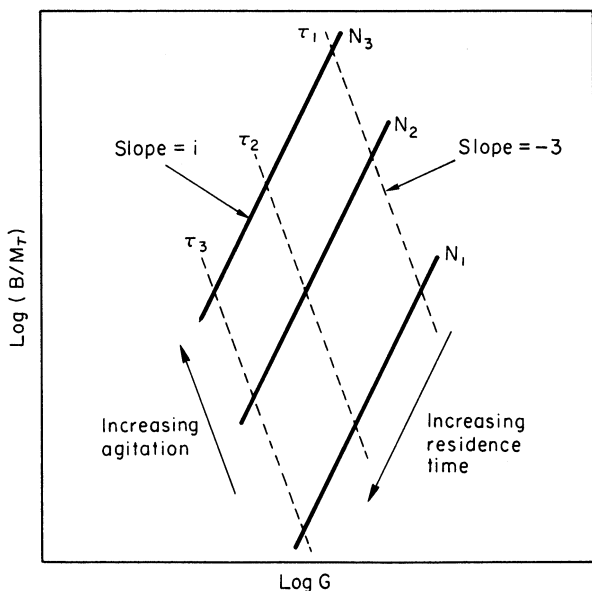


Figure 9.6. Combined effects of magma density, residence time and agitation

where N is the agitator speed. Assuming that $j = 1$, a plot of $\log(B/M_T)$ versus $\log G$ gives a sequence of lines of slope i for different values of N , and the resulting grid (Figure 9.6) can be used for identifying zones of acceptable operating conditions (Scrutton, 1978). In practical cases the exponent j tends to vary between 0.8 and 1, i between 1 and 2, and s between 2 and 3.

Most models for the scale-up of contact secondary nucleation rates are based on the Botsaris (1976) relationship

$$B = E_t F_1 F_2 \quad (9.60)$$

where E_t is the rate of energy transfer to the crystals by collision, F_1 the number of particles generated per unit of transferred energy and F_2 the fraction of particles that survive to become nuclei. The quantity E_t , which contains contributions from crystals of all sizes ($0 < L < \infty$), may be expressed by

$$E_t = \int_0^\infty E(L)\omega(L)n(L) dL \quad (9.61)$$

where $E(L)$, $\omega(L)$ and $n(L)$ are the collision energy, collision frequency and number of crystals of size L . Various models have been proposed for estimating $E(L)$ and $\omega(L)$ (Ottens and de Jong, 1973; Garside and Jančić, 1979), but the product $F_1 F_2$, normally considered to be a power function of the supersaturation, must be determined experimentally.

Although several different approaches have been made to this problem in recent years, all lead basically to the same nucleation rate equation (Garside and Davey, 1980) and tend to justify the use of empirical scale-up rules for crystallizers such as keeping the specific power input constant (section 9.3.4).

These rules, however, are probably not applicable to precipitation processes (section 8.10).

Size-dependent crystal growth

The simplifying assumption of size-independent crystal growth rate, utilized in the crystal population analyses so far, cannot always be justified. For one reason or another, many crystals exhibit size-dependent growth (section 6.2.7) and this leads to the generation of a different product CSD from that described previously under MSMPR conditions.

In order to accommodate the concept of size-dependent growth, several empirical relationships between G ($= dL/dt$) and L have been proposed, but the one currently most widely used is the ASL equation (Abegg, Stevens and Larson, 1968)

$$G(L) = G_0(1 + \gamma L)^b \quad b < 1 \quad (9.62)$$

where γ , b and G_0 are experimentally determined constants. Equation 9.62 satisfies a number of essential requirements, e.g. it is a continuous function of L and b including $L = 0$ and $b = 0$, it acknowledges that crystal nuclei ($L = 0$) grow at a finite rate, G_0 , and all positive moments of the CSD generated by the model converge. It does, however, suggest that as L increases to infinity so does G , but although this is unrealistic, it does not present any serious problems in dealing with crystal distributions in the size ranges normally encountered in industrial crystallizers.

An interesting critical analysis of the validity of empirical relationships for the assessment of size-dependent growth has been made by Rojkowski (1978) who proposes alternative relationships which merit consideration if a more rigorous assessment of the problem is considered necessary.

The population equation for an MSMPR crystallizer operated at steady state, with crystal growth rate independent of size ($dG/dL = 0$), may be written (equation 9.11)

$$G \frac{dn}{dL} = \frac{-n}{\tau} \quad (9.63)$$

For the case of size-dependent growth, this must be modified to

$$\frac{\partial(nG)}{\partial L} = \frac{-n}{\tau} \quad (9.64)$$

which, when combined with equation 9.62 and integrated, equating γ with $1/G_0\tau$, gives

$$n = n_0(1 - \gamma L)^{-b} \exp \left[\frac{1 - (1 + \gamma L)^{1-b}}{1 - b} \right] \quad (9.65)$$

For the case $b = 0$, equation 9.65 reduces to equation 9.12 and the population density plot is linear (*Figure 9.2b*). For $b > 0$ the plot begins to exhibit curvature which becomes very pronounced at values of $b > 0.5$. Considerable care

must be taken, however, when attempting to interpret curvature in population density plots based on experimental data since it is impossible to distinguish the independent effects of growth rate dispersion and size-dependent growth (section 6.2.7). Furthermore, curvature at the extremities of a population density plot can indicate a departure from ideal MSMPR behaviour (section 9.1.2). These and other aspects of the problem have been discussed in some detail by Jančić and Grootscholten (1984) and Randolph and Larson (1988).

9.1.2 Alternative operating modes

Crystallizers in series

Crystallizers are sometimes operated in a linked series of well-mixed vessels, with the magma flowing from one stage to another. The most frequent objective of series or ‘cascade’ operation is to economize on heat utilization, e.g. by dividing the overall temperature gradient over several stages and operating each stage at a lower temperature down the cascade. Further, in cooling crystallization, on account of the smaller temperature drops needed across the heat exchange elements, encrustation problems (section 9.5) may be significantly reduced.

There is also the possibility that cascade operation can influence the product CSD, although this is a complex problem to assess. For example, in a simple cascade of k vessels in which all act individually as basic MSMPR crystallizers operating at the same supersaturation, at constant crystal growth rate, and with nucleation confined to the first stage only, the mean crystal size and product CSD leaving the k^{th} stage may be represented by

$$L_k = \left(\frac{k+2}{3k} \right) L_1 \quad (9.66)$$

and

$$CV = 100/(k+3)^{1/2} \quad (9.67)$$

Equations 9.66 and 9.67 suggest that in this uncomplicated situation, which admittedly is hardly realistic from an industrial point of view, the mean crystal size and CSD would both decrease, e.g. from L_1 to $0.56 L_1$ and from 50 to 41% CV , at the end of a three-stage cascade, i.e. smaller crystals with a narrower size distribution.

For more practical operating conditions than the above, however, the analyses can be exceedingly complex (Robinson and Roberts, 1957; Randolph and Larson, 1962, 1988; Randolph, Deepak and Iskander, 1968; Hill, 1970; Abegg and Balakrishnan, 1971; Nývlt, 1971, 1973; Wey and Terwilliger, 1976; Rojkowski, 1977; Tavare and Chivate, 1978), and the benefits of cascade operation *as a means of CSD manipulation* are often negligible and can sometimes be negative.

CLO, FD and CPR

The expectation of perfect MSMPR operation is unrealistic for industrial crystallizers, and CSD analyses based on the strict simplifying assumptions

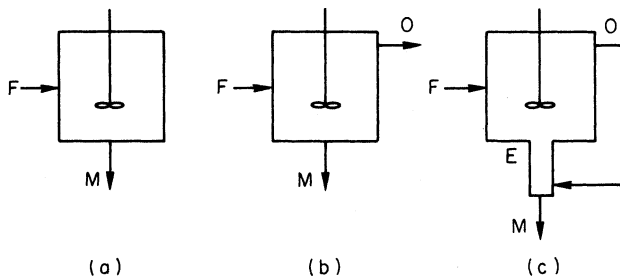


Figure 9.7. Three basic types of continuously operated mixed suspension crystallizer, (a) mixed product removal (MSMPR), (b) clear liquid overflow (CLO), (c) CLO with recycle through an elutriating leg (classified product removal MSCPR). F = feed, E = elutriating leg, M = magma outlet, O = overflow

outlined in section 9.1.1 need to be modified for application to practical situations. The effect of size-dependent growth, for example, which introduces curvature into population density plots and makes their interpretation difficult, has already been discussed in the previous section. There are other conditions, such as size-dependent nucleation, crystal attrition, breakage, agglomeration, classification and so on, that can exert equally profound influences. Analyses of these effects beyond the scope of the present work, are discussed in some detail by Randolph and Larson (1988) and Jančić and Grootscholten (1984).

It is appropriate, however, to make some comment here on a few common departures from MSMPR operation. Three basic types of continuously operated mixed-suspension crystallizer are shown in Figure 9.7. In the simple MSMPR unit (Figure 9.7a), where the outflow is of identical composition to that in the perfectly mixed vessel, the crystal and liquor residence times are equal:

$$\tau_c (= W/P) = \tau_l (= V/Q) \quad (9.68)$$

where Q is the feedstock rate ($\text{m}^3 \text{ h}^{-1}$) to a vessel of working volume V (m^3) containing a suspended mass of crystals W (kg). P is the crystal production rate (kg h^{-1}).

By allowing some clear liquor to overflow from the crystallizer (Figure 9.7b) the crystal residence time can be increased and rendered independent of the liquor residence time, i.e. $W/P \neq V/Q$. If required, the liquor overflow can be recycled back into the crystallizer through an elutriating leg, thus imposing some classifying action on the product crystals leaving the crystallizer (Figure 9.7c). This mode of operation is generally referred to as mixed-suspension, classified-product removal (MSCPR), an operating procedure that can be seen in several of the crystallizers described in section 8.4.

Clear liquor overflow (CLO), also known as *double draw-off* (DDO), increases the residence time of crystals in the growth zone and increases the magma density. This mode of operation also allows excess fine crystals to be removed from the system. Most crystallizers suffer from excessive nucleation, and to produce reasonably large crystals the excess fines must be removed. In terms of mass, the small crystals may appear insignificant; the cumulative masses of crystals in a mixed suspension varies as the fourth power of their size so, for

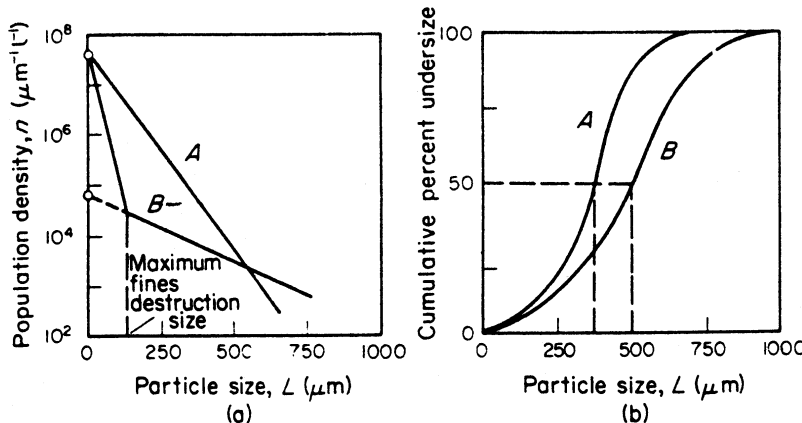


Figure 9.8. The effect of fines removal on (a) the population density and (b) the crystal size distribution. A, no fines destruction; B, fines destruction

example, crystals up to $\frac{1}{2}$ the mean product size constitute only $(\frac{1}{2})^4$, one-sixteenth, of the total mass in suspension. In terms of numbers, however, these small crystals in a crystallizer exert a dominant effect, often outnumbering the larger crystals by $> 1000 : 1$.

Fines destruction (FD) can be accomplished by recirculating the liquor overflow externally through a fines trap, e.g. a hydrocyclone or steam-heated dissolver, or internally as described by Saeman (1961). Figure 9.8 shows the effect of fines removal. The small-sized crystals undergo a very rapid decay up to the cut size of the fines trap (Figure 9.8a). Thereafter the decay proceeds at the rate appropriate to mixed product removal operation, and extrapolation of the population density line back to zero yields a lower *effective* density of nuclei appropriate to the crystallizer. The mean product size is increased by fines destruction (Figure 9.8b). A rough estimate of the rate of fines dissolution can be made by making the assumption that the Sherwood number = 2 (section 6.3.1).

Analyses of the influence of fines trapping on crystallizer performance have been made by Nauman (1971) and Nauman and Szabo (1971).

Classified product removal (CPR) is frequently adopted in crystallizer practice, e.g. with an elutriator or hydrocyclone. As Randolph (1970) has pointed out, however, although this practice may produce a narrower CSD it also leads to a smaller product mean size (Figure 9.9). The cases of mixed and classified product removal are compared on the population density plot in Figure 9.9a and the CSD implications are shown in Figure 9.9b.

9.1.3 Unsteady-state operation

Continuous crystallizers commonly develop unsteady-state behaviour. Feed rate or composition changes, temperature fluctuations, etc., will manifest themselves as transient disturbances in the product CSD until the system regains its original, or adjusts to a new, steady-state mode. A comprehensive

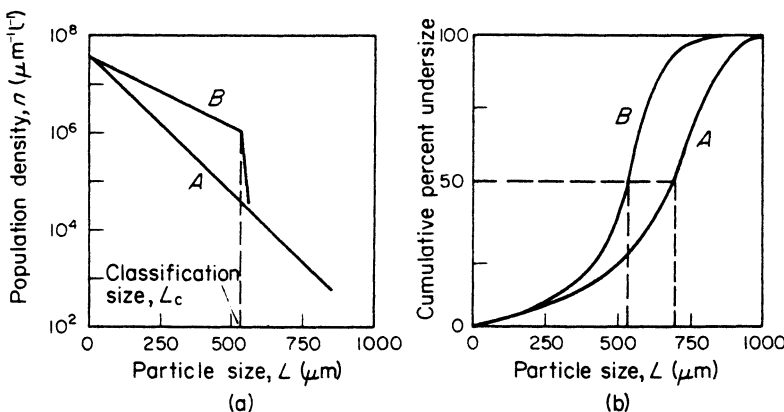


Figure 9.9. The effect of classified product removal on (a) the population density and (b) the crystal size distribution. A, mixed product removal; B, classified product removal

analysis of CSD transients resulting from step changes in operating conditions is given by Randolph and Larson (1988).

Even though operating conditions ostensibly remain constant, however, a crystallizer can exhibit unstable behaviour and develop periodic changes in crystal production rate and CSD, although it has often been suggested that a continuous crystallizer should be self-stabilizing. For example, an increase of the supersaturation would lead to a higher nucleation rate, but as this would give a total crystal surface area increase, owing to the growth of the nuclei, the supersaturation would then decrease and the nucleation rate would fall to its former value.

In practice, however, the dynamic behaviour of a continuous crystallizer is not so simple. The above stabilizing effect is subject to a considerable time lag, because newly formed nuclei have no appreciable surface area for a long time. Before stabilization can occur, therefore, large numbers of nuclei might be formed which will later reduce the supersaturation below its steady-state value. The resulting slow nucleation will lead to a decrease of the total crystal surface area, below its steady-state value, and this in turn will cause an increase of the supersaturation above its steady-state value, and so on.

The result of the above sequence of events will be the occurrence of limit cycles, and mathematical models of continuous crystallizers with perfect and imperfect mixing, with and without product classification have been developed (Nýlt and Mullin, 1970) to show how periodic changes of supersaturation, solids content, crystal size and production rate can readily occur. Periodic behaviour is most pronounced at the beginning of the crystallization process, and in most cases the fluctuations are subsequently damped. This means that under favourable conditions a steady state is usually reached (Figure 9.10a). However, under some operating conditions the damping is not effective and the cyclic behaviour may continue for a considerable time (Figure 9.10b). Indeed, in some cases the steady state may not be achieved at all.

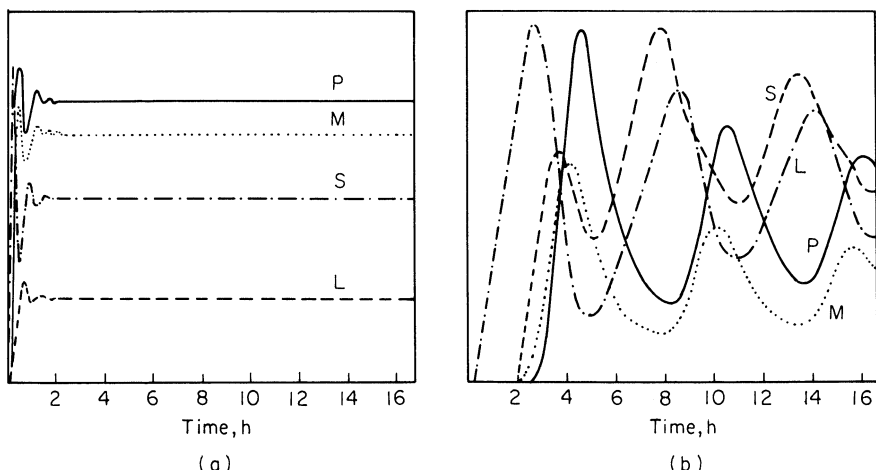


Figure 9.10. Dynamic behaviour of a mixed suspension crystallizer showing (a) mixed product removal – short period damped cycles; (b) classified product removal via elutriating leg – long period slowly damped cycles. P , production rate; M , magma density; S , supersaturation; L , median crystal size (various scales). (After Nývlt and Mullin, 1970)

The stability of a crystallizing system tends to increase with increasing crystal growth rate and magma density, and with decreasing nucleation ‘order’, minimum product size, and the relative amount of crystals withdrawn. Continuous seeding has the same effect as decreasing the effective nucleation order, and should lead to a stabilization of the system.

In general terms, clear liquor overflow (CLO) tends to reduce cycling behaviour while classified product removal (CPR) increases it. A common form of unintentional CPR is the use of a badly designed product outlet which causes segregated magma removal. Fines destruction (FD) can be used to control the population density of nuclei in the crystallizer. Much attention is being paid at the present time to ways in which on-line CSD measurement can be reliably used to assist the transmission of information to control systems to allow rapid adjustments to be made in temperature, feed rate, FD rate, etc. to stabilize the system.

Figure 9.11a shows schematically a mixed suspension crystallizer being operated with FD and CPR: the R-Z model of Randolph and Larson (1988). Figure 9.11b shows an idealized population density plot for the crystals suspended within the crystallizer. The CSDs in the three size ranges divided by the cut-sizes L_f and L_c may be expressed by

$$n = n_0 \exp(-RL/G\tau) \quad 0 < L < L_f \quad (9.69)$$

$$n = n_0 A \exp(-L/G\tau) \quad L_f < L < L_c \quad (9.70)$$

$$n = n_0 B \exp(-ZL/G\tau) \quad L_c < L < \infty \quad (9.71)$$

where A and B are exponential functions relating to R and Z , respectively. R , the ratio of the total fines removal rate to the flow through the crystallizer,

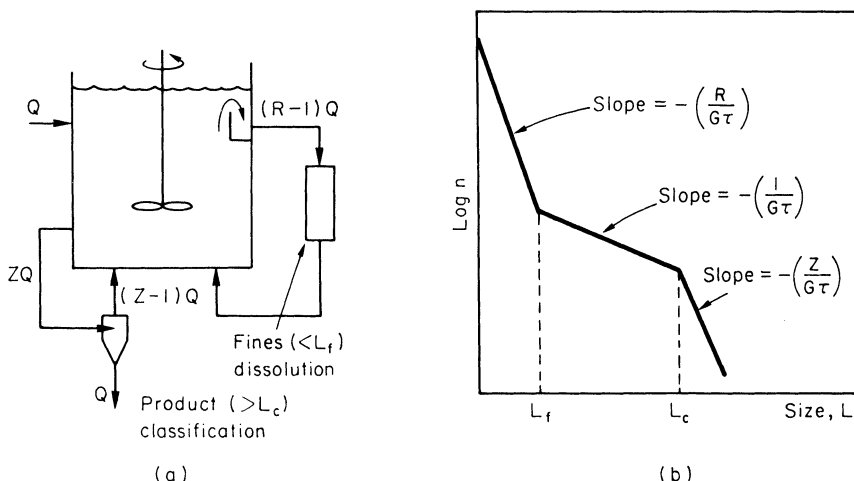


Figure 9.11. Mixed suspension crystallizer operating with fines destruction and classified product removal: (a) the R-Z model, (b) population density plot

expresses the decrease in residence time of the fine crystals ($< L_f$), i.e. $\tau_f = T/R$, where τ is the overall crystal mean residence time. Z , the ratio of the classified product removal rate to the total flow, expresses the increase in removal rate for the large crystals ($> L_c$), i.e. $\tau_c = \tau/Z$.

9.1.4 Batch crystallization

For batch crystallizers, which inevitably operate in the unsteady state, the simple population balance relationship, e.g. equation 9.63, must be modified to

$$\frac{\partial(nG)}{\partial L} = \frac{-\partial n}{\partial t} \quad (9.72)$$

and solved, with the relevant kinetic, mass balance and operating constraints, to predict the product CSD (Randolph and Larson, 1988). Methods for creating supersaturation include cooling, evaporating, reaction, salting out and combinations of these procedures.

Programmed (controlled) cooling

A typical batch cooling crystallization, for example, begins with a hot unsaturated feed liquor being charged to an agitated vessel equipped with a cooling jacket or coils. Supersaturation is created shortly after cooling is commenced, after which nucleation occurs, crystals grow and the supersaturation is depleted. The final product CSD is dependent on the supersaturation profile created over the batch time, so the cooling rate is of critical importance. Selective seeding can also be helpful (section 8.4.5).

If 'natural' cooling is employed, e.g. by passing coolant through the jacket or coils at a steady rate and constant inlet temperature, the temperature in the

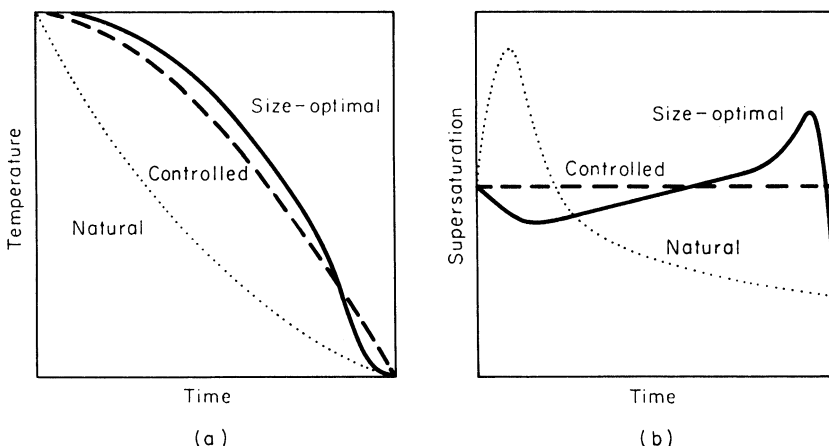


Figure 9.12. Natural, controlled (constant nucleation) and size-optimal cooling modes in a batch crystallizer: (a) temperature profiles, (b) supersaturation profiles

vessel will fall exponentially as shown in *Figure 9.12a*. On the other hand, the supersaturation increases very quickly in the early stages and peaks when nucleation occurs after exceeding the metastable limit (*Figure 9.12b*). This sequence of events leads to an uncontrolled performance and results in small crystals with a wide CSD.

A distinct improvement in performance can be obtained, however, if the supersaturation peak is eliminated. This may be done, for example, by choosing a working level of supersaturation at which the primary nucleation rate is likely to be negligible, seeding the solution with a predetermined mass of carefully sized seed crystals and maintaining the supersaturation within the metastable zone throughout the batch time. This mode of operation, called ‘controlled cooling’ requires that the cooling curve should fall slowly in the early stages and more quickly towards the end, i.e. the reverse of natural cooling (*Figure 9.12a*).

An early attempt to establish an ‘optimum’ cooling curve for batch cooling crystallization (Mullin and Nývlt, 1971) considered a controlled operation at constant supersaturation, and used a calculation method based on a supersaturation balance in which nuclei were generated in a sequence of discrete time steps.

A supersaturation balance on a batch cooling crystallizer gives

$$\frac{-d\Delta c}{dt} = \frac{dc^*}{dt} + k_g A \Delta c^g + k_b \Delta c^b \quad (9.73)$$

where c = concentration, c^* = equilibrium saturation, Δc = supersaturation ($= c - c^*$), t = time, A = total crystal area, k_g and k_b are growth and nucleation constants, and g and b are the ‘orders’ of growth and nucleation, respectively.

Equation 9.73 describes the rate of change of supersaturation in a seeded and nucleating solution. The first term on the right-hand side corresponds to the creation of supersaturation by cooling, taking advantage of the positive

temperature dependence of solubility. The second and third terms describe the desupersaturation rate caused by crystal growth and nucleation, respectively.

For a seeded system, making a number of simplifying assumptions such as constant supersaturation, negligible nucleation and growth only on the added seeds, a general expression of the optimum cooling curve becomes

$$-\frac{d\theta}{dt} = \frac{3W_{s0}G(t)L^2(t)}{\left[\frac{d\Delta c}{d\theta} - \frac{dc^*}{d\theta}\right]L_{s0}^3} \quad (9.74)$$

with mass of added seeds W_{s0} , seed size L_{s0} , batch temperature range θ_0 to θ_f , crystal growth rate G and size L . The batch time and corresponding cooling curve may be determined by numerically integrating equation 9.74. Further simplifying assumptions, e.g. if $G \neq G(L, \theta)$, $dc^*/d\theta = 0$ and $d\Delta c/d\theta = 0$, allows a very simple expression for predicting an approximate optimum cooling curve to be obtained:

$$\theta_t = \theta_0 - (\theta_0 - \theta_f)(t/\tau)^3 \quad (9.75)$$

where θ_0 , θ_f and θ_t are the temperatures at the beginning, end and at any time t during the process, and τ is the overall batch time. Equation 9.75 is often adequate for initial trials in a general industrial application (see example 9.3 in section 9.3.3). For *unseeded* solutions a modification of equation 9.75 is recommended:

$$\theta_t = \theta_0 - (\theta_0 - \theta_f)(t/\tau)^4 \quad (9.76)$$

which leads to an even more gentle decrease in temperature in the initial stages of the cooling process.

Figure 9.13 demonstrates the benefits of employing programme-controlled cooling during a seeded batch crystallization of potassium sulphate in which

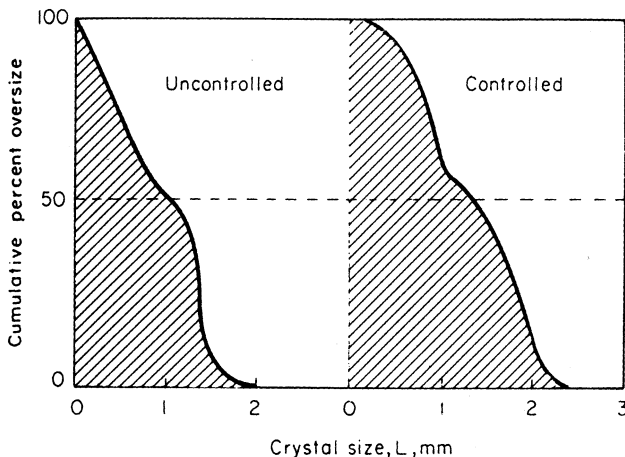


Figure 9.13. Cumulative product crystal size distributions for the uncontrolled and controlled seeded batch cooling crystallization of potassium sulphate. (After Mullin and Nývlt, 1971)

the median size was increased by about 40% above that obtained with uncontrolled cooling. The distribution curve, however, was bimodal and all product crystals contained some crystals smaller than the added seed size, demonstrating that secondary nucleation had occurred. Nevertheless, the median size was always significantly higher for controlled operation (Mullin and Nývlt, 1971).

The principle of controlled operation can be extended to other modes of supersaturation development, e.g. evaporation (Larson and Garside, 1973), salting-out (Tavare, Garside and Chivate, 1980) and reaction (Lindberg and Rasmussen, 2000). For the salting-out mode of operation Jones and Teodossiev (1988) have developed a simple microcomputer programme dosage rate system and demonstrated its utility for the controlled precipitation of potassium sulphate from aqueous solution using acetone.

Recognizing that some secondary nucleation inevitably occurs in seeded solutions, even at low supersaturation, the theory of programmed cooling crystallization was further developed by Jones and Mullin (1974) after which Jones (1974) demonstrated the application of optimal control theory to maximize product crystal size. Predicted ‘size-optimal’ cooling curves for seeded potassium sulphate solutions differ significantly from the ‘constant nucleation rate’ case considered above in that the supersaturated solution temperature is held relatively constant for a short period at the beginning of the operation, resulting in a desupersaturation as the seed crystals grow. Cooling is then commenced and increased, slowly at first and quickly later, creating a supersaturation peak towards the end of the process. Finally, the cooling rate is greatly reduced until the system approaches equilibrium (*Figure 9.12*).

Optimal control schemes have also been applied to batch cooling crystallization (Ajinkya and Ray, 1974; Morari, 1980; Chang and Epstein, 1982) and to the evaporative crystallization of sugar (Frew, 1973). A simplified model to obtain temperature-time trajectories for seeded batch cooling crystallization without resorting to optimization techniques has been proposed by Rohani and Bourne (1990).

Fines destruction

Even though significant improvements in product CSD can be made by employing controlled operation, the benefits are often diminished because fine crystals are created by secondary nucleation (Mullin and Nývlt, 1971; Jones and Mullin, 1974). In an attempt to combat this problem, the effects of fines destruction (FD), commonly employed to improve product CSD in continuous crystallizers (section 9.1.2) was investigated by Jones, Chianese and Mullin (1984).

Runs were made with potassium sulphate in a 30 L batch cooling crystallizer fitted with draft-tube agitator, the draft-tube also serving as a heat exchanger (Mullin and Nývlt, 1971; Jones and Mullin, 1973a) (*Figure 9.14*). A predetermined mass of seeds (500–600 µm) was added to the vessel when the solution had become supersaturated, after which programmed cooling, according to the constant nucleation rate mode, was commenced. The fines trap was a 100 × 50 mm cylinder located in the annular region which collected crystals

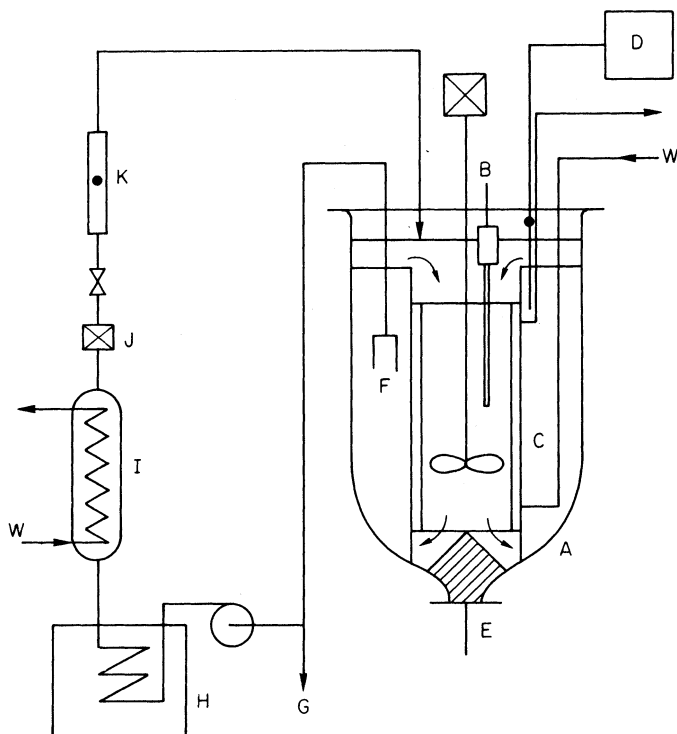


Figure 9.14. A batch cooling crystallizer for studying the effect of fines dissolution: A, 30 L crystallization vessel; B, immersion heater; C, draft-tube cooler; D, temperature indicator/controller; E, discharge plug with conical baffle; F, fines trap; G, sample point; H, oil bath; I, pre-cooler; J, filter ($5\text{ }\mu\text{m}$); K, Rotameter; W, cooling water inlet. (After Jones, Chianese and Mullin, 1984)

smaller than about $200\text{ }\mu\text{m}$, calculated from Stokes' law on the basis that the superficial velocity in the trap was about 5 mm s^{-1} . The total batch of liquor was circulated through the trap three times during a run.

A comparison of runs carried out under one particular set of conditions (Figure 9.15) shows the beneficial effects of FD operation, the fines content (< $600\text{ }\mu\text{m}$) of the product was decreased from about 25 to 10 per cent by mass, and the median product size was increased by about 25 per cent, from 1110 to $1380\text{ }\mu\text{m}$.

Two-stage batch cooling

Simple batch cooling crystallization can suffer from a serious defect if the hot feed solution is charged into an agitated vessel and uncontrolled cooling is commenced immediately. The large temperature difference between the solution and the surface of the cooling element, e.g., coil or jacket, often causes encrustation (scale) to form which not only reduces the effective

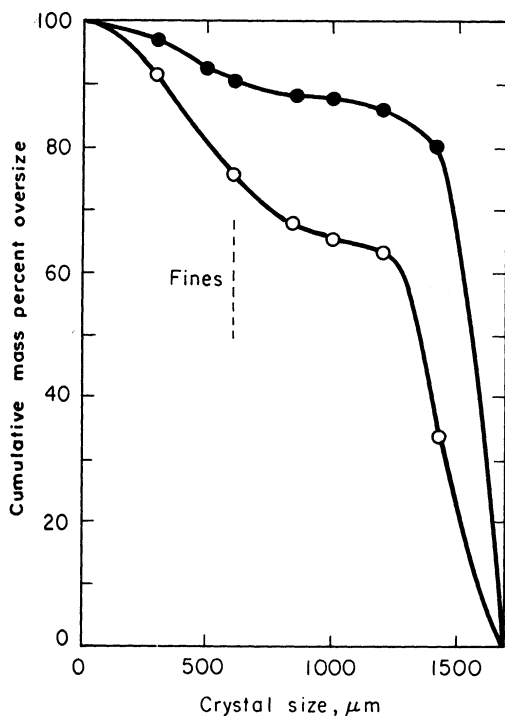


Figure 9.15. Experimental crystal size distributions for the batch cooling crystallization of potassium sulphate with and without fines destruction using the apparatus depicted in Figure 9.14. Added seeds $\sim 550 \mu\text{m}$; fines 'cut' $\sim 5 \mu\text{m}$. (After Jones, Chianese and Mullin, 1984)

temperature difference for heat transfer but also encourages the scale to continue to grow. The heat transfer rate consequently becomes slower and slower, the temperature difference rapidly falls and batch times can become excessively long and uneconomical.

To overcome these problems Nývlt (1992) proposes a technique which he calls *two-stage batch cooling*. If the intensity of heat flow is less than some critical value, characteristic of the given system, scaling will not occur on the cold surface and cooling can proceed with a high heat transfer coefficient. With a knowledge of this critical heat flow, or of the corresponding critical temperature difference, the cooling process can be divided into two stages with the result that the overall batch time can be substantially reduced. The rate of cooling may be simply expressed as

$$-\frac{d\theta}{dt} = K(\theta - \theta_w) \quad (9.77)$$

where θ and θ_w are the solution and cooling water temperatures ($^{\circ}\text{C}$) respectively, t is time (s) and K is a proportionality constant (s^{-1}). The solution of equation (9.77) is

$$\theta = \theta_{wt} + (\theta_0 + \theta_{w0}) \exp(-Kt) \quad (9.78)$$

where suffixes 0 and t refer to the initial and time t conditions respectively. The coefficient K is also a function of time, since scale continues to build up on the heat transfer surfaces during a run. As a first approximation

$$K_t = (K_0^{-1} + qt)^{-1} \quad (9.79)$$

where q is a constant that characterizes the rate of change of heat resistance of the scale:

$$q = (K_f^{-1} + K_0^{-1})t_b^{-1} \quad (9.80)$$

where t_b is the total batch time and the suffixes 0 and f denote the values of K at the start and end of the batch cooling. Equation 9.78 may then be written

$$\theta = \theta_{wt} + (\theta_0 - \theta_{w0}) \exp(-K_0 t / 1 + q K_0 t) \quad (9.81)$$

The batch time without any scale formation is therefore

$$t_{b0} = K_0^{-1} \ln[(\theta_0 - \theta_{w0})/(\theta_f - \theta_{wf})] \quad (9.82)$$

and with scale formation:

$$t_{bs} = t_{b0}/\{1 - q \ln[(\theta_0 - \theta_{w0})/(\theta_f - \theta_{wf})]\} \quad (9.83)$$

If the critical temperature in the crystallizer θ_m is known, below which no more scale is deposited, the cooling process may be divided into two stages.

In the first stage, the time taken to cool the charge, from the initial temperature θ_0 to the critical temperature θ_m is given by

$$t_1 = \frac{\ln[(\theta_0 - \theta_{w0})/(\theta_m - \theta_{wm})]}{K_0 \{1 - q \ln[(\theta_0 - \theta_{w0})/(\theta_m - \theta_{wm})]\}} \quad (9.84)$$

Some scale may form on the cooling surface during this stage, but the temperature difference between crystallizer contents and the coolant is still sufficiently large to permit efficient heat transfer. However, once the temperature falls below θ_m , even though no new scale is deposited, the temperature driving force becomes too low for efficient cooling so it would be better to continue the process with clean heat transfer surfaces. This could be achieved by removing any scale formed in the first stage, e.g., by thermal shock, but much better by transferring the magma to a second-stage vessel with fresh cooling surfaces. Any scale formed in the first-stage vessel can easily be removed by dissolution in hot feedstock entering for the next batch, and so on. The cooling time for the second stage, in the absence of any scale forming on the heat transfer surfaces, may be calculated from equation 9.82:

$$t_2 = K_0^{-1} \ln[(\theta_m - \theta_{wm})/(\theta_f - \theta_{wf})] \quad (9.85)$$

The overall batch time, $t_1 + t_2$, for two-stage cooling is usually very much shorter than for single-stage cooling because although the second stage proceeds with a smaller temperature difference than the first, the initial heat transfer coefficient is higher because of the cleaner surfaces. A worked example of two-stage cooling is given in section 9.3.

9.2 Kinetic data measurement and utilization

Brief reference has already been made to the experimental measurement of crystal nucleation and growth rates in section 6.2.5, and a continuous MSMPR crystallizer suitable for the purpose is depicted in *Figure 6.21*. For cooling crystallization studies, only one feedstock storage vessel and delivery point would be needed. The duplicate feed circuits depicted in *Figure 6.21* would be required if reaction crystallization, precipitation or salting-out studies are to be made.

Laboratory units as small as 250 mL, operating at low magma densities and for short residence times, have been widely and successfully used for measuring kinetic data for research purposes. To measure data useful for the design or scale-up of industrial crystallizers, however, it is necessary to operate on a larger scale and at magma densities nearer the industrial level ($>100 \text{ kg m}^{-3}$). It is recommended that the crystallizer working volume should not be smaller than at about 4 L, although units up to ten times this size have frequently been used. Large working volumes, however, can present problems with the maintenance of good mixing throughout the vessel and the need to store large volumes of solution at the required feedstock entry conditions. Since steady-state conditions are not normally achieved in much less than ten residence times, even the minimum recommended sized vessel would need $\sim 50 \text{ L}$ of solution to be stored to enable meaningful runs to be carried out.

There should be no crystal size classification at the magma discharge and sampling points. Every endeavour should be made to sample isokinetically, i.e. with the sample withdrawal velocity equal to that of the magma flowing at the point of removal.

A wide choice of agitators is available, e.g. draft-tube agitation or conventional agitators in vessels fitted with baffles (section 9.4.1). The important selection criteria are good mixing with a low impeller speed. For crystallization vessels operating with magma densities around industrial values it is helpful, for design and scale-up purposes, if measurements are made of the power input to the stirrer (section 9.3.4).

For continuous MSMPR evaporative crystallization studies, a suitably enclosed vessel fitted with a pressure regulator and appropriate vapour and magma removal means are required. Adequate vapour–liquid disengagement space must be provided in the vessel above the boiling liquid surface. It is very important that kinetic data needed for the design of an evaporative crystallizer be measured on an appropriate laboratory unit since hydrodynamic conditions in a boiling magma are very different from those in non-boiling magma at the same temperature. The boiling action can have a considerable influence on both the nucleation and crystal growth processes, although these effects have rarely been studied in a systematic manner.

Batch crystallization usually requires slightly less ancillary equipment than does continuous crystallization, although programmed operation requires appropriate control circuits. Magma discharge and sampling are usually carried out simultaneously at the end of a batch run. A typical unit for batch cooling crystallization is shown in *Figure 9.14*.

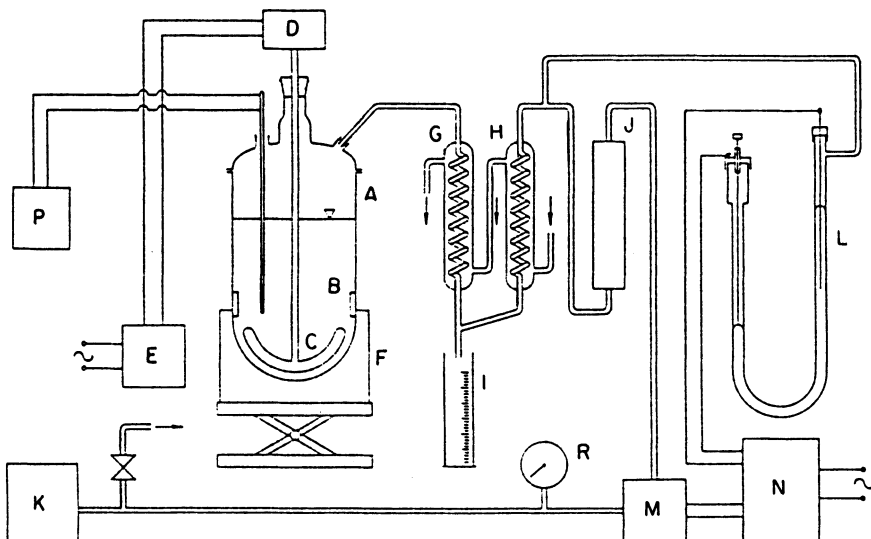


Figure 9.16. A pressure controlled batch evaporating crystallizer: A, 2 L crystallization vessel; B, baffle; C, stirrer; D, motor; E, variable speed controller; F, heating mantle; G, H, condensers; I, condensate receiver; J, drying tower; K, vacuum pump; L, contact manometer; M, electromagnetic valve; N, control box; P, electronic thermometer; R, vacuum gauge. (After Mullin and Broul, 1978)

Batch evaporative crystallization studies present the difficulty of maintaining a constant temperature because the solution boiling point, which depends on its vapour pressure, increases as the solution becomes more and more concentrated. Therefore, in order to keep the solution temperature constant while evaporation proceeds, it is necessary to change the system pressure accordingly. A simple way of doing this (*Figure 9.16*) is to change the internal pressure regularly, say at five minute intervals, by manually adjusting a movable contact in the manometer. With this arrangement it is possible to keep the temperature of a boiling aqueous solution constant $\pm 0.05^\circ\text{C}$ over the range $40\text{--}100^\circ\text{C}$ (Mullin and Broul, 1978).

Batch precipitating or salting-out crystallizers are generally operated in a semi-batch mode since, for example, a miscible liquid precipitant is normally added to the vessel continuously throughout most of the batch period. As described above, the precipitant addition rate may be regulated according to a 'controlled programme' (Jones and Teodossiev, 1988).

Several particle size measuring techniques are available for CSD determination (section 2.14). Electrical sensing zone (Coulter) and laser light scattering (Fraunhofer) methods are now quite popular in small-scale laboratory experimentation even though they often require a magma dilution step before measurements can be made. However, with larger crystallizers, operating at high magma densities and with the facility to take large samples, sieving is still by far the most common technique employed.

Whatever the size analysis method used, however, the main objective when measuring kinetic data should be to assess the characteristics of the crystals as

they were in the magma at the moment of sampling. This means that the CSD analysis should be made as quickly as possible. Reliable on-line analysis would be ideal, but this cannot always be achieved. If sieving is the chosen method, filtration of the magma sample, washing and subsequent drying of the crystals before analysis can cause significant changes in the sample and thus give misleading CSD information, and hence false kinetic data. Wet analysis, preferably using the original magma, can minimize these problems.

Evaluation of nucleation and growth rates

The following example demonstrates the procedure for evaluating nucleation and growth rates from data measured in a laboratory MSMPR crystallizer.

The size analysis of potash alum crystals (density, $\rho_c = 1770 \text{ kg m}^{-3}$; volume shape factor, $\alpha = 0.471$) leaving a continuous MSMPR crystallizer operated with a residence time $\tau = 15 \text{ min}$ (for both liquor and crystals) is shown in *Table 9.2*. When these data are plotted as $\log n$ versus L (*Figure 9.17*) the projected value of n at $\bar{L} = 0$ gives the *apparent* population density of nuclei (section 9.1.1) as $n_0 = 8.2 \times 10^8 \mu\text{m}^{-1} \text{ m}^{-3}$ (i.e. $8.2 \times 10^{14} \text{ m}^{-4}$). The slope of the line ($-1/G\tau$) is $-0.0129 \mu\text{m}^{-1}$, which gives a value of the growth rate $G = 8.6 \times 10^{-8} \text{ m s}^{-1}$. So the nucleation rate B (equation 9.15) = $n_0 G = 7.06 \times 10^7 \text{ m}^{-3} \text{ s}^{-1}$.

Other runs with the same crystallizer, made with different residence times, gave the following results:

$\tau \text{ min}$	$n_0 \text{ m}^{-4}$	$G \text{ m s}^{-1}$	$B \text{ m}^{-3} \text{ s}^{-1}$
10	1.1×10^{15}	1.3×10^{-7}	1.4×10^8
15	8.2×10^{14}	8.6×10^{-8}	7.1×10^7
30	6.7×10^{14}	4.2×10^{-8}	2.8×10^7

Table 9.2. Size analysis of potash alum crystals

Size range μm	ΔL μm	\bar{L} μm	\bar{L}^3 μm	dW^a g	$\alpha\rho\bar{L}^3\Delta L$ g μm	Population density ^b μm^{-1}
>710	—	—	—	—	—	—
710–500	210	605	2.21×10^8	1.20	3.88×10^{-2}	3.09×10^5
500–355	145	428	7.84×10^7	2.72	9.45×10^{-3}	2.88×10^6
355–250	105	303	2.78×10^7	4.27	2.43×10^{-3}	1.75×10^7
250–180	70	215	9.94×10^6	3.15	5.80×10^{-4}	5.43×10^7
180–125	55	153	3.58×10^6	1.69	1.64×10^{-4}	1.03×10^8
125–90	35	108	1.26×10^6	0.75	3.68×10^{-5}	2.04×10^8
90–63	27	77	4.57×10^5	0.28	1.03×10^{-5}	2.73×10^8
<63	(63)	(32)	3.28×10^4	0.12	1.72×10^{-6}	6.98×10^8

^aper 100 mL of slurry

^bper m^3 of slurry

$$n = 10^4 dW / \alpha \rho_c \bar{L}^3 \Delta L$$

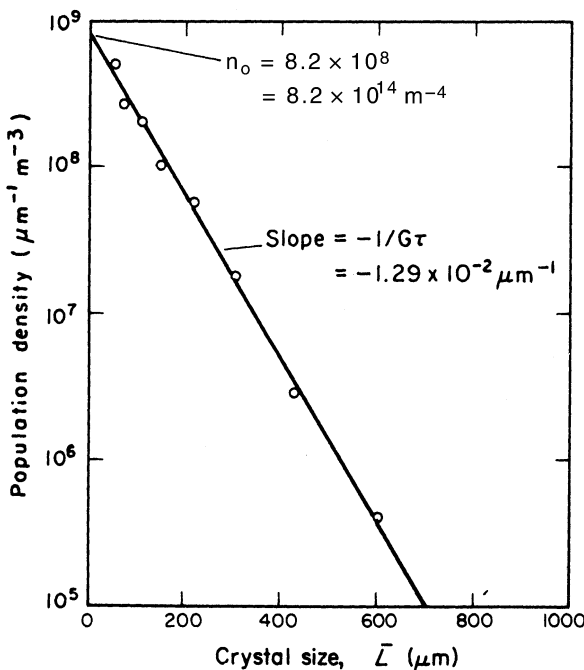


Figure 9.17. Population density plot (Example 9.1)

A plot of $\log n_0$ versus $\log G$ (as in Figure 9.2c, but not given here) in accordance with equation 9.18 gives a line of slope $i - 1$. Alternatively, a plot of $\log B$ versus $\log G$ gives a line of slope i . In the present case i is estimated as 1.7, and assuming that the order of the growth process $g = 1.6$ (section 6.2.4), then the order of the nucleation process $b = 2.7$.

Extrapolation of the linear portion of a population density plot to zero crystal size, to obtain an *apparent* value of n_0 , frequently has to ignore the fact that data points in the small size region, in this case below about $50 \mu\text{m}$, are not accommodated. Unfortunately the line often develops a pronounced upward curvature in this region, the estimation and interpretation of the n_0 value becomes quite speculative. This is a problem even in small laboratory crystallizers operating virtually in an ideal MSMPR manner, since small-crystal growth rates can be significantly size dependent (sections 6.2.7 and 9.1.1). The problem becomes very much more severe, however, when trying to assess data obtained from industrial crystallizers, where ideal MSMPR conditions are never achieved. In these cases, curvature and change of direction in the population density plot are commonly observed.

An interesting proposal to specify a standard procedure for deriving design oriented crystallization kinetics, avoiding reliance on fictitious extrapolated values of n_0 , is made by Jančić and Grootsholten (1984). The method involves using a value of n^* , corresponding to a chosen value of L^* lying within the range where the size data are considered to be reliable. The nucleation rate B is replaced by an effective rate B^* ($= n^*G^*$) which may require an evaluation of

the extent of growth rate size dependence. A successful application of the procedure is demonstrated with respect to data scale-up over the range 1 to 5 to 30 L.

9.3 Crystallizer specification

9.3.1 Crystallizer selection

The temperature–solubility relationship between the solute and solvent is of prime importance in the selection of a crystallizer. For solutions that yield appreciable quantities of crystals on cooling, the choice of equipment will generally lie between a simple cooling or a vacuum (flash cooling) crystallizer. For solutions that change little in composition with a reduction in temperature, an evaporating crystallizer would normally be used, although salting out might be considered in certain cases (section 8.4).

The required shape, size and size distribution of the crystalline product will also have an influence on the type of crystallizer selected. For the production of reasonably large uniform crystals the bias would be towards a crystallizer fitted with a suitable fines trap, and/or an elutriating leg which permits the discharge of a partially classified product.

Cost and space requirements are also important factors although few comparative up-to-date cost data are available. If the cost of a small crystallizer is known, however, a rough estimate of the cost of a larger one may be made by the six-tenths rule,

$$\text{Capital cost} \propto (\text{capacity})^{0.6}$$

for production capacities in the range 500–50 000 kg h⁻¹.

Although some of the simpler cooling crystallizers are relatively inexpensive, the initial cost of a mechanical unit can be fairly high. On the other hand, no costly vacuum-producing or condensing equipment is required. Dense crystal slurries can be handled in cooling units not requiring liquid circulation. Unfortunately, cooling heat exchange surfaces can easily become coated with a hard crystalline crust which reduces thermal efficiency. Direct contact cooling crystallizers (section 8.4.1) need no heat exchanger and do not suffer from this type of encrustation. Vacuum (flash cooling) crystallizers (section 8.4.3) do not need a heat exchanger either, but they cannot be used when the feed liquor has a high boiling point elevation.

Both vacuum and evaporating crystallizers generally have considerable height requirements to provide sufficient free space above the boiling liquor surface to allow entrained liquid droplets to disengage from the upflowing vapours. To minimize liquid droplet entrainment into the vapour space above the boiling liquid surface, a common cause of crystal encrustation on the walls, the evaporation rate must be controlled to limit the upward vapour velocity, u_{\max} , an estimate of which may be made from the relationship

$$u_{\max} = K / [\rho_V / (\rho_L - \rho_V)]^{0.5} \quad (9.86)$$

where ρ_L and ρ_V are the mother liquor and vapour densities respectively. K is an empirical constant which can be influenced by droplet size and surface tension, but an average working value of 0.017 m s^{-1} is suggested for evaporating crystallizers (Toussaint and Fortuin, 1976).

Despite all precautions being taken, some liquid droplets inevitably continue to flow upwards and, if not prevented, can exit the crystallizer and result in a loss of product. A number of impingement devices have been developed to facilitate liquid-vapour disengagement. The most widely used device is the demister pad, fabricated from knitted wire mesh, which provides a large surface area for droplet contact and coalescence, coupled with a very high open area and hence a negligible pressure drop. The installation of a demister allows a higher upward vapour velocity and hence a faster evaporation rate. Alternatively, it can reduce the height of the free-space required above the boiling liquor and hence the capital cost of the crystallizer. Gerunda (1981) and Wu (1984) give good accounts of the design of liquid-vapour separators.

Once a particular class of crystallizer is decided upon, the choice of a specific unit depends upon such considerations as the initial and operating costs, the space availability, the type and size of crystals required, the physical characteristics of the mother liquor and crystal slurry, the need for corrosion resistance, sterile operation, environmental protection, and so on.

In the design of a crystallizer, to minimize encrustation problems, particular attention should be paid to all liquor-mixing zones in the circuit. The liquor circulation loop generally includes several regions where flow streams of different temperature and composition meet, and these are all potential danger zones. Excessively high supersaturation may be created temporarily at the point of mixing, causing heavy nucleation which can lead to encrustation, erratic performance, operating instability, and so on. The composition and enthalpy of a mixed stream should always be such that only equilibrium phase can exist under the local temperature and pressure conditions – the so-called *mixing criterion* (see section 9.5).

Batch versus continuous crystallization

Continuous, steady-state operation is often regarded as the ideal procedure for many types of process plant equipment, but this is not always true for crystallization processes. Batch operation often offers considerable advantages, such as simplicity of equipment and minimization of encrustation on heat-exchanger surfaces. In many cases, only a batch crystallizer can produce the required crystal form, size distribution, or purity. On the other hand, the operating costs of a batch system can be significantly higher than those of a comparable continuous unit, and problems of product variation from batch to batch may be encountered.

The particular attraction of a continuous crystallizer is its built-in flexibility for control of temperature, supersaturation, nucleation, crystal growth, and all the other parameters that influence crystal size distribution. A continuous crystallizer, however, does not discharge its product under near equilibrium conditions

(a batch unit can, if the batch time is adjusted appropriately) so the product slurry may have to be passed to a holdup tank to allow equilibrium to be approached. Omission of this step may cause problems due to further crystallization occurring in other parts of the plant (e.g. unwanted deposition in pipelines and effluent tanks). A holdup (ageing) tank may also be necessary in a continuous system if the product exists in a phase (polymorph, hydrate, etc.) that differs from the one which appears initially (Ostwald's Rule of Stages – section 5.7).

A distinct advantage of batch crystallization, widely acknowledged in the pharmaceutical industry, is that the crystallizer can be cleaned thoroughly at the end of each batch to prevent contamination (seeding) of the next charge with any undesirable phase that might have arisen from transformation, rehydration, dehydration, air oxidation, etc., during the batch cycle. Continuous crystallization systems often self-seed undesirably after a certain operating time, which necessitates frequent shutdown and washout.

Semicontinuous crystallization processes often combine the best features of both batch and continuous operation. For example, a rapid mixer with a short residence time (possibly an on-line device, e.g. *Figure 9.14*) can discharge its product slurry into an agitated residence tank. In many cases, a series of tanks may have to be installed, which can then be operated as individual units or arranged in cascade (section 9.1.2).

Continuous crystallizers are generally more economical in operating and labour costs than are batch units, especially for large production rates. The batch units are usually cheaper in initial capital cost. One of the main advantages of a continuous unit is that the amount of mother liquor needing reworking is usually small, sometimes less than 5% of the feedstock handled. In batch units, as much as 50% of the mother liquor may require reworking.

The required crystal production rate and supply of feed liquor to the plant will generally be among the deciding factors in the choice between a batch and continuous unit. For example, for crystal production rates $> 100 \text{ kg h}^{-1}$ or feed liquor rates $> 1 \text{ m}^3 \text{ h}^{-1}$, continuous operation might be considered, but there is no general rule. Sugar, for example, is commonly produced batchwise at equivalent rates up to $20\,000 \text{ kg h}^{-1}$ per crystallizer.

9.3.2 Design strategies

Information for design

It is useful to know what sort of information a design engineer generally needs in order to specify an industrial crystallizer. A detailed description of the product should be given, including its full chemical name and formula, specifying if a hydrate is required or not. A realistic purity specification should be laid down. The production rate should be given, both as kg h^{-1} and ton year^{-1} or some other suitable long-term rate, making generous allowances for maintenance and other shutdown periods.

A reliable solubility curve of the product in the actual liquors should be established. Solubility data reported in the literature usually refer to pure

solutes and solvents, and these may be quite inapplicable to the industrial case. If impurities are known to be present in the working liquors, the relevant solubility data should be measured independently.

Measurements of the metastable zone width should be made in a manner relevant to the expected working conditions, if possible using the actual liquors to be processed, but most importantly *in the presence of crystalline phase* (section 5.3).

The size and size distribution of the required crystalline product should be specified, but it is important to remember that the more rigid the size specification the more difficult the crystallizer design becomes. An actual sample of the desired crystals, if available, is usually very helpful. Single-size specifications, such as 'about 450 µm', have no useful meaning, but upper and lower size limits may be quoted. For example, a specification such as '> 80% to be retained between 600 and 300 µm sieves' would be more helpful. Alternatively, the desired median size, MS, and coefficient of variation, CV, may be designated, as described in section 2.14.4.

The following liquor and solids data are also useful:

Liquor

- feedstock analysis and pH;
- density of the feedstock at the feed temperature;
- boiling-point elevation of the saturated solution;
- density and viscosity of the saturated solution over the working range of temperature.

Crystals

- true density of the substance;
- settling velocity of crystals of the desired size and shape in saturated solutions over a range of temperature;
- crystal growth and nucleation rates as functions of supersaturation and temperature;
- heat of crystallization.

Design procedures

Many approaches have been made over the past 30 years or more towards the mathematical modelling of crystallizer behaviour and the development of design strategies. All the methods occupy much common theoretical ground, despite their apparent differences, and they also suffer from a common defect in that they represent only idealized cases. The basic equations should only be used as qualitative guides to design. Uncritical application of set formulae to general industrial situations can often give very misleading results. No design equation is any more reliable than the data fed into it, but there is a particular problem with crystallization data which are in very short supply and of extremely variable quality. Great care should be taken, when attempting to measure reliable design data, to use experimental methods of appropriate scale and mode of operation in relation to the

envisioned large-scale equipment, and if at all possible to use actual process liquors.

The object of this section is simply to outline some typical initial approaches to design which in practice will have to be tailored for specific circumstances and data availability. There is no single ‘correct’ answer to the design of any crystallizer. The aim is to achieve a reasonable combination of design values within a specified framework, which should also include downstream requirement (section 9.7).

Amongst the first quantities that may have to be specified, or calculated, in a design procedure are the crystal production rate, a clearly defined ‘mean’ product crystal size, the crystallizer working volume, liquor circulation rate, magma density, mass of crystals in the suspension and the residence times of both crystals and liquor. Several of these quantities are interrelated and will not need separate calculation. Some are directly linked to the effective overall crystal growth rate, a sensitive system-specific quantity.

The following brief examples demonstrate the manipulation of some of the key relationships. In an actual design procedure the result of each calculation step should be assessed as to its reasonability, either in the light of experience with similar systems, or within restrictions set by existing equipment and operating procedures.

Since the population balance relationships have already been developed in some detail above (section 9.1.1) most of the following examples are based on the population balance approach and/or nomenclature, for reasons of continuity. It is important to understand, however, that other design methods are available, some based on mass or supersaturation balances rather than on population balances. For details of these other methods reference should be made to original literature sources, e.g., as summarized by Toyokura *et al.* (1984) and Nývlt (1978, 1992).

Example 9.1 Continuous cooling

A continuous cooling crystallizer is required to produce potassium sulphate crystals (density $\rho_c = 2660 \text{ kg m}^{-3}$, volume shape factor $\alpha = 0.7$) of $750 \mu\text{m}$ median size L_M at the rate $P_c = 1000 \text{ kg h}^{-1}$. On the basis of pilot-plant trials, it is expected that the crystallizer will operate with steady-state nucleation/growth kinetics expressed (equation 9.39 with $j = 1$ and $i = 2$) as $B = 4 \times 10^{18} M_T G^2 \text{ m}^{-3} \text{ s}^{-1}$. Assuming MSMPR conditions and a magma density $M_T = 250 \text{ kg m}^{-3}$, estimate the crystallizer volume and other relevant operating conditions.

The crystal growth rate G may be evaluated from equation 9.44:

$$\begin{aligned} G &= (30/\alpha\rho_c K_R L_M^4)^{1/i-1} \\ &= 30/0.7 \times 2.66 \times 10^3 \times 4 \times 10^{18} \times (7.5 \times 10^{-4})^4 \\ &= 1.27 \times 10^{-8} \text{ m s}^{-1} \end{aligned}$$

The residence time τ for both liquor and crystals under MSMPR conditions, is given by equation 9.37:

$$\begin{aligned}\tau &= L_M/3.67G \\ &= 7.5 \times 10^{-4}/(3.67 \times 1.27 \times 10^{-8}) = 1.61 \times 10^4 \text{ s} = 4.47 \text{ h}\end{aligned}$$

The magma discharge flow rate Q (and in this case of MSMPR operation, the feed liquor rate) is given by

$$\begin{aligned}Q &= P_c/M_T \\ &= 1000/250 = 4.0 \text{ m}^3 \text{ h}^{-1}\end{aligned}$$

The required vessel volume V , therefore, is

$$\begin{aligned}V &= Q\tau \\ &= 4.0 \times 4.47 = 17.9 \text{ m}^3\end{aligned}$$

The feed liquor concentration can be specified from a mass balance, knowing the inlet and outlet solution compositions.

Example 9.2 Continuous cooling with fines destruction

Using the data given or calculated in Example 9.1, calculate the liquor flow rate needed through a fines trap to remove 90% of the crystals smaller than 100 µm.

The crystal population decays exponentially with size (equation 9.12). If 90% of the crystals < 100 µm are removed, 10% are allowed to remain and grow to sizes > 100 µm, so

$$n/n_0 = \exp(-L/G\tau) = 0.1$$

and

$$\begin{aligned}L/G\tau &= \ln(1/0.1) = 2.303 \\ &= 10^{-4}/1.27 \times 10^{-8}\tau\end{aligned}$$

giving

$$\begin{aligned}\tau &= 10^{-4}/(1.27 \times 10^{-8} \times 2.303) = 3419 \text{ s} \\ &= 0.95 \text{ h} \\ &= V/(Q + Q_F)\end{aligned}$$

The required volumetric flow through the fines trap, Q_F , is therefore given by

$$\begin{aligned}Q_F &= (V/\tau) - Q \\ &= (12.5/0.95) - 2.5 \\ &= 10.7 \text{ m}^3 \text{ h}^{-1}\end{aligned}$$

Example 9.3 Batch cooling (seeded)

A seeded batch cooling crystallizer is required to produce 500 kg of potassium alum crystals of median size $L_p = 1500 \mu\text{m}$ using seeds of median size

$L_s = 100 \mu\text{m}$. Data: feedstock saturation temperature $\theta_0 = 55^\circ\text{C}$ (solution concentration = 0.249 kg/kg solution); final batch temperature $\theta_f = 15^\circ\text{C}$ (solution concentration = 0.113 kg/kg solution); crystal density $\rho_c = 1750 \text{ kg m}^{-3}$, crystal volume shape factor $\alpha = 0.47$, solution density $\rho_1 = 1100 \text{ kg m}^{-3}$. Maximum allowable growth rate $G = 5 \times 10^{-8} \text{ m s}^{-1}$.

Crystal yield

$$Y = 0.249 - 0.113 = 0.136 \text{ kg/kg solution}$$

The magma density can be calculated from

$$\begin{aligned} M_T &= Y/(\rho_c + 1/\rho_1) \\ &= 0.136/(0.136/1750 + 1/1100) \\ &= 138 \text{ kg/m}^3 \end{aligned}$$

Crystallizer volume

$$V = P_c/M_T = 500/138 = 3.6 \text{ m}^3$$

Mass of 100 μm seeds to be added (equation 8.25):

$$\begin{aligned} M_s &= P_c L_s^3 / (L_p^3 - L_s^3) \\ &= 500 \times (1 \times 10^{-4})^3 / [(1.5 \times 10^{-3})^3 - (1 \times 10^{-4})^3] \\ &= 0.148 \text{ kg} \end{aligned}$$

The batch time is given by

$$\begin{aligned} \tau &= (L_p - L_s)/G \\ &= (1.5 \times 10^{-3} - 1 \times 10^{-4})/(5 \times 10^{-8}) \\ &= 2.8 \times 10^4 \text{ s} = 7.8 \text{ h} \end{aligned}$$

In practice the batch time could be fixed at say 8 h. Seed crystals would be added as soon as the batch liquor temperature had cooled to its equilibrium saturation temperature (55°C), after which cooling would have to be carefully controlled, initially at a very slow rate, to prevent spurious nucleation.

There are many ways of predicting a controlled cooling programme, depending on the assumptions that can reasonably be made (section 9.1.4), but almost inevitably some modification will have to be made to a theoretical programme in the light of practical experience. The essential characteristics of a controlled cooling programme are demonstrated below using a simple relationship (equation 9.75) as the starting point:

$$\theta_t = \theta_0 - (\theta_0 - \theta_f)(t/\tau)^3$$

where θ_0 , θ_f and θ_t are the temperatures at the start, end and at any time t during the overall batch time τ . When applied to the present case ($\theta_0 = 55^\circ\text{C}$, $\theta_f = 15^\circ\text{C}$, $\tau = 8 \text{ h}$) equation 9.75 gives the following temperature profile:

$t \text{ (h)}$	0	1	2	3	4	5	6	7	8
$\theta^\circ\text{C}$	55.0	54.9	54.4	52.9	50.0	45.2	38.1	28.2	15.0

The very slow temperature decrease demanded in the early stages (in this case only 0.1 °C in the first hour) is typical of all controlled cooling programmes and emphasizes the need for precise temperature control.

If, after taking all precautions, excessive nucleation cannot be avoided, consideration should be given to the installation of a fines destruction circuit (Jones, Chianese and Mullin, 1984) to enhance the product crystal size (section 9.1.4).

Example 9.4 Two-stage batch cooling

A feedstock solution with an equilibrium saturation temperature of 75 °C is to be cooled from an initial temperature of 80 to 25 °C with cooling water at 20 °C. Preliminary tests showed that the initial feedstock can be cooled to 59.7 °C in 10 min. and that scale begins to form on the heat transfer surfaces at 60 °C. No scale is formed, however, if the temperature difference between the solution and coolant does not exceed 18 °C. Cooling the charge from 60 to 25 °C with the same flow of cooling water as above takes around 230 min. Estimate the optimum conditions for two-stage cooling (Nývlt, 1992).

The heat transfer coefficient K_0 for the first 10 min. cooling period, can be calculated from equation 9.82:

$$K_0 = 10^{-1} \ln [(80 - 20)/(59.7 - 20)] = 0.0413 \text{ min}^{-1}$$

and the time required for complete cooling, without any scale forming, would be

$$t_{b0} = (0.0413)^{-1} \ln [(80 - 20)/(25 - 20)] = 60.2 \text{ min.}$$

Below 60 °C, however, scale does form so the coefficient q must be estimated from equation 9.83:

$$\begin{aligned} q &= [1 - (t_{b0}/t_{bs})]/\ln [(\theta_0 - \theta_w)/(\theta_f - \theta_w)] \\ &= \{1 - [(60.2 - 10)/(230 - 10)]\}/\ln [(60 - 20)/(25 - 20)] \\ &= 0.371 \end{aligned}$$

The time required for the first stage to cool from 60 °C to θ_m ($= 20 + 18 = 38$ °C) calculated from equation 9.84 would be

$$\begin{aligned} t_1 &= \ln [(60 - 20)/(38 - 20)]/0.0413\{1 - 0.371 \ln [(60 - 20)/(38 - 20)]\} \\ &= 27.5 \text{ min.} \end{aligned}$$

and the time required for the second stage

$$\begin{aligned} t_2 &= (0.0413)^{-1} \ln [(38 - 20)/(25 - 20)] \\ &= 31.0 \text{ min.} \end{aligned}$$

giving an overall batch cooling time of $10 + 27.5 + 31.0 = 68.5$ min. This is a very considerable reduction (70%) from the single-stage cooling time of 230 min. noted above, which can be confirmed from equation 9.83:

$$t_{bs} = 10 + \{50.2/(1 - 0.371) \ln [(60 - 20)/(25 - 20)]\} = 230 \text{ min.}$$

Alternative design procedures

An alternative to the population balance approach to crystallizer design was developed in the 1960s by Nývlt and his co-workers (e.g. see Nývlt, 1971, 1992). An example of this method is given below, without any derivation of the key formulae but with explanatory notes where appropriate. For reasons of continuity, the original nomenclature has been changed slightly to blend with that used in the above sections. The following example deals with a continuous MSMPR crystallizer (Nývlt and Mullin, 1974) but the method can also be applied, with appropriate modification, to continuous-classifying and batch-operated crystallizers (Mullin and Nývlt, 1970; Nývlt and Mullin, 1977).

Example 9.5 Continuous cooling

Estimate the working volume of a continuous MSMPR cooling crystallizer, operating at 15 °C, to recover hydrated iron (II) sulphate ($\text{FeSO}_4 \cdot 7\text{H}_2\text{O}$) from an aqueous solution, saturated at 40 °C, fed at the rate of $10 \text{ m}^3 \text{ h}^{-1}$. The required product should contain at least 90 per cent by mass of crystals larger than 200 µm.

Data: solubility at 15 °C = 0.180 kg FeSO_4 /kg solution; solubility at 40 °C = 0.287 kg FeSO_4 /kg solution; feedstock solution density = 1290 kg m^{-3} ; ratio of molecular masses $R = (M_{\text{anh}}/M_{\text{hyd}}) = 152/278 = 0.547$; ratio of kinetic constants $i = (b/g) = 2.34$.

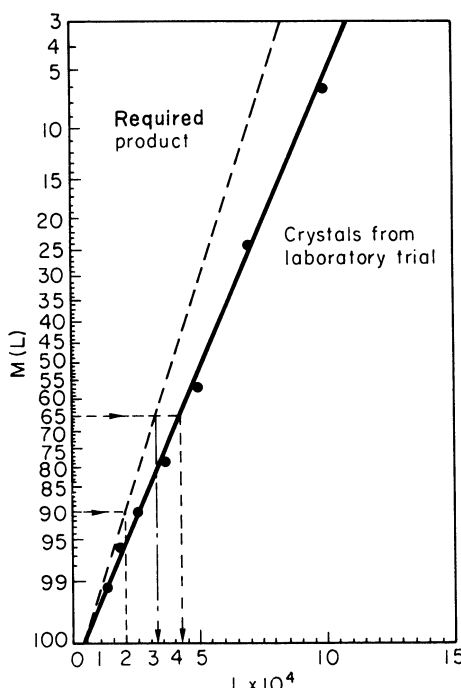


Figure 9.18. Linearized sieve analysis of ferrous sulphate heptahydrate crystals used in Example 9.4

Laboratory trials in a 4 L MSMPR cooling crystallizer operated at 15 °C with 3 L h⁻¹ of a feedstock saturated at 40 °C (i.e. residence time $\tau = 4/3 = 1.33$ h) gave a crystal product with the size analysis plotted in *Figure 9.18*, the ordinate scale of which corresponds with equation 9.30 describing the CSD in an MSMPR crystallizer. From this linearized plot of the laboratory trial data the dominant size L_D , at $M(L) = 65\%$, is found to be 430 µm, and by extrapolation to $M(L) = 100\%$, a hypothetical ‘initial’ crystal size may be estimated as $L_N = 40$ µm.

As the relevant solubilities of ferrous sulphate (expressed on an anhydrous basis) are 28.7 per cent by mass at 40 °C and 18.0 per cent at 15 °C, then from a materials balance, assuming no solvent loss, the magma density may be calculated from

$$\frac{m_c}{V\rho_l} = \frac{c_i - c_0}{R - c_0}$$

where m_c = mass of crystals, kg; c_i and c_0 = inlet (feedstock) and outlet (final) solution concentrations, kg anhydrous salt/kg of solution; $R = 0.547$ (above); ρ_l = solution density; V = crystallizer volume, m³. In this case, the magma density

$$\frac{m_c}{V\rho_l} = \frac{0.287 - 0.180}{0.547 - 0.180} = 0.292 \text{ kg FeSO}_4 \cdot 7\text{H}_2\text{O}/\text{kg solution}$$

and the specific production rate (= magma density ÷ residence time) is

$$\frac{\dot{m}_c}{V\rho_l} = \frac{0.292}{1.33} = 0.219 \text{ kg FeSO}_4/\text{h} \cdot \text{kg solution}$$

At this point a *system constant* **B** may be calculated, defined by

$$\mathbf{B} = L_D^{(i+3)/i} (m_c/V\rho_l)^{-1} (\dot{m}_c/V\rho_l)^{(i-1)/i}$$

This may be regarded as a basic design equation since it quantifies the complex interdependence of crystal size, production rate, magma density and the nucleation and growth kinetics. The units of **B** are m^(1+3*i*) s^(*i*-1) (solution concentration)^{-(1/*i*)}. For the present case

$$\begin{aligned} \mathbf{B} &= (4.3 \times 10^{-4})^{2.28} \times (0.292)^{-1} \times (0.219)^{0.573} \\ &= 3.03 \times 10^{-8} \end{aligned}$$

The broken line in *Figure 9.18*, representing the desired product crystals, is drawn through the points $L_N = 40$ µm at $M(L) = 100\%$ and $L = 200$ µm at $M(L) = 90\%$. From this line it can be read-off that the dominant size of the product crystals, L_D at $M(L) = 65\%$, should be 325 µm.

Applying the system constant equation to the required product crystals

$$3.03 \times 10^{-8} = (3.25 \times 10^{-4})^{2.28} \times (0.292)^{-1} \times (\dot{m}_c/V\rho_l)^{0.573}$$

so the specific production rate

$$\frac{\dot{m}_c}{V\rho_l} = 0.668 \text{ kg FeSO}_4 \cdot 7\text{H}_2\text{O}/\text{h} \cdot \text{kg solution}$$

The actual production rate is

$$\dot{m}_c = 10 \times 0.292 \times 1290 = 3767 \text{ kg FeSO}_4 \cdot 7\text{H}_2\text{O}/\text{h}$$

The crystallizer volume needed, therefore, is

$$V = \frac{3767}{0.668 \times 1290} = 4.4 \text{ m}^3$$

Example 9.6 Continuous cooling with clear liquor overflow

Using the data and product specification given in Example 9.4, estimate the working volume of an MSMPR crystallizer operating with $2 \text{ m}^3 \text{ h}^{-1}$ clear liquor overflow.

The magma density will be increased over that for the simple MSMPR case by the volumetric ratio (feed/feed – overflow):

$$\frac{m_c}{V\rho_l} = 0.292 \left[\frac{10}{10 - 2} \right] = 0.365 \text{ kg FeSO}_4 \cdot 7\text{H}_2\text{O/kg solution}$$

This value can now be used in the system constant equation to give

$$\left(\frac{\dot{m}_c}{V\rho_l} \right)^{-0.573} = \frac{(3.25 \times 10^{-4})^{2.28}}{3.03 \times 10^{-8} \times 0.365} = 1.008$$

Therefore the specific production rate

$$\frac{\dot{m}_c}{V\rho_l} = 0.986 \text{ kg FeSO}_4 \cdot 7\text{H}_2\text{O/h} \cdot \text{kg solution}$$

and the crystallizer volume

$$V = \frac{3767}{0.986 \times 1290} = 3.0 \text{ m}^3$$

i.e. some 30 per cent smaller than in Example 9.4.

Classifying crystallizers

Continuous classifying crystallizers, such as those shown in *Figure 8.46*, are widely used for the industrial production of relatively large ($> 1 \text{ mm}$) uniform crystals of a wide variety of substances. These units are usually designed on an *ad hoc* basis and over the years many ‘rules of thumb’, some more successful than others, have been devised to facilitate crystallizer specification.

Four basic quantities are generally needed for the design of a suspended (fluidized) bed crystallizer:

Liquor circulation rate, Q

Vessel cross-sectional area, A

Height of the crystal suspension, H

Over-all residence (draw-down) time, T

Although the calculations of these interrelated quantities are reasonably simple, they involve assumptions that can only be made on the basis of

either relevant experience or reliable experimental data. The basic relationships are:

$$Q = \frac{\text{crystal production rate, } P}{\text{effective supersaturation, } S} \quad (9.87)$$

$$A = \frac{\text{liquor circulation rate, } Q}{\text{liquor upflow velocity, } u} \quad (9.88)$$

$$H = \frac{\text{volume of suspension, } V}{\text{cross-sectional area, } A} \quad (9.89)$$

$$V = \frac{\text{mass of crystals in suspension, } W}{\text{suspension (magma) density, } d} \quad (9.90)$$

$$T = \frac{\text{mass of crystals in suspension, } W}{\text{crystal production rate, } P} \quad (9.91)$$

The quantity, T , which for a steady state system refers to both liquid and solid phases, must not be confused with the crystal growth time, i.e. the age of a product crystal, τ . In fact, it can be shown (Saeman, 1956) that for a classifying crystallizer $\tau = 4T$. However, the quantities that present considerable difficulty in measurement or estimation are S , u , and V or W . The last two are related through the crystal density ρ_c and the bed voidage ε :

$$\varepsilon = 1 - \frac{W}{\rho_c V} \quad (9.92)$$

These quantities will now be considered in turn.

Effective supersaturation, S

The choice of the working level of supersaturation should be based on reliable measurements of the metastable limits of the system which may be made in the laboratory under carefully controlled conditions. Metastable zone widths depend on many factors including the temperature, cooling rate, agitation, presence of impurities, etc., but the most important requirement is that they must be determined *in the presence of the crystalline phase* and, if possible, with the actual liquor to be processed.

The effective supersaturation, S , is that which is released during the passage of the liquor through the crystal bed in the crystallizer, i.e., the difference between the inlet and outlet supersaturations.

Solution upflow velocity, u

The solution upflow velocity, u , is not an easy quantity to specify. The solution upflow should balance the settling velocity of the crystals, but this is difficult to measure and virtually impossible to predict with accuracy. The trouble stems from the fact that the crystal suspension contains crystals of all sizes between product size and freshly generated nuclei. To choose the upflow velocity as the free settling velocity of a classified product crystal would result in the smaller crystals being swept out of the crystallizer. An upflow velocity taken as the free

settling velocity of the smallest crystals held up in the bed would at best demand that the product crystals be withdrawn through an elutriating leg, and at worst fail to fluidize the bed. The safest method, but admittedly the most tedious, is to measure the upper and lower fluidization velocities for the particular suspension and to use an intermediate value between these two limits. But the success of this method depends on the ability to specify accurately the suspension density or bed voidage to be used in the crystallizer (section 9.4.2).

Suspension volume, V

There is no generally successful method for estimating the suspension volume, V . Several methods are available and more than one should always be used in an attempt to arrive at a reasonable design value. A few of the more popular methods – and some are simply rough rules – include the following:

1. The suspension height H in a classifying crystallizer is frequently between one and two times the diameter of the vessel, which may be calculated from equation 9.88. This generalization, of course, can only give a very rough guide. It is well known, for example, that the production rate of a classifying crystallizer under given conditions is determined by its cross-sectional area and not by its height (Bamforth, 1965).
2. Two factors affect the height of a classified bed crystallizer: the relative desupersaturation γ (high values of γ require deep crystal beds), and the difference between the size of the smallest crystals held back in the bed, L_0 , and the size of the desired product crystals, L_p (the greater the difference the greater the depth of the bed).
3. As a rough guide to the relative desupersaturation, γ , substances with a first-order growth rate dependence on supersaturation ($g = 1$ in equation 6.61) may allow a desupersaturation of up to about 90 per cent, whereas for those with a second-order dependence the allowable desupersaturation may be lower than 50 per cent. It must be emphasized, however, that the relative desupersaturation is also a function of the crystallizer height, and the actual value of γ chosen for the operating conditions will determine the dimensions of the crystallizer.
4. The cross-sectional area of a classified bed crystallizer depends linearly on the production rate, the working supersaturation and the relative desupersaturation.
5. The separation intensity, SI, defined (Griffiths, 1947) as the mass of equivalent 1 mm crystals produced in 1 m^3 of crystallizer volume in 1 h, is a useful check quantity with values generally lying in the range 50 to $300\text{ kg/m}^3\text{ h}$. At operating temperatures near 30°C the lower limit is more frequent; an increase in temperature leads to higher values. For crystals larger (but not smaller) than 1 mm the relationship

$$\text{SI} = L_p P/V \quad (9.93)$$

may be used where L_p is the classified product size (mm), P the production rate (kg/h), and V the suspension volume (m^3). In other words, L_p is inversely proportional to the crystal production rate, P .

6. The over-all residence (draw-down) time, T , in many classifying crystallizers is about 2 h. Thus the mass of crystals in suspension, W , may be determined from the crystal production rate, P , by equation 9.91. After the appropriate value for the suspension density or bed voidage, ε , has been chosen the suspension volume may be calculated from equation 9.90 or 9.92.

The product crystal mean residence time, τ , i.e., the time it takes a crystal nucleus to grow to the classified product size, can be estimated in several ways:

1. Theoretical considerations (Saeman, 1956) suggest that the true crystal residence time, τ , i.e. the age of a product crystal in a classifying crystallizer, is four times the over-all residence time (draw-down time), T . Thus from point (6) above τ is about 8 h.
2. The crystallization rate in a classifying crystallizer is frequently equivalent to a mean deposition of 10–15% of the suspended crystal per hour. This is the same thing as saying that the product crystal growth time is around 7–10 h.
3. τ can be estimated from the linear crystal growth rate, G ($= dL/dt$), which can be measured directly or calculated from over-all growth data (section 6.2.4) by

$$\tau = \frac{L_p - L_0}{G} \quad (9.94)$$

where L_p is the product crystal size and L_0 is the size of the smallest crystals held up in the crystal bed. However, to make this calculation it is necessary to know or estimate the mean level of supersaturation in the crystallization zone in order to obtain the appropriate value of G .

4. τ can also be estimated from

$$\tau = \frac{L_p}{2G_p} \left(\frac{L_p^2}{L_0^2} - 1 \right) \quad (9.95)$$

which is derived (Nývlt, 1971) by assuming total desupersaturation of the solution passing through the crystal bed. In this equation G_p is the maximum linear crystal growth rate, i.e. at the bottom of the crystallization zone (product exit, liquor inlet).

Suspension (magma) density, M , or bed voidage, ε

Little general guidance can be given on the choice of a working value of the suspension density or bed voidage, ε . Pulley (1962), for example, suggests that values of ε lie between 0.5 at the bottom and 0.975 at the top of the suspension. However, in most cases over-all mean values in the range 0.8 to 0.9 are usually found in practice. This is confirmed if we make a linear interpolation for a mean voidage, $\varepsilon_{\text{mean}}$, and mean size, L_{mean} , in the suspension between Pulley's values of $\varepsilon_p = 0.5$ for the product size L_p and $\varepsilon_0 = 0.975$ for the smallest retained crystals, L_0 :

$$\varepsilon_{\text{mean}} = \varepsilon_p + \frac{\varepsilon_0 - \varepsilon_p}{L_p - L_0} \cdot L_{\text{mean}} \quad (9.96)$$

The mean crystal size in a perfectly classified suspension is given by

$$L_{\text{mean}} = 0.63L_p \quad (9.97)$$

and, putting this value into equation 9.96, we find that the mean bed voidage, $\varepsilon_{\text{mean}}$, varies from 0.8 for $L_0 \rightarrow 0$ to 0.9 for $L_0 = 0.25L_p$.

Utilizing the above factors, theoretical analyses of some possible design procedures for fluidized-bed classifying and mixed-suspension classified product removal crystallizers have been presented together with detailed worked examples by Mullin and Nývlt (1970) and Nývlt (1992).

9.3.4 Scale-up and operating problems

One of the basic problems of crystallizer design is the choice of method for measuring design data. The mode of operation, type of apparatus and scale of operation all have to be considered. Basically there are three choices: to measure the data on the laboratory, pilot-plant or industrial-plant scale. The last of these choices is not uncommon, because many crystallizers are designed on the basis of current experience. Generally, however, the choice lies somewhere between the laboratory unit and a pilot plant.

In terms of approximate physical dimensions, an example of the different scales of vessels being considered might be

	Laboratory	Pilot	Industrial
Volume, L	1	100	10 000
Diameter, mm	100	500	2 500

Despite the large volumetric differences in this example (100:1), the vessel diameter differences are really quite small (5:1). Therefore, since the vessel diameter is an important parameter in a crystallizer, laboratory-scale crystallization operations may not be vastly different from those in pilot-plant work, and pilot scale from industrial scale.

The perils of pilot-plant operation, however, are well known: they are expensive to design, construct and operate, and they are frequently unstable in operation owing to the ease of pipeline blockage and the need for carefully controlled low flow rates. There are many good reasons, therefore, to consider laboratory-scale operation at least for the initial gathering of design data, but it is recommended that the working volume of the experimental crystallizer should be at least 4 L. Even then, considerable caution should be exercised when applying the data. Problems associated with the scale-up of secondary nucleation data are discussed in section 9.1.1.

It is now generally accepted that much useful design information can be obtained in the laboratory so long as the fundamental differences between the laboratory and industrial plant scales of operation are fully appreciated. The two hydrodynamic conditions are quite different. For example, liquor paths and turn-over times are much shorter in the smaller vessels. The suspension circuit may only be a few centimetres in a laboratory vessel, whereas it may be 10 m or more in a full-scale plant. If the solution desupersaturates rapidly, very

high circulation rates would be needed in a large crystallizer to utilize fully the working volume. In a laboratory vessel this would not present a problem.

The conventional approach to the scale-up of process plant is based on the principle of similarity, aimed basically at maintaining similarity of equipment shape, flow characteristics, power input, temperature profiles, etc. The physical processes occurring in the small-scale unit should ideally be duplicates of those to be expected in the large-scale plant, but this is virtually impossible to achieve in practice.

The maintenance of *geometric* similarity requires identical ratios of corresponding dimensions in the two scales. *Kinematic* similarity requires identical ratios of instantaneous velocities between corresponding points; *dynamic* similarity requires identical ratios of forces, and so on. Successful scale-up ratios of the order of 1 : 100 based on volume or production rate, for example, are frequently achieved in practice (Johnstone and Thring, 1957). However, it is not possible to maintain complete similarity of all the different criteria simultaneously on scaling-up since there are usually many conflicting requirements. Attention is therefore normally directed to a limited number of key factors for the particular process under consideration and to attempt a reasonable scale-up of the most important.

Geometric similarity for most crystallization vessels is generally assessed by their height to diameter ratios. Kinematic similarity is achieved in a single-phase system if the ratios of the instantaneous velocities between corresponding points in units of different scale are identical. The situation is much more complicated in a crystallizer where both liquid and solid phases of changing composition can coexist. In such cases an assessment of the maintenance of kinematic similarity must include consideration of the crystal settling velocities (section 9.4.2) as well as the liquor flow.

The exact scale-up of crystallizers is not possible because it would be necessary to preserve similar flow characteristics of both liquid and solid phases together with identical temperatures and supersaturations in all equivalent regions. The scale-up of simple agitated vessels containing a liquid phase alone has long been recognized as a difficult problem. The two dimensionless numbers most frequently encountered in the analysis of stirrers and agitators are the Reynolds number, Re , and the Froude number, Fr :

$$Re = \frac{\rho n d^2}{\eta} \quad \text{and} \quad Fr = \frac{n^2 d}{g} \quad (9.98)$$

where d = agitator diameter, n = agitator speed (revolutions per unit time); ρ = liquid density; η = viscosity; g = gravitational acceleration. Re gives the ratio of the inertia and viscous forces, and Fr gives the ratio of centrifugal and gravitational acceleration.

For exact scale-up purposes, values of both Re and Fr should be kept constant but this is generally impossible. For example, if the agitator diameter is increased by a factor of 4, the agitator speed must be decreased by a factor of 2 if Fr is to be kept constant ($n \propto d^{-1/2}$) but by a factor of 16 if Re is to remain the same ($n \propto d^{-2}$). It is therefore impossible to satisfy both criteria, and some compromise must be made. For agitated crystallizers, more importance is

attached to Re (which influences fluid friction, heat and mass transfer) than to Fr (which is important only when gross vortexing occurs) so scale-up is generally based on the Reynolds number.

The power consumption, P , of an agitator is conventionally described by the relationship:

$$\frac{P}{\rho n^3 d^5} = Po \quad (9.99)$$

where the dimensionless quantity Po is usually called the Power number. In a turbulent fluid, at values of $Re > 10000$, Po is virtually a constant. Under these conditions, therefore, if the agitator speed is to be doubled the power input would have to be increased eightfold. If the agitator diameter is doubled, its speed remaining constant, the power input would have to be increased by a factor of 32.

Provided the same fluid is being agitated in two different units, the dependence of the agitator speed on the scale-up ratio assumes the form

$$n_1/n_2 = d_2/d_1 \quad (9.100)$$

and substitution into equation 9.99 leads to the power ratio

$$P_1/P_2 = (d_1/d_2)^2 \quad (9.101)$$

In other words, to maintain kinematic similarity the power consumption should increase as the square of the agitator diameter scale-up ratio.

The use of the empirical scale-up rule of keeping the specific power input (W m^{-3}) constant appears to be reasonable; at most it would be expected to produce only a modest increase in nucleation rate (section 9.1.1). Two other empirical scale-up criteria of keeping the agitator tip speed constant, or adjusting the agitator speed to the level where all the crystals are just in suspension, can also be justified since both might be expected to result in a decrease in a nucleation rate with increasing scale of operation (Nienow, 1976).

Another empirical rule based on considerable practical experience (Bennett, Fiedelman and Randolph, 1973) suggests that for scale-up at constant magma density and residence time, the quantity R^2/T should be kept constant, R = agitator tip speed and T = turnover time, i.e. crystallizer volume/volumetric liquor circulation rate.

The kinetics of crystal growth and nucleation are powerfully influenced by the system hydrodynamics (Ottens and de Jong, 1973) so the method of agitation in a crystallizer is very important. However, there is little reliable design information available for agitated vessels for solid–liquid systems, although the rapid advances now being made in computational fluid dynamics (CFD) modelling techniques (section 8.1.7) have the potential to provide a much better insight into the complex mixing effects involved.

Different types of agitator, and their position in the vessel, can produce substantially different flow patterns. For example, a centrally mounted propeller induces tangential flow and well-established pattern of circulation. A vortex is generally produced at high speeds, but the introduction of wall baffles creates

a chaotic turbulent motion. Off-centre stirring can do the same. Draft-tube agitation gives a very different type of circulation. This topic is discussed further in section 9.4.

9.4 Fluid-particle suspensions

9.4.1 Agitated vessels

There is, as yet, no completely satisfactory method for predicting the solids suspension characteristics of agitated vessels, although a considerable amount of attention has been paid to this intractable problem in recent years. It has long been known, for example, that the impeller geometry and speed, coupled with the vessel geometry and physical properties of the particulate system, are the important parameters. Several authors have presented relationships for predicting the minimum impeller speed to keep all the particles in suspension, i.e. to prevent particles resting on the bottom of the vessel. However, the spatial distribution of particles throughout the vessel is not easily predicted or assessed, but it is undoubtedly a function of the type of impeller and vessel geometry.

The equation due to Zweitering (1958) has been shown to be of wide applicability for estimating the minimum impeller speed, N , to suspend all the particles smaller than a certain size, d :

$$N = S[\nu^{0.1} d^{0.2} x^{0.13} D^{-0.85} (g\Delta\rho/\rho_l)^{0.45}] \quad (9.102)$$

where ν = kinematic viscosity of the liquid $\text{m}^2 \text{s}^{-1}$; d = normal particle size m ; x = fraction of solids in the system; D = impeller diameter m ; g = gravitational acceleration m s^{-2} ; ρ_l = liquid density, ρ_s = solid density, $\Delta\rho = \rho_s - \rho_l \text{ kg m}^{-3}$; and N = impeller speed rev s^{-1} .

The quantity S in equation 9.102 is a dimensionless constant and values are reported by Zweitering on graphs of S versus T/D with h/H as a parameter for a large number of different agitators (propeller, paddle, vaned disc turbine and fan disc turbine). T = vessel diameter, h = agitator clearance from bottom of vessel, H = liquid depth (*Figure 9.19*). In general,

$$S = (T/D)^a \quad (9.103)$$

where $a = 0.82$ for propeller agitators and 1.3 for radial flow impellers. For the suspension of crystals in a flat-bottomed vessel with baffles, using a flat-bladed turbine, Nienow (1968) suggested the relationship

$$N \propto d^{0.21} x^{0.12} D^{-2.2} \Delta\rho^{0.43} \quad (9.104)$$

which is compatible with equation 9.102 since the factor S is proportional to $(T/D)^{1.5}$, i.e. $N \propto D^{-2.35}$. *Figure 9.19* indicates a range of S values suggested for use with equation 9.102 for the case of a flat-bladed turbine impeller.

The terminal velocities of crystals suspended in agitated vessels may be predicted from the equations

$$u_t = 0.153 d^{1.14} g^{0.71} \Delta\rho^{0.71} / \rho_l^{0.29} \eta^{0.43} \quad (d < 500 \mu\text{m}) \quad (9.105)$$

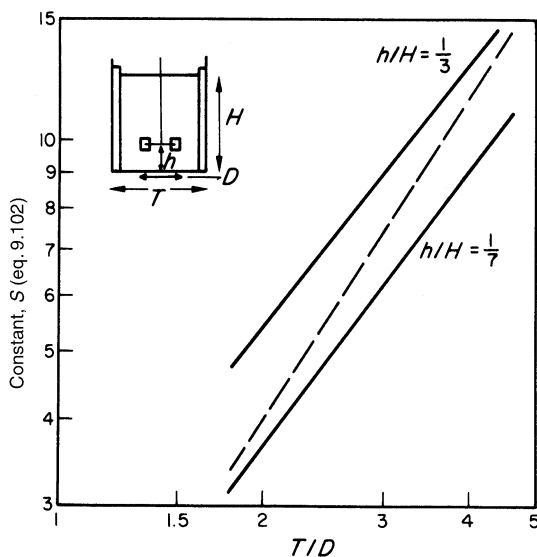


Figure 9.19. Suspension of crystals in a baffled, turbine-agitated vessel. Value of the constant S for equation 9.102. The broken line indicates data of Zweitering (1958). (After Nienow, 1968)

and

$$u_t = (4dg\Delta\rho/3\rho_1)^{1/2} \quad (d > 1500 \mu\text{m}) \quad (9.106)$$

For crystals of intermediate size, an interpolated mean value should be used.

The just-suspended slip velocity is given by

$$u_{js} = Ku_t \quad (9.107)$$

where K is based on a mass transfer enhancement factor evaluated from crystal dissolution rates. For ammonium alum crystals $K \sim 1.5$. The crystal slip velocity in the agitated vessel for different agitator speeds may be evaluated from

$$u_s = u_{js}(N/N_{js})^{0.8} \quad (9.108)$$

where N_{js} is the impeller speed needed to just suspend the crystals (Nienow, Bujac and Mullin, 1972).

The types of agitator commercially available to maintain crystals dispersed in a crystallizer are many and varied. They include anchors, gates, flat paddles, propellers, radial-flow flat-bladed turbines, axial-flow angle-bladed turbines, and so on. Each has its own fluid mixing and crystal dispersion characteristics. The selection of the most appropriate agitator for a given duty is a highly skilled task and reference should be made to specialist publications and technical brochures.

Good accounts of process mixing and agitation equipment for liquid–solid systems are given by Šterbáček and Tausk (1965), Uhl and Gray (1986), Oldshue (1983, 1992) and Harnby, Edwards and Nienow (1992).

Draft tubes

Draft-tube agitation is widely used in the chemical industry for suspending solids in liquids, but despite the longstanding popularity of these devices there is still very little published information available concerning their design or performance. The most common arrangement is a marine-type propeller acting as a pump within a draft tube located centrally in the vessel, e.g. as in *Figure 8.31b*. The flow pattern may be 'up' or 'down', i.e. the liquid or suspension is either sucked into the draft tube and then ejected into the top of the annular region between the wall and tube, or operated in the reverse manner. In the former case, any settling solids are sucked from the lower regions of the vessel and returned to the suspension at the top, and the whole suspension is circulated, e.g. as in a circulating magma crystallizer (section 8.4.3). In the latter case, the solids are normally kept suspended in the annular region and only liquor is circulated, together with any very small particles present, through the draft tube, as in a circulating liquor crystallizer where excessive secondary nucleation through crystal-agitator impact is prevented.

The important design parameters for a draft-tube agitated vessel are the diameters of the vessel and draft tube, the height of the draft tube and its position in the vessel, and the type and speed of the agitator. The liquid emerging from a down-flow draft tube under the action of the impeller has a radial component of velocity which may create an undesirable swirling motion in the annulus and induce a vortex at the free liquid surface. Vertical baffles located in the vessel wall can overcome this difficulty and produce a relatively stable suspended bed of particles.

The clearance of the draft tube from the base is important. A high clearance gives a low exit-liquid velocity and poor fluidization. A small clearance gives highly turbulent conditions and a high pressure drop at the tube exit which results in a greatly decreased draft-tube pumping efficiency.

There is an optimum vessel : tube diameter ratio for any given vessel and duty. For single-liquid mixing the optimum geometry is for equal areas of draft tube and annulus. For liquid-particle suspensions the optimum geometry is a function of the suspension characteristics, e.g. mass and fluidization velocity of particles, density of solid and liquid. The optimum draft tube diameter is always less than that in the single-phase case and decreases with increasing solids content as indicated in *Figure 9.20* for the suspension of K_2SO_4 crystals in their saturated solution using a down-flow draft tube (Jones and Mullin, 1973b). There is clearly no unique optimum draft tube diameter for all suspension densities, but the use of the hydraulic mean does have the beneficial effect that the superficial velocity in the annulus is lower than that in the draft tube, so particles will not settle in the region of the base.

9.4.2 Fluidized beds

A number of industrial crystallizers operate on the fluidized-bed principle, in which a mass of crystals is suspended in an upward flowing stream of liquor (*Figures 8.38* and *8.44*). One of the important parameters needed in the design

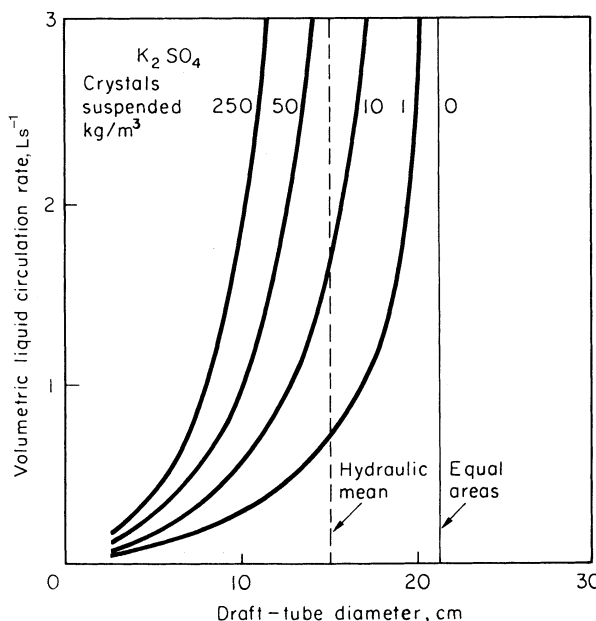


Figure 9.20. Optimum draft-tube diameters in a 30 cm diameter vessel. (After Jones and Mullin, 1973b)

of such crystallizers is the upflowing liquor velocity necessary to keep the crystals in suspension, but this is not easy to predict accurately. The crystals, being present in large quantities, are subjected to hindered settling and further complications arise if the crystals have irregular shape.

Free-fall velocity

The drag force, F , acting on a particle totally immersed in an infinite fluid is conventionally defined by the equation

$$F = c_D A_p \frac{1}{2} \rho u^2 \quad (9.109)$$

where c_D is the drag coefficient, which is a function of the particle Reynolds number ($Re_p = \rho n d / \eta$) and the particle shape. A_p = particle projected area, d = particle diameter, e.g. as measured by sieving, u = velocity, ρ = fluid density, and η = viscosity.

The free-fall or terminal settling velocity of a single particle in a fluid, u_0 , can be calculated by equating the drag force (equation 9.109) with the gravitational force. Thus for a spherical particle of density ρ_s

$$c_D A_p \frac{1}{2} \rho u_0^2 = \frac{\pi}{6} d^3 (\rho_s - \rho) g$$

i.e.

$$u_0 = \left[\frac{4d(\rho_s - \rho)g}{3\rho c_D} \right]^{1/2} \quad (9.110)$$

or

$$c_D = \frac{4d(\rho_s - \rho)g}{3\rho u_0^2} \quad (9.111)$$

For particle Reynolds numbers less than about 0.3, laminar flow conditions exist and Stokes' law indicates that, in this region, the drag force for spheres is given by

$$F = 3\pi u\eta d \quad (9.112)$$

Hence, for laminar flow conditions

$$c_D = \frac{3\pi u\eta d}{\frac{\pi}{4}d^2 \cdot \frac{1}{2}\rho u^2} = \frac{24}{Re_p} \quad (9.113)$$

and

$$u_0 = \frac{gd^2(\rho_s - \rho)}{18\eta} \quad (Re_p < 0.3) \quad (9.114)$$

For particle Reynolds numbers exceeding about 1000, the value of c_D becomes constant at approximately 0.44. The free-fall velocity in this region is thus given by

$$u_0 = 1.74 \left[\frac{gd(\rho_s - \rho)}{\rho} \right]^{1/2} \quad (Re_p > 1000) \quad (9.115)$$

Unfortunately the usual range of interest for crystallizer design lies between these two regions. For instance, the particle Reynolds numbers for individual crystals of potassium sulphate freely suspended in a saturated solution at 50 °C are about 3 and 550 for sizes of 100 µm and 2 mm, respectively. Within this intermediate region c_D is usually obtained from empirically derived values, but it cannot be used directly to determine the free-fall velocity, u_0 , because the term occurs in both c_D and Re_p . A trial and error procedure can be used but this is tedious and it is more convenient to combine c_D and Re_p , as $c_D Re_p^2$, to eliminate u_0 , i.e.,

$$c_D Re_p^2 = \frac{4d^3 \rho (\rho_s - \rho) g}{3\eta^2} \quad (9.116)$$

A plot of $c_D Re_p^2$ versus Re_p is given in Figure 9.21.

The use of the above relations is straightforward for the case of spheres. Crystals, however, are rarely spherical and irregular particles have drag characteristics that can differ appreciably from those of spheres. Drag coefficients for non-spherical particles have been reported by a number of authors, but to some extent these values are difficult to apply, since different shape factors have been used and not always defined.

Crystalline products are usually sized by sieving, so ideally the length term to be used should be that derived directly from the sieving operation, i.e. the second largest dimension of the particle (Figure 2.14).

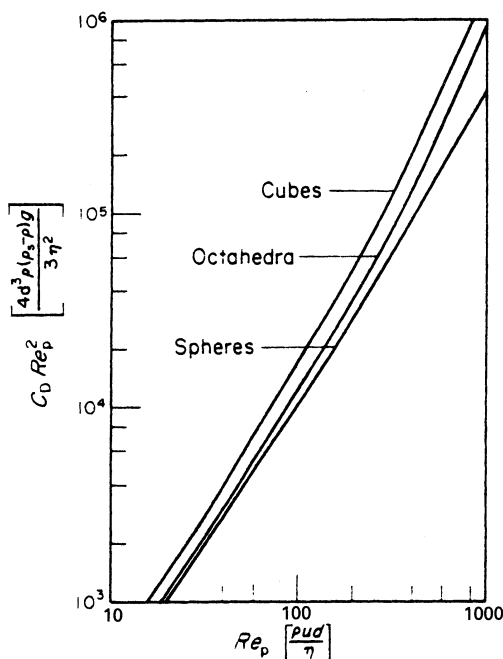


Figure 9.21. Variation of $C_D Re_p^2$ with Re_p

Measured terminal settling velocities of potash alum and potassium sulphate crystals give an indication of the behaviour of different crystal shapes under free-fall conditions (Mullin and Garside, 1970). The alum crystals were near-perfect octahedra, whereas those of potassium sulphate were elongated with a length to breadth ratio of about 3. Single crystals from a closely sized sieve fraction were allowed to fall through a stagnant saturated solution of the appropriate salt contained in a 70 mm internal diameter column. The time of fall through a fixed distance was measured for ten or more crystals of a given size and the average velocity calculated.

The measured free-fall velocities, u_0 , were corrected for the wall effect to give the free-fall velocities in an infinite medium, $u_{0(\infty)}$, with the equation (Richardson and Zaki, 1954)

$$u_{0(\infty)} = u_0(1 + 2.1d/D) \quad (9.117)$$

where D is the column diameter. Other correction factors have been quoted by various authors, but all these give very similar results for values of d/D below about 0.1.

The drag coefficients, calculated from $u_{0(\infty)}$ by use of equation 9.111 are plotted against the particle Reynolds number in Figure 9.22. The length term used in both these parameters is the arithmetic mean of the two adjacent sieve sizes between which the crystals were graded. Also shown in Figure 9.22 are the curves for spheres and two different isometric particles.

At low Reynolds numbers the drag coefficients for different shapes differ little from those for spheres. The effect of shape is more pronounced at high

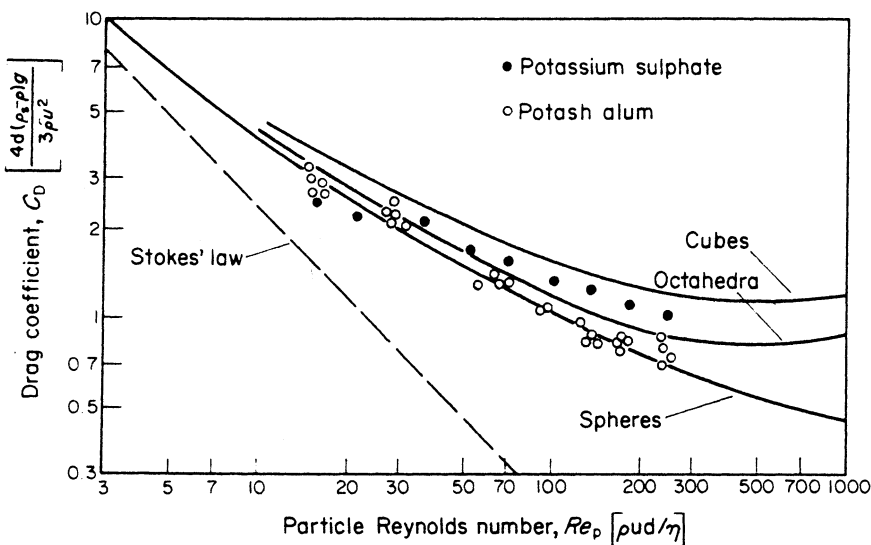


Figure 9.22. Variation of C_D with Re_p . (After Mullin and Garside, 1970)

Reynolds numbers, where the draft coefficients are appreciably higher than the corresponding values for spheres.

Superficial liquor velocity

In a liquid fluidized bed the superficial liquor velocity, u_s , and the bed voidage, ε , are related through the Richardson and Zaki (1954) equation:

$$u_s = u_i \varepsilon^z \quad (9.118)$$

The value of u_i is very nearly equal to the free-fall velocity of a single particle in an infinite fluid, $u_{0(\infty)}$, except when the ratio of particle size, d , to column diameter, D , is large, and, in general,

$$\log u_{0(\infty)} = \log u_i + \frac{d}{D} \quad (9.119)$$

The exponent z varies with the particle Reynolds number ($u_{0(\infty)}\rho d/\eta$) and the ratio d/D , and for the range of Reynolds numbers of interest in crystallizer design is given by

$$1 < Re_p < 200: \quad z = (4.4 + 18d/D) \cdot Re_p^{-0.1} \quad (9.120)$$

$$200 < Re_p < 500: \quad z = 4.4 Re_p^{-0.1} \quad (9.121)$$

$$Re_p < 500: \quad z = 2.4 \quad (9.122)$$

Although these equations have been shown to be reasonably accurate for spheres, there is little published information on the behaviour of non-spherical particles. Richardson and Zaki give a factor by which z must be multiplied when non-spherical particles are being handled, but this was only verified for particle Reynolds numbers above 500. A further difficulty is that when d/D is

not zero a discontinuity occurs in the calculated value of z at $Re_p = 200$, but in spite of these deficiencies the equations of Richardson and Zaki can be used to predict the performance of crystal suspensions.

For example, estimate the upflow velocity to maintain 1 mm ($d = 10^{-3}$ m) cubic crystals of sodium chloride ($\rho_c = 2170 \text{ kg m}^{-3}$) in their saturated solution ($\rho_l = 1200 \text{ kg m}^{-3}$, $\eta = 1.6 \text{ cP} = 1.6 \times 10^{-3} \text{ kg m}^{-1} \text{ s}^{-1}$) in a fluidized bed of voidage $\varepsilon = 0.8$.

From equation 9.116

$$c_D Re_p^2 = \frac{4 \times (10^{-3})^3 \times 1200 \times (2170 - 1200) \times 9.81}{3(1.6 \times 10^{-3})^2} = 5900$$

Using this value in *Figure 9.21* $Re_p = 50$, and from the definition of Re_p

$$\begin{aligned} u_0 &= Re_p(\eta/\rho_l d) \\ &= 50 \times 1.6 \times 10^{-3}/1200 \times 10^{-3} = 0.067 \text{ m s}^{-1} \\ &= 67 \text{ mm s}^{-1} \end{aligned}$$

Velocity–voidage relationships for crystals can be measured quite easily in the laboratory, which is recommended when accurate values are required. A simple apparatus for this purpose is shown in *Figure 9.23*. A glass column fluidization section, 25 mm diam. and 380 mm long surrounded by a 75 mm diam. calming section to prevent crystals being carried over into the pump. A scale attached to

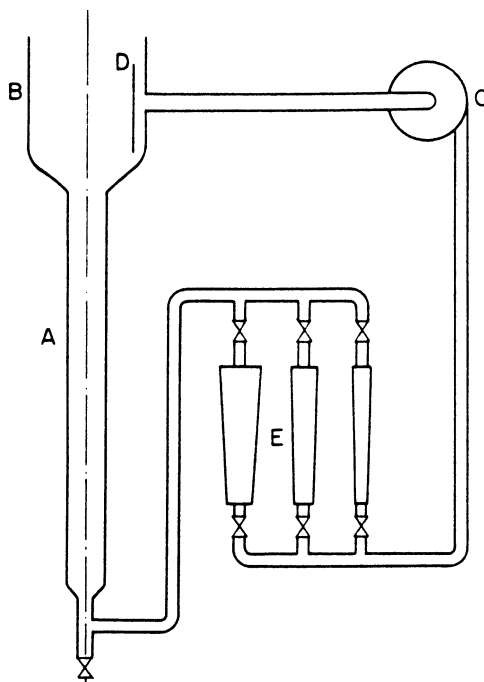


Figure 9.23. Apparatus for measuring velocity–voidage relationships: A, fluidization section; B, calming section; C, pump; D, baffle plate; E, flow meters

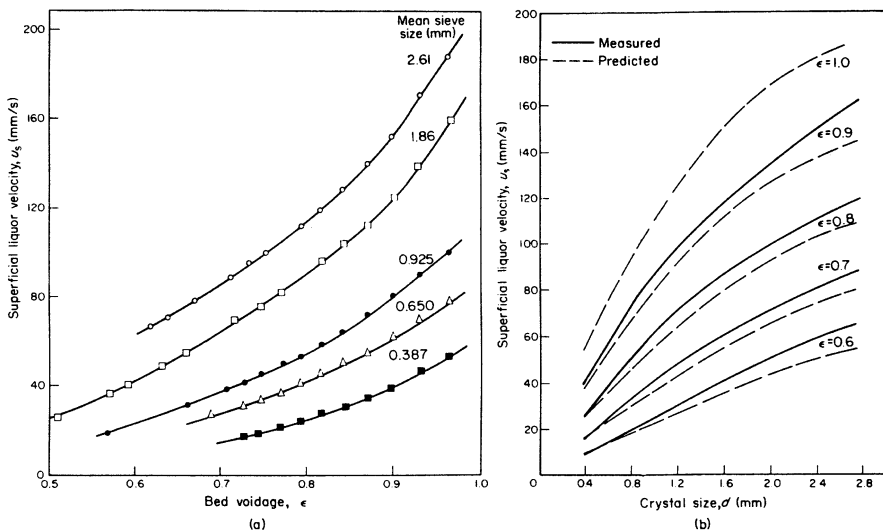


Figure 9.24. Potassium sulphate crystals suspended in saturated solution at 20 °C: (a) variation of superficial liquor velocity with bed voidage and crystal size; (b) comparison of measured and calculated (broken lines) velocities. (After Mullin and Garside, 1970)

the side of the fluidization section is used to measure crystal bed height. A given mass of crystals, graded into closely sized sieve fractions, is introduced into the fluidization zone. The solution circulation rate is varied and the crystal bed height measured at different solution velocities. From this height the voidage is calculated.

Some typical results for the variation of voidage with superficial velocity for several sizes of potassium sulphate crystals in saturated solution at 20 °C are shown in *Figure 9.24a*. Equations 9.118–9.120 are used to calculate the variation of superficial liquor velocity with crystal size and voidage. The measured values of $u_{0(\infty)}$ are used together with the values of z for spheres. *Figure 9.24b* compares calculated and experimental values and the agreement is reasonable, although errors of up to 20% occur for the larger sizes.

9.5 Encrustation

At some stage during their operating cycle, most crystallizers develop crystalline deposits on their internal surfaces. Such terms as scaling, fouling, salting, encrustation and encrustation are commonly used in this context. For convenience, however, only one term, *encrustation*, is used here to cover all types.

Encrustation is a serious problem in many crystallizer operations. On heat exchange surfaces, encrustation can reduce heat transfer and/or evaporation rates, and thereby reduce production rate or increase batch time. It can also lead to unstable operation. The need to remove encrustation from time to time often requires costly plant shutdown periods. Pipeline encrustation leads to greatly increased pumping power requirements and often to complete blockage.

Encrustation around an agitator shaft, commonly in the vicinity of the liquor surface, increases the agitator power requirements and may cause damage through out-of-balance rotation. Serious problems can occur if large lumps of encrustation break away inside the crystallizer and damage agitators or circulating pumps and block vessel outlets and liquor lines.

Encrustation can occur in the vapour space of evaporating and vacuum crystallizers (sections 8.4.2 and 8.4.3), particularly near the liquid–vapour interface. Severe build-up of deposits can increase the vapour velocity and intensify mother liquor droplet entrainment. Ideally, vapour velocities should be limited to not more than 1 m s^{-1} at atmospheric pressure and to not more than 3 m s^{-1} for low pressure operation (section 9.3.1).

The most common cause of encrustation in crystallizers is the creation of a zone of high supersaturation in the vicinity of a ‘receptive’ metal surface, e.g. a coil, jacket or heat exchanger tube. Other high-risk locations include vessel surfaces near vapour–liquor interfaces, regions of poor agitation or low flow rate and points at which different liquor streams meet and mix, e.g. at the feedstock inlet. Encrustation can start with crystalline fragments left behind after incomplete vessel cleaning, or embedded in the cracks and crevices of damaged surfaces, which act as nuclei and initiate growth when exposed to supersaturated liquor (section 5.2). For this reason, encrustations should never be chipped away from crystallizer surfaces because tiny scratches can easily become undesirable ‘seed centres’. Dissolution or melting are the only safe methods of crystal deposit removal.

The rates at which encrustations form and subsequently grow depend not only on the nature of the surface and the supersaturation encountered, but also on the nucleation and growth kinetics of the crystallizing system. Since the kinetics can be greatly influenced by trace impurities, these extraneous substances can have important effects on encrustation in a crystallizer. Any change in feed liquor composition or the addition of habit modifiers (section 6.4) may, therefore, alter the encrustation characteristics of the system for better or for worse. It is important to be aware that such changes are likely and, if possible, make initial trials on the pilot scale.

As high supersaturation is generally the root cause of encrustation problems, it might reasonably be expected to find some connection between the so-called metastable zone width (section 5.3) and the maximum undercooling allowed on a surface inside a crystallizer vessel. The study of Duncan and Phillips (1979) did in fact reveal such a connection and led to the postulation that the most likely mechanism was through deposition, e.g. on a cooling coil of secondary nuclei produced in the liquor layer close to the metallic surface. *Figure 9.25*, taken from the results of an extension of this work (Shock, 1983), demonstrates the approximate equality between the metastable zone width and the undercooling needed at a heat exchanger surface to initiate encrustation. For simplicity, all indications of the uncertainties of the individual experimental points, which can vary by several degrees Celsius, have been omitted, but the data do tend to justify the use of metastable zone width measurements, which can readily be made in the laboratory, as a rough guide to the specification of practical operating limits.

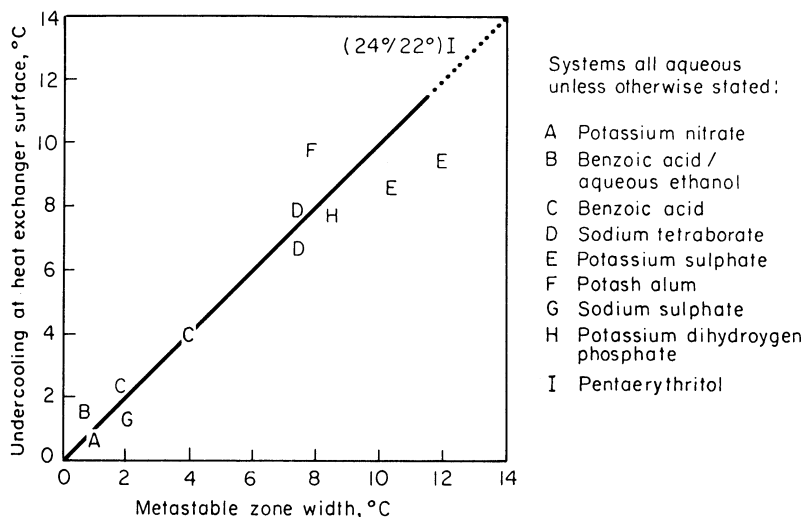


Figure 9.25. Comparison between metastable zone widths and the maximum undercooling permitted at a heat exchanger surface before the onset of encrustation: A, potassium nitrate; B, benzoic acid/aqueous ethanol; C, benzoic acid; D, sodium tetraborate; E, potassium sulphate; F, potash alum; G, sodium sulphate; H, potassium dihydrogen phosphate; I, pentaerythritol. (After Shock, 1983)

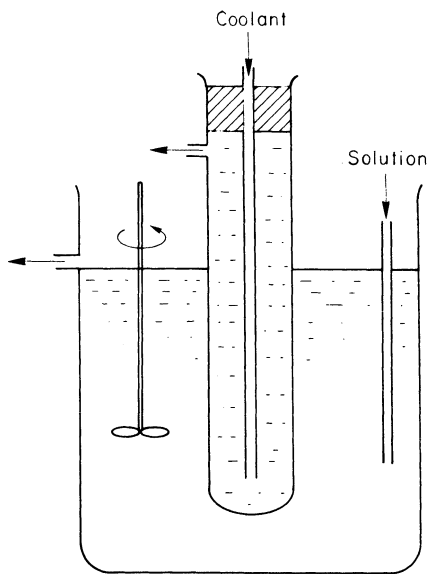


Figure 9.26. Cold-finger test for assessing encrustation behaviour

A rough assessment of the propensity for encrustation can be gained by using the simple cold-finger technique shown in *Figure 9.26*. Coolant is supplied at constant temperature and flow rate to the finger (e.g. 2.5 cm diameter, 15 cm long) which dips into solution flowing through the larger vessel. The maximum

temperature difference allowed between the coolant and solution without encrustation occurring can be determined by visual observation. This technique can also be used, with suitable modification, for crystallizing melts.

The mixing of saturated, or even unsaturated, flow streams in a crystallizer can produce a supersaturated mixture depending on their respective temperature, composition, flowrate and the solute solubility. Toussaint and Donders (1974) identified this particular problem, which so often leads to encrustation, and defined a *mixing criterion* for safe crystallizer operation which is satisfied when no supersaturation can occur whatever the ratio in which the flowstreams are mixed.

The temperature–concentration diagram in Figure 9.27 illustrates the mixing of a saturated solution A and unsaturated solution B to give a mixture with a composition and temperature represented by a point somewhere along line AB, determined by the mixture rule (section 4.4). A supersaturated mixture will be produced if the relative flowrates result in the mixture point lying in the sector below the solubility curve. For example, if A and B are mixed at equal mass flowrates, a supersaturated mixture M_1 would be produced (distance $AM_1 = BM_1$). For the mixture to enter the unsaturated zone, the B:A ratio would have to exceed about 7:2 in the case illustrated. The unsaturated mixture M_2 , for example, is the result of an 8:1 B:A ratio ($AM_2 = 8BM_2$).

The use of ultrasonic vibration to prevent crystal encrustation on cooling coils was demonstrated by Duncan and West (1972), who reported that the optimum range of vibration frequency was 10–100 kHz. Tests were carried out with *p*-xylene crystallizing from mixtures with its isomers and ice crystallizing from brine. Two mechanisms of encrustation were suggested, depending on the power level of the ultrasonic vibration. If the power level is high enough to cause cavitation in the liquid phase, the action appears to be the same as that in conventional ultrasonic cleaning, which depends on shock waves generated by the collapse of bubbles. At lower power levels the effect is attributed to the

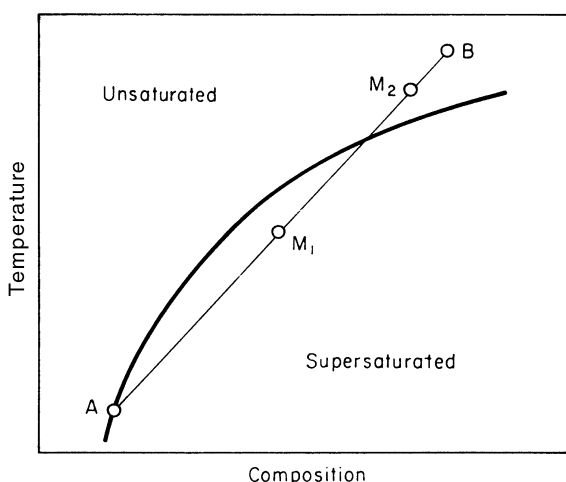


Figure 9.27. The mixing criterion (see text)

phenomenon of acoustic microstreaming at the solid–liquid interface. Although successful in small-scale pilot plant equipment, scale-up to large-scale industrial crystallizers has not yet been achieved.

The effect of an externally applied magnetic field on crystalline scale deposition, typically of CaCO_3 from hard water flowing in metal pipes, still remains a controversial subject despite the considerable number of investigations made over the past thirty years or so. There is still no general agreement on either the efficacy of commercially available devices or on the speculative mechanisms that have been proposed to explain their action (Söhnle and Mullin, 1988; Prasad *et al.*, 1999; Kotsinaris *et al.*, 1999).

Experimental techniques for studying the early stages of crystal encrustation have been reported by Chandler (1964), Veerka and Nývlt (1979), Duncan and Phillips (1979), Goldman and Spott (1981) and Chianese, Di Cave and Mazzarotta (1990). Examples of precautions that should be taken in the design and operation of crystallizers to minimize encrustation are given by Nývlt (1978), Wöhlk and Hofmann (1980), Shock (1983), and Söhnle and Garside (1992).

9.6 Caking of crystals

One of the most troublesome properties of crystalline materials is their tendency to bind together, or cake, on storage. Most crystalline products are required in a free-flowing form; they should, for example, flow readily out of containers, e.g. sugar and table salt, or be capable of being distributed evenly over surfaces, e.g. fertilizers. Handling, packaging, tabletting and many other operations are all made easier if the crystalline mass remains in a particulate state. Caking not only destroys the free-flowing nature of the product but also necessitates some crushing operation, either manual or mechanical, before it can be used.

The causes of caking may vary for different materials. Crystal size, shape, moisture content, the pressure under which the product is stored, temperature and humidity variations during storage and storage time can all contribute to the compacting of a granular crystalline product into a solid lump. In general caking is caused by the crystal surfaces becoming damp: the solution which is formed evaporates later and unites adjacent crystals with a cement of recrystallized solid. Crystal surfaces can become damp in a number of ways – the product may contain traces of solvent left behind due to inefficient drying, or the moisture may come from external sources.

Take, for example, the case of a water-soluble substance. If the partial pressure of water vapour in the atmosphere is greater than the vapour pressure that would be exerted by a saturated aqueous solution of the pure substance at that temperature, water will be absorbed by the crystals. If, later, the atmospheric moisture content falls to give a partial pressure below the vapour pressure of the saturated solution, the crystals will dry out and bind together. Small fluctuations in atmospheric temperature and humidity, sufficient to bring about these changes, can occur several times in one day.

A simple test for determining the atmospheric humidities at which a particular mass of crystals will absorb moisture consists of placing samples of the crystals in humidator vessels in which atmospheres of different known moisture content are created. Solutions of various strengths of sulphuric acid may be placed in the base of the humidator, the equivalent relative humidities of the resulting atmospheres can be calculated from vapour pressure data. Atmospheres of constant relative humidity can also be obtained by using saturated solutions of various salts in the base of the chamber of the humidator. *Table 9.3* gives a list of the percentage relative humidities of the atmospheres above various saturated salt solutions at 15 °C, and these can also be considered to be the critical humidities of the salts at 15 °C: if the atmospheric humidity is greater than the critical, the salt becomes hygroscopic. The term ‘deliquescence’ is usually reserved for the case where the substance absorbs atmospheric moisture and continues to do so until it becomes completely dissolved in the absorbed water. This will only occur if the vapour pressure of the salt solution

Table 9.3. Percentage relative humidities of the atmospheres above saturated solutions of various pure salts at 15 °C

Substance	Formula	Stable phase at 15 °C	Percentage relative humidity
Lead nitrate	Pb(NO ₃) ₂	anhyd.	98
Disodium phosphate	Na ₂ HPO ₄	12H ₂ O	95
Sodium sulphate	Na ₂ SO ₄	10H ₂ O	93
Sodium bromate	NaBrO ₃	anhyd.	92
Dipotassium phosphate	K ₂ HPO ₄	anhyd.	92
Potassium nitrate	KNO ₃	anhyd.	92
Sodium carbonate	Na ₂ CO ₃	10H ₂ O	90
Zinc sulphate	ZnSO ₄	7H ₂ O	90
Potassium chromate	K ₂ CrO ₄	anhyd.	88
Barium chloride	BaCl ₂	2H ₂ O	88
Potassium bisulphate	KHSO ₄	anhyd.	86
Potassium bromide	KBr	anhyd.	84
Ammonium sulphate	(NH ₄) ₂ SO ₄	anhyd.	81
Ammonium chloride	NH ₄ Cl	anhyd.	79
Sodium chloride	NaCl	anhyd.	78
Sodium nitrate	NaNO ₃	anhyd.	77
Sodium acetate	C ₂ H ₃ O ₂ Na	3H ₂ O	76
Sodium chlorate	NaClO ₃	anhyd.	75
Ammonium nitrate	NH ₄ NO ₃	anhyd.	67
Sodium nitrite	NaNO ₂	anhyd.	66
Magnesium acetate	Mg(C ₂ H ₃ O ₂) ₂	4H ₂ O	65
Sodium bromide	NaBr	2H ₂ O	58
Sodium dichromate	Na ₂ Cr ₂ O ₇	2H ₂ O	52
Potassium nitrite	KNO ₂	anhyd.	45
Potassium carbonate	K ₂ CO ₃	2H ₂ O	43
Calcium chloride	CaCl ₂	6H ₂ O	32
Lithium chloride	LiCl	H ₂ O	15

always remains lower than the partial pressure of the water vapour in the atmosphere. Calcium chloride, with a critical humidity of 32 per cent at 15°C, is a well-known example of a deliquescent salt. The term 'efflorescence' refers to the loss of water of crystallization from a salt hydrate: this occurs when the vapour pressure exerted by the hydrate exceeds the partial pressure of water vapour in the atmosphere. Sodium sulphate decahydrate, with a critical humidity of 93 per cent, is an example of an efflorescent salt.

Commercial crystalline salts frequently exhibit hygroscopy at atmospheric humidities lower than those given for the pure salts in *Table 9.3*. Usually impurities present in the product cause the trouble. For example, traces of calcium chloride in sodium chloride would render the crystals damp at very low atmospheric humidities. Removal of the hygroscopic impurity would be the answer, but this is not always economical. Coating of the crystals with a fine inert dust will often prevent the mass becoming damp; table salt, for instance, can be coated with magnesium carbonate or calcium aluminium silicate.

A number of precautionary measures can be taken to minimize the possibility of caking. One obvious method would be to pack perfectly dry crystals in a dry atmosphere, store them in an air-tight container and prevent any pressure being applied during storage. These desirable conditions, however, cannot always be obtained. Caking can also be minimized by reducing the number of contacts between the crystals, and this can be done by endeavouring to produce granular crystals of a uniform size. The crystals should be as large as possible: the smaller they are the larger will be the exposed surface area per unit mass. The actual size, however, is only of secondary importance in this respect. Shape and uniformity of the crystals, on the other hand, are extremely important factors affecting caking, as indicated in *Figure 9.28*.

The minimum caking tendency is shown by uniform granular crystals (*Figure 9.28a*). Even if caking did occur, the mass could easily be broken up because of the open structure and the relatively few points of contact per unit volume. Non-uniform granular crystals (*Figure 9.28b*) are more prone to caking: the voids in between the large granules are filled with the smaller particles, which results in a larger number of points of contact per unit volume, and the caked mass will not be broken up as easily as in the former case. Although the crystals depicted in *Figure 9.28c* are uniform, they are also elongated and may tend to cake badly. Here there are areas, as well as points, of contact: the needles can pack together and set hard on caking. The condition shown in *Figure 9.28d* is

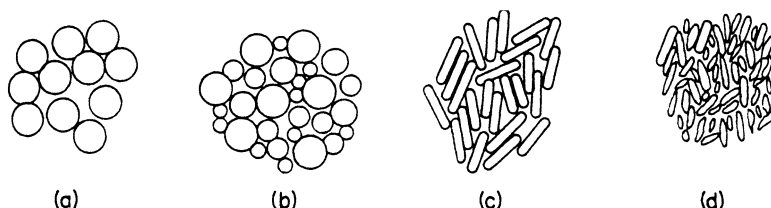


Figure 9.28. Effect of particle shape on the caking of crystals: (a) large uniform granular crystals (good); (b) non-uniform granular crystals (poor); (c) large uniform elongated crystals (poor); (d) non-uniform elongated crystals (very bad)

even worse. The crystals are both elongated and non-uniform: they can pack together very tightly into a mass with negligible voidage. When this sort of mass cakes, it is often quite impossible to transform it back to its original particulate state. Plate-like crystals also have bad caking characteristics.

Shape and uniformity of the particles also affect the behaviour of the product under storage. If the crystals are packed in bags and stacked on top of one another, the pressure in the bags near the bottom of the pile tends to force the crystals into closer contact: with non-uniform crystals this compaction may be quite severe and, in extreme cases, many of the crystals may be crushed. If the solubility of the salt in water increases with an increase in pressure, traces of solution may be formed under the high local pressure at the points of contact. The solution will then tend to flow into the voids, where the pressure is lower, and crystallize. Storage of crystalline materials under pressure should always be avoided if possible.

Controlled crystallization, coupled with some form of classifying action in the crystallizer, helps to produce crystals of uniform size. The production of granular crystals, however, may demand the careful control of other conditions of crystallization to modify the crystal habit; the rate of cooling, the degree of supersaturation and the pH of the crystallizing solution can exert considerable influence. The deliberate addition of traces of impurity, in the form of active ions or surface-active agents, may also help to produce the right type of crystal.

The use of habit modification (section 6.4) as a means of minimizing crystal caking is quite common. A good example is the novel method for preventing caking in water-soluble salts by treating the crystals with a very dilute solution of habit-modifying dyestuff, e.g. Acid Magenta. Should the crystals cake at some later stage, the cement of crystalline material, now consisting of a modified habit, will be very weak and the crystal mass will easily break down on handling. This method has proved effective with salts such as ammonium nitrate, ammonium sulphate and potassium nitrate (Whetstone, 1949a and b). The use of a large number of trace additives at the crystallization stage, and their effects on habit and caking of a number of inorganic salts including NaCl, KCl, K₂SO₄, NH₄Cl, NH₄NO₃ and (NH₄)₂SO₄ have been reported by Phoenix (1966).

The use of coating agents has already been mentioned above in connection with table salt, in the production of which magnesium carbonate and calcium aluminium silicate are frequently used. Icing sugar may be coated with 0.5 per cent of tricalcium phosphate or cornflour to prevent caking. Other anti-caking and flow conditioning agents used for industrial crystalline materials include

aluminium powder	magnesium carbonate
Acid Magenta dye	magnesium oxide
calcium silicate	paraffin wax
calcium aluminium silicate	phosphate rock
cellulose gums	silica dust
chalk	silica, hydrated
diatomaceous earth	sodium silico-aluminate

fuller's earth	surfactants
kaolin	synthetic resins
kieselguhr	tricalcium phosphate
magnesium aluminium silicate	

Finely divided substances used as dusting agents must have a good covering power so that very small quantities will produce the desired effect.

Several comprehensive accounts have been given of the methods employed for conditioning crystals and of testing procedures to determine the flow properties and caking tendency of crystalline materials (Shearon and Dunwoody, 1953; Whynes and Dee, 1957; Irani, Callis and Liu, 1959; Irani, Vandersall and Morgenthaler, 1961; Burak, 1966; Phoenix, 1966; Tanaka, 1978; Chen and Chou, 1993).

9.7 Downstream processes

An industrial crystallization process generally has to be followed by several separate operations in order to obtain the crystalline product in its final form. These *downstream* operations can include solid–liquid separation, washing, classification, drying and screening. Their requirements, or indeed the wish to avoid employing any one of them, can have an influence on the design of the crystallizer itself. The complete design of a crystallization plant, therefore, must take into consideration both upstream (feedstock supply and choice of processing mode, Wibowo and Ng, 2000) and downstream implications (Rossiter and Douglas, 1986; Sharratt, 1996).

Product specification can have an important bearing on the design of a crystallization plant. The specifications that have most influence on the downstream operations of those concerned with crystal purity, size distribution and moisture content. Since mother liquor contamination is a major cause of impurity appearing in a final product, an excessively tight purity specification can influence the choice of filter or centrifuge. It may also demand special washing facilities, a reslurrying step or even recrystallization. A tight crystal size distribution specification, for example, could necessitate a wet classification stage after the crystallizer, or a dry screening step after the dryer. In either case there could be consequential problems associated with recycling undersize and/or oversize material. The use of the term ‘mean size’ in crystal product specifications is a frequent cause of misunderstanding and disagreement between producer and customer. It should always be clearly established which of the many different mean sizes (see section 2.14.2) is intended. As noted in section 9.3.2, the product crystal size distribution can be quoted in terms of either upper and lower size limits or by the statistical median size and coefficient of variation (section 2.14.4).

In cases where crystal caking (section 9.6) is expected, a tight moisture content specification (surface moisture only) may be imposed on the final product. This will have a major influence on the choice of a dryer, which in turn will also have been influenced by the expected filter cake moisture content

in the solid–liquid separation stage. The cake moisture content can be reduced by compressing the cake, filtering under pressure or by increasing the centrifuge speed. The dryer heat load may be estimated from

$$\text{Heat load} = \frac{\text{evaporation rate} \times \text{enthalpy of vaporization}}{\text{thermal efficiency}}$$

For convective dryers thermal efficiencies in the range 0.4–0.7 may be expected, the lower values applying to heat sensitive products which require drying air temperatures < 100 °C. Vacuum dryers can have thermal efficiencies as high as 0.9, but their capital costs are also high.

The recommendation that a crystallizer should not be designed in isolation from its ancillary processes is strongly emphasized in a comprehensive series of papers by Rossiter and Douglas (1986). A proposed procedure for synthesizing process flowsheets for solids systems is applied to the optimization of a crystallizer–centrifuge–dryer system and illustrated by a case study based on a commercial common salt process. Sharratt (1996) addresses the ways in which environmental pressures can influence the total design of a crystallization plant. The underlying environmental driving forces, and their influence on the need for materials substitution, reduction of waste generation during downstream processing and the requirement for recycling, are identified as key problem areas (*Figure 9.29*).

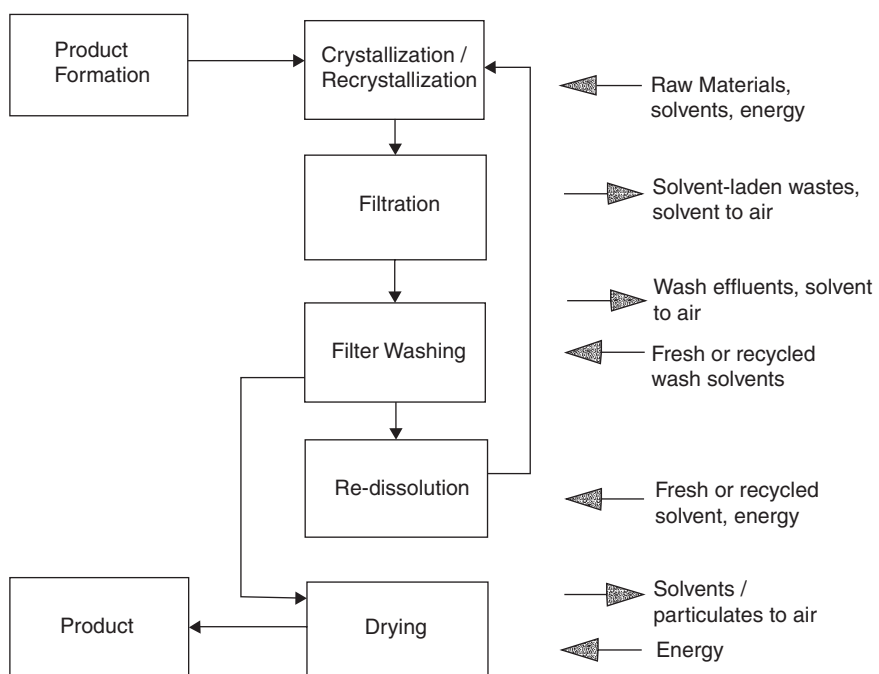


Figure 9.29. Potential environmental impacts and resource usage associated with the formation of solid products by crystallization from solution. (After Sharratt, 1996)

9.7.1 Laboratory tests

Some simple laboratory tests can be performed on the product magma from a crystallizer, or on the filtered and laboratory-dried crystals, to make an assessment of the potential downstream handling problems. Each test is capable of yielding a piece of useful information which, when added to that from the others, can give a useful picture of the slurry and crystal characteristics that will enable downstream process problems to be more clearly identified. The tests outlined below are not listed in any order of importance.

- One of the most commonly applied tests is a crystal size analysis, by sieving or any other appropriate technique. The median size and coefficient of variation, for example, may be used to characterize the crystals (section 2.14).
- Microscopic observation is highly recommended to assess the general appearance of the crystals (section 2.14.2). A Polaroid-type or digital camera attached to the microscope will allow rapid processing of photographs which can be quickly examined and kept as a permanent record. Poor shape may indicate the need for removing an undesirable impurity from the feedstock or for a habit modifier (section 6.4) to be added during the crystallization process. Needles, plates or irregular crystals with wide size distributions will indicate that potential problems of caking on storage may be encountered (section 9.6). Excessive agglomeration could warn of the possibility of a dusty product after drying.
- A sedimentation test may be performed very simply in a graduated glass cylinder to allow observation of both the rate and manner of the solid–liquid separation. Fast settling with a clear-cut interface would give an expectation of good filtration, washing and drying characteristics. Slow settling with an indistinct ‘cloudy’ interface would suggest the reverse. Experience should allow more precise interpretations relevant to subsequent operations.
- A simple filtration test, using a deep Buchner funnel ($>500\text{ mL}$ capacity) and vacuum flask to measure the rate of filtrate production (*Figure 9.30a*), is useful for assessing the ease or difficulty of the crystal-mother liquor separation step. The ‘parabolic law’ of filtration (Carman, 1938) suggests that, for an incompressible cake, the volume of filtrate V collected over a period of time t is given by

$$t = aV^2 + bV \quad (9.123)$$

i.e.

$$\frac{t}{V} = aV + b \quad (9.124)$$

so that a plot of t/V against V (*Figure 9.30b*) should give a straight line of slope a (the cake constant) and intercept b (the cloth constant). The cake constant can serve as a quantitative characterization of the filtrability of the magma (Purchas, 1981; Svarovsky, 1990). A subsequent washing rate test along similar lines would be relevant if the cake was compressible.

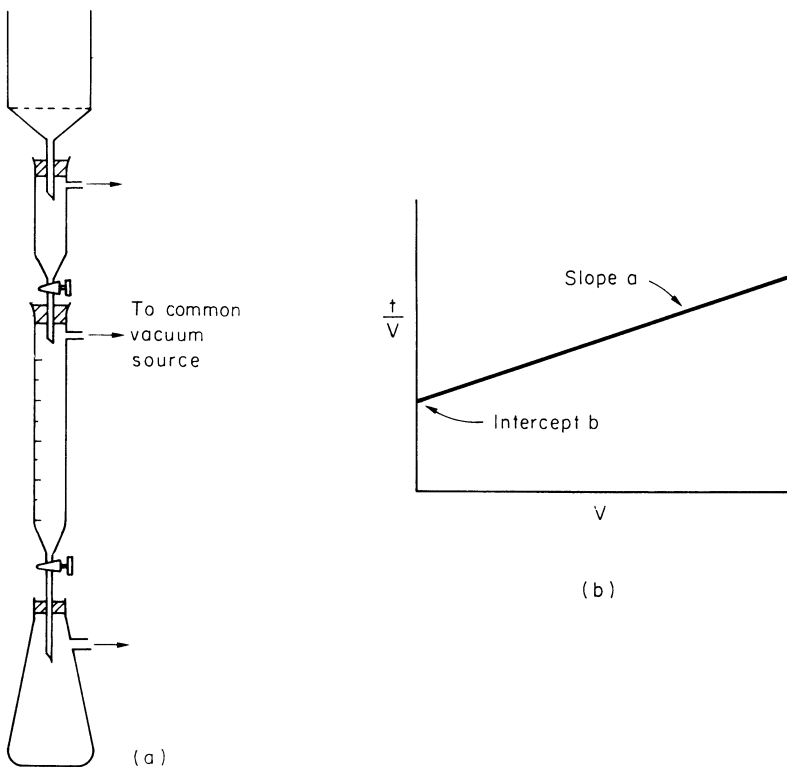


Figure 9.30. Filtration test for assessing magma characteristics: (a) simple apparatus, (b) plot of t/V versus V (equation 9.124)

- After filtration, the moisture content of the cake may be measured to give information for a subsequent drying operation. Even simple observations about the filter cake, such as whether it is dry and crumbly, hard packed, wet, pasty, etc., can be useful for assessing its subsequent processing problems.

Most crystalline materials in bulk quantities are to some extent friable, i.e., prone to attrition and breakage on handling, conveying, drying and undergoing operations such as screening (section 9.7.2). Crystalline agglomerates are particularly friable and can result in a dusty final product. A simple friability test may be made by tumbling a known mass of crystals in a rotating drum containing lifting flights to carry the crystals to the top of each revolution so that in addition to abrasion through rolling contact the crystals are submitted to mild impacts. A friability index (percentage) may be defined as

$$F = 100[(M_i - M_f)/M_i] \quad (9.125)$$

where M_i is the initial mass of crystals sieved to eliminate fine particles of a specified size, and M_f is the final mass of crystals, sieved to remove the pre-specified fines, after the test. The precise experimental details of the friability

test and the interpretation of the index F can be varied according to the material being handled and the information required.

9.7.2 Crystal washing

Even though the actual crystals produced in a crystallizer may themselves be essentially pure, after they have been separated from their mother liquor and dried the resultant crystalline mass may be relatively impure. Even if no inclusions are formed (section 6.6), the removal of mother liquor is frequently inadequate. Crystals retain a small quantity of mother liquor on their surfaces by adsorption and a larger amount within the voids of the particulate mass owing to capillary attraction. If the crystals are irregular, the amount of mother liquor retention within the crevices may be considerable; crystal clusters and agglomerates are notorious in this respect.

Industrial crystallization processes from the liquid phase must be followed by an efficient liquid–solid separation. Centrifugal filtration can often reduce the mother liquor content of granular crystalline masses to about 5–10 per cent, although irregular small crystals may retain more than 50 per cent. It is extremely important, therefore, not only to use the most efficient type of filter but to attempt to produce regular shaped crystals in the crystallizer.

After filtration, the product is usually given a wash to reduce still further the amount of impure mother liquor retained. Cakes of crystalline substances should not be too thick if a washing operation is required; otherwise the wash liquor becomes saturated long before it passes through the mass and the other liquor impurities are not removed effectively. If the crystals are very soluble in the mother solvent, another liquid, in which the substance is relatively insoluble, may be used for washing purposes. The wash liquid should be miscible with the mother solvent. For example, water could be used for washing substances crystallized from methanol; whereas methanol could be used for washing substances crystallized from benzene. Unfortunately, this two-solvent method of working usually means that a solvent recovery unit is required. Alternatively, a wash liquor consisting of a cold saturated solution of the pure substance in the pure mother solvent could be used if the crystals were appreciably soluble in the solvent. The contaminated wash liquor could then be recycled back to the crystallizer or reused in some other way.

When simple washing is inadequate, two mother liquor removal stages may be necessary: the wet crystals are removed from the filter, redispersed in wash liquor and then filtered again. There may be an appreciable loss of yield after such a washing process but this would be less than the loss after a complete recrystallization.

When crystallization has been carried out by the reaction method, the crystalline product may be relatively insoluble in the working solvent. On the other hand, the mother liquor may contain large quantities of another soluble material, resulting from the chemical reaction, and simple filtration and washing may be quite inadequate for its complete removal, especially if the crystalline particles are very small or irregular. For example, when barium sulphate is precipitated by mixing solutions of barium chloride and sodium sulphate, it

is difficult to remove the resulting sodium chloride contamination by conventional filtration and washing. In such cases, a sequence of dispersion-washing and decantation steps may be very effective.

The wash liquor requirements for decantation washing can be deduced by assuming, for simplicity, that all the soluble impurity is in solution and solution concentrations are constant throughout the dispersion vessel (Donald, 1937; Kirby, 1959).

Batch Operation. If I_0 and I_n denote the impurity concentrations in the crystalline material (kg of impurity/kg of product) initially and after washing stage n , respectively, and F is the fraction of liquid removed at each decantation, then from a mass balance:

$$I_n = I_0(1 - F)^n \quad (9.125)$$

which may be rewritten in the form:

$$\ln(I_n/I_0) = n \ln(1 - F) \quad (9.126)$$

Continuous Operation. For washing on a continuous basis, where fresh wash liquid enters the vessel continuously, and liquor is continually withdrawn through a filter screen, a mass balance over the unit gives:

$$V dI = -I dW \quad (9.127)$$

which may be written as:

$$\ln(I_n/I_0) = -W/V \quad (9.128)$$

where I_0 and I_n are the initial and final impurity concentrations. V and W are the volumes of the liquor in the vessel and wash water, respectively. Combination of equations 9.126 and 9.128 gives:

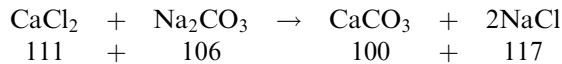
$$n \ln(1 - F) = -\frac{W}{V} \quad (9.129)$$

or, rearranging and dividing by F :

$$\frac{W}{nFV} = \frac{-\ln(1 - F)}{F} \quad (9.130)$$

W and nFV represent the wash liquor requirements for continuous and batch operations, respectively.

The utility of the above relationships may be demonstrated by a simple example: 100 kg of calcium carbonate is produced by the reaction



(a) Determine the number of washes required to reduce the NaCl concentration to 0.01 per cent in the final product. The fraction of liquid removed at each decantation is determined by observing the settling of the slurry in a graduated cylinder. In this case, assume $F = 0.7$:

$$I_0 = 117/100 = 1.17, I_n = 0.0001, I_n/I_0 = 8.55 \times 10^{-5}$$

From equation 9.126, for this value of I_n/I_0 and $F = 0.7$, $n = 7.8$. Therefore eight washes would be required.

(b) Calculate the volume of wash water required if the reaction mixture, containing 2 m^3 of liquor, is to be washed continuously to produce the same product as in (a):

For $V = 2.0\text{ m}^3$ and a value of $I_n/I_0 = 8.55 \times 10^{-5}$ using equation 9.128, the volume of wash water required, $W = 18.7\text{ m}^3$.

(c) Compare the wash water requirements of the batch and continuous processes:

The ratio of water consumption for the two methods can be determined from equation 9.130 written in the form

$$\frac{W_{\text{cont}}}{W_{\text{batch}}} = \frac{-\ln(1-F)}{F} = \frac{-\ln 0.3}{0.7} = 1.72$$

In this case, therefore, the continuous method would require 72 per cent more water than the batch method.

Descriptions of various modes of filter cake washing are discussed by Svarovksy (1990).

9.7.3 Crystal screening

Crystalline products are generally marketed in graded size ranges, and consequently dried crystals are frequently submitted to a screening process before final packaging. In some industrial processes screening followed by blending operations may be necessary to produce the final product.

Screening on an industrial scale is quite different from the laboratory procedures described in section 2.14.2 for test sieving purposes. In the latter operation sieving is continued to an end-point, i.e. until no more, or very little, of the material passes through the given sieve. In industrial screening there is neither the time nor indeed the necessity to approach this degree of perfection. The operation is usually continuous, feed material flowing at a steady rate on to a shaking or vibrating screen and remaining on the screening surface for a relatively short time. The passage of particles through the screen apertures is impeded by the motion of the screen and by the presence of other particles. Particle interference coupled with the short residence time of material on the screen lead to imperfect separation.

Descriptions of industrial screening equipment and modes of operation are given by Svarovksy (1990).

Screen capacity and efficiency

Particulate material fed to a screen can be considered to be composed of two fractions, an oversize fraction consisting of particles that are too large to pass through the screen apertures, and an undersize fraction consisting of particles

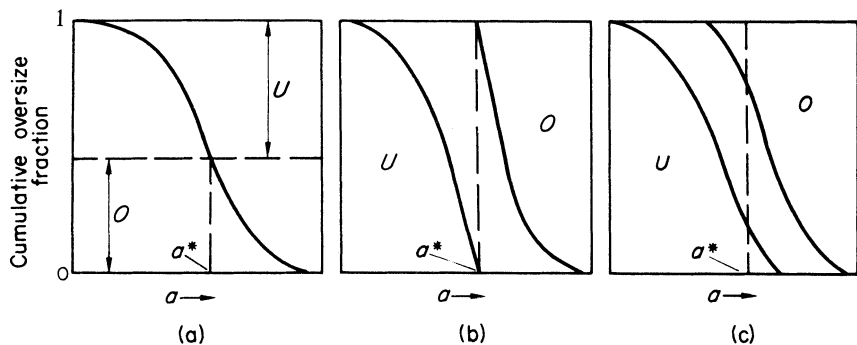


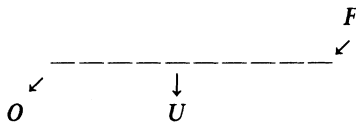
Figure 9.31. Cumulative oversize diagrams: (a) feedstock, (b) perfect screening, (c) actual screening

that are too small to be retained on the screen. The screening efficiency, or effectiveness of separation, therefore, should indicate the degree of success obtained in the segregation of these two fractions. In an industrial screening operation a ‘clean’ separation is never achieved; undersize particles are invariably left in the oversize fraction, mainly because the material does not remain on the sieve for a sufficiently long period, and oversize particles may be found in the undersize fraction if the screen mesh is non-uniform, punctured or inadequately sealed around its edges.

The capacity of a screen is the feed rate at which it performs the specified duty. In general, other factors remaining constant, the capacity, i.e. throughput, decreases as the required degree of separation, i.e. efficiency, increases. Some compromise, therefore, has to be made between capacity and efficiency. Various expressions of capacity are used. For a given screen, the specification kg/min or ton/h may be quite adequate. Capacity may also be quoted as mass per unit time per unit area of screening surface, but care must be taken here, because the length and width of the screen may be independent factors.

The term ‘efficiency’ applied to screening processes is not easy to define. In fact, there is no generally accepted definition of the term, and various industries adopt the one that most simply and adequately meets their needs. The following analysis indicates a few of the expressions commonly employed. The sieve-test data shown diagrammatically in *Figure 9.31a* point out the differences between perfect and actual screening operations. *Figure 9.31a* gives the sieve analysis (cumulative oversize fractions plotted against sieve aperture) of the feed material. Therefore, for an effective screen aperture a^* , fraction O represents the oversize particles and fraction U represents the undersize. For perfect separation, the sieve analyses of these two fractions would be as shown in *Figure 9.31b*: no particles smaller than a^* appear in the oversize fraction, none larger than a^* in the undersize fraction. In practice, however, unwanted particle sizes do appear in the undersize and oversize flow streams (*Figure 9.31c*).

A screening operation can be considered as the separation of a feedstock F into an oversize top product O and an undersize bottom product U , i.e.



Therefore, if F , O and U represent the masses of these flow streams, an overall mass balance gives

$$F = O + U \quad (9.131)$$

If x_F^o , x_O^o and x_U^o represent the mass fractions of oversize material, i.e. particles larger than a^* , in the feed, overflow and underflow, respectively, and x_F^u , x_O^u and x_U^u represent the corresponding undersize mass fractions, then a balance on the oversize material gives

$$Fx_F^o = Ox_O^o + Ux_U^o \quad (9.132)$$

and a balance on the undersize material gives

$$Fx_F^u = Ox_O^u + Ux_U^u \quad (9.133)$$

Thus, from equations 9.131 to 9.133,

$$\frac{O}{F} = \frac{x_F^o - x_U^o}{x_O^o - x_U^o} = \frac{x_U^u - x_F^u}{x_U^u - x_O^u} \quad (9.134)$$

and

$$\frac{U}{F} = \frac{x_O^o - x_F^o}{x_O^o - x_U^o} = \frac{x_F^u - x_O^u}{x_U^u - x_O^u} \quad (9.135)$$

For perfect screening, therefore,

$$Ox_O^o = Fx_F^o \quad (9.136)$$

and

$$Ux_U^u = Fx_F^u \quad (9.137)$$

For actual screening, two efficiencies can be defined:

$$E_O = \frac{Ox_O^o}{Fx_F^o} \quad (9.138)$$

and

$$E_U = \frac{Ux_U^u}{Fx_F^u} \quad (9.139)$$

Equation 9.138 gives a measure of the success of recovering oversize particles in the overflow stream, equation 9.139 of undersize material in the underflow stream. For perfect screening both E_O and E_U will be unity. Equations 9.138 and 9.139 require values of the mass flow rates F , O and U , but substitution from equations 9.132 and 9.133 can eliminate these quantities:

$$E_O = \frac{x_O^o(x_F^o - x_U^o)}{x_F^o(x_O^o - x_U^o)} \quad (9.140)$$

$$= \frac{(1 - x_O^u)(x_U^u - x_F^u)}{(1 - x_F^u)(x_U^u - x_O^u)} \quad (9.141)$$

Table 9.4. Sieve analyses (effective screen aperture $a^* = 460 \mu\text{m}$)

Aperture, μm	Feedstock	Cumulative mass fraction oversize Overflow	Underflow
850	0.02	0.06	—
710	0.12	0.29	—
600	0.26	0.52	0.02
500	0.45	0.78	0.08
425	0.68	0.90	0.22
355	0.81	0.96	0.46
300	0.90	1.00	0.68
212	0.98	—	0.84
—	1.00	—	1.00

and

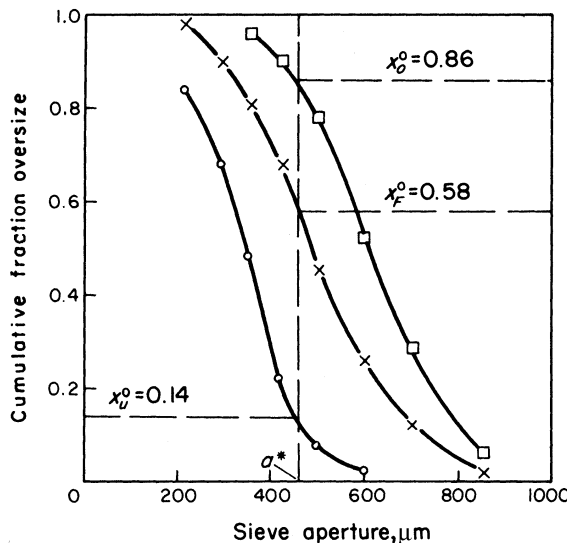
$$E_U = \frac{x_U^u(x_F^u - x_O^u)}{x_F^u(x_U^u - x_O^u)} \quad (9.142)$$

$$= \frac{(1 - x_U^o)(x_O^o - x_F^o)}{(1 - x_F^o)(x_O^o - x_U^o)} \quad (9.143)$$

An overall screen effectiveness, E , can be defined as the product of E_O and E_U .

Table 9.4 illustrates the calculation of these efficiencies. These data are plotted in Figure 9.32, where it can be seen that the values of x_F^o , x_O^o and x_U^o at $a^* = 460 \mu\text{m}$ are 0.58, 0.86 and 0.14, respectively. Therefore, from equations 9.138 and 9.141,

$$E_O = \frac{0.86(0.58 - 0.14)}{0.58(0.86 - 0.14)} = 0.91$$

**Figure 9.32.** Determination of screening efficiency ($a^* = 460 \mu\text{m}$)

and

$$E_U = \frac{(1 - 0.14)(0.86 - 0.58)}{(1 - 0.58)(0.86 - 0.14)} = 0.80$$

and the overall effectiveness

$$\begin{aligned} E &= E_O E_U = 0.91 \times 0.80 \\ &= 0.728 \text{ or } 73 \text{ per cent} \end{aligned}$$

A simpler form of equation 9.140 is often used to express the recovery of true undersize material in the overflow fraction, on the assumption that all the underflow stream consists of undersize material, i.e. $x_U^u = 1$:

$$E'_O = \frac{x_F^u - x_O^u}{x_F^u(1 - x_O^u)} \quad (9.144)$$

or

$$E'_O = \frac{x_O^o - x_F^o}{x_O^o(1 - x_F^o)} \quad (9.145)$$

The above assumption, of course, is not always valid.

Formulae of the above types have been criticized because they do not take into consideration the difference between an easy separation duty and a difficult one. For example, consider the sieving of two feedstocks *A* and *B* through, say, an 850 µm screen. In both cases 90% of the particles are smaller than 850 µm, but *A* contains a high proportion of particles smaller than, say, 250 µm, *B* a high proportion in the range 700–850 µm. Clearly, *A* can be sieved with ease, whereas the sieving of *B* is a difficult operation.

Some of the factors that can affect the capacity of a screen and the efficiency of separation are

- (a) *Feedstock properties*: particle shape and size; bulk density; moisture content; abrasion resistance.
- (b) *Screen characteristics*: percentage open area; aperture size and shape; length and width of screen; angle of inclination; material of construction; uniformity of mesh.
- (c) *Operating conditions*: feed rate; method of feeding; depth of layer on screen; frequency of vibration; amplitude of vibration; direction of vibration.

Appendix

Table A.1. International atomic weights

Name	Symbol	At. No.	At. Wt.	Valency
Actinium	Ac	89	227	—
Aluminium	Al	13	26.98	3
Antimony	Sb	51	121.76	3, 5
Argon	A	18	39.944	0
Arsenic	As	33	74.91	3, 5
Astatine	At	85	[210]	1, 3, 5, 7
Barium	Ba	56	137.36	2
Beryllium	Be	4	9.013	2
Bismuth	Bi	83	209.00	3, 5
Boron	B	5	10.82	3
Bromine	Br	35	79.916	1, 3, 5, 7
Cadmium	Cd	48	112.41	2
Calcium	Ca	20	40.08	2
Carbon	C	6	12.011	2, 4
Cerium	Ce	58	140.13	3, 4
Cesium	Cs	55	132.91	1
Chlorine	Cl	17	33.457	1, 3, 5, 7
Chromium	Cr	24	52.01	2, 3, 6
Cobalt	Co	27	58.94	2, 3
Copper	Cu	29	63.54	1, 2
Dysprosium	Dy	66	162.51	3
Erbium	Er	68	167.27	3
Europium	Eu	63	152.0	2, 3
Fluorine	F	9	19.00	1
Francium	Fr	87	[223]	1
Gadolinium	Gd	64	157.26	3
Gallium	Ga	31	69.72	2, 3
Germanium	Ge	32	72.60	4
Gold	Au	79	197.0	1, 3
Hafnium	Hf	72	178.50	4
Helium	He	2	4.003	0
Holmium	Ho	67	164.94	3
Hydrogen	H	1	1.0080	1
Indium	In	49	114.82	3
Iodine	I	53	126.91	1, 3, 5, 7
Iridium	Ir	77	192.2	3, 4
Iron	Fe	26	55.85	2, 3
Krypton	Kr	36	83.8	0
Lanthanum	La	57	138.92	3
Lead	Pb	82	207.21	2, 4
Lithium	Li	3	6.940	1

Lutecium	Lu	71	174.99	3
Magnesium	Mg	12	24.32	2
Manganese	Mn	25	54.94	2, 3, 4
Mercury	Hg	80	200.61	1, 2
Molybdenum	Mo	42	95.95	3, 4, 6
Neodymium	Nd	60	144.27	3
Neon	Ne	10	20.183	0
Nickel	Ni	28	58.71	2, 3
Niobium	Nb	41	92.91	3, 5
Nitrogen	N	7	14.008	3, 5
Osmium	Os	76	190.2	2, 3, 4, 8
Oxygen	O	8	16.000	2
Palladium	Pd	46	106.4	2, 4
Phosphorus	P	15	30.975	3, 5
Platinum	Pt	78	195.09	2, 4
Polonium	Po	84	210	—
Potassium	K	19	39.100	1
Praseodymium	Pr	59	140.92	3
Promethium	Pm	61	[145]	3
Protactinium	Pa	91	231	—
Radium	Ra	88	226.05	2
Radon	Rn	86	222	0
Rhenium	Re	75	186.22	—
Rhodium	Rh	45	102.91	3
Rubidium	Rb	37	85.48	1
Ruthenium	Ru	44	101.1	3, 4, 6, 8
Samarium	Sm(Sa)	62	150.35	2, 3
Scandium	Sc	21	44.96	3
Selenium	Se	34	78.96	2, 4, 6
Silicon	Si	14	28.09	4
Silver	Ag	47	107.880	1
Sodium	Na	11	22.991	1
Strontium	Sr	38	87.63	2
Sulphur	S	16	32.066 ± 0.003	2
Tantalum	Ta	73	180.95	5
Technetium	Tc	43	[99]	6, 7
Tellurium	Te	52	127.61	2, 4, 6
Terbium	Tb	65	158.93	3
Thallium	Tl	81	204.39	1, 3
Thorium	Th	90	232.05	4
Thulium	Tm	69	168.94	3
Tin	Sn	50	118.70	2, 4
Titanium	Ti	22	47.90	3, 4
Tungsten	W	74	183.86	6
Uranium	U	92	238.07	4, 6
Vanadium	V	23	50.95	3, 5
Xenon	Xe	54	131.3	0
Ytterbium	Yb	70	173.04	2, 3
Yttrium	Y	39	88.92	3
Zinc	Zn	30	65.38	2
Zirconium	Zr	40	91.22	4

Table A.2. Some physical properties of pure water

Temp., °C	Density, g cm ⁻³	Viscosity, cP	Surface tension, dyn cm ⁻¹	Vapour pressure, mm Hg	Dielectric constant	Refractive index*
0	0.99987 [†]	1.787	75.6	4.580	87.7	
5	0.99999	1.516	74.9	6.538	85.8	
10	0.99973	1.306	74.2	9.203	83.8	1.33410
15	0.99913	1.138	73.5	12.78	82.0	1.33377
20	0.99823	1.002	72.8	17.52	80.1	1.33335
25	0.99707	0.8903	72.0	23.75	78.3	1.33287
30	0.99568	0.7975	71.2	31.82	76.6	1.33228
40	0.99224	0.6531	69.6	55.34	73.2	1.33087
50	0.98807	0.5467	67.9	92.56	69.9	1.32930
60	0.9832	0.4666	66.2	149.5	66.8	1.32754
70	0.9778	0.405	64.4	233.8	63.9	1.32547
80	0.9718	0.355	62.6	355.3	61.0	1.32323
90	0.9653	0.316	60.7	525.9	58.3	1.32086
100	0.9584	0.283	58.9	760.0	55.7	1.31819

* Absolute index for sodium light.

† Density of ice at 0°C = 0.9168 g cm⁻³Density: 1 g cm⁻³ = 1000 kg m⁻³Viscosity: 1 cP = 10⁻³ N s m⁻² = 10⁻³ Pa s (= 10⁻³ kg m⁻¹ s⁻¹)Surface tension: 1 dyn cm⁻¹ = 10⁻³ N m⁻¹ (= 10⁻³ J m⁻²)

Triple point: 0.01 °C, 6.1 Pa

Critical point: 374 °C, 22 MPa

Pressure: 1 mm Hg = 133.3 N m⁻² (1 bar = 10⁵ N m⁻² = 10⁵ Pa)

Table A.3. Solubility products

Substance	Solubility product	Temperature, °C	Substance	Solubility product	Temperature, °C
Aluminium hydroxide	4×10^{-13}	15	Lead sulphate	1.1×10^{-8}	18
Aluminium hydroxide	1.1×10^{-15}	18	Lead sulphide	3.4×10^{-28}	18
Barium carbonate	7×10^{-9}	16	Lithium carbonate	1.7×10^{-3}	25
Barium chromate	1.6×10^{-10}	18	Lithium fluoride	2.6×10^{-3}	25
Barium fluoride	1.7×10^{-6}	18	Magnesium ammonium phosphate	2.6×10^{-13}	25
Barium hydroxide	2.5×10^{-4}	18	Magnesium carbonate	2.6×10^{-5}	12
Barium iodate ($2\text{H}_2\text{O}$)	6.5×10^{-7}	25	Magnesium fluoride	7.1×10^{-9}	18
Barium molybdate	3.4×10^{-8}	20	Magnesium hydroxide	1.2×10^{-11}	18
Barium oxalate ($2\text{H}_2\text{O}$)	1.2×10^{-7}	18	Magnesium oxalate	8.6×10^{-5}	18
Barium oxalate ($\frac{1}{2}\text{H}_2\text{O}$)	2.2×10^{-7}	18	Manganese hydroxide	4×10^{-14}	18
Barium sulphate	1.1×10^{-10}	18	Manganese sulphide	1.4×10^{-15}	18
Cadmium sulphide	3.6×10^{-29}	18	Mercuric sulphide	4×10^{-53} to 2×10^{-49}	18
Calcium carbonate (calcite)	0.99×10^{-8}	15	Mercurous bromide	1.3×10^{-21}	25
Calcium fluoride	3.4×10^{-11}	18	Mercurous chloride	2×10^{-18}	25
Calcium hydroxide	6.5×10^{-6}	25	Mercurous iodide	1.2×10^{-28}	25
Calcium oxalate (H_2O)	1.8×10^{-9}	18	Nickel sulphide	1.4×10^{-24}	18
Calcium sulphate	2.0×10^{-4}	10	Potassium acid tartrate		
Calcium tartrate ($2\text{H}_2\text{O}$)	0.77×10^{-6}	18	$[\text{K}^+] [\text{HC}_4\text{H}_4\text{O}_6]$	3.8×10^{-4}	18
Cobalt sulphide	3×10^{-26}	18	Silver bromate	4.0×10^{-5}	20
Cupric iodate	1.4×10^{-7}	25	Silver bromide	4.1×10^{-13}	18

Table A.3. (Continued)

Substance	Solubility product	Temperature, °C	Substance	Solubility product	Temperature, °C
Cupric oxalate	2.9×10^{-8}	25	Silver carbonate	6.2×10^{-12}	25
Cupric sulphide	8.5×10^{-45}	18	Silver chloride	1.6×10^{-10}	25
Cuprous bromide	4.2×10^{-8}	18–20	Silver chromate	9×10^{-12}	25
Cuprous chloride	1.0×10^{-6}	18–20	Silver cyanide $[\text{Ag}^+] [\text{Ag}(\text{CN})_2^-]$	2.2×10^{-12}	20
Cuprous iodide	5.1×10^{-12}	18–20	Silver hydroxide	1.5×10^{-8}	20
Cuprous sulphide	2×10^{-47}	16–18	Silver iodide	1.5×10^{-16}	25
Cuprous thiocyanate	1.6×10^{-11}	18	Silver sulphide	1.6×10^{-49}	18
Ferrous hydroxide	1.6×10^{-14}	18	Silver thiocyanate	0.49×10^{-12}	18
Ferric hydroxide	1.1×10^{-36}	18	Strontium carbonate	1.6×10^{-9}	25
Ferrous oxalate	2.1×10^{-7}	25	Strontium fluoride	2.8×10^{-9}	18
Ferrous sulphide	3.7×10^{-19}	18	Strontium molybdate	2.6×10^{-7}	20
Lead carbonate	3.3×10^{-14}	18	Strontium oxalate	5.6×10^{-8}	18
Lead chloride	1.7×10^{-5}	18	Strontium sulphate	3.8×10^{-7}	17.4
Lead chromate	1.8×10^{-14}	18	Zinc carbonate	1.0×10^{-10}	18
Lead fluoride	3.2×10^{-8}	18	Zinc hydroxide	6.3×10^{-17}	18
Lead iodate	1.2×10^{-13}	18	Zinc oxalate	1.4×10^{-9}	18
Lead iodide	7.5×10^{-9}	15	Zinc sulphide	1.2×10^{-23}	18
Lead oxalate	2.7×10^{-11}	18			

Table A.4. Solubilities of inorganic salts in water (g of anhydrous compound per 100 g of water)

Compound	Formula	Solubility, °C								Stable hydrates, 0–25 °C
		0	10	20	30	40	60	80	100	
Aluminium chloride sulphate nitrate	AlCl ₃		46		47					6
	Al ₂ (SO ₄) ₃	31.3	33.5	36.2	40.4	46.1	59.2	73.0	89.1	18
	Al(NO ₃) ₃	60	68	74	82	89	106	132	160	9
Ammonium alum bicarbonate bromide chloride dihydrogen phosphate iodide nitrate oxalate perchlorate sulphate thiocyanate vanadate	(NH ₄) ₂ Al ₂ (SO ₄) ₄	2.1	5.0	7.7	11.0	14.9	26.7		110 ^(95°)	24
	NH ₄ HCO ₃	12	16	21	27	35	decomp.			—
	NH ₄ Br	60.6	68.0	75.5	83.5	91.0	108	126	146	—
	NH ₄ Cl	29.7	33.4	37.2	41.4	45.8	55.2	65.6	77.3	—
	NH ₄ H ₂ PO ₄	22.0	28.0	36.5	45.8	56.6				—
	NH ₄ I	154	163	172	181	191	209	230	250	—
	NH ₄ NO ₃	118	150	192	242	297	421	580	870	—
	(NH ₄) ₂ C ₂ O ₄	2.1	3.1	4.4	6.0	8.0	14			1
	NH ₄ ClO ₄	11.7	16.4	21.8	27.9	34.4	50.2	67.8		—
Barium acetate bromide chlorate chloride hydroxide iodide nitrate	(NH ₄) ₂ SO ₄	71.0	73.0	75.4	78.0	81.0	88.0	95.3	103.3	—
	NH ₄ CNS	121		162						—
	NH ₄ VO ₃			4.8	8.4	13.2				—
	Ba(C ₂ H ₃ O ₂) ₂	58	63	72	75	79	74	74	74	3
	BaBr ₂	98	100	104	107	112	124	140	160	2
	Ba(ClO ₃) ₂	20.3	27.0	33.8	41.7	49.6	66.8	84.8	105	1
	BaCl ₂	31.6	33.2	35.7	38.2	40.7	46.4	52.4	58.3	2
	Ba(OH) ₂	1.6	2.5	3.9	5.6	8.2	21	101		8
	BaI ₂	170	186	203	220	232	247	261	272	6
Beryllium chloride nitrate sulphate	Ba(NO ₃) ₂	5.0	7.0	9.2	11.6	14.2	20.3	27.0	34.2	—
	BeCl ₂	68		73	77	79				4
	Be(NO ₃) ₂	98		107	110		177			4
	BeSO ₄	35	37	39	41	44	54	67	85	4

Table A.4. (Continued)

Compound	Formula	Solubility, °C								Stable hydrates, 0–25 °C
		0	10	20	30	40	60	80	100	
Boric acid	H ₃ BO ₃	2.59	3.62	4.95	6.64	8.79	14.9	23.6	38.0	—
Cadmium bromide	CdBr ₂	56.3	75.5	96.5	128	152			160	4
chloride	CdCl ₂	90	135	134	132	135	136	140	147	2½
iodide	CdI ₂	80	83	86	90				128	—
nitrate	Cd(NO ₃) ₂	120		140		220	400		660	4
sulphate	CdSO ₄	76.5	76.0	76.6		78.5	83.7		60.8	3
Caesium chloride	CsCl	161	175	187	197	208	230	250	271	—
chlorate	CsClO ₃	2.46	3.8	6.2	9.5	13.8	26.2	45.0	79.0	—
nitrate	CsNO ₃	9.3	14.9	23.0	33.9	47.2	83.8	134	197	—
perchlorate	CsClO ₄	0.1	1.0	1.6	2.6	4.0	7.3	14.4	30.0	—
sulphate	Cs ₂ SO ₄	167	173	179	184	190	200	210	220	—
Calcium acetate	Ca(C ₂ H ₃ O ₂) ₂	37.4	36.0	34.7	33.8	33.2	32.7	33.5	29.7	2
bicarbonate	Ca(HCO ₃) ₂	16.2	16.4	16.6	16.8	17.1	17.5	18.0	18.4	—
chloride	CaCl ₂	59.5	65.0	74.5	102		137	147	159	6
hydroxide	Ca(OH) ₂	0.19	0.18	0.17	0.15	0.14	0.12	0.09	0.08	—
iodide	CaI ₂	192	196	204	220	240			430	8
nitrate	Ca(NO ₃) ₂	102	115	129	153	196		359	363	4
sulphate	CaSO ₄	0.18	0.19	0.20	0.21	0.21	0.20	0.18	0.16	2
Cobalt ammonium sulphate	Co(NH ₄) ₂ (SO ₄) ₂	6.0	9.2	12.6	17.5	21.8	32.7	49.0		6
bromide	CoBr ₂	92		110		156	226		257	6
chloride	CoCl ₂	42	46	50	56		92	97	104	6
iodide	CoI ₂	138	160	185	234	300		400		1
nitrate	Co(NO ₃) ₂	85	89	97	110	126	167	211		6
sulphate	CoSO ₄	25.5	30.0	36.2	41.8	48	60	70	83	7
Copper (Cupric) chloride	CuCl ₂	69	71	74	76	81			98	2
nitrate	Cu(NO ₃) ₂	81.8	95.3	125		160	179	208	250	6
sulphate	CuSO ₄	14.3	17.4	20.7	25.0	28.5	40.0	55.0	75.4	5

Ferric ammonium sulphate	$\text{Fe}_2(\text{SO}_4)_3(\text{NH}_4)_2\text{SO}_4$		18	32	59	120			24
chloride	FeCl_3	74.4	81.9	91.8			526	540	6
Ferrous ammonium sulphate	$\text{FeSO}_4(\text{NH}_4)_2\text{SO}_4$	12.5		26.4		32.9	45.7		6
bromide	FeBr_2	102		115	122	128	144	160	177
chloride	FeCl_2	61	64	68	73	77	89	100	106
potassium sulphate	$\text{FeSO}_4\text{K}_2\text{SO}_4$	20	25	32	39	45	59		6
sulphate	FeSO_4	15.6	20.5	26.5	32.9	40.2			7
Lead acetate	$\text{Pb}(\text{C}_2\text{H}_3\text{O}_2)_2$	19.7	29.2	44.1	69.5	116			3
bromide	PbBr_2	0.45	0.62	0.85	1.2	1.5	2.4	3.3	4.8
chloride	PbCl_2	0.67	0.81	1.0	1.2	1.5	2.0	2.6	3.3
nitrate	$\text{Pb}(\text{NO}_3)_2$	39	48	57	66	75	95	115	139
Lithium bromide	LiBr	128	138	148	161	180	198	220	2
carbonate	Li_2CO_3	1.54	1.43	1.33	1.25	1.17	1.01	0.85	0.72
chloride	LiCl	64	70	80	90		102	112	125
fluoride	LiF			0.13		0.14	0.15		0.16
hydroxide	LiOH	12.6	12.7	12.8	13.0	13.2	13.9	15.4	17.5
iodate	LiIO_3			74.5		75.1	75.4	76.1	77.0
iodide	LiI	151	158	165	172	180			480
nitrate	LiNO_3	48	60	76					227
perchlorate	LiClO_4		51	56	63	72	93	125	3
sulphate	Li_2SO_4	35	35	34		33			29
Magnesium bromide	MgBr_2	92.0	95.0	96.5	99.2	101.6	107.5	113.7	120.6
chloride	MgCl_2	52.8	53.5	54.5	56.0	57.5	61.0	66.0	73.0
iodide	MgI_2	120		140		174			8
nitrate	$\text{Mg}(\text{NO}_3)_2$	66.5				84.7			137(90°)
sulphate	MgSO_4	22.3	27.8	33.5	39.6	44.8	55.3	56	50
Manganous chloride	MnCl_2	63.4	68.1	73.9	80.7	88.6	109	113	115
nitrate	$\text{Mn}(\text{NO}_3)_2$	50.5	54.1	58.8	67.4				6
sulphate	MnSO_4	53.2	60.0	64.5	66.4	68.8	55.0	48.0	34.0
Mercuric bromide	HgBr_2	0.3	0.4	0.6	0.7	1.0	1.7	2.8	4.9
chloride	HgCl_2	4.66	5.43	6.59	8.14	10.2	17.4	30.9	58.3
Mercurous perchlorate	$\text{Hg}_2(\text{ClO}_4)_2$	282		368	420	457	500	540	600

Table A.4. (Continued)

Compound	Formula	Solubility, °C								Stable hydrates, 0–25 °C
		0	10	20	30	40	60	80	100	
Nickel ammonium sulphate bromide chloride iodide nitrate sulphate	Ni(NH ₄) ₂ (SO ₄) ₂	1.6	4.0	6.5	9.0	12.0	17.5			6
	NiBr ₂	112	122	131	138	144	152	154	155	6
	NiCl ₂	54	60	64	69	73	82	87	88	6
	NiI ₂	124	135	147	157	174	184	187		6
	Ni(NO ₃) ₂	80	88	96	109	122	163		77	6
	NiSO ₄	26	32	37	43	47	55	63		6, 7
Potassium acetate aluminium sulphate bicarbonate bisulphate bromate bromide carbonate chlorate chloride chromate dichromate dihydrogen phosphate ferricyanide ferrocyanide hydrogen tartrate hydrogen oxalate hydrogen phthalate hydroxide iodate iodide	KC ₂ H ₃ O ₂	217	234	256	284	323	350	380		1½
	K ₂ Al ₂ (SO ₄) ₄	3.0	4.0	5.9	8.4	11.7	24.8	71.0		24
	KHCO ₃	22.5	27.7	33.2	39.1	45.4	60.0			—
	KHSO ₄	36.3		51.4		67.3			121.6	—
	KBrO ₃	3.1	4.0	6.8	10.0	13.1	22.5	33.9	50.0	—
	KBr	53.5	58.0	64.6	70.0	74.2	84.5	96.0	102.0	—
	K ₂ CO ₃	106	108	110	114	117	127	140	156	1½
	KClO ₃	3.3	5.0	7.0	10.5	14.0	24.5	38.5	57	—
	KCl	27.6	31.0	34.0	37.0	40.0	45.5	51.1	56.7	—
	K ₂ CrO ₄	58.2	60.0	61.7	63.4	65.2	68.6	72.1	75.6	—
	K ₂ Cr ₂ O ₇	5	7	12	20	26	43	61	80	—
	KH ₂ PO ₄	15.9	18.3	22.6	27.7	33.5	50.0	70.4		—
	K ₃ Fe(CN) ₆	31	36	43	50	60	66	72	81	—
	K ₄ Fe(CN) ₆	14	21	27	34	40	54	69	86	3
	KHC ₄ H ₄ O ₆	0.32	0.40	0.53	0.90	1.3	2.5	4.6	6.9	—
	KHC ₂ O ₄	2.2	3.4	5.2	7.4	11.0		34.7	51.0	—
	KHC ₂ O ₄ · C ₆ H ₄			11.0	12.7	16.3	27.0			—
	KOH	97	103	112	126				178	2
	KIO ₃	4.7	6.2	8.1	10.3	12.2	18	25	32	—
	KI	128	135	144	150	160	175	190	210	—

nitrate	KNO ₃	13.3	20.9	31.6	45.8	63.9	110	169	247	—
nitrite	KNO ₂	280	290	300	310	330			413	—
oxalate	K ₂ C ₂ O ₄	25.9	30.2	34.7	39.2	43.8		63.4	75	1
perchlorate	KClO ₄	0.75	1.1	1.8	2.6	4.4	9.0	14.8	21.8	—
permanganate	KMnO ₄	2.8	4.4	6.3	9.0	12.6	22.2			—
platinichloride	K ₂ PtCl ₆	0.74	0.90	1.12	1.41	1.76	2.64	3.79	5.18	—
sulphate	K ₂ SO ₄	7.4	9.3	11.1	13.1	14.9	18.3	21.4	24.2	—
sulphite	K ₂ SO ₃			107					113	1
thiocyanate	KCNS	176	189	242						—
Rubidium bromide	RbBr	89		110			150	175	190	—
chlorate	RbClO ₃	2.1	3.4	5.4	8.0	11.5	22.3	38.2	65	—
chloride	RbCl	70.6	77.4	83.6	89.5				128	—
nitrate	RbNO ₃	13.3	22.6	36.5	55.5	79.0	136	211	305	—
perchlorate	RbClO ₄		0.64	0.98	1.5	2.4	4.9	9.3	18	—
sulphate	Rb ₂ SO ₄	34.2	39.7	45.0	50.3	55.2			79.5	—
Silver acetate	AgC ₂ H ₃ O ₂	0.72	0.88	1.04	1.21	1.41	1.89	2.52		—
nitrate	AgNO ₃	122	170	222	300	376	525	669	952	—
sulphate	Ag ₂ SO ₄	0.57	0.70	0.80	0.89	0.98	1.15	1.30	1.41	—
Sodium acetate	NaC ₂ H ₃ O ₂	36.3	40.8	46.5	54.5	65.5	139	153	170	3
bicarbonate	NaHCO ₃	6.9	8.2	9.6	11.1	12.7	16.4	decomp.	—	—
borate (meta)	NaBO ₂	17	21	25	31	39	62	78	110	4
borate (tetra) (borax)	Na ₂ B ₄ O ₇	1.2	1.8	2.7	3.9	6.0	20.3	31.5	52.5	10
bromate	NaBrO ₃	27	30	35	42	50	63	76	91	—
bromide	NaBr	79.5	83.8	90.5	97.2	105		118	121	2
carbonate	Na ₂ CO ₃	7.1	12.5	21.4	38.8	48.5	46.4	45.8	45.5	10
chlorate	NaClO ₃	80	89	101	113	126	155	189	233	—
chloride	NaCl	35.6	35.7	35.8	36.1	36.4	37.1	38.1	39.8	—
chromate	Na ₂ CrO ₄	31.7	50.2	88.7	88.7	96.0	115	125	126	10
dichromate	Na ₂ Cr ₂ O ₇	163	170	178	196	220	275	380	430	2
dihydrogen phosphate	NaH ₂ PO ₄	58	70	85	107	138	179	207	247	2
ferrocyanide	Na ₄ Fe(CN) ₆	11	15	19	24	30	44	61		—
hydrogen arsenate	Na ₂ HAsO ₄	7.3	15.5	26.5	37	47	65	85		12
hydrogen phosphate	Na ₂ HPO ₄	1.7	3.6	7.7	20.8	51.8	82.9	92.4	102	12
hydroxide	NaOH	42.0	51.5	109	119	129	174		340	4, 3½
iodate	NaIO ₃	2.5	5.6	9.1	13.2		23	27	34	1½
iodide	NaI	159	169	179	196	210	250		302	2

Table A.4. (Continued)

Compound	Formula	Solubility, °C								Stable hydrates, 0–25 °C
		0	10	20	30	40	60	80	100	
Sodium nitrate	NaNO ₃	73	80	88	96	104	124	148	180	—
nitrate	NaNO ₂	72	78	85	92	98		133	163	—
oxalate	Na ₂ C ₂ O ₄	2.7	3.1	3.4	3.8	4.2	5.0	5.7	6.5	—
phosphate	Na ₃ PO ₄	1.5	4	11	20	31	55	81	108	12
pyrophosphate	Na ₄ P ₂ O ₇	3.2	3.9	6.2	10.0	13.5	21.8	30.0	40.3	10
sulphate	Na ₂ SO ₄	4.8	9.0	19.4	40.8	48.8	45.3	43.7	42.5	10
sulphide	Na ₂ S		15.4	18.8	22.5	28.5	39	49		9
sulphite	Na ₂ SO ₃	14.0	18.6	26.0	36.0	37	32	29	27	7
thiocyanate	NaCNS	98	112	134	170	174	186	202	223	1
thiosulphate	Na ₂ S ₂ O ₃	52	61	70	84	103	207	250	266	5
triphosphate	Na ₅ P ₃ O ₁₀	16.3	14.9	14.3	15.2	15.9	17.7			6
Stannous chloride	SnCl ₂	84		270 ^(15°)						—
iodide	SnI ₂			1.0	1.2	1.4	2.1	3.0	4.0	—
sulphate	SnSO ₄			19						—

Strontium acetate	$\text{Sr}(\text{C}_2\text{H}_3\text{O}_2)_2$	36.9	41.6	42	39.5		36.1	36.4	4, $\frac{1}{2}$
bromide	SrBr_2	85	93	102	112	124	150	182	223
chloride	SrCl_2	43.5	47.7	52.9	58.7	65.3	81.8	90.5	101
hydroxide	$\text{Sr}(\text{OH})_2$	0.9	1.2	1.7	2.3	3.2	7.8		8
iodide	SrI_2	164		179		198		370	6
nitrate	$\text{Sr}(\text{NO}_3)_2$	40	54	70	89	90	94	98	101
Thalium chlorate	TlClO_3	2		4			37	57	—
chloride	TlCl	0.21	0.25	0.33	0.42	0.52	0.8	1.2	1.8
hydroxide	TIOH	25.4			39.9	49.5	73.8	106	148
nitrate	TINO_3	3.91	6.22	9.55	14.3	20.9	46.2	111	414
sulphate	Tl_2SO_4	2.7	3.7	4.9	6.2	7.5	10.9	14.6	18.4
Uranyl nitrate	$\text{UO}_2(\text{NO}_3)_2$	97.5	110	125	143	169	252		6
Zinc bromide	ZnBr_2	390	420	440			620	640	670
chlorate	$\text{Zn}(\text{ClO}_3)_2$	145	153	200	209	223			6, 4
nitrate	$\text{Zn}(\text{NO}_3)_2$	95		118		207			6
sulphate	ZnSO_4	42	47	54	61	70		87	81

Table A.5. Solubilities of organic solids in water (g of anhydrous compound per 100 g of water)

Compound	Formula	Solubility, °C								Anhydrous melting point, °C
		0	10	20	30	40	60	80	100	
Acetamide	$\text{CH}_3 \cdot \text{CONH}_2$	138	175	230	310	440	850			81
Acetanilide	$\text{C}_6\text{H}_5\text{NH} \cdot \text{COCH}_3$		0.48	0.52	0.63	0.87	2.1	4.7		114
Adipic acid	$(\text{CH}_2)_4(\text{COOH})_2$	0.8	1.0	1.9	3.0	5.0	18	70	160	153
Alanine (D)	$\text{CH}_3\text{CH} \cdot \text{NH}_2 \cdot \text{COOH}$	12.7	14.2	15.8	17.6	19.6	24.3	30.0	37.3	~300(d.)
Alanine (D,L)	$\text{CH}_3\text{CH} \cdot \text{NH}_2 \cdot \text{COOH}$	12.1	13.8	15.7	17.9	20.3	26.3	33.9	44.0	~300(d.)
<i>o</i> -Aminophenol	$\text{C}_6\text{H}_4 \cdot \text{OH} \cdot \text{NH}_2$	1.7	1.9	2.0	2.2	2.4	2.7	3.0	7.0	173
<i>m</i> -Aminophenol	$\text{C}_6\text{H}_4 \cdot \text{OH} \cdot \text{NO}_2$		2.0	2.7	3.8	5.6	21	280	950	123
<i>p</i> -Aminophenol	$\text{C}_6\text{H}_4 \cdot \text{OH} \cdot \text{NO}_2$	1.1	1.3	1.6	1.9	2.3	3.6	7.9	37	184(d.)
Anthranilic acid (<i>o</i>)	$\text{C}_6\text{H}_4 \cdot \text{NH}_2 \cdot \text{COOH}$		0.3	0.35	0.6	0.9			95	145
Benzamide	$\text{C}_6\text{H}_5 \cdot \text{CONH}_2$		0.6	1.0	1.3	1.6	5	200	800	130
Benzoic acid	$\text{C}_6\text{H}_5 \cdot \text{COOH}$	0.17	0.20	0.29	0.40	0.56	1.16	2.72	5.88	122
Cinnamic acid	$\text{C}_6\text{H}_5 \cdot \text{CH}:\text{CH} \cdot \text{COOH}$		0.03	0.04	0.06				0.59	133
Citric acid*	$\text{C}_3\text{H}_4 \cdot \text{OH} \cdot (\text{COOH})_3$	96	115	137	173	210	280	370	530	153
Dicyandiamide	$\text{NH}_2 \cdot \text{C}(\text{:NH}) \cdot \text{NH} \cdot \text{CN}$	1.3	1.9	3.2	5.0	7.8	19	38		208
Fructose	$\text{CH}_2\text{OH}(\text{CHOH})_3\text{COCH}_2\text{OH}$	75		80		85	90			95–105
Fumaric acid (<i>trans</i>)	$\text{HOOC} \cdot \text{CH}:\text{CH} \cdot \text{COOH}$	0.23	0.35	0.50	0.72	1.1	2.3	5.2	9.8	287
Glucose (α -D) (dextrose)*	$\text{C}_6\text{H}_{12}\text{O}_6$	50	70	90	120	160	290	440		146
Glutamic acid (D)	$\text{COOH}(\text{CH}_2)_2\text{CH} \cdot \text{NH}_2 \cdot \text{COOH}$	0.34	0.50	0.72	1.0	1.5	3.2	6.5	14.0	198(d.)
Glycine	$\text{CH}_2 \cdot \text{NH}_2 \cdot \text{COOH}$	14.2	18.0	22.5	27	33	45	57	70	235(d.)
Hydroquinone (<i>p</i>)	$\text{C}_6\text{H}_4(\text{OH})_2$	4.0	5.4	7.2	9.6	13	35	88	198	170
<i>o</i> -Hydroxybenzoic acid	$\text{C}_6\text{H}_4 \cdot \text{OH} \cdot \text{COOH}$	0.13	0.15	0.20	0.28	0.42	0.91	2.26	8.12	159
<i>m</i> -Hydroxybenzoic acid	$\text{C}_6\text{H}_4 \cdot \text{OH} \cdot \text{COOH}$	0.35	0.55	0.86	1.3	2.0	4.5	12.4	58.7	200
<i>p</i> -Hydroxybenzoic acid	$\text{C}_6\text{H}_4 \cdot \text{OH} \cdot \text{COOH}$	0.25	0.35	0.53	0.80	1.25	4.29	13.7	49.9	215

Lactose*	C ₁₂ H ₂₂ O ₁₁	12.2	15.0	19.5	25.2	33.3	57.5	102	153	202
Maleic acid	HOOC · CH · COOH	39.3	50	70	90	115	178	283		130
Malic acid (D,L)	CH · OH · CH ₂ (COOH) ₂	89	105	126	150	180	270	460		128
Malonic acid	CH ₂ (COOH) ₂	108	128	153	180	212	292	455	810	135(d.)
Maltose*	C ₁₂ H ₂₂ O ₁₁	57	65	78	93	110	175	300		
Mannitol (D)	(CH ₂ OH) ₂ (CHOH) ₄	10.4	13.7	18.6	25.2	34.6	64.4	115	197	166
Melamine	C ₃ N ₃ (NH ₂) ₃	0.12	0.18	0.27	0.42	0.71	1.5	2.8	5.0	~250
Oxalic acid [†]	(COOH) ₂	3.5	6.0	9.5	14.5	21.6	44.3	84.4		189
Pentaerythritol	C(CH ₂ OH) ₄	3.0	4.0	5.8	8.2	11.4	21	40	80	262
Phenacetin (p)	C ₂ H ₅ O · C ₆ H ₄ · NHCOCH ₃			0.07					1.43	135
Phthalic acid (o)	C ₆ H ₄ (COOH) ₂	0.23	0.36	0.56	0.8	1.2	2.8	6.3	18.0	208
Picric acid (2,4,6)	C ₆ H ₂ · OH · (NO ₂) ₃	1.0	1.1	1.2	1.5	1.9	3.1	4.6	7.2	122
Pyrocatechol (o)	C ₆ H ₄ (OH) ₂			45.1		172	412	1120	8360	104
Raffinose [‡]	C ₁₈ H ₃₂ O ₁₆	3.4	6.6	13.6	27.1	49.9	86.9	153.8		118
Resorcinol (m)	C ₆ H ₄ (OH) ₂	66.2	85	123	170	225	390	634	1060	111
Salicylic acid (o)	C ₆ H ₄ · OH · COOH	0.13	0.15	0.20	0.28	0.42	0.91	2.26	8.12	159
Sorbitol	CH ₂ OH · (CHOH) ₄ · CH ₂ OH		179	222	275	355				95–100
Succinic acid	(CH ₂ · COOH) ₂	2.8	4.4	6.9	10.5	16.2	35.8	70.8	127	183
Succinimide	(CH ₂ CO) ₂ NH	10	16	26	48	83	140	213		125
Sucrose	C ₁₂ H ₂₂ O ₁₁	179	190	204	219	238	287	362	487	170–186(d.)
Sulphanilic acid (p)	C ₆ H ₄ · NH ₂ · SO ₃ H	0.45	0.80	1.12		2.03	3.01	4.51	6.67	> 280(d.)
Tartaric acid (D or L)	(CHOH · COOH) ₂	115	126	139	156	176	220	273	343	170
Tartaric acid (racemic)*	(CHOH · COOH) ₂	8.2	12.3	18.0	25.2	37.0	64.5	98.1	138	205
Taurine	NH ₂ CH ₂ CH ₂ SO ₃ H	3.9	6.0	8.8	12.4	16.8	27.4	38.4	45.7	~330(d.)
Thiourea	NH ₂ · CS · NH ₂	4.9	8.0	13.6	20.1	30.8	71	138	238	181
Triglycine sulphate	(NH ₂ CH ₂ COOH) ₃ H ₂ SO ₄	12	20	27	36	45	75			
Urea	NH ₂ · CO · NH ₂	67	85	105	135	165	250	400	730	133
Uric acid	C ₅ H ₄ O ₃ N ₄	0.002	0.004	0.006	0.009	0.012	0.023	0.039	0.062	(D)

* Crystallizes from water with 1H₂O † Crystallizes from water with 2H₂O ‡ Crystallizes from water with 5H₂O d = decomposes

Table A.6. Densities of crystalline inorganic solids

<i>Substance</i>		<i>Formula</i>	<i>Crystal system</i>	<i>Density g cm⁻³</i>
Aluminium	bromide	$\text{AlBr}_3 \cdot 6\text{H}_2\text{O}$		2.54
	chloride	$\text{AlCl}_3 \cdot 6\text{H}_2\text{O}$		2.40
	sulphide	Al_2S_3	hexagonal	2.02
	sulphate	$\text{Al}_2(\text{SO}_4)_3 \cdot 18\text{H}_2\text{O}$	monoclinic	1.69
Ammonium	acetate	$\text{NH}_4\text{C}_2\text{H}_3\text{O}_2$		1.17
	alum	$\text{NH}_4\text{Al}(\text{SO}_4)_2 \cdot 12\text{H}_2\text{O}$	octahedral	1.64
	arsenite (<i>o</i>)	$(\text{NH}_4)_2\text{HAsO}_4$	monoclinic	1.99
	bicarbonate	NH_4HCO_3	monoclinic	1.58
	bisulphate	NH_4HSO_4		1.78
	bisulphite	NH_4HSO_3		2.03
	bromide	NH_4Br	cubic	2.43
	chlorate	NH_4ClO_3		1.80
	chloride	NH_4Cl	cubic	1.53
	chromate	$(\text{NH}_4)_2\text{CrO}_4$	monoclinic	1.91
	cyanate	NH_4CNO		1.34
	dichromate	$(\text{NH}_4)_2\text{Cr}_2\text{O}_7$	monoclinic	2.15
	dihydrogen phosphate	$\text{NH}_4\text{H}_2\text{PO}_4$	tetragonal	1.80
	hydrogen phosphate	$(\text{NH}_4)_2\text{HPO}_4$	monoclinic	1.62
	iodate	NH_4IO_3	monoclinic	3.31
	iodide	NH_4I	cubic	2.51
	nitrate	NH_4NO_3	orthorhombic	1.73
	nitrite	NH_4NO_2		1.69
Barium	oxalate	$(\text{NH}_4)_2\text{C}_2\text{O}_4 \cdot \text{H}_2\text{O}$	orthorhombic	1.50
	perchlorate	NH_4ClO_4	orthorhombic	1.95
	permanganate	NH_4MnO_4		2.21
	sulphate	$(\text{NH}_4)_2\text{SO}_4$	orthorhombic	1.77
	thiocyanate	NH_4CNS	monoclinic	1.31
	thiosulphate	$(\text{NH}_4)_2\text{S}_2\text{O}_3$	monoclinic	1.68
	vanadate	NH_4VO_3		2.33
	acetate	$\text{Ba}(\text{C}_2\text{H}_3\text{O}_2)_2 \cdot 3\text{H}_2\text{O}$	triclinic	2.19
	bromate	$\text{Ba}(\text{BrO}_3)_2 \cdot \text{H}_2\text{O}$	monoclinic	3.99
	bromide	$\text{BaBr}_2 \cdot 2\text{H}_2\text{O}$	monoclinic	3.58
	carbonate	BaCO_3	orthorhombic	4.43
	chlorate	$\text{Ba}(\text{ClO}_3)_2 \cdot \text{H}_2\text{O}$	monoclinic	3.18
	chloride	$\text{BaCl}_2 \cdot 2\text{H}_2\text{O}$	monoclinic	3.10
	chromate	BaCrO_4	orthorhombic	4.50
	hydroxide	$\text{Ba}(\text{OH})_2 \cdot 8\text{H}_2\text{O}$	monoclinic	2.18
	iodate	$\text{Ba}(\text{IO}_3)_2$	monoclinic	5.00
	iodide	$\text{BaI}_2 \cdot 2\text{H}_2\text{O}$	hexagonal	5.15
	nitrate	$\text{Ba}(\text{NO}_3)_2$	cubic	3.24
	oxalate	BaC_2O_4		2.66
	perchlorate	$\text{Ba}(\text{ClO}_4)_2 \cdot 3\text{H}_2\text{O}$	hexagonal	2.74
	sulphate	BaSO_4	orthorhombic	4.50
	titanate	BaTiO_3	cubic	6.02

Beryllium	chloride	BeCl_2	orthorhombic	1.90
	nitrate	$\text{Be}(\text{NO}_3)_2 \cdot 3\text{H}_2\text{O}$		1.56
	sulphate	BeSO_4		2.44
		$\text{BeSO}_4 \cdot 4\text{H}_2\text{O}$	tetragonal	1.71
Borax		$\text{Na}_2\text{B}_4\text{O}_7 \cdot 10\text{H}_2\text{O}$	monoclinic	1.73
Boric	acid	H_3BO_3	triclinic	1.44
Cadmium	acetate	$\text{Cd}(\text{C}_2\text{H}_3\text{O}_2)_2 \cdot 3\text{H}_2\text{O}$	monoclinic	2.01
	borate	$\text{Cd}(\text{BO}_3)_2 \cdot \text{H}_2\text{O}$	orthorhombic	3.76
	bromide	CdBr_2	hexagonal	5.19
	carbonate	CdCO_3	trigonal	4.26
	chlorate	$\text{Cd}(\text{ClO}_3)_2 \cdot 2\text{H}_2\text{O}$		2.28
	chloride	CdCl_2	trigonal	4.05
		$\text{CdCl}_2 \cdot 2\frac{1}{2}\text{H}_2\text{O}$	monoclinic	2.84
	iodate	$\text{Cd}(\text{IO}_3)_2$		6.43
	iodide	CdI_2	hexagonal	5.67
	nitrate	$\text{Cd}(\text{NO}_3)_2 \cdot 4\text{H}_2\text{O}$		2.46
	sulphate	$\text{CdSO}_4 \cdot \text{H}_2\text{O}$	monoclinic	3.79
		$\text{CdSO}_4 \cdot 7\text{H}_2\text{O}$	monoclinic	2.48
	sulphide	CdS	hexagonal	4.82
Caesium	chloride	CsCl	cubic	3.99
	chlorate	CsClO_3	cubic	3.57
	iodate	CsIO_3	monoclinic	4.85
	iodide	CsI	monoclinic	4.51
	nitrate	CsNO_3	cubic	3.69
	perchlorate	CsClO_4	cubic	3.33
	sulphate	Cs_2SO_4	hexagonal	4.24
Calcium	bromide	CaBr_2	orthorhombic	3.55
		$\text{CaBr}_2 \cdot 6\text{H}_2\text{O}$	hexagonal	2.30
	carbonate (calcite)	CaCO_3	trigonal	2.71
	chlorate	$\text{Ca}(\text{ClO}_3)_2 \cdot 2\text{H}_2\text{O}$	orthorhombic	2.71
	chloride	$\text{CaCl}_2 \cdot 6\text{H}_2\text{O}$	trigonal	1.71
	fluoride	CaF_2	cubic	3.18
	iodide	$\text{CaI}_2 \cdot 6\text{H}_2\text{O}$	hexagonal	2.55
	nitrate	$\text{Ca}(\text{NO}_3)_2 \cdot 4\text{H}_2\text{O}$	monoclinic	1.90
	oxalate	$\text{CaC}_2\text{O}_4 \cdot \text{H}_2\text{O}$	cubic	2.2
	sulphate	$\text{CaSO}_4 \cdot 2\text{H}_2\text{O}$	monoclinic	2.32
	thiosulphate	$\text{CaS}_2\text{O}_3 \cdot 6\text{H}_2\text{O}$	triclinic	1.87
Cobalt	bromide	$\text{CoBr}_2 \cdot 6\text{H}_2\text{O}$		2.46
	chlorate	$\text{Co}(\text{ClO}_3)_2 \cdot 6\text{H}_2\text{O}$	cubic	1.92
	chloride	$\text{CoCl}_2 \cdot 6\text{H}_2\text{O}$	monoclinic	1.92
	iodate	$\text{Co}(\text{IO}_3)_2 \cdot 6\text{H}_2\text{O}$	octahedral	3.69
	iodide	$\text{CoI}_2 \cdot 6\text{H}_2\text{O}$	hexagonal	2.90
	nitrate	$\text{Co}(\text{NO}_3)_2 \cdot 6\text{H}_2\text{O}$	monoclinic	1.87
	sulphate	$\text{CoSO}_4 \cdot 7\text{H}_2\text{O}$	monoclinic	1.95
	sulphide	CoS_2	cubic	4.27

Table A.6. (Continued)

<i>Substance</i>		<i>Formula</i>	<i>Crystal system</i>	<i>Density g cm⁻³</i>
Copper	bromate	Cu(BrO ₃) ₂ · 6H ₂ O	cubic	2.6
	bromide	CuBr ₂	monoclinic	4.77
	carbonate	CuCO ₃	hexagonal	4.00
	chloride	CuCl ₂ · 2H ₂ O	orthorhombic	2.54
	iodate	Cu(IO ₃) ₂	monoclinic	5.24
	iodide	CuI	cubic	5.6
	nitrate	Cu(NO ₃) ₂ · 6H ₂ O		2.07
	sulphate	CuSO ₄ · 5H ₂ O	triclinic	2.28
Ferrous	ammonium sulphate	FeSO ₄ (NH ₄) ₂ SO ₄ · 6H ₂ O	monoclinic	1.86
	bromide	FeBr ₂	hexagonal	4.64
	chloride	FeCl ₂ · 2H ₂ O	monoclinic	2.36
		FeCl ₂ · 4H ₂ O	monoclinic	1.93
	sulphate	FeSO ₄ · 7H ₂ O	monoclinic	1.90
		FeSO ₄ · H ₂ O	monoclinic	2.97
Ferric	ammonium sulphate	FeNH ₄ (SO ₄) ₂ · 12H ₂ O	octahedral	1.71
	iodate	FeI(O ₃) ₂		4.8
	nitrate	Fe(NO ₃) ₃ · 9H ₂ O	monoclinic	1.68
	sulphate	Fe ₂ (SO ₄) ₃ · 9H ₂ O	orthorhombic	2.10
Lead	acetate	Pb(C ₂ H ₃ O ₂) ₂ · 3H ₂ O	monoclinic	2.55
	bromate	Pb(BrO ₃) ₂ · H ₂ O	monoclinic	5.53
	bromide	PbBr ₂	orthorhombic	6.63
	chlorate	Pb(ClO ₃) ₂ · H ₂ O	monoclinic	4.04
	chloride	PbCl ₂	orthorhombic	5.85
	chromate	PbCrO ₄	monoclinic	6.10
	fluoride	PbF ₂	orthorhombic	8.24
	iodate	Pb(IO ₃) ₂	hexagonal	6.16
	iodide	PbI ₂	hexagonal	6.16
	nitrate	Pb(NO ₃) ₂	cubic	4.53
	oxalate	PbC ₂ O ₄		5.28
	sulphate	PbSO ₄	monoclinic	6.20
Lithium	sulphide	PbS	cubic	7.50
	bromide	LiBr	cubic	3.46
	carbonate	Li ₂ CO ₃	monoclinic	2.11
	chloride	LiCl	cubic	2.07
		LiCl · H ₂ O	tetragonal	1.78
	fluoride	LiF	cubic	2.64
	hydroxide	LiOH · H ₂ O	monoclinic	1.51
	iodate	LiIO ₃	hexagonal	4.45
	iodide	LiI · 3H ₂ O	hexagonal	3.48
	nitrate	LiNO ₃	trigonal	2.38
	oxalate	Li ₂ C ₂ O ₄	orthorhombic	2.12
	sulphate	Li ₂ SO ₄	monoclinic	2.22

Magnesium	acetate	$\text{Mg}(\text{C}_2\text{H}_3\text{O}_2)_2$	orthorhombic	1.42
		$\text{Mg}(\text{C}_2\text{H}_3\text{O}_2)_2 \cdot 4\text{H}_2\text{O}$	monoclinic	1.45
	ammonium sulphate	$\text{MgSO}_4 \cdot (\text{NH}_4)_2\text{SO}_4 \cdot 6\text{H}_2\text{O}$	monoclinic	2.21
	bromate	$\text{Mg}(\text{BrO}_3)_2 \cdot 6\text{H}_2\text{O}$	cubic	2.29
	bromide	$\text{MgBr}_2 \cdot 6\text{H}_2\text{O}$	hexagonal	2.00
	chlorate	$\text{Mg}(\text{ClO}_3)_2 \cdot 6\text{H}_2\text{O}$	orthorhombic	1.80
	chloride	$\text{MgCl}_2 \cdot 6\text{H}_2\text{O}$	monoclinic	1.59
	iodate	$\text{Mg}(\text{IO}_3)_2 \cdot 4\text{H}_2\text{O}$	monoclinic	3.30
	nitrate	$\text{Mg}(\text{NO}_3)_2 \cdot 6\text{H}_2\text{O}$	monoclinic	1.64
	oxalate	$\text{MgC}_2\text{O}_4 \cdot 2\text{H}_2\text{O}$		2.45
	perchlorate	$\text{Mg}(\text{ClO}_4)_2 \cdot 6\text{H}_2\text{O}$	orthorhombic	1.80
	sulphate	MgSO_4	orthorhombic	2.66
	sulphide	$\text{MgSO}_4 \cdot 7\text{H}_2\text{O}$	orthorhombic	1.68
	sulphite	MgS	cubic	2.84
		$\text{MgSO}_3 \cdot 6\text{H}_2\text{O}$	orthorhombic	1.74
Manganese	acetate	$\text{Mn}(\text{C}_2\text{H}_3\text{O}_2)_2 \cdot 4\text{H}_2\text{O}$	monoclinic	1.59
	carbonate	MnCO_3	orthorhombic	3.13
	chloride	$\text{MnCl}_2 \cdot 4\text{H}_2\text{O}$	monoclinic	2.01
	nitrate	$\text{Mn}(\text{NO}_3)_2 \cdot 4\text{H}_2\text{O}$	monoclinic	1.82
	oxalate	MnC_2O_4		2.43
	sulphate	$\text{MnSO}_4 \cdot 7\text{H}_2\text{O}$	monoclinic	2.09
	sulphide	MnS	cubic	3.46
Mercuric	acetate	$\text{Hg}(\text{C}_2\text{H}_3\text{O}_2)_2$		3.27
	bromide	HgBr_2	orthorhombic	6.11
	chlorate	$\text{Hg}(\text{ClO}_3)_2$		5.00
	chloride	HgCl_2	orthorhombic	5.44
	fluoride	HgF_2	cubic	8.95
	iodide (α)	HgI_2	tetragonal	6.36
	iodide (β)	HgI_2	orthorhombic	6.09
	nitrate	$\text{Hg}(\text{NO}_3)_2 \cdot \text{H}_2\text{O}$		4.30
	sulphate	HgSO_4	orthorhombic	6.47
	sulphide (α)	HgS	hexagonal	8.10
	sulphide (β)	HgS	cubic	7.73
Mercurous	bromide	Hg_2Br_2	tetragonal	7.31
	chlorate	$\text{Hg}_2(\text{ClO}_3)_2$	orthorhombic	6.41
	chloride	Hg_2Cl_2	tetragonal	7.15
	fluoride	Hg_2F_2	cubic	8.73
	iodide	HgI_3	tetragonal	7.70
	nitrate	$\text{Hg}_2(\text{NO}_3)_2 \cdot 2\text{H}_2\text{O}$	monoclinic	4.79
	sulphate	Hg_2SO_4	monoclinic	7.56
Nickel	acetate	$\text{Ni}(\text{C}_2\text{H}_3\text{O}_2)_2 \cdot 4\text{H}_2\text{O}$	monoclinic	1.74
	ammonium sulphate	$\text{Ni}(\text{NH}_4)_2(\text{SO}_4)_2 \cdot 6\text{H}_2\text{O}$	monoclinic	1.92
	bromate	$\text{Ni}(\text{BrO}_3)_2 \cdot 6\text{H}_2\text{O}$	monoclinic	2.57
	bromide	NiBr_2	hexagonal	5.10
	carbonate	NiCO_3	cubic	2.6
	chlorate	$\text{Ni}(\text{ClO}_3)_2 \cdot 6\text{H}_2\text{O}$		2.07
	chloride	$\text{NiCl}_2 \cdot 2\text{H}_2\text{O}$	orthorhombic	2.58

Table A.6. (Continued)

<i>Substance</i>		<i>Formula</i>	<i>Crystal system</i>	<i>Density g cm⁻³</i>
	iodate	Ni(IO ₃) ₂		5.07
	iodide	NiI ₂	hexagonal	5.83
	nitrate	Ni(NO ₃) ₂ · 6H ₂ O	monoclinic	2.05
	sulphate	NiSO ₄ · 6H ₂ O	tetragonal	2.07
		NiSO ₄ · 7H ₂ O	orthorhombic	1.95
Potassium	acetate	KC ₂ H ₃ O ₂	monoclinic	1.57
	aluminium sulphate	KAl(SO ₄) ₂ · 12H ₂ O	octahedral	1.76
	bicarbonate	KHCO ₃	monoclinic	2.17
	bisulphate	KHSO ₄	orthorhombic	2.32
	bromate	KBrO ₃	trigonal	3.27
	bromide	KBr	cubic	2.75
	carbonate	K ₂ CO ₃ · 1½H ₂ O	monoclinic	2.04
	chlorate	KClO ₃	monoclinic	2.32
	chloride	KCl	cubic	1.98
	chromate	K ₂ CrO ₄	orthorhombic	2.73
	dichromate	K ₂ Cr ₂ O ₇	monoclinic	2.68
	dihydrogen phosphate	KH ₂ PO ₄	tetragonal	2.30
	ferricyanide	K ₃ Fe(CN) ₆	monoclinic	1.85
	ferrocyanide	K ₄ Fe(CN) ₆ · 3H ₂ O	monoclinic	1.85
	fluoride	KF	cubic	2.48
	formate	KCHO ₂	orthorhombic	1.91
	hydrogen oxalate	KHC ₂ O ₄	monoclinic	2.04
	hydrogen tartrate	KHC ₄ H ₄ O ₆	orthorhombic	1.98
	hydroxide	KOH	orthorhombic	2.04
	iodate	KIO ₃	monoclinic	3.93
	iodide	KI	cubic	3.13
	nitrate	KNO ₃	orthorhombic	2.11
	nitrite	KNO ₂	monoclinic	1.92
	oxalate	K ₂ C ₂ O ₄ · H ₂ O	monoclinic	2.13
	perchlorate	KClO ₄	orthorhombic	2.52
	permanganate	KMnO ₄	orthorhombic	2.70
	sodium tartrate	KNaC ₄ H ₄ O ₆ · 4H ₂ O	triclinic	1.79
	sulphate	K ₂ SO ₄	orthorhombic	2.66
	sulphide	K ₂ S	cubic	1.81
	thiocyanate	KCNS	orthorhombic	1.89
	thiosulphate	K ₂ S ₂ O ₃ · ½H ₂ O	monoclinic	2.23
Rubidium	bromate	RbBrO ₃	cubic	3.68
	bromide	RbBr	cubic	3.35
	chlorate	RbClO ₃	orthorhombic	3.19
	chloride	RbCl	cubic	2.80
	chromate	Rb ₂ CrO ₄	orthorhombic	3.52
	dichromate	Rb ₂ Cr ₂ O ₇	triclinic	3.13
	iodate	RbIO ₃	cubic	4.33
	iodide	RbI	cubic	3.55
	nitrate	RbNO ₃	cubic	3.11

	perchlorate	RbClO_4	orthorhombic	2.80
	sulphate	Rb_2SO_4	orthorhombic	3.61
	sulphide	Rb_2S		2.91
Silver	acetate	$\text{AgC}_2\text{H}_3\text{O}_2$		3.26
	bromate	AgBrO_3	tetragonal	5.21
	bromide	AgBr		6.47
	chlorate	AgClO_3	tetragonal	4.43
	chloride	AgCl	cubic	5.56
	iodate	AgIO_3	orthorhombic	5.53
	iodide	AgI	cubic	6.01
	nitrate	AgNO_3	orthorhombic	4.35
	oxalate	$\text{Ag}_2\text{C}_2\text{O}_4$		5.03
	sulphate	Ag_2SO_4	orthorhombic	5.45
	sulphide	Ag_2S	orthorhombic	7.33
Sodium	acetate	$\text{NaC}_2\text{H}_3\text{O}_2 \cdot 3\text{H}_2\text{O}$	monoclinic	1.45
	arsenate	$\text{Na}_3\text{AsO}_4 \cdot 12\text{H}_2\text{O}$	trigonal	1.76
	bicarbonate	NaHCO_3	monoclinic	2.16
	borate (tetra)	$\text{Na}_2\text{B}_4\text{O}_7 \cdot 10\text{H}_2\text{O}$	monoclinic	1.73
	borate (tetra)	$\text{Na}_2\text{B}_4\text{O}_7 \cdot 5\text{H}_2\text{O}$	monoclinic	1.82
	borate (meta)	$\text{NaBO}_2 \cdot 4\text{H}_2\text{O}$	triclinic	1.74
	bromate	Na_2BrO_3	cubic	3.34
	bromide	$\text{NaBr} \cdot 2\text{H}_2\text{O}$	monoclinic	2.18
	carbonate	$\text{Na}_2\text{CO}_3 \cdot 10\text{H}_2\text{O}$	monoclinic	1.44
	carbonate	$\text{Na}_2\text{CO}_3 \cdot \text{H}_2\text{O}$	orthorhombic	2.26
	chlorate	NaClO_3	cubic	2.49
	chloride	NaCl	cubic	2.17
	chlorite	$\text{NaClO}_2 \cdot 3\text{H}_2\text{O}$	triclinic	1.72
	chromate	$\text{Na}_2\text{CrO}_4 \cdot 10\text{H}_2\text{O}$	monoclinic	1.48
	citrate	$\text{C}_6\text{H}_5\text{O}_7\text{Na}_3$	orthorhombic	1.70
	cyanide	NaCN	orthorhombic	1.66
	dichromate	$\text{Na}_2\text{Cr}_2\text{O}_7 \cdot 2\text{H}_2\text{O}$	monoclinic	2.52
	dihydrogen phosphate	$\text{NaH}_2\text{PO}_4 \cdot 2\text{H}_2\text{O}$	orthorhombic	1.90
	ferrocyanide	$\text{Na}_4\text{Fe}(\text{CN})_6 \cdot 10\text{H}_2\text{O}$	monoclinic	1.46
	fluoride	NaF	cubic	2.56
	hydrogen arsenate	$\text{Na}_2\text{HAsO}_4 \cdot 7\text{H}_2\text{O}$	monoclinic	1.87
	hydrogen arsenate	$\text{Na}_2\text{HAsO}_4 \cdot 12\text{H}_2\text{O}$	monoclinic	1.74
	hydrogen phosphate	$\text{Na}_2\text{HPO}_4 \cdot 12\text{H}_2\text{O}$	orthorhombic	1.52
	hydroxide	NaOH	orthorhombic	2.13
	iodate	NaIO_3	orthorhombic	4.28
	iodide	$\text{NaI} \cdot 2\text{H}_2\text{O}$	monoclinic	2.45
	nitrate	NaNO_3	trigonal	2.26
	nitrite	NaNO_2	orthorhombic	2.17
	oxalate	$\text{Na}_2\text{C}_2\text{O}_4$	monoclinic	2.34
	perborate	NaBO_3	triclinic	1.73
	perchlorate	NaClO_4	orthorhombic	2.48
	perchlorate	$\text{NaClO}_4 \cdot \text{H}_2\text{O}$	monoclinic	2.10
	periodate	NaIO_4	tetragonal	4.12
	phosphate	$\text{Na}_3\text{PO}_4 \cdot 12\text{H}_2\text{O}$	trigonal	1.62
	potassium tartrate	$\text{NaKC}_4\text{H}_4\text{O}_6 \cdot 4\text{H}_2\text{O}$	triclinic	1.79

Table A.6. (Continued)

<i>Substance</i>		<i>Formula</i>	<i>Crystal system</i>	<i>Density g cm⁻³</i>
	pyrophosphate	Na ₄ P ₂ O ₇ · 10H ₂ O	monoclinic	1.82
	sulphate	Na ₂ SO ₄ · 10H ₂ O	monoclinic	1.46
	sulphide	Na ₂ S · 9H ₂ O	tetragonal	1.43
	sulphite	Na ₂ SO ₃ · 7H ₂ O	monoclinic	1.54
	thiosulphate	Na ₂ S ₂ O ₃ · 5H ₂ O	monoclinic	1.73
	triphsophate	Na ₅ P ₃ O ₁₀ · 6H ₂ O	triclinic	2.10
Stannous	bromide	SnBr ₂	orthorhombic	5.12
	chloride	SnCl ₂	orthorhombic	3.95
	iodide	SnI ₂	monoclinic	5.29
	sulphate	SnSO ₄ · 2H ₂ O	hexagonal	—
Strontium	acetate	Sr(C ₂ H ₃ O ₂) ₂		2.10
	bromate	Sr(BrO ₃) ₂ · H ₂ O	monoclinic	3.77
	bromide	SrBr ₂ · 6H ₂ O	hexagonal	2.39
	carbonate	SrCO ₃	orthorhombic	3.70
	chlorate	Sr(ClO ₃) ₂	orthorhombic	3.15
	chloride	SrCl ₂ · 6H ₂ O	trigonal	1.93
	hydroxide	Sr(OH) ₂ · 8H ₂ O	tetragonal	1.90
	iodate	Sr(IO ₃) ₂	triclinic	5.05
	iodide	SrI ₂ · 6H ₂ O	hexagonal	2.67
	nitrate	Sr(NO ₃) ₂ · 4H ₂ O	monoclinic	2.2
	sulphate	SrSO ₄	orthorhombic	3.96
	sulphide	SrS	cubic	3.70
Thallium	bromide	TlBr	cubic	7.56
	carbonate	Tl ₂ CO ₃	monoclinic	7.11
	chlorate	TlClO ₃	orthorhombic	5.05
	chloride	TlCl	cubic	7.00
	iodide	TlI	cubic	7.29
	nitrate	TlNO ₃	orthorhombic	5.56
	oxalate	Tl ₂ C ₂ O ₄	monoclinic	6.31
	sulphate	Tl ₂ SO ₄	orthorhombic	6.77
	sulphide	Tl ₂ S	tetragonal	8.46
Uranyl	acetate	UO ₂ (C ₂ H ₃ O ₂) ₂ · 2H ₂ O	orthorhombic	2.89
	nitrate	UO ₂ (NO ₃) ₂ · 6H ₂ O	orthorhombic	2.81
Zinc	acetate	Zn(C ₂ H ₃ O ₂) ₂ · 2H ₂ O	monoclinic	1.74
	bromate	Zn(BrO ₃) ₂ · 6H ₂ O	cubic	2.57
	bromide	ZnBr ₂	orthorhombic	4.20
	chlorate	Zn(ClO ₃) ₂ · 4H ₂ O	cubic	2.15
	chloride	ZnCl ₂	hexagonal	2.91
	iodate	Zn(IO ₃) ₂ · 2H ₂ O		4.22
	iodide	ZnI ₂	hexagonal	4.74
	nitrate	Zn(NO ₃) ₂ · 6H ₂ O	tetragonal	2.07
	sulphate	ZnSO ₄ · 7H ₂ O	orthorhombic	1.96
	sulphide	ZnS		3.98

Table A.7. Densities of crystalline organic solids

Substance	Formula	Crystal system	Density g cm ⁻³
Acetamide	CH ₃ · CONH ₂	trigonal	0.999
Acetanilide	C ₆ H ₅ NH · COCH ₃	orthorhombic	1.21
Acetylsalicylic acid	C ₆ H ₄ · OCOCH ₃ · COOH	monoclinic	1.39
Adipic acid	(CH ₂) ₄ (COOH) ₂	monoclinic	1.36
Alanine (DL)	CH ₃ · CH · NH ₂ · COOH	orthorhombic	1.40
<i>o</i> -Aminophenol	C ₆ H ₄ · OH · NO ₂	orthorhombic	1.29
<i>m</i> -Aminophenol	C ₆ H ₄ · OH · NO ₂	orthorhombic	1.28
<i>p</i> -Aminophenol	C ₆ H ₄ · OH · NO ₂	orthorhombic	1.30
Anthracene	C ₁₄ H ₁₀	monoclinic	1.25
Benzamide	C ₆ H ₅ · CONH ₂	monoclinic	1.08
Benzoic acid	C ₆ H ₅ · COOH	monoclinic	1.27
Cinnamic acid (<i>trans</i>)	C ₆ H ₅ · CH:CH · COOH	monoclinic	1.25
Citric acid	C ₃ H ₄ · OH · (COOH) ₃ · H ₂ O	orthorhombic	1.54
Cresol (<i>o</i>)	C ₆ H ₄ · OH · CH ₃	trigonal	1.05
Dicyandiamide	NH ₂ · C(NH) · NH · CN	orthorhombic	1.40
Fructose (D)	C ₆ H ₁₂ O ₆	orthorhombic	1.60
Fumaric acid (<i>trans</i>)	HOOC · CH:CH · COOH	monoclinic	1.64
Glucose (dextrose)	C ₆ H ₁₂ O ₆ · H ₂ O	orthorhombic	1.56
Glutamic acid (D)	(CH ₂) ₂ · CH · NH ₂ · (COOH) ₂		1.54
Glycine	CH ₂ · NH ₂ · COOH	monoclinic	0.83
Hydroquinone (<i>p</i>)	C ₆ H ₄ (OH) ₂	monoclinic	1.33
<i>o</i> -Hydroxybenzoic acid	C ₆ H ₄ · OH · COOH	monoclinic	1.44
<i>m</i> -Hydroxybenzoic acid	C ₆ H ₄ · OH · COOH	orthorhombic	1.47
<i>p</i> -Hydroxybenzoic acid	C ₆ H ₄ · OH · COOH	orthorhombic	1.47
Lactose	C ₁₂ H ₂₂ O ₁₁ · H ₂ O	monoclinic	1.59
Maleic acid (<i>cis</i>)	HOOC · CH:CH · COOH	monoclinic	1.59
Malic acid	HOOC · CH ₂ · CH(OH) · COOH		1.60
Maltose	C ₁₂ H ₂₂ O ₁₁ · H ₂ O		1.54
Melamine	C ₃ N ₃ (NH ₂) ₃	monoclinic	1.57
Mannitol (D)	(CH ₂ OH) ₂ (CHOH) ₄	orthorhombic	1.49
Naphthalene	C ₁₀ H ₈	monoclinic	1.15
Oxalic acid	(COOH) ₂ · 2H ₂ O	monoclinic	1.90
Pentaerythritol	C(CH ₂ OH) ₄	tetragonal	1.39
Phenol	C ₆ H ₅ OH	orthorhombic	1.07
Phthalic acid (<i>o</i>)	C ₆ H ₄ (COOH) ₂	monoclinic	1.59
Pyrocatechol (<i>o</i>)	C ₆ H ₄ (OH) ₂	monoclinic	1.37
Raffinose	C ₁₈ H ₃₂ O ₁₆ · 5H ₂ O	orthorhombic	1.47
Resorcinol (<i>m</i>)	C ₆ H ₄ (OH) ₂	orthorhombic	1.27
Salicylic acid (<i>o</i>)	C ₆ H ₄ · OH · COOH	monoclinic	1.44
Salol (<i>o</i>)	C ₆ H ₄ · OH · COOC ₆ H ₅	orthorhombic	1.26
Succinic acid	(CH ₂ · COOH) ₂	monoclinic	1.57
Succinimide	(CH ₂ CO) ₂ NH	orthorhombic	1.42
Sucrose	C ₁₂ H ₂₂ O ₁₁	monoclinic	1.59
Sulphanilic acid (<i>p</i>)	C ₆ H ₄ · NH ₂ · SO ₃ H	orthorhombic	1.49
Tartaric acid (racemic)	(CHOH · COOH) ₂ · H ₂ O	monoclinic	1.79
Thiourea	NH ₂ · CS · NH ₂	orthorhombic	1.41
Triglycine sulphate	(NH ₂ CH ₂ COOH) ₃ H ₂ SO ₄	monoclinic	1.68
Urea	NH ₂ · CO · NH ₂	tetragonal	1.33
Uric acid	C ₅ H ₄ O ₃ N ₄		1.89

Table A.8. Densities of some saturated aqueous solutions

	Solute	Densities (g cm^{-3}) at different temperatures ($^{\circ}\text{C}$)									
		0	10	20	30	40	50	60	70	80	90
Aluminium	potassium sulphate	1.03	1.04	1.05	1.07	1.10	1.14	1.21	1.29	1.44	
	sodium sulphate	1.26	1.30	1.31	1.33	1.31	1.32				
	thallium sulphate	1.03	1.04	1.06	1.08	1.12	1.18	1.28			
Ammonium	aluminium sulphate	1.03	1.04	1.05	1.06	1.09	1.12	1.17	1.21	1.29	
	benzoate			1.03	1.05						
	bromide		1.28	1.30							
	chloride	1.066	1.072	1.076	1.069	1.086	1.086	1.086	1.086	1.087	1.102
	dihydrogen phosphate	1.13	1.14	1.16	1.18	1.21	1.24	1.27	1.30		
	hydrogen phosphate		1.34								
	iodate		1.01	1.02							
	nitrate	1.26	1.29	1.31	1.33	1.35					
	oxalate		1.017	1.017	1.021	1.029	1.034				
	perchlorate	1.06	1.08	1.10	1.12	1.13	1.15	1.16	1.17	1.19	1.20
Barium	salicylate			1.14	1.15						
	sulphate	1.243	1.245	1.246	1.248	1.248	1.252	1.252	1.255		
	sulphite	1.18	1.19	1.20	1.21	1.22	1.23	1.24	1.26	1.27	
	bromide		1.70	1.73	1.75	1.76	1.80		1.90		2.10
	bromate		1.001	1.002	1.004						
	chlorate	1.20	1.23	1.27	1.32	1.36	1.40	1.43	1.47	1.51	1.55
	chloride		1.27	1.29	1.31	1.32	1.33				
	iodate		0.99	0.98							
	iodide	2.07	2.14	2.22	2.29	2.30	2.32	2.33	2.35		
	nitrate	1.04	1.05	1.06	1.09	1.10	1.12	1.14	1.15		
Beryllium	perchlorate	1.78		1.91		2.01		2.07		2.11	2.14
	sulphate	1.27	1.29	1.31		1.32		1.35			
Boric acid				1.025							

Cadmium	bromide	1.44	1.57	1.73	1.87	1.97	1.96	1.95	1.94	1.93
	chloride	1.64	1.69	1.74	1.78	1.84	1.83	1.82	1.82	1.82
	iodide	1.57		1.59		1.62		1.65		1.71
	nitrate			1.78						
	perchlorate		1.74	1.75	1.76	1.77	1.78	1.79	1.81	1.85
	potassium bromide	1.72	1.78	1.84	1.92	1.97	2.03	2.08	2.13	2.21
	potassium chloride	1.20	1.23	1.26	1.30	1.33	1.39		1.44	1.45
	bromate			1.02						
	bromide			1.69						
	chlorate			1.04						
Caesium	chloride	1.84	1.88	1.91	1.94	1.96	1.98	2.00	2.02	2.04
	iodate		1.01	1.02						
	iodide			1.54						
	nitrate	1.07	1.10	1.16	1.22	1.29	1.37	1.46	1.55	1.64
	sulphate	1.98	1.99	2.01	2.02	2.03	2.04	2.05	2.06	2.07
	aluminium sulphate	1.002	1.002	1.002	1.001	0.999	0.999	1.000	1.006	1.018
	perchlorate	1.00		1.01						
	chlorate			1.74	1.80					
	chloride	1.36	1.38	1.43	1.49	1.51				
	ferrocyanide			1.35	1.37	1.38	1.40	1.41	1.41	
Calcium	nitrate			1.46	1.62					
	sulphate			0.999	0.998	0.996				
	chlorate			1.86						
	nitrate			1.57						
	perchlorate	1.56	1.57	1.57	1.58	1.59				
Cupric	acetate			1.05						
	ammonium sulphate	1.01	1.11	1.13	1.16					
	bromide			1.84						
	chlorate			1.70						
	nitrate			1.69						
	sulphate	1.15	1.18	1.20	1.23	1.26	1.30	1.34	1.40	1.43
	chloride				1.79					
Ferric	perchlorate	1.61	1.63	1.65	1.66	1.68	1.70	1.71		

Table A.8. (Continued)

	<i>Solute</i>	0	10	20	<i>Densities (g cm⁻³) at different temperatures (°C)</i>						
					30	40	50	60	70	80	90
Ferrous	ammonium sulphate	1.14	1.16	1.19	1.22	1.25	1.29	1.32	1.35		
	chloride			1.44							
	nitrate		1.47	1.50	1.51						
Lead	perchlorate	1.54	1.55	1.56	1.57	1.58	1.57	1.58			
	acetate	1.14	1.20	1.26	1.41	1.60	1.88				
	bromate			1.01							
Lithium	bromide	1.004	1.005	1.006	1.006	1.006	1.005	1.004	1.002	1.000	0.999
	chlorate			1.20							
	chloride	1.006	1.008	1.007	1.006	1.005	1.003	1.001	0.998	0.995	0.991
Magnesium	iodide	1.000	1.000	0.999	0.997	0.993	0.989	0.985	0.980	0.976	0.969
	nitrate	1.30	1.35	1.42	1.48	1.55	1.59	1.63			
	benzoate			1.10							
Magnesium	bromate			1.83							
	chloride	1.27	1.28	1.29	1.30	1.30	1.31				
	citrate			1.21							
Magnesium	fluoride			1.002	0.998	0.994					
	formate			1.14							
	iodate			1.56	1.55						
Magnesium	iodide			1.83							
	nitrite			1.32							
	perchlorate	1.22	1.24	1.26	1.28	1.30					
Magnesium	salicylate			1.20	1.21						
	bromate	1.51	1.56	1.61	1.66	1.72	1.79	1.90	1.99	2.08	
	chlorate			1.60							
Magnesium	chloride			1.34							
	chromate			1.42							
	iodate	1.04	1.06	1.07	1.08	1.09	1.12				

	molybdate	1.12	1.14	1.15	1.16	1.16	1.18	1.20	1.15	1.12	1.09
Manganese	sulphate	1.24	1.26	1.29	1.33	1.35	1.38	1.41	1.42	1.43	1.40
	chloride			1.39	1.50	1.54	1.57	1.61	1.61		
	sulphate		1.47	1.49	1.51	1.53					
Mercuric	bromide				1.002						
	chloride	1.04	1.04	1.05	1.06	1.07	1.09	1.11	1.14	1.18	1.23
Nickel	ammonium sulphate		1.03	1.05	1.06						
	chlorate			1.85	1.55						
	perchlorate	1.57	1.58	1.58	1.59	1.592					
	sulphate		1.31	1.36	1.40	1.44	1.47	1.50			
Potassium	acetate	1.398	1.400	1.403	1.41	1.42	1.43				
	aluminium sulphate	1.03	1.04	1.05	1.07	1.10	1.14	1.21	1.29	1.44	
	bicarbonate			1.17							
	bromate	1.02	1.04	1.05	1.06	1.08					
	bromide	1.32	1.34	1.37	1.38	1.40	1.42				1.46
	carbonate	1.546	1.549	1.559	1.557		1.57		1.59		
	chlorate	1.02	1.03	1.05	1.06	1.07	1.09	1.12	1.14	1.17	1.19
	chloride	1.153	1.164	1.174	1.182	1.188	1.193	1.198	1.202	1.205	1.207
	citrate			1.51							
	chromate			1.38							
Potassium	dichromate		1.06	1.07							
	dihydrogen phosphate	1.11	1.12	1.15	1.17	1.20	1.23	1.26	1.31		
	ferricyanide	1.15	1.16	1.18	1.20	1.21	1.22	1.23			
	ferrocyanide		1.13	1.15	1.19	1.21	1.24	1.26	1.27	1.29	1.30
	formate			1.58							
	iodate	1.04	1.05	1.06	1.08		1.11		1.46	1.48	1.50
	iodide	1.67	1.69	1.71	1.73	1.75	1.76	1.77	1.78	1.80	1.81
	nitrate	1.05	1.11	1.17	1.22	1.28	1.33	1.39	1.44	1.49	1.53
	oxalate			1.21	1.22		1.25				
	perchlorate	1.005	1.007	1.009	1.016	1.022	1.026	1.032	1.04	1.05	1.06
	permanganate			1.03	1.05						
	sodium carbonate		1.30	1.39							
	sodium tartrate			1.30	1.31						
	sulphate	1.06	1.07	1.08	1.09	1.10	1.105	1.110	1.114	1.117	1.119

Table A.8. (Continued)

	<i>Solute</i>	0	10	20	30	40	50	60	70	80	90
		<i>Densities (g cm⁻³) at different temperatures (°C)</i>									
Rubidium	aluminium sulphate	1.01	1.01	1.01	1.02	1.02	1.03	1.05	1.08		
	bromide			1.62							
	chlorate			1.04							
	chloride	1.44	1.47	1.49	1.51	1.53	1.54	1.55	1.57	1.58	1.59
	iodate			1.03							
	iodide			1.84							
	nitrate	1.08	1.20	1.32	1.43	1.55	1.67	1.77	1.86	1.94	2.01
	perchlorate	1.007	1.008	1.010	1.013	1.017	1.022	1.03	1.04	1.05	1.06
Silver	sulphate	1.27	1.31	1.34	1.37	1.39	1.41	1.43	1.44	1.45	1.47
	acetate			1.004	1.006						
	bromate			0.999		0.993					
Sodium	chlorate			1.12	1.13						
	acetate	1.158	1.162	1.17	1.19	1.20	1.23	1.26			
	ammonium sulphate		1.17	1.18							
	benzene sulphonate			1.07	1.08						
	benzoate			1.15	1.16						
	bicarbonate			1.06	1.07	1.06	1.08				
	borate (borax)		1.018	1.025	1.035	1.040					
	bromate	1.18	1.21	1.25	1.28	1.30	1.34				
	bromide	1.44	1.49	1.52	1.56	1.58					
	carbonate	1.06	1.15	1.19	1.34	1.36	1.33				
	chlorate	1.39	1.40	1.43	1.45	1.47	1.49	1.51	1.54	1.56	1.58
	chloride	1.209	1.204	1.200	1.196	1.191	1.187	1.183	1.178	1.175	1.170
	citrate			1.26	1.28						
	chromate			1.43							
	dichromate			1.74							
	dihydrogen phosphate			1.39							

	ferrocyanide	1.06	1.09	1.11	1.12	1.14	1.19	1.22	1.26	1.28	1.29
	formate			1.32							
	hydrogen phosphate			1.05							
	iodate	1.02	1.04	1.07	1.09	1.10	1.12	1.14	1.16	1.190	1.192
	iodide	1.86	1.88	1.91	1.94	1.97	2.01	2.16	2.15		2.14
	molybdate			1.44							
	nitrate	1.35	1.37	1.38	1.40	1.41	1.43	1.44	1.46	1.48	1.49
	nitrite		1.34	1.36							
	oxalate			1.02	1.03						
	perchlorate		1.65	1.67	1.69	1.71	1.75				
	periodate		1.04	1.05	1.07	1.14	1.21	1.22			
	phosphate	1.068	1.071	1.09	1.12	1.17	1.26				
	salicylate			1.23	1.26						
Strontium	sulphate	1.04	1.08	1.15	1.29	1.32	1.31	1.29	1.28	1.27	1.26
	bromate	1.18	1.20	1.26	1.30	1.34	1.37	1.40	1.44	1.46	1.47
	chlorate	1.828	1.829	1.840	1.831	1.833	1.837	1.842	1.845	1.847	1.853
	chloride	1.33	1.35	1.38	1.42						
	nitrate	1.28	1.36	1.44	1.514	1.513	1.511	1.510	1.510	1.511	1.512
	nitrite			1.45							
Thallium	salicylate			1.01	1.02						
	chloride	1.001	1.002	1.001	0.999	0.998	0.995	0.992	0.989	0.986	0.982
	dihydrogen phosphate	2.54	2.69	2.83	2.95	3.15	3.20				
	hydroxide	1.23		1.32	1.34	1.45	2.19	2.79	4.17	4.69	5.71
	perchlorate	1.06	1.08	1.10	1.14	1.19	1.26	1.33	1.42	1.52	
	nitrate	1.03	1.06	1.08	1.11	1.16	1.23	1.33	1.48	1.72	2.14
Uranyl	sulphate	1.02	1.03	1.04	1.05	1.06	1.07	1.08	1.09	1.10	1.11
Zinc	chloride			2.75							
	acetate			1.16	1.17						
	benzene sulphonate			1.18	1.19						
	sulphate	1.38		1.46	1.52	1.59		1.59	1.55	1.51	1.49
Sucrose				1.32		1.33		1.33		1.35	
Urea							1.15	1.17			

Table A.9. Densities of some aqueous inorganic salt solutions at 20°C

Solution concentration is expressed as a percentage by mass (g anhydrous solute/100 g of solution)

mass %	NH ₄ Cl	NH ₄ NO ₃	NH ₄ OH	(NH ₄) ₂ SO ₄	NH ₄ H ₂ PO ₄	NH ₄ Al(SO ₄) ₂	(NH ₄) ₂ Ni(SO ₄) ₂	BaCl ₂
1	1.003	1.002	0.998	1.006	1.006	1.009	1.008	1.004
2	1.006	1.006	0.996	1.012	1.012	1.018	1.016	1.018
3	1.009	1.010	0.994	1.018	1.018	1.028	1.025	1.027
4	1.013	1.015	0.992	1.024	1.023	1.037	1.037	1.036
5	1.016	1.019	0.989	1.030	1.029	1.046	1.043	1.045
10	1.030	1.040	0.979	1.059	1.058			1.094
12	1.036	1.048	0.975	1.071	1.070			1.115
14	1.042	1.057	0.972	1.083	1.081			1.136
16	1.048	1.065	0.968	1.094	1.093			1.158
18	1.053	1.074	0.964	1.106	1.104			1.181
20	1.059	1.083	0.960	1.117	1.115			1.205
22	1.064	1.092	0.957	1.128	1.128			1.230
24	1.069	1.10	0.953	1.140	1.141			1.255
26		1.11	0.950	1.150				1.282
28		1.12	0.946	1.164				
30		1.13	0.943	1.176				
35			0.935					
40			0.926					

mass %	CaCl ₂	CsCl	CoCl ₂	CuSO ₄	FeCl ₃	Pb(NO ₃) ₂	LiCl	MgCl ₂
1	1.008	1.008	1.009	1.010	1.009	1.009	1.006	1.008
2	1.017	1.015	1.018	1.021	1.017	1.018	1.012	1.016
3	1.025	1.023	1.027	1.031	1.026	1.027	1.018	1.025
4	1.033	1.031	1.032	1.042	1.034	1.038	1.023	1.033
5	1.042	1.040	1.046	1.053	1.043	1.045	1.029	1.041
10	1.085	1.082	1.096	1.109	1.087	1.093	1.058	1.084

12	1.103	1.100	1.117	1.132	1.106	1.114	1.069	1.101
14	1.122	1.118	1.138	1.157	1.125	1.135	1.081	1.118
16	1.141	1.138	1.161	1.182	1.144	1.157	1.093	1.136
18	1.160	1.157	1.184	1.208	1.164	1.180	1.105	1.154
20	1.180	1.178	1.207		1.184	1.204	1.118	1.173
22	1.200	1.199			1.204	1.229	1.129	1.192
24	1.220	1.221			1.225	1.254	1.142	1.211
26		1.243			1.247	1.280	1.155	1.230
28		1.267			1.270	1.305	1.168	1.250
30		1.291			1.293	1.330	1.181	1.271
35		1.352			1.352			
40		1.425			1.420			

mass %	MgSO ₄	MnSO ₄	NiSO ₄	KBr	K ₂ CO ₂	KCl	K ₂ CrO ₄	K ₂ Cr ₂ O ₇
1	1.010	1.010	1.011	1.007	1.009	1.006	1.008	1.007
2	1.020	1.020	1.022	1.015	1.018	1.013	1.016	1.014
3	1.031	1.030	1.032	1.022	1.027	1.019	1.024	1.021
4	1.041	1.040	1.043	1.029	1.036	1.026	1.033	1.028
5	1.052	1.050	1.054	1.037	1.045	1.032	1.041	1.035
10	1.105	1.103		1.076	1.092	1.065	1.084	1.072
12	1.128	1.126		1.092	1.112	1.079	1.101	
14	1.150	1.149		1.109	1.131	1.092	1.120	
16	1.174	1.173		1.126	1.151	1.106	1.138	
18	1.198	1.197		1.144	1.171	1.120	1.157	
20	1.222	1.222		1.162	1.192	1.135	1.177	
22	1.247			1.181	1.213	1.149	1.196	
24	1.272			1.200	1.234	1.164	1.217	
26	1.298			1.220	1.256		1.238	
28				1.240	1.278		1.259	
30				1.262	1.300		1.281	
35				1.317	1.360		1.340	
40				1.377	1.417		1.399	

Table A.9. (Continued)

mass %	KI	KNO ₃	K ₂ C ₂ O ₄	KH ₂ PO ₄	K ₂ HPO ₄	K ₂ SO ₄	KAl(SO ₄) ₂	AgNO ₃
1	1.007	1.006	1.007	1.007	1.009	1.008	1.009	1.009
2	1.015	1.013	1.015	1.014	1.017	1.016	1.019	1.017
3	1.022	1.019	1.022	1.022	1.026	1.024	1.029	1.026
4	1.030	1.025	1.029	1.029	1.034	1.032	1.039	1.035
5	1.038	1.032	1.037	1.036	1.043	1.041	1.049	1.043
10	1.078	1.065	1.075	1.072	1.070	1.083		1.090
12	1.095	1.078						1.110
14	1.112	1.092						1.130
16	1.130	1.106						1.152
18	1.149	1.120						1.174
20	1.168	1.135						1.196
22	1.188	1.149						1.220
24	1.208	1.164						1.244
26	1.229							1.269
28	1.251							1.296
30	1.273							1.323
35	1.336							1.400
40	1.398							1.477
mass %	CH ₃ COONa	NaHCO ₃	NaBr	Na ₂ CO ₃	NaCl	NaOH	Na ₂ MoO ₄	NaNO ₃
1	1.005	1.007	1.008	1.010	1.007	1.011	1.009	1.007
2	1.010	1.015	1.016	1.021	1.014	1.022	1.017	1.014
3	1.015	1.022	1.024	1.031	1.021	1.033	1.026	1.020
4	1.021	1.029	1.032	1.042	1.029	1.045	1.035	1.027
5	1.026	1.036	1.040	1.052	1.036	1.056	1.044	1.034
10	1.051		1.082	1.105	1.073	1.111		1.069
12	1.062		1.100	1.126	1.088	1.133		1.084

14	1.072		1.118	1.148	1.103	1.155		1.090
16	1.083		1.137	1.168	1.118	1.177		1.114
18	1.093		1.157		1.134	1.199		1.129
20	1.104		1.177		1.150	1.221		1.145
22	1.115		1.197		1.166	1.243		1.161
24	1.126		1.218		1.183	1.265		1.177
26	1.137		1.240		1.199	1.287		1.194
28	1.148		1.263			1.309		1.211
30	1.160		1.286			1.330		1.228
35			1.350			1.380		1.270
40			1.416			1.432		1.320

mass %	Na ₂ HPO ₄	Na ₂ SO ₃	Na ₂ SO ₄	Na ₂ C ₄ H ₄ O ₆	Na ₂ S ₂ O ₃	Na ₂ WO ₄	SrCl ₂	ZnSO ₄
1	1.010	1.007	1.009	1.007	1.008	1.009	1.009	
2	1.020	1.018	1.018	1.014	1.017	1.018	1.018	1.021
3	1.030	1.028	1.027	1.021	1.025	1.028	1.027	1.031
4	1.040	1.038	1.037	1.028	1.033	1.037	1.036	1.042
5	1.050	1.048	1.046	1.036	1.042	1.047	1.046	1.053
10		1.095	1.093	1.072	1.085		1.094	1.109
12		0.115	1.113	1.087	1.102		1.115	1.133
14		1.134	1.133	1.102	1.120		1.136	1.157
16		1.155	1.153	1.118	1.139		1.158	1.183
18		1.175	1.173	1.133	1.157		1.180	
20		1.195	1.194	1.149	1.176		1.203	
22			1.215	1.165	1.195		1.226	
24			1.236	1.182	1.215		1.250	
26				1.198	1.235		1.275	
28				1.216	1.255		1.301	
30					1.276		1.327	
35					1.325			
40					1.385			

Table A.10. Viscosities of some aqueous solutions at 25°C

Solution concentrations are quoted in molality, m, i.e. gram-formula weight (anhydrous) per kg of water. Values in the final column marked with an asterisk (*) refer to saturated solutions at 25°C.

$$(1 \text{ cP} = 0.01 \text{ g cm}^{-1} \text{ s}^{-1} = 10^{-3} \text{ kg m}^{-1} \text{ s}^{-1} = 10^{-3} \text{ N s m}^{-2} = 1 \text{ mPa s}^{-1})$$

	Solute	Viscosity (cP) at 25°C		
		0.5m	1m	5m
(x)m				
Ammonium	aluminium sulphate			1.26*
	acetate	1.0	1.1	
	bromide	0.88	0.86	0.84
	chloride	0.88	0.88	0.91
	chromate	0.95	1.03	
	dichromate	0.92	0.95	
	dihydrogen phosphate	1.05	1.16	1.59
	iodide	0.86	0.83	0.80
	nitrate	0.88	0.87	0.90
	sulphate	0.98	1.36	2.1
Barium	acetate	1.3	1.8	
	chloride	1.0	1.1	1.3*
	nitrate		0.97	
Beryllium	sulphate	1.2		
Cadmium	chloride	1.00	1.02	
	nitrate	1.03	1.03	
	sulphate	1.20	1.19	
Calcium	acetate	1.3	1.9	
	chloride	1.03	1.2	4.1
	chromate	1.13		(6) 7.6
	nitrate	1.00	1.15	(3) 2.2
Cobalt	chloride	1.07	1.27	
	nitrate	1.03		
	sulphate	1.2		
Copper (cupric)	chloride	1.07	1.27	
	nitrate		1.26	4.6
	sulphate	1.21	1.67	
Ferric	chloride	1.21	1.64	10.0
Lead	acetate	1.15	1.39	
	nitrate	0.98	1.12	(1½) 1.3
Lithium	acetate	1.1	1.3	
	bromate	0.90	1.04	
	chlorate		1.01	1.78
	chloride	0.95	1.01	(35) 54 (20) 17

	iodate	1.23	(3) 2.7	
	hydroxide	1.0	(4) 2.6	
	nitrate	0.92	0.99	
	sulphate	1.15	1.48	
Magnesium	chloride	1.07	1.3	(3) 3.0
	nitrate	1.04	1.22	(3) 2.5
	sulphate	1.22	1.72	(2) 3.4
Manganese	chloride	1.07	1.28	(3) 2.6
	nitrate	1.04	1.22	(3) 2.2
	sulphate	1.21	1.69	(3) 7.1
Nickel	ammonium sulphate			1.10*
	chloride	1.07		
	nitrate	1.05		
	sulphate	1.21		
Potassium	acetate	1.01	1.10	(4) 1.94
	aluminium sulphate			1.22*
	bromide	0.88	0.86	0.94
	carbonate	1.04	1.19	(4) 2.9
	chlorate	0.89		
	chloride	0.89	0.89	(4) 0.94
	chromate	0.96	1.07	(2) 1.31
	bicarbonate	0.94	1.00	(2) 1.12
	bichromate			($\frac{1}{4}$) 0.90
	bisulphate	0.95	1.01	(2) 1.17
	ferricyanide	0.98		
	ferrocyanide	1.10		
	fluoride		1.01	1.42 (6) 1.85
	hydroxide		1.01	(6) 1.95
	iodide	0.85	0.83	0.85 (9) 1.07
	nitrate	0.87	0.87	(2) 0.89
	oxalate	0.99	1.09	
	phosphate	1.13	1.53	
Silver	hydrogen phosphate	1.07	1.34	(2) 1.94
	dihydrogen phosphate	1.11	1.15	
	sulphate	0.99		1.16*
	thiocyanate	0.87	0.85	0.93
	nitrate	0.98	0.94	1.33 (12) 2.4
Sodium	acetate	1.05	1.22	
	benzoate	1.12	1.41	
	bromate	0.94	0.99	
	bromide	1.19		
	carbonate	1.15	1.51	(2) 2.58
	bicarbonate	0.98	1.09	
	chlorate	0.93	0.96	1.52
	perchlorate		0.93	

Table A.10. (*Continued*)

<i>Solute</i>	<i>0.5 m</i>	<i>Viscosity (cP) at 25 °C</i>		
		<i>1 m</i>	<i>5 m</i>	<i>(x) m</i>
chloride	0.97	0.97	1.52	
chromate	1.11	1.46		
dihydrogen phosphate	1.17	1.30		
formate	0.97	1.07		
lactate	1.09	1.31		
iodide	0.90	0.92	1.16	(8) 1.81
nitrate	0.91	0.94	1.42	
sulphate	1.10	1.38		1.25*
bisulphate	0.99	1.11	2.55	
propionate	1.09	1.34		
salicylate	1.08	1.31		
tartrate	1.17	1.61		
thiosulphate				5.5*
Strontium	acetate	1.30	1.90	
	chloride	1.02	1.19	(3) 2.28
	nitrate	1.00	1.02	
Thallous	nitrate		0.85	
Zinc	chloride	1.06		
	nitrate	1.04		
	sulphate	1.22	1.69	(2) 3.36

Table A.11. Diffusion coefficients of concentrated aqueous electrolyte solutions at 25 °C ($D \times 10^{-9} \text{ m}^2 \text{ s}^{-1}$)

mol	BaCl ₂	CaCl ₂	KCl	KBr	KI	LiCl	NaCl
0	1.385	1.335	1.993	2.016	1.996	1.366	1.610
0.05	1.18	1.12	1.86	1.89	1.89	1.28	1.51
0.1	1.16	1.11	1.84	1.87	1.86	1.26	1.48
0.2	1.15	1.11	1.84	1.87	1.85	1.26	1.48
0.3	1.15	1.12	1.84	1.87	1.88	1.26	1.48
0.5	1.16	1.14	1.85	1.88	1.95	1.27	1.47
0.7	1.17	1.17	1.87	1.91	2.00	1.28	1.47
1.0	1.18	1.20	1.89	1.97	2.06	1.30	1.48
1.5	1.18	1.26	1.94	2.06	2.16	1.33	1.50
2.0		1.31	2.00	2.13	2.25	1.36	1.52
2.5		1.31	2.06	2.19	2.34	1.39	1.54
3.0		1.27	2.11	2.28	2.44	1.43	1.57
3.5		1.20	2.16	2.35	2.53	1.46	1.58
4.0			2.20	2.43			1.59
4.5							1.59
5.0							1.59
mol	NaBr	NaI	NH ₄ Cl	NH ₄ NO ₃	(NH ₄) ₂ SO ₄		
0	1.625	1.614	1.994	1.929		1.530	
0.05	1.53	1.52		1.79		0.80	
0.1	1.51	1.52	1.84	1.77		0.83	
0.2	1.50	1.53	1.84	1.75		0.87	
0.3	1.51	1.54	1.84	1.74		0.90	
0.5	1.54	1.58	1.86	1.72		0.94	
0.7	1.56	1.61	1.88	1.71		0.97	
1.0	1.59	1.66	1.92	1.69		1.01	
1.5	1.62	1.75	1.99	1.66		1.05	
2.0	1.66	1.84	2.05	1.63		1.07	
2.5	1.70	1.92	2.11	1.61		1.09	
3.0		1.99	2.16	1.58		1.11	
3.5			2.20	1.55		1.12	
4.0			2.24	1.52		1.14	
4.5			2.26	1.50			
5.0			2.26	1.47			

The values at zero concentration are the Nernst limiting values (see section 2.4)

Table A.12. *Activity coefficients of electrolytes at 25°C*
 (molality = gram-formula weight of anhydrous solute per kg of water)

Molality	AlCl ₃	Al ₂ (SO ₄) ₃	NH ₄ Cl	NH ₄ NO ₃	(NH ₄) ₂ SO ₄	BaCl ₂	BaBr ₂	BaI ₂
0.1	0.337	0.0350	0.770	0.740	0.423	0.508	0.517	0.536
0.2	0.305	0.0225	0.718	0.677	0.343	0.450	0.469	0.503
0.4	0.313	0.0153	0.665	0.606	0.270	0.411	0.440	0.504
0.6	0.356	0.0140	0.636	0.562	0.231	0.397	0.442	0.534
0.8	0.429	0.0149	0.617	0.530	0.206	0.397	0.452	0.581
1.0	0.539	0.0175	0.603	0.504	0.189	0.401	0.473	0.642
1.5	1.11		0.581	0.455	0.160	0.432	0.552	0.860
2.0			0.570	0.419	0.144		0.661	1.21
2.5			0.564	0.391	0.132			
3.0			0.561	0.368	0.125			
4.0			0.560	0.331	0.116			
5.0			0.562	0.302				
6.0			0.564	0.279				
Molality	BeSO ₄	CdCl ₂	CdBr ₂	CdSO ₄	CaCl ₂	CaBr ₂	CaI ₂	Ca(ClO ₄) ₂
0.1	0.150	0.228	0.190	0.150	0.518	0.532	0.552	0.557
0.2	0.109	0.164	0.132	0.103	0.472	0.491	0.524	0.532
0.4	0.0769	0.114	0.0890	0.0699	0.448	0.482	0.535	0.544
0.6	0.0639	0.0905	0.0699	0.0553	0.453	0.504	0.576	0.589
0.8	0.0570	0.0765	0.0591	0.0468	0.470	0.542	0.641	0.654
1.0	0.0530	0.0669	0.0518	0.0415	0.500	0.596	0.731	0.743
1.5	0.0490	0.0525	0.0416	0.0346	0.615	0.796	1.063	1.08
2.0	0.0497	0.0441	0.0361	0.0321	0.792	1.12	1.617	1.63
2.5	0.0538	0.0389	0.0328	0.0317	1.06	1.65		2.62
3.0	0.0613	0.0352	0.0305	0.0329	1.48	2.53		4.21
4.0	0.0875	0.0306	0.0278		2.93	6.27		10.8
5.0		0.0279			5.89	18.4		26.7
6.0		0.0263			11.1	55.7		63.7

Table A.12. (Continued)

Molality	KOH	KCl	KBr	KI	KClO ₃	KBrO ₃	KNO ₃	K acetate
0.1	0.776	0.770	0.772	0.778	0.749	0.745	0.739	0.796
0.2	0.739	0.718	0.722	0.733	0.681	0.674	0.663	0.766
0.4	0.713	0.666	0.673	0.689	0.599	0.585	0.576	0.750
0.6	0.712	0.637	0.646	0.667	0.541		0.519	0.754
0.8	0.721	0.618	0.629	0.654			0.476	0.766
1.0	0.735	0.604	0.617	0.645			0.443	0.783
1.5	0.791	0.583	0.600	0.636			0.380	0.840
2.0	0.863	0.573	0.593	0.637			0.333	0.910
2.5	0.947	0.569	0.593	0.644			0.297	0.995
3.0	1.05	0.569	0.595	0.652			0.269	1.09
4.0	1.31	0.577	0.608	0.673				
5.0	1.67		0.626					
6.0	2.14							
Molality	KCNS	KH ₂ PO ₄	K ₂ CrO ₄	K ₂ SO ₄	K ₃ Fe(CN) ₆	K ₄ Fe(CN) ₆	AgNO ₃	NaOH
0.1	0.769	0.731	0.466	0.436	0.268	0.139	0.734	0.764
0.2	0.716	0.653	0.390	0.356	0.212	0.0993	0.657	0.725
0.4	0.663	0.561	0.320	0.283	0.167	0.0693	0.567	0.695
0.6	0.633	0.501	0.282	0.243	0.146	0.0556	0.509	0.683
0.8	0.614	0.456	0.259		0.135	0.0479	0.464	0.677
1.0	0.599	0.421	0.240		0.128		0.429	0.677
1.5	0.573	0.358	0.215				0.363	0.687
2.0	0.556		0.200				0.316	0.707
2.5	0.546		0.194				0.280	0.741
3.0	0.538		0.194				0.252	0.782
4.0	0.529						0.210	0.901
5.0	0.524						0.181	1.07
6.0							0.159	1.30

Molality	NaCl	NaBr	NaI	NaClO ₃	NaClO ₄	Na ₂ SO ₄	Na ₂ CrO ₄	Na ₂ S ₂ O ₃
0.1	0.778	0.782	0.787	0.772	0.775	0.452	0.479	0.466
0.2	0.735	0.741	0.751	0.720	0.729	0.371	0.407	0.390
0.4	0.693	0.704	0.727	0.664	0.683	0.294	0.337	0.319
0.6	0.673	0.692	0.723	0.630	0.656	0.252	0.301	0.282
0.8	0.662	0.687	0.727	0.606	0.641	0.225	0.278	0.256
1.0	0.657	0.687	0.736	0.589	0.629	0.204	0.261	0.239
1.5	0.656	0.703	0.771	0.568	0.614	0.173	0.237	0.219
2.0	0.668	0.731	0.820	0.538	0.609	0.154	0.229	0.202
2.5	0.688	0.768	0.883	0.525	0.609	0.144	0.232	0.199
3.0	0.714	0.812	0.963	0.515	0.611	0.139	0.244	0.203
4.0	0.783	0.929			0.626	0.138	0.294	
5.0	0.874				0.649			
6.0	0.986				0.677			
Molality	NaBrO ₃	NaNO ₃	Na acetate	NaCNS	NaH ₂ PO ₄	SrCl ₂	SrBr ₂	SrI ₂
0.1	0.758	0.762	0.791	0.787	0.744	0.515	0.527	0.549
0.2	0.696	0.703	0.757	0.750	0.675	0.466	0.483	0.516
0.4	0.628	0.638	0.737	0.720	0.593	0.436	0.465	0.520
0.6	0.585	0.599	0.736	0.712	0.539	0.434	0.473	0.551
0.8	0.554	0.570	0.745	0.710	0.499	0.445	0.497	0.603
1.0	0.528	0.548	0.757	0.712	0.468	0.465	0.535	0.675
1.5	0.491	0.507	0.799	0.727	0.410	0.549	0.679	0.946
2.0	0.450	0.478	0.851	0.744	0.371	0.675	0.906	1.40
2.5	0.426	0.455	0.914	0.779	0.343	0.862		
3.0		0.437	0.982	0.814	0.320	1.14		
4.0		0.408		0.897	0.293	1.99		
5.0		0.386			0.276			
6.0		0.371			0.265			

Table A.12. (Continued)

Molality	Sr(NO ₃) ₂	UO ₂ (NO ₃) ₂	ZnCl ₂	ZnBr ₂	ZnI ₂	Zn(NO ₃) ₂	ZnSO ₄
0.1	0.478	0.543	0.518	0.547	0.572	0.530	0.150
0.2	0.410	0.512	0.465	0.510	0.550	0.487	0.104
0.4	0.348	0.518	0.413	0.504	0.573	0.467	0.0715
0.6	0.314	0.555	0.382	0.519	0.635	0.478	0.0569
0.8	0.292	0.608	0.359	0.537	0.713	0.499	0.0487
1.0	0.275	0.679	0.341	0.552	0.788	0.533	0.0435
1.5	0.251	0.899	0.306	0.568	0.936	0.650	0.0370
2.0	0.232	1.22	0.291	0.572	1.01	0.814	0.0357
2.5	0.223	1.60	0.287	0.582	1.05	1.05	0.0367
3.0	0.217	2.00	0.289	0.598	1.11	1.36	0.0408
4.0	0.212	2.64	0.309	0.664	1.24	2.30	
5.0		3.01	0.356	0.774	1.45	3.86	
6.0			0.420	0.930	1.75	6.38	

Table A.13. Molar ionic conductivities in water at infinite dilution, Λ_0

Cations	0	25	50	100 °C	Anions	0	25	50	100 °C
H ⁺	230	350	465	640	OH ⁻	105	198	284	440
Li ⁺	19	39		110	F ⁻			55	
Na ⁺	26	50	82	150	Cl ⁻	41	76	116	210
K ⁺	41	74	115	200	Br ⁻	43	78		
Rb ⁺	44	78			I ⁻	41	77		
Cs ⁺	44	77			NO ₃ ⁻	40	72	104	200
Ag ⁺	33	62	101	180	ClO ₃ ⁻			65	
NH ₄ ⁺	40	74	115	190	BrO ₃ ⁻			56	
Be ²⁺		45			IO ₂ ⁻			41	
Mg ²⁺	29	53		170	ClO ₄ ⁻	37	67		190
Ca ²⁺	31	60	98	190	IO ₄ ⁻			55	
Sr ²⁺	31	60			HCO ₃ ⁻			46	
Ba ²⁺	33	65	104	200	Formate ⁻			55	
Cu ²⁺		54			Acetate ⁻	20	41	67	130
Zn ²⁺		53			Propionate ⁻			36	
Co ²⁺		55			Butyrate ⁻			33	
Pb ²⁺		70			Benzoate ⁻			32	
Cd ²⁺		52			Oxalate ²⁻	39	73	115	210
					SO ₄ ²⁻	41	80	125	260
					CO ₃ ²⁻			69	
					P ₃ O ₉ ³⁻			84	
					P ₄ O ₁₂ ³⁻			94	
					Citrate ³⁻	36	70	113	210
					Fe(CN) ₆ ³⁻			100	
					Fe(CN) ₆ ⁴⁻	58	110	173	320
					P ₂ O ₇ ⁴⁻			96	
					P ₃ O ₁₀ ⁵⁻			110	

The values of Λ_0 are expressed as $\Omega^{-1} \text{cm}^2 \text{mol}^{-1}$ which, in SI units, become $\times 10^{-4} \text{S m}^2 \text{mol}^{-1}$.

Table A.14. Heats of solution of inorganic salts in water at approximately room temperature and infinite dilution

A positive value indicates an exothermic, a negative value an endothermic heat of solution
 $[1 \text{ kcal mol}^{-1} = 4.1868 \text{ kJ mol}^{-1}]$

<i>Substance</i>		<i>Formula</i>	<i>Heat of solution, kcal mol⁻¹</i>
Aluminium	ammonium sulphate	(NH ₄)Al(SO ₄) ₂	+30.5
	bromide	AlBr ₃	+86.1
	chloride	AlCl ₃	+77.9
	chloride	AlCl ₃ · 6H ₂ O	+13.1
	iodide	AlI ₃	+90.6
	sulphate	Al ₂ (SO ₄) ₃	+120
	sulphate	Al ₂ (SO ₄) ₃ · 18H ₂ O	+7.0
Ammonium	acetate	NH ₄ C ₂ H ₃ O ₂	+1.7
	alum	NH ₄ Al(SO ₄) ₂ · 12H ₂ O	-9.6
	bicarbonate	NH ₄ HCO ₃	-6.7
	bichromate	(NH ₄) ₂ Cr ₂ O ₇	-12.9
	bisulphate	(NH ₄) ₂ HSO ₄	+0.56
	bromide	NH ₄ Br	-4.5
	chloride	NH ₄ Cl	-3.8
	chromate	(NH ₄) ₂ CrO ₄	-5.7
	cyanide	NH ₄ CN	-4.6
	dihydrogen phosphate	NH ₄ H ₂ PO ₄	-3.86
	hydrogen phosphate	(NH ₄) ₂ HPO ₄	-3.13
	iodate	NH ₄ IO ₃	-7.6
	iodide	NH ₄ I	-3.6
	nitrate	NH ₄ NO ₃	-6.5
	nitrite	NH ₄ NO ₂	-4.0
	oxalate	(NH ₄) ₂ C ₂ O ₄	-8.0
	oxalate	(NH ₄) ₂ C ₂ O ₄ · H ₂ O	-11.5
	perchlorate	NH ₄ ClO ₄	-6.3
	sulphate	(NH ₄) ₂ SO ₄	-1.5
	sulphite	(NH ₄) ₂ SO ₃ · H ₂ O	-4.4
	thiocyanate	NH ₄ CNS	-5.5
	thiosulphate	(NH ₄) ₂ S ₂ O ₄	-6.2
Barium	acetate	Ba(C ₂ H ₃ O ₂) ₂	+6.0
	bromide	BaBr ₂	+5.2
	bromide	BaBr ₂ · 2H ₂ O	-3.9
	carbonate	BaCO ₃	-1.0
	chlorate	Ba(ClO ₃) ₂	-6.7
	chlorate	Ba(ClO ₃) ₂ · H ₂ O	-11.0
	chloride	BaCl ₂	+3.1
	chloride	BaCl ₂ · 2H ₂ O	-4.5
	cyanide	Ba(CN) ₂	+2.7
	fluoride	BaF ₂	-0.9
	hydroxide	Ba(OH) ₂	+11.4
	hydroxide	Ba(OH) ₂ · 8H ₂ O	-14.5
	iodide	BaI ₂	+10.3

	iodide	$\text{BaI}_2 \cdot 6\text{H}_2\text{O}$	-6.6
	nitrate	$\text{Ba}(\text{NO}_3)_2$	-9.6
	nitrite	$\text{Ba}(\text{NO}_2)_2$	-4.6
	phosphate	$\text{Ba}_3(\text{PO}_4)_2$	-16.6
	perchlorate	$\text{Ba}(\text{ClO}_4)_2$	-1.3
	sulphate	BaSO_4	-4.6
Beryllium	bromide	BeBr_2	+62.6
	chloride	BeCl_2	+51.1
	iodide	BeI_2	+72.6
	sulphate	BeSO_4	+18.1
	sulphate	$\text{BeSO}_4 \cdot 4\text{H}_2\text{O}$	+1.1
Boric acid		H_3BO_3	-5.4
Cadmium	bromide	CdBr_2	+0.43
	bromide	$\text{CdBr}_2 \cdot 4\text{H}_2\text{O}$	-7.3
	chloride	CdCl_2	+3.11
	chloride	$\text{CdCl}_2 \cdot 2\frac{1}{2}\text{H}_2\text{O}$	-3.0
	cyanide	$\text{Cd}(\text{CN})_2$	+8.7
	fluoride	CdF_2	+8.7
	iodide	CdI_2	-3.3
	nitrate	$\text{Cd}(\text{NO}_3)_2$	+8.1
	nitrate	$\text{Cd}(\text{NO}_3)_2 \cdot 4\text{H}_2\text{O}$	-5.1
	sulphate	CdSO_4	+12.8
Caesium	bromate	CsBrO_3	-12.1
	bromide	CsBr	-6.2
	bicarbonate	CsHCO_3	-4.0
	chloride	CsCl	-4.6
	fluoride	CsF	+9.0
	fluoride	$\text{CsF} \cdot \text{H}_2\text{O}$	+2.5
	hydroxide	CsOH	+17.0
	hydroxide	$\text{CsOH} \cdot \text{H}_2\text{O}$	+4.9
	iodide	CsI	-7.9
	nitrate	CsNO_3	-9.6
	perchlorate	CsClO_4	-13.3
	sulphate	Cs_2SO_4	-4.9
	sulphide	Cs_2S	+27.3
Calcium	acetate	$\text{Ca}(\text{C}_2\text{H}_3\text{O}_2)_2$	+7.0
	acetate	$\text{Ca}(\text{C}_2\text{H}_3\text{O}_2)_2 \cdot \text{H}_2\text{O}$	+5.9
	bromide	CaBr_2	+26.3
	chloride	CaCl_2	+19.8
	chloride	$\text{CaCl}_2 \cdot 6\text{H}_2\text{O}$	-4.1
	chromate	CaCrO_4	+6.4
	fluoride	CaF_2	-2.2
	iodide	CaI_2	+28.0
	iodide	$\text{CaI}_2 \cdot 8\text{H}_2\text{O}$	+1.7
	nitrate	$\text{Ca}(\text{NO}_3)_2$	+4.1
	nitrate	$\text{Ca}(\text{NO}_3)_2 \cdot 4\text{H}_2\text{O}$	-8.0

Table A.14. (Continued)

<i>Substance</i>		<i>Formula</i>	<i>Heat of solution, kcal mol⁻¹</i>
	nitrite	Ca(NO ₂) ₂	+2.2
	sulphate	CaSO ₄	+5.2
	sulphate	CaSO ₄ · 2H ₂ O	-0.18
	sulphide	CaS	+4.5
Cerium	chloride	CeCl ₃	+33.6
	iodide	CeI ₃	+49.5
Chromium	chloride	CrCl ₂	+18.6
Cobalt	bromide	CoBr ₂	+18.4
	bromide	CoBr ₂ · 6H ₂ O	-1.3
	chloride	CoCl ₂	+18.5
	chloride	CoCl ₂ · 6H ₂ O	-2.9
	fluoride	CoF ₂	+14.6
	iodate	Co(IO ₃) ₂	+1.6
	iodide	CoI ₂	+18.4
	nitrate	Co(NO ₃) ₂	+11.9
	nitrate	Co(NO ₃) ₂ · 6H ₂ O	-4.9
	sulphate	CoSO ₄	+25.0
	sulphate	CoSO ₄ · 7H ₂ O	-3.6
Copper	acetate	Cu(C ₂ H ₃ O ₂) ₂	+2.5
	bromide	CuBr ₂	+8.8
	chloride	CuCl ₂	+12.2
	iodide	CuI ₂	+6.2
	nitrate	Cu(NO ₃) ₂	+10.4
	nitrate	Cu(NO ₃) ₂ · 6H ₂ O	-10.7
	sulphate	CuSO ₄	+15.9
	sulphate	CuSO ₄ · 5H ₂ O	-2.86
Ferric	chloride	FeCl ₃	+31.7
	chloride	FeCl ₃ · 6H ₂ O	+5.6
Ferrous	bromide	FeBr ₂	+19.1
	chloride	FeCl ₂	+17.9
	chloride	FeCl ₂ · 4H ₂ O	+2.7
	iodide	FeI ₂	+19.1
	sulphate	FeSO ₄	+14.9
	sulphate	FeSO ₄ · 7H ₂ O	-4.4
Lead	acetate	Pb(C ₂ H ₃ O ₂) ₂	+2.1
	acetate	Pb(C ₂ H ₃ O ₂) ₂ · 3H ₂ O	-5.9
	bromide	PbBr ₂	-8.8
	chloride	PbCl ₂	-6.5
	iodide	PbI ₂	-15.5
	nitrate	Pb(NO ₃) ₂	-9.0

Lithium	bromate	LiBrO_3	-0.34
	bromide	LiBr	+11.5
	bromide	$\text{LiBr} \cdot \text{H}_2\text{O}$	+5.6
	bromide	$\text{LiBr} \cdot 2\text{H}_2\text{O}$	+2.1
	carbonate	Li_2CO_3	+3.1
	chloride	LiCl	+8.8
	chloride	$\text{LiCl} \cdot \text{H}_2\text{O}$	+4.6
	chloride	$\text{LiCl} \cdot 3\text{H}_2\text{O}$	-2.0
	fluoride	LiF	-1.1
	hydroxide	LiOH	+5.1
	hydroxide	$\text{LiOH} \cdot \text{H}_2\text{O}$	+1.6
	iodide	LiI	+14.9
	iodide	$\text{LiI} \cdot \text{H}_2\text{O}$	+7.1
	iodide	$\text{LiI} \cdot 2\text{H}_2\text{O}$	+3.5
	iodide	$\text{LiI} \cdot 3\text{H}_2\text{O}$	-0.17
	nitrate	LiNO_3	+0.47
	nitrate	$\text{LiNO}_3 \cdot 3\text{H}_2\text{O}$	-7.9
	nitrite	LiNO_2	+2.6
	nitrite	$\text{LiNO}_2 \cdot \text{H}_2\text{O}$	-1.7
	perchlorate	LiClO_4	+6.3
	sulphate	Li_2SO_4	+6.7
	sulphate	$\text{Li}_2\text{SO}_4 \cdot \text{H}_2\text{O}$	+3.8
Magnesium	bromide	MgBr_2	+43.5
	bromide	$\text{MgBr}_2 \cdot 6\text{H}_2\text{O}$	+19.8
	chloride	MgCl_2	+36.0
	chloride	$\text{MgCl}_2 \cdot 6\text{H}_2\text{O}$	+3.1
	chromate	MgCrO_4	+2.9
	iodide	MgI_2	+50.2
	nitrate	$\text{Mg}(\text{NO}_3)_2 \cdot 6\text{H}_2\text{O}$	-3.7
	nitrate	$\text{Mg}(\text{NO}_3)_2$	+20.4
	perchlorate	$\text{Mg}(\text{ClO}_4)_2$	+31.9
	sulphate	MgSO_4	+21.1
	sulphate	$\text{MgSO}_4 \cdot 7\text{H}_2\text{O}$	-3.18
Manganese	acetate	$\text{Mn}(\text{C}_2\text{H}_3\text{O}_2)_2$	+12.2
	bromide	MnBr_2	+19.4
	chloride	MnCl_2	+16.0
	chloride	$\text{MnCl}_2 \cdot 4\text{H}_2\text{O}$	+1.5
	fluoride	MnF_2	+20.2
	iodide	MnI_2	+19.7
	nitrate	$\text{Mn}(\text{NO}_3)_2$	+12.7
	nitrate	$\text{Mn}(\text{NO}_3)_2 \cdot 6\text{H}_2\text{O}$	-6.1
	sulphate	MnSO_4	+13.8
	sulphate	$\text{MnSO}_4 \cdot 7\text{H}_2\text{O}$	-1.7
Mercuric	acetate	$\text{Hg}(\text{C}_2\text{H}_3\text{O}_2)_2$	-4.2
	bromide	HgBr_2	-2.4
	chloride	HgCl_2	-3.3
Nickel	bromide	NiBr_2	+19.0
	chloride	NiCl_2	+19.3

Table A.14. (Continued)

<i>Substance</i>	<i>Formula</i>	<i>Heat of solution, kcal mol⁻¹</i>
chloride	NiCl ₂ · 6H ₂ O	-1.15
iodate	Ni(IO ₃) ₂	+0.6
iodide	NiI ₂	+19.4
nitrate	Ni(NO ₃) ₂	+11.7
nitrate	Ni(NO ₃) ₂ · 6H ₂ O	-7.5
sulphate	NiSO ₄	+15.1
sulphate	NiSO ₄ · 7H ₂ O	-4.2
Potassium	acetate	KC ₂ H ₃ O ₂
	aluminium sulphate	K ₂ Al ₂ (SO ₄) ₄
	aluminium sulphate	KAl(SO ₄) ₂ · 12H ₂ O
	bicarbonate	KHCO ₃
	bisulphate	KHSO ₄
	bromate	KBrO ₃
	bromide	KBr
	carbonate	K ₂ CO ₃
	carbonate	K ₂ CO ₃ · 1½H ₂ O
	chlorate	KClO ₃
	chloride	KCl
	chromate	K ₂ CrO ₄
	cyanate	KCNO
	cyanide	KCN
	dichromate	K ₂ Cr ₂ O ₇
	dihydrogen phosphate	KH ₂ PO ₄
	ferricyanide	K ₃ Fe(CN) ₆
	ferrocyanide	K ₄ Fe(CN) ₆ · 3H ₂ O
	fluoride	KF
	fluoride	KF · 2H ₂ O
	hydroxide	KOH
	hydroxide	KOH · H ₂ O
	hydroxide	KOH · 1½H ₂ O
	iodate	KIO ₃
	iodide	KI
	nitrate	KNO ₃
	nitrite	KNO ₂
	oxalate	K ₂ C ₂ O ₄
	oxalate	K ₂ C ₂ O ₄ · H ₂ O
	perchlorate	KClO ₄
	permanganate	KMnO ₄
	sulphate	K ₂ SO ₄
	sulphite	K ₂ SO ₃
	sulphite	K ₂ SO ₃ · H ₂ O
	thiocyanate	KCNS
	thiosulphate	K ₂ S ₂ O ₃
Rubidium	bicarbonate	RbHCO ₃
	bisulphate	RbHSO ₄

	bromate	RbBrO_3	-11.7
	bromide	RbBr	-6.0
	chlorate	RbClO_3	-11.4
	chloride	RbCl	-4.2
	fluoride	RbF	+6.3
	fluoride	$\text{RbF} \cdot \text{H}_2\text{O}$	+0.10
	fluoride	$\text{RbF} \cdot 1\frac{1}{2}\text{H}_2\text{O}$	-0.32
	hydroxide	RbOH	+15.0
	hydroxide	$\text{RbOH} \cdot \text{H}_2\text{O}$	+4.3
	hydroxide	$\text{RbOH} \cdot 2\text{H}_2\text{O}$	-0.21
	iodide	RbI	-6.2
	nitrate	RbNO_3	-8.8
	perchlorate	RbClO_4	-13.6
	sulphate	Rb_2SO_4	-6.7
Silver	acetate	$\text{AgC}_2\text{H}_3\text{O}_2$	-5.4
	chlorate	AgClO_3	-3.92
	fluoride	AgF	-4.85
	nitrate	AgNO_3	-5.4
	nitrite	AgNO_2	-10.5
	perchlorate	AgClO_4	-1.65
Sodium	acetate	$\text{NaC}_2\text{H}_3\text{O}_2$	+4.1
	acetate	$\text{NaC}_2\text{H}_3\text{O}_2 \cdot 3\text{H}_2\text{O}$	-4.7
	arsenate	Na_3AsO_4	+31.0
	arsenate	$\text{Na}_3\text{AsO}_4 \cdot 12\text{H}_2\text{O}$	-12.6
	bicarbonate	NaHCO_3	-4.2
	borate (tetra)	$\text{Na}_2\text{B}_4\text{O}_7$	+10.3
	borate (borax)	$\text{Na}_2\text{B}_4\text{O}_7 \cdot 10\text{H}_2\text{O}$	-25.8
	bromate	NaBrO_3	-6.4
	bromide	NaBr	+0.15
	bromide	$\text{NaBr} \cdot 2\text{H}_2\text{O}$	-4.6
	carbonate	Na_2CO_3	+5.6
	carbonate	$\text{Na}_2\text{CO}_3 \cdot 10\text{H}_2\text{O}$	-16.2
	chlorate	NaClO_3	-5.4
	chloride	NaCl	-0.93
	chlorite	NaClO_2	+1.15
	chlorite	$\text{NaClO}_2 \cdot 3\text{H}_2\text{O}$	-6.8
	chromate	Na_2CrO_4	+2.4
	chromate	$\text{Na}_2\text{CrO}_4 \cdot 10\text{H}_2\text{O}$	-15.8
	cyanate	NaCNO	-4.7
	cyanide	NaCN	-0.50
	cyanide	$\text{NaCN} \cdot \frac{1}{2}\text{H}_2\text{O}$	-0.79
	cyanide	$\text{NaCN} \cdot 2\text{H}_2\text{O}$	-4.4
	dihydrogen phosphate	NaH_2PO_4	+5.6
	fluoride	NaF	-0.06
	hydroxide	NaOH	+10.2
	iodate	NaIO_3	-4.8
	iodide	NaI	+1.5
	iodide	$\text{NaI} \cdot 2\text{H}_2\text{O}$	-3.9
	nitrate	NaNO_3	-5.0

Table A.14. (Continued)

<i>Substance</i>	<i>Formula</i>	<i>Heat of solution, kcal mol⁻¹</i>	
nitrite	NaNO ₂	-3.6	
oxalate	Na ₂ C ₂ O ₄	-5.5	
perchlorate	NaClO ₄	-3.6	
perchlorate	NaClO ₄ · H ₂ O	-5.4	
phosphate	Na ₃ PO ₄	+13.0	
phosphate	Na ₃ PO ₄ · 12H ₂ O	-15.0	
pyrophosphate	Na ₄ P ₂ O ₇	+12.0	
pyrophosphate	Na ₄ P ₂ O ₇ · 10H ₂ O	-12.0	
sulphate	Na ₂ SO ₄	+0.28	
sulphate	Na ₂ SO ₄ · 10H ₂ O	-18.7	
sulphide	Na ₂ S	+15.2	
sulphide	Na ₂ S · 9H ₂ O	-16.7	
tartrate	Na ₂ C ₄ H ₄ O ₆	-1.1	
tartrate	Na ₂ C ₄ H ₄ O ₆ · 2H ₂ O	-5.9	
thiocyanate	NaCNS	-1.8	
thiosulphate	Na ₂ S ₂ O ₃	+1.8	
thiosulphate	Na ₂ S ₂ O ₃ · 5H ₂ O	-11.4	
Stannous	bromide	SnBr ₂	-1.7
	chloride	SnCl ₂	+0.36
	iodide	SnI ₂	-5.8
Strontium	acetate	Sr(C ₂ H ₃ O ₂) ₂	+6.2
	acetate	Sr(C ₂ H ₂ O ₃) ₂ · $\frac{1}{2}$ H ₂ O	+5.9
	bromide	SrBr ₂	+16.0
	bromide	SrBr ₂ · 6H ₂ O	-6.4
	chloride	SrCl ₂	-11.5
	chloride	SrCl ₂ · 6H ₂ O	-7.1
	hydroxide	Sr(OH) ₂	+10.3
	hydroxide	Sr(OH) ₂ · 8H ₂ O	-14.3
	iodide	SrI ₂	+20.4
	iodide	SrI ₂ · 6H ₂ O	-4.5
	nitrate	Sr(NO ₃) ₂	-4.8
	nitrate	Sr(NO ₃) ₂ · 4H ₂ O	-12.4
	nitrite	Sr(NO ₂) ₂	-1.1
	sulphate	SrSO ₄	+2.1
Thallium	bromate	TlBrO ₃	-13.8
	bromide	TlBr	-13.7
	chloride	TlCl	-10.0
	hydroxide	TlOH	-3.2
	iodide	TlI	-17.7
	nitrate	TlNO ₃	-10.0
	sulphate	Tl ₂ SO ₄	-8.3
Uranyl	nitrate	UO ₂ (NO ₃) ₂	+19.0
	nitrate	UO ₂ (NO ₃) ₂ · 6H ₂ O	-5.5
	sulphate	UO ₂ SO ₄ · 3H ₂ O	+5.0

Zinc	acetate	$\text{Zn}(\text{C}_2\text{H}_3\text{O}_2)_2$	+9.8
	acetate	$\text{Zn}(\text{C}_2\text{H}_3\text{O}_2)_2 \cdot 2\text{H}_2\text{O}$	+4.0
	bromide	ZnBr_2	+15.0
	chloride	ZnCl_2	+15.7
	iodide	ZnI_2	+11.6
	nitrate	$\text{Zn}(\text{NO}_3)_2$	+20.1
	nitrate	$\text{Zn}(\text{NO}_3)_2 \cdot 6\text{H}_2\text{O}$	-5.9
	sulphate	ZnSO_4	+18.5
	sulphate	$\text{ZnSO}_4 \cdot 7\text{H}_2\text{O}$	-4.3

Table A.15. Heats of solution of organic solids in water at approximately room temperature and infinite dilution

A positive value indicates an exothermic, a negative value an endothermic heat of solution
 $[1 \text{ kcal mol}^{-1} = 4.1868 \text{ kJ mol}^{-1}]$

Substance	Formula	Heat of solution kcal mol ⁻¹
Acetamide	CH ₃ CONH ₂	-2.0
Aconitic acid	C ₃ H ₃ (COOH) ₃	-4.2
Benzoic acid	C ₆ H ₅ COOH	-6.5
Chloral hydrate	CCl ₃ CH(OH) ₂	-0.90
Chloroacetic acid	CH ₂ ClCOOH	-3.4
Citric acid	C ₃ H ₄ OH(COOH) ₃	-5.4
Dextrose (α -D-glucose)	C ₆ H ₁₂ O ₆	-2.6
Dextrose (hydrate)	C ₆ H ₁₂ O ₆ · H ₂ O	-5.0
Fumaric acid	HOOC · CH : CH · COOH	-5.9
Hydroquinone	C ₆ H ₄ (OH) ₂	-4.4
<i>o</i> -Hydroxybenzoic acid	C ₆ H ₄ OHCOOH	-6.3
<i>m</i> -Hydroxybenzoic acid	C ₆ H ₄ OHCOOH	-6.2
<i>p</i> -Hydroxybenzoic acid	C ₆ H ₄ OHCOOH	-5.8
Itaconic acid	HOOC · C(:CH ₂)CH ₂ COOH	-5.9
Lactose	C ₁₂ H ₂₂ O ₁₁	+2.5
Lactose (hydrate)	C ₁₂ H ₂₂ O ₁₁ · H ₂ O	-3.7
Maleic acid	HOOC · CH : CH · COOH	-4.4
Malic acid (DL)	CH · OH · CH ₂ (COOH) ₂	-3.3
Malonic acid	CH ₂ (COOH) ₂	-4.5
Mannitol (D)	(CH ₂ OH) ₂ (CHOH) ₄	-5.3
<i>p</i> -Nitroaniline	C ₆ H ₄ NH ₂ NO ₂	-3.7
<i>o</i> -Nitrophenol	C ₆ H ₄ OHNO ₂	-6.3
<i>m</i> -Nitrophenol	C ₆ H ₄ OHNO ₂	-5.2
<i>p</i> -Nitrophenol	C ₆ H ₄ OHNO ₂	-4.5
Oxalic acid	(COOH) ₂	-2.3
Oxalic acid (hydrate)	(COOH) ₂ · 2H ₂ O	-8.5
Oxamic acid	NH ₂ CO · COOH	-6.9
Pentaerythritol	C(CH ₂ OH) ₄	-6.1
Phloroglucinol (1,3,5)	C ₆ H ₃ (OH) ₃	-1.7
Phloroglucinol (hydrate)	C ₆ H ₃ (OH) ₃ · H ₂ O	-6.7
Phthalic acid	C ₆ H ₄ (COOH) ₂	-4.8
Picric acid (2,4,6)	C ₆ H ₂ OH(NO ₂) ₃	-7.1
Pyrocatechol	C ₆ H ₄ (OH) ₂	-3.5
Pyrogallol (1,2,3)	C ₆ H ₃ (OH) ₃	-3.7
Raffinose	C ₁₈ H ₃₂ O ₁₆	+8.4
Raffinose (hydrate)	C ₁₈ H ₃₂ O ₁₆ · 5H ₂ O	-9.7
Resorcinol	C ₆ H ₄ (OH) ₂	-3.9
Salicylic acid	C ₆ H ₄ OHCOOH	-6.3
Succinic acid	(CH ₂ COOH) ₂	-6.4
Sucrose	C ₁₂ H ₂₂ O ₁₁	-1.3
Tartaric acid (D)	(CHOH · COOH) ₂	-3.5
Tartaric acid (DL)	(CHOH · COOH) ₂	-5.4
Thiourea	NH ₂ CSNH ₂	-5.3
Urea	NH ₂ CONH ₂	-3.6
Urea nitrate	NH ₂ CONH ₂ · HNO ₃	-10.8

Table A.16. *Heats of fusion of organic substances*[$1 \text{ cal g}^{-1} = 4.1868 \text{ kJ kg}^{-1}$]

<i>Substance</i>	<i>Formula</i>	<i>Melting point,</i> $^{\circ}\text{C}$	<i>Heat of fusion</i> cal g^{-1}
<i>o</i> -Aminobenzoic acid	C ₆ H ₄ NH ₂ COOH	145	35.5
<i>m</i> -Aminobenzoic acid	C ₆ H ₄ NH ₂ COOH	180	38.0
<i>p</i> -Aminobenzoic acid	C ₆ H ₄ NH ₂ COOH	189	36.5
Anthracene	C ₁₄ H ₁₀	217	38.7
Anthraquinone	(C ₆ H ₄) ₂ (CO) ₂	282	37.5
Benzene	C ₆ H ₆	5.5	30.1
Benzoic acid	C ₆ H ₅ COOH	122	33.9
Benzophenone	(C ₆ H ₅) ₂ CO	48	23.5
<i>t</i> -Butyl alcohol	C ₄ H ₉ OH	25	21.9
Cetyl alcohol	CH ₃ (CH ₂) ₁₄ CH ₂ OH	49	33.8
Cinnamic acid	C ₆ H ₅ CH : CH · COOH	133	36.5
<i>p</i> -Cresol	CH ₃ · C ₆ H ₄ OH	35	26.3
Cyanamide	NH ₂ CN	43	49.5
Cyclohexane	C ₄ H ₁₂	6.7	7.57
<i>p</i> -Dibromobenzene	C ₆ H ₄ Br ₂	86	20.6
<i>p</i> -Dichlorobenzene	C ₆ H ₄ Cl ₂	53	29.7
<i>p</i> -Di-iodobenzene	C ₆ H ₄ I ₂	129	16.2
<i>o</i> -Dinitrobenzene	C ₆ H ₄ (NO ₂) ₂	117	32.3
<i>m</i> -Dinitrobenzene	C ₆ H ₄ (NO ₂) ₂	90	24.7
<i>p</i> -Dinitrobenzene	C ₆ H ₄ (NO ₂) ₂	174	40.0
Diphenyl	C ₁₂ H ₁₀	69	28.8
Ethyl alcohol	C ₂ H ₅ OH	-114	25.8
Hexamethylbenzene	C ₁₂ H ₁₈	166	30.5
Hydroquinone	C ₆ H ₄ (OH) ₂	172	58.8
Methyl alcohol	CH ₃ OH	-98	23.7
Naphthalene	C ₁₀ H ₈	80	35.6
α -Naphthol	C ₁₀ H ₇ OH	95	38.9
β -Naphthol	C ₁₀ H ₇ OH	121	31.3
<i>o</i> -Nitroaniline	C ₆ H ₄ NH ₂ NO ₂	70	27.9
<i>m</i> -Nitroaniline	C ₆ H ₄ NH ₂ NO ₂	113	41.0
<i>p</i> -Nitroaniline	C ₆ H ₄ NH ₂ NO ₂	147	36.5
Nitrobenzene	C ₆ H ₅ NO ₂	6	22.5
Phenanthrene	C ₁₄ H ₁₀	97	24.5
Phenol	C ₆ H ₅ OH	41	29.0
Pyrocatechol	C ₆ H ₄ (OH) ₂	104	49.4
Resorcinol	C ₆ H ₄ (OH) ₂	110	46.2
Stearic acid	C ₁₇ H ₃₅ COOH	68	47.6
Stilbene	C ₁₄ H ₁₂	124	40.0
Toluene	C ₆ H ₅ CH ₃	-95	17.2
<i>o</i> -Toluic acid	CH ₃ C ₆ H ₄ COOH	104	35.4
<i>m</i> -Toluic acid	CH ₃ C ₆ H ₄ COOH	109	27.6
<i>p</i> -Toluic acid	CH ₃ C ₆ H ₄ COOH	180	40.0
<i>p</i> -Toluidine	CH ₃ C ₆ H ₄ NH ₂	43	39.9
Thymol	C ₁₀ H ₁₃ OH	50	27.5
<i>p</i> -Xylene	C ₆ H ₄ (CH ₃) ₂	-25	30.6
<i>m</i> -Xylene	C ₆ H ₄ (CH ₃) ₂	-48	26.1
<i>p</i> -Xylene	C ₆ H ₄ (CH ₃) ₂	13	38.5

Table A.17. Common names of crystalline substances

Common name	Chemical name	Formula
Adamantane	tricyclodecane	$(\text{CH}_2)_8(\text{CH})_2$
ADP (see MAP)	ammonium dihydrogenphosphate	$\text{NH}_4\text{H}_2\text{PO}_4$
Alabaster	calcium sulphate	CaSO_4
Alum	$M_2^{\text{I}}\text{SO}_4 \cdot M_2^{\text{III}}(\text{SO}_4)_3 \cdot 24\text{H}_2\text{O}$	e.g. $\text{K}_2\text{SO}_4 \cdot \text{Al}_2(\text{SO}_4)_3 \cdot 24\text{H}_2\text{O}$
Alumina	aluminium oxide	Al_2O_3
Anhydrite	calcium sulphate	CaSO_4
Antifebrin	acetanilide (phenylacetamide)	$\text{C}_6\text{H}_5 \cdot \text{NH} \cdot \text{COCH}_3$
Antimonite	antimony trisulphide	Sb_2S_3
Apatite	tricalcium phosphate	$\text{Ca}_3(\text{PO}_4)_2$
Aragonite	calcium carbonate (orthorhombic)	CaCO_3
Arcanite	potassium sulphate	K_2SO_4
Argenite	silver sulphide	Ag_2S
Aspartic acid	aminosuccinic acid	$\text{CH}_3 \cdot \text{CH}(\text{NH}_2) \cdot (\text{COOH})_2$
Aspirin	acetylsalicylic acid	$\text{C}_6\text{H}_4 \cdot \text{OCOCH}_3 \cdot \text{COOH}$
Astracanite	magnesium sodium sulphate	$\text{MgSO}_4 \cdot \text{Na}_2\text{SO}_4 \cdot 4\text{H}_2\text{O}$
Baking soda	sodium bicarbonate	NaHCO_3
Baryta	barium oxide	BaO
Bayer hydrate	aluminium oxide trihydrate	$\text{Al}_2\text{O}_3 \cdot 3\text{H}_2\text{O}$
Bayerite	aluminium oxide trihydrate	$\text{Al}_2\text{O}_3 \cdot 3\text{H}_2\text{O}$
Beet sugar	sucrose	$\text{C}_{12}\text{H}_{22}\text{O}_{11}$
Berlin green	iron(III) ferricyanide	$\text{Fe}[\text{Fe}(\text{CN})_6]$
Berlinite	aluminium orthophosphate (α -)	AlPO_4
Berthollot's salt	potassium chlorate	KClO_3
Betol	β -naphthyl salicylate	$\text{C}_6\text{H}_4 \cdot \text{OH} \cdot \text{COOC}_{10}\text{H}_7$
Bischofite	magnesium chloride	$\text{MgCl}_2 \cdot 6\text{H}_2\text{O}$
Biuret	ureidoformamide	$\text{NH}(\text{CONH}_2)_2$
Blanc fixe	precipitated barium sulphate	BaSO_4
Blood sugar	dextrose (α -D-glucose)	$\text{C}_6\text{H}_{12}\text{O}_6 \cdot \text{H}_2\text{O}$
Blue vitriol	copper(II) sulphate	$\text{CuSO}_4 \cdot 5\text{H}_2\text{O}$
Bobierite	magnesium orthophosphate	$\text{Mg}_3(\text{PO}_4)_2 \cdot 4\text{H}_2\text{O}$
Boehmite	aluminium oxyhydroxide (α -)	$\text{AlO}(\text{OH})$
Boracic acid	boric acid	H_3BO_3
Boracite	magnesium chloride borate	$5\text{MgO} \cdot \text{MgCl}_2 \cdot 7\text{B}_2\text{O}_3$
Borax	sodium tetraborate	$\text{Na}_2\text{B}_4\text{O}_7 \cdot 10\text{H}_2\text{O}$
Bromyrite	silver bromide	AgBr
Brucite	magnesium hydroxide	$\text{Mg}(\text{OH})_2$
Brushite	calcium hydrogenphosphate	$\text{CaHPO}_4 \cdot 2\text{H}_2\text{O}$
Burkeite	sodium sulphate carbonate	$2\text{Na}_2\text{SO}_4 \cdot \text{Na}_2\text{CO}_3$
Calamine	zinc carbonate	ZnCO_3
Calcite	calcium carbonate (trigonal)	CaCO_3
Calomel	mercury(I) chloride	Hg_2Cl_2
Cane sugar	sucrose	$\text{C}_{12}\text{H}_{22}\text{O}_{11}$
Carbolic acid	phenol	$\text{C}_6\text{H}_5\text{OH}$
Carnallite	magnesium potassium chloride	$\text{MgCl}_2 \cdot \text{KCl} \cdot 6\text{H}_2\text{O}$
Caustic, lunar	silver nitrate	AgNO_3
Caustic potash	potassium hydroxide	KOH
Caustic soda	sodium hydroxide	NaOH

Celestite	strontium carbonate	SrCO_3
Cerargyrite	silver chloride	AgCl
Ceruse	basic lead carbonate	$2\text{PbCO}_3 \cdot \text{Pb}(\text{OH})_2$
Cerrussite	lead carbonate	PbCO_3
Chamber crystals	nitrosylsulphuric acid	NOHSO_4
Chevreul's salt	copper (I, II) sulphite	$\text{Cu}_2\text{SO}_3 \cdot \text{CuSO}_3 \cdot 2\text{H}_2\text{O}$
Chile saltpetre	sodium nitrate	NaNO_3
Chlorocalcite	potassium calcium chloride	$\text{KCl} \cdot \text{CaCl}_2$
Chrome alum	$\text{M}_2\text{SO}_4 \cdot \text{Cr}_2(\text{SO}_4)_3 \cdot 24\text{H}_2\text{O}$	e.g. $\text{K}_2\text{SO}_4 \cdot \text{Cr}_2(\text{SO}_4)_3 \cdot 24\text{H}_2\text{O}$
Chrome green	chromium(III) sesquioxide	Cr_2O_3
Chrome red	basic lead chromate	$\text{PbCrO}_4 \cdot \text{PbO}$
Chrome yellow	lead chromate	PbCrO_4
Cinnabar	mercury(II) sulphide	HgS
Colemanite	calcium borate	$2\text{CaO} \cdot 3\text{B}_2\text{O}_3 \cdot 5\text{H}_2\text{O}$
Collins' salt	strontium phosphate	$\text{Sr}_6\text{H}_3(\text{PO}_3)_5 \cdot 2\text{H}_2\text{O}$
Common salt	sodium chloride	NaCl
Copperas	iron(II) sulphate	$\text{FeSO}_4 \cdot 7\text{H}_2\text{O}$
Corn sugar	dextrose (α -D-glucose)	$\text{C}_6\text{H}_{12}\text{O}_6 \cdot \text{H}_2\text{O}$
Corrosive sublimate	mercury(II) chloride	HgCl_2
Corundum	aluminium oxide	Al_2O_3
Cream of tartar	potassium hydrogen tartrate	$\text{KHC}_4\text{H}_4\text{O}_6$
Crocoite	lead chromate	PbCrO_4
Cryolite	aluminium sodium fluoride	$\text{AlF}_3 \cdot 3\text{NaF}$
Crystal carbonate	sodium carbonate	$\text{Na}_2\text{CO}_3 \cdot \text{H}_2\text{O}$
Crystal violet	hexamethyl pararosaniline · HCl	$\text{C}_{19}\text{H}_{19}\text{N}_3\text{O} \cdot \text{HCl}$
DAP	diammonium phosphate	$(\text{NH}_4)_2\text{HPO}_4$
Darapskite	sodium sulphate nitrate	$\text{Na}_2\text{SO}_4 \cdot \text{Na}_2\text{NO}_3$
Dextrose	α -D-glucose	$\text{C}_6\text{H}_{12}\text{O}_6 \cdot \text{H}_2\text{O}$
Diaspose	aluminium oxide monohydrate	$\text{Al}_2\text{O}_3 \cdot \text{H}_2\text{O}$
Dithionite	sodium hydrosulphite	$\text{Na}_2\text{S}_2\text{O}_4 \cdot 2\text{H}_2\text{O}$
Diuretic salt	potassium acetate	CH_3COOK
Dolomite	magnesium calcium carbonate	$\text{MgCO}_3 \cdot \text{CaCO}_3$
Dung salt	disodium arsenate	Na_2HAsO_4
EDT	ethylenediamine tartrate	$(\text{CH}_2 \cdot \text{NH}_2)_2(\text{C}_4\text{H}_6\text{O}_6) \cdot \text{H}_2\text{O}$
Epsomite	magnesium sulphate	$\text{MgSO}_4 \cdot 7\text{H}_2\text{O}$
Epsom salts	magnesium sulphate	$\text{MgSO}_4 \cdot 7\text{H}_2\text{O}$
Erdmann's salt	ammonium tetranitro diammine cobaltate	$\text{NH}_4[\text{Co}(\text{NH})_2(\text{NO})_4]$
Everitt's salt	potassium iron(II) ferrocyanide	$\text{K}_2\text{Fe} \cdot \text{Fe}(\text{CN})_6$
Febrifuge salt	potassium chloride	KCl
Fischer's salt	potassium cobaltinitritite	$\text{K}_3[\text{Co}(\text{NO}_2)_6]$
Fixed nitre	potassium carbonate	K_2CO_3
Flowers of sulphur	sulphur	S
Fluorapatite	calcium fluophosphate	$\text{Ca}_5(\text{PO}_4)_3\text{F}$
Fluorite	calcium fluoride	CaF_2
Fremy's salt	potassium hydrogenfluoride	KHF_2
Fruit sugar	fructose	$\text{C}_6\text{H}_{12}\text{O}_6$
Gaylussite	sodium calcium carbonate	$\text{Na}_2\text{CO}_3 \cdot \text{CaCO}_3 \cdot 5\text{H}_2\text{O}$
Gibbsite	aluminium oxide trihydrate	$\text{Al}_2\text{O}_3 \cdot 3\text{H}_2\text{O}$

Table A.17. (Continued)

<i>Common name</i>	<i>Chemical name</i>	<i>Formula</i>
Glaserite	potassium sodium sulphate	$K_3Na(SO_4)_2$
Glauberite	sodium calcium sulphate	$Na_2SO_4 \cdot CaSO_4$
Glauber's salt	sodium sulphate decahydrate	$Na_2SO_4 \cdot 10H_2O$
Glycine	aminoacetic acid	$NH_2 \cdot CH_2 \cdot COOH$
Goethite	iron(III) oxyhydroxide	$FeO(OH)$
Graham's salt	sodium hexametaphosphate	$(NaPO_3)_6$
Grape sugar	dextrose (α -D-glucose)	$C_6H_{12}O_6 \cdot H_2O$
Green vitriol	iron(II) sulphate	$FeSO_4 \cdot 7H_2O$
Gypsum	calcium sulphate	$CaSO_4 \cdot 2H_2O$
Haematite	iron(III) oxide	Fe_2O_3
Halite	sodium chloride	$NaCl$
Hanksite	$[Na \cdot K \cdot SO_4 \cdot CO_3 \cdot Cl]$	$9Na_2SO_4 \cdot 2Na_2CO_3 \cdot KCl$
Hartshorn salt	ammonium carbonate	$(NH_4)_2CO_3$
Hexahydrate	magnesium sulphate	$MgSO_4 \cdot 6H_2O$
Hexamine	hexamethylenetetramine	$(CH_2)_6N_4$
Homberg's salt	boric acid	H_3BO_4
Hopeite	zinc phosphate	$Zn_3(PO_4)_2 \cdot 4H_2O$
Horn silver	silver chloride	$AgCl$
Hydargillite	aluminium oxide trihydrate	$Al_2O_3 \cdot 3H_2O$
Hydrohalite	sodium chloride dihydrate	$NaCl \cdot 2H_2O$
Hydromagnesite	basic magnesium carbonate	$3MgCO_3 \cdot Mg(OH)_2 \cdot 3H_2O$
Hydroxyapatite	calcium phosphate	$Ca_5(PO_4)_3OH$
Hypo	sodium thiosulphate	$Na_2S_2O_3 \cdot 5H_2O$
Iodrite	silver iodide	AgI
Iron alum	$M_2^I(SO_4) \cdot Fe_2(SO_4)_3 \cdot 24H_2O$	e.g. $(NH_4)_2SO_4 \cdot Fe_2(SO_4)_3 \cdot 24H_2O$
Iron black	precipitated antimony	Sb
Itaconic acid	methylene succinic acid	$CH_2:C(CO_2CH_3)CH_2CO_2H$
Kainite	$[Mg \cdot K \cdot Cl \cdot SO_4]$	$MgSO_4 \cdot KCl \cdot 3H_2O$
Kalicine	potassium bicarbonate	$KHCO_3$
Kalle's salt	acetone bisulphite	$CH_3 \cdot CO \cdot CH_3NaHSO_3$
KDP	potassium dihydrogen phosphate	KH_2PO_4
Kernite	sodium borate	$Na_2O \cdot 2B_2O_3 \cdot 4H_2O$
Kieserite	magnesium sulphate	$MgSO_4 \cdot H_2O$
Klee's salt	potassium hydrogen oxalate	$KHC_2O_4 \cdot H_2O$
Knorre's salt	sodium trimetaphosphate	$(NaPO_3)_3 \cdot 6H_2O$
Krugite	$[Ca \cdot Mg \cdot K \cdot SO_4]$	$4CaSO_4 \cdot MgSO_4 \cdot K_2SO_4 \cdot 2H_2O$
Langbeinite	magnesium potassium sulphate	$2MgSO_4 \cdot K_2SO_4$
Larch sugar	melezitose	$C_{18}H_{32}O_{16}$
Lemon chrome	barium chromate	$BaCrO_4$
Leonite	magnesium potassium sulphate	$MgSO_4 \cdot K_2SO_4 \cdot 4H_2O$
Litharge	red-brown lead monoxide	PbO
Liver of sulphur	potassium bisulphide	KHS
Löweite	magnesium sodium sulphate	$2MgSO_4 \cdot 2Na_2SO_4 \cdot 5H_2O$
Lunar caustic	silver nitrate	$AgNO_3$
Macquer's salt	potassium dihydrogenarsenate	KH_2AsO_4
Magnesite	magnesium carbonate	$MgCO_3$

Magnus' green salt	platinum tetrammine chloroplatinate	$\text{Pt}(\text{NH}_3)_4 \cdot \text{PtCl}_4$
Malic acid	hydroxysuccinic acid	$\text{CH}_2 \cdot \text{CH}(\text{OH})(\text{COOH})_2$
Malt sugar	maltose	$\text{C}_{12}\text{H}_{22}\text{O}_{11} \cdot \text{H}_2\text{O}$
Manganese alum	$\text{M}_2'\text{SO}_4 \cdot \text{Mn}_2(\text{SO}_4)_3 \cdot 24\text{H}_2\text{O}$	e.g. $\text{K}_2\text{SO}_4 \cdot \text{Mn}(\text{SO}_4)_3 \cdot 24\text{H}_2\text{O}$
Manganese white	manganese(II) carbonate	MnCO_3
Mandelic acid	hydroxyphenylacetic acid	$\text{CH}(\text{OH})(\text{C}_6\text{H}_5)\text{COOH}$
Manganite	manganese hydroxide	$\text{MnO}(\text{OH})$
MAP (see ADP)	monoammonium phosphate	$\text{NH}_4\text{H}_2\text{PO}_4$
Marignac's salt	potassium tin(II) sulphate	$\text{K}_2\text{Sn}(\text{SO}_4)_2$
Mascagnite	ammonium sulphate	$(\text{NH}_4)_2\text{SO}_4$
Massicot	yellow lead monoxide	PbO
Matt salt	ammonium hydrogen fluoride	NH_4HF_2
Maus' salt	potassium iron(III) sulphate	$\text{K}_5\text{Fe}_3(\text{SO}_4)_6(\text{OH})_2 \cdot 9\text{H}_2\text{O}$
Mercury fulminate	mercury(II) isocyanate	$\text{Hg}(\text{OCN})_2$
Mellitene	hexamethylbenzene	$\text{C}_{12}\text{H}_{18}$
Michler's ketone	tetramethyldiamino-benzophenone	$[(\text{CH}_3)_2\text{N} \cdot \text{C}_6\text{H}_4]_2\text{CO}$
Microcosmic salt	ammonium sodium phosphate	$\text{NH}_4\text{NaHPO}_4 \cdot 4\text{H}_2\text{O}$
Milk sugar	lactose	$\text{C}_{12}\text{H}_{22}\text{O}_{11}$
Mirabilite	sodium sulphate decahydrate	$\text{Na}_2\text{SO}_4 \cdot 10\text{H}_2\text{O}$
Miserite	potassium hydrogen sulphate	KHSO_4
Mohr's salt	iron(II) ammonium sulphate	$\text{FeSO}_4 \cdot (\text{NH}_4)_2\text{SO}_4 \cdot 6\text{H}_2\text{O}$
Monetite	calcium hydrogenphosphate	CaHPO_4
Mosaic gold	tin(IV) sulphide	SnS_2
Muriate of potash	potassium chloride	KCl
Nahcolite	sodium bicarbonate	NaHCO_3
Natron	sodium carbonate decahydrate	$\text{Na}_2\text{CO}_3 \cdot 10\text{H}_2\text{O}$
Newberyite	magnesium hydrogen phosphate	$\text{MgHPO}_4 \cdot 3\text{H}_2\text{O}$
Nickel, salt, single	nickel sulphate hexahydrate	$\text{NiSO}_4 \cdot 6\text{H}_2\text{O}$
Nickel salt, double	nickel ammonium sulphate	$\text{NiSO}_4 \cdot (\text{NH}_4)_2\text{SO}_4 \cdot 6\text{H}_2\text{O}$
Nickel vitriol	nickel sulphate heptahydrate	$\text{NiSO}_4 \cdot 7\text{H}_2\text{O}$
Nitre	potassium nitrate	KNO_3
Octacalcium phosphate	calcium phosphate	$\text{Ca}_8\text{H}_2(\text{PO}_4)_6 \cdot 5\text{H}_2\text{O}$
Paracetamol	p · hydroxyacetanilide	$\text{OH} \cdot \text{C}_6\text{H}_4 \cdot \text{NH} \cdot \text{COCH}_3$
Paris green	copper(II) hydrogen arsenite or heptamethylparosaniline · HCl	CuHAsO_3 or $\text{C}_{25}\text{H}_{30}\text{N}_3 \cdot \text{HCl}$
Paris yellow	lead chromate	PbCrO_4
Pearl ash	potassium carbonate	K_2CO_3
Pearl white	bismuth oxychloride or basic nitrate	BiOCl or $\text{Bi}(\text{OH})_2\text{NO}_3$
Penta salt	calcium potassium sulphate	$5\text{CaSO}_4 \cdot \text{K}_2\text{SO}_4 \cdot \text{H}_2\text{O}$
Perlate salt	disodium phosphate	Na_2HPO_4
Picric acid	trinitrophenol	$\text{OH} \cdot \text{C}_6\text{H}_2(\text{NO}_3)_3$
Pink salt	ammonium tin(IV) chloride	$2\text{NH}_4\text{Cl} \cdot \text{SnCl}_4$
Plaster of Paris	calcium sulphate hemihydrate	$\text{CaSO}_4 \cdot \frac{1}{2}\text{H}_2\text{O}$
Plimmer's salt	sodium antimony tartrate	$\text{NaSbO} \cdot \text{C}_4\text{H}_4\text{O}_6 \cdot 2\text{H}_2\text{O}$
Polyhalite	$[\text{K} \cdot \text{Mg} \cdot \text{Ca} \cdot \text{SO}_4]$	$\text{K}_2\text{SO}_4 \cdot \text{MgSO}_4 \cdot 2\text{CaSO}_4 \cdot 2\text{H}_2\text{O}$
Potash	potassium carbonate	K_2CO_3

Table A.17. (Continued)

<i>Common name</i>	<i>Chemical name</i>	<i>Formula</i>
Potash alum	potassium aluminium sulphate	$K_2SO_4 \cdot Al_2(SO_4)_3 \cdot 24H_2O$
Prismatic nitre	potassium nitrate	KNO_3
Prussian blue	Ferric ferrocyanide	$Fe_4[Fe(CN)_6]_3$
Prussiate of potash (yellow)	potassium ferrocyanide	$K_4Fe(CN)_6 \cdot 3H_2O$
Prussiate of potash (red)	potassium ferricyanide	$K_3Fe(CN)_6$
Preparing salt	sodium stannate	$Na_2SnO_3 \cdot 3H_2O$
Purging salt	sodium dihydrogenphosphate	$NaH_2PO_4 \cdot H_2O$
Quinol	hydroquinone (<i>p</i>)	$C_6H_4(OH)_2$
Quartz	silicon dioxide (hexagonal)	SiO_2
Racemic acid	DL-tartaric acid	$(CHOH \cdot COOH)_2$
Red precipitate	mercury(II) oxide	HgO
Rochelle salt	sodium potassium tartrate	$NaKC_4H_4O_6 \cdot 4H_2O$
Rock crystal	silicon dioxide (quartz)	SiO_2
Rock salt	sodium chloride	$NaCl$
Saccharose	sucrose	$C_{12}H_{22}O_{11}$
Sal-ammoniac	ammonium chloride	NH_4Cl
Salol	phenyl salicylate	$C_6H_4 \cdot OH \cdot COOC_6H_5$
Salt	sodium chloride	$NaCl$
Salt cake	sodium sulphate	Na_2SO_4
Salt of tartar	potassium carbonate	K_2CO_3
Saltpetre	potassium nitrate	KNO_3
Salts of lemon	potassium hydrogen oxalate or potassium tetroxalate	$KHC_2O_4 \cdot H_2O$ or $KHC_2O_4 \cdot H_2C_2O_4 \cdot 2H_2O$
Salts of sorrel	potassium hydrogen oxalate	$KHC_2O_4 \cdot H_2O$
Saturn salt	lead acetate	$Pb(C_2H_3O_2)_2$
Scheele's green	copper(II) hydrogen arsenite	$CuHAsO_3$
Scheelite	calcium tungstate	$CaWO_4$
Schlippe's salt	sodium thioantimonate	$Na_3SbS_4 \cdot 9H_2O$
Schoenite	magnesium potassium sulphate	$MgSO_4 \cdot K_2SO_4 \cdot 6H_2O$
Schutzenberger's salt	sodium hydrogensulphite	$NaHSO_3$
Seidlitz salt	magnesium sulphate	$MgSO_4 \cdot 7H_2O$
Seignette's salt	sodium potassium tartrate	$NaKC_4H_4O_6 \cdot 4H_2O$
Siderite	ferrous carbonate	$FeCO_3$
Silver salt	sodium anthraquinone β -sulphonate	$C_{14}H_7O_2 \cdot SO_3Na$
Single nickel salt	nickel sulphate hexahydrate	$NiSO_4 \cdot 6H_2O$
Smithsonite	zinc carbonate	$ZnCO_3$
Soda ash	sodium carbonate	Na_2CO_3
Soluble tartar	potassium DL-tartrate	$K_2C_4H_4O_6 \cdot 2H_2O$
Sörensen's salt	sodium monohydrogenphosphate	$Na_2HPO_4 \cdot 2H_2O$
Soubierom's salt	mercury ammonium nitrate	$(NH_2Hg_2O)NO_3$
Spinel	$M^{II}O \cdot M^{III}_2O_3$	e.g. $MgO \cdot Al_2O_3$
Stahl's salt	potassium sulphite	$K_2SO_3 \cdot 2H_2O$
Stibnite	antimony trisulphide	Sb_2S_3
Strengite	ferric orthophosphate	$FePO_4 \cdot 2H_2O$

Strontianite	strontium carbonate	SrCO_3
Styphnic acid	2:4:6 trinitroresorcinol	$\text{C}_6\text{H} \cdot (\text{OH})_2 \cdot (\text{NO}_2)_3$
Struvite	ammonium magnesium phosphate	$\text{NH}_4\text{MgPO}_4 \cdot 6\text{H}_2\text{O}$
Sugar	sucrose	$\text{C}_{12}\text{H}_{22}\text{O}_{11}$
Sugar of lead	lead acetate	$\text{Pb}(\text{CH}_3\text{COO})_2 \cdot 3\text{H}_2\text{O}$
Sugar of gelatin	aminoacetic acid	$\text{CH}_2 \cdot \text{NH}_2 \cdot \text{COOH}$
Sulphamic acid	aminosulphonic acid	$\text{NH}_2\text{SO}_3\text{H}$
Syngenite	potassium calcium sulphate	$\text{K}_2\text{SO}_4 \cdot \text{CaSO}_4 \cdot \text{H}_2\text{O}$
Sylvite	potassium chloride	KCl
Tachhydrite	calcium magnesium chloride	$\text{CaCl}_2 \cdot 2\text{MgCl}_2 \cdot 12\text{H}_2\text{O}$
Tartar emetic	potassium antimony tartrate	$\text{KSb} \cdot \text{C}_4\text{H}_4\text{O}_6 \cdot \frac{1}{2}\text{H}_2\text{O}$
Tartar, soluble	potassium D,L -tartrate	$\text{K}_2\text{C}_4\text{H}_4\text{O}_6 \cdot 2\text{H}_2\text{O}$
Tartrate	potassium hydrogen D,L -tartrate	$\text{KHC}_4\text{H}_4\text{O}_6$
Tetralin	tetrahydronaphthalene	$\text{C}_{10}\text{H}_{12}$
Tetryl	trinitrophenylmethylnitramine	$\text{C}_6\text{H}_3(\text{NO}_2)_3\text{N}(\text{CH}_3)\text{NO}_2$
TGS	triglycine sulphate	$(\text{NH}_2\text{CH}_2\text{COOH})_3\text{H}_2\text{SO}_4$
Thermodite	sodium sulphate	Na_2SO_4
Thermonatrite	sodium carbonate monohydrate	$\text{Na}_2\text{CO}_3 \cdot \text{H}_2\text{O}$
Tincal (borax)	sodium tetraborate	$\text{Na}_2\text{B}_4\text{O}_7 \cdot 10\text{H}_2\text{O}$
Tin crystals	tin(II) chloride	SnCl_2
TNT	2: 4: 6 trinitrotoluene	$\text{C}_6\text{H}_5 \cdot \text{CH}_3 \cdot (\text{NO}_2)_3$
Trimesic acid	benzenetricarboxylic acid	$\text{C}_6\text{H}_3(\text{COOH})_3$
Trona	sodium sesquicarbonate	$\text{Na}_2\text{CO}_3 \cdot \text{NaHCO}_3 \cdot 2\text{H}_2\text{O}$
Tutton salt	$M^{\text{I}}_2\text{SO}_4 \cdot M^{\text{II}}(\text{SO}_4) \cdot 6\text{H}_2\text{O}$	e.g. $(\text{NH}_4)_2\text{SO}_4 \cdot \text{NiSO}_4 \cdot 6\text{H}_2\text{O}$
Valentinite	antimony trioxide	Sb_2O_3
Vanthoffite	magnesium sodium sulphate	$\text{MgSO}_4 \cdot 3\text{Na}_2\text{SO}_4$
Variscite	aluminium orthophosphate	$\text{AlPO}_4 \cdot 2\text{H}_2\text{O}$
Vaterite	calcium carbonate (hexagonal)	CaCO_3
Vitamin C	L-ascorbic acid	$\text{C}_6\text{H}_8\text{O}_6$
Vivianite	ferrous orthophosphate	$\text{Fe}_3(\text{PO}_4)_2 \cdot 8\text{H}_2\text{O}$
Washing soda	sodium carbonate	$\text{Na}_2\text{CO}_3 \cdot 10\text{H}_2\text{O}$
White arsenic	arsenic oxide	As_2O_3
White lead	basic lead carbonate	$2\text{PbCO}_3 \cdot \text{Pb}(\text{OH})_2$
White precipitate	mercury (II) ammonium chloride	HgNH_2Cl
White vitriol	zinc sulphate	$\text{ZnSO}_4 \cdot 7\text{H}_2\text{O}$
Whiting	calcium carbonate	CaCO_3
Witherite	barium carbonate	BaCO_3
Wood sugar	xylose	$\text{C}_5\text{H}_{10}\text{O}_5$
Xylitol	pentanpentol	$\text{C}_5\text{H}_{12}\text{O}_5$
Yellowcake	ammonium polyuranate	$(\text{NH}_4)_2\text{U}_2\text{O}_7$

References

- Abegg, C.F. and Balakrishnan, N.S. (1971) The tanks-in-series concept as a model for imperfectly mixed crystallizers. *Chemical Engineering Progress Symposium Series No. 110*, **67**, 88–96.
- Abegg, C.F., Stevens, J.D. and Larson, M.A. (1968) Crystal size distributions in continuous crystallizers when growth rate is size-dependent. *AICheJ*, **14**, 118–122.
- Abrahart, E. (1977) *Dyes and their Intermediates*, 2nd edn., Arnold, London.
- Adams, J.R. and Ross, W.H. (1941) Relative caking tendencies of fertilizers. *Industrial and Engineering Chemistry*, **33**, 121–127.
- Adamski, T. (1963) Combination of crystal nucleation by a precipitation method. *Nature*, **197**, 894.
- AIChe (2000) *Profiles in Flue Gas Desulfurization*, AIChe, Washington; IChemE, Rugby.
- Ajinkya, M.B. and Ray, W.H. (1974) On the optimal operation of crystallization processes. *Chemical Engineering Communications*, **1**, 181–186.
- Akiya, T., Owa, M., Kawasaki, S., Goto, T. and Toyokura, K. (1976) The operation of a NaOH 3·5 H₂O crystallizer by direct contact cooling. In *Industrial Crystallization* (6th Symposium, Usti nad Labem), J.W. Mullin (ed.), Plenum Press, London, 421–429.
- Albertins, R., Gates, W.C. and Powers, J.E. (1967) Column crystallization. In *Fractional Solidification*, M. Zief and W.R. Wilcox (eds.), Dekker, New York.
- Albon, N. and Dunning, W.J. (1962) Growth of sucrose crystals: the behaviour of growth steps on sucrose crystals. *Acta Crystallographia*, **15**, 474–476.
- Alfassi, Z.B. and Mosseri, S. (1984) Solventing-out of electrolytes from their aqueous solution. *AICheJ*, **30**, 874–876.
- Allen, A.T., McDonald, M.P., Nicol, W.H. and Wood, R.M. (1972) Athermal concentration gradients in supersaturated solutions of sucrose. *Nature*, **235**, 36–37.
- Allen, T. (1990) *Particle Size Measurement*. 4th edn., Chapman and Hall, London.
- Al-Rashed, M.H. and Jones, A.G. (1999) CFD modelling of gas-liquid reactive precipitation. *Chemical Engineering Science*, **54**, 4779–4784.
- Altria, K.D. (2000) Capillary electrophoresis. *Chemistry in Britain*, **36**, (11), 38–41.
- Amin, A.B. and Larson, M.A. (1968) Crystallization of calcium sulphate from phosphoric acid. *Industrial and Engineering Chemistry Process Design and Development*, **7**, 133–137.
- Ananth, R. and Gill, W.N. (1991) Self-consistent theory of dendritic growth with convection. *Journal of Crystal Growth*, **108**, 173–189.
- Ang, H-M. and Mullin, J.W. (1979) Crystal growth rate determinations from desuper-saturation measurements: nickel ammonium sulphate hexahydrate. *Transactions of the Institution of Chemical Engineers*, **57**, 237–242.
- Anwar, J. and Boateng, P.K. (1998) Computer simulation of crystallization from solution. *Journal of the American Chemical Society*, **120**, 9600–9604.
- Aoyama, Y., Kawakami, G. and Miki, H. (1979) Pelletizing process of aluminium hydroxide for disposal of effluent from aluminium anodizing equipment. In *Industrial Crystallization 78* (7th Symposium, Warsaw), E.J. de Jong and S.J. Jančić (eds.), 465–472.

- Aquilano, D., Franchini-Angela, M., Rubbo, M., Mantovani, G. and Vaccari, G. (1983) Growth morphology of polar crystals: a comparison between theory and experiment in sucrose. *Journal of Crystal Growth*, **61**, 369–376.
- Arkenbout, G.F. (1995) *Melt Crystallization Technology*, Technomic, Basle.
- Arkenbout, G.J. (1976) Continuous fractional crystallization. *Chemtech*, **6**, 596–599.
- Arkenbout, G.J. (1978) Progress in continuous fractional crystallization. *Separation and Purification Methods*, **7**, (1), 99–134.
- Armstrong, A.J. (1969) The scraped shell crystallizer. *British Chemical Engineering*, **14**, 647–649.
- Arora, S.K. (1981) Advances in gel growth: a review. *Progress in Crystal Growth and Characterization of Materials*, **4**, 345–378.
- Asai, S. (1983) Various procedures for preferential crystallization of ionizable racemic mixtures. *Industrial and Engineering Chemistry*, **22**, 429–432.
- Aslund, B. and Rasmuson, Å.C. (1992) Semi-batch reaction crystallization of benzoic acid. *AIChEJ*, **38**, 328–342.
- ASTM E11 (1995) Wirecloth Sieves for Testing Purposes. American Society for Testing Materials, Philadelphia.
- Atwood, G.R. (1969) The progressive mode of multistage crystallization. *Chemical Engineering Progress Symposium Series No. 95*, **65**, 112–121.
- Autenrieth, H. (1953) Neuere Entwicklungen auf dem Gebiet der graphischen und rechnerischen Behandlung der Vorgänge bei der Gewinnung von Kalidigmitteln aus Rohsalzen. *Kali und Salz*, **2**, 3–17.
- Bailey, A.E. (1950) *Melting and Solidification of Fats and Waxes*, Interscience, New York [see Swern, D., (1979)].
- Baker, C.G.J. and Bergougnou, M.A. (1974) Precipitation of sparingly soluble salts. *Canadian Journal of Chemical Engineering*, **52**, 246–250.
- Baldyga, J. and Bourne, J.R. (1997) Interaction between chemical reactions and mixing on different scales. *Chemical Engineering Science*, **52**, 457–466.
- Baldyga, J. and Bourne, J.R. (1999) *Turbulent Mixing and Chemical Reactions*, Wiley, New York.
- Bamforth, A.W. (1965) *Industrial Crystallization*, Leonard Hill, London.
- Banerjee, S.C. and Doraiswamy, L.K. (1960) Enthalpy-concentration chart for the system urea-water. *British Chemical Engineering*, **5**, 269.
- Barba, D., Brandani, V. and di Giacomo, G. (1982) A thermodynamic model of CaSO₄ solubility in multicomponent aqueous solutions. *Chemical Engineering Journal*, **24**, 191–200.
- Barduhn, A.J. (1975) The status of freeze-desalination. *Chemical Engineering Progress*, **71**, (11), 80–87.
- Bartosch, K. and Mersmann, A. (1999) Design of a continuous melt crystallizer based on direct contact cooling. Paper 49 in *Industrial Crystallization* (14th Symposium, Cambridge). IChemE, Rugby.
- Bavin, M. (1989) Polymorphism in process development. *Chemistry and Industry*, 21 August, 527–529.
- Becker, R. and Döring, W. (1935) Kinetische Behandlung der Keimbildung in übersättigten Dämpfen. *Annalen der Physik*, **24**, 719–752.
- Beiny, D.H.M. and Mullin, J.W. (1987) Solubilities of higher normal alkanes in *m*-xylene. *Journal of Chemical Engineering Data*, **32**, 9–10.
- Beiny, D.H.M., Mullin, J.W. and Lewtas, K. (1990) Crystallization of n-dotricontane from hydrocarbon solution with polymeric additives. *Journal of Crystal Growth*, **106**, 801–806.

- Bell, D.J., Hoare, M. and Dunnill, P. (1983) The formation of protein precipitates and their centrifugal recovery. *Advances in Biochemical Engineering/Biotechnology*, **22**, 1–67.
- Belyustin, A.V. and Fridman, S.S. (1968) Trapping of solution by a growing crystal. *Soviet Physics Crystallography*, **13**, 298–300.
- Belyustin, A.V. and Rogacheva, E.D. (1966) Production of crystallization and nuclei in the presence of a seed crystal. In *Growth of Crystals*, A.V. Shubnikov and N.N. Sheftal (eds.), Consultants Bureau, New York.
- Bennema, P. (1968) Surface diffusion and the growth of sucrose crystals. *Journal of Crystal Growth*, **3/4**, 331–334.
- Bennema, P. (1969) The influence of surface diffusion for crystal growth from solution. *Journal of Crystal Growth*, **5**, 29–43.
- Bennema, P. (1984) Spiral growth and surface roughening: development since Burton, Cabrera and Frank. *Journal of Crystal Growth*, **69**, 182–197.
- Bennema, P. and Hartman, P. (1980) Attachment energy as a habit controlling factor. *Journal of Crystal Growth*, **49**, 145–156.
- Bennema, P. and Söhnle, O. (1990) Interfacial surface tension of crystallization and precipitation from aqueous solution. *Journal of Crystal Growth*, **102**, 547–556.
- Bennema, P. and van der Eerden, J.P. (1977) Crystal growth from solution: development in computer simulation. *Journal of Crystal Growth*, **42**, 201–213.
- Bennett, R.C. (1962) Product size distribution in commercial crystallizers. *Chemical Engineering Progress*, **58**, (9), 76–80.
- Bennett, R.C. (1992) Crystallizer selection and design. In Myerson, A.S. (ed.) (1992), pp. 103–130.
- Bennett, R.C., Fiedelman, H. and Randolph, A.D. (1973) Crystallizer influenced nucleation. *Chemical Engineering Progress*, **69**, 86–93.
- Bentivoglio, M. (1927) An investigation of the rate of growth of crystals in different directions. *Proceedings of the Royal Society*, **115**, 59–87.
- Berends, E.M., Bruinsma, O.S.L. and van Rosmalen, G.M. (1993) Nucleation and growth of fine crystals from supercritical CO₂. *Journal of Crystal Growth*, **128**, 50–56.
- Berg, W.F. (1938) Crystal growth from solutions. *Proceedings of the Royal Society, A164*, 79–95.
- Berglund, K.A., Kaufman, E.L. and Larson, M.A. (1983) Growth of contact nuclei of potassium nitrate. *AICHEJ*, **29**, 867–869.
- Berkeley, The Earl of, (1912) Solubility and supersolubility from the osmotic standpoint. *Philosophical Magazine*, **24**, 254–268.
- Berkovitch-Yellin, Z., Addadi, L., Idelson, M., Lahav, M. and Leiserowitz, L. (1982) Controlled modification of crystal habit by ‘tailor made’ impurities: application to benzamide. *Angewandt Chemie Supplement*, 1336–1345.
- Bernstein, J., Davey, R.J. and Henck, J-O. (2000) Concomitant Polymorphs. *Angewandte Chemie, Internat. Edn.*, **38**, 3440–3461.
- Berthoud, A. (1912) Theorie de la formation des faces d'un crystal. *Journal de Chimique Physique*, **10**, 624–635.
- Betts, W.D. and Girling, G.W. (1971) Continuous column crystallization. *Progress in Separation and Purification*, **4**, 31–91.
- Bilik, J. and Krupiczka, R. (1983) Heat transfer in the desublimation of phthalic anhydride. *Chemical Engineering Journal*, **26**, 169–180.
- Black, S.N., Davey, R.J. and Halcrow, M. (1986) The kinetics of crystal growth in the presence of tailor-made additives. *Journal of Crystal Growth*, **79**, 765–774.
- Blasdale, W.C. (1927) Equilibria in Saturated Salt Solutions. Chemical Catalog Co, New York.

- Bliznakov, G. (1965) Le mechanism de l'action des additives adsorbants dans la croissance cristalline. In Kern (1965), p. 283.
- Bliznakov, R. and Nikolaeva, R. (1967) Growth rate of {100} faces of KBr. *Kristall und Technik*, **2**, 161–166.
- Boistelle, R. (1976) Survey of crystal habit modification in solution. In *Industrial Crystallization* (6th Symposium, Usti nad Labem), J.W. Mullin (ed.), 203–214, Plenum Press, New York.
- Boistelle, R. (1982) Impurity effects in crystal growth from solution. In *Interfacial Aspects of Phase Transformations*, B. Mutaftschiev (ed.), 621–638, Reidel, Dordrecht.
- Boistelle, R. and Abbona, F. (1981) Morphology, habit and growth of Newberryite crystals ($MgHPO_4 \cdot 3H_2O$). *Journal of Crystal Growth*, **54**, 275–295.
- Boistelle, R., Abbona, F. and Madsen, H.E.L. (1983) On the transformation of struvite into newberryite in aqueous systems. *Physics and Chemistry of Minerals*, **9**, 216–222.
- Boistelle, R. and Madsen, H.E.L. (1978) Solubility of long chain n-alkanes in petroleum ether. *Journal of Chemical Engineering Data*, **23**, 28–29.
- Boistelle, R. and Simon, B. (1974) Épitaxes de $CdCl_2 \cdot 2NaCl \cdot 3H_2O$ sur les faces (100), (110), et (111) des NaCl. *Journal of Crystal Growth*, **26**, 140–146.
- Bolsaitis, P. (1969) Continuous column crystallization. *Chemical Engineering Science*, **24**, 1813–1825.
- Bonythan, C.W. (1966) Factors determining the rate of evaporation in the production of salt. *Proceedings of the 2nd Symposium on Salt*, Northern Ohio Geological Society, Cleveland, pp. 152–167.
- Bos, A.S. and Zuiderweg, F.J. (1985) Kinetics of continuous agglomeration in suspension. *Powder Technology*, **44**, 43–51.
- Botsaris, G.D. (1976) Secondary nucleation: a review. In *Industrial Crystallization* (6th Symposium, Usti nad Labem), J.W. Mullin (ed.), 3–22, Plenum Press, New York.
- Botsaris, G.D. (1982) Effects of impurities in crystallization processes. In *Industrial Crystallization 81* (8th Symposium, Budapest), S.J. Jančić and E.J. de Jong (eds.), 123–135, North-Holland, Amsterdam.
- Botsaris, G.D., Denk, E.G. and Chua, J. (1972) Nucleation in an impurity concentration gradient – a new mechanism of secondary nucleation. *AICHE Symposium Series No. 121*, **68**, 21–30.
- Bourne, J.R. and Davey, R.J. (1977) Growth of hexamethylenetetramine crystals from aqueous and ethanolic solutions. *Journal of Crystal Growth*, **39**, 267–274.
- Bourne, J.R., Davey, R.J., Gros, H. and Hungerbuhler, K. (1976) The rotating disc configuration in the measurement of crystal growth kinetics from solution. *Journal of Crystal Growth*, **34**, 221–229.
- Bovington, C.H. and Jones, A.L. (1970) Tracer studies of the kinetics of dissolution of lead sulphate. *Transactions of the Faraday Society*, **66**, 2088–2091.
- Bowden, F.P. and Tabor, D. (1964) *The Friction and Lubrication of Solids*, Clarendon, Oxford.
- Bowden, S.T. (1950) *The Phase Rule and Phase Reactions*, Macmillan, London.
- Bransom, S.H. (1960) Factors in the design of continuous crystallizers. *British Chemical Engineering*, **5**, 838–844.
- Bransom, S.H., Dunning, W.J. and Millard, B. (1949) Kinetics of crystallization in solution. *Discussions of the Faraday Society*, **5**, 83–103.
- Brečević, Lj. and Füredi-Milhofer, H. (1976) Transformation of amorphous calcium phosphate into crystalline hydroxyapatite. In *Industrial Crystallization* (6th Symposium, Usti nad Labem), J.W. Mullin (ed.), Plenum Press, New York, 277–283.

- Brečević, Lj. and Garside, J. (1981) On the measurement of crystal size distributions in the micrometer size range. *Chemical Engineering Science*, **36**, 867–869.
- Brečević, Lj. and Nielsen, A.E. (1990) Precipitation and properties of an amorphous calcium carbonate. In *Industrial Crystallization 90* (11th Symposium, Garmisch-Partenkirchen), A. Mersmann (ed.), GVC-VDI, Dusseldorf, 241–246.
- Bretherick, L. (1999) *Handbook of Reactive Chemical Hazards*, 6th edn., Butterworth-Heinemann, Oxford.
- Brice, J.C. (1965) *Growth of Crystals from the Melt*, North-Holland, Amsterdam.
- Brice, J.C. (1986) *Crystal Growth Processes*, Wiley, New York.
- British Pharmacopoeia* (2000) Appendix V: Determination of melting points and freezing points. The Stationery Office, London.
- Brodie, J.A. (1971) A continuous multistage melt purification process. *Mechanical and Chemical Engineering Transactions*, Institute of Engineers Australia, **7**, (1), 37–44.
- Bromley, L.A. (1973) Thermodynamic properties of strong electrolytes in aqueous solution. *AIChE Journal*, **19**, 313–320.
- Brookes, C.A., O'Neill, J.B. and Redfern, B.A.W. (1971) Anisotropy in the hardness of single crystals. *Proceedings of the Royal Society*, **A333**, 73–88.
- Brooks, R., Horton, A.T. and Torgesen, J.L. (1968) Occlusion of mother liquor in solution-growth crystals. *Journal of Crystal Growth*, **2**, 279–283.
- Brosheer, J.C. and Anderson, J.F. (1946) The system ammonia-phosphoric acid-water at 75 °C. *Journal of the American Chemical Society*, **68**, 902–904.
- Broul, M., Nývlt, J. and Söhnel, O. (1981) *Solubility in Inorganic Two-component Systems*, Academia, Prague.
- Brown, M.E. (1988) *Introduction to Thermal Analysis*, Chapman and Hall, London.
- Brown, P.M., Marquering, M. and Myerson, A.S. (1990) Purification of terephthalic acid by crystal ageing. *Industrial and Engineering Chemistry Research*, **29**, 2089–2093.
- Bryson, A.W., Glasser, D. and Lutz, W.F. (1976) Crystallization of ammonium paratungstate: a comparison between batch and continuous operation. *Hydrometallurgy*, **2**, 185–191.
- BS 188 (1993) Determination of the viscosity of liquids. British Standards Institution, London.
- BS 410 (2000) Test Sieves. British Standards Institution, London.
- BS 733 (1983) Pyknometers. Part 1: Specifications; Part 2: Calibration and use. British Standards Institution, London.
- BS 1796 (1990) Test Sieving. British Standards Institution, London.
- BS 3406 (1990) Determination of Particle Size of Powders: Part 1, Guide to powder sampling; Part 2, Gravitational liquid sedimentation; Part 3, Air elutriation; Part 4, Optical microscope and image analysis; Part 5, Electrical sensing zone (Coulter principle); Part 6, Centrifugal liquid sedimentation; Part 7, Single particle light interaction; Part 8, Porosimetry. British Standards Institution, London.
- BS 3625 (1963) Microscope eyepiece and screen graticule. British Standards Institution, London.
- BS 4359 (1984) Determination of Specific Surface of Powders: Part 1, Nitrogen adsorption (B.E.T.); Part 2, Air permeability. British Standards Institution, London.
- BS ISO 13317 (2000) Particle size analysis – gravitational sedimentation methods. British Standards Institution, London.
- BS ISO 13318 (2000) Particle size analysis – centrifugal sedimentation methods. British Standards Institution, London.
- BS ISO 13319 (2000) Particle size analysis – electrical sensing zone method. British Standards Institution, London.

- BS ISO 13320 (2000) Particle size analysis – laser diffraction methods. British Standards Institution, London.
- Buckley, H.E. (1952) *Crystal Growth*, Chapman and Hall, London.
- Buckton, G. and Darcy, P. (1999). Assessment of disorder in crystalline powders – a review of analytical techniques and their application. *International Journal of Pharmaceutics*, **179**, 141–158.
- Budz, J., Jones, A.G. and Mullin, J.W. (1986) Effect of selected impurities on the continuous precipitation of calcium sulphate (gypsum). *Journal of Chemical Technology and Biotechnology*, **36**, 153–161.
- Budz, J., Jones, A.G. and Mullin, J.W. (1987) Agglomeration of potassium sulphate crystals in an MSMPR crystallizer. *AICHE Symposium Series*, No. 253, **83**, 78–84.
- Budz, J., Karpinski, P.H., Mydlarz, J. and Nývlt, J. (1986) Salting-out precipitation of cocarboxylase hydrochloride from aqueous solutions by addition of acetone. *Industrial and Engineering Chemistry Product Research and Development*, **25**, 657–664.
- Bujac, P.D.B. (1976) Attrition and secondary nucleation in agitated crystal slurries. In *Industrial Crystallization* (6th Symposium, Usti nad Labem), J.W. Mullin (ed.), Plenum Press, New York, 23–31.
- Bujac, P.D.B. and Mullin, J.W. (1969) A rapid method for the measurement of crystal growth rates in a fluidized bed crystallizer. *Symposium on Industrial Crystallization*, Institution of Chemical Engineers, London, 121–129.
- Bunn, C.W. (1933) Adsorption, oriented overgrowth and mixed crystal formation. *Proceedings of the Royal Society*, **141**, 567–593.
- Bunn, C.W. (1949) Concentration gradients and the rates of growth of crystals. *Discussions of the Faraday Society*, **5**, 132–144.
- Bunn, C.W. (1961) *Chemical Crystallography*, 2nd edn., Clarendon Press, Oxford.
- Burak, N. (1966) Chemicals for improving the flow of powders. *Chemistry and Industry*, 844–850.
- Burton, W.K., Cabrera, N. and Frank, F.C. (1951) The growth of crystals and the equilibrium structure of their surfaces. *Philosophical Transactions*, **A243**, 299–358.
- Bushnell, J.D. and Eagen, J.F. (1975) Dewax process produces benefits. *The Oil and Gas Journal*, **73**, (20 October), 80–84.
- Butts, D.S. (1993) Elements of a well organized weather station and its use in solar pond design, operation and control. *Proceedings of the 7th Symposium on Salt*, Vol. 1. Elsevier, Amsterdam, 519–524.
- Cabrera, N. and Vermilyea, D.A. (1958) Growth of crystals from solution. In Doremus, Roberts and Turnbull (1958), 393–410.
- Capes, C.E. and Sutherland, J.P. (1967) Formation of spheres from finely divided solids in liquid suspension. *Industrial Engineering Chemistry Process Design and Development*, **6**, 146–154.
- Cardew, P.T. and Davey, R.J. (1982) Kinetic factors in the appearance and transformation of metastable phases. In *Symposium on the Tailoring of Crystal Growth*, Institution of Chemical Engineers, London, 1.1–1.9.
- Cardew, P.T. and Davey, R.J. (1985) The kinetics of solvent-mediated phase transformations. *Proceedings of the Royal Society*, **A398**, 415–428.
- Carless, J.E. and Foster, A.A. (1966) Accelerated crystal growth of sulphathiazole by temperature cycling. *Journal of Pharmacy and Pharmacology*, **18**, 697–702 and 815–820.
- Carman, P.C. (1934) A study of the mechanism of filtration. *Journal of the Society of Chemical Industry*, **53**, 159T–165T.
- Carman, P.C. (1938) Fundamental principles of industrial filtration: a critical review of present knowledge. *Transactions of the Institution of Chemical Engineers*, **16**, 168–188.

- Carr, R.L. (1970) Particle behaviour, storage and flow. *British Chemical Engineering*, **15**, 1541–1549.
- Cartwright, P.F.S., Newman, E.J. and Wilson, D.D. (1967) Precipitation from homogeneous solution: a review. *The Analyst*, **92**, 663–679.
- Casper, C. (1981) Investigation of evaporative freeze-crystallization. *German Chemical Engineering*, **4**, 219–225.
- Catone, D.L. and Matijevich, E. (1974) Aluminium hydrous oxide sols. *Journal of Colloid and Interface Science*, **48**, 291–301.
- Cayey, N.W. and Estrin, J. (1967) Secondary nucleation in agitated MgSO₄ solutions. *Industrial and Engineering Chemistry Fundamentals*, **6**, 13–20.
- Cedro, V. (1958) *Chemical Engineering*, **93**, (21), 5 (letter).
- Černý, J. (1963) Continuous crystallization of calcium nitrate tetrahydrate. British Patent 932215.
- Cerrata, M.K. and Berglund, K.A. (1987) Structure of aqueous solutions of some dihydrogen orthophosphates by laser Raman spectroscopy. *Journal of Crystal Growth*, **84**, 577–588.
- Cesar, M.A.B. and Ng, K.M. (1999) Improving product recovery in fractional crystallization processes: retrofit of an adipic acid plant. *Industrial and Engineering Chemistry Research*, **38**, 823–832.
- Chalmers, B. (1964) *Principles of Solidification*, Wiley, New York.
- Chandler, J.L. (1959) The wetted-wall column as an evaporative crystallizer. *British Chemical Engineering*, **4**, 83–87.
- Chandler, J.L. (1964) Effect of supersaturation and flow conditions on the initiation of scale formation. *Transactions of the Institution of Chemical Engineers*, **42**, 24–34.
- Chandrasekhar, S. (1992) *Liquid Crystals*, 2nd edn., University Press, Cambridge.
- Chang, C.J. and Randolph, A.D. (1989) Precipitation of microsized organic particles from supercritical fluids. *AIChEJ*, **35**, 1876–1882.
- Chang, C.T. and Epstein, M.A.F. (1982) Identification of batch crystallization control strategies using characteristic curves. *AIChE Symposium Series*, No. 215, **78**, 68–75.
- Chang, R.Y. and Wang, M.L. (1984) Modelling the batch crystallization process via shifted Legendre polynomials. *Industrial and Engineering Chemistry Process Design and Development*, **23**, 463–468.
- Chang, W-C. and Ng, K.M. (1998) Synthesis of the processing system around a crystallizer. *AIChEJ*, **44**, 2240–2251.
- Chaty, J.C. (1967) Rotary-drum techniques. In *Fractional Solidification*, M. Zief and W.R. Wilcox (eds.), Dekker, New York, Chapter 15.
- Chaty, J.C. and O'Hern, H.A. (1964) An engineering study of the rotary drum crystallizer. *AIChEJ*, **10**, 74–78.
- Chen, Y.L. and Chou, J.Y. (1993) Selection of anti-caking agents through crystallization. *Powder Technology*, **77**, 1–6.
- Chernov, A.A. (1961) The spiral growth of crystals. *Soviet Physics Uspekhi*, **4**, 116–148.
- Chernov, A.A. (1965) Some aspects of the theory on crystal growth forms in the presence of impurities. In Kern (1965), 1–13.
- Chernov, A.A. (1980) Modern Crystallography III: Crystal Growth. Springer-Verlag, Berlin.
- Chernov, A.A. (1989) Formation of crystals in solution. *Contemporary Physics*, **30**, 251–276.
- Chernov, A.A. (1993) Present-day understanding of crystal growth from aqueous solutions. *Progress in Crystal Growth and Characterization*, **26**, 121–151.

- Chernov, A.A., Zaitseva, N.P. and Rashkovich, L.N. (1990) Secondary nucleation induced by the cracking of a growing crystal (KDP and DKDP). *Journal of Crystal Growth*, **102**, 793–800.
- Chianese, A. (1988) Growth and distribution of sodium perborate in aqueous solution using the RDC technique. *Journal of Crystal Growth*, **91**, 39–49.
- Chianese, A., Di Cave, S. and Mazzarotta, B. (1990) Encrustation throughout sodium perborate crystallization. *Industrial Crystallization 90* (11th Symposium), A. Mersmann (ed.), Garmish, FRG, 453–458.
- Chivate, M.R. and Shah, S.M. (1956) Separation of m-cresol by extractive crystallization. *Chemical Engineering Science*, **5**, 232–241.
- Chlopin, V. (1925) Fractionierten Kristallisation radioaktiver Stoffe. *Zeitschrift für anorganische allgemeine chemie*, **143**, 97–117.
- Chu, J.C., Kalil, J. and Wetteroth, W.A. (1953) Mass transfer in a fluidized bed. *Chemical Engineering Progress*, **49**, 141–149.
- Ciborowski, J. and Wronski, S. (1962) Condensation of sublimable materials in a fluidized bed. *Chemical Engineering Science*, **17**, 481–489.
- Cise, M.D. and Randolph, A.D. (1970) Some aspects of crystal growth and nucleation of K_2SO_4 in a continuous-flow seeded crystallizer. *AICHE Symposium Series No. 121*, **68**, 42–56.
- Cisternas, L.A. (1999) Optimal design of crystallization-based separation schemes. *AICheJ*, **45**, 1477–1487.
- Clontz, N.A. and McCabe, W.L. (1971) Contact nucleation of $MgSO_4 \cdot 7H_2O$. *Chemical Engineering Progress Symposium Series, No. 110*, **67**, 6–17.
- Clydesdale, G. and Roberts, K.J. (1991) Structural stability and morphology of crystalline n-alkanes. *AICHE Symposium Series No. 284*, **87**, 130–142.
- COFFI Proceedings, (1968 ff) E. Roedder (ed.), US Geological Survey, Washington.
- Collet, A., Brienne, M-J. and Jacques, J. (1980) Optical resolution by direct crystallization of enantiomer mixtures. *Chemical Reviews*, **80**, 215–230.
- Collier, A.P. and Hounslow, N.J. (1999) Growth and aggregation rates for calcite and calcium oxalate monohydrate. *AICheJ*, **45**, 2298–2304.
- Collins, A.N., Sheldrake, G.N. and Crosby, J. (eds.) (1995) *Chirality in Industry*, Wiley, New York.
- Colônia, E.J., Dixit, A.B. and Tavare, N.S. (1998) Separation of chlorobenzoic acids through hydrotropy. *Industrial and Engineering Chemistry Research*, **37**, 1956–1969.
- Cooke, E.G. (1966) Influence of impurities on the growth and nucleation of NaCl. *Kristall und Technik*, **1**, 119–126.
- Coulson, J.M. and Richardson, J.F. (1991) *Chemical Engineering*, 4th edn., Vol. 1: *Fluid Flow, Heat and Mass Transfer*; Vol. 2: *Particle Technology and Separation Processes*, Pergamon, Oxford.
- Coulson, J.M. and Warner, F.E. (1949) A problem in chemical engineering design: the manufacture of mono-nitrotoluene. Institution of Chemical Engineers, London.
- Dauncy, L.A. and Still, J.E. (1952) Apparatus for the direct measurement of the saturation temperatures of solutions. *Journal of Applied Chemistry*, **2**, 399–404.
- Davey, R.J. (1976) The effect of impurity adsorption on the kinetics of crystal growth from solution. *Journal of Crystal Growth*, **34**, 109–119.
- Davey, R.J. (1979) The control of crystal habit. In *Industrial Crystallization 78* (7th Symposium, Warsaw), E.J. de Jong and S.J. Jančić (eds.), North-Holland, Amsterdam, 169–183.
- Davey, R.J. (1982) The role of additives in precipitation processes. In *Industrial Crystallization 81* (8th Symposium, Budapest), S.J. Jančić and E.J. de Jong (eds.), North-Holland, Amsterdam, 123–135.

- Davey, R.J. (1986) The role of the solvent in crystal growth from solution. *Journal of Crystal Growth*, **76**, 637–644.
- Davey, R.J., Black, S.N., Bromley, L.A., Cottier, D., Dobbs, B. and Rout, J.E. (1991) Molecular design based on recognition at inorganic surfaces. *Nature*, **353**, 10 October, 549–551. See also *Journal of the Chemical Society, Faraday Transactions*, **87** (1991), 3409–3414.
- Davey, R.J., Blagden, N., Potts, G.D. and Docherty, R. (1997) Polymorphism in molecular crystals: stabilization of a metastable form. *Journal of the American Chemical Society*, **119**, 1767–1772.
- Davey, R.J., Fila, W. and Garside, J. (1986) The influence of biuret on the growth kinetics of urea crystals from aqueous solution. *Journal of Crystal Growth*, **79**, 607–613.
- Davey, R.J. and Garside, J. (2000) *From Molecules to Crystallizers*, University Press, Oxford.
- Davey, R.J., Guy, P.D. and Ruddick, A.J. (1985) The IV–III polymorphic phase transition in aqueous slurries of ammonium nitrate. *Journal of Colloid and Interface Sciences*, **108**, 189–192.
- Davey, R.J., Hilton, A.M. and Garside, J. (1997) Crystallization from oil in water emulsions: particle synthesis and purification of molecular materials. *Chemical Engineering Research and Design*, **75**, 245–251.
- Davey, R.J. and Mullin, J.W. (1974) Growth of the {100} faces of ADP crystals in the presence of ionic species. *Journal of Crystal Growth*, **26**, 45–51.
- Davey, R.J. and Mullin, J.W. (1976) A mechanism for the habit modification of ADP crystals in the presence of ionic species in aqueous solution. *Kristall und Technik*, **11**, 229–233.
- Davey, R.J., Mullin, J.W. and Whiting, M.J.L. (1982) Habit modification of succinic acid crystals grown from different solvents. *Journal of Crystal Growth*, **58**, 304–312.
- Davey, R.J., Polywka, L.A. and Maginn, S.J. (1991) The control of morphology by additives: molecular recognition, kinetics and technology. In *Advances in Industrial Crystallization*, J. Garside, R.J. Davey and A.G. Jones (eds.), Butterworth-Heinemann, Oxford, 150–165.
- Davey, R.J. and Richards, J. (1985) A solvent mediated phase transformation in an aqueous suspension of an azo disperse dye. *Journal of Crystal Growth*, **71**, 597–601.
- David, R., Marchal, P., Klein, J-P. and Villermeaux, J. (1990) A discrete formulation of the agglomeration of crystals in a crystallization process. *Chemical Engineering Science*, **46**, 205–213.
- Davies, C.W. (1962) *Ion Association*, Butterworths, London.
- Davies, G.A., Ming, Y. and Garside, J. (1990) The selective separation and precipitation of salts in a liquid surfactant membrane system. In *Industrial Crystallization 90* (11th Symposium, Garmisch-Partenkirchen), A. Mersmann (ed.), GVC-VDI, 163–168.
- Deicha, G. (1955) *Lacunes des Cristeaux et leurs Inclusions Fluides*, Masson, Paris.
- De Jong, E.J. (1979) Nucleation: a review. In *Industrial Crystallization 78* (7th Symposium, Warsaw), E.J. de Jong and S.J. Jančić (eds.), North-Holland, Amsterdam, 3–17.
- Demopoulos, G.P., Kondos, P. and Papangelakis, V.G. (1988) Predictions of solubilities in chemical compounds precipitation systems. In *Crystallization and Precipitation* (Symposium proceedings, Saskatoon, October 1987), G.L. Strathdee, M.C. Klein, L.A. Melis (eds.), Pergamon Press, Oxford, 231–246.
- Demyanovich, R.J. and Bourne, J.R. (1989) Rapid micromixing by the impingement of thin liquid sheets. *Industrial and Engineering Chemistry Research*, **28**, 825–830.

- Denbigh, K.G. and White, E.T. (1966) Studies on liquid inclusions in crystals. *Chemical Engineering Science*, **21**, 739–754.
- Denk, E.G. and Botsaris, G.D. (1972) Fundamental studies in secondary nucleation from solution. *Journal of Crystal Growth*, **13/14**, 493–499.
- Denton, W.H. et al. (1970) Experimental studies on the immiscible refrigerant (butane) freezing process. In *3rd International Symposium on Fresh Water from the Sea (Dubrovnik)*, European Federation of Chemical Engineering, 51–58.
- Diepen, P.J., Bruinsma, O.S.L. and van Rosmalen, G.M. (2000) Melt crystallization by controlled evaporative cooling: the caprolactam-water system in batch operation. *Chemical Engineering Science*, **55**, 3575–3584.
- Dikshit, R.C. and Chivate, M.R. (1970) Separation of nitrochlorobenzenes by extractive crystallization. *Chemical Engineering Science*, **25**, 311–317.
- Dinsdale, A. and Moore, F. (1962) *Viscosity and its Measurement*, Institute of Physics, London.
- Dobbs, J.M., Wong, J.M. and Johnston, K.P. (1986) Nonpolar cosolvents for solubility enhancement in supercritical fluid carbon dioxide. *Journal of Chemical Engineering Data*, **31**, 303–308.
- Docherty, R. and Meenan, P. (1999) The study of molecular materials using computational chemistry. In Myerson, A.S. (ed.) (1999), pp. 106–165.
- Docherty, R. and Roberts, K.J. (1988) Modelling of the morphology of molecular crystals: anthracene, biphenyl and β -succinic acid. *Journal of Crystal Growth*, **88**, 159–168.
- Doerner, H.A. and Hoskins, W.M. (1925) The co-precipitation of radium and barium sulphates. *Journal of the American Chemical Society*, **47**, 662–675.
- Donald, M.B. (1937) Percolation leaching in theory and practice. *Transactions of the Institution of Chemical Engineers*, **15**, 77–104.
- Doremus, R.H., Roberts, B.W. and Turnbull, D. (1958) *Editors, Growth and Perfection of Crystals* (Symposium proceedings), Wiley, New York.
- Dow Chemical Co. (1978) *Three phase crystallization of bisphenyl A*, US Patent 4,079,087 14 March.
- Dufor, L. and Defay, R. (1963) *Thermodynamics of clouds*, Academic Press, New York.
- Dullien, F.A.L. and Shemilt, L.W. (1961) Diffusion coefficients for the liquid system ethanol-water. *Canadian Journal of Chemical Engineering*, **39**, 242–247.
- Duncan, A.G. and Phillips, R.H. (1976) Crystallization by direct cooling and its application to *p*-xylene production. *Transactions of the Institution of Chemical Engineers*, **54**, 153–159.
- Duncan, A.G. and Phillips, R.H. (1979) The dependence of heat exchanger fouling on solution undercooling. *Journal of Separation Process Technology*, **1**, 29–35.
- Duncan, A.G. and West, C.D. (1972) Prevention of incrustation on crystallizer heat exchanger surfaces by ultrasonic vibrations. *Transactions of the Institution of Chemical Engineers*, **50**, 109–114.
- Dunitz, J.D. and Bernstein, J. (1995) Disappearing polymorphs. *Accounts of Chemical Research*, **28**, 193–200.
- Dunning, W.J. (1969) General and theoretical introduction to nucleation. In Zettlemoyer (1969), 1–67.
- Dye, S.R. and Ng, K.M. (1995) By-passing eutectics with extractive crystallization: design alternatives and trade-offs. *AIChEJ*, **41**, 1456–1470.
- Dzyuba, A.S. (1983) Periodic capture of melt by a growing crystal. *Soviet Physics Crystallography*, **28**, 111–112.
- Eckert, C.A., Liotta, C.L. and Brown, J.S. (1993) Clean solution for chemical synthesis. *Chemistry and Industry*, 7 February, 94–97.

- Edie, D.D. and Kirwan, D.J. (1973) Impurity trapping during crystallization from melts. *Industrial and Engineering Chemistry Fundamentals*, **12**, 100–106.
- Egan, C.J. and Luthy, R.V. (1955) Separation of xylenes. *Industrial and Engineering Chemistry*, **47**, 250–253.
- Eggers, H.H., Ollman, D., Heinz, D., Drobot, D.W. and Nokolajew, A.W. (1986) Sublimation und Desublimation im System AlCl₃ – FeCl₃. *Zeitschrift für Physikalische Chemie*, **267**, 353–363.
- Eidelmann, N., Azoury, R. and Sarig, S. (1986) Reversal of trends in impurity effects on crystallization parameters. *Journal of Crystal Growth*, **74**, 1–9.
- Elwell, D. (1980) High-temperature solution growth. In *Crystal Growth*, B.R. Pamplin (ed.), 2nd edn., Pergamon, Oxford, 463–483.
- Elwell, D. and Scheel, H.J. (1975) *Crystal Growth from High-Temperature Solution*, Academic Press, London.
- Enüstün, B.V. and Turkevich, J. (1960) The solubility of fine particles of strontium sulphate. *Journal of the American Chemical Society*, **82**, 4502–4509.
- Enyedy, G. (1962) Continuous vacuum crystallization process: material balance for maximum yield. *Chemical Engineering Progress Symposium Series, No. 58*, **37**, 10–27.
- Espitalier, F., Biscans, B., Authelin, J-R. and Laguerie, C. (1997) Modelling of the mechanism of formation of spherical grains obtained by the quasi-emulsion crystallization process. *Chemical Engineering Research and Design*, **75**, 257–267.
- Estrin, J., Sauter, W.A. and Karshina, G.W. (1969) On size dependent growth rate expressions. *AICHEJ*, **15**, 289–290.
- Evans, T.W., Margolis, G. and Sarofim, A.F. (1974) Models of secondary nucleation attributable to crystal-crystallizer and crystal-crystal collisions. *AICHEJ*, **20**, 959–965.
- Ewing, G.W. (1997). *Analytical Instrumentation Handbook*, 2nd edn., Marcel Dekker, New York.
- Faktor, M.M. and Garrett, I. (1974) *Growth of Crystals from the Vapour*, Chapman and Hall, London.
- Faraday Discussions (1949) No. 5: *Crystal Growth*, The Chemical Society, London.
- Faraday Discussions (1957) No. 24: *Interaction in Ionic Solutions*, The Chemical Society, London.
- Faraday Discussions (1967) No. 43: *The Structure and Properties of Liquids*, The Chemical Society, London.
- Faraday Discussions (1976) No. 61: *Precipitation*, The Chemical Society, London.
- Faraday Discussions (1978) No. 66: *Structure and Motion in Molecular Liquids*, The Chemical Society, London.
- Faraday Discussions (1998) No. 109: *Chemistry and Physics of Molecules and Grains in Space*, The Chemical Society, London.
- Fasoli, U. and Conti, R. (1976) Secondary nucleation in agitated crystallizers. In *Industrial Crystallization* (6th Symposium, Usti nad Labem), J.W. Mullin (ed.), Plenum Press, New York, 77–87.
- Feilchenfeld, H. and Sarig, S. (1985) Calcium chloride hexahydrate: A phase-changing material for energy storage. *Industrial and Engineering Chemistry Product Research and Development*, **24**, 130–133.
- Fernandez-Lozano, J.R. (1976) Recovery of potassium magnesium sulphate from sea-water bittern. *Industrial and Engineering Chemistry Process Design and Development*, **15**, 445–449.
- Fernandez-Lozano, J.R. and Wint, A. (1979) Production of potassium sulphate by an ammoniation process. *The Chemical Engineer*, No. 349, 688–690.
- Findlay, A. (1973) *Practical Physical Chemistry*, 9th edn., B.P. Levitt (ed.), Longmans Green, London.

- Findlay, A. and Campbell, A.N. (1951) *The Phase Rule and its Applications*, 9th edn., Longmans, London.
- Findlay, R.A. and Weedman, J.A. (1958) Separation and purification by crystallization. *Advances in Petroleum Chemistry and Refining*, Vol. 1, K.A. Kobe and J.J. McKetta (eds.), Interscience, New York.
- Finkelstein, E. (1983). On solar ponds: critique, physical fundamentals and engineering aspects. *Journal of Heat Transfer Recovery Systems*, **3**, 431–437.
- Fischer, O., Jančić, S.J. and Saxer, K. (1984) Purification of compounds forming eutectics and solid solutions by fractional crystallization. In *Industrial Crystallization 84* (9th Symposium, The Hague), S.J. Jančić and E.J. de Jong (eds.), Elsevier, Amsterdam, 153–157.
- Fitch, B. (1970) How to design fractional crystallization processes. *Industrial and Engineering Chemistry*, **62**, (12), 6–31.
- Fitch, B. (1976) Design of fractional crystallization processes involving solid solutions. *AICHE Symposium Series, No. 153*, **72**, 79–86.
- Follner, H. and Schwarz, H. (1982) Morphology and crystal growth of structurally related A_2BX_4 and A_2BX_3 compounds. *Zeitschrift für Kristallographie*, **161**, 35–43.
- Foust, A.S., Wenzel, L.A., Clump, C.W., Maus, L. and Andersen, L.B. (1960) *Principles of Unit Operations*, Wiley, New York.
- Franck, R., David, R., Villermaux, J.A. and Klein, J-P. (1998) A chemical reaction engineering approach to salicylic acid precipitation: modelling of batch kinetics and application to continuous operation. *Chemical Engineering Science*, **43**, 69–77.
- Frank, F.C. (1949) The influence of dislocations on crystal growth. *Discussions of the Faraday Society*, **5**, 48–54.
- Frank, F.C. (1958) Kinematic theory of crystal growth and dissolution processes. In Doremus, Roberts and Turnbull (1958), 411–420.
- Franke, J. and Mersmann, A. (1995) Influence of operational conditions on the precipitation process. *Chemical Engineering Science*, **50**, 1737–1753.
- Frankel, N.A. and Acrivos, A. (1967) On the viscosity of concentrated suspensions of solid spheres. *Chemical Engineering Science*, **22**, 847–853.
- Franks, F. (ed.) (1972–1982) *Water – A Comprehensive Treatise* (6 volumes), Plenum Press, New York.
- Franks, F. and Ives, D.J.G. (1966) Structural properties of alcohol-water mixtures. *Quarterly Reviews of the Chemical Society*, **20**, 1–44.
- Fredenslund, A., Jones, R.L. and Prausnitz, J.M. (1975) Group contribution estimations of activity coefficients in non-ideal liquid mixtures. *AICHEJ*, **25**, 1086–1099.
- Freundlich, H. (1926) *Colloid and Capillary Chemistry*, Methuen, London, p. 154.
- Frew, J.A. (1973) Optimal control of batch raw sugar crystallization. *Industrial and Engineering Chemistry Process Design and Development*, **12**, 460–467.
- Füredi-Milhofer, H. and Walton, A.G. (1969) Principles of precipitation of fine particles. Chapter 5 in *Dispersion of Powders in Liquids*, G.D. Parfitt (ed.), Elsevier, Amsterdam.
- Füredi, H. (1967) Complex precipitating systems. *The Formation and Properties of Precipitates*. A.G. Walton, ed., Interscience, New York, Chapter 6.
- Gaikar, V.G., Mahapatra, A. and Sharma, M.M. (1989) Separation of close boiling point mixtures through dissociation extractive crystallization. *Industrial and Engineering Chemistry Research*, **28**, 199–204.
- Garabedian, H. and Strickland-Constable, R.F. (1972) Collision breeding of crystal nuclei: sodium chlorate. *Journal of Crystal Growth*, **13/14**, 506–509.
- Garber, H.J. and Goodman, A.W. (1941) Fractional crystallization. *Journal of Physical Chemistry*, **45**, 573–588.

- Gardner, G.L. (1976) Kinetics of the dehydration of calcium oxalate trihydrate crystals in aqueous solution. *Journal of Colloid and Interface Science*, **54**, 298–310.
- Garrett, D.E. (1958) Industrial crystallization at Trona. *Chemical Engineering Progress*, **54**, (12), 65–69.
- Garside, J. (1971) The concept of effectiveness factors in crystal growth. *Chemical Engineering Science*, **26**, 1425–1431.
- Garside, J. (1977) Kinetics of crystallization from solution. In *Crystal Growth and Materials*, E. Kaldis and H.J. Scheel (eds.), 483–513, North-Holland, Amsterdam.
- Garside, J. (1985) Industrial crystallization from solution. *Chemical Engineering Science*, **40**, 3–26.
- Garside, J. (1991) The role of transport processes in crystallization. In *Advances in Industrial Crystallization*, J. Garside, R.J. Davey and A.G. Jones (eds.), Butterworth-Heinemann, Oxford, 92–104.
- Garside, J. and Davey, R.J. (1980) Secondary contact nucleation: kinetics, growth and scale-up. *Chemical Engineering Communications*, **4**, 393–424.
- Garside, J. and Jančić, S.J. (1979) Measurement and scale-up of secondary nucleation kinetics for the potash alum-water system. *AICheJ*, **25**, 948–958.
- Garside, J. and Larson, M.A. (1978) Direct observation of secondary nuclei production. *Journal of Crystal Growth*, **43**, 694–704.
- Garside, J. and Mullin, J.W. (1968) Crystallization of aluminium potassium sulphate: a study in the assessment of crystallizer design data. III: Growth and dissolution rates. *Transactions of the Institution of Chemical Engineers*, **46**, 11–18.
- Garside, J. and Tavare, N.S. (1981) Non-isothermal effectiveness factors for crystal growth. *Chemical Engineering Science*, **36**, 863–866.
- Garside, J. and Tavare, N.S. (1985) Mixing, reaction and precipitation: limits of micromixing in an MSMPR crystallizer. *Chemical Engineering Science*, **40**, 1485–1493.
- Garside, J., Davey, R.J. and Jones, A.G. (eds.) (1991) *Advances in Industrial Crystallization*, Butterworth-Heinemann, Oxford.
- Garside, J., Gaska, C. and Mullin, J.W. (1972) Crystal growth rate studies with potassium sulphate in a fluidized bed crystallizer. *Journal of Crystal Growth*, **13/14**, 510–516.
- Garside, J., Gibilaro, L.G. and Tavare, N.S. (1982) Evaluation of crystal growth kinetics from a desupersaturation curve using initial derivatives. *Chemical Engineering Science*, **37**, 1625–1628.
- Garside, J., Mersmann, A. and Nývlt, J. (eds.) (1990) *Measurement of Crystal Growth Rates*, European Federation of Chemical Engineering Working Party on Crystallization.
- Garside, J., Mullin, J.W. and Das, S.N. (1973) Importance of crystal shape in crystal growth rate determinations. *Industrial and Engineering Chemistry Process Design and Development*, **12**, 369–371.
- Garside, J., Phillips, V.R. and Shah, M.B. (1976) On size-dependent crystal growth. *Industrial and Engineering Chemistry Fundamentals*, **15**, 230–238.
- Garside, J., Rusli, I.T. and Larson, M.A. (1979) Origin and size distribution of secondary nuclei. *AICheJ*, **25**, 57–64.
- Garten, V.A. and Head, R.B. (1963) Crystalloluminescence and the nature of the critical nucleus. *Philosophical Magazine*, **8**, 1793–1803.
- Garten, V.A. and Head, R.B. (1966) Homogeneous nucleation and the phenomenon of crystalloluminescence. *Philosophical Magazine*, **14**, 1243–1253.
- Gates, W.C. and Powers, J.E. (1970) Determination of the mechanics causing and limiting separation by column crystallization. *AICheJ*, **16**, 648–657.

- Gee, E.A., Cunningham, W.K., Heindl, R.A. (1947) Production of iron-free alum. *Industrial and Engineering Chemistry*, **39**, 1178–1188.
- Gel'perin, N.I. and Nosov, G.A. (1977) Fractional crystallization of melts in drum crystallizers. *Soviet Chemical Industry*, **9**, 713–716.
- Gel'perin, N.I., Nosov, G.A. and Parokonyi, V.D. (1978) Crystallization of a superheated melt on cooled surfaces. *International Chemical Engineering*, **18**, 129–133.
- Gerunda, A. (1981) How to size liquid-vapour separators. *Chemical Engineering*, 4 May, 81–84.
- Gibbs, J.W. (1948) *Collected Works*, Vol. I, *Thermodynamics*, Yale University Press, New Haven.
- Gibson, R.E. (1934) The calculation of the solubility of certain salts in water at high pressure from data obtained at low pressure. *Journal of the American Chemical Society*, **56**, 865–870.
- Gill, W.N. (1989) Heat transfer in crystal growth dynamics. *Chemical Engineering Progress*, **85**, (7), 33–42.
- Gillot, J. and Goldberger, W.M. (1969) Separation by thin-film fractional sublimation. *Chemical Engineering Progress Symposium Series*, **65**, (91), 36–42.
- Gilman, J.J. (ed.) (1963) *The Art and Science of Growing Crystals*, Wiley, New York.
- Gilmer, G.H., Ghez, R. and Cabrera, N. (1971) An analysis of combined surface and volume diffusion processes in crystal growth. *Journal of Crystal Growth*, **8**, 79–93.
- Ginde, R.M. and Myerson, A.S. (1992) Cluster size estimation in binary supersaturated solutions. *Journal of Crystal Growth*, **116**, 41–47.
- Gmehling, J.G., Anderson, T.F. and Prausnitz, J.M. (1978) Solid-liquid equilibria using UNIFAC. *Industrial and Engineering Chemistry Fundamentals*, **17**, 269–273.
- Gnyra, B., Jooste, R.F. and Brown, N. (1974) Polycrystallization of aluminium trihydroxide. *Journal of Crystal Growth*, **21**, 141–145.
- Goldman, G. and Spott, G. (1981) Krustenbildung in Kristallisationsanlagen: eine neue praxisnahe Meßmethode. *Chemie Ingenieur Technik*, **53**, 713–716.
- Gordon, L., Salutsky, M.L. and Willard, H.H. (1959) *Precipitation from Homogeneous Solution*, Wiley, New York.
- Grønvold, F. and Meisingset, K.K. (1982) Thermodynamic properties and phase transitions of salt hydrates between 270 and 400 K: $\text{NH}_4\text{Al}(\text{SO}_4)_2 \cdot 12\text{H}_2\text{O}$, $\text{KAl}(\text{SO}_4)_2 \cdot 12\text{H}_2\text{O}$, $\text{Al}_2(\text{SO}_4)_3 \cdot 17\text{H}_2\text{O}$, $\text{ZnSO}_4 \cdot 7\text{H}_2\text{O}$, $\text{Na}_2\text{SO}_4 \cdot 10\text{H}_2\text{O}$, and $\text{Na}_2\text{S}_2\text{O}_3 \cdot 5\text{H}_2\text{O}$. *Journal of Chemical Thermodynamics*, **14**, 1083–1098.
- Gray, G.W. (ed.) (1987) *Thermotropic Liquid Crystals*, Wiley, Chichester.
- Griffiths, H. (1925) Mechanical crystallization. *Journal of the Society of Chemical Industry*, **44**, 7T–18T.
- Griffiths, H. (1947) Crystallization. *Transactions of the Institution of Chemical Engineers*, **25**, xiv–xviii.
- Grimmett, E.S. (1964) Kinetics of particle growth in the fluidized bed calcination process. *AICHEJ*, **10**, 717–722.
- Gunn, D.J. and Murthy, M.S. (1972) Kinetics and mechanisms of precipitations. *Chemical Engineering Science*, **27**, 1293–1313.
- Gupta, R.B. and Heidemann, R.A. (1990) Solubility models for amino acids and antibiotics. *AICHEJ*, **36**, 333–341.
- Gutoff, E.B. and Swank, T.F. (1980) Dispersions of spherical dye particles by continuous precipitation. *AICHE Symposium Series No. 193*, **76**, 43–51.
- Gyulai, Z. (1948) Beiträge zur Kenntnis der Kristallwachstumsvorgänge. *Zeitschrift für Physik*, **125**, 1–17.
- Haase, T. and Schöner, H. (1969) *Solid-Liquid Equilibrium*, Pergamon, Oxford.

- Hadzerga, P. (1967) Dynamic equilibria in the solar evaporation of Great Salt Lake brine. *Society of Mining Engineers Transactions*, **238**, 413–419.
- Halasz, S. and Mullin, J.W. (1987) Precipitation studies in a foam column: potash alum from aqueous solution using 2-propanol. *Crystal Research and Technology*, **22**, 193–197.
- Halfon, A. and Kaliaguine, S. (1976) Alumina trihydrate crystallization. *Canadian Journal of Chemical Engineering*, **54**, 160–172.
- Halstead, W.D. (1970). Some aspects of the behaviour of K_2SO_4 in aqueous solutions. *Journal of Applied Chemistry*, **20**, 45–47
- Hanitzsch, E. and Kahlweit, M. (1969) Ageing of precipitates. *Symposium on Industrial Crystallization*, Institution of Chemical Engineers, London, 130–141.
- Harbury, L. (1946) Solubility and melting point as functions of particle size. *Journal of Physical Chemistry*, **50**, 190–199.
- Harnby, N., Edwards, M.F. and Nienow, A.W. (1992) *Mixing in the Process Industries*, 2nd edn., Butterworths, London.
- Harned, H.S. and Owen, B.B. (1958) *The Physical Chemistry of Electrolytic Solutions*, 3rd edn., Reinhold, New York.
- Hartman, P. (1963) Structure, growth and morphology of crystals. *Zeitschrift für Kristallographie*, **119**, 65–78.
- Hartman, P. (1980) Attachment energy as a habit controlling factor. *Journal of Crystal Growth*, **49**, 157–165.
- Hartman, P. and Perdok, W.G. (1955) On the relations between structure and morphology of crystals. *Acta Crystallographica*, **8**, 49–52.
- Hartshorne, N.H. and Stuart, A. (1969) *Practical Optical Crystallography*, 2nd edn., Arnold, London.
- Hasson, D., Addai-Mensah, J. and Metcalf, J. (1990) Filterability of gypsum crystallized in phosphoric acid solution in the presence of ionic impurities. *Industrial and Engineering Chemistry Research*, **29**, 867–875.
- Hatschek, E. (1928) *The Viscosity of Liquids*, Bell, London.
- Heist, J.A. (1981) Freeze crystallization: waste water recycling and reuse. *AICHE Symposium series*, No. 209, **77**, 259–272.
- Henisch, H.K. (1988) *Crystals in Gels and Liesegang Rings*, Cambridge University Press, Cambridge.
- Henning, S. and Ulrich, J. (1997) Migration of liquid inclusions in growing crystal layers. *Chemical Engineering Research and Design*, **75**, 233–236.
- Henry, J.D. and Powers, J.E. (1970) Experimental and theoretical investigation of continuous flow column crystallization. *AICHEJ*, **16**, 1055–1063.
- Her, Y-S., Matijevic, E. and Wilcox, W.R. (1990) Continuous precipitation of mono-dispersed yttrium basic carbonate powders. *Powder Technology*, **61**, 173–177.
- Herington, E.F.G. (1963) *Zone Melting of Organic Compounds*, Wiley, New York.
- Hildebrand, J.H., Prausnitz, J.M. and Scott, R.L. (1971) *Regular and Related Solutions*, Van Nostrand, New York.
- Hill, S. (1970) Residence time distribution in continuous crystallizers. *Journal of Applied Chemistry*, **20**, 300–304.
- Hiquily, N. and Laguerie, C. (1984) Inclusion formation in ammonium perchlorate crystals: influence of surfactants. *Industrial Crystallization 84* (9th Symposium, The Hague), S.J. Jančić and E.J. de Jong (eds.), Elsevier, Amsterdam, 79–83.
- Hirth, J.P. and Loethe, J. (1968) *Theory of Dislocations*, McGraw-Hill, New York.
- Hoare, M. (1982) Protein precipitation and ageing. *Transactions of the Institution of Chemical Engineers*, **60**, 79–87 and 157–163.

- Hoare, M.R. and McInnes, J. (1976) Statistical mechanics and morphology of very small atomic clusters. *Discussions of the Faraday Society*, **61**, 12–24.
- Holden, A.N. (1949) Growing single crystals from solution. *Discussions of the Faraday Society*, **5**, 312–318.
- Holden, C.A. and Bryant, H.S. (1969) Purification by sublimation. *Separation Science*, **4**, (1), 1–13.
- Holeci, I. (1965) Emulsion crystallization of organic substances. *CSSR SNTL Technical Digest*, **71**, 515.
- Holland, A.A. (1951) A new type of evaporator. *Chemical Engineering*, **58**, (1), 106–107.
- Holven, A.L. (1942) Supersaturation in sugar boiling operations. *Industrial and Engineering Chemistry*, **34**, 1234–1240.
- Honig, P. (ed.) (1959) *Principles of Sugar Technology*, 2 vols., Elsevier, Amsterdam.
- Honigmann, B. and Horn, D. (1973) α – β transformations of copper phthalocyanine in organic suspensions. In *Particle Growth in Suspensions*, A.L. Smith (ed.), Academic Press, London, 283–294.
- Hooks, I.J. and Kerze, F. (1946) Nomograph predicts crystal sizes. *Chemical and Metallurgical Engineering*, **53**, (7), 140.
- Hoppe, A. (1964) Dewaxing with urea. *Advances in Petroleum Chemistry and Refining*, Vol. 8, J.J. McKetta (ed.), Interscience, New York.
- Hostomský, J. and Jones, A.G. (1991) Calcium carbonate crystallization, agglomeration and form during continuous precipitation from solution. *Journal of Physics, D: Applied Physics*, **24**, 165–170.
- Hou, T-P. (1942) *Manufacture of Soda*, 2nd edn., Reinhold, New York.
- Hougen, D.A., Watson, K.M. and Ragatz, R.A. (1943) *Chemical Process Principles*, Part 1, 2nd edn., Wiley, New York.
- Hounslow, M.J. (1990) Nucleation, growth and aggregation rates from steady-state experimental data. *AICHEJ*, **36**, 1748–1752.
- Hughmark, G.A. (1969) Mass transfer for suspended solid particles in agitated liquids. *Chemical Engineering Science*, **24**, 291–287.
- Hui, Y.H. (ed.) (1996). *Bailey's Industrial Oil and Fat Products*, 5th edn. (5 vols.), Wiley, New York.
- Hulbert, H.M. and Katz, S. (1964) Some problems in particle technology: a statistical mechanical formulation. *Chemical Engineering Science*, **19**, 555–574.
- Humphreys-Owen, S.P.F. (1949) Crystal growth from solution. *Proceedings of the Royal Society*, **A197**, 218–237.
- Hunt, J.D. and Jackson, K.A. (1966) Nucleation of solid in an undercooled liquid by cavitation. *Journal of Applied Physics*, **37**, 254–257.
- Hurle, D.T.J. (1961) Constitutional supercooling during crystal growth from stirred melts. *Solid State Electronics*, **3**, 37–44.
- Hurle, J.C.G. (1993) *Handbook of Crystal Growth* (3 vols.), North-Holland, Amsterdam.
- Irani, R.R., Callis, C.F. and Liu, T. (1959) Flow conditioning and anti-caking agents. *Industrial and Engineering Chemistry*, **51**, 1285–1288.
- Irani, R.R., Vandersall, H.L. and Morgenthaler, W.W. (1961) Water vapour sorption in flow conditioning and cake inhibition. *Industrial and Engineering Chemistry*, **53**, 141–142.
- ISO 13322 (2001) *Image Analysis Methods*, International Organization for Standardization, Zurich.
- ISO 2591 (1989) *Sieve testing*, International Organization for Standardization, Zurich.
- ISO 3310 (2000) *Test Sieves*. International Organization for Standardization, Zurich.

- ISO 565 (1990) *Test sieves: woven wire, perforated plate and electroformed sheet*, International Organization for Standardization, Zurich.
- ISO 5725 (1992) *Precision of Test Methods*, International Organization for Standardization, Zurich.
- IUPAC (1980–91) *Solubility Data Series*, Vol. 1–48, J.W. Lorimer (ed.), Pergamon Press, Oxford.
- Jackson, K.A. (1958) *Liquid metals and solidification*, American Society of Metals, Cleveland.
- Jackson, K.A. (1974) Theory of crystal growth from the melt. *Journal of Crystal Growth*, **24/25**, 130–136.
- Jacques, J., Collet, A. and Wilen, S.H. (1981) *Enantiomers, Racemates and Resolutions*, Wiley, New York.
- Jadhan, V.K., Chivate, M.R. and Tavare, N.S. (1991) Separation of p-cresol from its mixture with 2,6 xylene by adductive crystallization. *Chemical Engineering Data*, **36**, 249–251.
- Jadhan, V.K., Chivate, M.R. and Tavare, N.S. (1992) Separation of phenol from its mixture with o-cresol by adductive crystallization. *Journal of Chemical Engineering Data*, **37**, 232–235.
- Jager, J., de Wolf, S., Kramer, H.J.M. and de Jong, E.J. (1991) Estimation of nucleation and attrition kinetics from CSD transients in a continuous crystallizer. *Chemical Engineering Research and Design*, **69**, 53–62.
- Jančić, S.J. (1989) Fractional crystallization. In *Industrial Crystallization 87* (10th Symposium, Bechyně), J. Nývlt and S. Žáček (eds.), Elsevier, Amsterdam, 57–70.
- Jančić, S.J. and Grootscholten, P.A.M. (1984) *Industrial Crystallization*, University Press, Delft.
- Janse, A.H. and de Jong, E.J. (1978) On the width of the metastable zone. *Transactions of the Institution of Chemical Engineers*, **56**, 187–193.
- Jeremiassen, F. and Svane, H. (1932) Supersaturation control attains close crystal sizing. *Chemical and Metallurgical Engineering*, **39**, 594–596.
- Johnson, A.I. and Huang, C.J. (1955) Estimation of heat capacities of organic liquids. *Canadian Journal of Technology*, **33**, 421.
- Johnston, K.P., Barry, S.F., Read, W.K. and Holcomb, T.R. (1987) Separation of isomers using retrograde crystallization from supercritical fluids. *Industrial and Engineering Chemistry Research*, **26**, 2372–2377.
- Johnson, R.T., Rousseau, R.W. and McCabe, W.L. (1972) Factors affecting contact nucleation. *AICHE Symposium Series No. 121*, **68**, 31–41.
- Johnstone, R.E. and Thring, M.W. (1957) *Pilot Plants, Models and Scale-up Methods in Chemical Engineering*, McGraw-Hill, New York.
- Jones, A.G. (1974) Optimal operation of a batch cooling crystallizer. *Chemical Engineering Science*, **29**, 1075–1087.
- Jones, A.G., Chianese, A. and Mullin, J.W. (1984) Effect of fines destruction on batch cooling crystallization of potassium sulphate solutions. In *Industrial Crystallization 84* (9th Symposium, The Hague), S.J. Jančić and E.J. de Jong (eds.), 191–195.
- Jones, A.G., Ewing, C.M. and Melvin, M.V. (1981) Biotechnology of solar saltfields. *Hydrobiologia*, **82**, 391–406.
- Jones, A.G. and Mullin, J.W. (1973a) Crystallization kinetics of potassium sulphate in a draft-tube agitated vessel. *Transactions of the Institution of Chemical Engineers*, **51**, 302–308.
- Jones, A.G. and Mullin, J.W. (1973b) The design of a draft-tube agitated vessel. *Chemistry and Industry*, 21 April, 387–388.

- Jones, A.G. and Mullin, J.W. (1974) Programmed cooling crystallization of potassium sulphate solutions. *Chemical Engineering Science*, **29**, 105–118.
- Jones, A.G. and Teodossiev, N.M. (1988) Microcomputer programming of dosage rate during batch precipitation. *Crystal Research and Technology*, **23**, 957–966.
- Jones, C.M., Larson, M.A., Ristic, R.I. and Sherwood, J.N. (2000) The role of dislocations, strain and supersaturation on the growth of NaNO₃. *Journal of Crystal Growth*, **208**, 520–524.
- Jones, W.J. (1913a) Über die Grösse der Oberflächenenergie fester Stoffe. *Zeitschrift für Physikalische Chemie*, **82**, 448–456.
- Jones, W.J. (1913b) Über die Beziehung zwischen geometrischer Form und Dampfdruck, Löslichkeit und Formenstabilität. *Annalen der Physik*, **41**, 441–448.
- Jones, W.J. and Partington, J.R. (1915) A theory of supersaturation. *Philosophical Magazine*, **29**, 35–40.
- Joy, E.F. and Payne, J.H. (1955) Fractional precipitation or crystallization systems. *Industrial and Engineering Chemistry*, **47**, 2157–2161.
- Juzaszek, P. and Larson, M.A. (1977) Influence of fines dissolving on crystal size distribution in an MSMPR crystallizer. *AICHeJ*, **23**, 460–468.
- Kabascı, S., Althaus, W. and Weinspach, P.M. (1996). Batch precipitation of calcium carbonate from highly supersaturated solutions. *Chemical Engineering Research and Design*, **74**, 765–772.
- Kahlweit, M. (1975) Ostwald ripening of precipitates. *Advances in Colloid and Interface Science*, **5**, 1–35.
- Karel, M. and Nývlt, J. (1989) Measurement of growth rates for single crystals and pressed tablets of CuSO₄ · 5H₂O on a rotating disc. *Collections of the Czechoslovak Chemical Communications*, **54**, 2951–2961.
- Kashchiev, D. (2000) *Nucleation*, Butterworth-Heinemann, Oxford.
- Kaufmann, D.W. (ed.) (1960) *Sodium Chloride*, Reinhold, New York.
- Kawashima, Y. (1984) Spherical crystallization and pharmaceutical systems. *Pharmacy International*, **5**, 40–43.
- Kawashima, Y., Handa, T., Takeuchi, H., Takenaka, H. and Lin, S.Y. (1986) Spherical agglomeration of calcium carbonate dispersed in aqueous medium containing sodium oleate. *Powder Technology*, **46**, 61–66.
- Kawashima, Y., Okumura, M. and Takenaka, H. (1984) The effects of temperature on the spherical crystallization of salicylic acid. *Powder Technology*, **39**, 41–47.
- Kelly, F.D. and Chimowitz, E.H. (1989) Experimental data for the crossover process on a model supercritical system. *AICHeJ*, **35**, 981–987.
- Kelly, F.H.C. and Mak, F.K. (1975) *The Sucrose Crystal and its Solution*, University Press, Singapore.
- Kemp, S.D. (1958) Sublimation and vacuum freeze drying. In *Chemical Engineering Practice*, Vol. 6, H.W. Cremer and T. Davies (eds.), Butterworths, London, 567–600.
- Kendall, K. (1978) The impossibility of comminuting small particles by compaction. *Nature*, **272**, 710–711.
- Kenner, C.T. and Busch, K.W. (1979) *Quantitative Analysis*, Macmillan, New York.
- Kern, R. (ed.) (1965) Adsorption et Croissance Cristalline. *Colloquium No. 152* (Symposium proceedings), C.N.R.S., Paris.
- Khamskii, E.V. (1969) *Crystallization from Solutions*, Consultants Bureau, New York.
- Kim, K.-J. and Mersmann, A. (1997) Melt crystallization with direct contact cooling techniques. *Chemical Engineering Research and Design*, **75**, 176–182.
- Kimura, H. (1980) Nucleation of molten Na₂S₂O₃ · 5H₂O and some other similar hydrates: a thermodynamic observation. *Industrial and Engineering Chemistry Fundamentals*, **19**, 251–253.

- King, R.J. (1984) Mechanical vapour recompression crystallizers. *Chemical Engineering Progress*, **80**, (7), 63–69.
- Kirby, T. (1959) Find wash liquor requirements fast. *Chemical Engineering*, **66**, 20 April, 169–170.
- Kirwan, D.J. and Pigford, R.L. (1969) Crystallization kinetics of pure and binary melts. *AIChEJ*, **15**, 442–449.
- Kishishita, A., Kishimoto, S. and Nagashima, N. (1996) Characterization of organic crystal products. *Journal of Crystal Growth*, **167**, 729–733.
- Kitaigorodskii, A.I. (1961) *Organic Crystal Chemistry*, Consultants Bureau, New York.
- Kitamura, M. (1989) Polymorphism in the crystallization of L-glutamic acid. *Journal of Crystal Growth*, **96**, 541–546.
- Kitamura, M., Furukawa, H. and Asaeda, M. (1994) Solvent effect of ethanol on crystallization and growth of L-histidine polymorphs. *Journal of Crystal Growth*, **141**, 193–199.
- Kitamura, M. and Tanake, T. (1994) Crystallization behaviour of polymorphous Ni-complex clathrates. *Journal of Crystal Growth*, **142**, 165–170.
- Kitamura, M., Yamamoto, M., Yoshinaga, Y. and Masuoka, H. (1997). Crystal size control of sulfathiazole using high pressure CO₂. *Journal of Crystal Growth*, **178**, 378–386.
- Kitano, Y., Okumara, M. and Idogaki, M. (1980) Abnormal behaviours of copper and zinc ions in parent solution at the early stage of calcite formation. *Geochemical Journal*, **14**, 167–175.
- Klein, M.O., Sareen, B.K., Strathdee, G.L. and Storer, D.K. (1987) Low temperature crystallization using the natural climate of Saskatchewan: computer modelling of a pond crystallizer. *Crystallization and Precipitation Symposium Proceedings*, Strathdee, G.L. et al. (eds.) (1987), Pergamon Press, Oxford, 21–31.
- Klug, D.L. (1992) The influence of impurities and solvents on crystallization. In Myerson, A.S. (ed.) (1992), pp. 65–87.
- Knapp, L.F. (1922) The solubility of small particles and the stability of colloids. *Transactions of the Faraday Society*, **17**, 457–465.
- Knuth, M. and Weinspach, P.M. (1976) Experimentelle Untersuchung des Warme und Stoffübergangs an die Partikeln einer Wirbelschicht bei der Desublimation. *Chemie Ingenieur Technik*, **48**, 893.
- Kolař, V. (1958) Collections of the Czechoslovak Chemical Communications, **23**, 1680 [see also **24**, (1959), 301].
- Kolthoff, I.M., Sandell, E.B., Meehan, E.J. and Bruckensteine, S. (1969) *Quantitative Chemical Analysis*, 4th edn., Macmillan, London.
- Komarov, V.F., Garside, J. and Mullin, J.W. (1976) A technique for investigating primary nucleation in stagnant solutions. *Chemistry and Industry*, 7 February, 119–120.
- Kossel, W. (1934) Zur Energetik von Oberflächenvorgängen. *Annalen der Physik*, **21**, 457–480.
- Kotsinaris, A., van Rosmalen, G.M. and Hounslow, M.J. (1999) Magnetic water treatment. Paper 228 in *Industrial Crystallization* (14th Symposium, Cambridge), IChemE, Rugby.
- Krabbes, E. (1995) Vapour Growth. In *Science and Technology of Crystal Growth*, J.P. van der Eerden and O.S.L. Bruinsma (eds.), Kluwer, Dordrecht, 123–136.
- Krupiczka, R. and Pyschny, J. (1990) Mathematical modelling of the desublimation of phthalic anhydride. *Chemical Engineering and Processing*, **28**, 29–34.
- Kuboi, R., Nienow, A.W. and Conti, R. (1984) Mechanical attrition of crystals in stirred vessels. In *Industrial Crystallization 84* (9th Symposium, The Hague), S.J. Jančić and E.J. de Jong (eds.), North-Holland, Amsterdam, 211–216.

- Kubota, N. and Fujiwara, M. (1990) Minimum seed crystal size for secondary nucleation of potassium alum in a stirred-vessel crystallizer. *Journal of Chemical Engineering Japan*, **23**, 691–696.
- Kubota, N. and Mullin, J.W. (1995) A kinetic model for crystal growth from aqueous solution in the presence of impurities. *Journal of Crystal Growth*, **152**, 203–208.
- Kubota, N., Fugisawa, Y., Yokota, M. and Mullin, J.W. (1999) Pseudo-solubilities of potassium sulphate in water in the presence of Fe(III) impurities. *Journal of Crystal Growth*, **197**, 388–392.
- Kubota, N., Fukazawa, J., Yashiro, H. and Mullin, J.W. (1994) Pseudo-solubilities of potassium sulphate caused by traces of Cr(III) salts under controlled pHs. *Journal of Crystal Growth*, **143**, 287–293.
- Kubota, N., Ito, K. and Shimizu, K. (1986) Chromium ion effect on contact nucleation of ammonium sulphate. *Journal of Crystal Growth*, **76**, 272–278.
- Kubota, N., Kawakami, T. and Tadaki, T. (1986) Calculation of supercooling temperature for primary nucleation of potassium nitrate from aqueous solution by the two-kind active site model. *Journal of Crystal Growth*, **74**, 259–274.
- Kubota, N., Uchiyama, I., Nakai, K., Shimizu, K. and Mullin, J.W. (1988) Change of solubility of K_2SO_4 in water by traces of Cr(III). *Industrial and Engineering Chemistry Research*, **27**, 930–934.
- Kubota, N., Yokota, M. and Mullin, J.W. (1997) Supersaturation dependence of crystal growth in solution in the presence of impurities. *Journal of Crystal Growth*, **182**, 86–94.
- Kubota, N., Yokota, M. and Mullin, J.W. (2000) The combined influence of supersaturation and impurity concentration on crystal growth. *Journal of Crystal Growth*, **212**, 480–488.
- Kudela, L. and Sampson, M.J. (1986) Understanding sublimation technology. *Chemical Engineering*, **93**, No. 12, 93–98.
- Lacmann, R. and Stranski, I.N. (1958) The effect of adsorption of impurities on the equilibrium and growth forms of crystals. In Doremus, Roberts and Turnbull (1958), 427–439.
- Lancia, A., Musmarra, D. and Priciandaro, M. (1999) Measuring induction periods for $CaSO_4 \cdot 2H_2O$ precipitation. *AICheJ*, **45**, 390–397.
- Land, T.A. et al. (1999) Recovery of surfaces from impurity poisoning during crystal growth. *Nature*, **399**, 3 June, 442–445.
- Larson, M.A. (1982) Secondary nucleation: an analysis. In *Industrial Crystallization 81* (8th Symposium, Budapest), S.J. Jančić and E.J. de Jong (eds.), North-Holland, Amsterdam, 55–60.
- Larson, M.A. and Garside, J. (1973) Crystallizer design techniques using the population balance. *The Chemical Engineer*, 318–328.
- Larson, M.A. and Garside, J. (1986) Solute clustering in supersaturated solutions. *Chemical Engineering Science*, **41**, 1285–1289.
- Larson, M.A. and Mullin, J.W. (1973) Crystallization kinetics of ammonium sulphate. *Journal of Crystal Growth*, **20**, 183–191.
- Larson, M.A., Timm, D.C. and Wolff, P.R. (1968) Effect of suspension density on crystal size distribution. *AICheJ*, **14**, 448–457.
- Laudise, R.A. (1970) *The Growth of Single Crystals*, Prentice-Hall, Englewood Cliffs.
- Laudise, R.A. and Sullivan, R.A. (1959) Pilot plant production of synthetic quartz. *Chemical Engineering Progress*, **55**, (5), 55–59.
- Leci, C.L. and Mullin, J.W. (1968) Refractive index measurement in liquids rendered opaque by the presence of suspended solids. *Chemistry and Industry*, 1517.

- Lee, M-Y. *et al.* (1996) Influence of metal ion inclusion on the morphology of Gibbsite. *Chemical Engineering Research and Design*, **74**, 739–743.
- Leeuwen, M.L.J.van (1998) *Precipitation and Mixing*. PhD Thesis. University Press, Delft.
- Leeuwen, M.L.J.van, Bruinsma, O.S.L. and van Rosmalen, G.M. (1996) Influence on mixing on the product quality in precipitation. *Chemical Engineering Science*, **51**, 2595–2600.
- Leigh, T. (1977) Resolution of racemic bases. *Chemistry and Industry*, 1 January, 36–37.
- Letan, R. (1973) A direct contact cooled crystallizer. *Industrial and Engineering Chemistry Process Design and Development*, **12**, 300–305.
- Leubner, I.H. (1987) Crystal formation (nucleation) under kinetically controlled and diffusion-controlled growth conditions. *Journal of Physical Chemistry*, **91**, 6069–6073.
- Leubner, I.H., Jaganathan, R. and Wey, J.S. (1980) Formation of silver bromide in double-jet precipitation. *Photographic Science and Engineering*, **24**, 268–272.
- Levins, D.M. and Glastonbury, J.R. (1972) Particle-liquid hydrodynamics and mass transfer in a stirred vessel. *Transactions of the Institution of Chemical Engineers*, **50**, 32–41 and 132–146.
- Lewin, S. (1960) *The Solubility Product Principle*, Pitman, London.
- Lewis, B. (1980) Nucleation and growth theory. In *Crystal Growth*, 2nd edn., B.R. Pamplin (ed.), Pergamon Press, Oxford, 23–63.
- Lewtas, K., Tack, R.D., Beiny, D.H.M. and Mullin, J.W. (1991) Wax crystallization in diesel fuel: habit modification and growth of n-alkane crystals. In *Advances in Industrial Crystallization*, J. Garside, R.J. Davey and A.G. Jones (eds.) (1991), Butterworth-Heinemann, Oxford, 166–179.
- Liao, J.C. and Ng, K.C. (1990) Effect of ice nucleators on snow making and spray freezing. *Industrial and Engineering Chemistry Research*, **29**, 361–366.
- Liesegang, R.E. (1911) Über die Reifung von Silberhaloidemulsionen. *Zeitschrift für Physikalische Chemie*, **75**, 374–377.
- Lindberg, M. and Rasmuson, Å.C. (2000) Supersaturation generation at the feedpoint in reaction crystallization of a molecular compound. *Chemical Engineering Science*, **55**, 1735–1746.
- Linford, R.G. (1972) Surface energy of solids. *Chemical Society Reviews*, **1**, 445–464.
- Liu, G-T. and Nagahama, K. (1996) Application of rapid expansion of supercritical solutions in crystallization separation. *Industrial and Engineering Chemistry Research*, **35**, 4626–4634.
- Liu, S.T. and Nancollas, G.H. (1973) The crystallization of magnesium hydroxide. *Desalination*, **12**, 75–80.
- Lo, P.Y. and Myerson, A.S. (1990) Diffusion and cluster formation in supersaturated solution. *Journal of Crystal Growth*, **99**, 1048–1052.
- Lobachev, A.N. (1971) *Hydrothermal Synthesis of Crystals*, Consultants Bureau, New York.
- Long, F.A. and McDevit, W.F. (1952) Activity coefficients of non-electrolyte solutes in aqueous salt solution. *Chemical Reviews*, **51**, 119–169.
- Lowell, S. and Shields, J.E. (1984) *Powder Surface Area and Porosity*, Chapman and Hall, London.
- Lukes, J.A. and Lukes, G.C. (1993) Solar evaporation correlations at the Salar de Atacama. *Proceedings of the 7th Symposium on Salt*, Vol. 1. Elsevier, Amsterdam, pp. 525–532.
- Lyle, O. (1957) *Technology for Sugar Refinery Workers*, 3rd edn., Chapman and Hall, London.

- Lyman, W.J., Reehl, W.F. and Rosenblatt, D.H. (1982) *Handbook of Chemical Property Estimation Methods*, McGraw-Hill, New York.
- Macedo, E.A., Skovborg, P. and Rasmussen, P. (1990) Calculations of phase equilibria for solutions of strong electrolytes in solvent-water mixtures. *Chemical Engineering Science*, **45**, 875–882.
- Manguo, J.L. and Schwartz, J.C. (1985) Simulation of an evaporative solar salt pond. *Industrial and Engineering Chemistry Process Design and Development*, **24**, 1245–1251.
- Mantovani, G., Vaccari, G., Squaldino, G., Aquilano, D. and Rubbo, M. (1985) Sucrose crystal colour as a function of some industrial crystallization parameters. *L'Industria Saccarifera Italiana*, **78**, 7–14 and 79–86.
- Marc, R. (1908) Über die Kristallisation aus wässrigen Lösungen. *Zeitschrift für Physikalische Chemie*, **61**, 385–398.
- Marcant, B. and David, R. (1991) Experimental evidence for and prediction of micro-mixing effects in precipitation. *AICHeJ*, **37**, 1698–1710.
- Margolis, G. and Gutoff, E.B. (1974) Simulation of the precipitation of silver bromide photographic emulsions. *AICHeJ*, **20**, 467–474.
- Markvart, M., Vaneček, V. and Drbohlav, R. (1962) The drying of low melting point substances and evaporation of solutions in fluidized beds. *British Chemical Engineering*, **7**, 503–506.
- Marshall, W.L. and Slusher, R. (1966) Thermodynamics of $\text{CaSO}_4 \cdot 2\text{H}_2\text{O}$ in aqueous NaCl solutions 0–110 °C. *Journal of Physical Chemistry*, **70**, 4015–4027.
- Maruscak, A., Baker, C.G.J. and Bergougnou, M.A. (1971) Calcium carbonate precipitation in a continuous stirred tank reactor. *Canadian Journal of Chemical Engineering*, **49**, 819–824.
- Mason, B.J. (1957) *The Physics of Clouds*, Clarendon, Oxford.
- Matijević, E. (1994) Uniform inorganic colloidal dispersions – achievements and challenges. *Langmuir*, **10**, 8–16.
- Matsuoka, M. (1984) Rates of nucleation and growth of organic condensates of mixed vapours. *Industrial Crystallization 84* (9th Symposium, The Hague), S.J. Jančić and E.J. de Jong (eds.), Elsevier, Amsterdam, 357–360.
- Matsuoka, M. (1991) Developments in melt crystallization. In *Advances in Industrial Crystallization* (Symposium proceedings), J. Garside and A.G. Jones (eds.), Butterworth-Heinemann, Oxford, 229–244.
- Matsuoka, M. and Ozawa, R. (1989) Determination of solid-liquid phase equilibria of binary organic systems by differential scanning calorimetry. *Journal of Crystal Growth*, **96**, 596–604.
- Matthews, G.P. (1985) *Experimental Physical Chemistry*, Clarendon Press, Oxford.
- Matusevich, L.N. (1968) *Crystallization from Solutions* (in Russian), Moscow.
- Matz, G. (1958) Fließbett-Sublimation. *Chemie Ingenieur Technik*, **30**, 319–329.
- Matz, G. (1966) Die Sublimation im Rahmen der thermischen Trennverfahren. *Chemie Ingenieur Technik*, **38**, 299–308.
- Matz, G. (1969) *Kristallization*, 2nd edn., Springer-Verlag, Berlin.
- Matz, G. (1970) Mittlere Kristallwachstumsgeschwindigkeit des Einzelkorns. *Chemie Ingenieur Technik*, **4**, 1134–1141.
- Max, M. and Dillon, W. (2000) Natural gas hydrates: a frozen asset. *Chemistry and Industry*, 10 January, 16–18.
- Mazzarotta, B. (1989) Crystallization of potassium sulphate from glaserite. *Crystal Research and Technology*, **24**, 503–511.
- McCabe, W.L. (1929) Crystal growth in aqueous solutions. *Industrial and Engineering Chemistry*, **21**, 30–33 and 112–119.

- McCabe, W.L. (1935) The enthalpy-concentration chart – a useful device for chemical engineering calculations. *Transactions of the American Institute of Chemical Engineers*, **31**, 129–164.
- McCabe, W.L. (1963) 'Crystallization' in *Chemical Engineers' Handbook*, 4th edn., J.H. Perry (ed.), McGraw-Hill, New York.
- McCabe, W.L. and Smith, J.C. (1976) *Unit Operations of Chemical Engineering*, 3rd edn., McGraw-Hill, New York.
- McCabe, W.L., Smith, J.C. and Harriott, P. (1985) *Unit Operations of Chemical Engineering*, 4th edn., McGraw-Hill, New York.
- McCabe, W.L. and Stevens, R.P. (1951) Rate of growth of crystals in aqueous solution. *Chemical Engineering Progress*, **47**, 168–174.
- McCandless, F.P. (1980) Separation of C₉ alkylbenzenes by induced extractive crystallization. *Industrial and Engineering Chemistry Product Research and Development*, **19**, 612–616.
- McCauley, J.A. (1991) Detection and characterization of polymorphs in the pharmaceutical industry. *AIChE Symposium Series No. 284*, **87**, 58–63.
- McKay, D.L. (1967) Phillips fractional solidification process. In *Fractional Solidification*, M. Zief and W.R. Wilcox (eds.), Dekker, New York, Chapter 16.
- McKay, D.L. and Goard, H.W. (1965) Continuous fractional crystallization, *Chemical Engineering Progress*, **61**, (11), 99–104.
- McKie, D. and McKie, C. (1974) *Crystalline Solids*, 3rd edn., Nelson, London.
- Meissner, H.P. and Kusik, C.L. (1979) Double salt solubilities. *Industrial and Engineering Chemistry, Process Design and Development*, **18**, 391–397.
- Meissner, H.P. and Manning, M.P. (1983) In *Chemical Engineering Thermodynamics*, S.A. Newman (ed.), Ann Arbor Science, Chapter 28.
- Meissner, H.P. and Tester, J.W. (1972) Activity coefficients of strong electrolytes in aqueous solution. *Industrial and Engineering Chemistry, Process Design and Development*, **11**, 128–133.
- Melia, T.P. and Moffitt, W.P. (1964) Secondary nucleation from aqueous solution. *Industrial and Engineering Chemistry Fundamentals*, **3**, 313–317.
- Melikhov, I.V. and Kelebeev, A.S. (1979) Coagulative growth of barium sulphate crystals from a strongly supersaturated aqueous solution. *Soviet Physics Crystallography*, **24**, 239–241.
- Mellor, J.D. (1978) *Fundamentals of Freeze Drying*, Academic Press, London.
- Meranda, D. and Furter, W.F. (1977) Elevation of the boiling point of water by salts at saturation. *Journal of Chemical and Engineering Data*, **22**, 315–317.
- Mersmann, A. (1990) Calculation of interfacial tensions. *Journal of Crystal Growth*, **102**, 841–847.
- Mersmann, A. (ed.) (1995) *Crystallization Technology Handbook*, Marcel Dekker, New York.
- Mersmann, A. and Bartosch, K. (1998) How to predict the metastable zone width. *Journal of Crystal Growth*, **183**, 240–250.
- Mersmann, A. and Kind, M. (1988) Chemical engineering aspects of precipitation from solutions. *Chemical Engineering and Technology*, **11**, 264–276.
- Mersmann, A. and Kind, M. (1989) Modelling of chemical process equipment: the design of crystallizers. *International Chemical Engineering*, **29**, 616–626.
- Metheny, D.E. and Vance, S.W. (1962) Particle growth in fluidized bed dryers. *Chemical Engineering Progress*, **58**, (6), 45–48.
- Michaels, A.S. and Colville, A.R. (1960) The effect of surface active agents on crystal growth rate and crystal habit. *Journal of Physical Chemistry*, **64**, 13–19.

- Middleman, S. (1965) Mass transfer from particles in agitated systems: applications of Kolmogoroff theory. *AICheJ*, **11**, 750–752.
- Miers, H.A. (1904) The concentration of the solution in contact with a growing crystal. *Philosophical Transactions*, **A202**, 492–515.
- Miers, H.A. and Isaac, F. (1906) Refractive indices of crystallizing solutions. *Journal of the Chemical Society*, **89**, 413–454.
- Miers, H.A. and Isaac, F. (1907) The spontaneous crystallization of binary mixtures. *Proceedings of the Royal Society*, **A79**, 322–351.
- Miller, P. and Saeman, W.C. (1947) Continuous vacuum crystallization of ammonium nitrate. *Chemical Engineering Progress*, **43**, 667–690.
- Mina-Mankarios, G. and Pinder, K.L. (1991). Salting out crystallization of sodium sulphate. *Canadian Journal of Chemical Engineering*, **69**, 308–324.
- Misra, C. and White, E.T. (1971) Kinetics of crystallization of aluminium trihydroxide from seeded aluminate solutions. *Chemical Engineering Progress Symposium Series*, No. 110, **67**, 53–65.
- Moates, G.H. and Kennedy, J.K. (1967) Continuous-zone melting. In *Fractional Solidification*, M. Zief and W.R. Wilcox (eds.), Dekker, New York, 342–373.
- Mohamed, R.S., Debenedetti, P.G. and Prudhomme, R.K. (1989) Effects of process conditions on crystals obtained from supercritical mixtures. *AICheJ*, **35**, 325–328.
- Mohan, R., Kaytancioglu, O. and Myerson, A.S. (2000) Diffusion and cluster formation in supersaturated solutions of ammonium sulphate at 289K. *Journal of Crystal Growth*, **217**, 393–403.
- Molinari, J.G.D. (1967a) The Proabd refiner. In *Fractional Solidification*, M. Zief and W.R. Wilcox (eds.), Dekker, New York, Chapter 13.
- Molinari, J.G.D. (1967b) Newton Chambers Process. In *Fractional Solidification*, M. Zief and W.R. Wilcox (eds.), Dekker, New York, Chapter 14.
- Molinari, J.G.D. and Dodgson, B.V. (1974) Theory and practice related to the Brodie purifier. *The Chemical Engineer*, Jul/Aug, 460–464.
- Monhemius, A.J. (1977) Precipitation diagrams for metal hydroxides, sulphides, arsenates and phosphates. *Transactions of the Institution of Mining Metallurgy*, **86**, C202–C206.
- Montillon, G.H. and Badger, W.L. (1927) Rate of growth of crystals in aqueous solution. *Industrial and Engineering Chemistry*, **19**, 809–816.
- Moore, W.J. (1972) *Physical Chemistry*, 5th edn., Longmans, London.
- Morari, M. (1980) Some comments on the optimal operation of batch crystallizers.
- Moritoki, M. (1984) Crystallization and sweating of p-cresol by application of high pressure. In *Industrial Crystallization 84* (9th Symposium, The Hague), S.J. Jančić and E.J. de Jong (eds.), Elsevier, Amsterdam, 373–376.
- Moyers, C.G. and Olson, J.H. (1974) Dense-bed column crystallizer: An experimental and analytical study. *AICheJ*, **20**, 1118–1124.
- Muir, R.F. and Howatt, C.S. (1982) Predicting solid-liquid equilibrium data from vapour-liquid data. *Chemical Engineering*, 22 Feb, 89–92.
- Mullin, J.B., Straughan, B.W. and Bricknell, W.S. (1965) Liquid encapsulation techniques. *Physics and Chemistry of Solids*, **26**, 782.
- Mullin, J.W. (1960) The analysis of sieve test data. *The Industrial Chemist*, **36**, 272–278.
- Mullin, J.W. (1973) Solution concentration and supersaturation units and their conversion factors. *The Chemical Engineer*, No. 274, 316–317.
- Mullin, J.W. and Amatavivadhana, A. (1967) Growth kinetics of ammonium and potassium dihydrogenphosphate crystals. *Journal of Applied Chemistry*, **17**, 151–156.

- Mullin, J.W. and Ang, H-M. (1974) Crystal size measurement: a comparison of the technique of sieving and Coulter counter. *Powder Technology*, **10**, 153–156.
- Mullin, J.W. and Ang, H-M. (1976) Nucleation characteristics of aqueous nickel ammonium sulphate solutions. *Faraday Society Discussions*, No. **61**, 141–148.
- Mullin, J.W. and Ang, H-M. (1977) Supersaturation and crystal size distribution changes during the precipitation of nickel ammonium sulphate hexahydrate. *Kristall und Technik*, **12**, 105–115.
- Mullin, J.W. and Broul, M. (1978) A laboratory scale evaporative crystallizer. *Chemistry and Industry*, 1 April, 226–228.
- Mullin, J.W. and Cook, T.P. (1963) Diffusivity of ammonium dihydrogen phosphate in aqueous solutions. *Journal of Applied Chemistry*, **13**, 423–429.
- Mullin, J.W. and Cook, T.P. (1965) Diffusion and dissolution of the hydroxybenzoic acids in water. *Journal of Applied Chemistry*, **15**, 145–151.
- Mullin, J.W. and Garside, J. (1967) Crystallization of aluminium potassium sulphate: a study in the assessment of crystallizer design data: I: Single crystal growth rates, II: Growth in a fluidized bed. *Transactions of the Institution of Chemical Engineers*, **45**, 285–295.
- Mullin, J.W. and Garside, J. (1970) Voidage-velocity relationships in the design of suspended-bed crystallizers. *British Chemical Engineering*, **15**, 773–775.
- Mullin, J.W. and Gaska, J. (1969) Growth and dissolution of potassium sulphate in a fluidized bed. *Canadian Journal of Chemical Engineering*, **47**, 483–489.
- Mullin, J.W. and Jančić, S.J. (1979) Interpretation of metastable zone widths. *Transactions of the Institution of Chemical Engineers*, **57**, 188–193.
- Mullin, J.W. and Leci, C.L. (1969a) Evidence of molecular cluster formation in supersaturated solutions of citric acid. *Philosophical Magazine*, **19**, 1075–1077.
- Mullin, J.W. and Leci, C.L. (1969b) Some nucleation characteristic of aqueous citric acid solutions. *Journal of Crystal Growth*, **5**, 75–76.
- Mullin, J.W. and Leci, C.L. (1972) Desupersaturation of seeded citric acid solutions in a stirred vessel. *AICHE Symposium Series*, No. **121**, **68**, 8–20.
- Mullin, J.W. and Nývlt, J. (1970) Design of classifying crystallizers. *Transactions of the Institution of Chemical Engineers*, **48**, 7–14.
- Mullin, J.W. and Nývlt, J. (1971) Programmed cooling of batch crystallizers. *Chemical Engineering Science*, **26**, 369–377.
- Mullin, J.W. and Osman, M.M. (1973) Nucleation and precipitation of nickel ammonium sulphate crystals from aqueous solution. *Kristall und Technik*, **8**, 471–481.
- Mullin, J.W. and Raven, K.D. (1961) Nucleation in agitated solutions. *Nature*, **190**, 251.
- Mullin, J.W. and Raven, K.D. (1962) Influence of mechanical agitation on the nucleation of aqueous salt solutions. *Nature*, **195**, 35–38.
- Mullin, J.W. and Šipek, M. (1982) Solubility and density isotherms for potassium aluminium sulphate water-alcohol systems. *Journal of Chemical Engineering Data*, **26**, 164–165.
- Mullin, J.W. and Söhnel, O. (1977) Expressions of supersaturation in crystallization studies. *Chemical Engineering Science*, **32**, 683–686 and **33**, 1535–1538.
- Mullin, J.W. and Williams, J.R. (1984) A comparison between indirect contact cooling methods for the crystallization of potassium sulphate. *Chemical Engineering Research and Design*, **62**, 296–302.
- Mullin, J.W. and Žáček, S. (1981) Precipitation of potash alum from aqueous solution. *Journal of Crystal Growth*, **53**, 515–518.
- Mullin, J.W., Amatavivadhana, A. and Chakraborty, M. (1970) Crystal habit modification studies with ADP and KDP. *Journal of Applied Chemistry*, **20**, 153–158.

- Mullin, J.W., Chakraborty, M. and Mehta, K. (1970) Nucleation and growth of ammonium sulphate crystals. *Journal of Applied Chemistry*, **20**, 367–371.
- Mullin, J.W., Teodosiev, N. and Söhnle, O. (1989) Potassium sulphate precipitation from aqueous solution by salting-out with acetone. *Chemical Engineering and Processing*, **26**, 93–99.
- Mullin, J.W., Murphy, J.D., Söhnle, O. and Spoors, G. (1989) Ageing of precipitated magnesium hydroxide. *Industrial and Engineering Chemistry Research*, **28**, 1725–1730.
- Murata, Y. and Honda, T. (1977) Growth of m-chloronitrobenzene crystals. *Journal of Crystal Growth*, **39**, 315–327.
- Murray, D.C. and Larson, M.A. (1965) Size distribution dynamics in a salting-out crystallizer. *AICheJ*, **11**, 728–733.
- Myerson, A.S. (ed.) (1992) *Handbook of Industrial Crystallization*, Butterworth-Heinemann, Oxford.
- Myerson, A.S. (ed.) (1999) *Molecular Modelling Applications in Crystallization*, University Press, Cambridge.
- Myerson, A.S. and Kirwan, D.J. (1977) Impurity trapping during dendritic crystal growth. *Industrial and Engineering Chemistry Fundamentals*, **16**, 414–424.
- Myerson, A.S. and Lo, P.Y. (1990) Diffusion and cluster formation in supersaturated solutions. *Journal of Crystal Growth*, **99**, 1048–1052.
- Myerson, A.S. and Saska, M. (1984) Formation of solvent inclusions in terephthalic acid crystals. *AICheJ*, **30**, 865–867.
- Myerson, A.S. and Senol, D. (1984) Diffusion coefficients near the spinodal curve. *AICheJ*, **30**, 1004–1006.
- Nagashima, Y. and Maeda, S. (1980) Design of desalination plant employing a direct contact refrigerant. *Heat Transfer Research Japan*, **8**, 71–75.
- Nagashima, Y. and Yamasaki, T. (1979) The results of direct cooling in a crystallizer for a caustic soda purification process. *AIChe Symposium Series*, No. 189, **75**, 250–255.
- Nakai, T. and Nakamura, H. (1979) Nucleation mechanism of calcium carbonate accompanying Ostwald ripening. In *Industrial Crystallization 78* (7th Symposium, Warsaw), E.J. de Jong and S.J. Jančić (eds.), North-Holland, Amsterdam, 75–79.
- Nancollas, G.H. (1966) *Interactions in Electrolyte Solutions*, Elsevier, Amsterdam.
- Nancollas, G.H. and Gardner, G.L. (1974) Kinetics of crystal growth of calcium oxalate monohydrate. *Journal of Crystal Growth*, **21**, 267–272.
- Nancollas, G.H. and Gill, J.S. (1979) Formation and dissolution of high-temperature forms of CaSO₄ scales: influence of inhibitors. *Society of Petroleum Engineers Journal*, December, 423–429.
- Nancollas, G.H. and Purdie, N. (1964) The kinetics of crystal growth. *Quarterly Reviews of the Chemical Society*, **18**, 1–20.
- Nancollas, G.H. and Reddy, M.M. (1974) The kinetics of crystallization of scale-forming materials. *Society of Petroleum Engineers Journal*, April, 117–126.
- Nancollas, G.H. and Tomazic, B. (1974) Growth of calcium phosphate on hydroxyapatite crystals. *Journal of Physical Chemistry*, **78**, 2218–2225.
- Nancollas, G.H. and Zawacki, S.J. (1984) Inhibitors of crystallization and dissolution. In *Industrial Crystallization 84* (9th Symposium, The Hague), S.J. Jančić and E.J. de Jong (eds.), Elsevier, Amsterdam, 51–60.
- Nass, K.K. (1991) Process implications of polymorphism in organic compounds. *AIChe Symposium Series No. 284*, **87**, 72–81.
- Nass, K.K. (1994) Rational solvent selection for cooling crystallization, *Industrial and Engineering Chemistry Research*, **33**, 1580–1584.

- Nauman, E.B. (1971) Selective fines destruction in recycle crystallizers. *Chemical Engineering Progress Symposium Series, No. 110*, **67**, 116–120.
- Nauman, E.B. and Szabo, T.T. (1971) Non-selective fines destruction in recycle crystallizers. *Chemical Engineering Progress Symposium Series, No. 110*, **67**, 108–115.
- Nelson, C.D. and Glatz, C.E. (1985) Primary particle formation in protein precipitation. *Biotechnology and Bioengineering*, **27**, 1434–1444.
- Nernst, W. (1904) Theorie der Reaktionsgeschwindigkeit in heterogenen Systemen. *Zeitschrift für Physikalische Chemie*, **47**, 52–55.
- Ness, J.N. and White, E.T. (1976) Collision nucleation in an agitated crystallizer. *Chemical Engineering Progress Symposium Series, No. 72*, **153**, 64–73.
- Newman, H.H. and Bennett, R.C. (1959) Circulating magma crystallizers. *Chemical Engineering Progress*, **55**, (3), 65–70.
- Nicol, W.M. (1969) The effect of superheating on boiling point elevation measurement. *International Sugar Journal*, **71**, 325–328.
- Nicolau, I.F. (1971) Purification process by solution zone passages. *Journal of Materials Science*, **6**, 1049–1052.
- Nielsen, A.E. (1964) *Kinetics of Precipitation*, Pergamon, Oxford.
- Nielsen, A.E. (1969) Nucleation and growth of crystals at high supersaturation. *Kristall und Technik*, **4**, 17–38.
- Nielsen, A.E. (1979) Kinetics of crystal growth during precipitation of a binary electrolyte. In *Industrial Crystallization 78* (7th Symposium, Warsaw), E.J. de Jong and S.J. Jančić (eds.), North-Holland, Amsterdam, 159–168.
- Nielsen, A.E. (1984) Electrolyte crystal growth mechanisms. *Journal of Crystal Growth*, **67**, 289–310.
- Nielsen, A.E. and Söhnle, O. (1971) Interfacial tensions, electrolyte crystal-aqueous solution, from nucleation data. *Journal of Crystal Growth*, **11**, 233–242.
- Nienow, A.W. (1968) Suspension of solid particles in turbine agitated baffled vessels. *Chemical and Engineering Science*, **23**, 1453–1459.
- Nienow, A.W. (1969) Dissolution mass transfer in a turbine agitated vessel. *Canadian Journal of Chemical Engineering*, **47**, 243–258.
- Nienow, A.W. (1976) The effect of agitation and scale-up on crystal growth rates and on secondary nucleation. *Transactions of the Institution of Chemical Engineers*, **54**, 205–207.
- Nienow, A.W. and Conti, R. (1978) Particle abrasion at high solids concentration in stirred vessels. *Chemical Engineering Science*, **33**, 1077–1086.
- Nienow, A.W., Bujac, P.D.B. and Mullin, J.W. (1972) Slip velocities in agitated vessel crystallizers. *Journal of Crystal Growth*, **13/14**, 488–492.
- Nienow, A.W., Unahabokha, R. and Mullin, J.W. (1966) Concentration-dependent physical properties and rates of mass transport. *Industrial and Engineering Chemistry Fundamentals*, **5**, 578–579.
- Nienow, A.W., Unahabokha, R. and Mullin, J.W. (1968) Diffusion and mass transfer of ammonium and potassium chloride in aqueous solution. *Journal of Applied Chemistry*, **18**, 154–156.
- Nobbs, J.H. and Patterson, D. (1977) Studies of the kinetics of nucleation and growth of pigment dispersions using a laser light-scattering apparatus in a flow system. *Journal of the Chemical Society Faraday Transactions*, **I 73**, 558–568.
- Novomeysky, M.A. (1936) The Dead Sea: a storehouse of chemicals. *Transactions of the Institution of Chemical Engineers*, **14**, 60–84.
- Novotný, P. and Söhnle, O. (1988) Density of aqueous salt solutions. *Journal of Chemical Engineering Data*, **33**, 49–55.

- Nowlan, M.F., Thi, H.D. and Sangster, J. (1980) Prediction of the viscosity of mixed electrolyte solutions from single-salt data. *Canadian Journal of Chemical Engineering*, **58**, 637–642.
- Noyes, A.A. and Whitney, W.R. (1897) Rate of solution of solid substances in their own solution. *Journal of the American Chemical Society*, **19**, 930–934.
- Nývlt, J. (1968) Kinetics of crystallization in solution. *Journal of Crystal Growth*, **3/4**, 377–383.
- Nývlt, J. (1971) *Industrial Crystallization from Solutions*, Butterworths, London.
- Nývlt, J. (1973) Design of continuous agitated crystallizers. *Kristall und Technik*, **8**, 603–610.
- Nývlt, J. (1973) The effect of periodic change on the shape of crystals. In *Particle Growth in Suspensions*, A.L. Smith (ed.), Academic Press, London, 131–136.
- Nývlt, J. (1977) *Solid-Liquid Phase Equilibria*, Elsevier, Amsterdam.
- Nývlt, J. (1978) *Industrial Crystallization: The Present State of the Art*, Verlag Chemie, Weinheim.
- Nývlt, J. (1983) Induction period of nucleation and metastable zone width. *Collections of the Czechoslovak Chemical Communications*, **48**, 1977–1983.
- Nývlt, J. (1989) Calculation of the kinetics of crystallization based on a single batch experiment. *Collections of the Czechoslovak Chemical Communications*, **54**, 3187–3197.
- Nývlt, J. (1992) *Design of Crystallizers*, CRC Press, Boca Raton.
- Nývlt, J. (1995) The Ostwald Rule of Stages. *Crystal Research and Technology*, **30**, 445–451.
- Nývlt, J. and Mullin, J.W. (1970) Periodic behaviour of continuous crystallizers. *Chemical Engineering Science*, **25**, 131–147.
- Nývlt, J. and Mullin, J.W. (1974) Design of continuous mixed-suspension crystallizers. *Kristall und Technik*, **9**, 141–155.
- Nývlt, J. and Mullin, J.W. (1977) Design of batch agitated crystallizers. *Kristall und Technik*, **12**, 1243–1249.
- Nývlt, J., Söhnel, O., Matuchová, M. and Broul, M. (1985) *The Kinetics of Industrial Crystallization*, Academia, Prague.
- O'Hara, M. and Reid, R.C. (1973) *Modelling Crystal Growth Rates from Solution*, Prentice-Hall, Englewood Cliffs.
- Oldshue, J.Y. (1983) *Fluid Mixing Technology*, McGraw-Hill, New York.
- Oldshue, J.Y. (1992) Agitation and mixing. In Myerson, A.S. (ed.) (1992), pp. 165–177.
- Ostwald, W. (1896) *Lehrbuch der Allgemeinen Chemie*, 2, Englemann, Leipzig, p. 444.
- Ostwald, W. (1897) Studien über die Bildung und Umwandlung fester Körper. *Zeitschrift für Physikalische Chemie*, **22**, 289–330.
- Ostwald, W. (1900) Über die vermeintliche Isomeric des roten und gelben Quecksilberoxyds und die Oberfläschen spannung fester Körper. *Zeitschrift für Physikalische Chemie*, **34**, 495–503.
- Ostwald, W. (1901) *Analytische Chemie*, 3rd edn., Englemann, Leipzig, pp. 23 ff.
- Othmer, D.F. and Frohlich, G.H. (1960) Correlating vapour pressures and heats of solution for the ammonium nitrate-water system. *AICHeJ*, **6**, 210–214.
- Othmer, D.F. and Thakar, M.S. (1953) Correlating diffusion coefficients in liquids. *Industrial and Engineering Chemistry*, **45**, 589–593.
- Otpushchennikov, N.F. (1962) Determination of the size of the elementary crystal nucleus from acoustic measurement. *Soviet Physics Crystallography*, **7**, 237–240.
- Ottens, E.P.K. and de Jong, E.J. (1973) A model for secondary nucleation in a stirred vessel cooling crystallizer. *Industrial and Engineering Chemistry Fundamentals*, **12**, 179–184.

- Palermo, J.A. (1967) Studies of crystallization and melting processes in small equipment. *Chemical Engineering Progress Symposium Series, No. 70*, **63**, 21–27.
- Palmer, K. (1970) Product size performance from Oslo-Krystal crystallizers. In *Industrial Crystallization*, Institution of Chemical Engineers Symposium, London, 190–201.
- Pamplin, B.R. (1980) *Crystal Growth*, 2nd edn., Pergamon, Oxford.
- Parr, N.L. (1960) *Zone Refining and Allied Techniques*, Newnes, London.
- Paterson, W.R. and Hayhurst, A.N. (2000) Mass or heat transfer from a sphere to a flowing liquid. *Chemical Engineering Science*, **55**, 1925–1927.
- Peet, R.B. (1931) *Theory of continuous vacuum crystallization, Report No. V-45*, American Potash & Chemical Corporation, Trona, California.
- Petric, B. and Petric, N. (1980) Investigations of the rate of sedimentation of magnesium hydroxide obtained from seawater. *Industrial and Engineering Process Design and Development*, **19**, 329–335.
- Pfann, W.G. (1966) *Zone Melting*, 2nd edn., Wiley, New York.
- Pfefer, G. and Boistelle, R. (1996) Control of molecular crystals morphology. *Chemical Engineering Research and Design*, **74**, 744–749.
- Phillips, F.C. (1980) *An Introduction to Crystallography*, 4th edn., Longmans Green, London.
- Phillips, V.A., Kolbe, J.L. and Opperhauser, H. (1977) The growth of Mg(OH)₂ crystals from MgCl₂ and Ca(OH)₂ in a brine environment. *Journal of Crystal Growth*, **41**, 235–244.
- Phillips, V.R. (1974) The quantitative recovery of crystals from mother liquor in experiments on crystallization from solution. *Chemistry and Industry*, 16 November, 922–974.
- Phillips, V.R. and Mullin, J.W. (1976) Surface perfection as a factor influencing growth layers on the 100 faces of ADP crystals. In *Industrial Crystallization*, J.W. Mullin (ed.) (1976), Plenum Press, New York.
- Phoenix, L. (1966) How trace additives inhibit the caking of inorganic salts. *British Chemical Engineering*, **11**, 34–38.
- Pirttimaki, J., Laine, E., Ketolainen, J. and Paronen, P. (1993) Effects of grinding and compression on crystal structure of anhydrous caffeine. *International Journal of Pharmaceutics*, **95**, 93–99.
- Plasari, E., Grisoni, P. and Villermaux, J. (1997) Influence of process parameters on the precipitation of organic nanoparticles by drowning-out. *Chemical Engineering Research and Design*, **75**, 237–244.
- Player, M.R. (1969) Mathematical analysis of column crystallization. *Industrial and Engineering Chemistry Process Design and Development*, **8**, 210–217.
- Plewes, A.C. and Klassen, J. (1951) Mass transfer rates from the solid to the gas phase. *Canadian Journal of Technology*, **29**, 322.
- Popovitz-Biro, R., Weissbuch, I., Jacquemain, D., Leveiller, F., Leiserowitz, L. and Lahav, M. (1991) Studies on the early stages of crystal nucleation. In *Advances in Industrial Crystallization* (Symposium Proceedings), J. Garside, R.J. Davey and A.G. Jones (eds.), Butterworth-Heinemann, Oxford, 3–19.
- Porter, M.W. and Spiller, R.C. (eds.) (1951) *The Barker Index of Crystals* (3 Vols.), Heffer, Cambridge.
- Powers, H.E.C. (1948) Determination of the grist of sugars. *International Sugar Journal*, **50**, 149–151.
- Powers, H.E.C. (1963) Nucleation and early crystal growth. *The Industrial Chemist*, **39**, 351–353.
- Powers, H.E.C. (1969/70) Sucrose crystals: inclusions and structure. *Sugar Technology Reviews*, **1**, 85.

- Prasad, K.V.R., Ristic, R.I., Sherwood, J.N. and Zikic, A.M. (1999) Influence of magnetic fields on the crystallization of materials. Paper 34 in *Industrial Crystallization* (14th Symposium, Cambridge), IChemE, Rugby.
- Pulley, C.A. (1962) The Krystal crystallizer. *The Industrial Chemist*, **38**, 63–66, 127–132, 175–178.
- Purchas, D.B. (1981) *Solid-Liquid Separation Technology*, Uplands Press, Croydon.
- Purdon, F.F. and Slater, V.W. (1946) *Aqueous Solutions and the Phase Diagram*, Arnold, London.
- Qui, Y. and Rasmussen, Å.C. (1990) Growth and dissolution of succinic acid crystals in a batch stirred crystallizer. *AIChEJ*, **36**, 665–676.
- Rajagopal, S., Ng, K.M. and Douglas, J.M. (1991) Design and economic trade-offs of extractive crystallization processes. *AIChEJ*, **37**, 437–447.
- Raju, K. and Atkinson, G. (1988) Thermodynamics of ‘scale’ mineral solubilities: BaSO₄ in aqueous NaCl. *Journal of Chemical Engineering Data*, **33**, 490–495.
- Raju, K. and Atkinson, G. (1989) Thermodynamics of ‘scale’ mineral solubilities: SrSO₄ in aqueous NaCl. *Journal of Chemical Engineering Data*, **34**, 361–364.
- Randolph, A.D. (1964) A population balance for countable entities. *Canadian Journal of Chemical Engineering*, **42**, 280–281.
- Randolph, A.D. (1965) Mixed suspension, mixed product removal crystallizer as a concept in crystallizer design. *AIChEJ*, **11**, 424–430.
- Randolph, A.D. (1970) How to approach problems of crystallization. *Chemical Engineering*, 4 May, 80–84.
- Randolph, A.D. and Larson, M.A. (1962) Transient and steady stage size distribution in continuous mixed suspension crystallizers. *AIChEJ*, **8**, 639–645.
- Randolph, A.D. and Larson, M.A. (1988) *Theory of Particulate Processes*, 2nd edn., Academic Press, New York.
- Randolph, A.D. and Sikdar, S.K. (1974) Effect of a soft impeller coating on the net formation of secondary nuclei. *AIChEJ*, **20**, 410–412.
- Randolph, A.D. and Sikdar, S.K. (1976) Creation and survival of secondary crystal nuclei (K₂SO₄). *Industrial and Engineering Chemistry Fundamentals*, **15**, 64–71.
- Randolph, A.D., Deepak, C. and Iskander, M. (1968) On the narrowing of particle-size distributions in staged vessels with classified product removal. *AIChEJ*, **14**, 827–830.
- Read, W.T. (1953) *Dislocation in Crystals*, McGraw-Hill, New York.
- Reddy, M.M. (1978) Kinetic inhibitions of CaCO₃ formation by waste water constituents. In *Chemistry of Waste Water Technology*, A.J. Rubin (ed.), Science Publications, Ann Arbor, Chapter 3.
- Reddy, M.M. and Nancollas, G.H. (1976) The crystallization of calcium carbonate: effect of Mg²⁺, Sr²⁺ and SO₄²⁻. *Journal of Crystal Growth*, **35**, 33–38.
- Redman, T., Rohani, S. and Strathdee, G.L. (1997) Control of the crystal mean size in a pilot plant potash crystallizer. *Chemical Engineering Research and Design*, **75**, 183–192.
- Reich, R. and Kahlweit, M. (1968) Zur Kinetic des Kristallwachstums in wässrigen Lösungen. *Berichte der Bunsengesellschaft*, **72**, 66–69, 70–74.
- Reid, R.C., Prausnitz, J.M. and Poling, B.E. (1987) *The Properties of Gases and Liquids*, 4th edn., McGraw-Hill, New York.
- Ricci, J.E. (1966) *The Phase Rule and Heterogeneous Equilibrium*, Dover Publications, New York.
- Rice, R.W. and Baud, R.E. (1990) The role of micromixing in the scale-up of geometrically similar batch reactors. *AIChEJ*, **36**, 293–298.
- Richardson, J.F. and Zaki, W.N. (1954) Sedimentation and fluidization. *Transactions of the Institution of Chemical Engineers*, **32**, 35–55.

- Richardson, P., Hoare, M. and Dunnill, P. (1990) A new biochemical engineering approach to the fractional precipitation of proteins. *Biotechnology and Bioengineering*, **36**, 354–366.
- Ridgway, K. (1970) School of Pharmacy, University of London (Private communication).
- Ristic, R.I., Sherwood, J.N. and Shripathi, T. (1991) The role of dislocations and mechanical deformation in growth rate dispersion in potash alum crystals. In *Advances in Industrial Crystallization* (Symposium proceedings), J. Garside, R.J. Davey and A.G. Jones (eds.), Butterworth-Heinemann, Oxford, 77–91.
- Roberts, A.G. and Shah, K.D. (1975) The large scale application of prilling. *The Chemical Engineer*, 748–750.
- Robinson, J.N. and Roberts, J.E. (1957) A mathematical study of crystal growth in a cascade of agitators. *Canadian Journal of Chemical Engineering*, **35**, 105–112.
- Robinson, R.A. and Stokes, R.H. (1970) *Electrolyte Solutions*, 2nd edn., Butterworths, London.
- Rohani, S. and Bourne, J.R. (1990) A simplified approach to the operation of a batch crystallizer. *Canadian Journal of Chemical Engineering*, **68**, 799–806.
- Rojkowski, Z. (1977) Crystal size distribution from cascade of mixed tanks. *Kristall und Technik*, **12**, 1129–1138.
- Rojkowski, Z. (1978) Two parameter kinetic equation of size dependent crystal growth. *Kristall und Technik*, **13**, 1277–1284.
- Roques, H. and Girou, A. (1974) Kinetics of the formation conditions of carbonate tartars. *Water Research*, **8**, 907–920.
- Rosenberg, H.M. (1978) *The Solid State*, Clarendon Press, Oxford.
- Rossiter, A.P. and Douglas, J.M. (1986) Design and optimization of solids processes. *Chemical Engineering Research and Design*, **64**, Part 1: A hierarchical decision procedure for process synthesis of solids system, 175–183. Part 2: Optimization of crystallizer, centrifuge and dryer systems, 184–190. Part 3: Optimization of a crystalline salt plant using a novel procedure, 191–196.
- Rousseau, R.W. and O'Dell, F.P. (1980) Separation of solutes by selective nucleation. *Industrial and Engineering Chemistry Process Design and Development*, **19**, 603–608.
- Rousseau, R.W., Li, K.K. and McCabe, W.L. (1976) The influence of seed crystal size on nucleation rates. *AICHE Symposium Series No. 153*, **72**, 48–52.
- Rowe, P.N. and Claxton, K.T. (1965) Heat and mass transfer from a single sphere to fluid flowing through an array. *Transactions of the Institution of Chemical Engineers*, **43**, 321–331.
- RSC/CEC (1986) *Organic-Chlorine Solvents: Health Risks*, Royal Society of Chemistry, London.
- RSC/CEC (1988) *Solvents in Common Use: Health Risks*, Royal Society of Chemistry, London.
- Rubin, B. (1969) Growth of single crystals by controlled diffusion in silica gel. *AICHEJ*, **15**, 206–208.
- Rumford, F. and Bain, J. (1960) The controlled crystallization of sodium chloride. *Transactions of the Institution of Chemical Engineers*, **38**, 10–20.
- Ruskam, R.P. (1978) Prilling versus granulation for nitrogen fertilizer production. *Chemical Engineering*, 7 June, 114–118.
- Rusli, I.T., Schrader, G.L. and Larson, M.A. (1989) Raman spectroscopic study of NaNO₃ clustering in supersaturated solutions. *Journal of Crystal Growth*, **97**, 345–351.
- Rutner, E., Goldfinger, P. and Hirth, J.P. (eds.) (1964) *Condensation and Evaporation of Solids*, Gordon and Breach, New York.

- Rychlý, R. and Nývlt, J. (1974) Measuring and calculating heats of crystallization, *Kristall und Technik*, **9**, 799–810.
- Saeman, W.C. (1956) Crystal size distribution in mixed suspensions. *AICHEJ*, **2**, 107–112.
- Saeman, W.C. (1961) Crystallization equipment design. *Industrial and Engineering Chemistry*, **8**, 612–622.
- Saeman, W.C., McCamy, I.W. and Houston, E.C. (1952) Production of ammonium nitrate by continuous vacuum crystallization. *Industrial and Engineering Chemistry*, **44**, 1912–1915.
- Saito, N., Yokota, M., Sato, A. and Kubota, N. (1998) Liquid inclusion formation in a NaCl crystal triggered by adhesion of small crystals. *Kagaku Kogaku Ronbunshu*, **24**, 486–490.
- Saito, N., Yokota, M., Sato, A. and Kubota, N. (1999) Growth enhancement and liquid inclusion formation by mechanical contacts on a NaCl crystal. *AICHEJ*, **45**, 1153–1156.
- Sako, T., Satu, M. and Yamane, S. (1990) Purification of polycyclic aromatic compounds using retrograde crystallization in supercritical CO₂. *Journal of Chemical Engineering Japan*, **23**, 770–772.
- Samant, R.N. and Chandalla, S.B. (1985) Separation of racemic mixtures: optical resolution of DL-2-amino-1-butanol. *Industrial and Engineering Chemistry Process Design and Development*, **24**, 426–429.
- Samoilov, O.Y. (1965) *Structure of Aqueous Electrolyte Solutions and the Hydration of Ions*, Consultants Bureau, New York.
- Santhanam, C.J. (1966) Adductive crystallization processes. *Chemical Engineering*, **73**, 6 June, 165–170.
- Sarig, S. and Mullin, J.W. (1980) The size reduction of crystals in slurries by the use of habit modifiers. *Industrial and Engineering Chemistry Process Design and Development*, **19**, 490–494.
- Sarig, S. and Mullin, J.W. (1982) Effect of trace impurities on calcium sulphate (gypsum) precipitation. *Journal of Chemical Technology and Biotechnology*, **32**, 525–531.
- Sarig, S., Glasner, A. and Epstein, J.A. (1975) Crystal habit modifiers: the relationship between the structure of the additive and the crystal lattice. *Journal of Crystal Growth*, **28**, 295–299.
- Sato, K. (1988) Observations of spatial correlation between growth spirals and inclusions in stearic acid crystals grown from solution. *Japanese Journal of Applied Physics*, **19**, 1257–1264 and 1829–1836.
- Sato, K. and Boistelle, R. (1984) Stability and occurrence of polymorphic modifications of stearic acid in polar and nonpolar solutions. *Journal of Crystal Growth*, **66**, 441–450.
- Sato, K., Suzuki, K. and Okada, M. (1985) Solvent effects on kinetics of solution-mediated transition of stearic acid polymorphs. *Journal of Crystal Growth*, **72**, 699–704.
- Savitt, S.A. and Othmer, D.F. (1952) Separation of m- and p-cresols from their mixtures. *Industrial and Engineering Chemistry*, **44**, 2428–2431.
- Sax, N.I. (1992) *Dangerous Properties of Industrial Materials*, R.J. Lewis (ed.), 8th edn., 3 vols., Van Nostrand-Reinhold, New York.
- Scheffler, P. and Henning, R. (1979) Design of spray towers for the granulation of melts (in German). *Chemische Technik*, **31**, 610–614.
- Schierholz, P.M. and Stevens, J.D. (1975) Determination of the kinetics of precipitation in a dilute system. *AICHE Symposium Series No. 151*, **71**, 248–256.
- Schildknecht, H. (1966) *Zone Melting*, Academic Press, London.
- Scholle, S. and Brunclíková, Z. (1968) *Chemický Průmysl*, **18**, 533–538 (in Czech).

- Scholle, S. and Szmigielská, M. (1965) *Chemický Průmysl*, **15**, 520–534 and 557–559 (in Czech).
- Schott, H. (1961) A mathematical extrapolation for the method of wet residues. *Journal of Chemical Engineering Data*, **6**, 324–325.
- Schreinemakers, F.A.H. (1893) Graphische Ableitung aus den Lösung-Isothermen eines Dopplesalz und seiner Komponenten. *Zeitschrift für Physikalische Chemie*, **11**, 75–109.
- Schweizer, P. von, Corelli, B. and Widmer, F. (1975) Dimensionierung eines Prillturmes. *Separatabdruck aus Chimia*, **29**, 78–84.
- Schwenk, W. and Raouzeos, G. (1995) Sublimation: a non-fluid thermal separation process. *Chemical Technology Europe*, **2**, (2), 14–17.
- Schwenker, R.F. and Garn, P.D., eds. (1969) *Thermal Analysis* (2 vols.), Academic Press, New York.
- Scrutton, A. (1978) Laboratory study of the crystallization of sodium chloride from brine. *Proceedings of the 5th International Symposium on Salt*, Hamburg, Northern Ohio Geological Society, Cleveland, 383–395.
- Sears, G.W. (1958) The effect of poisons on crystal growth. In Doremus, Roberts and Turnbull (1958), 441–445.
- Seavoy, G.E. and Caldwell, H.B. (1940) Vacuum and mechanical crystallizers. *Industrial and Engineering Chemistry*, **32**, 627–636.
- Secor, R.M. (1963) Resolution of optical isomers. *Chemical Reviews*, **63**, 297–309.
- Seidell, A. (1958) *Solubilities of Inorganic and Metalorganic Compounds*, 4th edn., W.F. Linke (ed.), Vol. 1, Van Nostrand, New York, Vol. 2, American Chemical Society, Washington.
- Seth, K.K. and Stahel, E.P. (1969) Heat transfer from helical coils immersed in agitated vessels. *Industrial Engineering Chemistry*, **61** (6), 39–49.
- Shah, B.C., McCabe, W.L. and Rouseau, R.W. (1973) Polyethylene versus stainless steel impellers for crystallization processes. *AIChEJ*, **19**, 194.
- Shah, J.S. (1980) Zone refining and its application. In *Crystal Growth*, 2nd edn., B.R. Pamplin (ed.), Pergamon, Oxford, 301–351.
- Shakova, N.A., Polyakov, N.N., Mikhailov, V.V. and Tikhonov, I.D. (1973) Investigation of the granulation of ammonium nitrate in a fluidized bed under industrial conditions. *International Chemical Engineering*, **13**, 658–661.
- Shamlou, P.A., Jones, A.G. and Djamarani, K. (1990) Hydrodynamics of secondary nucleation in suspension crystallization. *Chemical Engineering Science*, **45**, 1405–1416.
- Sharratt, P.N. (1996) Crystallization: meeting the environmental challenge. *Chemical Engineering Research and Design*, **74**, 732–738.
- Shaviv, F. and Letan, R. (1979) Effect of operating conditions on crystallization by cooling. *AIChE Symposium Series, No. 189*, **75**, 186–189.
- Shearon, W.H. and Dunwoody, W.B. (1953) Ammonium nitrate. *Industrial and Engineering Chemistry*, **45**, 496–504.
- Shekunov, B.Yu., Hanna, M. and York, P. (1999) Crystallization process in turbulent supercritical flows. *Journal of Crystal Growth*, **198/199**, 1345–1351.
- Sheldon, R.A. (ed.) (1993) *Chirotechnology*, Marcel Dekker, New York.
- Shepherd, T.J., Rankin, A.H. and Alderton, D.H.M. (1985) *A Practical Guide to Fluid Inclusion Studies*, Blackie, Glasgow.
- Sherwin, M.B., Shinnar, R. and Katz, S. (1967) Dynamic behaviour of the well-mixed isothermal crystallizer. *AIChEJ*, **13**, 1141–1154.
- Sherwood, P. (1965) Separating aromatic hydrocarbons by clathration. *British Chemical Engineering*, **10**, 382–385.

- Sherwood, T.K. and Johannes, C. (1962) The maximum rate of sublimation of solids. *AIChEJ*, **8**, 590–593.
- Shirley, A.R., Nunelly, L.M. and Cartney, F.T. (1982) Melt granulation of urea by the falling-curtain process. *Industrial and Engineering Chemistry Product Research and Development*, **21**, 617–620.
- Shock, R.A.W. (1983) Encrustation of crystallizers. *Journal of Separation Process Technology*, **4**, 1–13.
- Short, M.A. (1957) Methods of growing crystals. *The Industrial Chemist*, **33**, 3.
- Sikdar, S.K., Ore, F. and Moore, J.H. (1980) Crystallization of calcium sulphate hemihydrates in reagent-grade phosphoric acid. *AICHE Symposium Series, No. 193*, **76**, 82–89.
- Skelland, A.H.P. (1958) Correlatin of scraped-film heat transfer in the Votator. *Chemical Engineering Science*, **7**, 166–175.
- Skold-Jorgensen, S., Rasmussen, P. and Fredenslund, A. (1982) On the concentration dependence of the UNIQUAC/UNIFAC models. *Chemical Engineering Science*, **37**, 99–111.
- Skřivánek, J., Žáček, S., Hostomský, J. and Vacek, V. (1976) Recrystallization in suspensions. In *Industrial Crystallization* (6th Symposium, Usti nad Labem), J.W. Mullin (ed.), Plenum Press, New York, 173–185.
- Sloan, E.D. (1997) *Clathrate Hydrates of Natural Gases*, Marcel Dekker, New York.
- Sloan, G.J. and McGhie, A.R. (1988) Techniques of melt crystallization. In *Techniques of Chemistry*, Vol. 19, A. Weissberger and W. Saunders (eds.), Wiley, New York.
- Smith, P.G. and Nienow, A.W. (1983) Particle growth mechanisms in fluidized bed granulation. *Chemical Engineering Science*, **38**, 1223–1240.
- Smoluchowski, M. von (1918) Versuch einer mathematischen Theorie der Koagulations kinetic kolloider Lösungen. *Zeitschrift für Physikalische Chemie*, **92**, 129–168.
- Smythe, B.M. (1967) Sucrose crystal growth. *Australian Journal of Chemistry*, **20**, 1087, 1097, 1115.
- Sobczak, E. (1990) A simple method of determination of mass transfer coefficients and surface reaction constants for crystal growth. *Chemical Engineering Science*, **45**, 561–564.
- Société Proabd (1959) Process and apparatus for refining crude naphthalene. British Patent 837295 [see also British Patent 899799; 1961 (benzene)].
- Söhnel, O. (1983) Metastable zone of solutions. *Chemical Engineering Research and Design*, **61**, 186–190.
- Söhnel, O. and Garside, J. (1992) *Precipitation: Basic Principles and Industrial Applications*, Butterworth-Heinemann, Oxford.
- Söhnel, O. and Maraček, J. (1978) Precipitation of magnesium hydroxide. *Kristall und Technik*, **13**, 253–262.
- Söhnel, O. and Mullin, J.W. (1978a) Expressions of supersaturation for systems containing hydrates, partially dissociated electrolytes and mixtures of electrolytes. *Chemical Engineering Science*, **33**, 1537–1538.
- Söhnel, O. and Mullin, J.W. (1978b) A method for the determination of precipitation induction periods. *Journal of Crystal Growth*, **44**, 377–382.
- Söhnel, O. and Mullin, J.W. (1982) Precipitation of calcium carbonate. *Journal of Crystal Growth*, **60**, 239–250.
- Söhnel, O. and Mullin, J.W. (1987) Influence of mixing on batch precipitation. *Crystal Research and Technology*, **22**, 1235–1240.
- Söhnel, O. and Mullin, J.W. (1988a) Interpretation of crystallization induction periods. *Journal of Colloid and Interface Science*, **123**, 43–50.

- Söhnel, O. and Mullin, J.W. (1988b) The role of time in metastable zone width determinations. *Chemical Engineering Research and Design*, **66**, 537–540.
- Söhnel, O. and Mullin, J.W. (1988c) Some comments on the influence of a magnetic field on crystalline scale formation. *Chemistry and Industry*, 6 June, 356–358.
- Söhnel, O. and Mullin, J.W. (1991) Agglomeration in batch precipitated suspensions. *AICHE Symposium Series*, No. 284, **87**, 182–190.
- Söhnel, O. and Novotný, P. (1985) *Densities of Aqueous Solutions of Inorganic Substances*, Academia, Prague.
- Söhnel, O., Chianese, A. and Jones, A.G. (1991) Theoretical approaches to design of precipitation systems: the present state of the art. *Chemical Engineering Communications*, **106**, 151–175.
- Söhnel, O., Mullin, J.W. and Jones, A.G. (1988) Crystallization and agglomeration in the batch precipitation of strontium molybdate. *Industrial and Engineering Chemistry Research*, **27**, 1721–1728.
- Sonnenfeld, P. (1984) *Brines and Evaporites*, Academic Press, New York.
- Stahly, G.P. and Byrn, S.R. (1999). Solid state structure of chiral organic pharmaceuticals. In Myerson, A.S. (ed.) (1999), pp. 313–345.
- Stávek, J., Šípek, M., Hirasawa, I. and Toyokura, K. (1992) Controlled double-jet precipitation of sparingly soluble salts. *Chemical Materials*, **4**, 545–555.
- Stephen, H. and Stephen, T. (1963) *Solubilities of Inorganic and Organic Compounds* (5 vols.), Pergamon, London.
- Šterbáček, Z. and Tausk, P. (1965) *Mixing in the Chemical Industry*, Pergamon Press, Oxford.
- Stevenson, D.G. (1964) Theory of the design and operation of continuous precipitators, *Transactions of the Institution of Chemical Engineers*, **42**, 316–322.
- Stokes, R.H. and Mills, R. (1965) *Viscosity of Electrolytes*, Pergamon, Oxford.
- Strickland-Constable, R.F. (1968) *Kinetics and Mechanism of Crystallization*, Academic Press, London.
- Strickland-Constable, R.F. (1979) Mechanism of production and growth inhibition of collision crystallites. *Journal of the Chemical Society Faraday Transactions*, **I**, **75**, 921–924.
- Sugimoto, T. (1978) Kinetics of reaction-controlled Ostwald ripening of precipitates in the steady state. *Journal of Colloid and Interface Science*, **63**, 369–377.
- Sun, Y-C. (1971) Water: key to new crystallization process for purifying organics. *Chemical Engineering*, 12 July, 87–90.
- Sung, C.Y., Estrin, J. and Youngquist, G.R. (1973) Secondary nucleation of MgSO₄ by fluid shear. *AICHEJ*, **19**, 957–962.
- Sunier, A.A. (1929) A critical consideration of some schemes of fractionalism. *Journal of Physical Chemistry*, **33**, 577–589.
- Suzuki, M., Ogaki, T. and Sato, K. (1985) Crystallization and transformation mechanism of α, β and γ-polymorphs of ultra-pure oleic acid. *Journal of the American Oil and Color Chemists' Society*, **62**, 1600–1604.
- Svalov, G.V. (1970) Estimating drum crystallizers. *British Chemical Engineering*, **15**, 1153.
- Svanoe, H. (1940) Krystal classifying crystallizer. *Industrial and Engineering Chemistry*, **32**, 636–639.
- Svarovsky, L. (1990) *Solid-Liquid Separation*, 3rd edn., Butterworths, London.
- Tai, C.Y. and Cheng, C.-S. (1997) Crystal morphology of naphthalene in processes involving supercritical CO₂. *Chemical Engineering Research and Design*, **75**, 228–232.
- Takegami, K. (1993) The 4C melt crystallization with adiabatic cooling. In *Industrial Crystallization 93* (12th Symposium, Warsaw), Rojkowski, Z.H. (ed.), Supplementary, pp. 1–5.

- Takegami, K., Nakamaru, N. and Morita, M. (1984) Industrial molten fractional crystallization. In *Industrial Crystallization 84* (9th Symposium, The Hague), S.J. Jančić and E.J. de Jong (eds.), Elsevier, Amsterdam, 143–146.
- Tamman, G. (1925) *States of Aggregation* (Translated by R.F. Mehl), van Nostrand, New York.
- Tamme, R. (1987) Low-temperature energy storage. *CHEMTECH*, August, 496–500.
- Tanaka, T. (1978) Evaluating the caking strength of powders. *Industrial and Engineering Chemistry Product Research and Development*, **17**, 241–246.
- Tare, J.P. and Chivate, M.R. (1976a) Selection of a solvent for adductive crystallization. *Chemical Engineering Science*, **31**, 893–899.
- Tare, J.P. and Chivate, M.R. (1976b) Separation of close boiling isomers by addutive and extractive crystallization. *AICHE Symposium Series, No. 153*, **72**, 95–99.
- Tavare, N.S. (1991) Batch crystallizers. *Reviews in Chemical Engineering*, **7**, 213–353.
- Tavare, N.S. (1995) *Industrial Crystallization: process simulation, analysis and design*, Plenum Press, New York.
- Tavare, N.S. and Chivate, M.R. (1978) CSD analysis from a single stage and two stage cascade of MSCPR crystallizers. *Canadian Journal of Chemical Engineering*, **56**, 758–761.
- Tavare, N.S. and Garside, J. (1990) Simulation of reactive precipitation in a semi-batch crystallizer. *Transactions of the Institution of Chemical Engineers*, **68**, 115–122.
- Tavare, N.S., Garside, J. and Chivate, M.R. (1980) Analysis of batch crystallizers. *Industrial and Engineering Chemistry Process Design and Development*, **19**, 653–665.
- Teeple, J.E. (1929) *The Industrial Development of Searles Lake Brines*, Chemical Catalog Co, New York.
- Tempkin, D.E. (1964) *Crystallization Processes*, Consultants Bureau, New York, p. 15.
- Tezak, B. (1966) Coulombic and stereochemical factors of colloid stability of precipitating systems. *Discussions of the Faraday Society*, No. 42, 175–186.
- Thompson, A.R. and Molstad, M.C. (1945) Solubility and density isotherms for potassium and ammonium nitrates in isopropanol solutions. *Industrial and Engineering Chemistry*, **37**, 1244–1248.
- Thomson, W. (1871) On the equilibrium of a vapour at a curved surface of a liquid. *Philosophical Magazine*, **42**, 448–452 (First reported in *Proceedings of the Royal Society of Edinburgh*, **7** (1869/70), 63–68).
- Thorp, D. (1946) Solubility as a criterion of purity. *Journal of the Society of Chemical Industry*, **65**, 414–419.
- Timms, R. (1991) Crystallization of fats. *Chemistry and Industry*, 20 May, 342–345.
- Ting, H.H. and McCabe, W.L. (1934) Supersaturation and crystal formation in seeded solutions of MgSO₄. *Industrial Engineering Chemistry*, **26**, 1201–1207.
- Tipson, R.S. (1956) Crystallization and recrystallization. In *Techniques of Organic Chemistry*, Vol. III, Part 1. A. Weissberger (ed.), Interscience, New York.
- Tomi, D.T. and Bagster, D.F. (1978) The behaviour of aggregates in stirred vessels. *Transactions of the Institution of Chemical Engineers*, **56**, 1–18.
- Torgesen, J.L. and Horton, A.T. (1963) Electrolytic conductance of ammonium dihydrogen phosphate solutions in the saturated region. *Journal of Physical Chemistry*, **67**, 376–381.
- Torgesen, J.L., Horton, A.T. and Saylor, C.P. (1963) Equipment for single growth from aqueous solution. *Journal of Research, National Bureau of Standards*, Washington, **67C**, 25–32.

- Toussaint, A.G. and Donders, A.J.M. (1974) The mixing criterion in crystallization by cooling. *Chemical Engineering Science*, **29**, 237–245.
- Toussaint, A.G. and Fortuin, J.M.H. (1975) Design criteria for DTB vacuum crystallizers. In *Industrial Crystallization* (6th Symposium, Usti nad Labem), J.W. Mullin (ed.), Plenum Press, New York, 311–318.
- Toyokura, K. et al. (1976a) Growth of naphthalene from molten naphthalene-benzoic acid crystallized on a cooled cylindrical surface. *AICHE Symposium Series No. 153*, **72**, 87–93.
- Toyokura, K. et al. (1976b) The operation of a NaOH 3.5 H₂O crystallizer by direct contact cooling. In *Industrial Crystallization* (6th Symposium, Usti nad Labem), J.W. Mullin (ed.), Plenum Press, London, 421–429.
- Toyokura, K. et al. (1984) Design of fluidized bed crystallizers. In *Industrial Crystallization 84* (9th Symposium, The Hague), S.J. Jančić and E.J. de Jong (eds.), North-Holland, Amsterdam, 463–466 and 467–470.
- Toyokura, K., Mogi, J. and Hirasawa, I. (1977) Secondary nucleation of K-alum by minimum size seeds in a stirred vessel. *Journal of Chemical Engineering of Japan*, **10**, 35–39.
- Toyokura, K., Yamazoe, K. and Mogi, J. (1976) Secondary nucleation rate of alum in a fluidized bed. *AICHE Symposium Series, No. 153*, **72**, 53–60.
- Tsuge, H., Yoshizawa, S. and Tsuzuki, M. (1996) Reactive crystallization of calcium phosphate. *Chemical Engineering Research and Design*, **74**, 797–802.
- Turnbull, D. (1950) Kinetics of heterogeneous nucleation. *Journal of Chemical Physics*, **18**, 198–203.
- Turnbull, D. (1953) Kinetics of precipitation of BaSO₄. *Acta Metallurgica*, **1**, 17.
- Turnbull, D. and Fisher, J.C. (1949) Rate of nucleation in condensed systems. *Journal of Chemical Physics*, **17**, 71–73.
- Tyner, M. (1955) Enthalpy-concentration diagrams of binary aqueous mixtures of hydrazine, sodium carbonate and glycerol. *AICheJ*, **1**, 87–92.
- Tyrrell, H.J.V. (1961) *Diffusion and Heat Flow in Liquids*, Butterworths, London.
- Ubbelohde, A.R. (1965) *Melting and Crystal Structure*, Clarendon, Oxford.
- Ueda, H. and Takashima, Y. (1977) Desublimation of two-component systems. *Journal of Chemical Engineering, Japan*, **10**, 6–12.
- Uemaki, O. and Mathur, K.B. (1976) Granulation of ammonium sulphate fertilizer in a spouted bed. *Industrial and Engineering Chemistry Process Design and Development*, **15**, 504–508.
- Uhl, V.W. and Gray, J.B. (1986) *Mixing: Theory and Practice* (3 vols.), Academic Press, New York.
- Ulrich, J. (1989) Growth rate dispersion – a review. *Crystal Research and Technology*, **24**, 249–257.
- Ulrich, J. (1992) Melt Crystallization. In Myerson, A.S. (ed.) (1992), pp. 151–164.
- Ulrich, J. and Kruse, M. (1989) Ultra-microhardness measurements of non-metallic crystals and an attempt for their calculation. *Crystal Research and Technology*, **24**, 181–186.
- Ulrich, J. and Offermann, H. (1985) On the difference in growth rates of fragmented and non-fragmented crystals during industrial crystallization. *Journal of Crystal Growth*, **73**, 397–399.
- Valeton, J.J.P. (1924) Wachstum und Auflösung der Kristalle. *Zeitschrift für Kristallographie*, **59**, 483.
- Van Bueren, H.G. (1960) *Imperfections in Crystals*, Interscience, New York.
- Van den Berg, P.J. and Hallie, G. (1960) New developments in granulation techniques. *Proceedings of the Fertilizer Society*.

- Van der Eerden, J.P., Bennema, P. and Cherepanova, T.A. (1978) Survey of Monte Carlo simulations of crystal surfaces and crystal growth. *Progress in Crystal Growth and Characterization*, **1**, 219–264.
- van der Voort, E. (1991) The morphology of succinic acid crystals: the role of solvent interaction. *Journal of Crystal Growth*, **110**, 662–68.
- Van Hook, A. (1961) *Crystallization: Theory and Practice*, Reinhold, New York.
- Van Rosmalen, G.M. and Bennema, P. (1990) Characterization of additive performance on crystallization: habit modification. *Journal of Crystal Growth*, **99**, 1053–1060.
- Van Rosmalen, G.M., Daudsey, R.J. and Marchée, W.G.J. (1981) An analysis of growth experiments of gypsum crystals in suspension. *Journal of Crystal Growth*, **52**, 801–811.
- Van Rosmalen, G.M., Marchée, W.G.J. and Bennema, P. (1976) A comparison of gypsum crystals grown in silica gel and agar in the presence of additives. *Journal of Crystal Growth*, **35**, 169–176.
- Van Rosmalen, G.M., Witkamp, G.J. and de Vreugd, C.H. (1989) Additive and impurity effects in crystallization processes. In *Industrial Crystallization 87* (10th Symposium, Bechyně), J. Nývlt and S. Žáček (eds.), Elsevier, Amsterdam, 15–20.
- van't Hoff, J.H. (1903) *Physical Chemistry in the Service of Science*, University Press, Chicago, p. 116.
- van't Land, C.M. and Wienk, B.G. (1976) Control of particle size in industrial NaCl-crystallization. In *Industrial Crystallization* (6th Symposium, Usti nad Labem), J.W. Mullin (ed.), Plenum Press, New York, 51–60.
- Vega, R. and Funk, E.W. (1974) Solid-liquid equilibrium in concentrated aqueous salt solution: systems with a common ion. *Desalination*, **15**, 225–241.
- Verma, A.R. (1953) *Crystal Growth and Dislocations*, Butterworths, London.
- Verma, A.R. and Krishna, P. (1966) *Polymorphism and Polytypism in Crystals*, Wiley, New York.
- Neverká, F. and Nývlt, J. (1979) Growth of scale on a cooling surface during the stirring of a crystal suspension. *Chemiký Průmysl*, **29**, 123–127, 580–582, 623–626.
- Neverká, V., Söhnel, O., Bennema, P. and Garside, J. (1991) Concentration gradients in supersaturated solutions: a thermodynamic analysis. *AICHEJ*, **37**, 490–498.
- Villermaux, J. (1988) The role of energy dissipation in contacting and mixing devices. *Chemical Engineering and Technology*, **11**, 276–287.
- Vitovec, J., Smolík, J. and Kugler, J. (1978) Separation of sublimable compounds by partial crystallization from their vapour mixtures. *Collections of the Czechoslovak Chemical Communications*, **43**, 396–400.
- Vold, R.D. and Vold, M.J. (1949) Determination of solubility. In *Techniques of Organic Chemistry*, A. Weissberger (ed.), Vol. 7, Part I. Physical Methods. Interscience, New York.
- Volmer, M. (1939) *Kinetic der Phasenbildung*, Steinkopff, Leipzig.
- Volmer, M. and Schultz, W. (1931) Kondensation an Kristallen. *Zeitschrift für Physikalische Chemie*, **156**, 1–22.
- Vonnegut, B. (1948) Variation with temperature of the nucleation rate of supercooled tin and water drops. *Journal of Colloid Science*, **3**, 563–569.
- Wachi, S. and Jones, A.G. (1991) Mass transfer with chemical reaction and precipitation. *Chemical Engineering Science*, **46**, 1027–1033.
- Wachi, S. and Jones, A.G. (1995) Aspects of gas-liquid reactors for precipitate particle formation. *Reviews in Chemical Engineering*, **11**, 1–51.
- Wallach, D.L. (1997) Ammonium sulphate as a by-product in flue gas desulphurization. *ACS Symposium Series No. 668*, 244–254.

- Walton, A.G. (1967) *The Formation and Properties of Precipitates*, Interscience, New York.
- Wanklyn, B.M. (1983) The present status of flux growth. *Journal of Crystal Growth*, **65**, 533–540.
- Wei, H. and Garside, J. (1997) Application of CFD modelling to precipitation systems. *Chemical Engineering Science*, **75**, 219–227.
- Weimarn, P.P. von (1926) The precipitation laws. *Chemical Reviews*, **2**, 217–242.
- Weingaertner, D.A., Lynn, S. and Hanson, D.N. (1991) Extractive crystallization of salts from concentrated aqueous solution. *Industrial and Engineering Chemistry Research*, **30**, 490–501.
- Wells, A.F. (1946) Crystal growth. *Annual Reports on the Progress of Chemistry*. The Chemical Society, London, **43**, 62–87.
- Wells, A.F. (1962) *Structural Inorganic Chemistry*, 3rd edn., Clarendon Press, Oxford.
- Wey, J.S. and Estrin, J. (1972) On the growth of secondary nuclei. *AICHE Symposium Series*, No. 121, **68**, 74–87.
- Wey, J.S. and Terwilliger, J.P. (1976) Design considerations for a multistage cascade crystallizer. *Industrial and Engineering Chemistry Process Design and Development*, **15**, 467–469.
- Wey, J.S., Terwilliger, J.P. and Gingello, A.D. (1980) Analysis of AgBr precipitation in a continuous suspension crystallizer. *AICHE Symposium Series*, No. 193, **76**, 34–42.
- Whetstone, J. (1949a) Anti-caking treatment for ammonium nitrate. *The Industrial Chemist*, **25**, 401–403.
- Whetstone, J. (1949b) The effect of crystal habit modification on the setting of inorganic oxy salts. *Discussions of the Faraday Society*, **5**, 261–266.
- White, E.A.D. (1964) Crystal growth techniques. *GEC Journal*, **31**, (1), 43.
- White, E.T. and Wright, P.G. (1971) Magnitude of size dispersion effects in crystallization. *Chemical Engineering Progress Symposium Series No. 110*, **67**, 81–87.
- White, M.L. and Frost, A.A. (1959) The rate of nucleation of supersaturated KNO₃ solutions. *Journal of Colloid Science*, **14**, 247–251.
- Whynes, A.L. and Dee, T.P. (1957) The caking of granular fertilizers: a laboratory investigation. *Journal of the Science of Food and Agriculture*, **8**, 577–591.
- Wibowo, C. and Ng, K.M. (2000) Unified approach for synthesizing crystallization-based separation processes. *AICHEJ*, **46**, 1400–1421.
- Wiechers, H.N.S., Sturrock, P. and Marias, G.R. (1975) Calcium carbonate crystallization kinetics. *Water Research*, **9**, 835–838.
- Wilcox, W.R. (1968) Removing inclusions from crystals by gradient techniques. *Industrial and Engineering Chemistry*, **60**, 12–23.
- Wilke, C.R. and Chang, P. (1955) Correlation of diffusion coefficients in dilute solutions. *American Institute of Chemical Engineers Journal*, **1**, 264–270.
- Willard, H.W., Merritt, L.M., Dean, J.A. and Settle, F.A. (1988) *Instrumental Methods of Analysis*, 7th edn., Wadsworth, Belmont.
- Williams, A.J. (1981) Explosives Research Establishment, Waltham Abbey. (Private communication.)
- Winn, D. and Doherty, M.F. (2000) Modelling crystal shapes of organic materials grown from solution. *AICHEJ*, **46**, 1348–1364.
- Wintermantel, K. and Wellinghoff, G. (1994) Melt crystallization: theoretical premises and technical limitations. *International Chemical Engineering*, **34**, 17–27.
- Wintermantel, K., Holzknecht, A. and Thoma, P. (1987) Density of sublimed layers. *Chemical Engineering and Technology*, **10**, 205–210.
- Winzer, A. and Emons, H-H. (1976) Investigations on the Ostwald ripening of well soluble salts by means of radioactive isotopes. In *Industrial Crystallization* (6th

- Symposium, Usti nad Labem), J.W. Mullin (ed.), Plenum Press, New York, 163–171.
- Wise, W.S. and Nicholson, E.B. (1955) Solubilities and heats of crystallization of sucrose etc. in aqueous solution. *Journal of the Chemical Society*, 2714–2716.
- Wisniak, J. and Herskowitz, M. (1984) *Solubility of Gases and Solids – A Literature Source Book*, Elsevier, Amsterdam.
- Wöhlk, W. (1982) Industrial crystallization under the aspect of energy economic operation. In *Industrial Crystallization 81* (8th Symposium, Budapest), S.J. Jančić and E.J. de Jong (eds.), North-Holland, Amsterdam, 227–235.
- Wöhlk, W. and Hofmann, G. (1980) Verkrustungsprobleme – verhindernsmöglichkeiten. *Chemie Ingenieur Technik*, **52**, 898–900.
- Wojciechowski, B. (1981) Structural phase transitions in saturated aqueous solutions. *Journal of Crystal Growth*, **52**, 824–828.
- Woodward, G.D. and McCrone, W.C. (1975) Unusual crystallization behaviour. *Journal of Applied Crystallography*, **8**, 342.
- Wright, J.D. (1987) *Molecular Crystals*, University Press, Cambridge.
- Wu, F.H. (1984) Drum separator design: a new approach. *Chemical Engineering*, 2 April, 74–80.
- Wyckoff, R.W.G. (1963–8) *Crystal Structures* (5 vols.), 2nd edn., Interscience, New York.
- Yamamoto, T. (1939) The influence of cations in aqueous solution on the growth of crystals. *Scientific Papers of the Institute of Physical Chemistry Research Japan*, **35**, 228–289.
- Yokota, M., Takahashi, Y., Sato, A., Kubota, N., Masumi, F. and Takeuchi, H. (1998) Purity drop in optical resolution of DL-methionine by the diastereomer method. *Chemical Engineering Science*, **53**, 1473–1497.
- Young, S.W. (1911) Mechanical stimulus to crystallization in supercooled liquids. *Journal of the American Chemical Society*, **33**, 148–162.
- Žáček, S., Nývlt, J., Garside, J. and Nienow, A.W. (1982) A stirred tank for continuous crystallization studies. *Chemical Engineering Journal*, **23**, 111–113.
- Zauner, R. and Jones, A.G. (2000a) Determination of nucleation, growth, agglomeration and disruption kinetics from experimental data: the calcium oxalate system. *Chemical Engineering Science*, **55**, 4219–4232.
- Zauner, R. and Jones, A.G. (2000b) Scale-up of continuous and semi-batch precipitation processes. *Industrial and Engineering Chemistry Research*, **39**, 2392–2403.
- Zernike, J. (1938) *Phase Equilibria*, Elsevier, Amsterdam.
- Zettlemoyer, A.C. (ed.) (1969) *Nucleation*, Dekker, New York.
- Zhang, J. and Nancollas, G.H. (1991) Dissolution kinetics of calcium phosphates involved in biomineralization. In *Advances in Industrial Crystallization*, J. Garside, R.J. Davey and A.G. Jones (eds.), Butterworth-Heinemann, Oxford, 47–62.
- Zief, M. and Wilcox, W.R. (1967) *Fractional Solidification*, Marcel Dekker Interscience, New York.
- Zimmerman, H.K. (1952) The experimental determination of solubilities, *Chemical Reviews*, **51**, 25–65.
- Zumstein, R.C. and Rousseau, R.W. (1987) Utilization of industrial data in the development of a model for crystallizer simulation. *AICHE Symposium Series*, No. 253, **83**, 130–139.
- Zweitering, Th. N. (1958) Suspension of solid particles in liquids by agitators. *Chemical Engineering Science*, **8**, 244–253.

Author index

- Abbona, F., 271, 283
Abegg, C.F., 417, 418
Abrahart, E., 337
Acrivos, A., 39
Adamski, T., 190
Ajinkya, M.B., 426
Akiya, T., 376
Albertins, R., 349
Albon, N., 257
Alderton, D.H.M., 288
Alfassi, Z.B., 394
Allen, T., 66, 69, 71, 72, 75
Allen, A.T., 134
Al-Rashed, M.H., 342
Althaus, W., 336
Altria, K.D., 114
Amatvivadhana, A., 238, 255, 277, 254
Amin, A.B., 366
Ananth, R., 236
Anderson, J.F., 119
Anderson, T.F., 100, 122
Ang, H-M., 73, 211, 248, 323
Anwar, J., 214, 271
Aoyama, Y., 340
Aquilano, D., 271, 285, 288
Arkenbout, G.J., 351, 353
Armstrong, A.J., 348
Arnold, P.M., 349
Arora, S.K., 311
Asaeda, M., 283
Asai, S., 298
Aslund, B., 395
Atkinson, G., 122
Autenreith, H., 179
Authelin, J-R., 401
Azoury, R., 273
- Badger, W.L., 403
Bagster, D.F., 317
Bailey, A.E., 155, 348
Bain, J., 253
Baker, C.G.J., 336, 339
Balakrishnan, N.S., 418
Baldyga, J., 341
Bamforth, A.W., 354, 373–375, 383, 394,
 446
Banerjee, S.C., 147
Barba, D., 121
Barduhn, A.J., 398
- Barone, S.P., 131
Bartosch, K., 347, 355, 377
Baud, R.E., 341
Bavin, M., 300, 301
Becker, R., 182
Beiny, D.H.M., 99, 278
Bell, D.J., 111
Belyustin, A.V., 199, 286
Bennema, P., 134, 223, 231, 233, 271
Bennett, R.C., 387, 412, 450
Bentivoglio, M., 238
Berends, E.M., 303
Berg, W.F., 230
Berglund, K.A., 134, 254, 258
Bergougnou, M.A., 336, 339
Berkeley, Earl of, 181
Berkovitch-Yellin, Z., 274, 275
Bernstein, J., 199, 201, 280, 281, 301
Berthoud, A., 226
Betts, W.D., 349
Bilik, J., 363
Biscans, B., 401
Black, S.N., 256
Blagden, N., 284
Blasdale, W.C., 112, 123, 179
Bliznakov, G., 258, 273
Boateng, P.K., 214, 270
Boistelle, R., 256, 271, 273, 278, 283
Bolsaitis, P., 349
Bonython, C.W., 378
Bos, A.S., 402
Bose, E., 2
Botsaris, G.D., 195, 199, 206, 278, 416
Bourne, J.R., 249, 285, 341, 342, 426
Bovington, C.H., 229, 260
Bowden, F.P., 49
Bowden, S.T., 136
Brandani, V., 121
Bransom, S.H., 246, 406, 407
Bravais, A., 14, 15, 269
Brečević, Lj., 73, 322, 325
Bretherick, L., 90
Brice, J., 236
Bricknell, W.S., 313
Brienne, M-J., 298, 300
Brodie, J.A., 350
Bromley, L.A., 122
Brookes, C.A., 48
Brooks, R., 286

- Brosheer, J.C., 119
 Broul, M., 94, 123, 195, 216, 431
 Brown, J.S., 303
 Brown, N., 324
 Brown, M.E., 154
 Brown, P.M., 322
 Bruinsma, O.S.L., 303, 342, 356
 Bruncíková, Z., 146
 Bryant, H.S., 359, 366
 Bryson, A.N., 340
 Buckley, H.E., 30, 199, 216, 276
 Buckton, G., 326
 Budz, J., 273, 336
 Bujac, P.D.B., 196, 246, 248, 452
 Bunn, C.W., 30, 230, 256, 287
 Burak, N., 467
 Burton, W.K., 221
 Bushnell, J.D., 376
 Butts, D.S., 378
 Byrn, S.R., 298
- Cabrera, N., 221, 256
 Caldwell, H.B., 372, 373
 Callis, C.F., 467
 Campbell, A.N., 136
 Capes, C.E., 402
 Cardew, P.T., 214, 283
 Carless, J.E., 322
 Carman, P.C., 469
 Cartney, F.T., 357
 Cartwright, P.F.S., 333
 Casper, C., 362, 377, 399
 Catone, J.L., 339
 Cayey, N.W., 198
 Černý, J., 376
 Cerrata, M.A., 134
 Cesar, M.A.B., 179, 293
 Chakraborty, M., 202, 204, 205, 255, 277
 Chandalla, S.B., 298
 Chandler, J.L., 384, 463
 Chandrasekhar, S., 30
 Chang, P., 302
 Chang, C.T., 426
 Chang, C.J., 42, 302
 Chang, W-C., 179, 293,
 Chaty, J.C., 354
 Chen, Y.L., 467
 Cheng, C.S., 303
 Cherepanova, T.A., 231
 Chernov, A.A., 31, 197, 216, 223, 253,
 Chianese, A., 340, 426, 427, 428, 441, 463
 Chimowitz, E.H., 303
 Chivate, M.R., 340, 396, 397, 418, 426
 Chlopin, V., 293, 327
 Chou, J.Y., 467
 Chu, J.C., 263
- Chua, J.O., 206
 Ciborowski, J., 362
 Cisternas, L.A., 293
 Claxton, K.T., 263
 Clontz, N.A., 196
 Collet, A., 22, 296–300
 Clydesdale, G., 271
 Collier, A.P., 318
 Collins, A.N., 298
 Colônia, E.J., 334
 Colville, A.R., 255
 Conti, R., 196
 Cook, T.P., 42
 Cooke, E.G., 277, 278
 Corelli, B., 357
 Coulson, J.M., 146, 345
 Crosby, J., 298
 Cunningham, W.K., 394
 Currie, P., 217
- Darcy, P., 294, 326
 Das, S.N., 75, 76, 244
 Dauncy, L.A., 117
 Davey, R.J., 195, 214, 221, 233, 242, 248,
 253, 255–257, 271–278, 281–285,
 301, 401, 416,
 David, R., 341, 395
 Davies, G.A., 401
 Davies, C.W., 101, 122
 De Jong, E.J., 195, 197, 202, 416, 450
 De Vreugd, 278
 Dean, J.A., 115
 Debendetti, P.G., 303
 Dee, T.P., 467
 Deepak, C., 418
 Defay, R., 214
 Deicha, G., 288
 Demopoulos, G.P., 123
 Demyanovich, R.J., 342
 Denbigh, K.G., 285, 286, 287
 Denk, E.G., 199, 206
 Denton, W.H., 398
 Diepen, P.J., 356
 Di Cave, S., 463
 Di Giacomo, G., 121
 Dikshit, R.C., 397
 Dillon, W., 400
 Dixit, A.B., 334
 Djamarani, K., 196
 Dobbs, J.M., 303
 Dodgson, B.V., 351
 Doerner, H.A., 292, 293, 327
 Docherty, R., 271, 284,
 Doherty, M.F., 278
 Donald, M.B., 472
 Donders, A.J.M., 462

- Donnay, J.D.H., 15
 Doraiswamy, L.K., 147
 Döring, W., 182
 Douglas, J.M., 397, 467, 468
 Drbohlav, R., 402
 Dufor, L., 214
 Dühring, U., 57, 132
 Dullien, F.A.L., 44
 Duncan, A.G., 376, 460, 462, 463
 Dunitz, J.D., 199, 201, 280
 Dunnill, P., 111, 338
 Dunning, W.J., 214, 256, 406, 407
 Dunwoody, W.B., 356, 467
 Dye, S.R., 397
 Dzyuba, A.J., 287
 Eagen, J.F., 376
 Eckert, C.A., 303
 Edwards, M.F., 452
 Egan, C.J., 396
 Eggers, H.H., 361
 Eidelman, N., 273
 Einstein, A., 38, 41
 Elwell, D., 310
 Enüstün, B.V., 109
 Epstein, J.A., 274
 Epstein, M.A.F., 426
 Espitalier, F., 401
 Estrin, J., 195, 198
 Ewing, C.M., 378
 Ewing, G.W., 115
 Eyring, H., 41
 Faktor, M.M., 309, 314
 Fasoli, U., 196
 Feilchenfeld, H., 144
 Fernandez-Lozano, J.R., 335, 394
 Fiedelman, H., 450
 Fila, W., 274
 Findlay, R.A., 396
 Findlay, A., 39, 114, 119, 136
 Finkelstein, E., 378
 Fischer, O., 353
 Fisher, J.C., 187
 Fitch, B., 179, 293
 Föllner, H., 271
 Fortuin, J.M.H., 435
 Foster, A.A., 322
 Foust, A.S., 146
 Franchini-Angela, M., 271
 Franck, R., 395
 Frank, F.C., 220, 221, 223
 Frankel, N.A., 39
 Franks, F., 133
 Fredenslund, A., 122
 Freundlich, H., 108
 Frew, J.A., 426
 Fridman, S.S., 286
 Frohlich, G.H., 146
 Frost, A.A., 189
 Fugisawa, Y., 111, 256, 262
 Fugiwara, M., 198, 256
 Fukasawa, J., 111, 256
 Funk, E.W., 123
 Füredi, H., 328–330
 Füredi-Milhofer, H., 316, 322, 324
 Furter, W.F., 56
 Furukawa, H., 283
 Gaikar, V.G., 397
 Garabedian, H., 197
 Garber, H.J., 293
 Gardner, G.L., 131, 322
 Garrett, D.E., 336, 370, 394
 Garrett, I., 309, 314
 Garside, J., 73–76, 130, 134, 189, 195, 197,
 205, 228, 229, 234, 238, 244–250, 253,
 254, 261, 263, 267, 268, 274–278, 316,
 318, 340–342, 401, 416, 426, 456
 Garten, V.A., 189
 Gaska, C., 229, 244, 262, 268
 Gates, W.C., 349
 Gee, E.A., 394
 Gel'perin, N.I., 354
 Gerunda, A., 435
 Giacalone, A., 61
 Gibbs, J.W., 108, 135, 182, 216, 320
 Gibilaro, L.G., 248
 Gibson, R.E., 119
 Gill, W.N., 236
 Gill, J.S., 336
 Gillot, J., 361, 365
 Ginde, R.M., 134
 Gingello, A.D., 339
 Girling, G.W., 349
 Girou, A., 336
 Glasner, A., 274
 Glasser, D., 340
 Glastonbury, J.R., 264
 Glatz, C.E., 338
 Gmehling, J.G., 100, 122
 Gnyra, B., 324
 Goard, H.W., 348
 Goldberger, W.M., 361, 365
 Goldfinger, P., 359
 Goldman, G., 463
 Goodman, A.W., 293
 Gordon, L., 328, 332, 333
 Gray, J.B., 452
 Griffiths, H., 372, 392, 446
 Grimmett, E.S., 402
 Grisoni, P., 338

- Grønvold, F., 144
 Grootscholten, P.A.M., 71, 73, 418, 419,
 433
 Groves, G., 30
 Gupta, R.B., 122
 Guth, E., 39
 Gutoff, E.B., 337, 339
 Guy, P.D., 284
 Gyulai, Z., 195
- Haase, T., 136
 Hadziriga, P., 179
 Halasz, S., 334, 335
 Halfon, A., 337
 Halcrow, M., 256
 Hallie, G., 357
 Halstead, W.D., 111
 Hanitzsch, E., 321
 Hanna, M., 273, 303
 Hanson, D.N., 394, 397
 Harbury, L., 110
 Harnby, N., 452
 Harned, H.S., 40
 Harriott, P., 146
 Hartman, P., 269, 271
 Hartshorne, N.H., 18, 30
 Hatschek, E., 36
 Hayhurst, A.N., 266
 Haiyü, R.J., 3, 13, 16, 217
 Head, R.B., 189
 Heidemann, R.A., 122
 Heindl, R.A., 394
 Heist, J.A., 399
 Henisch, H.K., 311
 Henk, J-O., 281,
 Henning, R., 357
 Henning, S., 288
 Her, Y-S., 339
 Herington, E.F.G., 308
 Herskowitz, M., 123
 Heywood, H., 75
 Henry, J.D., 349
 Hill, S., 418
 Hilton, A.M., 401
 Hiquily, N., 288
 Hirasawa, I., 198, 342
 Hirth, J.P., 30, 359
 Hoare, M.R., 182
 Hoare, M., 111, 338
 Hofmann, G., 463
 Holden, C.A., 359, 366
 Holden, A.N., 310, 359
 Holeci, I., 400
 Holland, A.A., 401,
 Holven, A.L., 131
 Holzknecht, A., 367
- Honda, T., 287
 Honigmann, B., 283, 322
 Hooke, R., 13
 Hooks, I.J., 404
 Hoppe, A., 396
 Horn, D., 283, 322
 Horton, A.T., 48, 286, 310
 Hoskins, W.M., 292, 293, 327
 Hostomský, J., 336, 371
 Hou, T-P., 394
 Hougen, D.A., 146
 Hounslow, M.H., 318, 463
 Huang, C.J., 52
 Hughmark, G.A., 269, 420
 Humphreys-Owen, S.P.F., 287
 Hunt, J.D., 181
 Hurle, J.C.G., 309, 313, 314
- Idogaki, M., 336
 Irani, R.R., 467
 Isaac, F., 123
 Iskander, M., 418
 Ito, K., 206
 Ives, D.J.G., 133
- Jackson, K.A., 182, 233
 Jacques, J., 22, 296–300
 Jadhav, V.K., 396
 Jagannathan, R., 337
 Jager, J., 196
 Jančić, S.J., 71, 73, 202, 353, 345, 416, 418,
 419, 433
 Jánecke, E., 171, 176
 Janse, A.H., 202
 Jeremiassen, F., 374
 Johannes, C., 362
 Johnson, A.I., 52
 Johnson, R.T., 196
 Johnston, K.P., 303
 Johnstone, R.E., 449
 Jones, A.G., 196, 248, 273, 318, 319, 334,
 336, 340–343, 393, 395, 426–428,
 431, 441, 453
 Jones, A.L., 229, 260
 Jones, C.M., 254
 Jones, R.L., 122
 Jones, W.J., 110
 Jooste, R.F., 324
 Joy, E.F., 293, 328
- Kabascı, S., 336
 Kahlweit, M., 229, 321, 322
 Kai, J., 144
 Kaliaguine, S., 337
 Kalil, J., 263
 Karel, M., 249

- Kashchiev, D., 189, 191
 Kaufman, E.L., 254
 Kawakami, G., 340
 Kawakami, T., 202
 Kawasaki, S., 376
 Kawashima, Y., 402
 Kaytancioglu, O., 134
 Kelebeev, J.S., 324
 Kelly, A., 30
 Kelly, F.D., 303
 Kelly, F.H.C., 338
 Kelvin, Lord, 108
 Kemp, S.D., 359
 Kern, R., 278
 Kerze, F., 404
 Khamskii, E.V., 133, 181
 Kim, K.J., 347, 355, 377
 Kimura, H., 144
 Kind, M., 251, 279, 340
 King, R.J., 381
 Kirby, T., 472
 Kirwan, D.J., 235, 288
 Kishimoto, S., 326
 Kishishita, A., 326
 Kitamura, M., 283, 335, 396
 Kitano, Y., 336
 Klassen, J., 362
 Klein, J-P., 395
 Klein, M.O., 378
 Klug, D.L., 256
 Knapp, L.F., 110
 Knuth, M., 362, 368
 Kolař, V., 269
 Kolbe, J.L., 337
 Kolthoff, I.M., 315, 325–327
 Komarov, V.F., 189
 Kondos, P., 123
 Kossel, W., 220, 255
 Kotsinaris, A., 420, 463
 Krabbes, E., 314
 Krishna, P., 18
 Krupiczka, R., 363
 Kruse, M., 49
 Kuboi, R., 196
 Kubota, N., 111, 198, 202, 206, 256–260,
 262, 288, 299
 Kudela, L., 359
 Kugler, J., 361, 368
 Lacmann, R., 253
 Laguerie, C., 288, 401
 Lahav, M., 274, 276
 Lancia, A., 213
 Land, T.A., 243
 Larson, M.A., 134, 197, 249, 254, 277,
 336, 407, 412, 417, 419, 421, 426
 Laudise, R.A., 309
 Leci, C.L., 47, 133, 187, 198
 Lee, M.Y., 278
 Leeuwen, M.J.L. van, 342, 343
 Leiserowitz, L., 274, 276
 Letan, R., 376
 Leubner, I.H., 323, 337
 Levins, D.M., 264
 Lewin, S., 106
 Lewis, B., 216
 Lewtas, K., 278
 Li, K.K., 198
 Liao, J.C., 198
 Liesegang, R.F., 320
 Lindberg, M., 342, 426
 Linford, R.G., 214
 Liotta, C.L., 303
 Liu, G.T., 303
 Liu, S.T., 131
 Liu, T., 467
 Lo, P.Y., 127
 Long, F.A., 111
 Lobachev, A.N., 310
 Loeth, J., 30
 Lowell, S., 72
 Lukes, G.C. and J.A., 378
 Luthy, R.V., 396
 Lutz, W.F., 340
 Lynn, S., 394, 397
 Macedo, E.A., 122
 Madsen, H.E.L., 283
 Maginn, S.J., 276, 278
 Mahapatra, A., 397
 Mak, F.K., 338
 Manguo, J.L., 378
 Manning, M.P., 123
 Mantovani, G., 271, 285, 288
 Maraček, J., 337
 Marais, G.R., 131
 Marcant, B., 341
 Marché, W.G.J., 271
 Margolis, G., 337, 339
 Markwart, M., 402
 Marquering, G.M., 322
 Marshall, W.L., 125
 Maruscak, A., 336
 Mason, B.J., 192
 Masumi, F., 299
 Mathur, K.B., 402
 Matijević, E., 333, 339
 Matsuoka, H., 335
 Matsuoka, M., 154, 345, 361
 Matthews, G.P., 114, 119
 Matuchová, M., 195, 216
 Matz, G., 232, 293, 294

- Max, M., 400
 Mazzarotta, B., 336, 463
 McCabe, W.L., 146, 195, 196, 198, 403–406
 McCandless, F.P., 396
 McCauley, J.A., 301
 McCrone, W.C., 199, 280
 McDevit, W.F., 111
 McDonald, M.P., 134
 McGhie, A.R., 308, 313
 McInnes, J., 182
 McKay, D.L., 349
 McKie, C. and D., 31
 Meenan, P., 271
 Mehta, K., 202, 204, 205
 Meisingset, K.K., 144
 Meissner, H.P., 122
 Melia, T.P., 189, 198
 Melikhov, I.V., 324
 Mellor, J.D., 359
 Melvin, M.V., 378
 Meranda, D., 56
 Merritt, L.M., 115
 Mersmann, A., 213, 249–251, 279, 340,
 341, 355, 377
 Metheny, D.E., 401
 Michaels, A.S., 255
 Middleman, S., 269
 Miers, H.A., 123, 226
 Miki, H., 340
 Millard, B., 406, 407
 Miller, W.H., 10
 Mills, R., 36, 43
 Mina-Mankarios, G., 394
 Ming, Y., 401
 Misra, C., 337
 Mitscherlich, E., 16
 Moffit, W.P., 189, 198
 Mogi, J., 196, 198
 Mohamed, R.S., 303
 Mohan, R., 134
 Molinari, J.G.D., 347, 351
 Monhemius, A.J., 330
 Montillon, G.H., 403
 Moore, J.H., 336, 339
 Moore, W.J., 103
 Morgenthaler, W.W., 467
 Morari, M., 426
 Morita, M., 351
 Moritoki, M., 358
 Mosseri, S., 394
 Mullin, J.W., 42, 46, 47, 73, 75, 76, 99,
 113, 119, 126–130, 134, 187–190,
 197, 198, 202, 203, 205–213, 221,
 229, 238–240, 242, 244–248, 255–
 263, 267, 268, 271–273, 277, 278,
 316–319, 322–325, 334–337, 341,
 376, 393, 421, 424–426, 431, 441,
 442, 448, 452, 453, 456, 463
 Mullin, J.B., 312
 Murata, Y., 287
 Murphy, J.D., 322, 337
 Musmarra, D., 213
 Myerson, A.S., 134, 192, 271, 276, 278,
 286, 288, 322
 Nagahama, K., 303
 Nagashima, N., 326
 Nagashima, Y., 376
 Nagashima, N., 326
 Nakai, K., 111, 262
 Nakamaru, N., 351
 Nancollas, G.H., 101, 131, 188, 260, 262,
 278, 282, 322, 336
 Nass, K.K., 301
 Nauman, E.B., 420
 Nelson, C.D., 338
 Nernst, W., 46, 225
 Ness, J.N., 196
 Newman, E.J., 333
 Newman, H.H., 387
 Ng, K.C., 198
 Ng, K.M., 179, 293, 397, 467
 Nicholson, E.B., 118
 Nicol, W.H., 57, 134
 Nicolaeva, R., 258
 Nicolau, I.F., 308
 Nielsen, A.E., 188, 205, 207, 213, 229, 233,
 321, 325, 330
 Nienow, A.W., 45, 196, 246, 267, 269, 402,
 451, 452
 Nobbs, J.H., 337
 Nosov, G.A., 354
 Novomeysky, M.A., 377
 Novotný, P., 34, 115
 Nowlan, M.F., 37
 Noyes, A.A., 225
 Nunelly, L.M., 357
 Nývlt, J., 75, 94, 113, 117, 121, 123, 136,
 189, 195, 202, 205, 214, 216, 248,
 249, 318, 322, 370, 393, 418, 421,
 424–428, 438, 441, 442, 448, 463
 O'Dell, F.P., 199
 O'Hara, M., 231
 O'Hern, H.A., 354
 O'Neill, J.B., 48
 Ogaki, T., 284
 Okada, M., 283
 Okumara, M., 336, 402
 Oldshue, J.Y., 452
 Opperhauser, H., 337
 Ore, F., 336, 339

- Osman, M.M., 208, 211
 Ostwald, W., 108, 123, 214, 320
 Othmer, D.F., 42, 146, 396
 Otpushchennikov, N.F., 190
 Ottens, E.P.K., 416, 450
 Owen, B.B., 40
 Ozawa, R., 154
- Palermo, J.A., 235
 Palmer, K., 413
 Pamplin, B.R., 313, 314
 Papangelakis, V.G., 123
 Parokonyi, V.D., 354
 Parr, N.L., 307
 Partington, J.R., 110
 Pasteur, L., 22
 Paterson, W.R., 266
 Patterson, D., 377
 Payne, J.H., 293, 328
 Peet, R.B., 407
 Perdok, W.G., 269, 271
 Petric, B. and M., 337
 Pfann, W.G., 303, 308
 Pfefer, G., 278
 Phillips, V.R., 242, 244
 Phillips, V.A., 337
 Phillips, F.C., 31
 Phillips, R.H., 376, 460, 463
 Phoenix, L., 277, 466
 Pigford, R.L., 235
 Pinder, K.L., 394
 Pirttimaki, J., 301
 Plasari, E., 338
 Player, M.R., 349
 Plewes, A.C., 362
 Poiseuille, J.L., 37
 Poling, B.E., 37, 62
 Polywka, L.A., 276, 278
 Popovitz-Biro, R., 276
 Potts, G.D., 284
 Powers, J.E., 349
 Powers, H.E.C., 82, 195, 285, 288
 Prasad, K.V.R., 420, 463
 Prausnitz, J.M., 37, 62, 100, 122
 Priciandaro, M., 213
 Prud'homme, R.K., 303
 Pulley, C.A., 447
 Purchas, D.B., 469
 Purdie, N., 188
 Purdon, F.F., 112, 169, 179
 Pyschny, J., 363
- Qui, Y., 248
 Ragatz, R.A., 146
 Rajagopal, S., 397
- Raju, K., 122
 Randolph, A.D., 196, 249, 302, 407, 412,
 418–423, 450
 Rankin, A.H., 288
 Raouzeos, G., 367
 Rashkovich, L.N., 197
 Rasmussen, P., 122
 Rasmuson, Å.C., 248, 342, 395, 426
 Raven, K.D., 190
 Ray, W.H., 426
 Read, W.T., 221
 Reddy, M.M., 322, 336
 Redfern, B.A.W., 48
 Reich, R., 229
 Reid, R.C., 37, 62, 231
 Ricci, J.E., 136, 169
 Rice, R.W., 341
 Richardson, J.F., 146, 456–458
 Richardson, P., 338
 Ridgway, K., 49
 Ristic, R.I., 196, 254, 420, 463
 Roberts, A.G., 357
 Roberts, K.J., 271
 Roberts, J.E., 407, 418
 Robinson, R.A., 43, 48, 122, 129
 Robinson, J.N., 407, 418
 Rogacheva, E.D., 199
 Rohani, S., 426
 Rojkowski, Z., 417, 418
 Roozeboom, H.W.B., 167
 Roques, H., 336
 Rosenberg, H.M., 31
 Rossiter, A.P., 467, 468
 Rousseau, R.W., 196, 198, 199
 Rowe, P.N., 263
 Rubbo, M., 271, 285, 288
 Rubin, B., 311
 Ruddick, A.J., 284
 Rumford, F., 253
 Ruskam, R.P., 357
 Rusli, I.T., 134, 197, 254
 Rutner, E., 359
- Saeman, W.C., 389, 390, 406, 445, 447
 Saito, T., 288
 Sako, T., 303
 Salutsky, M.L., 328, 332, 333
 Samant, R.N., 298
 Samoilov, O.V., 133
 Sampson, M.J., 359
 Sangster, J., 37
 Santhanam, C.J., 396
 Sarig, S., 144, 197, 206, 274, 336
 Saska, M., 286
 Sato, A., 288, 299
 Sato, K., 283, 284, 287

- Satu, M., 303
 Savitt, S.A., 396
 Sax, N.I., 90
 Saxon, K., 353
 Saylor, C.P., 310
 Scheel, H.J., 310
 Scheffler, P., 357
 Schierholz, P.M., 336
 Schildknecht, H., 308, 349
 Scholle, S., 147
 Schönert, H., 136
 Schott, H., 169
 Schrader, G.L., 134
 Schreinemakers, F.A.H., 116, 169
 Schultz, W., 220
 Schwarz, H., 271
 Schwartz, J.C., 378
 Schweizer, P., 357
 Schwenk, W., 367
 Scrutton, A., 416
 Sears, G.W., 262
 Seavoy, G.E., 372, 373
 Secor, R.M., 298
 Seidell, A., 123
 Senol, D., 192
 Settle, F.A., 115
 Shah, B.C., 196
 Shah, J.S., 308
 Shah, K.D., 357
 Shah, S.M., 397
 Shakova, N.A., 402
 Shamlou, P.A., 196
 Sharma, M.M., 397
 Sharratt, P.N., 467, 468
 Shaviv, F., 376
 Shearon, W.H., 356, 467
 Shekunov, B.Yu., 303
 Sheldon, R.A., 298
 Sheldrake, G.N., 298
 Shemilt, L.W., 44
 Shepherd, T.J., 288
 Sherwood, T.K., 362
 Sherwood, J.N., 196, 254, 463
 Sherwood, P., 396
 Shields, J.E., 72
 Shimizu, K., 111, 206, 262
 Shirley, A.R., 357
 Shock, R.A.W., 460, 461, 463
 Shripathi, T., 196, 254
 Shuvalov, L.A., 31
 Sikdar, S.K., 196, 336, 339
 Simha, R., 39
 Simon, B., 273
 Šípek, M., 118, 342
 Skold-Jorgensen, S., 122
 Skřivánek, J., 372
 Skelland, A.H.P., 348
 Skovborg, P., 122
 Slater, V.W., 112, 169, 179
 Sloan, E.D., 399
 Sloan, G.J., 308, 313
 Slusher, R., 121
 Smith, P.G., 402
 Smith, J.C., 146
 Smolik, J., 361, 368
 Smoluchowski, M. von, 316, 317
 Smythe, B.M., 253
 Sobczak, E., 228
 Söhnel, O., 34, 94, 115, 123, 129, 130, 134,
 189, 190, 195, 202, 205–211, 213,
 216, 316–319, 322, 334, 336–342, 463
 Sonnenfeld, P., 377
 Spoors, G., 322, 337
 Spot, G., 463
 Squaldino, G., 271, 285, 288
 Stahly, G.P., 298, 299
 Stávek, J., 298, 299, 342
 Steno, N., 3
 Stephen, H. and T., 123
 Šterbáček, Z., 452
 Stevens, J.D., 336, 417
 Stevens, R.P., 195
 Stevenson, D.G., 340
 Still, J.E., 117
 Stokes, G.G., 37, 69, 455
 Stokes, R.H., 36, 43, 48, 122, 129
 Stranski, I.N., 256
 Straughan, B.W., 313
 Strickland-Constable, R.F., 189, 195–197,
 205, 216, 235, 359, 362
 Stuart, A., 18, 30
 Sturrock, P., 131
 Sugimoto, T., 322
 Sun, Y-C., 401
 Sung, C.Y., 195
 Sunier, A.A., 293
 Sutherland, J.P., 402
 Suzuki, M., 283, 284
 Svalov, G.V., 354
 Svanoé, H., 374
 Svarovsky, L., 469, 473
 Swank, T.F., 337
 Swern, D., 155, 348
 Szabo, T.T., 420
 Szmigiel'ská, M., 147
 Tabor, D., 49
 Tack, R.D., 278
 Tadaki, T., 202
 Tai, C.Y., 303
 Takahashi, Y., 299
 Takashima, Y., 362

- Takegami, K., 351, 355
 Takeuchi, H., 299
 Tamman, G., 186, 235
 Tamme, R., 144
 Tanaka, T., 396, 467
 Tare, J.P., 397
 Tausk, P., 452
 Tavare, N.S., 228, 248, 254, 334, 340, 341,
 342, 396, 418
 Teeple, J.E., 112, 123, 179
 Tekenaka, H., 402
 Tempkin, D.E., 233
 Teodosiev, N., 334, 431
 Terwilliger, J.P., 339, 418
 Tester, J.W., 122
 Tezak, B., 328, 329
 Thakar, M.S., 42
 Thi, H.D., 37
 Thoma, P., 367
 Thomson, W., 108, 320
 Thring, M.W., 449
 Timms, R., 348
 Ting, H.H., 195
 Tipson, R.S., 291–293
 Tomazic, B., 322
 Tomi, D.T., 317
 Torgesen, J.L., 48, 286, 310
 Toussaint, A.G., 435, 462
 Toyokura, K., 196, 198, 320, 342, 354,
 376, 438
 Tsuge, H., 395
 Tsuzuki, M., 395
 Turkevich, J., 102
 Turnbull, D., 187, 195, 232
 Tyner, M., 147
 Tyrrell, H.J.V., 43
 Ubbelohde, A.R., 236
 Uchiyama, I., 111, 262
 Ueda, H., 362
 Uemaki, O., 402
 Uhl, V.W., 452
 Ulrich, J., 49, 254, 288
 Unahabokha, R., 45, 267
 Vaccari, G., 271, 285, 288
 Vacek, V., 371
 Vainshtein, B.K., 31
 Valeton, J.J.P., 226
 Van den Berg, P.J., 357
 Van Hook, A., 260
 Van der Eerden, J.P., 231, 233
 Van Bueren, H.G., 31
 Van Rosmalen, G.M., 271, 278, 303, 342,
 356, 420, 463
 Van der Voort, E., 273
 Van't Hoff, J.H., 179
 Van't Land, C.M., 196
 Vance, S.W., 401
 Vandersall, H.L., 467
 Vaneček, V., 402
 Vega, R., 123
 Verma, A.R., 18, 221
 Vermilyea, D.A., 256
 Veverká, F., 134, 463
 Villermaux, J., 338, 341, 395
 Vitovec, J., 361, 368
 Vold, M.J. and R.D., 112, 113
 Volmer, M., 182, 185, 194, 218, 220
 Vonnegut, B., 189
 Wachi, S., 395
 Wallach, D.L., 357, 395
 Walton, A.G., 188, 316, 323, 327
 Wanklyn, B.M., 310
 Warner, F.E., 345
 Watson, R.A., 62
 Watson, K.M., 146
 Weedman, J.A., 396
 Wei, H., 342
 Weimarn, P.P. von, 323
 Weingaertner, D.A., 394, 397
 Weinspach, P.M., 336, 362, 368
 Wellinghoff, G., 343
 Wells, A.F., 31, 216
 West, A.J.M., 462
 Wetteroth, W.A., 263
 Wey, J.S., 337, 339, 418
 Whetstone, J., 463
 White, E.T., 196, 254, 286, 287
 White, M.L., 189
 Whiting, M.J.L., 271, 272
 Whitney, W.R., 225
 Whynes, A.L., 467
 Wibowo, C., 179, 293, 467
 Widmer, F., 357
 Wiechers, H.N.S., 131
 Wienk, B.G., 196
 Wilcox, W.R., 288, 308, 339
 Wilen, S.H., 22, 296–300
 Wilke, C.R., 42
 Willard, H.H., 115, 328, 332
 Williams, A.J., 285, 286
 Williams, J.R., 376
 Wilson, D.D., 333
 Winn, D., 278
 Wint, A., 335
 Wintermantel, K., 343, 367
 Wise, W.S., 118
 Wisniak, J., 123
 Witkamp, G.J., 278
 Wöhlk, W., 381, 463

- Wojciechowski, B., 133
Wong, J.M., 303
Wood, R.M., 134
Woodward, G.D., 199
Wright, J.D., 31, 254
Wronski, S., 362
Wu, F.H., 435
Wulff, G., 217

Yamamoto, M., 335
Yamamoto, T., 286, 287
Yamane, S., 303
Yamasaki, T., 376
Yamazoe, K., 196
Yokota, M., 111, 256–260, 262, 288, 299
York, P., 303
Yashiro, H., 111, 256

Yoshinaga, Y., 335
Yoshizawa, S., 395
Young, S.W., 181
Youngquist, G.R., 195

Žáček, S., 213, 250, 371
Zaitseva, N.P., 197
Zaki, W.N., 456–458
Zauner, R., 318, 342, 343
Zawacki, S.J., 262, 278
Zettlemoyer, A.C., 189
Zhang, J., 260, 282
Zikic, A.M., 420, 463
Zief, M., 308
Zimmerman, H.K., 112
Zuiderweg, F.J., 402
Zweitering, Th.N., 451, 452

Subject index

- Acid Magenta, 466
Activation energy, 47, 251
Activity:
 coefficients, 100, 514–518
 optical, 18
 solubility product, 104
Adipic acid, 255
Adducts, 395
Adsorption layer theories, 218
Ageing of precipitates, 320
Agitated vessels, 369, 451
Agitators, scale-up, 448
Agglomeration, 316, 402
Aitken nuclei, 193
Alanine, 21
Alkanes, 271
Allotropy, 17
Alpha factor, 233, 272
Alumina hydrate, 324, 336
Aluminium:
 hydroxide, 340
 chloride, 359
 nitrate, 402
 sulphate, 385
Alums, 8, 16, 25, 165
Aminophenol, 359
Ammonium:
 alum, 49, 166, 204, 237, 246, 248
 chloride, 46, 204, 464, 385
 dihydrogen phosphate, 49, 134, 204,
 237, 256, 261, 285, 464
 diuranate, 340
 nitrate, 17, 146, 204, 237, 284, 354,
 402, 464
 enantiotropy, 17
 paratungstate, 340
 perchlorate, 285, 288
 sulphate, 13, 141, 167, 204, 237, 334,
 383, 394, 402, 464
Amorphous precipitates, 325
Andreassen pipette, 70
Anthracene, 16, 271, 359
Anthranilic acid, 359
Archimedean solids, 6
Arrhenius equation, 102, 184, 219,
 251
Astrakanite, 166
Atomic weights, table of, 478
p-Azoxyphenetole, 2
- Barium:
 acetate, 93
 chloride, 385, 464
 hydroxide, 374
 nitrate, 294, 385
 sulphate, 122, 289, 291, 292
 tungstate, 318
Batch crystallization, 392, 423, 435, 439,
 441
Bayer hydrate, 324, 336, 337
BCF equation, 222
Benzamide, 275
Benzanthrone, 359
Benzene-naphthalene, 140
Benzoic acid, 275, 359, 461
Benzophenone, 139, 200, 362
Benzoquinone, 359
BET adsorption, 72
Boiling point, 55
 elevation, 56, 132
Borax, 146, 204
Boric acid, 146
Bose's swarm theory, 2
Boundary layers, 248, 264
Bravais lattices, 14
Bravais rule, 15, 269
Bridgman–Stockbarger technique, 314
Brines, natural, 180, 336, 377, 394
Brodie purifier, 350
Burgers vector, 28
- Caking of crystals, 463
Calcite, 13, 48
Calcium:
 acetate, 93
 carbonate, 17, 130, 131, 211, 282, 284,
 336, 339, 402
 chloride, 144, 146, 385, 402, 464
 hydroxide, 92
 nitrate, 146, 354, 377, 402
 oxalate, 138, 322, 329
 phosphate, 138, 322
 sulphate, 121, 271, 322, 336, 339
 tartrate, 311
Camphor, 359
Caprolactam, 356
Carbon, polymorphs, 17
Carnallite, 180
Carotene, 302

- Cascades, 418
 Chirality, 18, 22, 295
 Chlopin equation, 327
 Chlorobenzenes, 351
 Cholesteric state, 3
 Chromium chloride, 359
 Citric acid, 133, 198, 204, 237
 Clapeyron equation, 59
 Clathrate compounds, 296
 Clausius–Clapeyron equation, 61
 Clear liquor overflow, 419
 Clusters, solute, 132–134, 190
 Coefficient of variation (CV), 82, 412
 Common ion effect, 107
 Common names of salts, 530–535
 Compatible salts, 174, 335
 Compatible polymorphs, 281
 Conductivity:
 electrical, 48
 ionic, 103
 thermal, 54
 Congruent melting point, 142
 Coning and quartering, 65
 Constitutional supercooling, 305
 Controlled crystallization 392, 423
 Controlled seeding, 392, 439
 Cooling:
 crystallization, 369
 direct contact, 375
 programmed, 392, 423, 439
 Copper:
 chloride, 385
 phthalocyanine, 283, 322
 sulphate, 8, 13, 93, 95, 204, 385
 Cost estimation, 434
 Cresol, *m-p-* separation, 396
 Cristobalite, 17
 Critical humidity of salts, 464
 Critical nucleus, 183, 190, 219
 Critical point, 137, 302
 Cryohydrates, 141
 Cryoscopic constant, 56
 Crystal growth:
 dendritic, 236
 diffusion controlled, 225
 effect of impurities, 254, 269
 effect of crystal size, 253
 effect of strain, 196, 253, 254
 effect of temperature, 251
 expressions of, 236
 in gels, 310
 inhibition of, 254
 faces, 238
 layers, 218, 242
 measurement of, 236
 mechanisms of, 216
 overall, 243
 rate expressions, 236
 size dependent, 253
 spiral, 29, 221
 theories, 216
 Crystal habit, 3, 22, 269
 Crystallization:
 adductive, 395
 batch, 392, 423, 435, 439, 441
 choice of method, 92, 434
 controlled, 392, 423
 cooling, 369
 emulsion, 400
 evaporative, 377
 extractive, 397
 fractional, 289, 349
 freeze, 347, 398
 high-pressure, 357
 hydrothermal, 310
 melt, 234, 343–358
 pressure, 357
 salting-out, 333, 393
 spherical, 402
 spray, 401
 reaction, 394
 vacuum, 385
 yield, 96, 391
 Crystallizers:
 agitated vessels, 369
 batch, 392, 423, 439, 441
 belt, 354
 cascade of, 418
 Cerny, 377
 choice of, 434
 classification of, 368
 column, 349
 cooling, 369
 cooling disc, 373
 cost estimation of, 434
 design of, 403, 436
 direct contact cooling, 355, 375
 double propellor, 389
 draft-tube, 386
 drum, 354, 374
 DTB, 387
 evaporating, 377
 fluidized bed, 388
 in series, 418
 MSMPR, 249, 408
 multiple-effect, 379
 multistage vacuum, 390
 open tank, 369
 operating problems, 403
 Oslo-Krystal, 375, 383
 Pachuca, 369
 periodic behaviour, 420

- ponds, 377
 programme-cooled, 392, 423, 439
 rotary, 354, 374
 scale-up of, 488
 scraped-surface, 347, 374
 solar ponds, 377
 spray, 401
 Sulzer MWB, 353
 Sweat-tank, 347
 Swenson–Walker, 372
 TNO column, 351
 trough, 371
 TSK, 351
 turbulence, 388
 twin, 371
 unsteady-state operation, 420
 vacuum, 382, 385
 wetted-wall, 385
 Wuiff–Bock, 372
 Crystallographic symmetry, 4
 Crystalloluminescence, 189
 Crystals:
 agglomeration of, 316
 caking of, 463
 composite, 25
 covalent, 15
 dendritic, 24, 236
 dissolution of, 260
 equilibrium shape, 216
 hardness, 48
 imperfections in, 27
 inclusions in, 284
 ionic, 15
 liquid, 2
 maximum size of, 278
 metallic, 15
 mixed, 16
 molecular, 15
 morphology of, 269, 323
 piezo-electric, 309
 purity of, 141, 297
 semiconducting, 309
 single, 309
 symmetry of, 4
 twin, 25
 Crystal-size distribution (CSD), 403–429
 measurement of, 64–85
 MS/CV, 76–85, 412
 Cyclic behaviour of crystallizers, 420
 Cycling, temperature, 320
 Cyclonite, 406
 Czochralski technique, 312
 Damköhler number, 229
 Davies equation, 101, 122
 Dead Sea salts, 377
 Debye–Hückel equation, 101, 122
 Defects in crystals, 27
 Deliquescence, 465
 Dendrites, 24, 236
 Dendritic salt, 277
 Density, 32–35
 of inorganic salts, 492–498
 of organic solids, 499
 of solutions, 500–509
 of bulk solids/slurries, 34
 Desalination, 377, 398
 Dewaxing of oils, 376
 Diamond, 8, 17, 48
 Differential thermal analysis, 153
 Diffusion:
 coefficients, 41, 513
 measurement of, 41–47
 boundary layer, 264
 Dilatometry, 155
 Direct contact cooling, 355, 375
 Dislocations, 28, 221
 Dissolution, 260
 Doerner–Hoskins equation, 327
 Double draw-off, 419
 Double jet mode, 341
 Downstream processes, 467
 Draft tube agitation, 453
 Draft tube crystallizer (DTB), 387
 Driving force for mass transfer, 266
 Drying-up point, 161, 163, 165
 DSC/DTA, 153
 Dühring's rule, 56, 132
 Dulong and Petit's rule, 51
 Ebullioscopic constant, 56
 Effectiveness factors, 229, 256
 Efflorescence, 465
 Emulsion crystallization, 400
 Enantiomorphism, 18
 Enantiotropy, 17, 139, 282
 Encrustation, 459
 Enthalpy-concentration diagrams,
 146–151
 Equilibrium:
 determination of, 112–120, 169
 shape of crystal, 216
 Euler relationship, 7
 Eutectic mixtures, 140, 158
 Eutonic point, 160, 164
 Evaporative crystallization, 377
 Extractive crystallization, 397
 Fats and waxes, 155, 348, 374
 Fatty acids, 354
 Ferric chloride, 143, 359
 Ferrous sulphate, 93, 204, 374, 442

- Fick's law, 44
 Filtration of crystals, 469
 Fines destruction, 420, 426, 439
 Flash cooling, 382, 385
 Fluidized beds, 453
 Flux growth, 310
 Fourier equation, 54
 Fractional crystallization, 289, 349, 361, 365
 Freeze crystallization, 347, 398
 Freeze drying, 359
 Freezing point, 55
 Frössling equation, 241
 Froude number, 449
 Fusion, enthalpy of, 59, 529
- Gamma function, 84
 Garnet, 6
 Gas hydrates, 399
 Gaussian (normal) distribution, 82
 Gels, crystallization from, 310
 Gibbs–Thomson (Kelvin) formula, 108–110, 184, 320
 Gilliland–Sherwood equation, 362
 Glaserite, 336
 Glutamic acid, 283
 Goethite, 325
 Goniometers, 3
 Graphite, 8, 17
 Grashof number, 241
 Growth rate dispersion, 254
 Güntelberg equation, 101
 Gypsum, 48, 271, 322, 336
- Habit modification, 22, 269
 Hafnium tetrachloride, 366
 Hardness of crystals, 48
 Hartman–Perdok theory, 269
 Haüy's laws, 3, 11, 16, 217
 Heat capacity, 50–54
 Heat (enthalpy) of:
 crystallization, 62
 fusion, 59, 529
 solution, 62, 520–527
 sublimation, 59
 transition, 59
 vaporization, 61
 Heat, units of, 49
 Heat storage hydrates, 144
 Hemibedral class, 9
 Hertz–Knudsen equation, 362
 Hexamine, 271, 285
 High-pressure crystallization, 357
 Histidine, 144
 Holohedral class, 9
 Humidity, critical, of salts, 464
- Hydrates, for heat storage, 144
 Hydrazine, 146, 335
 Hydrothermal crystallization, 310
 Hydroxybenzoic acids, 43
 Hydrotropes, 111, 334
- Ice, 8, 359, 398
 Ice cream, 348
 Iceland spar, 1
 Ideal and non-ideal solutions, 98–108
 Imperfections, crystal, 27
 Impurities, effect on:
 caking, 463
 growth, 254, 269
 habit, 269
 nucleation, 205
 solubility, 110
 Inclusions, 284
 Incompatible salts, 174, 335
 Incongruent melting point, 142
 Incrustation, 459
 Induction period, 206–210
 Interfacial tension 39, 193, 210
 Invariant growth, 217
 Iodine, 8, 359
 Ionic strength, 101
 Isokinetic sampling, 65, 430
 Isomorphism, 16
 Isotropy, 1
- j*-factors, 263
 Jänecke's projection, 172–179, 345
- Kolmogoroff theory, 269, 317
 Kopp's rule, 51
 Kossel model, 220, 255
 Kozeny equation, 72
 Kyropoulos technique, 312
- Lactic acid, 20
 Latent heats, 58
 Latent period, 206
 Lattice density, 15, 217, 269
 Law of:
 Bravais, 15
 constant interfacial angles, 3, 217
 mass action, 106
 rational intercepts, 11
 Lead:
 iodate, 338
 nitrate, 273, 294
 sulphate, 321
 Le Chatelier's principle, 93
 Lever arm principle, 147
 Liquid crystals, 2
 Lithium chloride, 464

- Lixivation, 471
 Log-normal distribution, 84
- McCabe AL law, 404
 McCabe–Thiele diagram, 294
 Macle, 25
 Macromixing, 341
 Magma density, 34, 414
- Magnesium:
 acetate, 464
 chloride, 376
 hydroxide, 138, 322, 337
 sulphate, 63, 146, 150, 199, 204, 237,
 385, 403
 enthalpy chart, 150
 phosphate, 283
- Manganous chloride, 385
 Manganous nitrate, 142
 Margarine, 348
 Mass transfer, 260–269
 correlations, 263
 driving force, 266
 Maximum crystal size, 278
 Melt crystallization, 234, 343–358
 Melting point, 55
 congruent and incongruent, 142
 Meritectic point, 143
 Merkel charts, 146–151
 Mesitylene, 358
 Mesomorphic state, 2
 Metastable supersaturation, 123, 201–205
 Metathesis, 171, 335
 Methanol, aqueous, solubilities in, 334
 Microscopy, 69
 Micromixing, 341
 Miller indices, 10
 Mimetic twinning, 25
 Mitscherlich's law, 16
 Mixed crystals, 16
 Mixing criterion, 435, 462
 Mixture rule, 141, 147, 157, 162, 345
 Mohs hardness scale, 48
 Molal and molar solutions, 90
 Mole fractions, 91
 Molecular clusters, 133, 190
 Monotropy, 18, 139, 282
 Morphology of crystals, 269, 323
 MS/CV size specification, 82
 MSMPR crystallizer, 249, 408
- Naphthalene, 48, 347, 351, 359, 368, 400
 -benzene, 140
 - β -naphthol, 145
 - β -naphthylamine, 145
 β -naphthol, 359
 Nematic state, 2
- Newberryite, 271
 Nickel:
 ammonium sulphate, 212, 237, 248, 323
 sulphate, 8, 17, 204, 334
- Nitrochlorobenzenes, 397
 Nitrophenol, eutectics, 158
 Nitrotoluene, eutectics, 345
- Nucleation:
 classical theory, 182–189
 effect of impurities, 205
 heterogeneous, 192–195
 homogeneous, 182–189
 'order' of, 201, 249, 409
 primary, 182
 secondary, 195–201, 416
 spinodal, 191
 surface, two-dimensional, 219
 thermal history, 205
- Nuclei:
 Aitken, 193
 critical, 182, 190
 growth of, 206
 population density of, 408
- Occlusions, 284
 Oleic acid, 284
 Optical activity, 18
 Ostwald–Freundlich equation, 108–110
 Ostwald ripening, 320, 322
 Ostwald's rule of stages, 180, 197, 214,
 280, 282, 322, 436
- Overgrowth, 17
 Overlapping, 217
 Oxalic acid, 8, 51
- Pachuca vessels, 370
 Paneth–Fajans–Hahn rule, 326
 Parallel growth, 26
 Parametral plane, 10
 Particle size, 64–85
 and crystal growth, 253
 and solubility, 108
 and surface area, 66
- Pentaerythritol, 461
 Periodic behaviour of crystallizers, 420
 Periodic bond chains, 271
 Phase diagrams, 135–180
 Phase rule, 135
 Phase transformation, 58, 280, 322
 Phenol, 347
 Phthalic anhydride, 359, 363, 368
 Phthalimide, 359
 Piezo-electric crystals, 309
 Pinacoids, 23
 Point groups, 15
 Poiseuille's equation, 37

- Polymorphs, 16, 137, 280
 phase diagrams, 139, 282
 transformation of, 17, 137, 138, 280–284
- Polytypism, 18
- Ponchon–Savarit diagram, 294
- Population balance, 407
- Potassium:
 acetate, 385
 alum, 26, 49, 167, 204, 237–247, 385,
 461
 bromide, 167, 204
 carbonate, 464
 chlorate, 8
 chloride, 8, 46, 141, 167, 204, 237, 248,
 274, 372
 chromate, 93, 464
 dichromate, 8
 dihydrogen phosphate, 49, 204, 237,
 255, 286, 461
 iodide, 36, 204, 285
 nitrate, 8, 204, 237, 385, 461
 $\text{NaNO}_3\text{--H}_2\text{O}$, 160
 nitrite, 204
 permanganate, 372
 sulphate, 21, 49, 126, 167, 204, 237,
 248, 262, 271, 334, 377, 385, 425,
 461
- Power number, 450
- Precipitates, 315
 ripening of, 320
 agglomeration of, 316
 amorphous, 325
- Precipitation, 315–343
 diagrams, 328
 double-jet, 341
 from homogeneous solution, 332
 processes, 336
 techniques, 331
- Pressure melt crystallization, 357
- Prilling, 356
- Primary nucleation, 182
- Proabd refiner, 347
- Programmed cooling, 392, 423, 439
- Propane hydrates, 398
- Proteins, 338
- Pseudomorphs, 18
- Purity of crystals, 141, 297
- Pyrogallol, 359
- Quartz, 17, 48, 310
- Quaternary systems, 169
- Racemates, 21, 295
- Raoult's law, 55
- Reciprocal salt pairs, 171, 335
- Recrystallization, 289, 349, 361, 365
- Refractive index of solutions, 47
- Reticular density, 15, 217, 269
- Reynolds number, 241, 249, 263–268, 449
- Riffles, 66
- Ripening of precipitates, 320
- Rittinger's law, 196
- Roozeboom phase types, 167
- Rosin–Rammier–Sperling plot, 84
- Rotating disc, 248
- Ruby, 8
- Rutile, 8
- Salicylic acid, 43, 363, 402
- Salting-in, 107
- Salting-out, 107, 111, 333, 393
- Sampling:
 isokinetic, 65, 430
 of solids, 64
 of solutions, 113
- Scale-up of crystallizers, 448
- Scaling, crystal, 459
- Schmidt number, 241, 263, 265
- Scraped surface crystallizer, 347, 374
- Screening, industrial, 473
- Screw dislocations, 29, 221
- Secondary nucleation, 195, 416
- Seeding, 197, 392, 439
- Sedimentation, 69
- Shape factors, 73–76
- Sherwood number, 241, 263, 266, 420
- Sieves and sieving, 67, 78
- Silicon dioxide, 17, 338
- Silver:
 bromide, 330, 339
 chloride, 332
 halides, 232, 337
 iodide, 8, 332
 nitrate, 8
- Single crystals, 309
- Size classification, 64–85
 coefficient of variation, 82
 graphical analyses, 78–81
 mean size, 76
- Slip velocity, 451
- Slurry density, 34
- Smectic state, 2
- Sodium:
 acetate, 93, 95, 98, 144, 204, 372, 391,
 464
 bicarbonate, 394
 broniate, 464
 bromide, 204, 464
 carbonate, 63, 146, 204, 394
 enthalpy chart, 148
 heat of solution, 63
 chlorate, 13, 199, 286, 464

- chloride, 8, 24, 93, 140, 204, 237, 253, 274, 286, 324, 394, 464
hydrate, 140
 $\text{--H}_2\text{O--Na}_2\text{SO}_4$, 163
chromate, 93, 95, 204
cyanide, 402
dichromate, 464
hydroxide, 146, 376, 380, 402
Dühring plot, 57
iodide, 204
nitrate, 8, 134, 190, 204, 354, 464
 $\text{--H}_2\text{O--KNO}_3$, 160
nitrite, 204, 464
perchlorate, 286
phosphates, 144, 204, 373
sulphate, 93, 97, 144, 146, 204, 283, 354, 372, 373, 382, 402, 403, 461
enthalpy chart, 149
 $\text{--H}_2\text{O--NaCl}$, 163
sulphite, 271, 372
thiosulphate, 13, 49, 144, 204, 237, 372, 375
Solar pond evaporation, 377
Solid solutions, 16, 144, 166
Solubility:
correlations, 92–95
determination of, 112–120, 169
diagrams, 93, 95
expression and conversion, 90–92
ideal, 98
impurities and, 110
inorganic salts in water, 483–489
isothermal methods, 118
organic solids in water, 490–491
particle size and, 108
prediction of, 120
pressure effect, 119
product, 104–108, 119, 481–482
sparingly soluble salts, 119
supersolubility diagram, 124
Solution:
analysis of, 114
composition expressions, 90–92
heat of, 62, 520–527
ideal and non-ideal, 98–108
refractive index of, 47
structure of, 132
Solvents, choice of, 86–90
Space lattices, 12
Specific heat capacity, 50
Specific surface area, 72
Spherulization, 354, 402
Spiral growth, 29, 221
Spinodal decomposition, 191, 134
Spray crystallization, 401
Stagnant film, 226, 234, 264
Stearic acid, 283
Stokes' law, 37, 69, 455
Stopped-flow technique, 208
Strontium carbonate, 211
sulphate, 122
Structure of solutions, 132
Sublimation, 300, 358–368
enthalpy of, 61
yield from, 364
Succinic acid, 248, 271, 272
Sucrose, 8, 13, 32, 49, 126, 132, 134, 195, 238, 253, 271, 285, 337, 426
Sugar, see sucrose
Sulphur, 8, 137, 333, 359
Supercritical fluids, 137, 302
Supersaturation, 123–132
balance, 424
conversion factors for, 127
thermodynamic, 128
Surface:
area, of crystals, 66, 72
energy, 183, 193, 216
reaction (integration), 225
tension, 39–41
Symmetry, crystal, 4
Synthetic complex method, 116, 169
Systems, crystal, 7
Tartaric acid, 19, 21
Temperature cycling, 322
Terephthalic acid, 286, 359
Terminal solid solutions, 142
Ternary systems, 156
Tetrahedral class, 9
Thaw-melt method, 153
Thermal analysis, 151–156
Thermal conductivity, 54
Thiourea adducts, 396
Thymol, 359
Titanium hexafluoride, 359
Transition point, 95, 143
Triangular diagrams, 157
Tridymite, 17
Triple point, 137
Trouton's rule, 61
Tutton salts, 166
Twin crystals, 25
Ultrasonics, effects of, 181, 462
Unstable salt pair, 171
Uranium hexafluoride, 359
Urea, 134, 146, 274, 354
adducts, 396

- Vacuum:
 cooling, 385
 crystallizers, 382, 385
- Van't Hoff equation, 98
- Verneuil furnace, 314
- Vicinal faces, 12
- Viscosity, 35–39
 of solutions, 510–512
 of suspensions, 38
- Washing of crystals, 244, 471
- Water, properties of, 41, 55–56, 136, 480
- Watering-out, 333
- Waxes and fats, 155, 348, 374
- Wet residue method, 169
- Xylene, *p*-, 350, 358, 376, 396,
 462
- Xylitol, 199
- Yield, theoretical crystal, 96, 391
- Yttrium carbonate, 338
- Zinc sulphate, 464
- Zircon, 8
- Zirconium tetrachloride, 366
- Zone refining, 303